Universidad Autónoma de Madrid

Facultad de Ciencias

Departamento de Química Orgánica

Tesis Doctoral

Development of Novel Photocatalytic Strategies and Visible Light Photocatalysts

Thomas Rigotti

Madrid, 2020

La presente tesis ha sido realizada en el Departamento de Química Orgánica de la Universidad Autónoma de Madrid, bajo la supervisión del Prof. Dr. José Julián Alemán Lara**.** La financiación de este trabajo ha provenido del Consejo Europeo de Investigación (ERC-CG, número de contrato 647550), del Ministerio de Economía y Competitividad (CTQ-2015-64561-R y RTI2018-095038- B-I00), de la "Comunidad de Madrid" y de los Fondos Estructurales y de Inversión Europeos (S2018/NMT-4367).

La tesis se presenta como un compendio de publicaciones. Las publicaciones están distribuidas en cinco diferentes capítulos, teniendo cada capítulo su propia introducción. Además, el documento contiene una presentación de la tesis doctoral, una introducción general a la fotocatálisis, unos objetivos de la tesis doctoral, un resumen de los resultados y unas conclusiones finales comunes a toda la tesis.

La parte experimental de cada uno de los capítulos está recogida en la memoria electrónica adjunta a la tesis doctoral, aunque también han sido descritos los compuestos principales al final de cada uno de ellos. Los espectros de RMN y las descripciones detalladas de los procedimientos experimentales quedan, por tanto, recogidas en la memoria USB.

El idioma en el que está escrita la tesis es el inglés. Conforme a la normativa, la presentación de la tesis doctoral y las conclusiones finales están redactadas en castellano.

Abbreviations and Acronyms

The abbreviations and acronyms used in this PhD thesis are the ones recommended in the "Guidelines for Authors" (*The Journal of Organic Chemistry*, Standard Abbreviations and Acronyms). The structure of the photocatalysts that have been discussed are the ones reported in the "Photoredox Catalysis - Desk Reference and User's Guide" available at the Merck - Sigma Aldrich website. In addition, the following abbreviations and acronyms have been used:

A	Acceptor
AC	Aminocatalyst
BET	Back electron transfer
BODIPYs	4,4-Difluoro-4-bora-3a,4a-diaza-*s*-indacenes
BOX	Bisoxazoline
CFL	Compact Fluorescent Lamp
D	Donor
DAC	Donor-Acceptor Cyclopropane
DBFOX	(*R*,*R*)-4,6-dibenzofurandiyl-2,2'-bis(4-phenyloxazoline)
DFT	Density Functional Theory
DIPEA	*N*,*N*-Diisopropylethylamine
EDA	Electron Donor-Acceptor
EDG	Electron-donating Group
EnT	Energy Transfer
E_S	Singlet Energy
E_T	Triplet Energy
EWG	Electron-withdrawing Group
FC	Flash Chromatography
HAT	Hydrogen atom transfer
Het	Heterocycle
IBX	2-Iodoxybenzoic acid
L	Ligand
LA	Lewis acid
LED	Light Emitting Diode
LG	Leaving group

M	Metal
Mes	Mesityl
MLCT	Metal-to-ligand Charge Transfer
MS	Mass spectrometry or Molecular Sieves
m-DNB	*meta*-Dinitrobenzene
PC	Photocatalyst
PCET	Proton-coupled Electron Transfer
PG	Protecting Group
Phth	Phthalimide
PMP	Paramethoxyphenyl
PTH	10-Phenylphenothiazine
PyBOX	Bis(oxazolinyl)pyridine
$Rh_2(esp)_2$	Bis[rhodium(α,α,α′,α′-tetramethyl-1,3-benzenedipropionic acid)]
SCE	Saturated Calomel Electrode
SET	Single-electron transfer
TDDFT	Time-Dependent DFT
TDS	*tert*-Hexyldimethylsilyl
TMS	Trimethylsilyl
TPP	Tetraphenylporphyrin

Presentación de la tesis doctoral

La presente tesis doctoral se ha desarrollado en el Departamento de Química Orgánica de la Universidad Autónoma de Madrid, bajo la supervisión del Prof. Dr. José Julián Alemán Lara (grupo de investigación FRONCAT). En la tesis doctoral se han desarrollado distintos proyectos de fotocatálisis y fotocatálisis enantioselectiva, utilizando fotocatalizadores homogéneos, catalizadores bifuncionales o irradiación directa de intermedios fotoactivos. Además, la síntesis de compuestos fluorescentes se ha llevado a cabo mediante catálisis metálica enantioselectiva.

Debido al gran interés para el desarrollo de nuevas metodologías y nuevas reacciones en el campo de la química orgánica, la fotocatálisis ha tenido un rápida evolución en las últimas dos décadas gracias al desarrollo de nuevas fuentes de irradiación y a nuevas estrategias para la formación de radicales e intermedios excitados, utilizando la luz visible como fuente de energía renovable. Esto es principalmente debido a la reactividad única de los intermedios excitados que permite llevar a cabo transformaciones que sería imposible obtener mediante la síntesis orgánica convencional, basada en estrategias polares y en rupturas heterolíticas. Además, la fotocatálisis puede generar intermedios radicalarios mediante oxidación o reducción de varios sustratos sin tener que utilizar reactivos tóxicos o condiciones de reacción drásticas, aprovechándose de la enorme energía de los fotones para inducir procesos redox desde el estado electrónico excitado del fotocatalizador. Asimismo, la combinación de procesos redox con otros tipos de catálisis permite la generación de intermedios que serían imposible de obtener mediante otras metodologías, evidenciando una vez más como esta disciplina permite conseguir procesos únicos.

Durante el desarrollo de esta tesis doctoral se han estudiado diferentes modos de activación que pueden ser utilizados en fotocatálisis para llevar a cabo transformaciones muy diferentes desde un punto de vista mecanístico. Esto nos ha permitido expandir nuestros conocimientos en el campo de la química orgánica con un particular interés para las nuevas estrategias fotocatalíticas disponibles que incluyen procesos a transferencia de un electrón, transferencias de energía y excitación directa de intermedios de reacción. Además se han estudiado nuevos procesos fotocatalíticos enantioselectivos, ya que el número limitado de estrategias disponibles hasta el momento es debido a la gran dificultad en inducir de manera efectiva altos niveles de estereocontrol en transformaciones que tienen lugar sobre sustratos e intermedios excitados. Esto es esencialmente debido a la gran reactividad de los mismos, impidiendo el desarrollo de procesos asimétricos mediados por un catalizador enantiopuro. En el primer capítulo de la tesis, hemos descrito algunas de las estrategias básicas de la fotocatálisis al igual que los distintos procesos fotocatalíticos asimétricos publicados hasta el momento.

Teniendo en cuenta todas las consideraciones expuestas arriba, en el capítulo 2 hemos investigado una reacción fotocatalítica de expansión estereoespecifica de ciclopropanos para conseguir compuestos enantioenriquecidos a través de una apertura de anillo de ciclopropanos dando lugar a anillos de cinco miembros. Normalmente, estas reacciones de expansión se obtienen mediante la utilización de “Donor-Acceptor Cyclopropanes” y permitiendo la apertura del anillo tensionado mediante el uso de diferentes tipos de activaciones. Sin embargo, esto limita fuertemente el rango de sustratos que se pueden emplear para estas reacciones de expansión. Por tanto decidimos estudiar la apertura mediante el uso de una estrategia fotocatalítica.

En el capítulo 3, debido al creciente interés de la comunidad científica para el desarrollo de procesos fotocatalíticos, hemos decidido investigar la reacción de α-alquilación asimétrica de aldehídos que está basada en procesos de transferencia de un electrón. En este contexto se ha llevado a cabo la síntesis de un foto-aminocatalizador bifuncional que no se había descrito hasta el momento en la bibliografía, estudiando su actividad catalítica y comparándolo con otros sistemas fotocatalíticos.

Por otro lado, en el capítulo 4, hemos estudiado una reacción [2+2] fotocatalítica asimétrica. Esta constituye una de las reacciones fotoquímicas más utilizadas e investigadas debido a la construcción inusual de múltiples enlaces en un único paso, que sería muy difícil conseguir mediante química polar y activaciones convencionales. Estas reacciones han sido ampliamente utilizadas en fotoquímica, principalmente a través de irradiación directa de sustratos orgánicos con luz ultravioleta, mientras que las correspondientes cicloadiciones [2+2] bajo irradiación de luz visible han sido desarrolladas gracias al uso de fotocatalizadores o modulación de las propiedades fotofísicas de sus intermedios. Sin embargo, el desarrollo de procesos catalíticos eficientes de cicloadiciones [2+2] enantioselectivas ha sido descrito recientemente. Estas están basadas en el uso de ácidos de Lewis o catalizadores de enlace de hidrógeno, limitando el rango de posibles sustratos que se pueden emplear para conseguir una reacción enantioselectiva. Por estas razones se planteó utilizar una estrategia aminocatalítica para intentar activar de manera covalente los sustratos y poder expandir el tipo de ciclobutanos enantioenriquecidos obtenidos.

Adicionalmente, en el capítulo 5, hemos desarrollado unos nuevos fotocatalizadores de acridinio con el objetivo de mejorar las prestaciones de los catalizadores análogos descritos en la bibliografía.

Por último, en el capítulo 6, nos planteamos la síntesis de cromóforos orgánicos que pudieran ser utilizados como biosensores. Entre ellos, los colorantes basados en estructuras de BODIPY han sido ampliamente empleados en este campo. Además, debido a la particular estructura de los mismos, su posición *meso* esta activada hacia reacciones de adición nucleofila. Por estas razones se pensó en preparar unas pirrolidinas funcionalizadas con un BODIPY mediante una reacción de ciclación asimétrica catalizada por un metal. De esta forma, los compuestos resultantes podrían ser utilizados como biosensores o permitir la funcionalización de péptidos.

Finalmente cabe destacar que la presente tesis doctoral está compuesta de una introducción general a la fotocatálisis y a la fotocatálisis enantioselectiva donde se han indicado los objetivos generales de la tesis doctoral. Después de esta parte introductoria están presentes cinco capítulos, con una introducción específica para cada uno, relativos a diferentes temáticas estudiadas durante la tesis con correspondientes publicaciones y partes experimentales representativas. Para la parte experimental completa se ha incluido una memoria USB donde está recogida tosa esa información. Además, al término de la tesis, se han recogido unas conclusiones generales en castellano.

El autor de esta tesis doctoral ha aportado una contribución original distinta en cada capítulo, evidenciado por el orden en el que el doctorando figura en cada una de las publicaciones, ya sea como autor principal o como coautor.

En el capítulo 2 el autor ha contribuido a la optimización de las condiciones de reacción, la evaluación del alcance estructural de la reacción de expansión de ciclopropanos a dihidrofuranos (Tabla 1) y a la realización de las pruebas mecanísticas (Esquema 3).

En el capítulo 3 el autor ha contribuido mediante el diseño del catalizador bifuncional (Esquema 1), la optimización de las condiciones de reacción (Tabla 2), la evaluación de parte del alcance estructural de la reacción fotocatalítica (Tablas 3 y 4) y la realización de las pruebas mecanísticas (Esquemas 4 y 5 y Figuras 4 y 6).

En el capítulo 4 el autor ha contribuido al diseño del sistema catalítico, la optimización de las condiciones de reacción (Tabla 1), la evaluación del alcance estructural de la reacción de cicloadición (Tabla 2) y la realización de las pruebas mecanísticas (Figura 2 y Esquema 1).

En el capítulo 5 el autor ha contribuido a la primera publicación mediante el diseño del sistema catalítico y la realización de las reacciones fotocatalíticas (Esquema 3), mientras que en la segunda publicación el autor ha realizado una parte de las pruebas mecanísticas mediante técnicas espectrométricas (Figuras 2 y 3).

En el capítulo 6 el autor ha contribuido mediante la realización de la optimización de las condiciones de reacción (Tabla 1) y la evaluación del alcance estructural de la reacción de cicloadición (Tabla 2).

Además, en cada una de las publicaciones anteriormente mencionadas, el autor ha contribuido a la escritura de las mismas.

INDEX

1. Introduction to Photocatalysis and Enantioselective Photocatalysis

1.1 Photochemistry

Photochemistry has been envisioned as a powerful and innovative tool that could have been applied for organic synthesis since the end of the 19th century. Many chemists such as Stanislao Cannizzaro, Emanuele Paternò and in particular Giacomo Ciamician recognized the potential of this unexplored research area that was enabling interesting transformations and permitting unique reactivities.[1] Due to the absence of appropriate artificial irradiation systems, photochemistry started as a solar discipline, employing natural sunlight as the energy source and leaving the reaction mixtures exposed to sun irradiation for long periods of time. Ciamician and his collaborator Paul Silber discovered a wide range of photochemical reactions as photoreductions, photoisomerizations, photopinacolizations, photocleavages and photocycloadditions.[2] The most brilliant example of Ciamician's chemistry was the intramolecular [2+2] photocycloaddition that led to the obtainment of carvonecamphor after a long exposure to sunlight of a solution of carvone (Scheme 1a).[3] Another example of the synthetic value of photochemistry is demonstrated by the photopinacolization achieved upon irradiation of an ethanol solution of benzophenone to obtain the corresponding pinacol product (Scheme 1b).[4] In addition, Ciamician envisioned that photochemistry could have been employed as an environmentally friendly strategy in organic synthesis and as an alternative green energy source for the future humankind.[5]

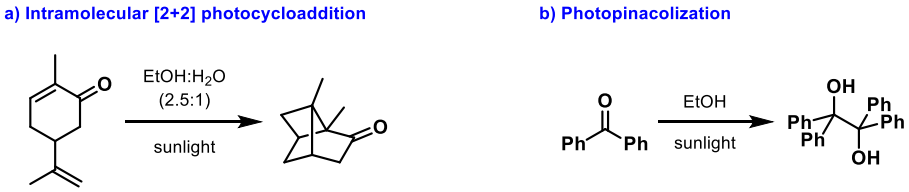

Scheme 1. First examples of photochemical reactions developed by Giacomo Ciamician.

Since then, photochemistry has been widely employed in organic synthesis, mainly employing UV irradiation, as many organic molecules are not absorbing light in the visible light region. It has been employed for both the production of important building blocks in organic synthesis and for the construction of complex molecules in total synthesis.[6] Nevertheless, photochemical reactions that are carried out under UV irradiation present some drawbacks: I) the unselective excitation of several functional groups in polyfunctionalized molecules, II) the high reactivity of open-shell radicals that can lead to consecutive reactions or undesired transformations, III) the special and unpractical equipment required for UV light irradiation, IV) the high challenge of developing catalytic enantioselective strategies. In particular, the latter is due to the employed highly energetic UV irradiation that leads to an indiscriminate excitation of the substrate without any pre-association with the chiral catalyst, obtaining a racemic background process without any stereoinduction. For these reasons, photochemistry has been remained sideline from conventional organic chemistry research until the appearance of suitable irradiation sources that can operate in the visible light region and the development of

[1] M. Oelgemöller, *Chem. Rev.* **2016**, *116*, 9664-9682.
[2] A. Albini, V. Dichiarante, *Photochem. Photobiol. Sci*. **2009**, *8*, 248-254.
[3] (a) G. Ciamician, P. Silber, *Ber. Dtsch. Chem. Ges*. **1908**, *41*, 1928-1935; the structure of the cyclobutane was confirmed by subsequent studies: (b) G. Büchi, I. M. Goldman, *J. Am. Chem. Soc*. **1957**, *79*, 4741-4748; (c) J. Meinwald, R. A. Schneider, *J. Am. Chem. Soc*. **1965**, *87*, 5218-5229.
[4] G. Ciamician, P. Silber, *Ber. Dtsch. Chem. Ges*. **1900**, *33*, 2911-2913.
[5] G. Ciamician, *Science* **1912**, *36*, 385-394.
[6] M. D. Kärkäs, J. A. Porco Jr., C. R. J. Stephenson, *Chem. Rev*. **2016**, *116*, 9683-9747.

new activation strategies, photocatalysts and photosensitizers that permit predictable and controlled transformations, a part from unique activation modes.[7]

1.2 Different Strategies in Photochemistry and Photocatalysis

The excitation of an organic substrate can be achieved through direct irradiation with the appropriate light source, nevertheless, since many organic compounds does not absorb light in the visible region, it is often necessary to employ UV irradiation with all the drawbacks and limitations highlighted above (Figure 1a). Upon irradiation, the singlet ground-state compound reaches a singlet excited state (S) which can be the active species that is undergoing different chemical transformations or it can lead to a triplet excited state (T) through intersystem crossing (ISC).[7a] The nature of the excited state (singlet or triplet) effectively involved in the different reactions is strongly dependent to the specific transformation and reaction conditions.

To avoid the use of UV light, and to overcome some of the limitations associated with the direct excitation of organic substrates, different strategies have been developed to carry out the reaction under visible light irradiation (Figure 1b-d). The one that has undoubtedly found more applications is photoredox catalysis which relies on the ability of excited state photocatalysts in engaging SET processes with various organic substrates (Figure 1b).[8] This can be explained by the fact that SET processes are more intensively studied, highly predictable, and similar to radical chemistry. Therefore, the previously known reactivity of open-shell intermediates has provided a strong background for the development of catalytic photoredox processes. Moreover the constant development of new photocatalysts, with a wide range of photophysical properties and excited state redox potentials, has enormously expanded the number of radical precursors that can be employed in the reactions. In some cases a base or acid-assisted SET can be achieved, leading to a proton-coupled electron transfer (PCET) that permits to carry out otherwise unfavorable photoredox transformations.[9] Hence, a good planning for the desired transformation, that is taking into account the various steps of the photocatalytic cycle, is permitting to identify reasonable conditions prior having to face the experimental challenges.

Furthermore, the employment of a catalytic or stoichiometric photosensitizer, which is absorbing light in the visible light region, can enable the indirect excitation of a targeted compound through the formation of an excited complex (exciplex) or through an energy transfer (Figure 1c).[7a-b,10] An exciplex is formed between an excited photosensitizer and a ground-state substrate upon sharing of the electronic excitation between the two components.[10] On the other hand, an energy transfer occurs between an excited photosensitizer and a ground-state substrate, leading to a ground-state photosensitizer and an excited substrate. The photosensitization can occur from either the singlet or the triplet excited states leading to singlet or triplet excited exciplexes or substrates. The employment of a photosensitizer for the formation of an exciplex is challenging since it is not easily rationalizable and depends on the specific combination of the components. On the other hand, triplet energy transfer has been widely employed in photochemistry to achieve a spin-forbidden transition, obtaining a triplet

[7] (a) C. R. J. Stephenson, T. P. Yoon, D. W. C. MacMillan "Visible Light Photocatalysis in Organic Chemistry", **2018**, Wiley-VCH; (b) R. Brimioulle, D. Lenhart, M. M. Maturi, T. Bach, *Angew. Chem. Int. Ed*. **2015**, *54*, 3872-3890; (c) E. Meggers, *Chem. Commun*. **2015**, *51*, 3290-3301; (d) A. F. Garrido-Castro, M. C. Maestro, J. Alemán, *Tetrahedron Lett.* **2018**, *59*, 1286-1294. (e) C. Jiang, W. Chen, W.-H. Zheng, H. Lu, *Org. Biomol. Chem*. **2019**, *17*, 8673-8689.

[8] (a) C. Prier, D. Rankic, D. W. C. MacMillan, *Chem. Rev*. **2013**, *113*, 5322-5363; (b) J. M. R. Narayanam, C. R. J. Stephenson, *Chem. Soc. Rev*. **2011**, *40*, 102-113; (c) N. A. Romero, D. A. Nicewicz, *Chem. Rev.* **2016**, 116, 10075-10166; (d) M. H. Shaw, J. Twilton, D. W. C. MacMillan, *J. Org. Chem.* **2016**, *81*, 6898-6926. (e) b) J. Twilton, C. Le, P. Zhang, M. H. Shaw, R. W. Evans, D. W. C. MacMillan, *Nat Rev Chem*. **2017**, *1*, 0052.

[9] E. C. Gentry and R. R. Knowles, *Acc. Chem. Res*. **2016**, *49*, 1546-1556.

[10] G. J. Kavarnos, N. J. Turro, *Chem. Rev.* **1986**, *86,* 401-449.

excited substrate through the employment of a triplet photosensitizer.[11] The photosensitizer is usually a compound that can absorb light in the visible region and that can easily undergo an intersystem crossing to reach its triplet excited state. From this excited state the triplet sensitization can occur, overcoming the impossible direct excitation of the substrate to its triplet excited state. A special case of energy transfer is the triplet-triplet annihilation (TTA).[7a] This occurs between two triplet excited state molecules that upon reaction lead to a singlet ground-state and a singlet excited state molecule. It is important to notice that the resulting singlet energy is higher than the corresponding triplet energies for the excited molecules and the process is known as photon upconversion.

Another way to carry out a reaction under visible light irradiation is taking advantage of the formation of colored ground-state Electron Donor-Acceptor (EDA) complexes (Figure 1d).[12] These transient generated intermediates can be formed between an electron-rich and an electron-poor substrate through association and interaction of them in the ground-state. The formation of an EDA complex is evidenced by the fact that a new absorption band appears in the visible light region upon preparation of the reaction mixtures. Therefore, this permits to employ visible light to obtain an excited EDA complex which can undergo different chemical transformations or can carry out a single-electron transfer (SET) between the electron-rich and the electron-poor substrate, leading to the free radical ions which can eventually react in a variety of reactions.

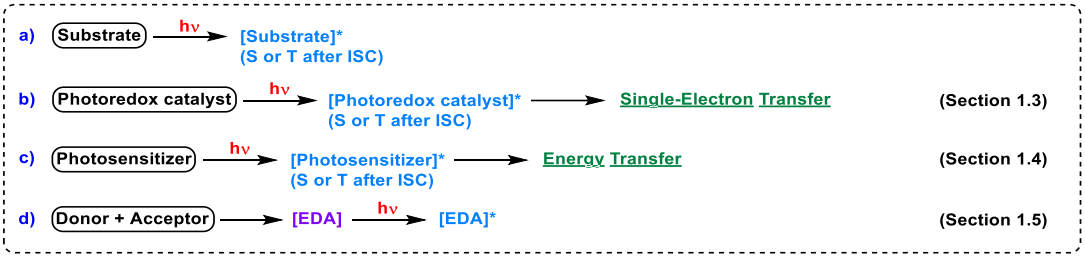

Figure 1. Different strategies in photochemistry and photocatalysis.

In the following sections, we will describe some of the reported photocatalytic strategies (Sections 1.3-1.5) and the most significant enantioselective strategies developed to induce an asymmetric photocatalytic process (Section 1.6).

1.3 First Examples and Modern Advances of Photoredox Catalysis through SET

The development of an increasing number of new photocatalysts and photosensitizers in the last decades has been triggered by the fact that photoredox catalysis enables the achievement of new activation modes and new reactivities that are often complementary in comparison to the conventional polar methodologies, giving access to products that would be impossible to obtain in a different way.[7a,8,11] The usually employed photocatalysts are metal complexes or organic dyes that permit the use of visible light as the irradiation source. The lifetime of their excited states is relatively high (from ns to µs), permitting a bimolecular single-electron transfer process to occur with a wide range of substrates. Upon irradiation, the singlet ground-state photocatalyst can reach different electronic singlet excited states that rapidly undergo an internal conversion to the lowest singlet excited state. The singlet excited state can revert to the ground-state through thermal and vibrational deactivation or, in some cases, through emission (fluorescence). The lowest singlet excited state can undergo an intersystem crossing to the triplet state depending on the nature of the photocatalyst, the spin-orbit coupling and various

[11] Q.-Q. Zhou, Y.-Q. Zou, L.-Q. Lu, W.-J. Xiao, *Angew. Chem. Int. Ed.* **2019**, *58*, 1586-1604.
[12] C. G. S. Lima, T. de M. Lima, M. Duarte, I. D. Jurberg, M. W. Paixão, *ACS Catal.* **2016**, *6*, 1389-1407.

photophysical parameters (Figure 2). This excited state can be deactivated through emission of radiation (phosphorescence) or through thermal deactivation. Metal complexes present a high rate of ISC and usually, for this reason, their excited active species are triplets. Nevertheless, many photocatalysts react from their singlet excited state (the majority of the organophotocatalysts for example),[8c] evidencing that the real photocatalytic active intermediate is dictated by the specific combination of reaction, photocatalyst, substrate and reaction conditions.

These ground-state compounds are poor oxidants and poor reductants but, upon excitation, they become strong oxidants and strong reductants in their electronic excited state (Figure 2a).[8a] In the case of a metal complex photocatalyst, the electronic transition with one electron being excited from the metal-centered orbitals to the ligand-centered π* orbitals, named as metal-to-ligand charge transfer (MLCT), is leading to a triplet excited state after intersystem crossing. Since radiative deactivation to the singlet ground-state is a spin-forbidden transition, the lifetime of the triplet excited state is higher than the lifetime of the singlet excited state. Therefore, in the case of a rapid ISC, the triplet excited species is the responsible of the redox processes, having the remarkably characteristic of being both a stronger oxidant and a stronger reductant than the ground-state photocatalyst.[8a] This is essentially due to the fact that upon excitation the photocatalyst presents an electron in a higher-energy orbital that can easily engage a single-electron transfer (SET) with an appropriate substrate, acting as a reductant. On the other hand, as a result of the lower-energy hole created in the catalyst orbitals upon excitation, the photocatalyst can act as an oxidant species receiving one electron from an appropriate substrate.

Under photoredox catalysis net reductive, net oxidative or redox neutral reactions can be carried out, with the excited state of the catalyst implied through an oxidative quenching or a reductive quenching cycle (Figure 2b).[8d] In net reductive and in net oxidative reactions an electron donor or an electron acceptor are respectively required as stoichiometric additives to close the cycle, whereas in redox neutral reactions the two redox processes required to regenerate the photoredox catalyst are carried out in different steps of the reaction mechanism involving only the substrates. In addition, redox neutral reactions can be achieved through the synergistic employment of dual-catalytic systems in which the photoredox catalyst is combined with a redox-active co-catalyst.

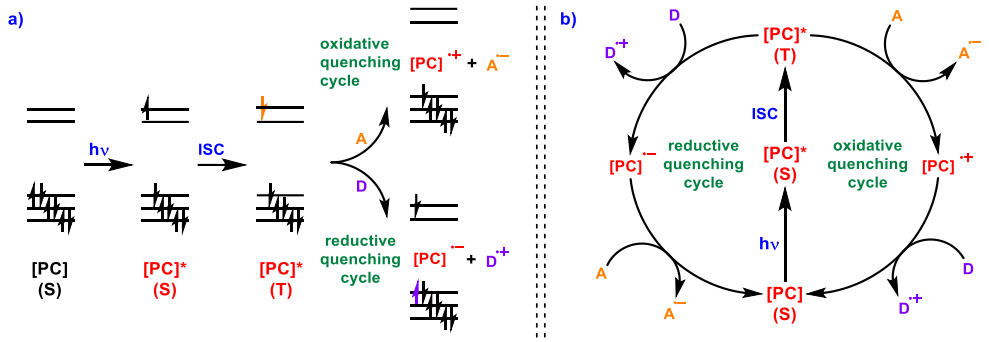

Figure 2. (a) Simplified molecular orbital representation for a photoredox catalyst. (b) Photocatalytic cycles (reductive and oxidative quenching cycles).

The first example of a net reductive photocatalytic reaction was reported by Kellog in 1978 (Scheme 2a),[13] while the first examples of a net oxidative and a redox neutral photocatalytic reactions were published some years later by Cano-Yelo and Deronzier (Scheme

[13] D. M. Hedstrand, W. M. Kruizinga, R. M. Kellogg, *Tetrahedron Lett*. **1978**, *19*, 1255-1258.

2b,c).[14,15]Although a general methodology for the addition of radicals, photocatalitically generated from redox active esters, to Michael acceptors has been reported by Okada and Oda in 1991 (Scheme 2d),[16] the employment of photoredox catalysis has been maintained definitely underexplored since the late 2000s.[8]

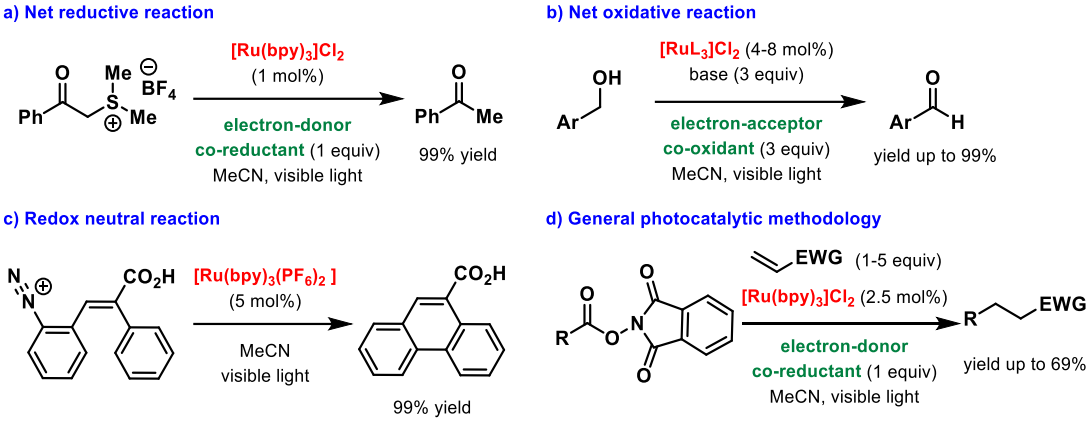

Scheme 2. First examples of net reductive, net oxidative and redox neutral photoredox reactions.

During the first decade of the 21st century, the research groups of Bach[17] (Scheme 3a), Yoon[18a] (Scheme 3b), MacMillan[19] (Scheme 3c) and Stephenson[20] (Scheme 3d) reported the use of photoredox catalysis for synthetically highly valuable single-electron transfer processes, pushing a growing interest of the research community in this area and opening the pathway for the advent of modern photocatalysis. In 2008, the Yoon's research group reported a Lewis acid-mediated intramolecular [2+2] photocycloaddition of enones employing photoredox catalysis through a reductive quenching cycle (Scheme 3b).[18] The use of the lithium cation as a Lewis acid permitted the lowering of the ground state reduction potential of the substrate, activating the enone towards the single-electron transfer reduction and leading to a radical anion intermediate that carry out the cyclization. The presence of a chain propagation mechanism was demonstrated successively by the same authors.[21] Another pioneering example which highlighted the potential of visible light-mediated methods was presented by Stephenson's research group in 2009 (Scheme 3d).[20] Through a mild photocatalytic methodology, they achieved the dehalogenation of acyl and benzyl halides in high efficiency and with high yields.

Soon after the previously described [2+2] photocycloaddition of enones,[18] the Yoon's research group reported an intramolecular [2+2] photocycloaddition of styrene derivatives through the employment of an oxidative quenching cycle, highlighting that by means of choosing the correct combination of substrate and additive the same photocatalyst can unlock mechanistically different transformations (Scheme 4a).[22] An important example of the high synthetic value of photocatalytic processes was disclosed by Yoon's lab, in which an intermolecular radical cation Diels-Alder reaction was achieved (Scheme 4b).[23]

[14] H. Cano-Yelo, A. Deronzier, *Tetrahedron Lett*. **1984**, *25*, 5517-5520.
[15] H. Cano-Yelo, A. Deronzier, *J. Chem. Soc., Perkin Trans. 2* **1984**, 1093-1098.
[16] K. Okada, K. Okamoto, N. Morita, K. Okubo, M. Oda, *J. Am. Chem. Soc.* **1991**, *113*, 9401-9402.
[17] A. Bauer, F. Westkamper, S. Grimme, T. Bach, *Nature* **2005**, *436*, 1139-1140.
[18] (a) M. A. Ischay, M. E. Anzovino, J. Du, T. P. Yoon, *J. Am. Chem. Soc.* **2008**, *130*, 12886-12887; for a closely related intermolecular version reported by the same research group see: (b) J. Du, T. P. Yoon, *J. Am. Chem. Soc.* **2009**, *131*, 14604-14605.
[19] D. A. Nicewicz, D. W. C. MacMillan, Science 2008, 322, 77-80.
[20] J. M. R. Narayanam, J. W. Tucker, C. R. J. Stephenson, *J. Am. Chem. Soc.* **2009**, *131*, 8756-8757.
[21] M. A. Cismesia, T. P. Yoon, *Chem. Sci.*, **2015**, *6*, 5426-5434.
[22] (a) M. A. Ischay, Z. Lu, T. P. Yoon, *J. Am. Chem. Soc.* **2010,** *132*, 8572-8574; for a closely related intermolecular version reported by the same research group see: (b) M. A. Ischay, M. S. Ament, T. P. Yoon, *Chem. Sci.*, **2012**, *3*, 2807-2811.
[23] (a) S. Lin, M. A. Ischay, C. G. Fry, T. P. Yoon, *J. Am. Chem. Soc*. **2011**, *133*, 19350-19353; for a closely related intramolecular version reported by the same research group see: (b) S. Lin, C. E. Padilla, M. A. Ischay, T. P. Yoon, *Tetrahedron Lett.* **2012**, *53*, 3073-3076.

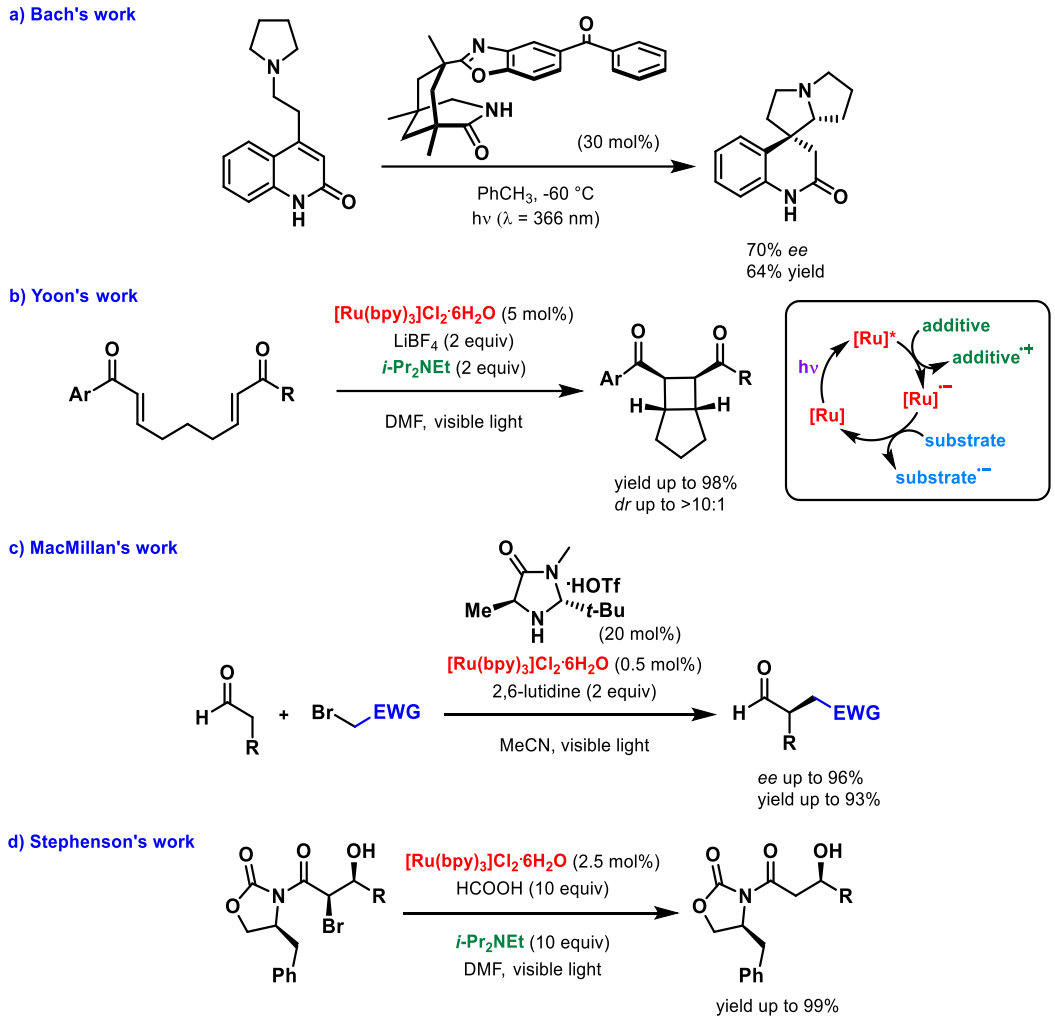

Scheme 3. Landmark examples reported in photoredox catalysis.

This photochemical [4+2] cycloaddition represents an impressive example of an umpolung of reactivity in comparison with the thermal Diels-Alder reaction. Indeed, through this strategy, the overall regiochemistry of the Diels-Alder is completely reverted since upon one-electron oxidation the dienophile presents opposite electronic characteristics, giving access to natural products such as *Heitziamide A*.

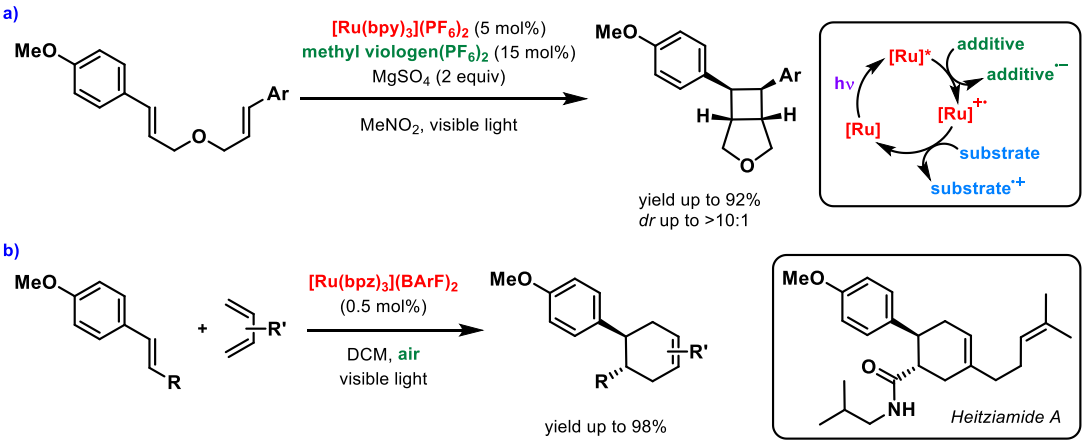

Scheme 4. (a) Intramolecular [2+2] photocycloaddition of styrene derivatives through photoredox catalysis. (b) Intermolecular photocatalytic radical cation Diels-Alder reaction.

Similar strategies for the achievement of [3+2] cycloadditions and [4+2] annulations were developed in the laboratory of Zheng, employing cyclopropylamines or cyclobutylamines and styrene or acetylene derivatives, respectively (Scheme 5).[24,25] Upon photoredox oxidation of the amine by the excited ruthenium catalyst, the 3- or 4-membered ring is easily opened leading to an iminium ion radical intermediate. The latter can carry out the cycloaddition event and, after a SET to regenerate the photocatalyst, the corresponding ring-expanded product is obtained by a redox neutral reaction.

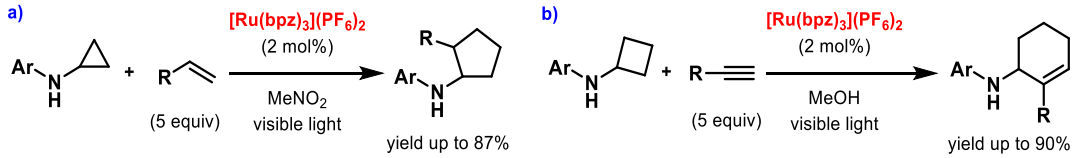

Scheme 5. (a) [3+2] and (b) [4+2] photocatalytic annulation reactions of cyclopropyl and cyclobutyl amines.

Another interesting example of the synthetic value of photoredox catalysis can be appreciated by the anti-Markovnikov hydroetherification of alkenes reported by the Nicewicz's lab in 2012 which represents a redox neutral reaction (Scheme 6).[26] The employment of a highly oxidizing Fukuzumi's acridinium catalyst permitted the generation of a radical cation intermediate from a styrene derivative, which can be trapped by a nucleophile, either in an intramolecular or intermolecular fashion. Then, the corresponding benzyl radical can undergo a hydrogen atom transfer (HAT) with a redox-active HAT co-catalyst to furnish the desired product. Thus, a SET between the two catalysts restores the ground-state of each of them. During the last years the Nicewicz's lab has developed other acridinium-based photoredox catalysts with enhanced photophysical properties and efficiencies in many photocatalytic reactions.[27] The unique excited state redox potentials of this class of catalysts permitted to achieve the oxidation of normally unreactive substrates and their implementation in the synthesis of valuable products.

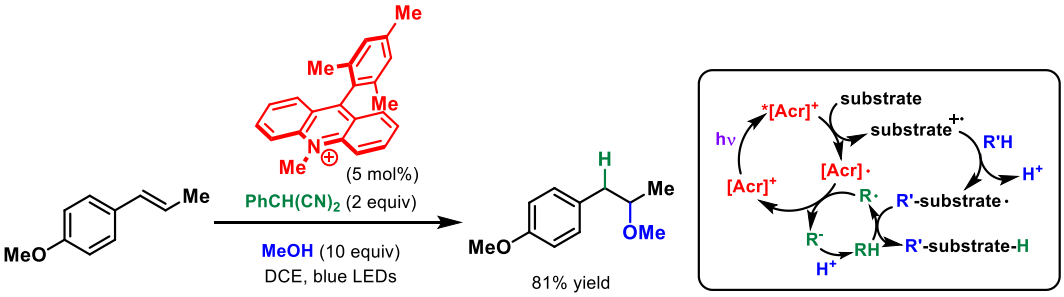

Scheme 6. Anti-Markovnikov hydroetherification of styrene derivatives through a radical cation intermediate.

On the other hand, the development of highly reducing photocatalysts has permitted the reduction of a wide range of substrates. For instance, normally inert substrates like aryl chlorides could be dehalogenated through the employment of 10-phenylphenothiazine.[28] This methodology allowed to carry out the dehalogenation of aryl iodides, aryl bromides, aryl chlorides and some alkyl bromides in high efficiency. Furthermore the reaction could be performed under air, observing just a slight decrease of reactivity and yields, since the catalyst works from its singlet excited state. Other highly reducing organic photocatalysts have been

[24] S. Maity, M. Zhu, R. S. Shinabery, N. Zheng, *Angew. Chem. Int. Ed.* **2012**, *51*, 222-226.
[25] J. Wang, N. Zheng, *Angew. Chem. Int. Ed.* **2015**, *54*, 11424-11427.
[26] D. S. Hamilton, D. A. Nicewicz, *J. Am. Chem. Soc.* **2012**, *134*, 18577-18580.
[27] (a) K. A. Margrey, D. A. Nicewicz, *Acc. Chem. Res.* **2016**, *49*, 1997-2006; (b) A. R. White, L. Wang, D. A. Nicewicz, *Synlett* **2019**, *30*, 827-832.
[28] E. H. Discekici, N. J. Treat, S. O. Poelma, K. M. Mattson, Z. M. Hudson, Y. Luo, C. J. Hawker, J. Read de Alaniz, *Chem. Commun.*, **2015**, *51*, 11705-11708.

developed by Akita's research group and their efficiency was demonstrated by the generation of different radicals from normally inert substrates.[29] The employment of these and other metal-based photocatalysts led to a wide range of fluoromethylative difunctionalization of alkenes as a representative potentiality of photoredox catalysis.[30] On the other hand, an innovative strategy for the generation of radicals was reported by Melchiorre's group through the development of a nucleophilic organic catalyst (Scheme 7).[31] Indeed, by means of a polar S_N2 reaction photocatalytically inert alkyl electrophiles could be activated after displacement of a chlorine leaving group by the dithiocarbamate anion catalyst. Then, the resulting photoactive intermediate can undergo a homolytic cleavage to afford the corresponding radical. This methodology could be applied to radical conjugate additions, late-stage functionalization, and to dual-catalytic systems to achieve asymmetric photocatalytic processes.

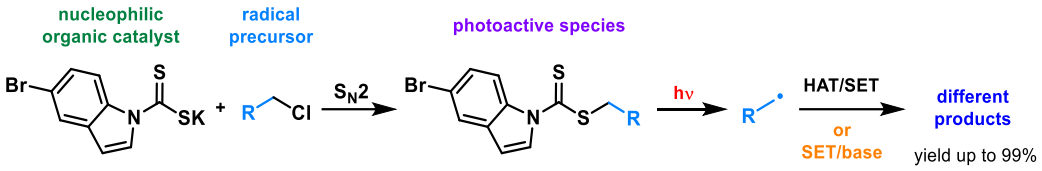

Scheme 7. Photocatalytic reduction of alkyl chlorides through homolytic cleavage of a photoactive species.

A recent development in this field through the merging of photoredox catalysis and nickel catalysis was simultaneously reported by Molander's,[32a] and MacMillan-Doyle's[32b] research groups with two pioneering examples in 2014 (Scheme 8). The use of amino acids, dimethylanilines, benzylic or (α-alkoxy)alkyl trifluoroborates as the nucleophilic partners and radical precursors permitted the achievement of *Csp*^{3}-*Csp*^{2} cross-coupling reactions under exceptionally mild conditions from simple and available organic substrates. The employment of photoredox catalysis for the predictable generation of radicals and the use of nickel as the metal catalyst led to the development of an impressive number of cross-coupling methodologies achievable through metallaphotoredox catalysis.[8e]

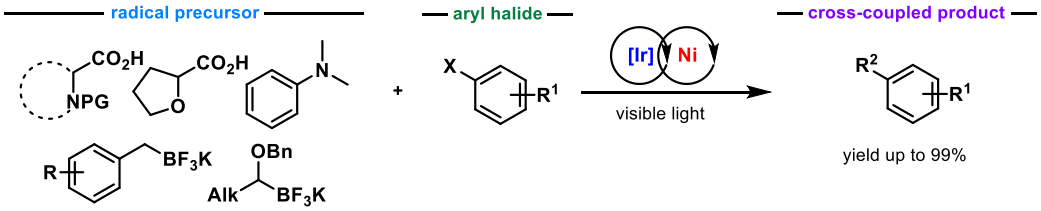

Scheme 8. Merging of photocatalysis and transition metal catalysis (metallaphotoredox catalysis).

A special case of a single-electron transfer mechanism in photoredox catalysis is the proton-coupled electron transfer (PCET). A PCET is a redox process composed by a single-electron transfer and a proton transfer which are performed in a concerted manner.[9] The use of PCET in synthetic organic chemistry has been maintained relatively unexplored even if there are numerous examples of biological redox reactions that are working through concerted PCET mechanism.[33] The net result of a PCET is a HAT but the two mechanisms are presenting huge differences in regards of the thermodynamics that are involved. Indeed, in a HAT process the proton and the electron are exchanged between a single donor and a single acceptor. On the other hand, in PCET the electron and the proton can be exchanged between a substrate or a radical and two different acceptors or donors, respectively. The appropriate combination of a

[29] N. Noto, T. Koike, M. Akita, *ACS Catal.* **2019**, *9*, 4382-4387.
[30] T. Koike, M. Akita, *Chem* **2018**, *4*, 409-437.
[31] B. Schweitzer-Chaput, M. A. Horwitz, E. de Pedro Beato, P. Melchiorre, *Nat. Chem.* **2019**, *11*, 129-135.
[32] (a) J. C. Tellis, D. N. Primer, G. A. Molander, *Science,* **2014**, *345*, 433-436; (b) Z. Zuo, D. T. Ahneman, L. Chu, J. A. Terrett, A. G. Doyle, D. W. C. MacMillan, *Science,* **2014**, *345*, 437-440.
[33] S. Y. Reece, J. M. Hodgkiss, J. Stubbe, D. G. Nocera, *Philos. Trans. R. Soc., B* **2006**, *361*, 1351-1364.

photocatalyst (as a photoreductant or a photooxidant) and an acid or a base is enabling PCET under visible light irradiation, allowing homolytic activations and bond cleavages that are inaccessible by conventional PCET strategies. Thus, reductive PCET-based (photoreductant and acid) and oxidative PCET-based (photooxidant and base) reactions can be obtained. Furthermore, the chemoselectivity of PCET-based reactions relies on the fact that this activation mechanism requires hydrogen bonding interactions between the substrate and the acid or the base prior to the electron transfer, unlocking selective homolytic activations and cleavages. The pioneering works regarding photocatalytic PCET catalysis were reported by Knowles' group.[9] A ketyl-radical cyclization reaction was achieved through a reductive PCET-based mechanism employing ruthenium photocatalyst, an acid co-catalyst and a stoichiometric hydrogen atom donor (Scheme 9a).[34] The initial homolytic activation was carried out through the synergistic action of the photocatalyst and the acid to give a ketyl radical which can undergo an intramolecular cyclization to obtain the bicyclic product after lactonization. On the other hand an oxidative PCET-based intermolecular reaction was accomplished through the selective bond homolysis of an amide substrate to furnish an amidyl radical (Scheme 9b).[35] The latter can engage a radical conjugate addition with an activated olefin to give, after electron and proton transfer, the corresponding cyclic product, restoring the catalysts. The employment of these strategies allowed to obtain a wide range of reactions like hydroaminations, hydroamidations, ring-expansions and remote C-H bond alkylation reactions among others.[36] Furthermore, DiRocco and co-workers reported that a photoredox PCET-based strategy could be employed for the efficient late-stage functionalization of biologically active heterocycles in a Minisci-type photocatalytic reaction.[37] In all the discussed cases the direct photoreduction or photooxidation of the substrates by the photocatalyst was thermodynamically disfavored and allowed only once the acid or the base employed as hydrogen donor or acceptor was coordinated to the specific substrate.

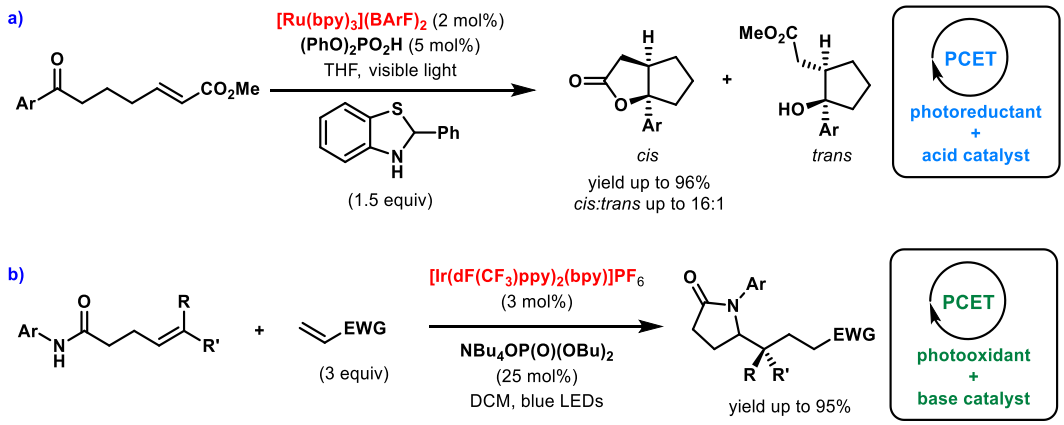

Scheme 9. Proton-coupled electron transfer (PCET) strategies employed in photoredox catalysis.

[34] K. T. Tarantino, P. Liu, R. R. Knowles, *J. Am. Chem. Soc.* **2013**, *135*, 10022-10025.

[35] G. J. Choi, R. R. Knowles, *J. Am. Chem. Soc*. **2015**, *137*, 9226-9229.

[36] (a) A. J. Musacchio, L. Q. Nguyen, G. H. Beard, R. R. Knowles, *J. Am. Chem. Soc.* **2014**, *136*, 12217-12220; (b) A. J. Musacchio, B. C. Lainhart, X. Zhang, S. G. Naguib, T. C. Sherwood, R. R. Knowles, *Science* **2017**, *355*, 727-730; (c) D. C. Miller, J. M. Ganley, A. J. Musacchio, T. C. Sherwood, W. R. Ewing, R. R. Knowles, *J. Am. Chem. Soc.* **2019**, *141*, 16590-16594; (d) David C. Miller, G. J. Choi, H. S. Orbe, R. R. Knowles, *J. Am. Chem. Soc*. **2015**, *137*, 13492-13495; (e) K. Zhao, K. Yamashita, J. E. Carpenter, T. C. Sherwood, W. R. Ewing, P. T. W. Cheng, R. R. Knowles, *J. Am. Chem. Soc*. **2019**, *141*, 8752-8757; (f) G. J. Choi, Q. Zhu, D. C. Miller, C. J. Gu, R. R. Knowles, *Nature* **2016**, *539*, 268-271.

[37] D. A. DiRocco, K. Dykstra, S. Krska, P. Vachal, D. V. Conway, M. Tudge, *Angew. Chem. Int. Ed.* **2014**, *53*, 4802-4806.

1.4 First Examples and Modern Advances of Photocatalysis by Triplet Energy Transfer

The first example of a [2+2] photocycloaddition of norbornadiene derivatives through a triplet energy transfer mechanism was reported by Kutal's Group in 1986 (Scheme 10a).[38] The use of a ruthenium complex as a triplet photosensitizer permitted the excitation of the norbornadiene to its triplet excited state, which subsequently carried out the [2+2] photocycloaddition to give the corresponding quadricyclene. In this example, the ruthenium complex is effectively working as a triplet photosensitizer and not as a photoredox catalyst since the excited state redox potentials of the ruthenium complex are not enough to engage a SET process with the norbornadiene due to the higher ground-state redox potentials of the substrate. On the other hand Castellano's research group reported that a ruthenium photosensitizer can be selectively photoexcited to give a triplet energy transfer towards an anthracene substrate, which can undergo a photodimerization through a triplet-triplet annihilation (TTA) mechanism (Scheme 10b).[39]

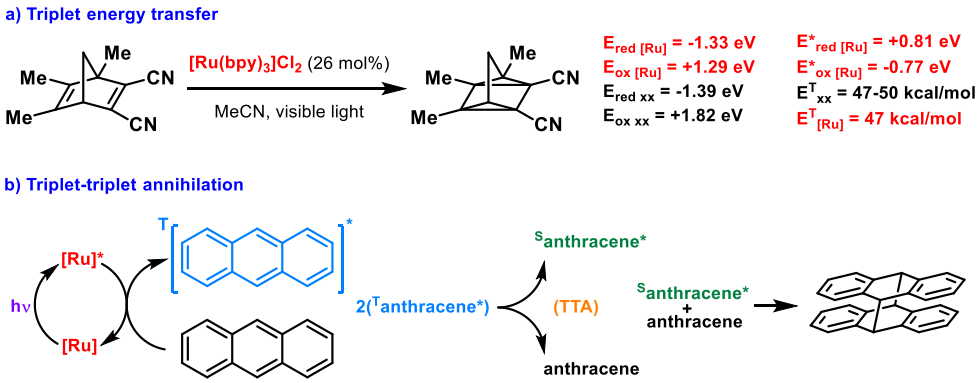

Scheme 10. First examples of photocatalytic reactions mediated by an energy transfer mechanism.

Some years later the research groups of Bach,[40] Yoon,[41] and Xiao[42] employed triplet energy transfer methodologies in modern synthetic applications of photocatalysis. In 2009, Bach's group described that a chiral xanthone catalyst could be employed as a triplet photosensitizer to achieve a highly efficient enantioselective [2+2] photocycloaddition (Scheme 11a).[40] In 2012, the Yoon's lab reported an intramolecular [2+2] photocycloaddition of styrene derivatives to obtain the corresponding cyclobutanes through a triplet energy transfer mechanism enabled by the use of an iridium photosensitizer (Scheme 11b).[41] In this case, the iridium complex worked as a triplet photosensitizer since the excited state redox potentials of the catalyst are not sufficient to participate in any SET process, precluding any redox pathway. In addition, the Xiao's group simultaneously reported a [2+2] photodimerization to spirooxindoles derivatives through a ruthenium catalyzed triplet energy transfer, as supported by mechanistic investigations.[42]

Relatively recently the Wu's research group reported a [2+2] photodimerization of chalcones and cinnamic acid derivatives to the corresponding cyclobutanes achieved by means of a triplet energy transfer mechanism, employing an iridium photosensitizer under visible light irradiation (Scheme 12).[43] This represented a simple methodology for the construction of dimeric cyclobutanes in high yields, overcoming the drawbacks and low efficiency of the previously reported solid-state and molten-state photochemical dimerization reactions.

[38] H. Ikezawa, C. Kutal, K. Yasufuku, H. Yamazaki, *J. Am. Chem. Soc.* **1986,** *108,* 1589-1594.
[39] R. R. Islangulov, F. N. Castellano, *Angew. Chem.* **2006**, *118*, 6103-6105.
[40] C. Müller, A. Bauer, T. Bach, *Angew. Chem. Int. Ed*. **2009**, *48*, 6640-6642.
[41] Z. Lu, T. P. Yoon, *Angew. Chem. Int. Ed*. **2012**, *51*, 10329-10332.
[42] Y.-Q. Zou, S.-W. Duan, X.-G. Meng, X.-Q. Hu, S. Gao, J.-R. Chen, W.-J. Xiao, *Tetrahedron* **2012**, *68*, 6914-6919.
[43] T. Lei, C. Zhou, M.-Y. Huang, L.-M. Zhao, B. Yang, C. Ye, H. Xiao, Q.-Y. Meng, V. Ramamurthy, C.-H. Tung, L.-Z. Wu, *Angew. Chem. Int. Ed*. **2017**, *56*, 15407-15410.

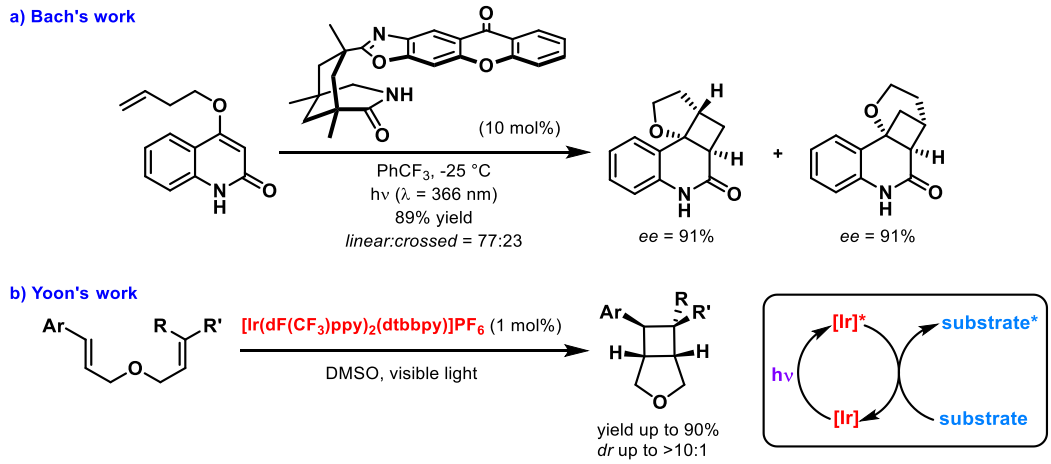

Scheme 11. Triplet energy transfer-mediated intramolecular [2+2] reactions: (a) enantioselective [2+2] photocycloaddition of quinolones and (b) diastereoselective [2+2] photocycloaddition of styrene derivatives.

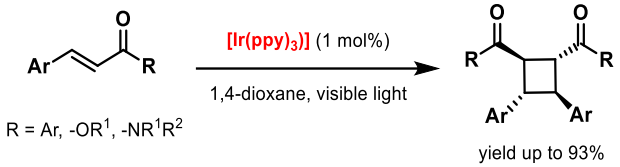

Scheme 12. [2+2] Photodimerization of chalcones and cinnamic acid derivatives by energy transfer.

Another fascinating example of a triplet energy transfer pathway was described by Smith's research group in the photo-mediated 6π heterocyclization of 2-aryloxyketones, 2-arylthioketones and 2-arylaminoketones (Scheme 13).[44] Six-electron cyclizations have been intensively investigated in conventional thermal processes but the achievement of a simple and efficient photochemical methodology that relies on a triplet energy transfer represents an interesting application of photocatalysis. The possibility of having redox pathways was excluded by the high reduction potential of cyclic 2-aryloxyketones, which lies outside the range of the reducing ability of the majority of the photocatalysts. On the other hand, the triplet energy of the substrate was below the triplet energy value of the iridium photosensitizer, leading to a favorable energy transfer mechanism.

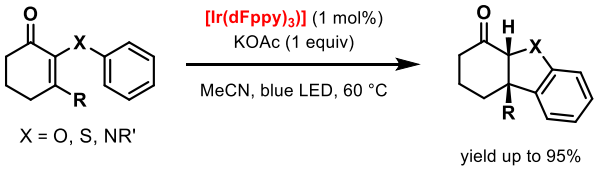

Scheme 13. Photocatalytic 6π heterocyclization achieved through an energy transfer mechanism.

In addition, evidences of triplet energy transfer mechanisms has been observed and employed for the successful development of metallaphotoredox catalytic reactions (Scheme 14).[8e] Upon mechanistic investigations energy transfer processes have been found to be operative in various reported metallaphotoredox methodologies like in the cross-coupling of carboxylic acids with aryl halides.[45,46] This is in accordance with previously disclosed works involving triplet energy transfer to organometallic species in photocatalytic reactions.[47]

[44] N. Münster, N. A. Parker, L. van Dijk, R. S. Paton, M. D. Smith, *Angew. Chem. Int. Ed.* **2017**, *56*, 9468-9472.
[45] D. R. Heitz, J. C. Tellis, G. A. Molander, *J. Am. Chem. Soc.* **2016**, *138*, 12715-12718.
[46] E. R. Welin, C. Le, D. M. Arias-Rotondo, J. K. McCusker, D W. C. MacMillan, *Science* **2017**, *355*, 380-385.
[47] (a) M. Osawa, H. Nagai, M. Akita, *Dalton Trans.* **2007**, *8*, 827-829; (b) W.-J., Yoo, T. Tsukamoto, S. Kobayashi, *Org. Lett.* **2015**, *17*, 3640-3642.

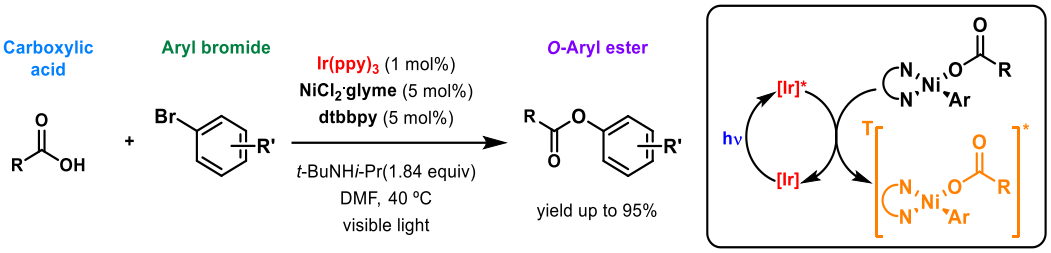

Scheme 14. Cross-coupling reaction through metallaphotoredox catalysis and triplet energy transfer.

A nice example of two different light-induced processes that can be synergistic employed into a photocascade reaction was provided by the group of Xiao (Scheme 15).[48] Energy transfer and single-electron transfer mechanisms were efficiently coupled to give tetrasubstituted pyrroles under mild conditions. The photosensitization of vinyl azides was carried out through an energy transfer mechanism to give an azirine intermediate which could be opened by means of a SET photooxidation employing Fukuzumi's acridinium catalyst. The resulting radical cation could then react with an electron-deficient alkyne undergoing a ring closing event.

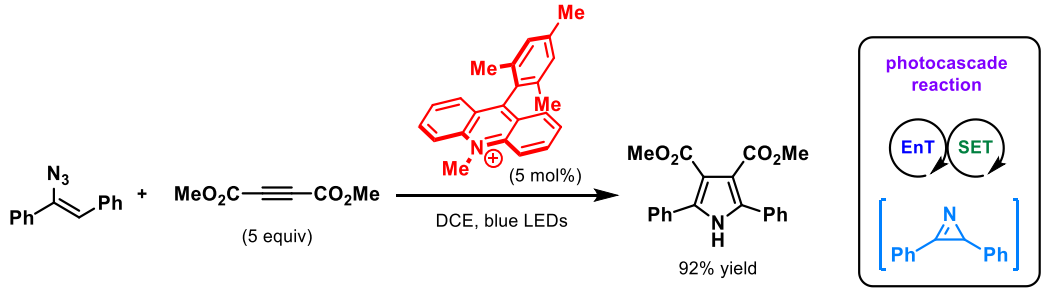

Scheme 15. Photocascade reaction involving a single-electron transfer and an energy transfer sequence.

1.5 First Examples and Modern Advances of Photocatalysis by EDA Complex Formation

Since the formulation of Mulliken's charge-transfer theory regarding the existence of molecular complexes between an electron donor and an electron acceptor almost 70 years ago,[49] the formation of different EDA complexes has been identified and intensively studied.[50] However, the synthetic importance of this phenomena has not been recognized by the whole organic research community until quite recently and their employment in photocatalysis has been maintained almost unexplored until the last decade.[12,51] The intermediacy of charge-transfer complexes was proposed by MacMillan's and Chatani's groups in the α-trifluoromethylation of silylketene acetals and in the arylation of heteroarenes using diaryliodonium salts (Scheme 16).[52,53] Nevertheless, the most intensive research work was reported by Melchiorre's group disclosing a large number of asymmetric EDA complex-mediated reactions.[54] Indeed, different strategies were described, leading to the enantioselective α-alkylation of aldehydes (Scheme 17 and Scheme 28a, Section 1.6) and ketones and to the

[48] J. Xuan, X.-D. Xia, T.-T. Zeng, Z.-J. Feng, J.-R. Chen, L.-Q. Lu, W.-J. Xiao, *Angew. Chem. Int. Ed*. **2014**, *53*, 5653-5656.
[49] R. S. Mulliken, *J. Am. Chem. Soc*. **1950**, *72*, 600-608. (b) R. S. Mulliken, *J. Am. Chem. Soc*. **1952**, *74*, 811-824.
[50] For some selected examples see: (a) S. Fukuzumi, K. Mochida, J. K. Kochi, *J. Am. Chem. Soc.* **1979**, *101*, 5961-5972; (b) H. C. Gardner, J. K. Kochi, *J. Am. Chem. Soc*. **1976**, *98*, 2460-2469; (c) D. Cantacuzène, R. Dorme, *Tetrahedron Lett.* **1975**, *16*, 2031-2034; (d) M. A. Fox, J. Younathan, G. E. Fryxell, *J. Org. Chem.* **1983**, *48*, 3109-3112; (e) M. Patz, S. Fukuzumi, *J. Phys. Org. Chem*. **1997**, *10*, 129-137.
[51] Y. Weia, Q.-Q. Zhou, F. Tan, L.-Q. Lu, W-J Xiao, Synthesis **2019**, *51*, 3021-3054.
[52] P. V. Pham, D. A. Nagib, D. W. C. MacMillan, *Angew. Chem. Int. Ed.* **2011**, *50*, 6119-6122.
[53] M. Tobisu, T. Furukawa, N. Chatani, *Chem. Lett.* **2013**, *42*, 1203-1205.
[54] (a) E. Arceo, I. D. Jurberg, A. Álvarez-Fernández, P. Melchiorre, *Nat. Chem*. **2013**, *5*, 750-756; (b) E. Arceo, A. Bahamonde, G. Bergonzini, P. Melchiorre, *Chem. Sci*., **2014**, *5*, 2438–2442; (c) Ł. Woźniak, J. J. Murphy, P. Melchiorre, *J. Am. Chem. Soc*. **2015**, *137*, 5678-5681; (d) Z.-Y. Cao, T. Ghosh, P. Melchiorre, *Nat. Commun*. **2018**, *9*, 3274.

asymmetric α-perfluoroalkylation of β-ketoesters, representing the first examples of enantioselective photocatalytic reactions enabled by the formation of an EDA complex.[54a-c] Moreover, the same group reported various racemic charge-transfer-mediated methodologies such as aromatic perfluoroalkylation of α-cyano arylacetates and alkylation of indoles.[55]

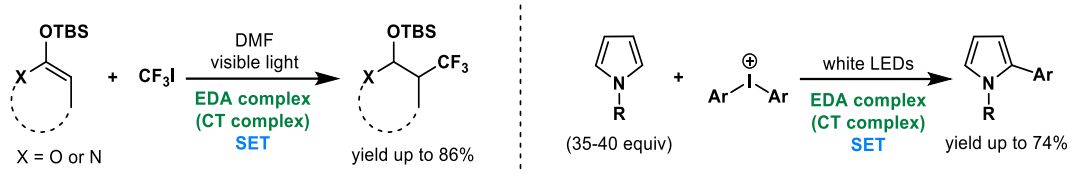

Scheme 16. Representative examples of EDA complex-mediated reactions in the absence of an external photocatalyst.

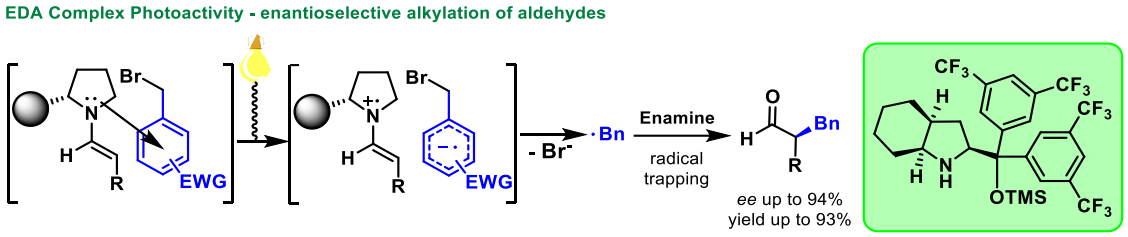

Scheme 17. First EDA complex-mediated enantioselective strategy.

An interesting example in which for the first time an electron donor was used as an external catalyst, triggering the generation of radicals through the formation of a transient EDA complex, was reported by Bach's group in 2019 (Scheme 18).[56] The catalyst employed was 3-acetoxyquinuclidine that in combination with a redox-active ester led to the formation of an EDA complex. The subsequent SET from the donor to the acceptor generates a carbon-centered radical and loss of carbon dioxide. The so-generated radicals have been employed for intramolecular cyclizations, hydrodecarboxylations, aminodecarboxylations and dimerizations.

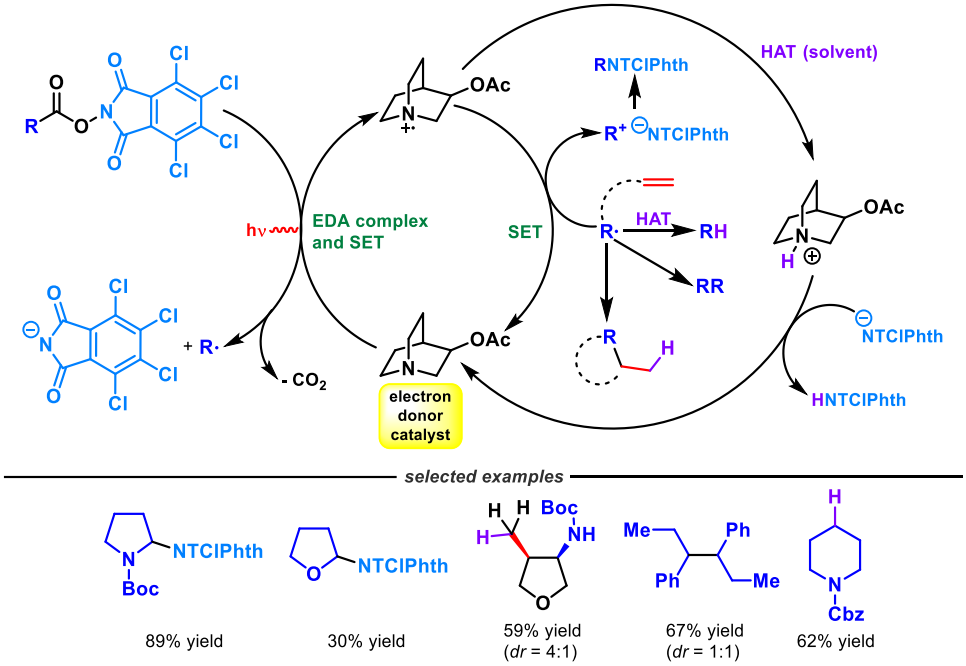

Scheme 18. Example of an electron donor employed as a catalyst to trigger the formation of an EDA complex.

[55] (a) M. Nappi, G. Bergonzini, P. Melchiorre, *Angew. Chem. Int. Ed.* **2014**, *53*, 4921-4925; (b) S. R. Kandukuri, A. Bahamonde, I. Chatterjee, I. D. Jurberg, E. C. Escudero-Adán, P. Melchiorre, *Angew. Chem.Int. Ed.* **2015**, *54*, 1485-1489.

[56] I. Bosque, T. Bach, *ACS Catal*. **2019**, *9*, 9103-9109.

1.6 Enantioselective Photocatalysis

Although asymmetric catalysis of polar reactions has been intensively investigated and studied in the last decades, with the development of a myriad of different catalytic systems to achieve highly enantioselective reactions, the research community has reserved limited attention and efforts for the development of asymmetric strategies in photocatalysis.[7b-d] This is essentially due to the different characteristics of polar-catalyzed reactions in comparison with photo-catalyzed reactions. Indeed, in conventional thermal processes, the activation mode of the catalyst is through the lowering of the activation energy of the transition state, leading to a preferential or selective catalyzed reaction pathway. The use of a chiral catalyst is permitting to carry out stereoinduced processes that are faster than the racemic background reactions, which in some cases can be virtually inexistent. On the other hand, in most of the photochemical reactions, the catalyst is not working through the lowering of any activation barrier, since upon absorption of a photon, the substrate has enough energy to carry out either the stereocontrolled or the racemic background processes. Thus, the necessary discrimination between them is obstructed by the nature of photochemical reactions and excited state intermediates that are challenging the possibility of a stereoinduced transformation mediated by a chiral catalyst. Nevertheless, in the last decades, a growing interest in photocatalysis has driven chemists into approaching the challenging area of enantioselective photocatalysis and a multitude of new activation strategies have been developed to overcome background processes or to permit that only catalyst-mediated transformations could be carried out.

The first enantioselective photochemical reaction was reported by Hammond and Cole in 1965 (Scheme 19a).[57] The *cis-trans* isomerization of 1,2-diphenylcyclopropane was achieved through the use of a chiral naphthalene derivative as the photosensitizer through the formation of an exciplex upon irradiation. After reaching a stationary state for the *cis-trans* isomerization (51:49 ratio), the optical rotation of the *trans* isomer was measured, observing the corresponding asymmetric induction due to a preferential sensitization of one of the *trans* enantiomers and leading to an enantioenrichment of the other. This was essentially due to the formation of diastereoisomeric exciplexes that presented different excited state lifetimes.

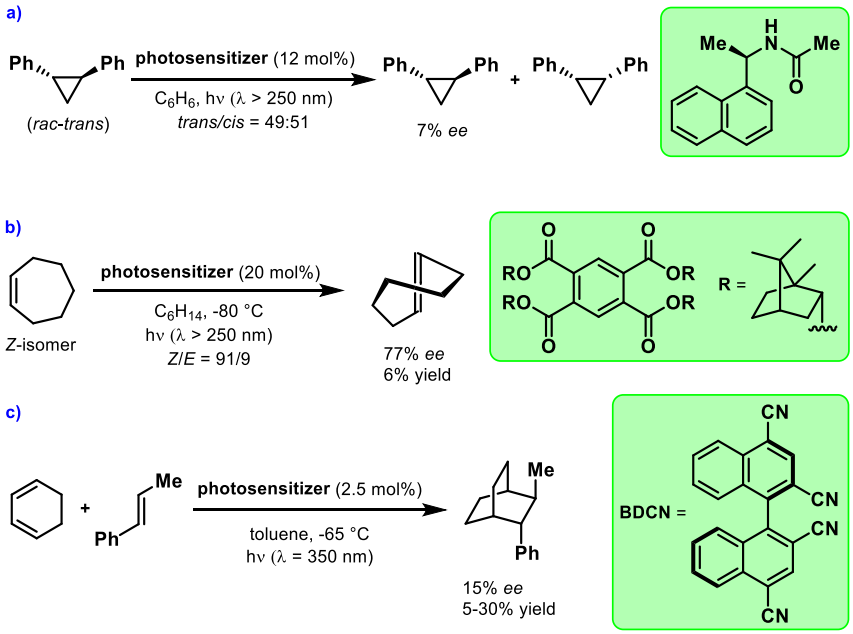

Scheme 19. First examples of enantioselective photocatalytic reactions achieved employing a photosensitizer.

[57] G. S. Hammond, R. S. Cole, *J. Am. Chem. Soc.* **1965**, *87*, 3256-3257.

Despite the fact that the possibility of performing asymmetric photochemical transformations was recognized more than 50 years ago, the first example of a highly enantioselective photochemical reaction was reported by Inoue's research group in 1999 (Scheme 19b).[58] The photoisomerization through exciplex sensitization of (*Z*)-cycloheptene led to the obtainment of the (*S*)-*E*-isomer with a 77% of enantiomeric excess (*ee*) in low yield (6%). Another important example is the Diels-Alder reaction reported by Schuster's group in 1990 that was achieved through the formation of a three-component exciplex (triplex) between an enantioenriched bis-anthracene derivative photosensitizer (70% *ee*), *trans*-β-methylstyrene and 1,3-cyclohexadiene to give the Diels-Alder product in 15% *ee* and yields in the range of 5-30%. The latter represents the first example of an enantioselective photocycloaddition reported in the literature (Scheme 19c).[59]

The first example of an enantioselective photocatalytic reaction, in which the corresponding products were obtained in synthetically useful yields and moderate enantioselectivity, was achieved through the use of a dual-catalytic system by Córdova's research group in 2004 (Scheme 20).[60] The enantioselective α-oxygenation of aldehydes was accomplished through a photocatalytic sensitization of molecular oxygen to its reactive singlet excited state and consequent reaction with a ground-state enamine. The peroxide intermediate was then reduced by $NaBH_4$ to furnish the corresponding enantioenriched diol.

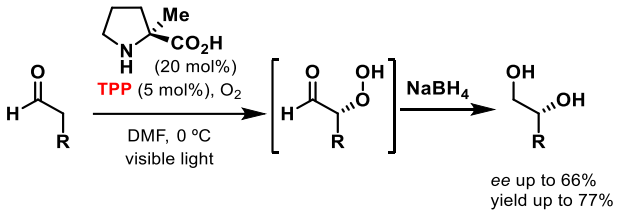

Scheme 20. First asymmetric photocatalytic reaction by means of photosensitization through a dual-catalytic system.

40 years after the pioneering work of Hammond and Cole, the research group of Bach reported the first highly enantioselective photocatalytic reaction, in which a substrate underwent a stereocontrolled photoredox process under the control of an excited state chiral catalyst (Scheme 21).[17] In this pioneering work, the pyrrolidine-tethered lactam was converted into the spirocyclic pyrrolizidine with high enantioselectivity (70% *ee*) and high yield (64%). The benzophenone moiety worked as a photocatalyst through a photoinduced hydrogen atom transfer (PHAT), that can be seen as a combination of a photoredox single-electron transfer process (photo-oxidation) and a subsequent proton transfer.[8c] Upon oxidation, the generated α-amino radical can carry out an intramolecular radical conjugate addition to the lactam, furnishing the spirocyclic pyrrolizidine. The stereoinduction was achieved through the employment of a specially tailored bifunctional photocatalyst that can efficiently coordinate with the substrate through hydrogen bonding due to the lactam binding motif present in its structure. The binding interactions between the catalyst and the substrate are also favoring the occurrence of a preferential PHAT between the benzophenone moiety and the coordinated substrate, limiting possible intermolecular SET events involving uncoordinated substrate that would lead to a racemic background reaction.

[58] (a) R. Hoffmann, Y. Inoue, *J. Am. Chem. Soc.* **1999**, *121*, 10702-10710; for a similar pioneering study achieving a 41% of *ee* see: (b) Y. Inoue, T. Yokoyama, N. Yamasaki, A. Tai, *Nature* **1989**, *341*, 225-226.

[59] J.-I. Kim, G. B. Schuster, *J. Am. Chem. Soc.* **1990**, *112*, 9635-9637.

[60] A. Córdova, H. Sundén, M. Engqvist, I. Ibrahem, J. Casas, *J. Am. Chem. Soc.* **2004**, *126*, 8914-8915.

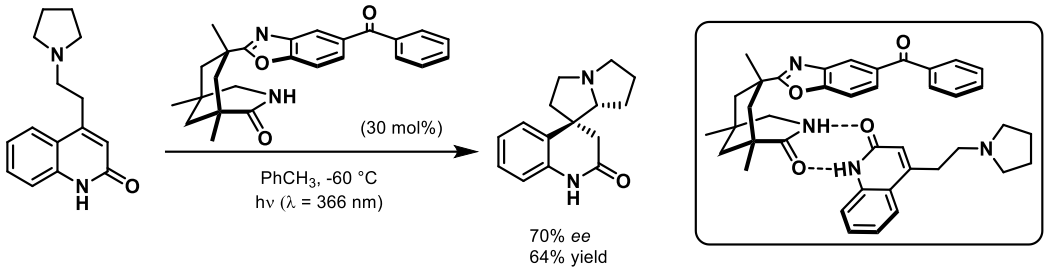

Scheme 21. First enantioselective photocatalytic reaction through bifunctional catalysis and PHAT.

Another brilliant pioneering example in asymmetric photocatalysis was reported by MacMillan's group in 2008 (Scheme 22).[19] The enantioselective α-alkylation of aldehydes was achieved through the merging of enamine and photoredox catalysis, offering a solution to a long-standing issue in organocatalysis and organic synthesis.[61] The use of a ruthenium photocatalyst permitted the generation of electron-deficient radicals from different bromo derivative as radical precursors that can react with an electron-rich ground-state chiral enamine intermediate. This strategy relies on the fact that a photoredox catalytic cycle, which is responsible of the radical generation, is working in a synergistic manner with the ground-state aminocatalytic cycle that is responsible of the stereoselectivity observed. The combination of them into a dual catalytic system is avoiding the possibility of an undesired racemic background process since the stereodefining event is not involving any excited state intermediates.

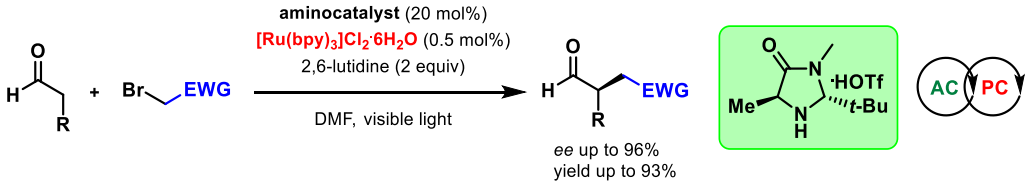

Scheme 22. First enantioselective photoredox reaction achieved through a dual-catalytic system.

Another milestone in asymmetric photocatalysis was reported by Bach's research group in 2009.[40] A highly enantioselective [2+2] photocycloaddition was achieved through the use of a chiral xanthone bifunctional catalyst (Scheme 23). The higher rigidity and planarity of the xanthone derivative in comparison with the above reported benzophenone analogue permitted a higher association of the substrate through hydrogen bonding leading to an efficient and enantioselective transformation. Furthermore, the higher triplet energy of xanthone (E_T = 74 Kcal/mol) in comparison with benzophenone (E_T = 69 Kcal/mol) might favoring the triplet sensitization of the substrate as well. The triplet energy transfer was preferentially accomplished between the xanthone moiety and the substrate due to the close proximity of them in the catalyst-substrate complex formed upon hydrogen bonding interaction. The product was obtained in 89% yield as a mixture of two regioisomers (regioisomeric ratio, *rr* = 77:23) derived from linear and crossed cyclobutane ring formation and with high enantioselectivities (91% *ee* for both regioisomers). Some years later a similar thioxanthone-based catalyst was employed for the asymmetric [2+2] photocycloaddition of 4-alkylquinolones under visible light irradiation.[62]

[61] P. Melchiorre, *Angew. Chem. Int. Ed.* **2009**, *48*, 1360-1363.
[62] R. Alonso, T. Bach, *Angew. Chem. Int. Ed*. **2014**, *53*, 4368-4371.

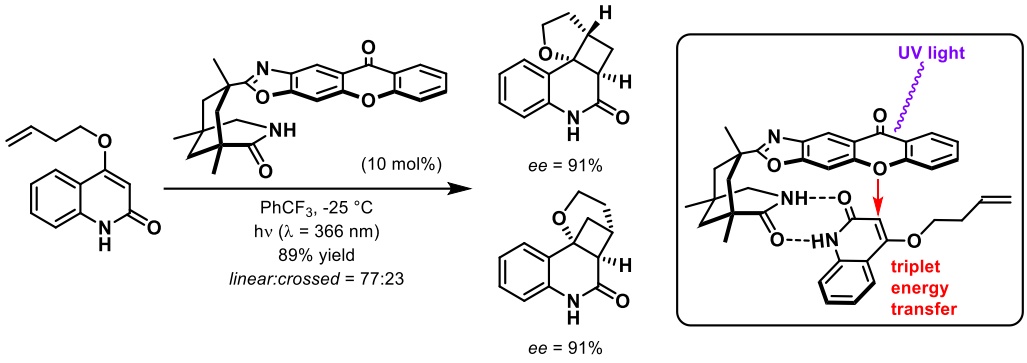

Scheme 23. Enantioselective [2+2] photocycloaddition through hydrogen-bonding catalysis and triplet energy transfer.

In 2010 the research group of Bach reported an enantioselective [2+2] photocycloaddition over coumarins through a new activation strategy enabled by the employment of a chiral Lewis acid as the catalyst (Scheme 24).[63] This activation mode hinge on the observation that coumarins do not undergo [2+2] photocycloadditions in the absence of an appropriate additive since their excited state is rapidly deactivated to the ground-state. The use of an oxazaborolidine Lewis acid is increasing the ISC rate to the triplet with a subsequent increase of the excited state lifetime. Therefore, the Lewis acid-mediated process is leading efficiently to a stereocontrolled [2+2] photocycloaddition. The use of a chiral oxazaborolidine Lewis acid was employed by the same research group to carry out an asymmetric [2+2] photocycloaddition starting from enones.[64] In this case the Lewis acid provoked a strong bathochromic shift upon coordination, permitting the selective excitation of the Lewis acid-coordinated substrate complex.

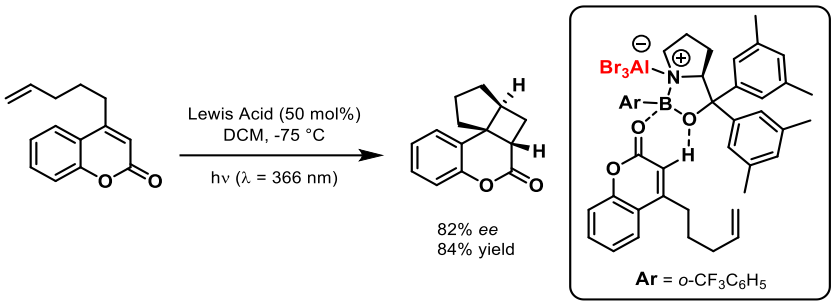

Scheme 24. Enantioselective [2+2] photocycloaddition of coumarins mediated by a Lewis acid catalyst.

In 2014, Yoon's group reported a highly enantioselective dual-catalytic strategy to achieve intermolecular [2+2] photocycloadditions of acyclic enones through visible light irradiation (Scheme 25a).[65] This methodology permitted to achieve crossed products between an aryl enone (which can be reduced through a Lewis acid-mediated photoredox process to the corresponding radical anion) and an alkyl enone (that cannot be reduced under the reaction conditions). In the context of [2+2] cycloadditions, the Yoon's group reported the first enantioselective Lewis acid-catalyzed intermolecular [2+2] photocycloaddition enabled by a triplet energy transfer to obtain enantioenriched cyclobutanes in high efficiency.[66,67,68,69]

[63] H. Guo, E. Herdtweck, T. Bach, *Angew. Chem. Int. Ed.* **2010**, *49*, 7782-7785.
[64] R. Brimioulle, T. Bach, *Science* **2013**, *342*, 840-843.
[65] J. Du, K. L. Skubi, D. M. Schultz, T. P. Yoon, *Science* **2014**, *344*, 392-396.
[66] T. R. Blum, Z. D. Miller, D. M. Bates, I. A. Guzei, T. P. Yoon, *Science* **2016**, *354*, 1391-1395.
[67] Z. D. Miller, B. J. Lee, T. P. Yoon, *Angew. Chem. Int. Ed*. **2017**, *56*, 11891-11895.
[68] M. E. Daub, H. Jung, B. J. Lee, J. Won, M.-H. Baik, T. P. Yoon, *J. Am. Chem. Soc*. **2019**, *141*, 9543-9547.
[69] For asymmetric [2+2] photocycloadditions enabled by the use of a chiral hydrogen-bonding Iridium photocatalyst reported by the Yoon's lab, see: (a) K. L. Skubi, J. B. Kidd, H. Jung, I. A. Guzei, M.-H. Baik, T. P. Yoon, *J. Am. Chem. Soc*. **2017**, *139*, 17186-17192; (b) J. Zheng, W. B. Swords, H. Jung, K. L. Skubi, J. B. Kidd, G. J. Meyer, M.-H. Baik, T. P. Yoon, *J. Am. Chem. Soc*. **2019**, *141*, 13625-13634.

Moreover the same group employed dual-catalytic photoredox strategies to achieve an intramolecular enantioselective [3+2] photocycloaddition of aryl cyclopropyl ketones[70] and an enantioselective radical conjugate addition of α-amino radicals to Michael acceptors (Scheme 25b).[71] In the latter case the combination of Lewis acid catalyst and a photocatalyst permitted the obtainment of enantioenriched γ-aminocarbonyl adducts through the generation of α-amino radicals from α-silyl aniline derivatives.

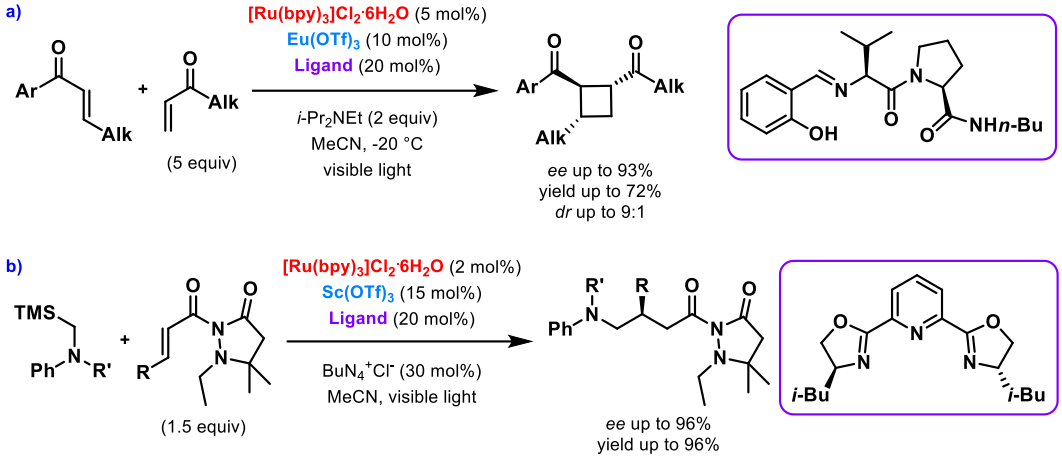

Scheme 25. Enantioselective intermolecular [2+2] cycloaddition (a) and radical conjugate addition (b) achieved through dual-catalytic photoredox strategies.

In 2012 the Rovis' research group reported the addition of linear alkyl aldehydes to iminium ions generated from the photo-oxidation of *N*-phenyltetrahydroisoquinoline derivatives (Scheme 26).[72] The synergistic combination of *N*-heterocyclic carbene (NHC) catalysis and photoredox catalysis in a dual-catalytic system led to the obtainment of the corresponding products in high yield and enantioselectivity. A similar stereocontrolled interception of an iminium ion by a nucleophile was accomplished by Jacobsen's and Stephenson's research groups through the combination of photoredox and anion binding catalysis.[73]

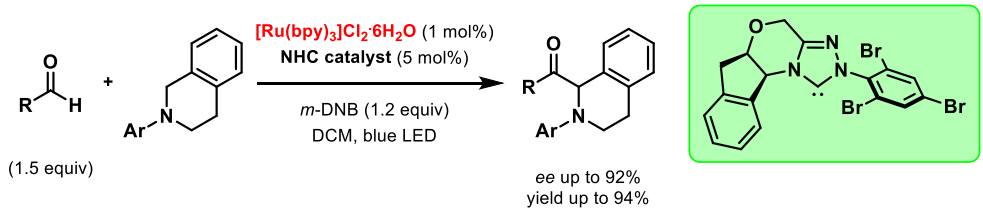

Scheme 26. Asymmetric nucleophilic addition to photo-generated iminium ions by NHC catalysis.

A brilliant asymmetric aza-pinacol cyclization reaction enabled by a reductive proton-coupled electron transfer (PCET) was reported by the research group of Knowles in 2013, being the first example of an asymmetric photocatalytic reaction achieved through PCET activation (Scheme 27).[74] The concerted PCET was achieved through the employment of a chiral phosphoric acid (Brønsted acid) and an iridium photocatalyst to give a stable ketyl phosphate H-bond complex, which is undergoing an intramolecular radical reaction to furnish the enantioenriched cyclic product. On the other hand, the synergistic action of a photoredox catalyst and an ionic Brønsted

[70] A. G. Amador, E. M. Sherbrook, T. P. Yoon, *J. Am. Chem. Soc*. **2016**, *138*, 4722-4725.
[71] L. Ruiz Espelt, I. S. McPherson, E. M. Wiensch, T. P. Yoon, *J. Am. Chem. Soc.* **2015**, *137*, 2452-2455.
[72] D. A. DiRocco, T. Rovis, *J. Am. Chem. Soc*. **2012**, *134*, 8094-8097.
[73] G. Bergonzini, C. S. Schindler, C.-J. Wallentin, E. N. Jacobsen, C. R. J. Stephenson, *Chem. Sci.* **2014**, *5*, 112-116.
[74] L. J. Rono, H. G. Yayla, D. Y. Wang, M. F. Armstrong, R. R. Knowles, *J. Am. Chem. Soc.* **2013**, *135*, 17735-17738.

acid was employed by the group of Ooi to obtain an asymmetric radical coupling between α-amino radicals and aldimine-derived anion-radicals.[75]

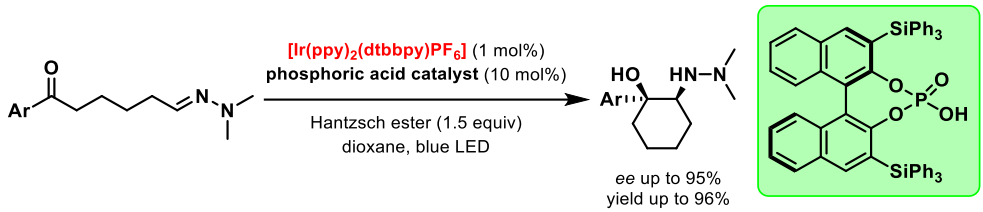

Scheme 27. Enantioselective aza-pinacol cyclization enabled by a photocatalytic PCET strategy.

Melchiorre's research group has demonstrated that it is possible to take advantage of the photoactivity of transient generated EDA complex intermediates to carry out highly enantioselective photoredox reactions without the use of an external photocatalyst (Scheme 28a).[54a] This represented the first example of an enantioselective photocatalytic reaction allowed by an EDA complex formation. Following this pioneering example, similar asymmetric strategies were reported by the same group to achieve the α-alkylation of ketones and the α-perfluoroalkylation of β-ketoesters.[54a-c] Other outstanding strategies reported by the same group rely on the ability of photoactive chiral enamine and iminium ion intermediates to reach, under visible light irradiation, an excited state from which they can act as strong reductants or strong oxidants, respectively (Scheme 28b,c). By these means the enantioselective α-alkylation of aldehydes was achieved through enamine catalysis,[76,77,78] while a variety of β-functionalizations of enals was achieved through the employment of iminium ion catalysis, leading to enantioenriched products that it was not possible to obtain through polar and established methodologies.[79] The same research group reported as well an unprecedented enantioselective radical conjugate addition to cyclic enones through an iminium ion-catalyzed process that relies for its success on an electron-relay mechanism (Scheme 29).[80] The nucleophilic carbon-centered radical is generated through the photooxidation of benzodioxole or aniline derivatives, employing a decatungstenate or an iridium photocatalyst (PC), respectively. The radical is then added to the β-position of cyclic enones in an iminium-catalyzed reaction to forge a quaternary stereocenter in high stereoselectivity. The usually prevalent back electron transfer (BET), that is restoring the radical and the α,β-unsaturated compound, is avoided through an internal SET from the electron-rich carbazole moiety to the highly unstable α-iminyl radical. Then, a favorable enamine-imine tautomerism is shifting the equilibrium towards the product. Furthermore, another similar strategy has been employed by the same group without using an external photocatalyst since, upon generation of an intramolecular EDA complex, a transient carbazole oxidant species can initiate a chain propagation reaction through the generation of an α-amino radical from an α-silylamine as the radical precursor.[54d]

[75] D. Uraguchi, N. Kinoshita, T. Kizu, T. Ooi *J. Am. Chem. Soc.* **2015**, *137*, 13768-13771 (in this case a PCET mechanism is unlikely as reported by the authors).

[76] M. Silvi, E. Arceo, I. D. Jurberg, C. Cassani, P. Melchiorre, *J. Am. Chem. Soc*. **2015**, *137*, 6120-6123.

[77] For mechanistic studies regarding the α-alkyation of enamines, see: A. Bahamonde, P. Melchiorre, *J. Am. Chem. Soc.* **2016**, *138*, 8019-8030.

[78] G. Filippini, M. Silvi, P. Melchiorre, *Angew. Chem. Int. Ed.* **2017**, *56*, 4447-4451.

[79] (a) M. Silvi, C. Verrier, Y. P. Rey, L. Buzzetti, P. Melchiorre, *Nat. Chem*. **2017**, *9*, 868-873; (b) C. Verrier, N. Alandini, C. Pezzetta, M. Moliterno, L. Buzzetti, H. B. Hepburn, A. Vega-Peñaloza, M. Silvi, P. Melchiorre, *ACS Catal*. **2018**, *8*, 1062-1066; (c) L. Woźniak, G. Magagnano, P. Melchiorre, *Angew. Chem. Int. Ed*. **2018**, *57*, 1068-1072; (d) D. Mazzarella, G. E. M. Crisenza, P. Melchiorre, *J. Am. Chem. Soc.* **2018**, *140*, 8439-8443; (e) P. Bonilla, Y. Rey, C. Holden, P. Melchiorre, *Angew. Chem. Int. Ed*. **2018**, *57*, 12819-12823. (f) L. A. Perego, P. Bonilla, P. Melchiorre, *Adv. Synth. Catal.* **2020**, *362*, 302-307.

[80] J. J. Murphy, D. Bastida, S. Paria, M. Fagnoni, P. Melchiorre, *Nature* **2016**, *532*, 218-222.

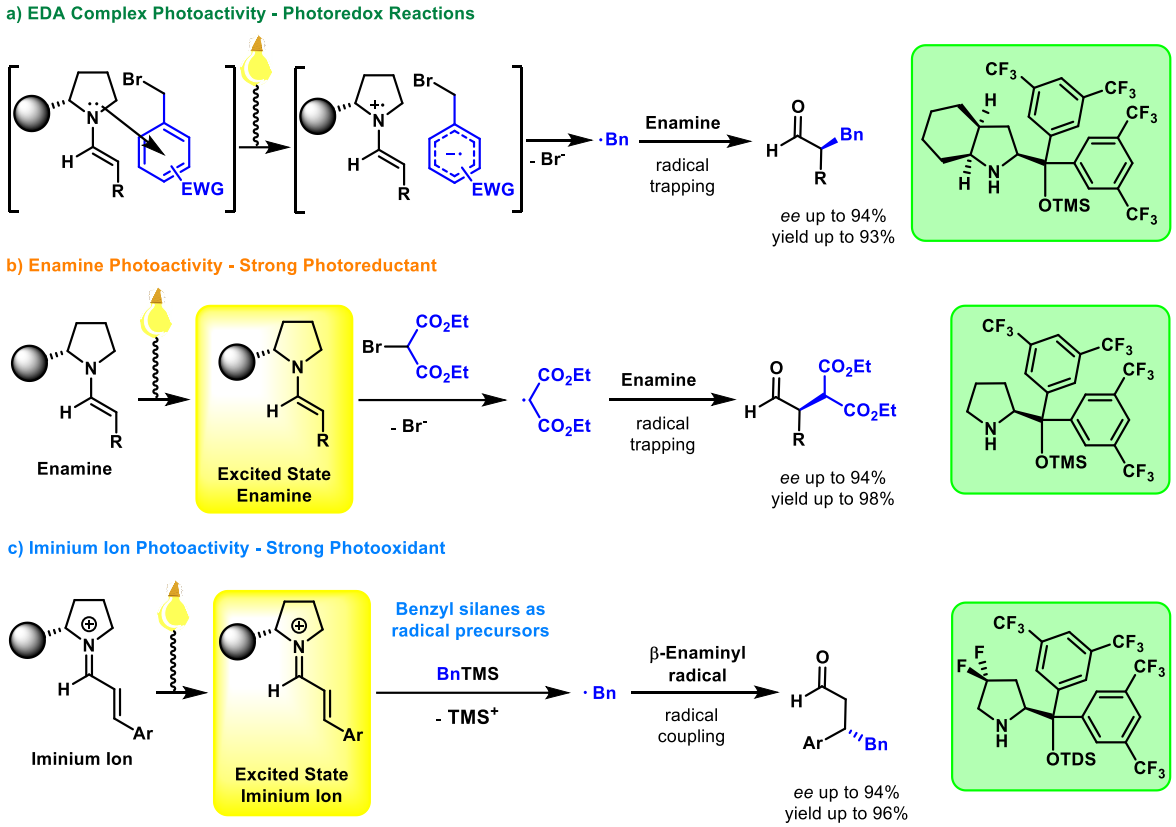

Scheme 28. Asymmetric reactions achieved by the intermediacy of photoactive EDA complexes (a), enamines (b) and iminium ions (c), leading to α- and β-functionalization reactions.

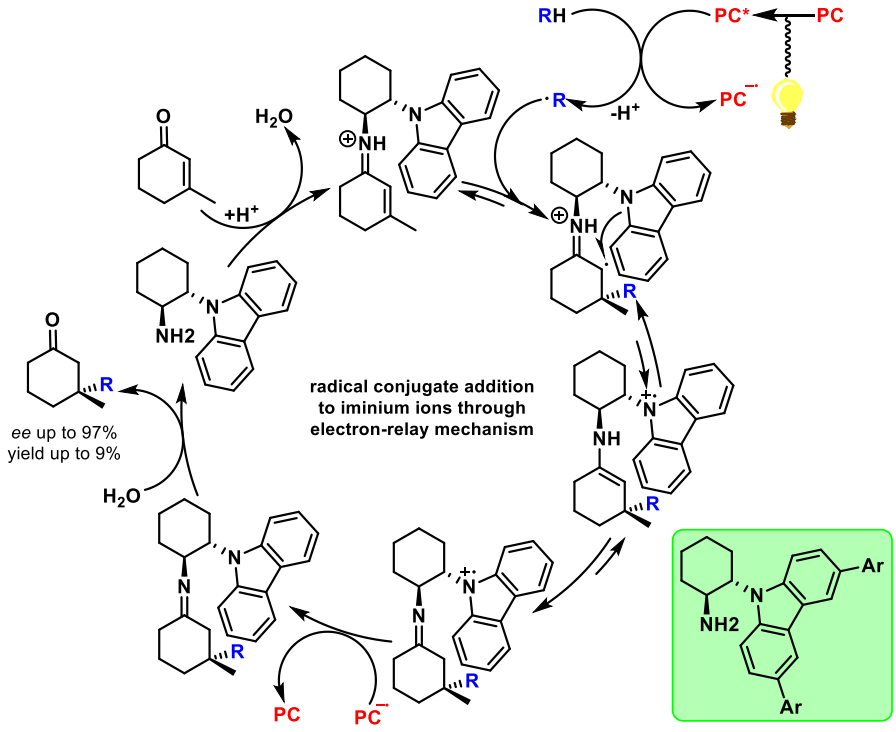

Scheme 29. Enantioselective radical conjugate addition to enones through an electron-relay mechanism.

In the last years chiral-at-metal iridium and rhodium catalysts were developed in the laboratories of Meggers' research group, showcasing their high potentiality in asymmetric photocatalytic reactions.[81] The chiral bifunctional catalyst can work as a Lewis acid and as a photocatalyst (after binding with the substrate and formation of a metal-enolate, metal-enone or metal-ketone complex), without the requirement of employing dual catalytic systems. Indeed, the first photocatalytic reaction reported by this research group regarded the use of an iridium catalyst for the α-alkylation of 2-acyl imidazoles, which was accomplished in high efficiency and enantioselectivity (Scheme 64, Chapter 3).[82] After this seminal work a multitude of different asymmetric reactions (α-aminoalkylations, α-trichloromethylations, α-aminations, radical couplings and β-functionalizations) were achieved by the same group using chiral iridium or rhodium complexes (Scheme 30a-c).[83] Relatively recently Meggers' group reported that the rhodium catalyst could be efficiently employed in [2+2] and [3+2] photocycloaddition reactions[84] and in an interesting sequential HAT-hetero-Diels-Alder reaction (Scheme 30d).[85] Chiral-at-metal iridium complexes have been also developed by the Yoon's lab, allowing the achievement of highly enantioselective [2+2] photocycloadditions.[69] The particular feature of these catalyst is that they have been properly design to permit hydrogen-bonding interactions with the substrate and thus inducing stereocontrolled transformations.

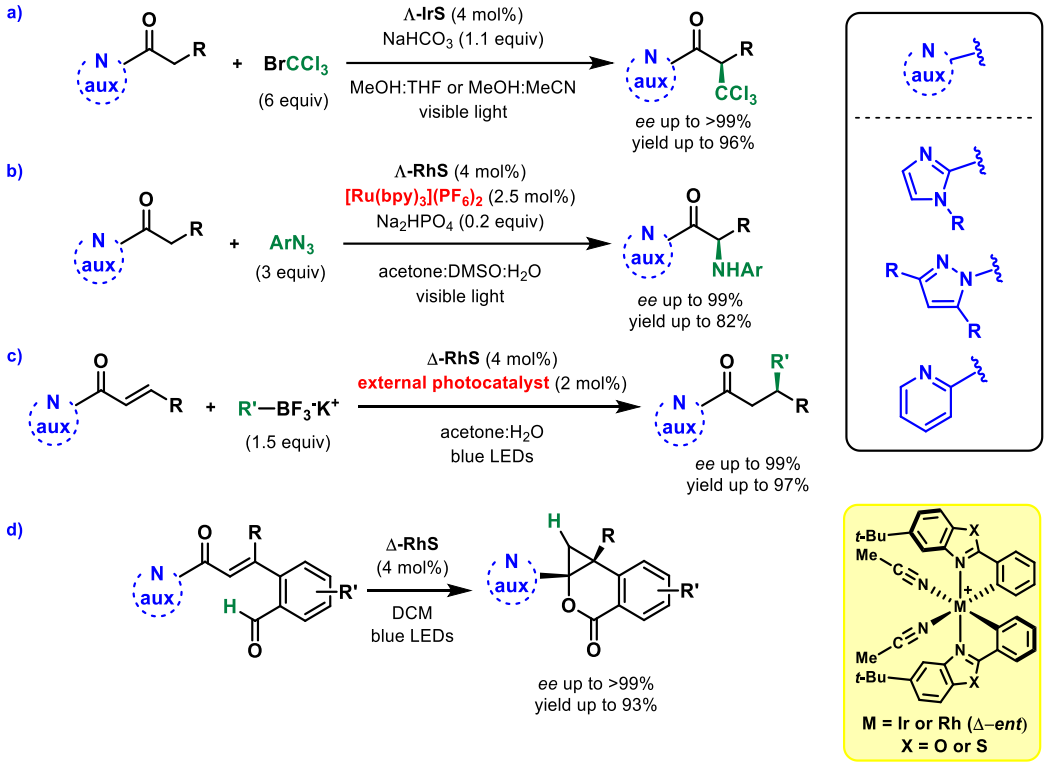

Scheme 30. Different asymmetric reactions achieved through a chiral-at-metal catalyst.

[81] X. Huang, E. Meggers, *Acc. Chem. Res.* **2019**, *52*, 833-847.

[82] H. Huo, X. Shen, C. Wang, L. Zhang, P. Röse, L.-A. Chen, K. Harms, M. Marsch, G. Hilt, E. Meggers, *Nature* **2015**, *515*, 100-103.

[83] (a) C. Wang, Y. Zheng, H. Huo, Philipp Röse, L. Zhang, K. Harms, G. Hilt, E. Meggers, *Chem. Eur. J.* **2015**, *21*, 7355-7359; (b) H. Huo, C. Wang, K. Harms, E. Meggers, *J. Am. Chem. Soc*. **2015**, *137*, 9551-9554; (c) X. Huang, R. D. Webster, K. Harms, E. Meggers, *J. Am. Chem. Soc.* **2016**, *138*, 12636-12642; (d) C. Wang, J. Qin, X. Shen, R. Riedel, K. Harms, E. Meggers, Angew. Chem. Int. Ed. **2016**, *55*, 685-688; (e) H. Huo, K. Harms, and E. Meggers, *J. Am. Chem. Soc.* **2016**, *138*, 6936-6939.

[84] (a) X. Huang, T. R. Quinn, K. Harms, R. D. Webster, L. Zhang, O. Wiest, E. Meggers, *J. Am. Chem. Soc*. **2017**, *139*, 9120-9123; (b) N. Hu, H. Jung, Y. Zheng, J. Lee, L. Zhang, Z. Ullah, X. Xie, K. Harms, M.-H. Baik, E. Meggers, *Angew. Chem. Int. Ed.* **2018**, *57*, 6242-6246. For an example of [3+2] photocycloaddition developed by the same group, see: (c) X. Huang, X. Li, X. Xie, K. Harms, R. Riedel, E. Meggers, *Nat. Commun*. **2017**, *8*, 2245.

[85] C. Zhang, S. Chen, C.-X. Ye, K. Harms, L. Zhang, K. N. Houk, E. Meggers, *Angew. Chem. Int. Ed*. **2019**, *58*, 14462-14466.

In 2016, Fu's and Peters' research groups reported a highly enantioselective copper-catalyzed carbon-nitrogen cross-coupling reaction enabled by the intermediacy of a photoactive copper species under visible light irradiation (Scheme 31).[86] This activation strategy permitted to achieve a stereocontrolled cross-coupling between alkyl chlorides and indoles or carbazoles. Indeed, the nitrogen-containing nucleophilic species is generating a transient chiral copper intermediate which can be photoexcited under blue LED irradiation to carry out the reduction of the alkyl chloride, delivering the subsequent C-N cross-coupled product.

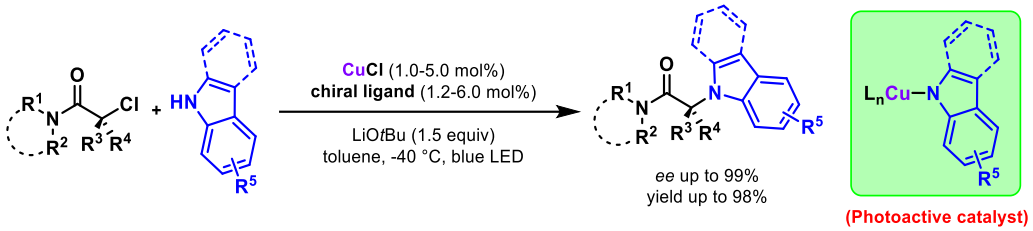

Scheme 31. Asymmetric carbon-nitrogen cross-coupling catalyzed by a photoactive copper species.

Although the possibility of performing an asymmetric cross-coupling reaction through metallaphotoredox catalysis was reported in the seminal work of Molander's group (achieving an enantiomeric excess of 50%),[32a] the only highly enantioselective example reported in the literature appeared in 2016 through a collaboration between MacMillan's and Fu's research groups (Scheme 32).[87] The use of amino acids as radical precursors and the employment of a semicorrine-like ligand furnished the corresponding enantioenriched cross-coupled products in high yield and enantioselectivity. Following this strategy, an enantioselective desymmetrization of cyclic meso-anhydrides was achieved by Rovis' and Doyle's labs to give the corresponding enantioenriched ketoacids.[88]

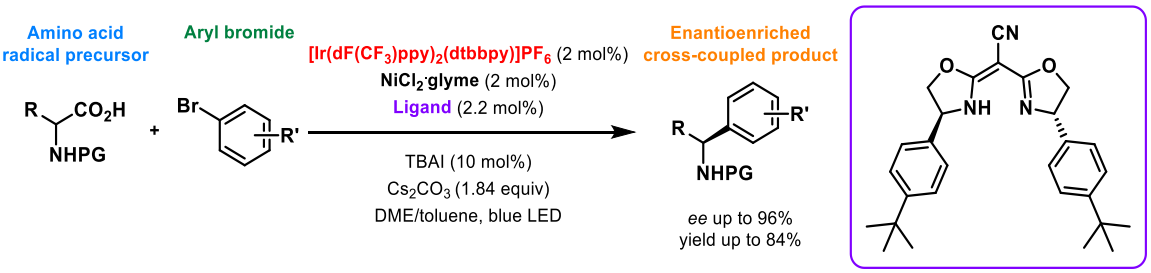

Scheme 32. Enantioselective cross-coupling of amino acids and aryl bromides under metallaphotoredox catalysis.

Although the first developed stereocontrolled photochemical reaction was obtained through an enantioselective photosensitization, leading to a deracemization process,[57] only very recently high levels of stereoinduction were achieved by these means. Indeed, a groundbreaking example of a highly efficient photocatalytic deracemization strategy was reported by Bach's research group in 2018 (Scheme 33a).[89] Through the use of a bifunctional thioxanthone catalyst, that can coordinate with an allene-containing cyclic lactam, a triplet energy transfer was achieved with different sensitization rates between the two enantiomers, leading to an enantioenrichment of one of them over the other. This catalytic system was then applied to the deracemization of cyclopropyl derivatives and for the deracemization of chiral sulfoxides.[90,91] Another brilliant example of a highly efficient deracemization process was reported by Knowles' and Miller's groups through the synergistic employment of photocatalysis, phosphate base catalysis and HAT catalysis to achieve enantioenriched cyclic ureas as the products (Scheme

[86] Q. M. Kainz, C. D. Matier, A. Bartoszewicz, S. L. Zultanski, J. C. Peters, G. C. Fu, *Science* **2016**, *351*, 681-684.
[87] Z. Zuo, H. Cong, W. Li, J. Choi, G. C. Fu, D. W. C. MacMillan, *J. Am. Chem. Soc.* **2016**, *138*, 1832-1835.
[88] E. E. Stache, T. Rovis, A. G. Doyle, *Angew. Chem. Int. Ed*. **2017**, *56*, 3679-3683.
[89] A. Hölzl-Hobmeier, A. Bauer, A. Vieira Silva, S. M. Huber, C. Bannwarth, T. Bach, *Nature* **2018**, *564*, 240-243.
[90] A. Tröster, A. Bauer, C. Jandl, T. Bach, *Angew. Chem. Int. Ed*. **2018**, *58*, 3538-3541.
[91] L. Wimberger, T. Kratz, T Bach, *Synthesis* **2019**, 51, 4417-4416.

33b).[92] After initial photo-oxidation of a racemic urea the chiral phosphate catalyst carry out an enantioselective proton transfer over the chiral radical cation to generate an achiral radical intermediate. Then, this intermediate can undergo an enantioselective HAT by employment of a chiral thiol catalyst. Thus, the synergistic and matched combination of these two chiral catalysts is accomplishing the preferential formation of one enantiomer from a racemate.

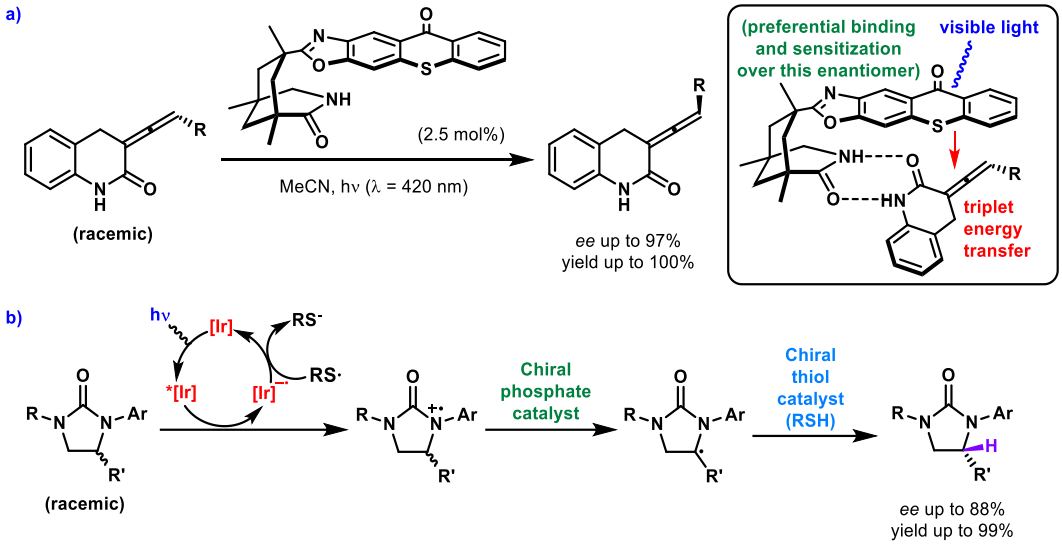

Scheme 33. First examples of photocatalytic deracemization processes developed by Bach's group (a) and by Knowles' and Miller's groups (b).

[92] N. Y. Shin, J. M. Ryss, X. Zhang, S. J. Miller, R. R. Knowles, *Science* **2019**, *366*, 364-369.

1.7 General Objectives of the Present PhD Thesis

Although catalytic strategies have been intensively employed and studied in the last decades, photochemistry and in particular photocatalysis have received limited attentions by the research community. Furthermore, the application of photocatalytic strategies to organic synthesis have been maintained underexplored until the last decade and intensive efforts are undergoing nowadays to develop new and efficient methodologies. This can be highlighted by the fact that during the last years an increasing and growing number of publications have been reported in this research field, showcasing the huge interest of the whole research community worldwide. This is undoubtedly due to the increasing interest for the developing of new methodologies that are in accordance with the green chemistry principles. In this context, the use of light as a renewable and cheap energy source that can be converted into chemical energy, and the use of catalysis to promote many challenging reactions is showcasing the great potential of this discipline, both for academic research and for industrially relevant applications. The reasons of this renewed interest in photochemistry and photocatalysis can be essentially attributable to the ability and complementary reactivity of excited state intermediates to undergo a number of different transformations that it would be not possible to achieve employing conventional polar chemistry and catalysis. Furthermore, the possibility to generate open-shell radical intermediates under mild, chemoselective conditions, avoiding the use of toxic reagents have helped this discipline to grow faster being one of the chosen methods for the late-stage functionalization or derivatization of pharmaceutical targets. Moreover, the construction of library of compounds, by means of high-throughput screening and analysis is getting more attention and finding more applications in the laboratories worldwide.

During the development of the PhD thesis, we decided to study different activation modes that can be used in photocatalysis to carry out mechanistically different transformations, to expand our knowledge in this context and to understand the fundamental and modern principles that are at the base of photocatalysis, taking into consideration the advantages and disadvantages of every activation mode. For these reasons we decided to study single-electron transfer, triplet energy transfer and selective direct excitation processes (Figure 1).

Furthermore we decided to focus our efforts in the challenging area of enantioselective photocatalysis. Enantiopure compounds are products with a high added value that can be obtained through asymmetric catalytic strategies. Furthermore, following the Food and Drug Administration (FDA) and European Medicines Agency (EMA) regulations on “chiral drugs” which encourages the marketing of drugs as single enantiomers, the academic and pharmaceutical research worlds are endeavoring to develop highly enantioselective processes. The limited number of asymmetric strategies in photocatalysis reported until the last decade can be due to the high difficulty in inducing a stereocontrolled transformation over highly reactive excited state intermediates. Thus, the delivering of chiral information from an enantiopure catalyst is really challenging, with few effective catalytic methodologies reported nowadays.

Taking into consideration all the above described challenges and synthetic interests, we started studying a stereospecific cyclopropane ring-expansion reaction to afford enantiomerically enriched five-membered products by means of an energy transfer mechanism (Figure 3, Chapter 2). One of the most versatile methods to achieve a ring-expansion of cyclopropane derivatives is employing donor-acceptor cyclopropanes, which are three-membered ring-containing compounds opportunely substituted to induce a polarization of one of the bonds, which can be easily cleaved to give transient zwitterionic intermediates. To overcome the limitations of this strategy and to obtain a wider range of differently substituted five-membered rings as possible products, we decided to investigate the possibility of employing visible light photocatalysis to achieve a rearrangement of vinyl cyclopropanes and corresponding heteroatom-containing analogues under mild conditions. In addition, since the obtainment of

enantiopure products is highly desirable we envisioned that if the starting materials would have been enantioenriched, we would had the possibility of achieving a stereospecific transformation with retention of the chiral information over the photocatalytic process.

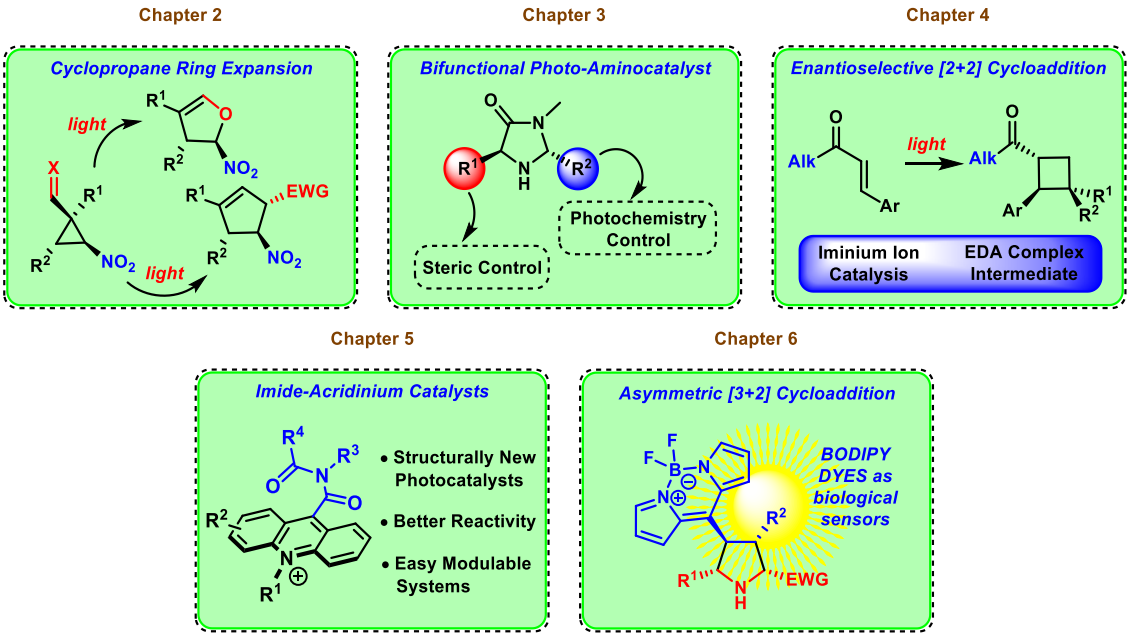

Figure 3. Objectives of the present PhD thesis.

On the other hand, photoredox catalytic reactions have attracted increased attention in the last decades, with a huge number of synthetic methodologies that rely on photocatalytic single-electron transfer processes. Consequently we decided to investigate an asymmetric α-alkylation of aldehydes that relies on SET events (Figure 3, Chapter 3). For this purpose we envisioned that the synthesis of a new bifunctional photo-aminocatalyst would have provided an unprecedented example for what is regarding its synthesis and its implementation in enantioselective photocatalysis. Moreover, the study of the mechanistic differences between a bifunctional and a dual-catalytic system encouraged us to attempt the synthesis of it, aiming at the observation of its behavior in an asymmetric reaction.

One of the most important and widely employed photocatalytic reactions is the [2+2] photocycloaddition. This represents an incomparable reaction for the construction of multiple bonds in a single step that organic chemists have in their synthetic toolbox. Nevertheless, asymmetric strategies for the obtainment of enantioenriched cyclobutanes are often limited to few reported activation modes. The lack of aminocatalytic methods that are available to organic chemists for the asymmetric synthesis of cyclobutanes prompted us to investigate the combination of iminium ion catalysis and visible light irradiation as a new activation mode in enantioselective [2+2] photocycloadditions (Figure 3, Chapter 4).

In the context of photoredox catalysis, the development of new organic photocatalysts that present increased efficiencies and versatile properties is highly desirable. The employment of photocatalysts with enhanced photophysical properties in SET processes can expand the scope of the reaction, achieving single-electron reduction or oxidations over normally inert substrates, or unlock new chemical transformations. One family of organic photocatalysts that has found wide use in the last decade relies on an acridinium-based structure. Since these catalysts present a charge-transfer behavior and a relatively high intersystem-crossing rate the population of its triplet excited state is taking place to a high extent. Nevertheless, the photoactive species which is acting as a strong oxidant is, in most of the cases, the singlet excited state. For these reasons we envisioned the synthesis of a new family of acridinium catalysts which would present enhanced photocatalytic properties (Figure 3, Chapter 5).

In the last chapter, we decided to investigate the BODIPY moiety as an electron-withdrawing group. Indeed, although some organic chromophores present enhanced photocatalytic properties that make suitable their use as photocatalyst, another important and useful application of them is by their implementation as biological sensors. BODIPY dyes represent a class of organic chromophores that have unique photophysical properties and they have been intensively used for cell imaging purposes. Interestingly, the electron-withdrawing character of the BODIPY core is activating its *meso* position but there were not reported uses of BODIPY as electron-withdrawing group in asymmetric catalysis. In addition, the ubiquitous presence of pyrrolidine derivatives in biologically relevant compounds has prompted us to evaluate an asymmetric copper-catalyzed [3+2] cycloaddition using the BODIPY as an electron-withdrawing group, to afford tetrasubstituted pyrrolidines which contain this fluorescent unit (Figure 3, Chapter 6).

Photocatalytic Cyclopropane Ring Expansion

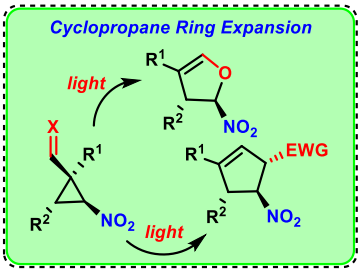

Chapter 2

2. Photocatalytic Cyclopropane Ring Expansion

2.1 Introduction to Cyclopropane Ring-opening Reactions

Cyclopropanes are synthetically useful building blocks in organic synthesis since, due to their particular geometry, they present uncommon strained structures and enhanced reactivity. Moreover, upon ring-opening, they permit to access medium-sized rings and particularly constrained molecules that it would be difficult to achieve through other strategies.[93] Indeed, the synthesis and the subsequent transformations of cyclopropane derivatives have been intensively exploited in organic chemistry for the preparation of a variety of industrially relevant compounds and in several total synthesis of natural products.[94] The derivatization of cyclopropanes can be essentially achieved through ring-opening reactions. While nucleophilic and electrophilic attacks would lead to functionalized acyclic products, bimolecular cycloaddition and rearrangement reactions leads to interesting products by means of ring-expansion reactions.

2.2 Donor-acceptor Cyclopropanes (DACs)

One of the most straightforward methods to achieve a cyclopropane ring expansion to the corresponding five-membered (or larger) rings employs Donor-Acceptor-Cyclopropanes (DACs).[95] These are synthetically useful and widely versatile cyclopropanes that can be easily opened under Lewis acid catalysis, if the cyclopropane ring is appropriately substituted with an electron-withdrawing and an electron-donating group (EWG and EDG). This allows the obtainment of a polarized carbon-carbon bond in the three-membered ring through a "push-pull" effect (Scheme 34). The resulting dipole (zwitterionic intermediate) can then react in a [3+2] or other cycloaddition reactions with a dipolarophile, both in an intermolecular or in an intramolecular fashion. Another way to achieve a ring-expansion reaction is through an intramolecular rearrangement of the dipole, in which the acceptor moiety of the DAC is incorporated into the corresponding five-membered ring.

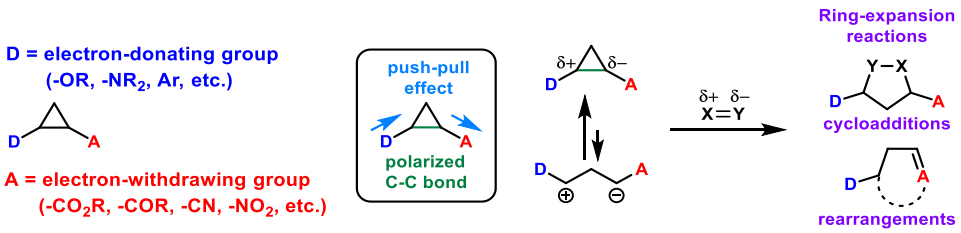

Scheme 34. Polarization and reactivity of donor-acceptor cyclopropanes (DACs).

In the last decades, the use of Lewis acid catalysis has provided a suitable and effective activation strategy for the ring-opening of DACs under mild conditions, giving access to valuable ring-expanded products and to an enormous variety of functionalizations. The first pioneering example of a Lewis acid-assisted ring expansion was reported by Stork's research group in 1969 (Scheme 35a).[96] The use of stannic chloride as the Lewis acid led to a cyclopropane ring-opening and following trapping of the carbocation intermediate by the metal-enolate. Several years

[93] J. Liu, R. Liu, Y. Wei, M. Shi, *Trends in Chemistry* **2019**, *1*, 779-793.
[94] (a) C. Ebner, E. M. Carreira, *Chem. Rev.* **2017**, *117*, 11651-11679; (b) S. J. Gharpure, L. N. Nanda, Tetrahedron Lett. **2017**, *58*, 711-720.
[95] (a) T. F. Schneider, J. Kaschel, D. B. Werz, *Angew. Chem. Int. Ed.* **2014**, *53*, 5504-5523; (b) M. A. Cavitt, L. H. Phun, S. France, *Chem. Soc. Rev.* **2014**, *43*, 804-818; (c) H. K. Grover, M. R. Emmett, M. A. Kerr, *Org. Biomol. Chem.* **2015**, *13*, 655-671.
[96] G. Stork, P. A. Grieco, *J. Am. Chem. Soc.* **1969**, *91*, 2407-2408.

later, the Snider's group reported one of the first methodologies to obtain an intermolecular cyclopropane ring-expansion reaction with a wide variety of different substituted alkenes by the use of an over-stoichiometric amount of Lewis acid (Scheme 35b).[97]

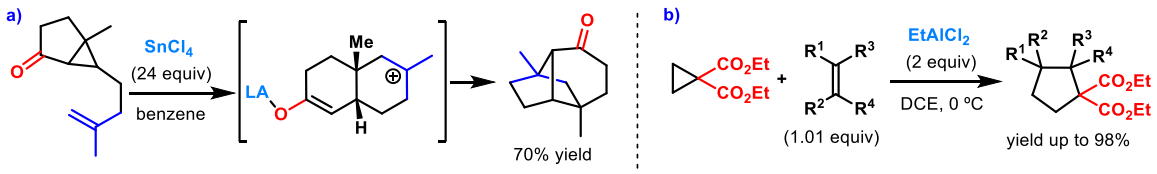

Scheme 35. Seminal examples of intramolecular and intermolecular reactions of DACs.

Since then, several research groups have intensively investigated ring-opening reactions of donor-acceptor cyclopropanes employing Lewis acid catalysis, achieving outstanding expansion reactions with retention of the chiral information of the starting materials or developing asymmetric transformations. Nevertheless, under these reaction conditions, this ring-opening strategy usually requires the presence of two geminal electron-withdrawing groups or a strong electron-donating group to achieve a sufficient degree of polarization of one of the three-membered ring bonds and the subsequent ring-opening. One outstanding enantioselective example of a DAC ring-expansion was provided by Johnson's group in 2009 (Scheme 36).[98] The use of a magnesium-PyBOX ligand catalytic system permitted to carry out a dynamic kinetic asymmetric cycloaddition of racemic donor-acceptor cyclopropanes over different aldehydes as the hetero-dipolarophiles to obtain the corresponding tetrahydrofuran derivatives.

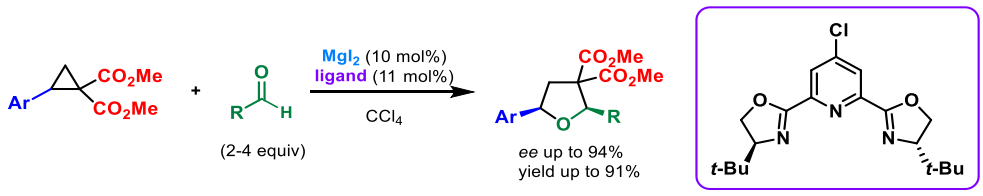

Scheme 36. Enantioselective dynamic kinetic cycloaddition over a hetero-dipolarophile.

A related intramolecular ring-expansion over hetero-dienophiles was reported by the group of Wang in 2010 (Scheme 37a).[99] The employment of scandium (III) triflate as the Lewis acid allowed the synthesis of interesting tri-cyclic structures by means of an intramolecular reaction between the transient zwitterionic species and the dipolarophile. In addition, a one-pot procedure for the preparation of nitrogen-containing analogues was achieved in high efficiency by an initial imine formation and subsequent ring-expansion reaction (Scheme 37b).

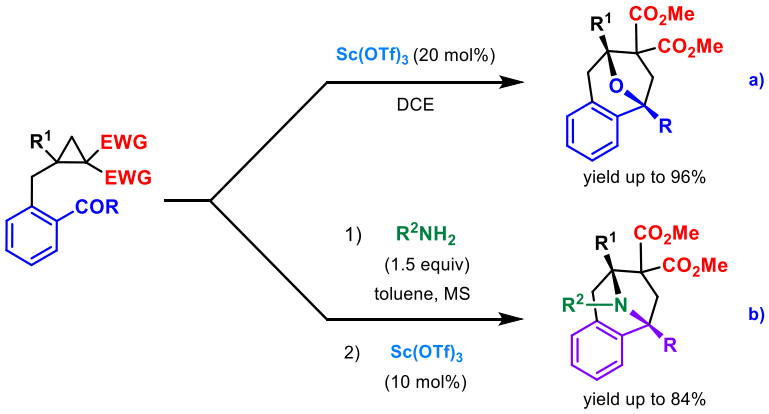

Scheme 37. Intramolecular reaction of a donor-acceptor cyclopropanes.

[97] R. B. Beal, M. A. Dombroski, B. B. Snider, *J. Org. Chem*. **1986**, *51*, 4391-4399.
[98] A. T. Parsons, J. S. Johnson, *J. Am. Chem. Soc*. **2009**, *131*, 3122-3123.
[99] S. Xing, W Pan, C Liu, J Ren, Z. Wang, *Angew. Chem. Int. Ed*. **2010**, *49*, 3215-3218.

The potentiality of this strategies are highlighted by the fact that the reaction works even over dipolarophiles containing a carbon-carbon double bond like in the case of an indole derivative (Scheme 38).[100] The corresponding annulated product was obtained in high yield and enantioselectivity, showcasing the utility of this method for the synthesis of the main core of a natural product.

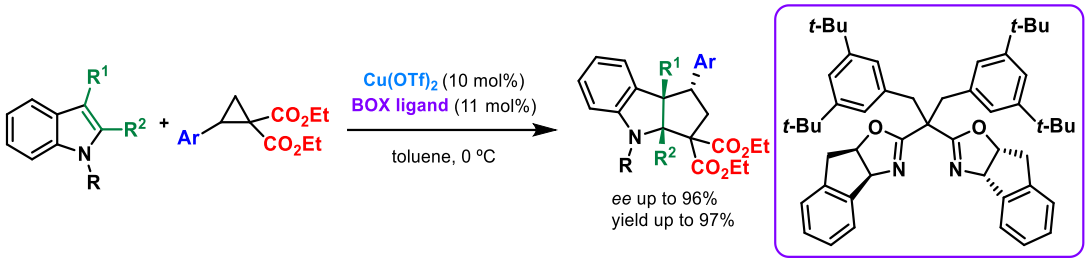

Scheme 38. Enantioselective cycloaddition over indole derivatives as the dipolarophiles.

On the other hand, Jørgensen's group employed organocatalysis as a complementary and efficient activation strategy for the ring-opening of donor-acceptor cyclopropanes.[101] The use of a pyrrolidine-based aminocatalyst or a chiral thiourea bifunctional catalyst allowed the achievement of enantioenriched four-membered and five-membered ring derivatives, respectively (Scheme 39a,b). The cyclobutane adducts are obtained after ring-opening and formation of a dienamine as the chiral active species, whereas in the other case the formation of a stabilized anion is responsible of the first nucleophilic attack over the nitrostyrene derivative.

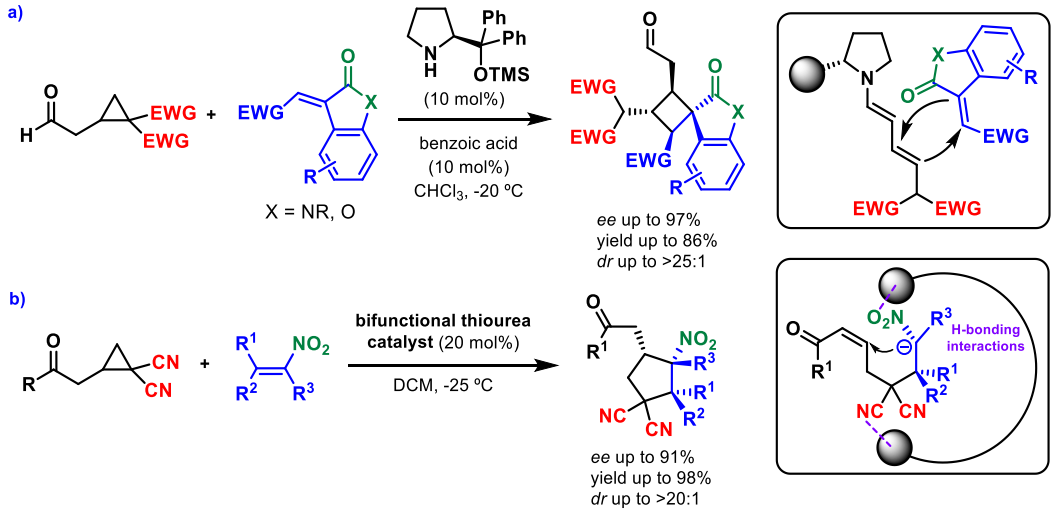

Scheme 39. Organocatalytic asymmetric [2+2] (a) and [3+2] (b) cycloadditions.

2.3 Vinyl Cyclopropane and Related Rearrangements

Another way to achieve an intramolecular ring expansion of a cyclopropane is through a rearrangement of vinyl cyclopropanes and corresponding heteroatom-containing analogues.[102]

[100] H. Xiong, H. Xu, S. Liao, Z. Xie, Y. Tang, *J. Am. Chem. Soc*. **2013**, *135*, 7851-7854.

[101] (a) K. S. Halskov, F. Kniep, V. H. Lauridsen, E. H. Iversen, B. S. Donslund, K. A. Jørgensen, *J. Am. Chem. Soc.* **2015**, *137*, 1685-1691; (b) J. Blom, A. Vidal-Albalat, J. Jørgensen, C. L. Barløse, K. S. Jessen, M. V. Iversen, K. A. Jørgensen, *Angew. Chem. Int. Ed.* **2017**, *56*, 11831-11835; for an iminium ion strategy reported by Vicario's group, see: (c) E. Sanchez-Diez, D. L. Vesga, E. Reyes, U. Uria, L. Carrillo, J. L. Vicario, *Org. Lett*. **2016**, *18*, 1270-1273.

[102] (a) T. Hudlicky, J. W. Reed, *Angew. Chem. Int. Ed*. **2010**, *49*, 4864-4876, (b) M. Meazza, H Guo, R. Rios, *Org. Biomol. Chem*. **2017**, *15*, 2479-2490.

This reaction can be achieved thermally (at high temperature or under pyrolysis conditions), under Lewis acid catalysis or aminocatalysis (employing DACs), and photochemically (mainly employing UV light). Although the first thermal vinyl cyclopropane rearrangement was discovered in 1959 by Neureiter (Scheme 40a), achieving the thermal transformation of dichlorovinylcyclopropane to dichlorocyclopentene, the corresponding rearrangement of nitrogen- and oxygen-containing analogues were precedently discovered by Cloke and Wilson in 1929 and 1947, respectively (Scheme 40b,c).[102a,103] On the other hand, UV light irradiation has been widely employed to achieve the same rearrangements without the need of high temperatures and harsh reaction conditions (Scheme 40d,e).[104]

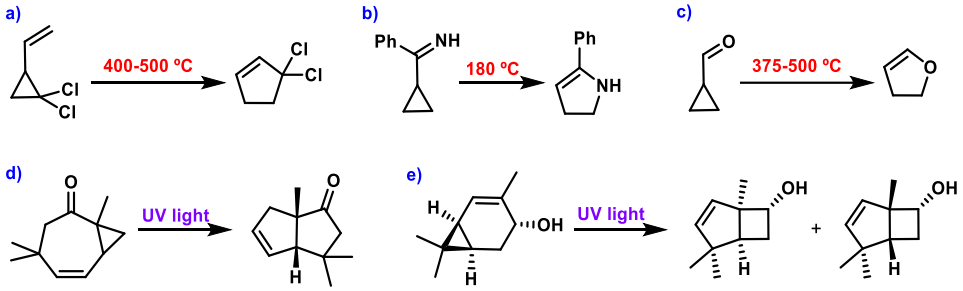

Scheme 40. a-c) First vinyl cyclopropane rearrangements. d-e) Photochemical rearrangements.

A modern rearrangement of DACs to dihydrofuranes was reported by Johnson's research group in 2006 through the use of a Ni(0) catalytic system, which allowed the obtainment of a wide variety of differently substituted products in high yield and with retention of enantiomeric excess (Scheme 41).[105] Another elegant example of a donor-acceptor cyclopropane transformation was provided by Werz's group to achieve the rearrangement of a nitro cyclopropane derivative with the following incorporation of the nitro acceptor moiety into the final product (Scheme 42).[106] The use of a rhodium catalyst permitted the in situ generation of the nitro cyclopropane derivative without the need of its isolation, leading smoothly to the final product in high efficiency. Worth to mention is that other electron-withdrawing group has never been found incorporated into the final ring stucture. The different reactivity of the two acceptor groups has been highlighted by means of DFT analysis, revealing that the transition state which is leading to the cyclic nitronate presents a lower activation barrier in comparison with the alternative insertion of the other electron-withdrawing group.

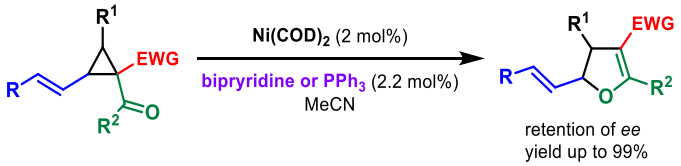

Scheme 41. Nickel catalyzed rearrangement to dihydrofuranes derivatives.

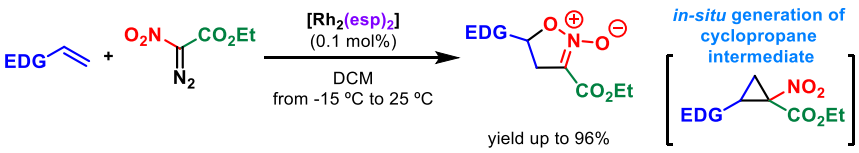

Scheme 42. Rhodium catalyzed rearrangement to cyclic nitronates.

[103] (a) N. Neureiter, *J. Org. Chem.* **1959**, *24*, 2044-2046; (b) J. B. Cloke, *J. Am. Chem. Soc*. **1929**, *51*, 1174-1187; (c) C. L. Wilson, *J. Am. Chem. Soc*. **1947**, *69*, 3002-3004.

[104] (a) L. A. Paquette, G. V. Meehan, R. P. Henzel, R. F. Eizember, *J. Org. Chem*. **1973**, *38*, 3250-3256. (b) H. R. Sonawane, B. S. Nanjundiah, V. G. Shah, D. G. Kulkarni, J. R. Ahuja, *Tetrahedron Lett*. **1991**, *32*. 1107-1108.

[105] R. K. Bowman, J. S. Johnson, *Org. Lett* **2006**, *8*, 573-576.

[106] C. D. Schmidt, J. Kaschel, T. F. Schneider, D. Kratzert, D. Stalke, D. B. Werz, *Org. Lett*. **2013**, *15*, 6098-6101.

A nice example, which is showcasing the potential of organocatalysis in the rearrangement of donor-acceptor cyclopropanes, was reported by Vicario's research group in 2018 (Scheme 43).[107] The corresponding dihydrofuranes derivatives were achieved in high enantioselectivity and, in some cases, the reaction worked properly with just one electron-withdrawing group that was efficiently incorporated into the five-membered ring.

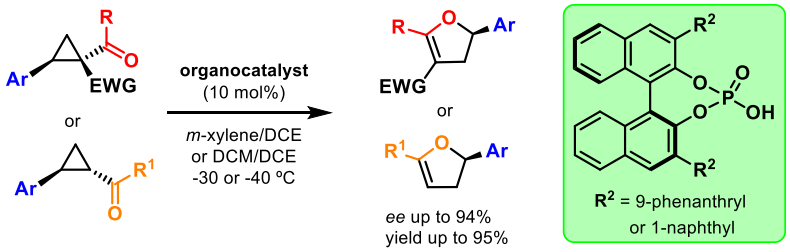

Scheme 43. Organocatalytic asymmetric rearrangement to dihydrofuranes derivatives.

An interesting rearrangement involving a cyclopropane bond-breaking between two acceptor moieties was reported through the use of *N*-heterocyclic carbene catalysis (Scheme 44a).[108] By means of an umpolung of reactivity, the final six-membered ring products were obtained in high yield and in an enantiospecific manner. Another nice example was achieved by Trushkov's group in 2018 through Lewis acid catalysis over a stiryl cyclopropane that present a geminal substitution with two electron-withdrawing groups, leading to cyclopentene derivatives (Scheme 44b).[109]

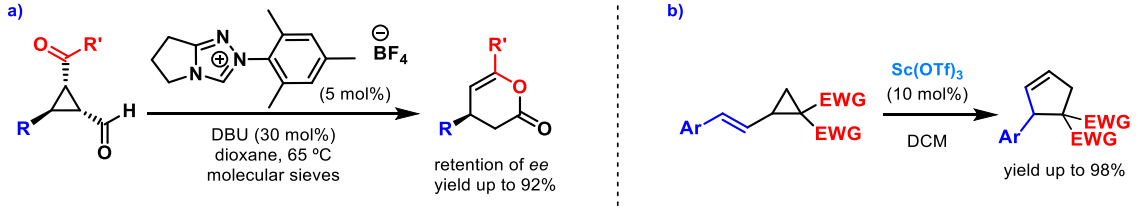

Scheme 44. a) Reactivity umpolung by NHC catalysis. b) Lewis acid-catalyzed rearrangement to cyclopentene derivatives.

2.4 Photocatalytic Strategies

To overcome some of the reactivity limitations of heterolytic cleavage-mediated methodologies of DACs and to avoid the use of high energetic UV irradiation, the Yoon's research group reported two different photocatalytic Lewis acid strategies, being one an intramolecular racemic and the other one an intermolecular asymmetric version, to achieve a distonic radical anion intermediate that can react with a wide range of unactivated olefins to give cyclopentanes under visible light irradiation (Scheme 45 and Scheme 46).[110] Both intramolecular and intermolecular reactions can be carried out without the requirement of a dipolarophile as the reaction partner, obtaining the corresponding products in high efficiency. The aryl cyclopropyl ketone was activated through the lowering of its redox potential by coordination of a Lewis acid, which permitted its selective reduction by a ruthenium photocatalyst, leading to a cyclopropane ring opening and subsequent reaction.

[107] A. Ortega, R. Manzano, U. Uria, L. Carrillo, E. Reyes, T. Tejero, P. Merino, J. L. Vicario, *Angew. Chem. Int. Ed.* **2018**, *57*, 8225-8229.
[108] G.-Q. Li, L.-X. Dai, S.-L. You, *Org. Lett.* **2009**, *11*, 1623-1625.
[109] O. A. Ivanova, A. O. Chagarovskiy, A. N. Shumsky, V. D. Krasnobrov, I. I. Levina, I. V. Trushkov, *J. Org. Chem.* **2018**, *83*, 543-560.
[110] (a) Z. Lu, M. Shen, T. P. Yoon, *J. Am. Chem. Soc.* **2011**, *133*, 1162-1164; (b) A. G. Amador, E. M. Sherbrook, T. P. Yoon, *J. Am. Chem. Soc.* **2016**, *138*, 4722-4725.

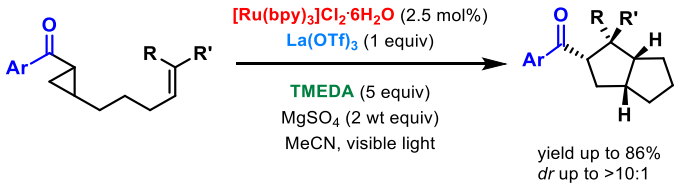

Scheme 45. Intramolecular photocatalytic cyclopropane ring-expansion to cyclopentane derivatives.

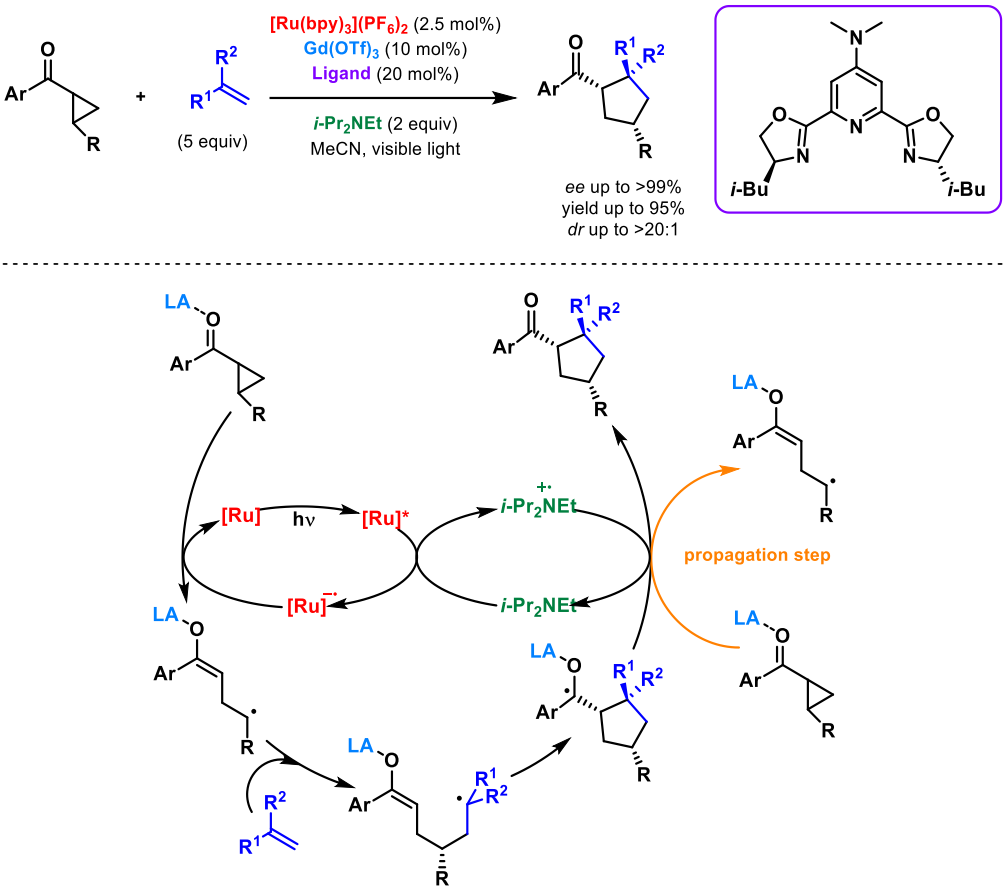

Scheme 46. Intermolecular photocatalytic cyclopropane ring-expansion to enantioenriched cyclopentane derivatives under Lewis acid catalysis.

Another racemic example that is worth to mention is an intermolecular reaction developed by the research group of Lu, in which a lithium cation-mediated intermolecular cyclopropane ring expansion was obtained between nitrocyclopropanes and styrenes, in analogy with Yoon's report (Scheme 47).[111]

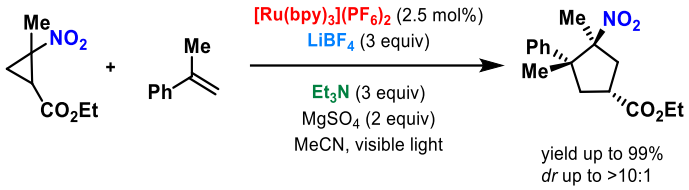

Scheme 47. Intermolecular photocatalytic ring-expansion of nitro cyclopropanes to cyclopentanes.

[111] C. Wang, X. Ren, H. Xie, Z. Lu, *Chem. Eur. J.* **2015**, *21*, 9676-9680.

In 2018, Meggers' group efficiently employed a chiral-at-metal rhodium catalyst for an enantioselective cyclopropane ring-expansion reaction to cyclopentanes and cyclopentenes with alkenes and alkynes as the reaction partners (Scheme 48).[112]

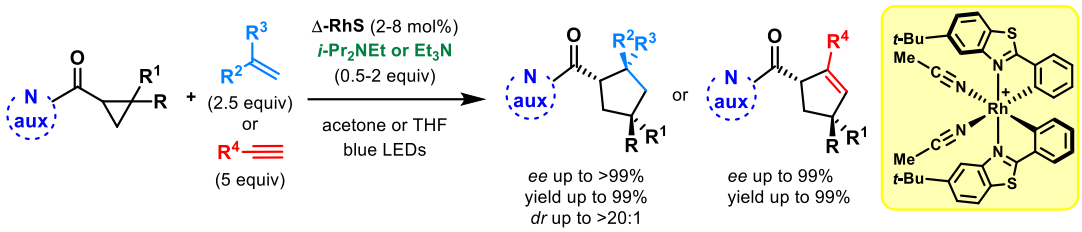

Scheme 48. Enantioselective cyclopropane ring-expansion to cyclopentane and cyclopentene derivatives by a chiral-at-metal rhodium photocatalyst.

Through a complementary photocatalytic strategy the Zheng's research group reported that cyclopropylamines can undergo a ring-expansion reaction with styrene derivatives, leading to the corresponding cyclopentanes (Scheme 49).[24] By means of a single-electron transfer the cyclopropylamine could be photooxidized to an amine radical cation, which led to the cyclopropane ring-opening and formation of an iminium ion. The carbon-centered radical can then carry out the cyclization reaction with various styrene derivatives, followed by the restoring of the ground-state photocatalyst.

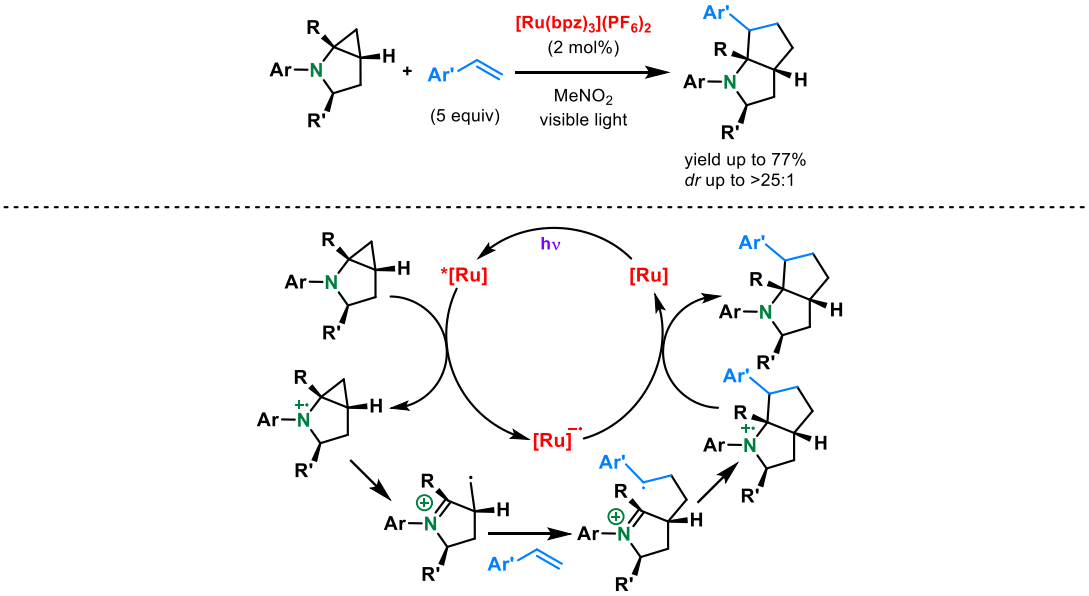

Scheme 49. Photocatalytic ring-expansion of cyclopropylamine derivatives.

An enantioselective strategy to achieve a cyclopropane ring-expansion reaction through the use of a catalytic photoactive chiral iminium ion species was reported by Melchiorre's research group in 2018 (Scheme 50).[79c] Based on the initial observations of Mariano's research group of photoredox-mediated ring-opening and radical addition of cyclopropanols,[113] the Melchiorre's group developed an asymmetric photo-organocascade reaction. The cyclopropanols can be photooxidized by an excited iminium ion species, which is acting as a strong oxidant to give a SET between them. Upon ring-opening and loss of a proton the cyclopropanol gives a neutral radical species which can undergo a radical coupling with the β-enaminyl radical to afford a β-

[112] X. Huang, J. Lin, T. Shen, K. Harms, M. Marchini, P. Ceroni, E. Meggers, *Angew. Chem. Int. Ed.* **2018**, *57*, 5454-5458.

[113] (a) J. Stavinoha, E. Bay, A. Leone, P. S. Mariano, *Tetrahedron Lett*. **1980**, *21*, 3455-3458; (b) P. S. Mariano, J. Stavinoha, E. Bay, *Tetrahedron* **1981**, *37*, 3385-3395.

functionalized intermediate. The latter can then carry out an intramolecular aldol reaction to afford the final enantioenriched five-membered ring product after hydrolysis.

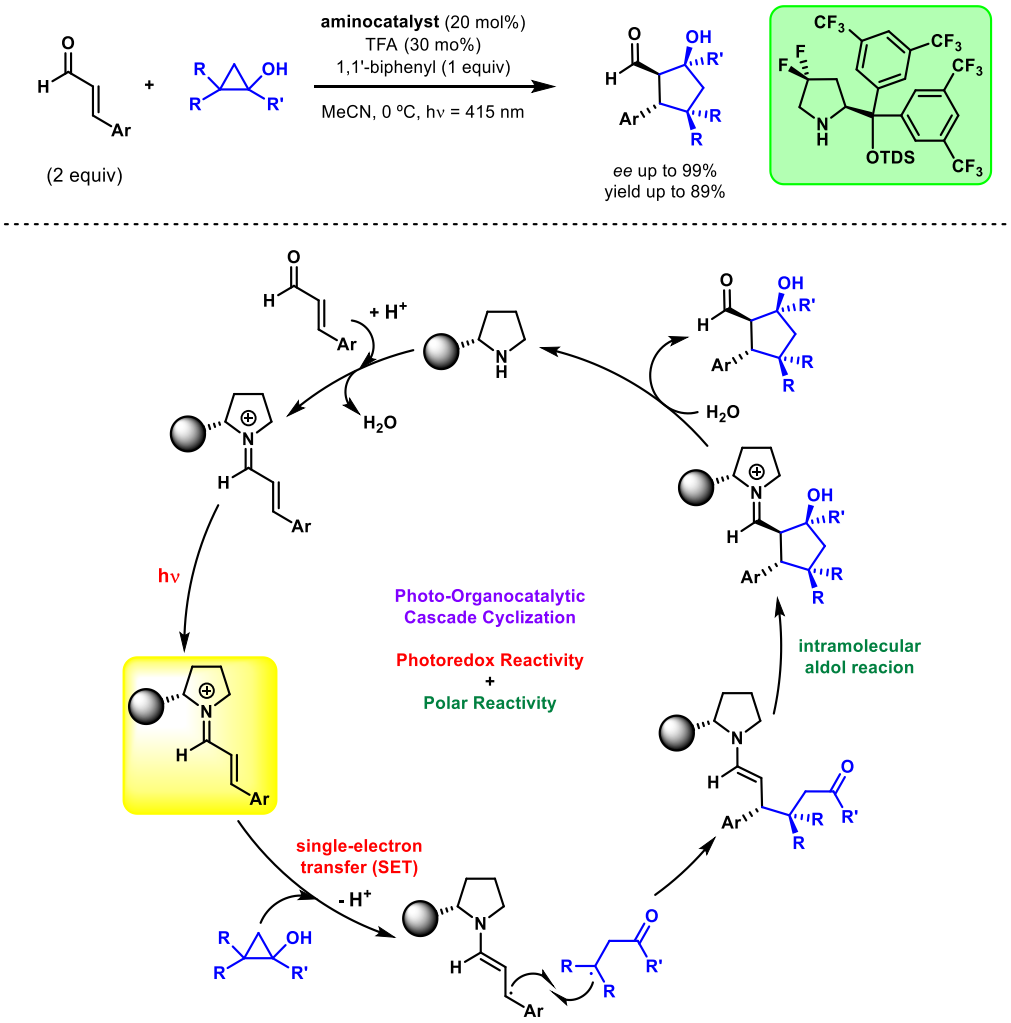

Scheme 50. Enantioselective ring-expansion of cyclopropanols through a photocascade reaction.

An brilliant enantioselective intermolecular cyclopropane ring-expansion reaction was reported by Maruoka's research group in 2014 (Scheme 51).[114] The employment of an enantiopure thiol catalyst permitted the photochemical generation of a chiral thilyl radical, which can be added to the vinyl cyclopropane to give a subsequent ring-opening. The stereoinduced cyclization is then taking place under the control of the chiral catalyst to furnish the corresponding enantioenriched vinyl cyclopentane after restoring of the thilyl radical.

In the context of photocatalytic rearrangements of cyclopropyl derivatives two examples that are worth to mention are the visible light-induced ring-expansions to dihydrofuranes reported by Plietker's and Wenger's group (Scheme 52a,b).[115] The use of an iron or a molybdenum photocatalyst allowed the synthesis of these compounds in high efficiency through single-electron transfer mechanisms.

[114] T. Hashimoto, Y. Kawamata, K. Maruoka, *Nat. Chem*. **2014**, *6*, 702-705.

[115] (a) C.-H. Lin, D. Pursley, J. E. M. N. Klein, J. Teske, J. A. Allen, F. Rami, A. Köhn, B. Plietker, *Chem. Sci*. **2015**, *6*, 7034-7043; (b) L. A. Bîldt, X. Guo, A. Prescimone, O. S. Wenger, *Angew. Chem. Int. Ed*. **2016**, *55*, 11247-11250.

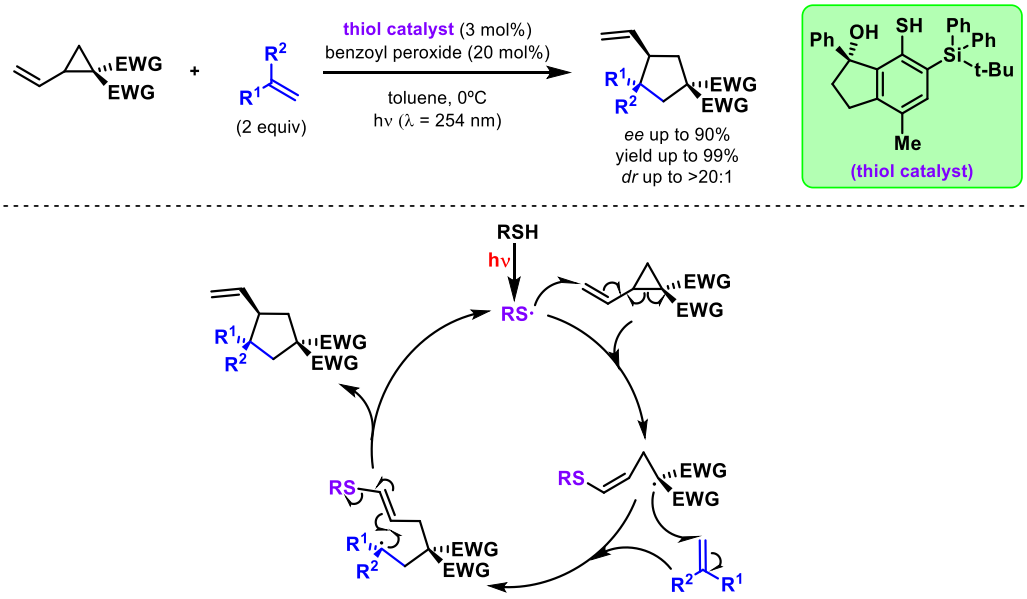

Scheme 51. Enantioselective strategy for the obtainment of vinyl cyclopentanes by a thilyl radical.

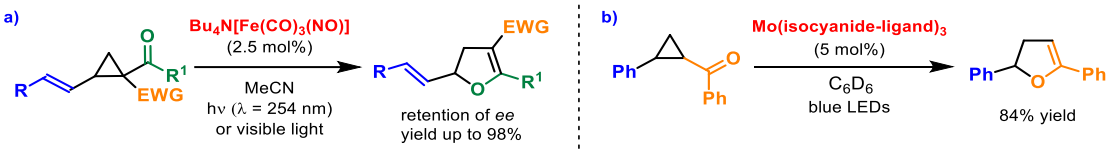

Scheme 52. Photocatalytic ring-expansion reactions to dihydrofuranes.

2.5 Objectives of this Chapter

Due to the few reported methodologies for the achievement of a stereospecific intramolecular cyclopropane-ring expansion reaction to dihydrofuranes and cyclopentenes until 2016, we started considering about the possibility of exploiting a rearrangement of vinyl cyclopropanes and corresponding heteroatom-containing analogues through the use of photocatalysis. This would have the advantages of not being necessary the presence of one electron-donating and one electron-withdrawing substituents on the three-membered ring like in polar DAC cycloadditions. Furthermore, employing photocatalysis it would be possible to achieve a carbon-carbon bond breaking between two acceptor moieties, leading to a complementary reactivity in comparison with the intramolecular DAC cycloadditions. For this purpose, we choose enantioenriched nitrocyclopropane carboxaldehydes and related vinyl derivatives to achieve a ring expansion to optically enriched dihydrofuranes and cyclopentenes, respectively (Scheme 53).

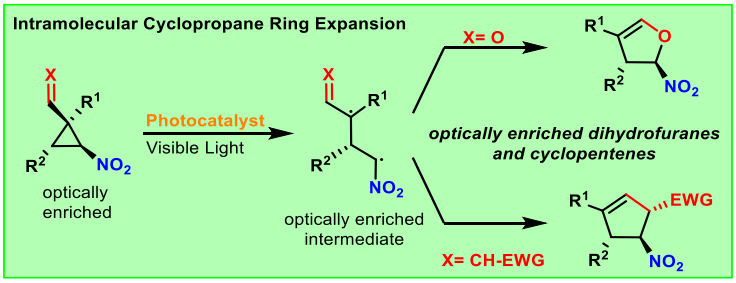

Scheme 53. Proposed photocatalytic strategy for the ring-expansion of nitro cyclopropane derivatives.

The targeted starting materials have been chosen since the Lu's lab reported that nitrocyclopropanes could be reduced through a photoredox strategy and since our group has reported an organocatalytic methodology to obtain the desired nitrocyclopropanes in an enantiopure form (Scheme 54).[111,116] Moreover the corresponding possible products, 2,3-dihydrofuranes and cyclopentanes, are important structures that are found in a wide number of natural products (Scheme 55).[117]

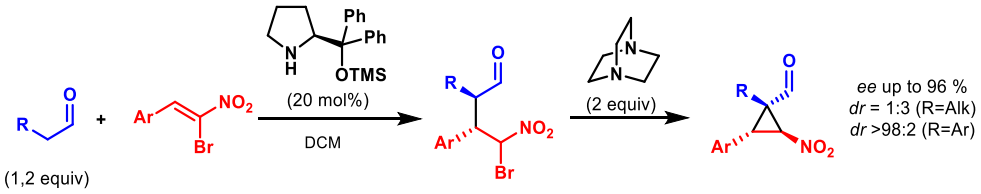

Scheme 54. Asymmetric organocatalytic methodology for the preparation of nitro cyclopropanes.

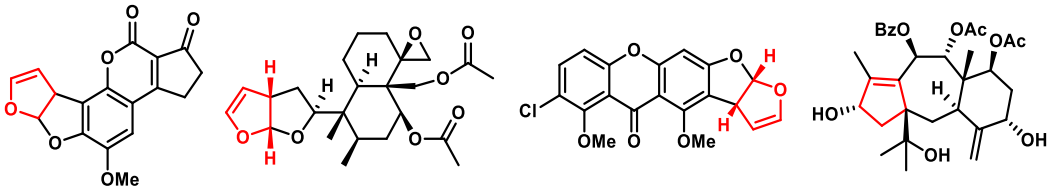

Scheme 55. Examples of dihydrofurane scaffolds present in biologically relevant compounds.

In order to achieve this goal, we proposed the following sub-objectives:

1) Searching of the appropriate reaction conditions as photocatalyst, solvent, temperature and corresponding irradiation set-up (type of photoreactor).
2) Evaluation of the reaction scope and exploration of different starting materials in the ring expansion reaction.
3) DFT calculations and mechanistic investigations in order to elucidate the photocatalytic rearrangement mechanism.

[116] J. Luis-Barrera, R. Mas-Ballesté, J. Alemán, *ChemPlusChem* **2015**, *80*, 1595-1600.

[117] (a) G. S. Bbosa, D. Kitya, A. Lubega, J. Ogwal-Okeng, W. W. Anokbonggo, D. B. Kyegombe, "Review of the Biological and Health Effects of Aflatoxins on Body Organs and Body Systems, Aflatoxins - Recent Advances and Future Prospects (Chapter 12)", *IntechOpen*, **2013**, 239-265. (b) D. H. R. Barton, H. T. Cheung, A. D. Cross, L. M. Jackman, M. Martin-Smith, *J. Chem. Soc.* **1961**, 5061-5072. (c) P. S. Steyn, R. Vleggaar, *J. Chem. Soc., Perkin Trans. 1* **1974**, 2250-2256. (d) R. Kaur, S. K. Chattopadhyay, A. Chatterjee, O. Prakash, F. Khan, N. Suri, D. Priya, A. K. Saxena, *Med. Chem. Res.* **2014**, *23*, 4138-4148.

2.6 Publications and Experimental Section

Visible-Light Photocatalytic Intramolecular Cyclopropane Ring Expansion

Javier Luis-Barrera, Víctor Laina-Martín, Thomas Rigotti, Francesca Peccati, Xavier Solans-Monfort, Mariona Sodupe, Rubén Mas-Ballesté, Marta Liras, and José Alemán*

Angew. Chem. Int. Ed. **2017**, *56*, 7826-7830

The experimental section was taken from the "Supporting Information" document associated with the specific publication and is including the corresponding numeration. The characterization data have been shown only for the final products that appear in the scope of the reaction. The complete "Supporting Information" documents, with all the characterization data, NMR spectra, SFC or HPLC traces and other experimental procedures have been included in the enclosed USB memory.

Photocatalysis

International Edition: DOI: 10.1002/anie.201703334
German Edition: DOI: 10.1002/ange.201703334

Visible-Light Photocatalytic Intramolecular Cyclopropane Ring Expansion

*Javier Luis-Barrera, Víctor Laina-Martín, Thomas Rigotti, Francesca Peccati, Xavier Solans-Monfort, Mariona Sodupe, Rubén Mas-Ballesté, Marta Liras, and José Alemán**

Dedicated to Professor Carmen Navarro Ranninger

Abstract: *Described herein is a new visible-light photocatalytic strategy for the synthesis of enantioenriched dihydrofurans and cyclopentenes by an intramolecular nitro cyclopropane ring expansion reaction. Mechanistic studies and DFT calculations are used to elucidate the key factors in this new ring expansion reaction, and the need for the nitro group on the cyclopropane.*

The [3+2] cycloaddition reactions of donor–acceptor cyclopropanes (DACs), having double bonds, under Lewis acid catalysis are one of the most commonly used methods for the construction of different cycles through ring expansion reactions.[1] Therefore, in the presence of a Lewis acid, 1,3-zwitterions can be generated and trapped by different double bonds, that is C=C, C=N, C=O. Brilliant examples of intermolecular cycloadditions (Scheme 1a) from the groups of Maulide,[2a] Trushkov,[2b] Tang,[2c] Doyle,[2d] Tomilov,[2e] and Werz[2f–h] have been reported recently, while the group of Wang and others have developed related intramolecular cross-cycloadditions (IMCC; Scheme 1b).[3]

Visible-light photocatalysis has received significant attention during the last few years because of its ability to achieve bond constructions that are not possible using other procedures.[4] However, although thermal DAC reactions have been studied in the literature, only two examples of intermolecular cyclopropane ring expansion using photocatalysis have been reported.[5] Lu and co-workers have published on the cyclopropane ring opening under visible-light photocatalysis, and its intermolecular addition to a double bond to generate racemic cyclopentanes with a moderate diastereomeric ratio (Scheme 2a).[5a] More recently, Yoon and co-workers published a very elegant investigation in which photocatalysis is used in combination with a chiral Lewis acid to access cyclopentanes through an intermolecular process (Scheme 2a).[5b]

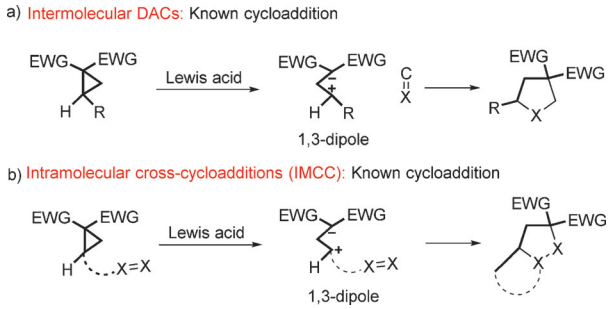

Scheme 1. DAC- and IMCC-type reactions. EWG = electron-withdrawing group.

Based on these investigations, we hypothesized that enantiomerically enriched cyclopropanes could be used as starting materials for the intramolecular visible-light photocatalytic ring expansion, a process that has remained elusive up to now. Very recently, the synthesis of chiral cyclopropanes which contain a chiral center flanked by an aldehyde and a nitro group was reported by our group.[6] We thought that the formation of the chiral intermediate **A**, which could preserve the chiral information to the final product, would be

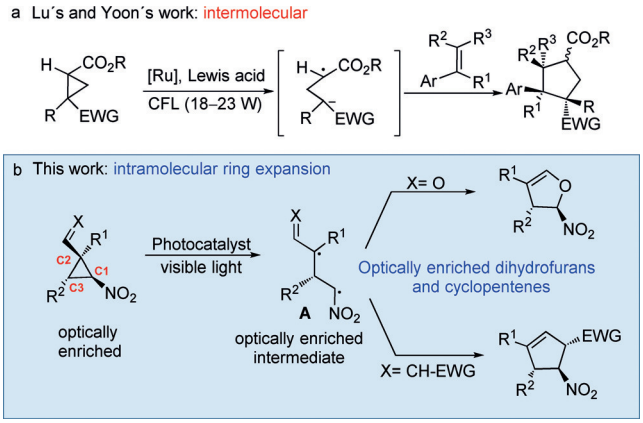

Scheme 2. Different strategies for the intermolecular reaction of cyclopropanes with double bonds and the expansion shown in this work.

[*] J. Luis-Barrera, V. Laina-Martín, T. Rigotti, Prof. Dr. J. Alemán
Organic Chemistry Department, Módulo 1
Universidad Autónoma de Madrid
28049 Madrid (Spain)
E-mail: jose.aleman@uam.es
Homepage: http://www.uam.es/jose.aleman
Dr. F. Peccati, Prof. Dr. X. Solans-Monfort, Prof. Dr. M. Sodupe
Departament de Química, Universidad Autónoma de Barcelona
08193 Bellaterra (Spain)
Prof. Dr. R. Mas-Ballesté
Inorganic Chemistry Deparment, Universidad Autónoma de Madrid
28049 Madrid (Spain)
Dr. M. Liras
Imdea Energy Institute
28935 Móstoles (Madrid)

Supporting information for this article can be found under: https://doi.org/10.1002/anie.201703334.

an appropriate strategy for its intramolecular expansion reaction (Scheme 2b). This approach is challenging because two other plausible C–C bond ruptures might take place (C2–C3 and C3–C1), but only the C1–C2 bond breaking will lead to **A** for the expansion reaction. This ring enlargement (C1–C2 cleavage) stands in contrast to the common expansion of DACs (C2–C3 cleavage).[3e,f] Therefore, the first visible-light photocatalytic strategy for the synthesis of enantioenriched dihydrofurans and cyclopentenes,[7] by an intramolecular cyclopropane expansion reaction is presented.

First, we studied the expansion of the aldehyde **1a** to **2a** (for structures see Table 1) using different photocatalysts such as acridinium salts, eosin Y, and different iridium and ruthenium complexes. Only two iridium complexes were active, and **3b** [Ir(dFppy)$_3$] allowed higher conversion than **3a** [Ir(ppy)$_3$], with CH_2Cl_2 as the best solvent and irradiation of blue light into the reaction media, through a glass bar, thus achieving full conversion of **2a** after 4 hours (see the Supporting Information for full optimization of reaction conditions). The scope of the reaction was studied with different cyclopropanes (**1**[8]; Table 1). Regarding R^2, different aromatic groups, having substitutions at the *para* position, and alkyl groups were studied. Excellent yields for the compounds **2a–c** were achieved. In addition, different R^1 groups were studied, thus showing that the reaction takes place with primary alkyl groups (**2d**), aromatics (**2e** and **2f**), and hydrogen (**2g** and **2h**).[9] In all cases, we observed similar final *ee* values for the products **2** as those for the reactants **1** (*ee* value within parentheses), thus indicating that no loss of stereochemical information at C3 was observed. The absolute configuration of the starting material **1f** was unequivocally determined by its X-ray diffraction structure (see structure in Table 1).[10]

To expand the scope of the reaction, we studied cyclopropanes bearing a double bond instead of an aldehydic group (Table 2). Firstly, the aldehydes **1** were treated with different commercially available Wittig reagents to give the cyclopropane starting materials **4** (see the Supporting Information). The reaction worked with the cyclopropane **4a** to give **5a**, with a good *ee* value, by using the same reaction conditions as those used for the expansion of the aldehydes **1**, but with slightly longer reaction times compared to that of the aldehydes. Substrates with other aromatic residues, such as methoxy and bromo substituents (**4b** and **4c**), also underwent the ring expansion reaction in moderate to good yields. Other groups at R^1, such as *n*Pr (**4d**), were also tolerated. Unexpectedly, the aromatic group at R^1 (**4e**) did not yield the desired product **5e**. Other double bonds bearing benzyl esters (**4f**), ketones (**4g**), or nitriles (**4h**) also worked, giving moderate to good yields, without any loss in the final enantioselectivity. The absolute configuration of the starting material **4c** was unequivocally determined by its X-ray diffraction structure (see structure in Table 2).[10]

Furthermore, the photocatalytic cyclopropanation expansion reaction worked with other functional groups (Scheme 3). When the reaction was performed with the ketone **6**, the reaction was much slower (3 days) in comparison with the aldehyde derivatives **1**, yielding **7** in moderate yield. The α-keto-ester **8** was more reactive (24 h), thus giving the trisubstituted dihydrofuran **9** in good yield.

Table 1: Different ring expansions of **1** using the photocatalyst **3b**.[a]

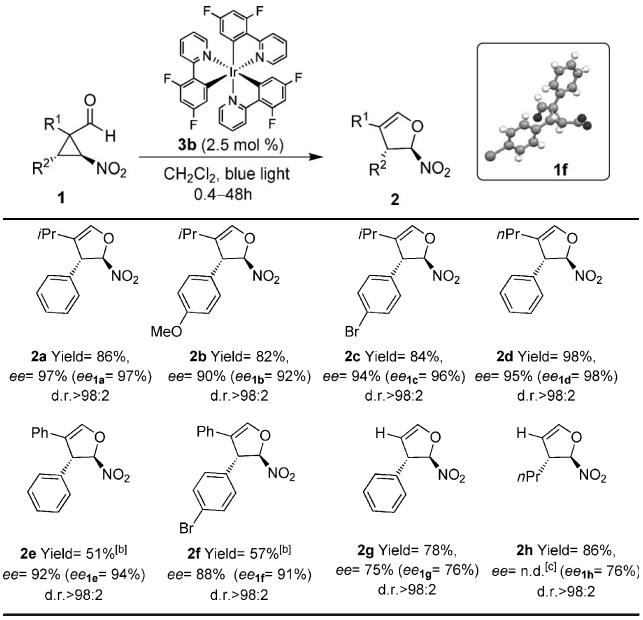

[a] All the reactions were performed at 0.1 mmol scale of **1** in 1.0 mL CH_2Cl_2. The *ee* value of the starting cyclopropane **1** (given within parentheses) and final dihydrofurans (**2**) were determined by SFC. Yield of product isolated after flash chromatography. [b] Yield based on conversion as determined by ^{1}H NMR spectroscopy. [c] The *ee* value could not be determined by SFC, although possess optical rotation activity.

Table 2: Different ring expansion of **4** using the photocatalyst **3b**.[a]

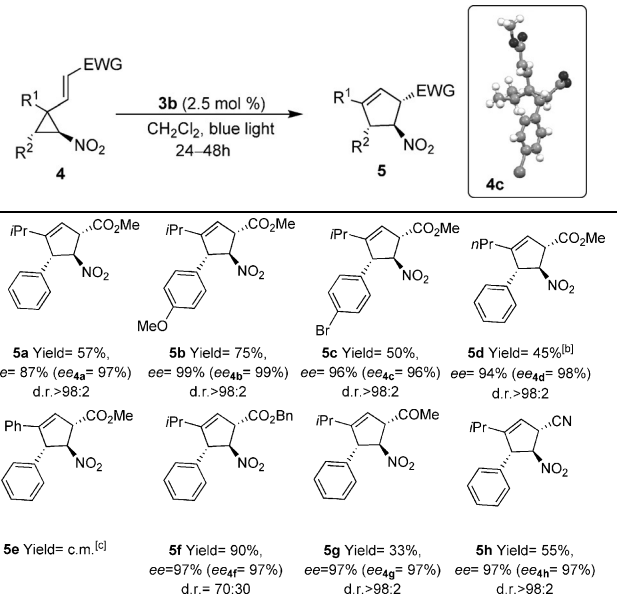

[a] All the reactions were performed at 0.1 mmol scale of **4** in 1.0 mL CH_2Cl_2. The *ee* value of the starting material cyclopropane **4** (given within parentheses) and the final cyclopentenes **5** were determined by SFC. Yield of product isolated after flash chromatography. [b] Yield based on conversion as determined by ^{1}H NMR spectroscopy. [c] Complex mixture.

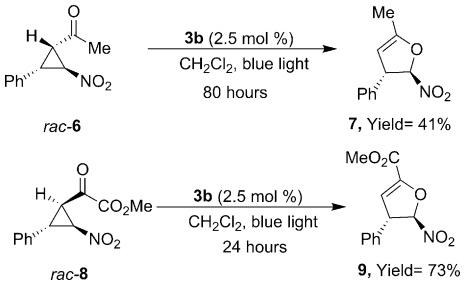

Scheme 3. Reaction with ketone and α-ketoester cyclopropane derivatives.

To understand this process, we carried out additional experiments and DFT(M06/6-31+G(d,p)) calculations,[11a] including the SMD implicit solvent model[11b] (see the Supporting Information for details). The process starts with the excitation of the photocatalyst **3b** to **3b*** using visible-light irradiation. To evaluate the possibility of a photo-redox mechanism, cyclic voltammetry measurements were carried out for **1a** and compared with the reported redox potentials for the excited state of **3b**[12] (see the Supporting Information). Electrochemical characterization rules out photocatalytic oxidation as a mechanism of activation since no oxidation features below +1.5 V (vs. Ag/AgCl) were observable in the cyclic voltammogram of **1a**. However, one irreversible reduction of **1a** at half-wave potential of −1.06 V (vs. Ag/AgCl) was observed. Although photoreduction of **1a** by **3b*** ($Ir^{4+}/Ir^{3+*} = -1.39$ V vs. Ag/AgCl) would be possible, we found that the use of Eosin Y as a photo reductor catalyst [$E°(EY^{+}/EY^{*}) = -1.11$ V vs. Ag/AgCl[4d]] did not result in any conversion (see the Supporting Information). Furthermore, despite the higher reducing power of [$Ir(ppy)_3$] (**3a**) in its excited state [$E°(Ir^{4+}/Ir^{3+*}) = -1.67$ V vs. Ag/AgCl], the conversion into the observed product using **3a** is very poor in comparison with the results obtained with **3b** (27% vs. >98%; see the Supporting Information). Therefore, an energy-transfer process should be considered as an alternative mechanism.[13] Considering that we did not observe any overlap in the emission of the photocatalyst **3b** ($\lambda_{max} = 453$ nm) and the absorption of the nitrocyclopropane **1a** ($\lambda_{max} = 229$ nm; see the Supporting Information), the energy-transfer process from **3b*** to the substrate should proceed through a Dexter-type mechanism (instead of a Forster pathway). Such a mechanism implies that triplet spin state in the substrate is induced by short distance interaction with the triplet excited state of photocatalyst. Indeed, the calculated values of singlet–triplet gap in **1a** and the emission energy of **3a** are in good agreement (see below). In a quest for evidence of an energy-transfer mechanism, the cyclopropane **8** was irradiated with UV light ($\lambda_{max} = 365$ nm), and the expansion reaction was observed with a moderate conversion (23%) after 24 hours. Although a value of the quantum yield less than one does not exclude a possible radical-chain mechanism, we measured the Φ of the reaction of **1a** in the presence of **3b** (see the Supporting Information). The observed value ($\Phi = 0.05$) could suggest that a radical-chain propagation is not taking place.

Considering that changes in R^1, R^2, and CHO/CH=EWG did not suppress the observed reactivity, we hypothesized that the nitro group must play a key role in the photocatalytic activation of cyclopropane. Indeed, when the nitro group was substituted by an ester or a ketone (**10** and **11**; see Figure 1),

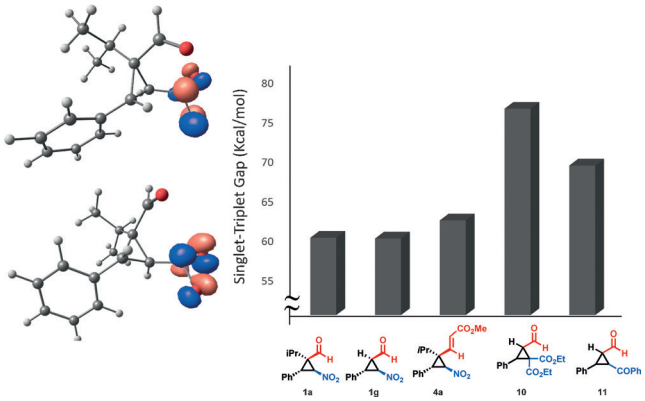

Figure 1. SOMO orbitals calculated for triplet state of **1a** (left) and singlet–triplet energy gap for a range of cyclopropane reagents (right).

the reaction under visible-light photocatalytic conditions did not take place, thus indicating that the presence of the nitro group is essential for the ring-expansion process. With the aim of gaining a deeper insight into this point, the singlet–triplet Gibbs energy gap was calculated for **1a** and other related structures where the nitro group was substituted by different functional groups (Figure 1). Interestingly, the lowest singlet–triplet gaps are computed for molecules enclosing the nitro group. In fact, such an energetic difference between the spin states of the organic reagent, reasonably matches the reported emission energy for **3b** (ca. 60 kcal mol^{-1}).[12] Certainly, when the nitro group is substituted by COPh or two esters, the gap substantially increases (>70 kcal mol^{-1}), thus hindering the photocatalytic process, which is in agreement with the absence of reactivity of **10** and **11**. The two SOMO orbitals of the triplet state are localized on the NO_2 group, in agreement with the role of such a fragment on lowering the excitation energy of the reagent.

The first step is the opening of the cyclopropane ring that leads to the formation of the first biradical ^{3}**IIa** (Figure 2, right). Three C–C bond breaks are possible (paths a, b, or c), and give three different isomers (^{3}**IIa**, ^{3}**IIb**, and ^{3}**IIc**). Ring expansion from ^{3}**IIa** enables the final observed five-membered ring isomer (**2a**) whereas that from ^{3}**IIb** would lead to the five-membered ring ^{1}**IVb** which is not observed experimentally. Finally, ^{3}**IIc** is an unproductive pathway because of the disposition of the aldehyde group. Product formation through pathways a and b requires the conformational change from ^{3}**II** to another biradical, ^{3}**III**, to properly orient the reacting groups before ring closure occurs. This ring closure implies a spin crossing from the triplet to the singlet state and can occur either before or after ^{3}**II**→^{3}**III** interconversion. To understand the reaction mechanism, we explored the reactivity of **1a** as a representative example (for **4a**, see the

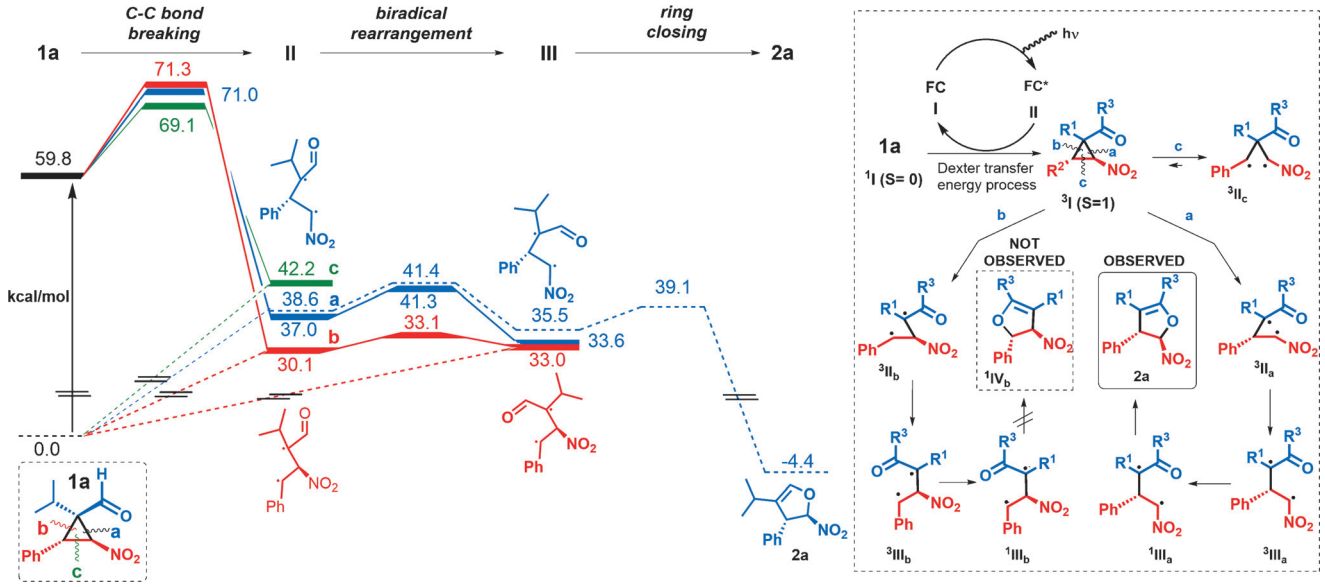

Figure 2. Gibbs energy profile calculated for reaction pathway from **1a** to **2a** (left). Solid lines correspond to species in the triplet state, whereas dashed lines refer to the energies of the spin-corrected singlet state.[11c] Possible reaction pathways of triplet excited state of **1a** (right).

Supporting Information), considering both the triplet and open-shell singlet states for all biradical intermediates.

Figure 2 shows the Gibbs energy profiles for pathways a, b, and c of **1a**. The three possible C–C cleavages are kinetically and thermodynamically favored. Energy barriers are low (9–12 kcal mol^{-1}) and the reaction ΔG ranges from −18 to −30 kcal mol^{-1}. Noteworthy, the most stable biradical corresponds to ^{3}**IIb**. In these species, the radical character lies at the two carbon centers which are able to better stabilize the unpaired electrons: the tertiary carbon atom presents the stabilizing CHO group and the benzyl carbon atom (see the Supporting Information for details). However, this cleavage pathway would lead to the ring expansion product ^{1}**IVb** which is not experimentally observed (Figure 2), thereby indicating that other factors determine the observed reactivity. In particular, the evolution of intermediates ^{3}**IIa** and ^{3}**IIb** differs significantly. That is, although for both intermediates the Gibbs energy barrier for the biradical rearrangement (^{3}**II**→ ^{3}**III**) is low, this process is exergonic for path a and endergonic for path b. This data suggests that ^{3}**IIIa** would be a more long-lived species than ^{3}**IIa**, whereas the opposite is expected for pathway b. Moreover, open-shell singlet-state optimizations of ^{1}**IIa** and ^{1}**IIIa** yield to two minima with very similar geometries and energetics to those of the triplet states. ^{1}**IIa** evolves to reactants in an essentially barrierless process, whereas ^{1}**IIIa** leads to the final product observed, after overcoming a low-energy barrier of 3.6 kcal mol^{-1}. This process suggests that spin crossing probably occurs after biradical rearrangement, that is, at geometries close to that of ^{3}**IIIa**. In contrast, all attempts to locate open-shell singlet-state structures for **IIb** and **IIIb** collapsed to reactants, thus suggesting that spin crossing always leads to the initial reactants.[14] Thus, spin crossing in pathway b appears to be unproductive, and is in agreement with the non-observation of ^{1}**IVb** as the resulting product[15] and the low value of the quantum yield.

The calculations suggest that the key point is that the biradical intermediates of pathway a can evolve into products, whereas those of pathway b can only return to reactants. This difference seems to originate from three key points: 1) The biradical rearrangement is only exergonic for pathway a, and favors the species which leads to the final product. It suggests that it is more likely that spin crossing occurs after biradical rearrangement. 2) There is almost no overlap between the carbon p orbitals of both species (**IIa** and **IIIa**) involved in the formation of dihydrofuran in pathway a, and is in contrast to the overlap observed in **IIb**. Furthermore, the S^2 expectation value obtained for open-shell singlets is around 1. Indeed, this value is observed for **IIa** and **IIIa**, whereas in the case of **IIb** the calculated value is 0.86 (Figure 3). Consequently, the latter intermediate exhibits a smaller biradical character. Therefore, after spin-crossing in pathway b the reactant is easily recovered, but not the product, which requires a larger electronic reorganization. 3) The partial charges of the atoms involved in the new C–O bond formation in the ring-closure step are both negative for **IIIb**, and they present opposite signs in **IIIa** (Figure 3). That is, the NO_2 electron-withdrawing character induces a positive charge on the carbon atom directly bonded to it, thus resulting in a Coloumbic attraction in **IIIa** with the negatively charged oxygen fragment. Therefore, this could favor the orientation of the reacting fragments and overall facilitate the reaction along pathway a.

In conclusion, a new visible-light photocatalytic strategy for the synthesis of enantioenriched dihydrofurans and cyclopentenes by an intramolecular cyclopropane ring expansion reaction has been developed. This process proceeds under mild reaction conditions, achieving good to excellent yields with excellent enantioselectivities in the final products. Moreover, DFT calculations have been carried out to elucidate the role of the nitro group and the origin of product selectivity.

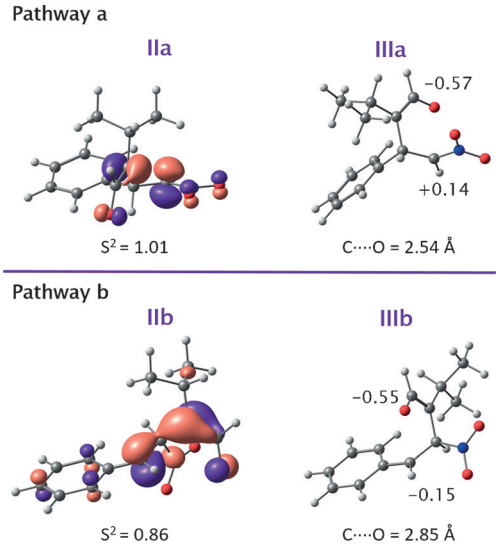

Figure 3. Lowest-energy singly occupied orbital of the unrestricted broken shell singlet at the ^{3}**IIa** and ^{3}**IIb** geometries (left). Partial charges of the oxygen and carbon atoms involved in the formation of the five-membered ring in the ^{3}**IIIa** and ^{3}**IIIb** structures (right).

Acknowledgments

The Spanish Government (CTQ2015-64561-R, CTQ2014-59544-P) and the European Research Council (ERC-CG, contract number: 647550) are acknowledged. We acknowledge the generous allocation of computing time at the CCC (UAM). V.L.-M. and M.L. thank the UAM and MINECO for a predoctoral fellowship-UAM and Ramon y Cajal contract, respectively. X.S.-M. is grateful for a Professor Agregat Serra-Húnter position and M.S. financial support from an ICREA award.

Conflict of interest

The authors declare no conflict of interest.

Keywords: density functional calculations · small ring systems · photocatalysis · reaction mechanisms · ring expansion

How to cite: *Angew. Chem. Int. Ed.* **2017**, *56*, 7826–7830
Angew. Chem. **2017**, *129*, 7934–7938

[1] For recent review, see: T. F. Schneider, J. Kaschel, D. B. Werz, *Angew. Chem. Int. Ed.* **2014**, *53*, 5504; *Angew. Chem.* **2014**, *126*, 5608.

[2] For intermolecular processes, see e.g.: a) J. Sabbatani, N. Maulide, *Angew. Chem. Int. Ed.* **2016**, *55*, 6780; *Angew. Chem.* **2016**, *128*, 6892; b) O. A. Ivanova, E. M. Budynina, V. N. Khrusta-lev, D. A. Skvortsov, I. V. Trushkov, M. Y. Melnikov, *Chem. Eur. J.* **2016**, *22*, 1223; c) H. Xu, J.-L. Hu, L. Wang, S. Liao, Y. Tang, *J. Am. Chem. Soc.* **2015**, *137*, 8006; d) Q.-Q. Cheng, Y. Qian, P. Y. Zavalij, M. P. Doyle, *Org. Lett.* **2015**, *17*, 3568; e) D. D. Borisov, R. A. Novikov, Y. V. Tomilov, *Angew. Chem. Int. Ed.* **2016**, *55*, 12233; *Angew. Chem.* **2016**, *128*, 12421; f) L. K. B. Garve, M. Petzold, P. G. Jones, D. B. Werz, *Org. Lett.* **2016**, *18*, 564.

[3] For a recent review of intramolecular cyclopropane expansion, see: a) M. A. Cavitt, L. H. Phun, S. France, *Chem. Soc. Rev.* **2014**, *43*, 804. For some selected references, see: b) J. Zhang, S. Xing, J. Ren, S. Jiang, Z. Wang, *Org. Lett.* **2015**, *17*, 218; c) W. Zhu, J. Fang, Y. Liu, J. Ren, Z. Wang, *Angew. Chem. Int. Ed.* **2013**, *52*, 2032; *Angew. Chem.* **2013**, *125*, 2086; d) Y. Bai, W. Tao, J. Ren, Z. Wang, *Angew. Chem. Int. Ed.* **2012**, *51*, 4112; *Angew. Chem.* **2012**, *124*, 4188; e) C. Brand, G. Rauch, M. Zanoni, B. Dittrich, D. B. Werz, *J. Org. Chem.* **2009**, *74*, 8779; f) T. F. Schneider, J. Kaschel, S. I. Awan, B. Dittrich, D. B. Werz, *Chem. Eur. J.* **2010**, *16*, 11276.

[4] For some selected reviews in photocatalysis, see: a) C. Prier, D. Rankic, D. W. C. MacMillan, *Chem. Rev.* **2013**, *113*, 5322; b) J. M. R. Narayanam, C. R. J. Stephenson, *Chem. Soc. Rev.* **2011**, *40*, 102; c) N. A. Romero, D. A. Nicewicz, *Chem. Rev.* **2016**, *116*, 10075.

[5] a) C. Wang, X. Ren, H. Xie, Z. Lu, *Chem. Eur. J.* **2015**, *21*, 9676; b) A. G. Amador, E. M. Sherbrook, T. P. Yoon, *J. Am. Chem. Soc.* **2016**, *138*, 4722.

[6] J. Luis-Barrera, R. Mas-Balleste, J. Alemán, *ChemPlusChem* **2015**, *80*, 1595.

[7] For examples, see: a) D. H. R. Barton, H. T. Chung, A. D. Gross, L. M. Jackman, M. Martin-Smith, *J. Chem. Soc.* **1961**, 5061; b) R. B. von Dreele, G. R. Pettit, R. H. Ode, R. E. Perdue, J. D. White, P. S. Manchand, *J. Am. Chem. Soc.* **1975**, *97*, 6236; c) R. Kaur, S. K. Chattopadhyay, A. Chatterjee, O. Prakash, F. Khan, N. Suri, D. Priya, A. K. Saxena, *Med. Chem. Res.* **2014**, *23*, 4138.

[8] The absolute configuration at C2 with aromatic groups of the starting material **1** possess opposite configuration to those with hydrogen or alkyls groups. See Ref. [6] and the Supporting Information for more details.

[9] The synthesis of cyclopropanes **1g** and **1h** were obtained following procedures described in the literature, see: a) J. Vesely, G.-L. Zhao, A. Bartoszewicz, A. Córdova, *Tetrahedron Lett.* **2008**, *49*, 4209.

[10] CCDC 1404743 (**1f**) and 1529711 (**4c**) contain the crystallographic data. These data can be obtained free of charge from The Cambridge Crystallographic Data Centre. Because the chiral center configuration supporting R^2 did not change during the ring expansion process, we assumed the same configuration at this carbon atom in the final product **2** or **5**, whereas the configuration of the α-nitro carbon atom (C1) and α-EWG carbon atom in products **5** were confirmed by ^{1}H NMR experiments (see the Supporting Information).

[11] a) Y. Zhao, D. G. Truhlar, *Theor. Chem. Acc.* **2008**, *120*, 215; b) A. V. Marenich, C. J. Cramer, D. G. Truhlar, *J. Phys. Chem. B* **2009**, *113*, 6378; c) K. Yamaguchi, F. Jensen, A. Dorigo, K. N. Houk, *Chem. Phys. Lett.* **1988**, *149*, 537.

[12] T. B. Demissie, K. Ruud, J. H. Hansen, *Organometallics* **2015**, *34*, 4218.

[13] For a related study, see: T. R. Blum, Z. D. Miller, D. M. Bates, I. A. Guzei, T. P. Yoon, *Science* **2016**, *354*, 1391.

[14] The unique transition state leading to ^{1}**IVb**, one that we have been able to locate, is a closed-shell singlet which connects **1a** with ^{1}**IVb** and can be associated with a high-energy barrier ($\Delta G^{\neq} = 34.2$ kcal mol^{-1}) by a thermal process.

[15] To understand why racemization processes are not taking place with pathways b and c, we also calculated the unproductive racemization pathways (see the Supporting Information). Interestingly, all intermediates that would involve a loss of enantioselectivity are higher in energy than the most stable biradical, ^{3}**II**, of each pathway by between 2.9 and 8.5 kcal mol^{-1}.

Manuscript received: March 31, 2017
Revised manuscript received: April 28, 2017
Accepted manuscript online: May 10, 2017
Version of record online: June 6, 2017

Experimental Part
Chapter 2

(The complete “Supporting Information” documents, with all the characterization data, NMR spectra, SFC or HPLC traces and other experimental procedures have been included in the enclosed USB memory)

General procedure for the synthesis of dihydrofuranes (2)

The photocatalyst tris[2-(4,6-difluorophenyl)pyridinato-C^2,*N*]iridium(III) **3b** (0.0025 mmol) was transferred to a Schlenk tube followed by the corresponding nitrocyclopropanecarbaldehyde **1** (0.1 mmol) dissolved in 1 mL of CH_2Cl_2. The mixture was deoxygenated by three cycles of "freeze-pump-thaw", the photoreactor (blue LEDs) was switched on and the reaction mixture was stirred during the indicated time. In the end, after removal of the solvent, the crude mixture was purified through filtration over celite or by flash chromatography over Iatrobeads silica gel (cyclohexane : ethyl acetate).

Characterization data for dihydrofuranes (2)

(2*R*,3*R*)-4-Isopropyl-2-nitro-3-phenyl-2,3-dihydrofuran (2a)

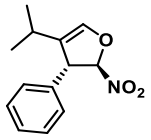

2a

The product was obtained following the general procedure starting from **1a** after 4h of irradiation. The final filtration over celite afforded the pure product **2a** as a pale yellow oil (86% yield).

$[\alpha]^{20}_D$ = - 213.1 (*c* = 0.765, $CHCl_3$).

^{1}H NMR (300 MHz, $CDCl_3$): δ 7.42-7.32 (m, 3H), 7.26-7.20 (m, 2H), 6.45 (t, *J* = 1.6 Hz, 1H), 5.72 (d, *J* = 1.9 Hz, 1H), 4.30 (m, 1H), 2.22-2.06 (m, 1H), 1.05 (d, *J* = 6.8 Hz, 3H), 0.94 (d, *J* = 6.9 Hz, 3H) ppm.

^{13}C NMR (75 MHz, $CDCl_3$): δ 138.8, 137.5, 129.3, 128.3, 127.5, 127.0, 111.9, 57.3, 24.3, 21.9, 20.9 ppm.

HRMS (EI): calculated for $C_{13}H_{14}O^+$ $[M -H,-NO_2]^+$: 186.1039; found: 186.1029. The enantiomeric excess was determined by SFC using a *Daicel Chiralpak* IA column: CO_2/MeOH 97:3, flow rate 3.0 mL/min, τ_{major} = 1.95 min, τ_{minor} = 2.45 min, *ee* = 97%.

(2*R*,3*R*)-4-Isopropyl-3-(4-methoxyphenyl)-2-nitro-2,3-dihydrofuran (2b)

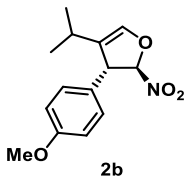

2b

The product was obtained following the general procedure starting from **1b** after 4h of irradiation. The crude reaction mixture was purified by flash chromatography affording the product **2b** as a pale yellow oil (82% yield).

$[\alpha]^{20}_D$ = - 181.2 (*c* = 0.46, $CHCl_3$).

^{1}H NMR (300 MHz, $CDCl_3$): δ 7.14 (d, *J* = 8.6 Hz, 2H), 6.90 (d, *J* = 8.6 Hz, 2H), 6.42 (d, *J* = 1.4 Hz, 1H), 5.68 (d, *J* = 1.6 Hz, 1H), 4.25 (m, 1H), 3.74 (s, 3H), 2.22-2.06 (m, 1H), 1.04 (d, *J* = 6.8 Hz, 3H), 0.94 (d, *J* = 6.9 Hz, 3H) ppm.

^{13}C NMR (75 MHz, $CDCl_3$): δ 138.6, 130.1, 129.4, 128.6, 127.0, 114.6, 112.1, 56.7, 55.3, 24.3, 21.9, 20.9 ppm.

HRMS (TOF-ESI): calculated for $C_{14}H_{17}O_2^+$ [M -NO_2]$^+$: 217.1223; found: 217.1221. The enantiomeric excess was determined by SFC using a *Daicel Chiralpak* IA column: CO_2/MeOH 97:3, flow rate 3.0 mL/min, τ_{major} = 2.47 min, τ_{minor} = 3.04 min, *ee* = 90%.

(2*R*,3*R*)-3-(4-Bromophenyl)-4-isopropyl-2-nitro-2,3-dihydrofuran (2c)

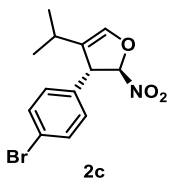

2c

The product was obtained following the general procedure starting from **1c** after 4h of irradiation. The final filtration over Celite afforded the pure product **2c** as a pale yellow oil (84% yield).

$[\alpha]^{20}_D$ = - 97.9 (*c* = 0.58, $CHCl_3$).

^{1}H NMR (300 MHz, $CDCl_3$): δ 7.52 (d, *J* = 8.5 Hz, 2H), 7.12 (d, *J* = 8.4 Hz, 2H), 6.46 (t, *J* = 1.6 Hz, 1H), 5.67 (d, *J* = 1.8 Hz, 1H), 4.27 (m, 1H), 2.21-2.06 (m, 1H), 1.04 (d, *J* = 6.8 Hz, 3H), 0.94 (d, *J* = 6.9 Hz, 3H) ppm.

^{13}C NMR (75 MHz, $CDCl_3$): δ 139.2, 136.5, 132.4, 129.1, 126.6, 122.4, 111.3, 56.7, 24.3, 21.9, 20.9 ppm.

HRMS (EI): calculated for $C_{13}H_{13}BrO^+$ [M -H,-NO_2]$^+$: 264.0144; found: 264.0198. The enantiomeric excess was determined by SFC using a *Daicel Chiralpak* IA column: CO_2/MeOH 97:3, flow rate 3.0 mL/min, τ_{major} = 2.83 min, τ_{minor} = 3.40 min, *ee* = 94%.

(2*R*,3*R*)-2-Nitro-3-phenyl-4-propyl-2,3-dihydrofuran (2d)

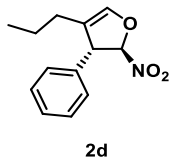

2d

The product was obtained following the general procedure starting from **1d** after 4h of irradiation. The final filtration over Celite afforded the pure product **2d** as a pale yellow oil (98% yield).

$[\alpha]^{20}_D$ = - 191.4 (*c* = 0.84, $CHCl_3$).

^{1}H NMR (300 MHz, $CDCl_3$): δ 7.36-7.27 (m, 3H), 7.20-7.12 (m, 2H), 6.40 (m, 1H), 5.66 (d, *J* = 1.8 Hz, 1H), 4.15 (m, 1H), 1.92-1.72 (m, 2H), 1.42-1.18 (m, 2H), 0.78 (t, *J* = 7.3 Hz, 3H) ppm.

^{13}C NMR (75 MHz, $CDCl_3$): δ 139.7, 137.2, 129.3, 128.3, 127.5, 120.2, 111.6, 58.1, 25.9, 20.8, 13.6 ppm.

HRMS (TOF-ESI): calculated for $C_{13}H_{15}O$ [M-NO_2]$^+$: 187.1117; found: 187.1115. The enantiomeric excess was determined by SFC using a *Daicel Chiralpak* IA column: CO_2/MeOH 97:3, flow rate 3.0 mL/min, τ_{major} = 2.16 min, τ_{minor} = 2.85 min, *ee* = 95%.

(*2R,3R*)-2-Nitro-3,4-diphenyl-2,3-dihydrofuran (2e)

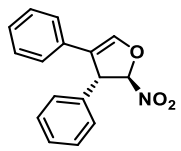

2e

The product was obtained following the general procedure starting from **1e** after 20 minutes, and the crude was purified by FC (9:1 cyclohexane : ethyl acetate), affording the pure product as a yellow oil (51% yield based on a conversion of 52% by ^{1}H-NMR).

$[\alpha]^{20}_D$ = - 180.5 (*c* = 0.60, $CHCl_3$).

^{1}H NMR (300 MHz, $CDCl_3$): δ 7.40 – 7.13 (m, 11H), 5.80 (d, *J* = 1.7 Hz, 1H), 4.81 (t, *J* = 1.7 Hz, 1H) ppm.

^{13}C NMR (75 MHz, $CDCl_3$): δ 141.5, 137.1, 130.3, 129.6, 128.9, 128.7, 127.6 (x2), 125.6, 120.2, 111.9, 56.7 ppm.

HRMS (EI): calculated for $C_{16}H_{12}O^+$ [M -H, -NO_2]$^+$: 220.0883; found: 220.0926. The enantiomeric excess was determined by SFC using a *Daicel Chiralpak* IA column: CO_2/MeOH 90:10, flow rate 2.0 mL/min, τ_{major} = 4.5 min, τ_{minor} = 5.3 min, *ee* = 92%.

(*2R,3R*)-3-(4-Bromophenyl)-2-nitro-4-phenyl-2,3-dihydrofuran (2f)

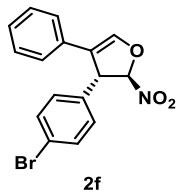

2f

The product was obtained following the general procedure starting from **1e** after 20 minutes, and the crude was purified by FC (9:1 cyclohexane : ethyl acetate), affording the pure product as a yellow oil (57% yield based on a conversion of 60% by ^{1}H-NMR).

$[\alpha]^{20}_D$ = - 26.5 (*c* = 0.23, $CHCl_3$).

^{1}H NMR (300 MHz, $CDCl_3$): δ 7.51 (d, *J* = 8.5 Hz, 2H), 7.28 – 7.10 (m, 8H), 5.76 (d, *J* = 1.7 Hz, 1H), 4.78 (bs, 1H) ppm.

^{13}C NMR (75 MHz, $CDCl_3$): δ 141.6, 135.9, 132.7, 129.8, 129.2, 128.9, 127.7, 125.4, 122.7, 119.7, 111.3, 55.9 ppm.

HRMS (EI): calculated for $C_{16}H_{11}OBr^+$ [M -H, -NO_2]$^+$: 297.9988; found: 298.0061. The enantiomeric excess was determined by SFC using a *Daicel Chiralpak* IB-3 column: CO_2/MeOH 97:3, flow rate 2.0 mL/min, τ_{minor} = 2.0 min, τ_{major} = 2.5 min, *ee* = 88%.

(2*R*,3*S*)-2-Nitro-3-phenyl-2,3-dihydrofuran (2g)

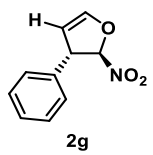

2g

Following the general procedure described above, the compound was obtained in 78% yield as a yellow oil (time 21h). The crude was purified by flash column chromatography cyclohexane:AcOEt (9:1 → 7:3) as eluent.

$[\alpha]^{20}_D$ = - 81.7 (*c* = 0.75, $CHCl_3$).

^{1}H NMR (300 MHz, $CDCl_3$): δ 7.44-7.31 (m, 3H), 7.30-7.24 (m, 2H), 6.77 (t, *J* = 2.3 Hz, 1H), 5.80 (d, *J* = 2.1 Hz, 1H), 5.41 (t, *J* = 2.8 Hz, 1H), 4.45 (q, *J* = 2.2 Hz, 1H).

^{13}C NMR (75 MHz, $CDCl_3$): δ 145.8, 137.9, 129.2, 128.4, 127.2, 110.9, 105.3, 55.5.

HRMS (EI): calculated for $C_{10}H_8O^+$ [M –H, -NO_2]$^+$: 144.0570; found: 144.0560. The enantiomeric excess was determined by SFC using *Daicel Chiralpak* IA column [CO_2/MeOH (97:3)]; flow rate 3 ml/min; τ_{major} = 2.7 min, τ_{minor} = 3.1 min, *ee* = 76 %.

(2*R*,3*R*)-2-Nitro-3-propyl-2,3-dihydrofuran (2h)

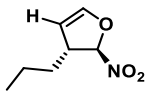

2h

Following the general procedure described above, the compound was obtained in 86% yield as a yellow oil (time 48h). The crude was purified by flash column chromatography using 9:1 cyclohexane:AcOEt as eluent in 86% yield.

$[\alpha]^{20}_D$ = - 11.2 (*c* = 0.60, $CHCl_3$).

^{1}H NMR (300 MHz, $CDCl_3$): δ 6.51 (t, *J* = 2.3 Hz, 1H), 5.67 (d, *J* = 2.1 Hz, 1H), 5.22 (t, *J* = 2.8 Hz, 1H), 3.26 – 3.17 (m, 1H), 1.55 – 1.39 (m, 4H) 0.97 (t, *J* = 7.0 Hz, 3H).

^{13}C NMR (75 MHz, $CDCl_3$): δ 144.6, 109.8, 105.9, 50.5, 36.0, 19.8, 13.8. The enantiomeric excess could not be determined because the lack of UV active groups of **2h**. However, the optical activity of the sample demonstrates that the compuound **2h** is enantiomerically enriched.

HRMS (EI): calculated for $C_7H_{11}O^+$ [M, -NO_2]$^+$: 111.0804; found: 111.0881.

General procedure for the synthesis of cyclopentenes (5)

The photocatalyst tris[2-(4,6-difluorophenyl)pyridinato-C^2,*N*]iridium(III) **3b** (0.0025 mmol) was transferred to a Schlenk tube followed by the corresponding vinylcyclopropane **4** (0.1 mmol) dissolved in 1 mL of CH_2Cl_2. Then, three cycles of "freeze-pump-thaw" deoxygenation were carried out and the reaction was stirred in the presence of blue light until complete conversion was observed by ^{1}H-NMR. After that, the solvent was evaporated under reduced pressure and the crude reaction mixture was purified by flash chromatography (cyclohexane : ethyl acetate) using Iatrobeads silica gel or filtration over celite.

Characterization data for cyclopentenes (5)

Methyl (*1S,4S,5S*)-3-isopropyl-5-nitro-4-phenylcyclopent-2-ene-1-carboxylate (5a)

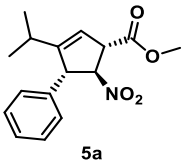

5a

The product was obtained following the general procedure starting from **4a** after 24h, and the crude was purified by FC (9:1 cyclohexane : ethyl acetate), affording the pure product as a yellow oil (57% yield).

$[\alpha]^{20}_D$ = - 60.4 (*c* = 1.40, $CHCl_3$).

^{1}H NMR (300 MHz, $CDCl_3$): δ 7.32 – 7.08 (m, 5H), 5.49 (m, 1H), 5.32 (t, *J* = 5.8 Hz, 1H), 4.34 (d, *J* = 6.0 Hz, 1H), 4.28 – 4.23 (m, 1H), 3.73 (s, 3H), 1.90 (m, 1H), 0.99 (d, *J* = 6.7 Hz, 3H), 0.84 (d, *J* = 7.0 Hz, 3H) ppm.

^{13}C NMR (75 MHz, $CDCl_3$): δ 171.6, 152.9, 139.8, 129.1, 128.2, 127.8, 118.5, 93.7, 58.2, 54.3, 52.7, 27.5, 21.1, 20.4 ppm.

HRMS (TOF-ESI): calculated for $C_{16}H_{19}NO_4Na^+$ $[M+Na]^+$: 312.1206; found: 312.1201. The enantiomeric excess was determined by SFC using a *Daicel Chiralpak* IG-3 column: CO_2/MeOH 98:2, flow rate 2.0 mL/min, τ_{major} = 2.8 min, τ_{minor} = 3.0 min, *ee* = 87%.

Methyl (*1S,4S,5S*)-3-isopropyl-4-(4-methoxyphenyl)-5-nitrocyclopent-2-ene-1-carboxylate (5b)

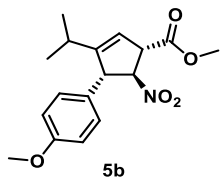

5b

The product was obtained following the general procedure starting from **4b** after 24h, and the crude was purified by FC (9:1 cyclohexane : ethyl acetate), affording the pure product as a yellow oil (75% yield).

$[\alpha]^{20}_D$ = - 31.2 (c = 0.34, $CHCl_3$).

^{1}H NMR (300 MHz, $CDCl_3$): δ 7.09 (d, *J* = 8.7 Hz, 2H), 6.88 (d, *J* = 8.6 Hz, 2H), 5.54 (bs, 1H), 5.34 (t, *J* = 5.9 Hz, 1H), 4.35 (d, *J* = 5.8 Hz, 1H), 4.30 – 4.24 (m, 1H), 3.80 (s, 3H), 3.79 (s, 3H), 2.03 – 1.95 (m, 1H), 1.06 (d, *J* = 6.6 Hz, 3H), 0.90 (d, *J* = 7.0 Hz, 3H) ppm.

^{13}C NMR (75 MHz, $CDCl_3$): δ 171.6, 159.2, 153.0, 131.7, 129.3, 118.2, 114.4, 93.9, 57.7, 55.3, 54.1, 52.7, 27.5, 21.0, 20.4 ppm.

HRMS (TOF-ESI): calculated for $C_{17}H_{21}NO_5Na^+$ $[M+Na]^+$: 342.1317; found: 342.1320. The enantiomeric excess was determined by SFC using a *Daicel Chiralpak* IA column: CO_2/MeOH 97:3, flow rate 3.0 mL/min, τ_{major} = 2.2 min, τ_{minor} = 3.1 min, *ee* = 99%.

Methyl (*1S,4S,5S*)-4-(4-bromophenyl)-3-isopropyl-5-nitrocyclopent-2-ene-1-carboxylate (5c)

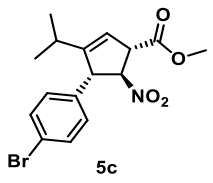

5c

The product was obtained following the general procedure starting from **4c** after 24h, and the crude was purified by FC (9:1 cyclohexane : ethyl acetate), affording the pure product as a yellow oil (50% yield).

$[\alpha]^{20}_D$ = - 9.5 (*c* = 0.20, $CHCl_3$).

^{1}H NMR (300 MHz, $CDCl_3$): δ 7.32 – 7.08 (m, 4H), 5.49 (m, 1H), 5.32 (t, *J* = 5.8 Hz, 1H), 4.34 (d, *J* = 6.0 Hz, 1H), 4.28 – 4.23 (m, 1H), 3.73 (s, 3H), 1.90 (m, 1H), 0.99 (d, *J* = 6.7 Hz, 3H), 0.84 (d, *J* = 7.0 Hz, 3H) ppm.

^{13}C NMR (75 MHz, $CDCl_3$): δ 171.6, 152.9, 139.8, 129.1, 128.2, 127.8, 118.5, 93.7, 58.2, 54.3, 52.7, 27.5, 21.1, 20.4 ppm.

HRMS (TOF-ESI): calculated for $C_{16}H_{18}NO_4NaBr^+$ $[M+Na]^+$: 390.0311; found: 390.0316. The enantiomeric excess was determined by SFC using a *Daicel Chiralpak* IC column: CO_2/MeOH 98:2, flow rate 2.0 mL/min, τ_{minor} = 6.6min, τ_{minor} = 7.0 min, *ee* = 96%.

Methyl (*1S,4S,5S*)-5-nitro-4-phenyl-3-propylcyclopent-2-ene-1-carboxylate (5d)

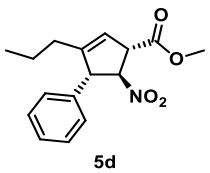

5d

The product was obtained following the general procedure starting from **4d** after 48h, and the crude was purified by FC (9:1 cyclohexane : ethyl acetate), affording the pure product as a yellow oil (45% yield yield based on conversion by ^{1}H-NMR).

$[\alpha]^{20}_D$ = - 34.2 (*c* = 0.74, $CHCl_3$).

^{1}H NMR (300 MHz, $CDCl_3$): δ 7.42 – 7.08 (m, 5H), 5.58 (bs, 1H), 5.40 (t, *J* = 5.6 Hz, 1H), 4.36 – 4.28 (m, 2H), 3.79 (s, 3H), 1.92 – 1.71 (m, 2H), 1.49 – 1.31 (m, 2H), 0.84 (t, *J* = 7.3 Hz, 3H) ppm.

^{13}C NMR (75 MHz, $CDCl_3$): δ 171.6, 146.9, 139.6, 129.1, 128.1, 127.9, 120.2, 93.4, 59.2, 54.5, 52.7, 31.1, 20.2, 13.7 ppm.

HRMS (TOF-ESI): calculated for $C_{16}H_{19}NO_4Na^+$ $[M+Na]^+$: 312.1206; found: 312.1195. The enantiomeric excess was determined by SFC using a *Daicel Chiralpak* IG-3 column: CO_2/MeOH 90:10, flow rate 3.0 mL/min, τ_{major} = 1.0 min, τ_{minor} = 1.1 min, *ee* = 94%.

Benzyl (*1S,4S,5S*)-3-isopropyl-5-nitro-4-phenylcyclopent-2-ene-1-carboxylate (5f)

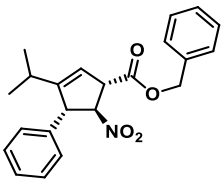

5f

The product was obtained following the general procedure starting from **4a** after 24h, and the crude was purified by FC (19:1 cyclohexane : ethyl acetate), affording the pure product as a yellow oil (90% yield, *d.r.* = 2:1).

$[\alpha]^{20}_D$ = - 100.0 (*c* = 0.66, $CHCl_3$).

^{1}H NMR (300 MHz, $CDCl_3$): *major diastereoisomer* δ 7.42 – 7.27 (m, 8H), 7.18 – 7.14 (m, 2H), 5.58 (dd, *J* = 3.8, 2.1 Hz, 1H), 5.40 (t, *J* = 5.7 Hz, 1H), 5.22 (d, *J* = 1.9 Hz, 2H), 4.41 (d, *J* = 1.9 Hz, 1H), 4.35 (ddd, *J* = 5.8, 3.8, 2.1 Hz, 1H), 1.97 (m, 1H), 1.05 (d, *J* = 6.8 Hz, 3H), 0.90 (d, *J* = 6.8 Hz, 3H) ppm.

^{13}C NMR (75 MHz, $CDCl_3$): δ 171.1, 153.2, 139.9, 135.4, 129.2, 128.8, 128.7, 128.4, 128.3, 118.7, 93.8, 67.6, 58.4, 54.7, 29.9, 27.7, 21.2, 20.6 ppm.

^{1}H NMR (300 MHz, $CDCl_3$): *minor diastereoisomer* δ 7.41 – 7.18 (m, 10H), 5.74 – 5.67 (m, 1H), 5.16 – 5.09 (m, 3H), 4.64 (d, *J* = 5.4 Hz, 1H), 4.21 – 4.13 (m, 1H), 2.10 – 1.97 (m, 1H), 1.06 (d, *J* = 6.8 Hz, 3H), 0.89 (d, *J* = 6.8 Hz, 3H) ppm.

HRMS (EI): calculated for $C_{22}H_{22}O_2^+$ $[M-H, -NO_2]^+$: 318.1614; found: 318.1595. The enantiomeric excess of the major diastereoisomer was determined by SFC using a *Daicel Chiralpak* IG-3 column: CO_2/MeOH 95:5, flow rate 2.0 mL/min, τ_{major} = 4.0 min, τ_{minor} = 4.7 min, *ee* = 97%.

1-((4*S*,5*S*)-3-Isopropyl-5-nitro-4-phenylcyclopent-2-en-1-yl)ethan-1-one (5g)

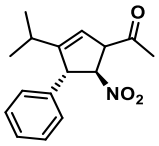

5g

The product was obtained following the general procedure starting from **4g** after 2h of irradiation. The crude was purified by FC (cyclohexane : ethyl acetate) affording the pure product as a pale yellow oil (33% yield).

$[\alpha]^{20}_D$ = - 49.1 (*c* = 0.38, $CHCl_3$).

^{1}H NMR (300 MHz, $CDCl_3$): δ 7.39-7.28 (m, 3H), 7.17-7.11 (m, 2H), 5.57 (dd, *J* = 3.7, 1.9 Hz, 1H), 5.49 (t, *J* = 5.4 Hz, 1H), 4.45 (d, *J* = 5.3 Hz, 1H), 4.34 (dd, *J* = 4.9, 1.9 Hz, 1H), 2.37 (s, 3H), 2.05-1.90 (m, 1H), 1.05 (d, *J* = 6.7 Hz, 3H), 0.92 (d, *J* = 6.9 Hz, 3H).

^{13}C NMR (75 MHz, $CDCl_3$): δ 203.7, 153.4, 139.9, 129.0, 128.2, 127.7, 117.7, 91.8, 62.8, 57.7, 28.8, 27.5, 21.1, 20.5.

HRMS (EI): calculated for $C_{16}H_{18}O^+$ $[M -H,-NO_2]^+$: 226.1352; found: 226.1334. The enantiomeric excess was determined by SFC using a *Daicel Chiralpak* IA column: CO_2/MeOH 98:2, flow rate 2.0 mL/min, τ_{major} = 3.86 min, τ_{minor} = 4.16 min, *ee* = 97%.

(*1S,4S,5S*)-3-Isopropyl-5-nitro-4-phenylcyclopent-2-ene-1-carbonitrile (5h)

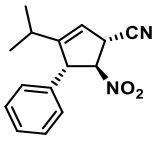

5h

The product was obtained following the general procedure starting from **4h** after 24h, and the crude was purified by FC (9:1 cyclohexane : ethyl acetate), affording the pure product as a colorless oil (55% yield).

$[\alpha]^{20}_D$ = - 37.2 (*c* = 2.03, $CHCl_3$).

^{1}H NMR (300 MHz, $CDCl_3$): δ 7.50 – 7.07 (m, 5H), 5.54 (bs, 1H), 5.15 (t, *J* = 5.0 Hz, 1H), 4.43 (d, *J* = 5.0 Hz, 2H), 2.11 – 2.02 (m, 1H), 1.10 (d, *J* = 6.7 Hz, 3H), 0.92 (d, *J* = 7.0 Hz, 3H).

^{13}C NMR (75 MHz, $CDCl_3$): δ 155.9, 138.0, 129.5, 128.5, 127.9, 118.0, 115.8, 93.9, 58.5, 38.8, 27.7, 20.9, 20.3.

HRMS (EI): calculated for $C_{15}H_{16}N^+$ $[M -NO_2]^+$: 210.1277; found: 210.1325. The enantiomeric excess was determined by SFC using a *Daicel Chiralpak* IA column: CO_2/MeOH 97:3, flow rate 2.0 mL/min, τ_{major} = 4.0 min, τ_{minor} = 4.3 min, *ee* = 97%.

Synthesis and characterization data for racemic compounds 7 and 9

5-Methyl-2-nitro-3-phenyl-2,3-dihydrofuran (7)

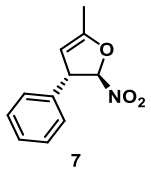

7

The product was obtained following the general procedure for the synthesis of dihydrofuranes starting from ***rac*-6**. After 80 hours the crude was purified by FC (19:1 cyclohexane : ethyl acetate) affording the pure product as a colorless oil (51% yield).

^{1}H NMR (300 MHz, CD_2Cl_2): δ 7.34 – 7.16 (m, 5H), 5.69 (d, *J* = 1.9 Hz, 1H), 4.96 – 4.93 (m, *J* = 2.7, 1.3 Hz, 1H), 4.32 – 4.28 (m, 1H), 2.02 (t, *J* = 1.5 Hz, 3H) ppm.

^{13}C NMR (75 MHz, CD_2Cl_2): δ 156.6, 139.5, 129.5, 128.5, 127.6, 111.9, 100.2, 56.9, 13.4 ppm.

HRMS (EI): calculated for $C_{11}H_{10}O^+$ $[M\text{-}NO_2]^+$: 158.0726; found: 158.0689.

Methyl-4-nitro-3-phenylcyclopent-1-ene-1-carboxylate (9)

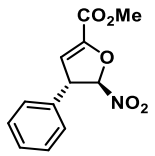

9

The compound was obtained following the general procedure for the synthesis of dihydrofuranes starting from ***rac*-8**. After 24h of irradiation the crude product was purified over celite to obtain the pure product as a pale yellow oil (73% yield).

^{1}H NMR (300 MHz, $CDCl_3$): δ 7.45-7.35 (m, 3H), 7.27-7.22 (m, 2H), 6.28 (d, *J* = 3.1 Hz, 1H), 5.92 (d, *J* = 2.3 Hz, 1H), 4.60-4.55 (m, 1H), 4.93 (s, 3H)

^{13}C NMR (75 MHz, $CDCl_3$): δ 158.8, 148.0, 136.2, 129.5, 128.9, 127.2, 114.2, 110.4, 56.3, 52.8

HRMS (TOF-ESI): calculated for $C_{12}H_{11}NO_5Na$ $[M+Na]^+$: 272.0529; found: 272.0526.

Synthesis of a Bifunctional Photo-Aminocatalyst

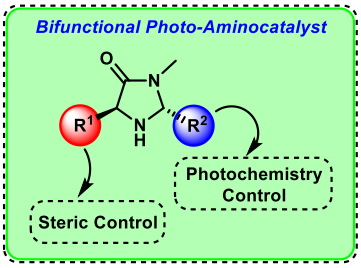

Chapter 3

3. Synthesis of a Bifunctional Photo-Aminocatalyst

3.1 Introduction to Aminocatalysis and to the Enantioselective α-Alkylation of Aldehydes

In the last years enamine and iminium ion catalysis have been intensively investigated, expecially after the discovery of proline as an efficient organocatalyst and after the development of Jørgensen-Hayashi's pyrrolidine-based[118a] and MacMillan's imidazolidinone-based[118b] catalysts (Scheme 56). Their uses range from enamine catalysis (with nucleophilic addition to carbonyl compounds, Michael acceptors or cycloaddition reactions) to iminium ion catalysis (with β-functionalizations or Diels-Alder reactions, among many others).[119]

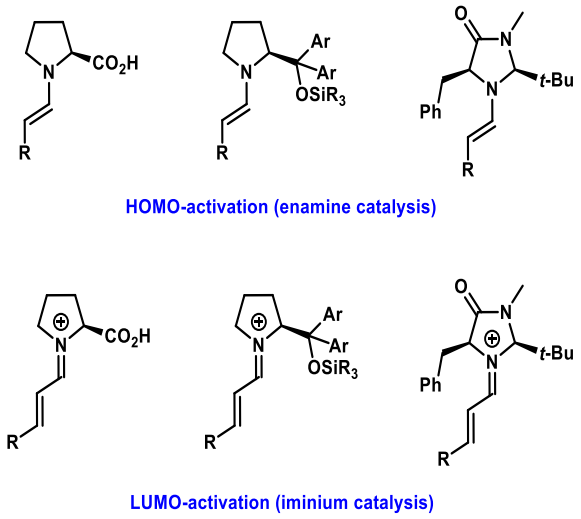

Scheme 56. HOMO and LUMO activation strategies in enamine and iminium ion catalysis.

Some years after the advent of organocatalysis, MacMillan's group reported a new activation mode for the enantioselective α-functionalization of aldehydes through singly occupied molecular orbital (SOMO) catalysis (Scheme 57).[120] The employment of a stoichiometric amount of ceric ammonium nitrate (CAN) permitted the selective oxidation of an enamine intermediate to obtain a chiral SOMO-activated species, which can react with a wide range of SOMOphiles (such as allylsilanes or silyl enol ethers) to give, after a second electron oxidation, the desired enantioenriched products.[120,121] This has been enormously increased the range of possible reaction partners for α-functionalization reactions but it did not permit the use of simple alkylating reagents such as alkyl halides for this purpose. Indeed, the only aminocatalytic example of α-alkylation of aldehydes described in the literature at that time was reported by List's research group, which enabled an asymmetric intramolecular S_N2 reaction of haloaldehydes through enamine activation in a base-assisted process (Scheme 58).[122]

---

[118] (a) S. Bertelsen, K. A. Jørgensen, *Chem. Soc. Rev*., **2009**, *38*, 2178-2189; (b) G. Lelais, D. W. C. MacMillan, *Aldrichimica Acta* **2006**, *39*, 79-87.

[119] (a) A. Erkkilä, I. Majander, P. M. Pihko, *Chem. Rev*. **2007**, *107*, 5416-5470; (b) S. Mukherjee, J. W. Yang, S. Hoffmann, B. List, *Chem. Rev*. **2007**, *107*, 5471-5569; (c) P. Melchiorre, M. Marigo, A. Carlone, G. Bartoli, *Angew. Chem. Int. Ed*. **2008**, *47*, 6138- 6171; (d) D. W. C. MacMillan, *Nature* **2008**, *455*, 304-308.

[120] T. D. Beeson, A. Mastracchio, J.-B. Hong, K. Ashton, D. W. C. MacMillan, *Science* **2007**, *316*, 582-585.

[121] (a) H.-Y. Jang, J.-B. Hong, D. W. C. MacMillan, *J. Am. Chem. Soc*. **2007**, *129*, 7004-7005; (b) T. H. Graham, C. M. Jones, N. T. Jui, D. W. C. MacMillan, *J. Am. Chem. Soc*. **2008**, *130*, 16494-16495; (c) H. Kim, D. W. C. MacMillan, *J. Am. Chem. Soc*. **2008**, *130*, 398-399; (d) M. Amatore, T. D. Beeson, S. P. Brown, D. W. C. MacMillan, *Angew. Chem. Int. Ed*. **2009**, *48*, 5121-5124; (e) J. C. Conrad, J. Kong, B. N. Laforteza, D. W. C. MacMillan, *J. Am. Chem. Soc*. **2009**, *131*, 11640-11641; (f) A. Mastracchio, A. A. Warkentin, A. M. Walji, D. W. C. MacMillan, *PNAS* **2010**, *107*, 20648-20651.

[122] (a) N. Vignola, B. List, *J. Am. Chem. Soc*. **2004**, *126*, 450-451; (b) A. Fu, B. List, W. Thiel, *J. Org. Chem*. **2006**, *71*, 320-326.

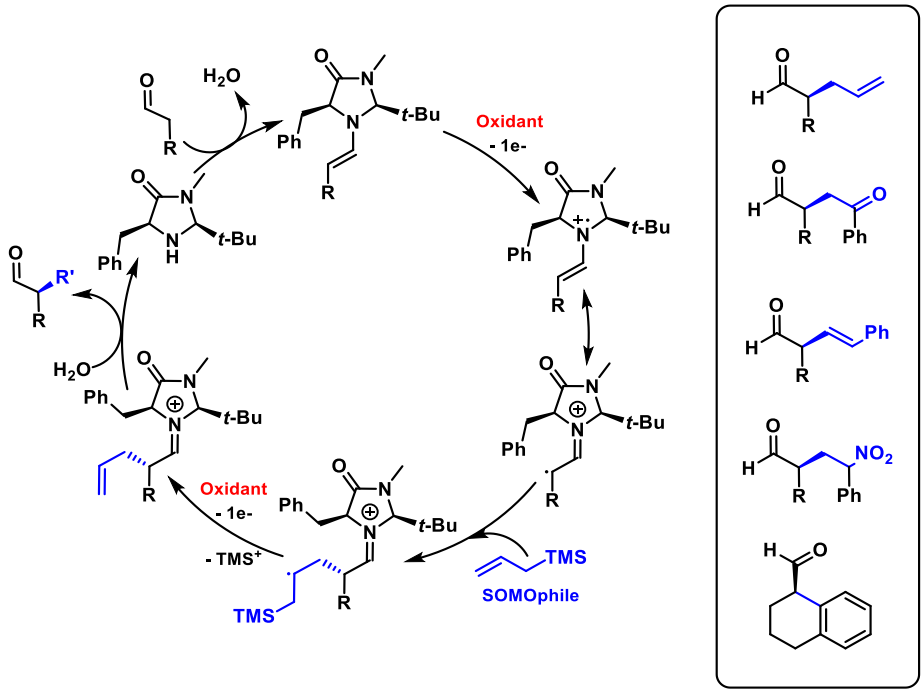

Scheme 57. SOMO activation over chiral enamine intermediate for the enantioselective α-functionalization of aldehydes through SOMO catalysis and representative functionalized products.

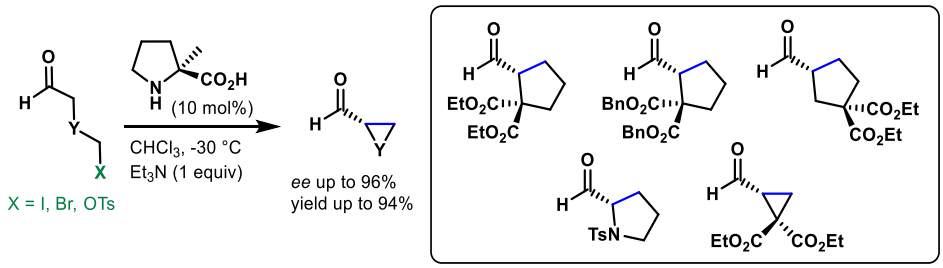

Scheme 58. Aminocatalytic enantioselective intramolecular α-alkylation of haloaldehydes.

In 2008, MacMillan's lab solved this long-standing problem combining enamine catalysis and photoredox catalysis (Scheme 59).[19,61] The use of an external ruthenium photocatalyst permitted the initiation step for the generation of a carbon-centered radical from different bromo derivatives. Then, the electron-deficient radical can enter into the aminocatalytic cycle to give an α-amino radical which can be oxidized by another molecule of bromo derivative to generate another carbon-centered radical in a propagation step of a chain propagation mechanism.[21] It is important to notice that a sacrificial amount of enamine is initially quenching the excited state of the photocatalyst to give a $[Ru(bpy)_3]^+$ that is responsible of the generation of the first radical from the bromo derivative. On the other hand, after hydrolysis, the iminium ion leads to the desired enantioenriched α-alkylated aldehyde. The same research group reported a wide range of different α-functionalization reactions achieved through the employment of enamine and photoredox catalysis, choosing the opportune combination of aminocatalyst, radical precursor and appropriate photocatalyst.[123]

[123] (a) D. A. Nagib, M. E. Scott, D. W. C. MacMillan, *J. Am. Chem. Soc*. **2009**, *131*, 10875-10877; (b) H.-W. Shih, M. N. Vander Wal, R. L. Grange, D. W. C. MacMillan, *J. Am. Chem. Soc*. **2010**, *132*, 13600-13603; (c) E. R. Welin, A. A. Warkentin, J. C. Conrad, D. W. C. MacMillan, *Angew. Chem. Int. Ed*. **2015**, *54*, 9668-9672; for a photocatalyst-free strategy employing a photoactive radical precursor, see: (d) G. Cecere, C. M. König, J. L. Alleva, D. W. C. MacMillan, *J. Am. Chem. Soc.* **2013**, *135*, 11521-11524.

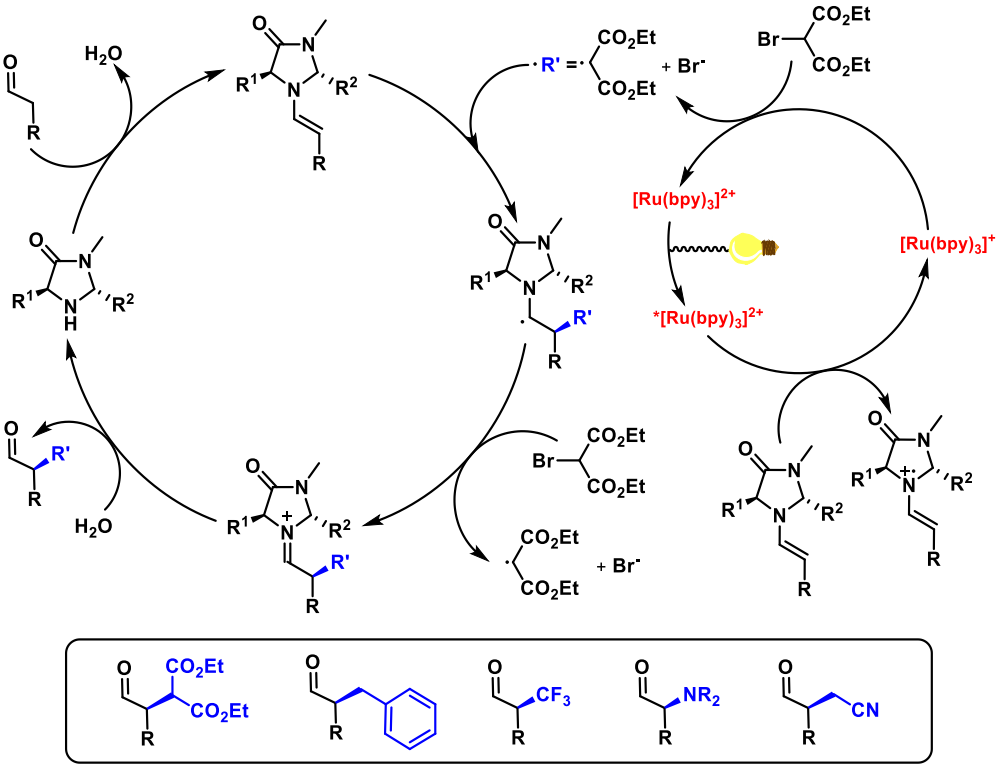

Scheme 59. Mechanistic proposal for the enantioselective α-alkylation of aldehydes through the merging of enamine and photoredox catalysis.

Some years later, Melchiorre's research group reported that enamine itself could act as a photoactive species to carry out the α-alkylation reaction of aldehydes in the absence of any external photocatalyst employing a pyrrolidine-based organocatalyst (Scheme 60).[76] Indeed, upon visible light absorption, the enamine can reach an electronic excited state, acting as a strong reducing agent capable of initiating the same process through reduction of a molecule of diethyl bromomalonate. Even in this case, a chain propagation mechanism has found to be operative. Moreover, both pyrrolidine-based and imidazolidinone-based catalysts could be employed for the reaction since both the corresponding enamines can work as sacrificial initiators of the photoredox process.[77] The same group has also explored the use of iodo-sufonyl derivatives as radical precursors to achieve an asymmetric formal methylation and benzylation of aldehydes.[78]

Another strategy employed by the Melchiorre's lab take advantage of the photoactivity of EDA complexes to achieve the α-functionalization of aldehydes without the requirement of an external photocatalyst (Scheme 61).[54a] The combination of an aminocatalyst, an aldehyde and an electron-poor benzyl halide led to the formation of a colored ground state EDA complex, recognized by the fact that a new absorption band appeared in the absorption spectra upon preparation of the reaction mixture. In this case, a transient generated enamine intermediate works as the donor while the electron-poor benzyl halide as the acceptor. Upon visible light irradiation an excited EDA complex is obtained which can carry out an intermolecular SET from the enamine to the benzyl halide to generate the corresponding radical ions. The presence of bromide as a suitable leaving group is triggering the process, competing with the usually prevalent back electron transfer (BET) that regenerates the ground-state complex. Finally, a stereocontrolled radical recombination is leading to the enantioenriched α-benzylated aldehyde. Nevertheless, the presence of a radical chain propagation mechanism was demonstrated by quantum yield measurements (ϕ>1).[77] Indeed, an electrophilic benzyl radical can react with a ground-state enamine, accounting for the generation of an α-amino radical that can give the subsequent propagation step.

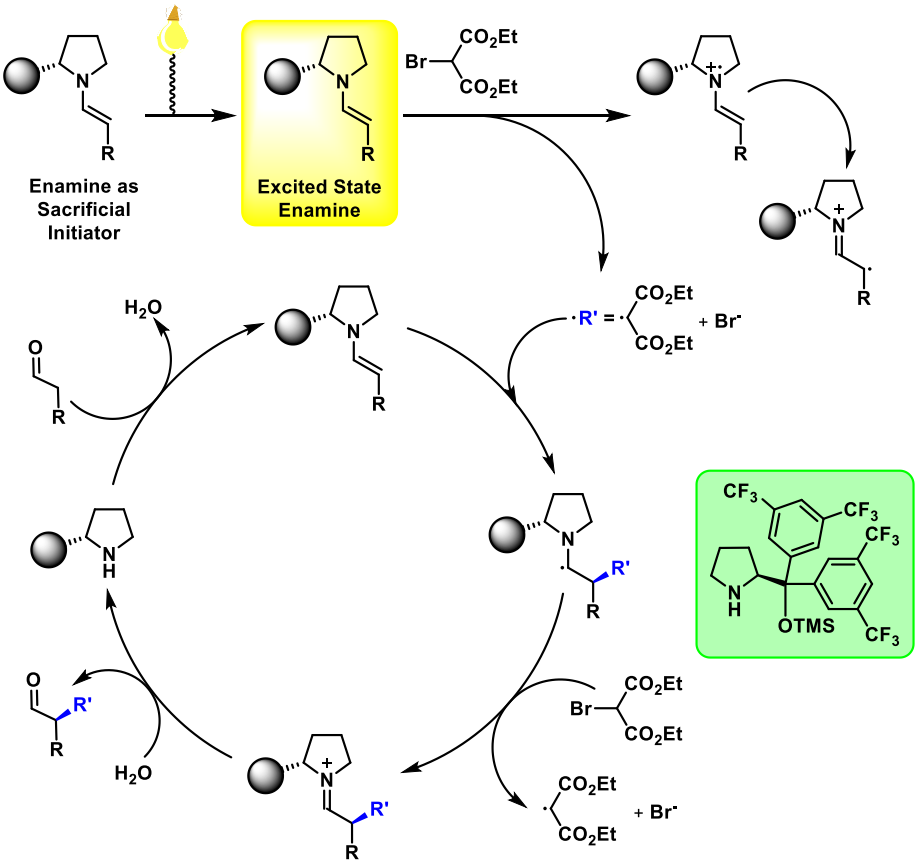

Scheme 60. Mechanistic proposal for the enantioselective α-alkylation through a photoactive enamine.

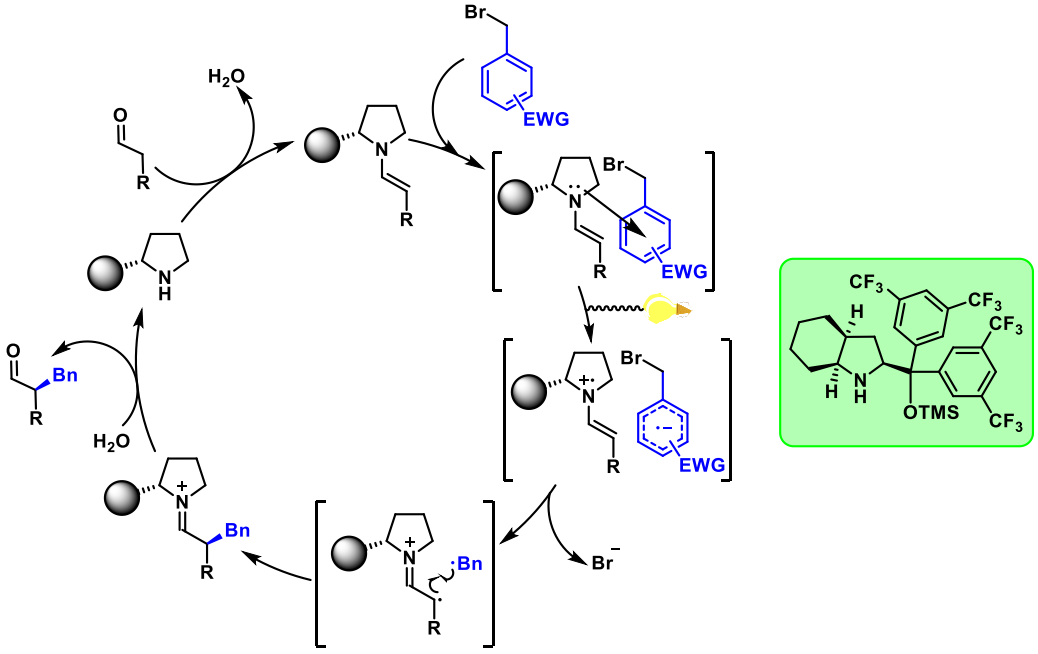

Scheme 61. Mechanistic proposal for the enantioselective α-alkylation of aldehydes through the photoactivity of a transient generated EDA complex intermediate.

Recently, MacMillan's research group reported a new methodology to achieve the enantioselective α-functionalization of aldehydes employing unactivated olefins as the reaction partners and without the required use of an external stoichiometric oxidant like CAN. The highly selective and synergistic combination of enamine catalysis, photoredox catalysis and hydrogen

atom transfer (HAT) catalysis gave access to enantioenriched products that were not possible to obtain employing other strategies (Scheme 62).[124] Upon visible light excitation the iridium photocatalyst is selectively oxidizing the chiral enamine intermediate to give an electrophilic SOMO-activated species, which can react with a wide range of unactivated olefins, leading to a nucleophilic carbon-centered radical. The subsequent HAT from an appropriate thiol catalyst is generating the product, whereas a SET process has to occur between the iridium and the thiol radical to restore the photocatalyst and the HAT catalyst, after protonation. It is important to notice that the three catalytic cycles are working together with complete selectivity to furnish the desired product due to polarity matches.

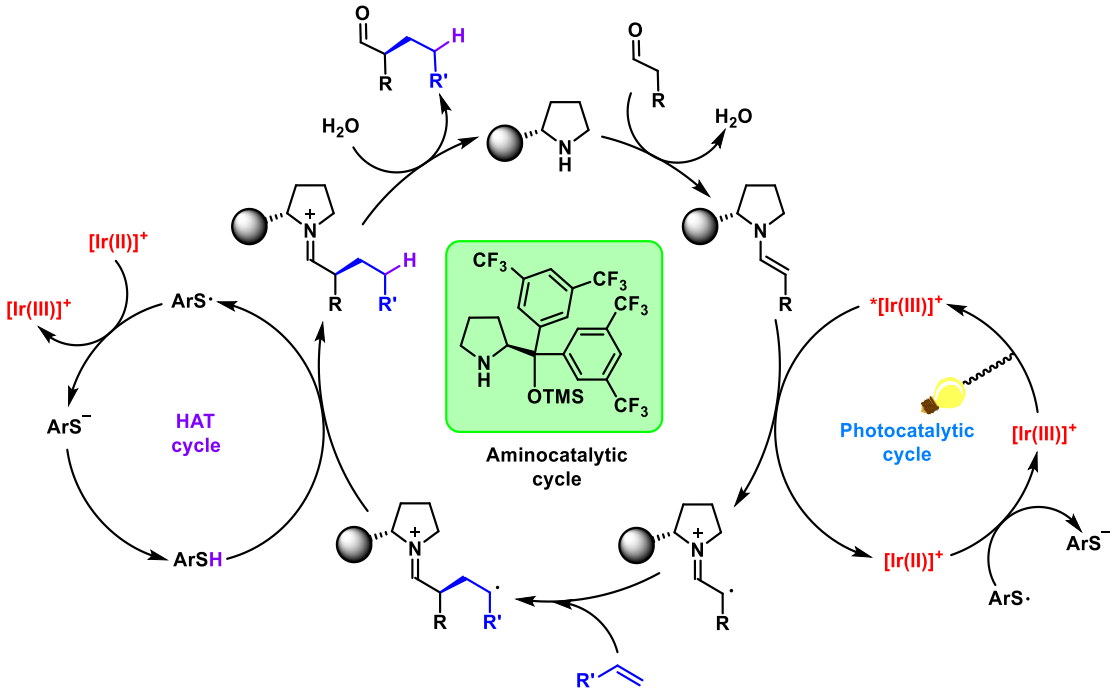

Scheme 62. Mechanistic proposal for the enantioselective α-alkylation of aldehydes through the merging of enamine, photoredox and HAT catalysis.

3.2 Introduction to Bifunctional Photocatalysis

Since the development and employment of bifunctional catalysts for organocatalytic reactions have had a beneficial impact on both reactivity and stereoselectivity, we thought about the possibility of synthetizing a bifunctional photo-aminocatalyst and to study its behavior in the α-alkylation of aldehydes as a model reaction. Indeed, just few precedents regarding the synthesis and employment of bifunctional photocatalysts in photocatalytic reactions were reported in the literature. In some cases it permitted the achievement of highly enantioselective transformations that were not possible to obtain through dual catalytic systems, whereas in other cases an increased reactivity and enantioselectivity was observed. On the other hand the employment of a chiral metal complex, which works as a Lewis acid and as a photocatalyst, allowed the development of a single-catalyst system.

The first bifunctional photocatalyst was reported by the research group of Bach in 2005 to achieve an intramolecuar radical conjugate addition over a pyrrolidine-tethered lactam (Scheme 63).[17] The corresponding spirocyclic pyrrolizidine product was obtained in high enantioselectivity (70% *ee*) and high yield (64%). The bifunctional catalyst was composed by a

[124] A. G. Capacci, J. T. Malinowski, N. J. McAlpine, J. Kuhne, D. W. C. MacMillan, *Nat. Chem*. **2017**, *6*, 1073-1077.

benzophenone moiety as the photocatalytic unit and a lactam binding motif, which worked as a hydrogen-bonding organocatalytic scaffold. The α-amino radical was generated through a photoinduced hydrogen atom transfer (PHAT), which is a common activation mode of benzophenone organophotocatalysts.[8c] Upon formation, the α-amino radical can carry out an intramolecular radical conjugate addition to the lactam, furnishing the spirocyclic pyrrolizidine (Scheme 63, right). The binding interactions between the bifunctional catalyst and the substrate are determining the stereoinduction since one prochiral face of the lactam is shielded by the benzophenone moiety, leading to a necessary approach of the radical from the opposite face. The hydrogen bonding coordination is also favoring the occurrence of a preferential PHAT between the catalyst-coordinated substrate limiting possible intermolecular SET events with uncoordinated lactam molecules that would lead to a racemic background reaction. Similar bifunctional photocatalytic systems were reported by the same research group in the following years.[40,62] The developed bifunctional catalysts relied on a xanthone or thioxanthone chromophore moiety, which allowed a preferential triplet energy transfer to a catalyst-coordinated substrate. The lactam binding motif was crucial to achieve a selective coordination with the quinolone substrate, allowing a preferential short-distance triplet sensitization in comparison with an intermolecular photosensitization.

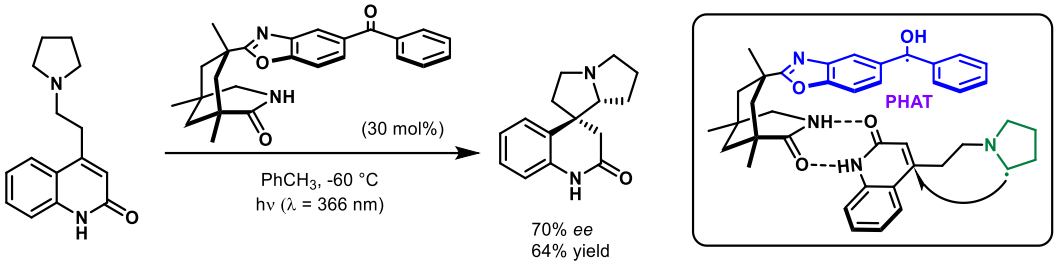

Scheme 63. First bifunctional catalyst employed in enantioselective photocatalysis.

On the other hand the research group of Meggers reported the synthesis of an iridium chiral-at-metal complex and the employment of it as a bifunctional photocatalyst to achieve the α-alkylation of 2-acyl imidazoles (Scheme 64).[82] The iridium catalyst works as a Lewis acid by selective binding of the 2-acyl imidazoles, leading to the generation of a chiral enolate and as a photocatalyst through the generation of different radicals from the corresponding bromo derivatives. Therefore, highly enantioenriched products are obtained by means of a single-catalyst system, which works effectively in the ground-state as a Lewis acid and in the excited state as a photocatalyst.

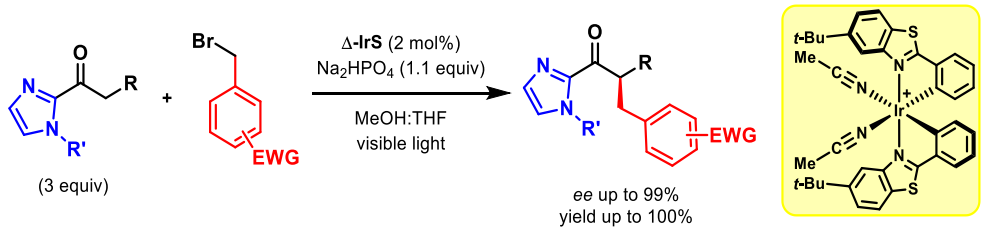

Scheme 64. Chiral-at-metal bifunctional iridium catalyst for the asymmetric α-alkylation reaction.

In 2017, the research group of Xiao reported the synthesis of a bifunctional photocatalyst for the photohydroxylation of β-ketoesters under aerobic conditions (Scheme 65).[125] The catalyst combines a Ni(II) salt as the Lewis acid and a chiral bisoxazoline ligand which contains a thioxanthone moiety as the photosensitizer. Through visible light absorption the thioxanthone chromophore reaches an excited state and permits the photosensitization of oxygen to singlet oxygen. This excited species is attacking the enolate of the β-ketoesters to give, due to the chiral

[125] W. Ding, L.-Q. Lu, Q.-Q. Zhou, Y. Wei, J.-R. Chen, W.-J. Xiao, *J. Am. Chem. Soc.* **2017**, *139*, 63-66.

environment, a stereocontrolled transformation. It is worth to mention that the authors demonstrated the superiority of the bifunctional catalytic system over an analogous dual-catalytic system composed by a bisoxazoline ligand and a thioxanthone derivative as the external photosensitizer. Indeed, both reactivity and enantioselectivity were found to be higher for the bifunctional system, indicating that the tethered thioxanthone is also changing the steric hindrance around the nickel active center to induce a higher degree of stereocontrol in the transformation.

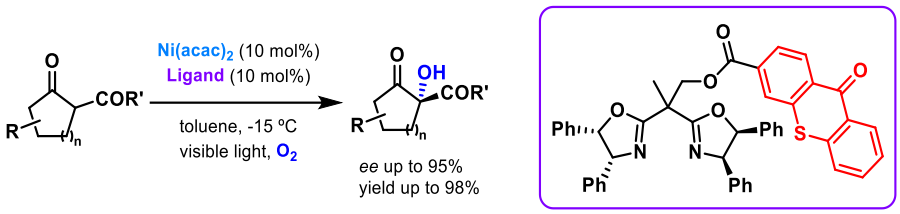

Scheme 65. Photohydroxylation of β-ketoesters under the mediation of a bifunctional catalyst.

A Lewis acid bifunctional photocatalyst which rely on a nickel-DBFOX ligand system was employed by the research group of Gong to achieve a radical conjugate addition over *N*-acyl pyrazole as the Michael acceptors (Scheme 66).[126] The α-amino radicals were generated from α-silyl amines as the radical precursors by a metal-ligand or a metal-ligand-substrate complex, which acts as a photooxidant. Indeed, both these possible photoactive species have an excited state reduction potential which is higher than the required value to carry out an exoergonic single-electron transfer process with the substrate.

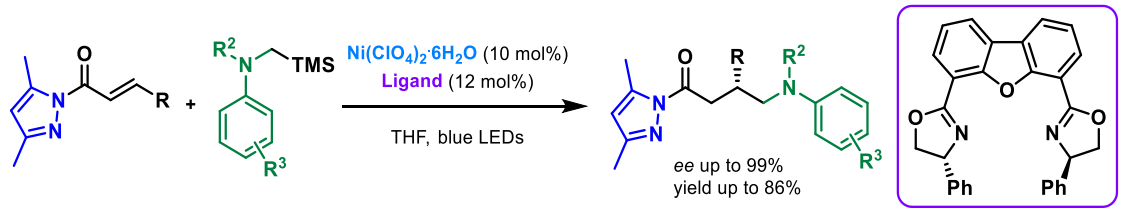

Scheme 66. Nickel/DBFOX bifunctional system for asymmetric radical conjugate additions.

A related copper-based bifunctional photocatalyst was developed by the same research group in 2018 (Scheme 67).[127] The bifunctional system was composed by a copper salt and a chiral bisoxazoline ligand, while the generation of carbon-centered radicals from alkyl and benzyl trifluoroborate salts allowed to carry out a highly enantioselective radical addition to imines in high efficiency. However, the Lewis acid-ligand complex does not present an excited state reduction potential capable of engaging a thermodynamically feasible SET to oxidize the trifluoroborates salts. Indeed, the authors proposed that a light induced homolysis is taking place over an organocopper species, which is obtained after ligand exchange with the trifluoroborates salt, as supported by mechanistic investigations. Furthermore, in both Gong's methodologies (Scheme 66 and 67), control experiments evidenced that the bifunctional photocatalyst needs both the metal center and the appropriate ligand to enable the SET event.

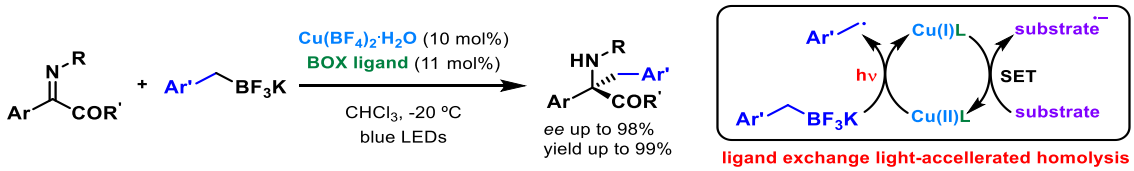

Scheme 67. Copper/BOX ligand bifunctional system for the enantioselective radical addition to imines.

[126] X. Shen, Y. Li, Z. Wen, S. Cao, X. Hou, L. Gong, *Chem. Sci.* **2018**, *9*, 4562-4568.
[127] Y. Li, K. Zhou, Z. Wen, S. Cao, X. Shen, M. Lei, L. Gong, *J. Am. Chem. Soc.* **2018**, *140*, 15850-15858.

Another example of a bifunctional copper-based photocatalyst is the one reported by Fu's and Peter's groups in 2016 (Scheme 68).[86] After ligand exchange between the carbazole (or indole) and the metal salt a photoactive copper species is obtained which can engage a SET with a tertiary alkyl chloride. A subsequent highly enantioselective carbon-nitrogen cross-coupling is achieved. Indeed the copper-carbazole species is acting in a bifunctional manner, as a photoredox active species and as a transition metal complex by means of mediating the cross-coupling reaction.

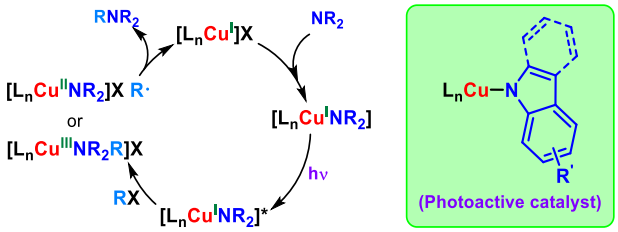

Scheme 68. Copper bifunctional photocatalyst for asymmetric carbon-nitrogen cross-coupling reactions.

3.3 Objectives of this Chapter

Although various bifunctional photocatalytic systems have been developed in the last years, these are mainly based on Lewis acid catalytic systems, transition metal complexes or lactam hydrogen binding interactions. On the other hand, to the best of our knowledge, a similar concept was not reported in photo-aminocatalysis. Based on the previous examples, different authors have shown the use of dual-catalytic systems for the α-alkylation of aldehydes, employing different metal-based or organic photocatalysts (Scheme 69left).[128] Therefore, we hypothesized that we could have designed a single chiral scaffold, which contained both the aminocatalyst and the photocatalyst (Scheme 69right). The designed catalyst would help to understand the α-alkylation process and the corresponding advantages and disadvantages of the bifunctional catalytic system. For this purpose we envisioned different sub-objectives:

1) Design and facile synthesis of a new bifunctional photo-aminocatalyst which would permit an easy modulation of the steric and photocatalytic properties.
2) Employment of this bifunctional photo-aminocatalyst in the α-alkylation of aldehydes to study its efficiency.
3) Mechanistic studies, DFT calculations and laser flash photolysis to better elucidate the behavior of the bifunctional catalyst in comparison with dual-catalytic systems.

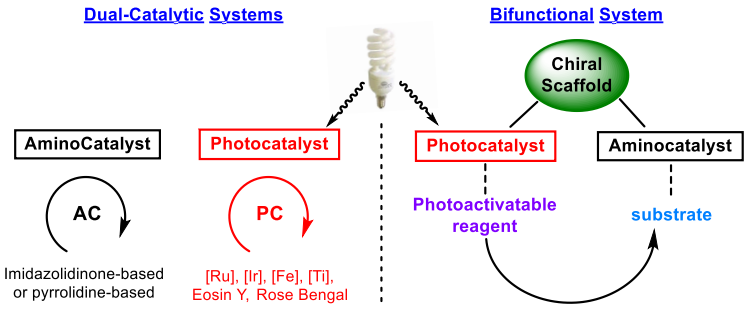

Scheme 69. Dual-catalytic and bifunctional catalytic systems.

[128] (a) A. Gualandi, M. Marchini, L. Mengozzi, M. Natali, M. Lucarini, P. Ceroni, P. G. Cozzi, *ACS Catal*. **2015**, *5*, 5927-5931; (b) P. Riente, M. Matas Adams, J. Albero, E. Palomares, M. A. Pericàs, *Angew. Chem. Int. Ed*. **2014**, *53*, 9613-9616; (c) M. Cherevatskaya, M. Neumann, S. Füldner, C. Harlander, S. Kümmel, S. Dankesreiter, A. Pfitzner, K. Zeitler, B. König, *Angew. Chem. Int. Ed*. **2012**, *51*, 4062-4066; (d) M. Neumann, S. Füldner, B. König, K. Zeitler, *Angew. Chem. Int. Ed*. 2011, *50*, 951-954; (e) K. Fidaly, C. Ceballos, A. Falguières, M. Sylla-Iyarreta Veitia, A. Guy, C. Ferroud, *Green Chem*. **2012**, *14*, 1293-1297.

3.4 Publications and Experimental Section

A Bifunctional Photoaminocatalyst for the Alkylation of Aldehydes: Design, Analysis, and Mechanistic Studies

Thomas Rigotti, Antonio Casado-Sánchez, Silvia Cabrera, Raúl Pérez-Ruiz, Marta Liras, Víctor A. de la Peña O'Shea, and José Alemán*

ACS Catal. **2018**, *8*, 5928-5940

(*Highlighted* in *Synfacts*, **2018**, *14*, 984)

The experimental section was taken from the "Supporting Information" document associated with the specific publication and is including the corresponding numeration. The characterization data have been shown only for the final products that appear in the scope of the reaction. The complete "Supporting Information" documents, with all the characterization data, NMR spectra, SFC or HPLC traces and other experimental procedures have been included in the enclosed USB memory.

ACS Catalysis

Research Article

Cite This: ACS Catal. 2018, 8, 5928−5940

pubs.acs.org/acscatalysis

A Bifunctional Photoaminocatalyst for the Alkylation of Aldehydes: Design, Analysis, and Mechanistic Studies

Thomas Rigotti,[†] Antonio Casado-Sánchez,[†] Silvia Cabrera,[‡,§] Raúl Pérez-Ruiz,[∥] Marta Liras,[∥] Víctor A. de la Peña O'Shea,[∥] and José Alemán*[,†,§]

[†]Organic Chemistry Department, Módulo 1, Universidad Autónoma de Madrid, 28049 Madrid, Spain

[‡]Inorganic Chemistry Department, Módulo 7, Universidad Autónoma de Madrid, 28049 Madrid, Spain

[§]Institute for Advanced Research in Chemical Sciences (IAdChem), Universidad Autónoma de Madrid, 28049 Madrid, Spain

[∥]Photoactivated Processes Unit, IMDEA Energy, Av. Ramón de la Sagra 3, 28935 Móstoles, Madrid, Spain

Supporting Information

ABSTRACT: A bifunctional photoaminocatalyst based on imidazolidinone and thioxanthone is presented. The preparation of these catalysts proceeds in a two-step synthesis that allows an easy tuning of the steric properties. The photophysical and electrochemical data of the imidazolidinone photocatalysts have been determined, indicating that the catalysts can work under visible light conditions. To corroborate the experimental observations, ground state geometry optimization and energy transition studies of thioxanthone and bifunctional catalyst **4c** were optimized by time-dependent density functional theory (TD DFT) calculations. The alkylation of aldehydes with this photoaminocatalyst works with high enantioselectivities and yields due to the stereoelectronic properties of the catalyst. A rational mechanistic cycle based on different mechanistic experiments, TD DFT calculations, and laser flash photolysis is presented.

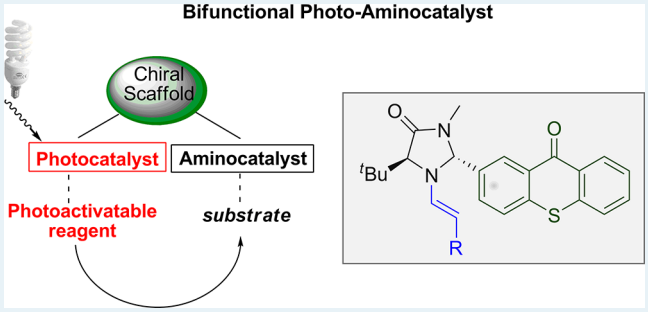

KEYWORDS: *bifunctional photocatalyst, organocatalysis, pyrrolidines, photochemistry, mechanism*

INTRODUCTION

Photocatalysis has emerged as one of the best strategies for the development of sustainable and novel processes for the synthesis of organic compounds.[1] In spite of the enormous growth in this area, the vast majority of the developed methodologies provide achiral or racemic compounds using either metallic complexes or organic molecules as the photocatalysts. The main reason for this is the difficulty of combining a chiral catalyst to induce a stereochemical control, with high reactivity and low activation barriers of radical intermediates.[2] In spite of this difficulty, asymmetric photocatalytic transformations have been successfully accomplished by the use of a dual-catalyst approach using a combination of a photocatalyst and a chiral organocatalyst.[3] The use of only one catalyst that combines chirality and photoredox properties is not only more convenient but also more challenging and, consequently, less explored. The pioneering work performed by Bach's group developed the photoasymmetric [2+2] cycloaddition by employing a chiral bifunctional catalyst, containing a chromophore unit, that induced a stereocontrol by hydrogen bond interactions.[4] A similar strategy was applied by Xiao's group who developed a bifunctional metal photocatalyst for an enantioselective aerobic oxidation in which the photosensitizer is linked to a chiral bisoxazoline metal complex.[5] Recently, Meggers and co-workers have developed new chiral iridium and rhodium complexes that simultaneously act as photocatalysts and as chiral Lewis acids to provoke the asymmetric induction.[6] However, to the best of our knowledge, a bifunctional photoaminocatalyst that contains a photocatalyst and aminocatalyst has not been developed yet.

During the past few years, the asymmetric α-alkylation of aldehydes and ketones[7] has become an attractive topic because of the synthetic utility of the products obtained. In 2008, MacMillan developed a pioneering and remarkable example in which the photoredox catalyst $Ru(bpy)_3^{2+}$ and an imidazolidinone organocatalyst were employed in a dual catalytic system[3a] to furnish the α-alkylation of aldehydes using different radical precursors (left, Figure 1). Since then, diverse dual catalytic systems based on other metal complexes[8] and semiconductors[9] as photocatalysts have also been reported. Alternatively, the α-alkylation of aldehydes using metal-free photocatalysts was developed by Zeitler's[10] and Ferroud's[11] groups using the dyes Eosin Y and Rose Bengal, respectively. The combination of an organic photocatalyst (Eosin Y or Rose Bengal) and MacMillan's imidazolidinone catalyst made possible the alkylation of aldehydes with alkyl halides, but the enantioselectivity achieved was in some cases lower compared to that of metal-based dual catalytic systems.

Received: April 5, 2018
Revised: May 9, 2018
Published: May 15, 2018

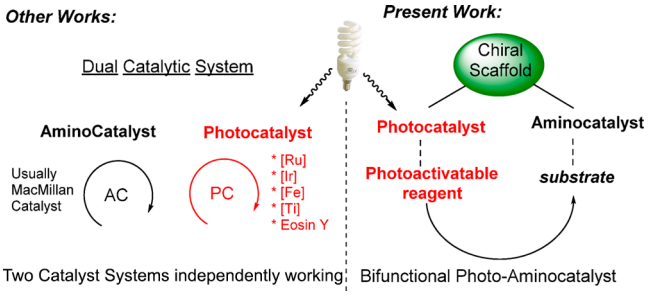

Figure 1. Comparison of the two catalytic systems, dual catalytic and bifunctional photoaminocatalyst systems.

These findings emphasize that the α-alkylation of aldehydes is not a trivial process and that there are difficulties in finding the appropriate conditions for the compatibility of two different catalytic systems. In addition, the development of a general photo-organocatalyst for the α-alkylation of aldehydes (instead of using an external photocatalyst for each photoactivatable reagent) will be a significant advance in the field of visible light photoredox catalysis. The design of a unique metal-free catalyst, called a bifunctional photoaminocatalyst, capable of activating both the photoactivatable reagent and the substrate simultaneously, would be highly desirable (right, Figure 1). In the field of organocatalysis, the dual activation of reagents by a bifunctional organocatalyst is an area of great importance, which has led to the development of novel transformations.[12] Most of the reported bifunctional catalysts are combinations of a Lewis base with a Lewis acid moiety. However, the incorporation of a photo-organocatalyst in a bifunctional catalyst is much scarcer, and more particularly, the combination of a photo-organocatalyst and an aminocatalyst has not been developed yet.[7]

For the design of the new photoaminocatalysts, different factors need to be taken into account (Figure 2). First, the election of the chiral scaffold that will incorporate the two catalytic moieties is crucial for the success of its application. 4-Imidazolidinone has been chosen for two reasons. (i) The catalysts usually employed for the alkylation of aldehydes in most of the dual catalytic systems are MacMillan's imidazolidinone catalysts, which are chiral 4-imidazolidinone derivatives. (ii) These catalysts possess two groups (R^1 and R^2) that could allow the incorporation of two different units (Figure 2, top). The R^1 group would permit the easy modulation of the steric hindrance of the aminocatalyst, whereas the second (R^2) would also incorporate the photocatalytic unit. Moreover, the synthesis of chiral 4-imidazolidinones is simple and short and assembles the R^1 and R^2 groups from two separate reactants that allows an easy fine-tuning of the properties of the catalyst. With regard to the photocatalytic unit, thioxanthones have been widely studied as photoinitiators in polymerization processes[13] and as efficient photocatalysts in energy- and electron-transfer proceses.[14] In addition, Bach's group has reported that thioxanthones can also be used as visible light photocatalysts in asymmetric transformations.[15] We envisaged that thioxanthones would be good candidates as the photocatalytic unit for the synthesis of the bifunctional photoaminocatalyst. In particular, 2-substituted thioxanthones were chosen as building blocks for the synthesis of the photoaminocatalyst.[16] The second consideration is related to the geometry of the enamine in the aminocatalyst that has been studied in depth by MacMillan and others.[3] Therefore, in our case, because the incorporation of the aromatic photocatalytic unit (R^2) is required, and to control the geometry in the enamine, the R^1 group must be of a different relative size compared to R^2 (Figure 1, bottom).

Herein, we present a bifunctional photoaminocatalyst by a combination of both an amino-organocatalyst (imidazolidinone) and a photo-organocatalyst (thioxanthone) in the same molecule. In addition, the photophysical and electrochemical data of photoaminocatalysts, their application in the alkylation of aldehydes and a rational catalytic cycle based on different mechanistic studies, time-dependent density functional theory (TD DFT) calculations, and laser flash photolysis are also presented.

RESULTS AND DISCUSSION

Synthesis of the Bifunctional Photocatalysts and Characterization. The photoaminocatalysts **4** were prepared in two steps, starting from commercially available amino acids (Scheme 1). First, amino acids **1a−c** were easily transformed into *N*-methyl aminoamides **2a−c** in high yields. The aminoacetylation of the corresponding carboxythioxanthone[17] **3** with amides **2a−c** led to the desired photoaminocatalysts **4a−d** with moderate to good *trans*/*cis* ratios. The absolute configuration of the major diastereoisomer of catalysts **4b** and **4c** was determined by single-crystal X-ray analysis[18] (see the bottom of Scheme 1). In the structures, both substituents (R^1 and thioxanthone) are in *trans* geometry with the thioxanthone moiety in a pseudo-equatorial disposition.

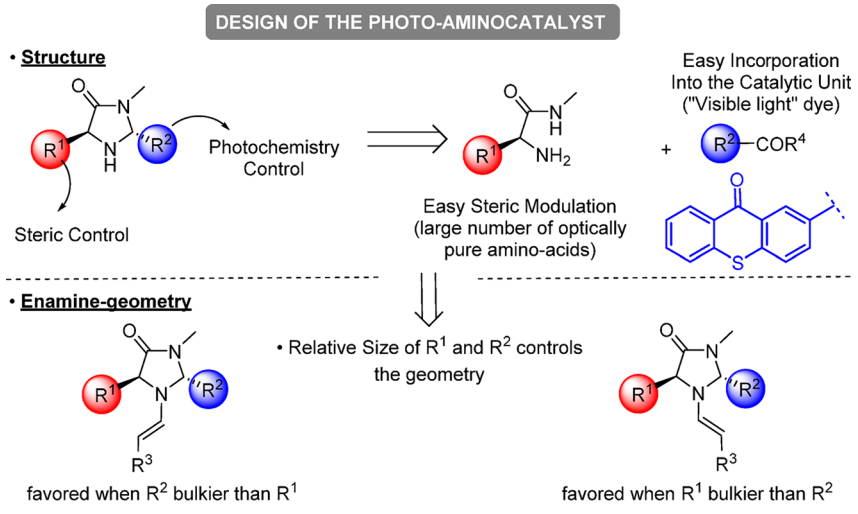

Figure 2. Design of the photoaminocatalysts and initial considerations.

DOI: 10.1021/acscatal.8b01331
ACS Catal. 2018, 8, 5928−5940

Scheme 1. Synthesis of Photoaminocatalysts 4 and X-ray Crystal Structures of 4b and 4c

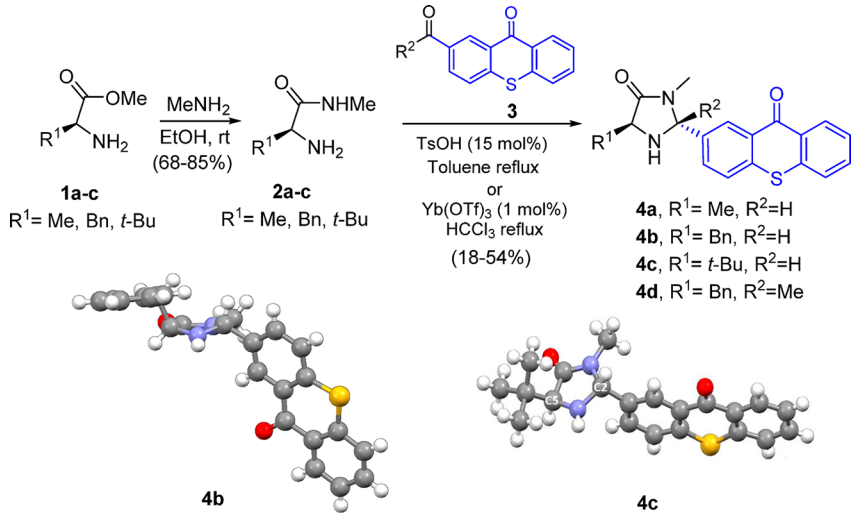

Table 1. Photophysical and Electrochemical Data of Thioxanthone and Catalysts 4a–d, and Structures of Parent Imidazolidinone Catalysts 4e and 4f

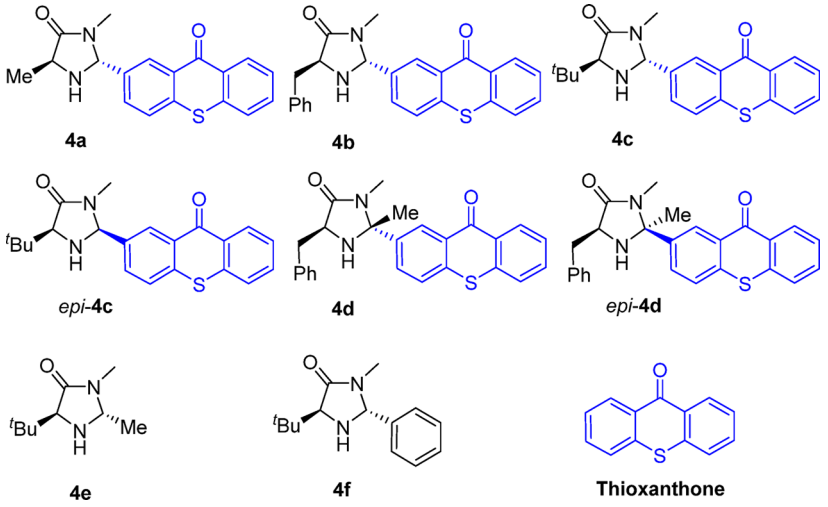

compound	absorption (λ_{max}, nm)[a]	emission (λ_{max}, nm)[b]	S_1 energy (eV)[c]	E_{ox} (V vs SCE)[d]	E^*_{ox} (V vs SCE)[e]	E_{red} (V vs SCE)[d]	E^*_{red} (V vs SCE)[e]
thioxanthone	381	409	3.13	+1.82	−1.31	−1.48	+1.65
4a	381	412	3.14	+1.32 +1.83	−1.31	−1.45	+1.69
4b	381	416	3.12	+1.44 +1.80	−1.32	−1.50	+1.62
4c	381	413	3.13	+1.36 +1.80	−1.33	−1.50	+1.63
epi-**4c**	379	420	3.14	+1.08 +1.82	−1.32	−1.35	+1.79
4d	380	414	3.13	+1.49 +1.84	−1.29	−1.44	+1.69
epi-**4d**	379	413	3.15	+1.50 +1.84	−1.31	−1.41	+1.74

[a]UV–vis spectra recorded in 0.025 mM CH_2Cl_2 solutions at room temperature. [b]Fluorescence recorded in 0.25 mM CH_2Cl_2 solutions at room temperature. [c]Determined from the intersection of the normalized absorbance and emission spectra (converted into electronvolts). [d]Conditions: 50 mV s^{-1} scan rate, 1 mM solution of the compound in an argon-saturated CH_3CN solution, 0.1 M solution of a Bu_4NPF_6 glassy carbon disk (2.8 mm diameter) as a working electrode, platinum wire as a counter electrode, and Ag/AgCl as a reference electrode. [e]Excited state redox potentials of the thioxanthone moiety estimated using the equation $E^*_{ox} = E_{ox} - E_{0-0}$ or $E^*_{red} = E_{red} + E_{0-0}$, where E_{0-0} is the singlet state energy.

Next, we studied the photophysical and electrochemical properties of bifunctional catalysts **4** to understand their suitability for a photocatalytic process (Table 1). For comparison, the same study was also performed using thioxanthone under identical experimental conditions. The ultraviolet–visible (UV–vis) absorption spectrum of thioxanthone presents an absorption maximum

DOI: 10.1021/acscatal.8b01331
ACS Catal. 2018, 8, 5928–5940

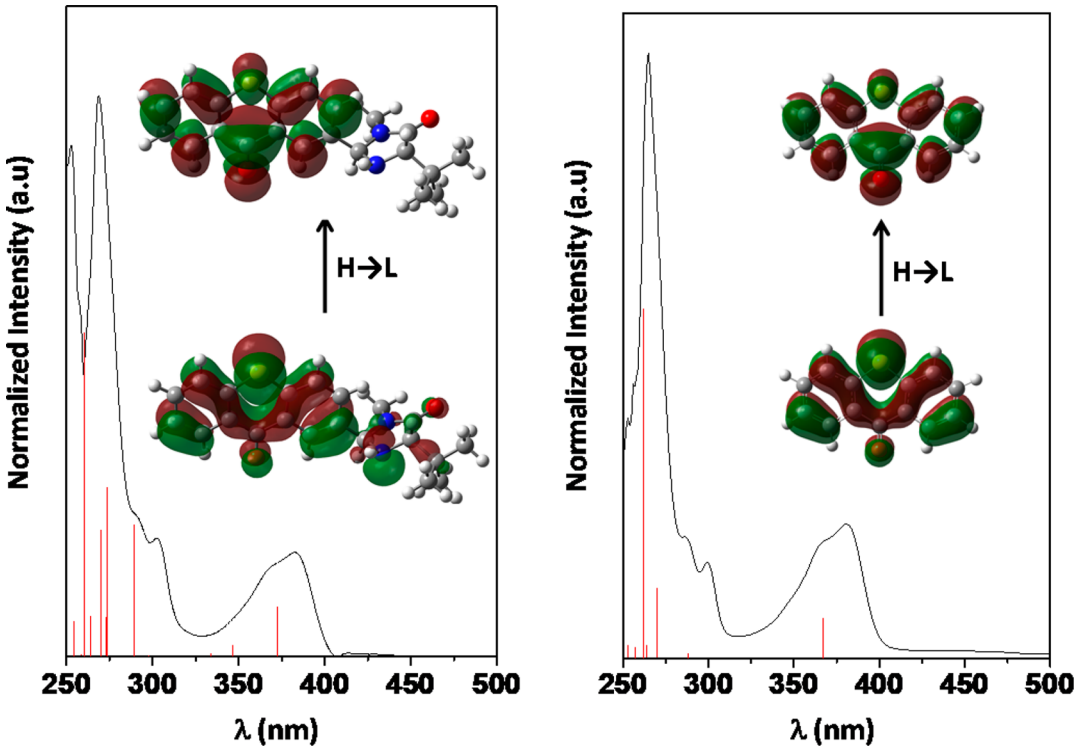

Figure 3. Comparison between the experimental (black line) and calculated vertical (red bars) excitation by TD DFT B3LYP (6-311++G**) for catalyst **4c** (left) using dimethylformamide as a solvent and thioxanthone (right) using DCM as a solvent. The inset shows molecular orbitals involved in the S_1 transition.

(λ_{max}) at 381 nm with a significant part of the absorption band in the visible region. The different structures and stereochemistry of the amino-thioxanthone catalysts **4** showed little effect on the maximum absorption (λ_{max} = 380 ± 1 nm). Similar findings were described by Neumann et al., who reported that the 2-substitution in the aromatic ring of the thioxanthone did not produce any significant effect on the absorption maximum, or on the molar absorption coefficients, regardless of the nature of the substituent.[16] Moreover, strong emissions at λ_{max} values of 413−420 nm were observed for all catalysts upon photoexcitation of the absorption maximum at room temperature. The excited singlet state energy of the photoaminocatalyst was estimated to be at the intersection of the normalized absorption and emission spectra. As we expected, all the S_1 energy values are very close to that of thioxanthone, which indicates that the imidazolidinone fragment has little effect on the photophysical properties of the thioxanthone moiety.

The ground state redox potentials of the catalysts were determined by cyclic voltammetry (CV) in acetonitrile as a solvent (Table 1). Amino-thioxanthone catalysts **4** show two irreversible oxidation peaks: the most positive corresponds to the oxidation of the thioxanthone moiety and the less cathodic to the amine moiety (see the Supporting Information for further details). This assignment was confirmed by comparing the redox values of bifunctional catalysts **4** with the oxidation peaks of thioxanthone and imidazolidinone catalysts **4f** (1.40 V vs SCE in CH_3CN). In addition, one reversible reduction potential was also determined, which corresponds to the thioxanthone reduction. When the redox potentials and the singlet state energy are taken into account, the oxidation and reduction excited state potentials of catalysts **4** were estimated. Both oxidation and reduction potentials in the excited state of bifunctional catalysts **4** are similar to those calculated for thioxanthone, which indicates the preservation of the electrochemical properties of the thioxanthone moiety on the bifunctional catalyst properties, which confirms the adequate design of bifunctional catalysts **4**.

To corroborate the experimental photophysical observations, the ground state geometry optimization of thioxanthone and bifunctional catalyst **4c**, as well as their energy transition studies, were optimized by TD DFT calculations (see Figure 3 and the Supporting Information). Geometry optimization of the thioxanthone ground state (S_0) revealed a planar structure with C_{2v} symmetry similar to that previously described in the literature (Figure 3, right).[19,20] Other possible conformations such as nonplanar structures with C_s symmetry described by Rubio Pons et al.[21] were not considered because they are less stable conformations.[22] The absorption spectra of thioxanthone exhibited a first band located at 381 nm that, by taking our calculations into account, can be assigned to the $\pi-\pi^*$ transitions from HOMO to LUMO orbitals (see the Supporting Information for further details). In addition, an $n-\pi^*$ optically forbidden transition (S_2), energetically close to S_1, was also observed, which is in agreement with Ishijima's studies.[23] On the other hand, Mundt et al.[19] observed a change in the energy of these excited states with a lower $n-\pi^*$ transition under vacuum conditions. These variations are due to the solvent effect, which stabilizes the $\pi-\pi^*$ excited state of the thioxanthone. In addition, the optimization of the triplet state leads to an energy of 2.73 eV that is close to the experimental value of 2.84 eV.[24] As described above (see Table 1), the UV−vis spectrum of **4c** has a profile similar to that of thioxanthone (Figure 3, left). The TD DFT calculations showed that the S_1 transition takes place between the HOMO, which is delocalized over the whole molecule with a contribution from the amine moiety, and the LUMO localized predominantly on the thioxanthone (Figure 3). We found that the triplet state of **4c**

DOI: 10.1021/acscatal.8b01331
ACS Catal. 2018, 8, 5928−5940

exhibited an energy value of 2.73 eV, which is identical to that of free thioxanthone.

The α-alkylation of aldehydes with diethyl bromomalonate was chosen as a model reaction[3a] to evaluate the catalytic activity of bifunctional photocatalysts **4** (see Table 2). Moreover, using

Table 2. Screening of Different Bifunctional Photo-Organocatalysts 4 in the α-Alkylation of Aldehyde 5a[a]

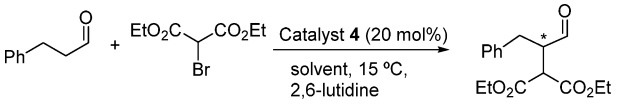

5a **6a** **7a**

	catalyst (mol %)	solvent	conversion[b] (%)	ee (%)[c]
1	**4e** (20)	DMF	41	91
2	**4f** (20)	DMF	<5	–
3	**4e** (20) and $Ru(bpy)_3^{2+}$ (1)	DMF	85	91
4	**4f** (20) and $Ru(bpy)_3^{2+}$ (1)	DMF	59	97
5	**4a** (20)	DMF	100	64
6	**4b** (20)	DMF	77	57
7	**4c** (20)	DMF	100	>99
8	*epi*-**4c** (20)	DMF	11	8[d]
9	**4d** (20)	DMF	71	37
10	*epi*-**4d** (20)	DMF	30	29
11	**4c** (20)	DMSO	60	>99
12	**4c** (20)	CH_2Cl_2	14	>99
13	**4c** (20)	toluene	5	96
14	**4c** (10)	DMF	35	91
15[e]	**4c** (20)	DMF	100	70
16	**4f** (20) and thioxanthone (20)	DMF	97	97

[a]**5a** (0.3 mmol), **6a** (0.15 mmol), 2,6-lutidine (0.3 mmol), and catalyst **4** in 0.3 mL of the indicated solvent were stirred at 15 °C for 18 h under visible light irradiation (CFL-23 W). [b]Conversion of **7a** determined by ^{1}H NMR. [c]Determined by SFC on the chiral stationary phase after derivatization (see the Supporting Information). [d]Opposite enantiomer obtained. [e]Reaction performed under blue LED (385 mW) irradiation.

the usual formulation for the determination of the free energies of a photoinduced electron-transfer (PET) process [ΔG_{PET} = 23.06(E_{ox} − E_{red}) − E^*(S_1 or T_1)], we can estimate the thermodynamic driving force of the PET between the diethyl bromomalonate as the reactant *vide infra* (E_{red} = −1.0 V vs SCE in CH_3CN) and catalysts **4** (see E_{ox} and E^* values in Table 1). All the estimated ΔG_{PET} values are negative (ranging from −9.0 to −9.9 kcal/mol), which indicates that the process is thermodynamically favorable for all the catalysts **4**.

Optimization Studies and Scope of the Reaction. Initially, the α-alkylation of hydrocinnamaldehyde (**5a**) was performed using MacMillan's imidazolidinone catalyst **4e** (20 mol %) without any external photosensitizer (entry 1) under visible light irradiation (23 W commercial fluorescent bulb) using dimethylformamide (DMF) as a solvent. The reaction furnished α-alkylated product **7a** with a 41% conversion and a 91% enantiomeric excess. Catalyst **4f** was then employed under the same reaction conditions (entry 2), yielding a negligible conversion (<5%), indicating that this catalyst did not work under these reaction conditions. Then, catalysts **4e** and **4f** have been employed in combination with $Ru(bpy)_3^{2+}$ as an external photocatalyst (entries 3 and 4), obtaining 85% (91% ee) and 59% (97% ee) conversion, respectively. We then tested our bifunctional photocatalysts **4a**−**d** (entries 5−15). To our delight, bifunctional photocatalyst **4a** allowed the synthesis of **7a** with complete conversion and a moderate enantiomeric excess (64% ee, entry 5). The use of catalyst **4b** with a slightly bulky substituent, such as the benzyl group (R^1 = Bn), provided comparable enantioselectivity (57%, entry 6), whereas the catalyst with the bulkier *tert*-butyl moiety (**4c**) achieved an outstanding >99% ee and full conversion (entry 7). By contrast, the epimer photocatalyst *epi*-**4c** showed very low reactivity and enantioselectivity (entry 8). Furthermore, catalysts **4d** and *epi*-**4d** with a quaternary stereocenter showed enantiomeric excesses and conversions smaller than those of catalyst **4c** (entries 9 and 10). Using the best catalyst **4c**, other solvents such as dimethyl sulfoxide (DMSO) or CH_2Cl_2 were also studied, yielding in all cases identical enantioselectivities but lower conversions (entries 11 and 12). Conversely, an apolar solvent such as toluene afforded the product with a low conversion (entry 13). Moreover, the decrease in catalyst loading involved a large conversion decrease (entry 14), and the use of blue LEDs (λ_{max} = 450 nm) as an irradiation source afforded aldehyde **7a** in lower enantioselectivity (entry 15). We then performed the reaction in the presence of catalyst **4f** and thioxanthone (dual catalytic system), and the results were compared to those of catalyst **4c** (entries 7 and 16). As it can be observed, only a very slightly better result was obtained in the case of the bifunctional catalytic system (**4c**). The latter result forced us to investigate the mechanistic differences between the dual catalytic system and the bifunctional catalyst (see below).

Once the optimal conditions had been determined (Table 2, entry 8), we studied the scope of the α-alkylation of aldehyde **5a** using a variety of alkylating reagents (Table 3). Bromomalonates **6a** and **6b** (a tertiary bromide) were reduced by catalyst **4c** to give aldehydes **7a** and **7b**, respectively, with an excellent yield and enantioselectivies. Later, the electron reduction of bromonitrile species (bromoacetonitrile, E_{red} = −1.23 V vs SCE in CH_3CN; see the Supporting Information for cyclic voltammetry) by photoorganocatalyst **4c** was explored, and the negative value of the free energy (ΔG_{PET} = −2.3 kcal/mol) guarantees the thermodynamic driving force of the process. The reaction with nitriles **6c** and **6d** provided aldehydes **7c** and **7d**, respectively, in high yields and excellent enantioselectivities. It is worth mentioning that these results are better than those previously described in the literature.[7] α-Bromoketone derivatives **6e**−**g** (e.g., bromoacetophenone; E_{red} = −0.89 V vs SCE) were also reduced using our catalytic system, yielding ketones **7e**−**g**, respectively, with an excellent yield and high levels of enantiocontrol (84−95% ee). Furthermore, the reaction of benzyl derivative **6h** with aldehyde **5a** was successfully catalyzed by bifunctional thioxanthone **4c** to afford **7h** in 97% ee.

Next, the applicability of the photocatalyst was evaluated using different aldehydes (**5**) with bromomalonate **6a** as a bromo derivative (Table 4). Primary and secondary β-alkyl aldehydes **5i** and **5j** exhibited good reactivity, affording aldehydes **7i** and **7j**, respectively, with excellent enantioselectivies (96 and 97% ee, respectively). The bifunctional catalytic system also allowed the successful alkylation of functionalized aldehydes **1k** and **1l**. Accordingly, alkylated aldehydes **7l** and **7k**, containing an *N*-Boc-piperidine and a double bond, respectively, were isolated in good yields and high enantioselectivities (96 and 99% ee, respectively). It must be highlighted that the level of enantioselectivity achieved for the α-alkylation of aldehydes using bifunctional catalyst **4c** is not only comparable to but also better than those reported in the literature using dual catalytic systems. These better enantioselectivities are due to the more sterically hindered nature of bifunctional photocatalyst **4c** compared

DOI: 10.1021/acscatal.8b01331
ACS Catal. 2018, 8, 5928−5940

Table 3. Scope of the α-Alkylation of 5a with Bromo Derivatives 6[a]

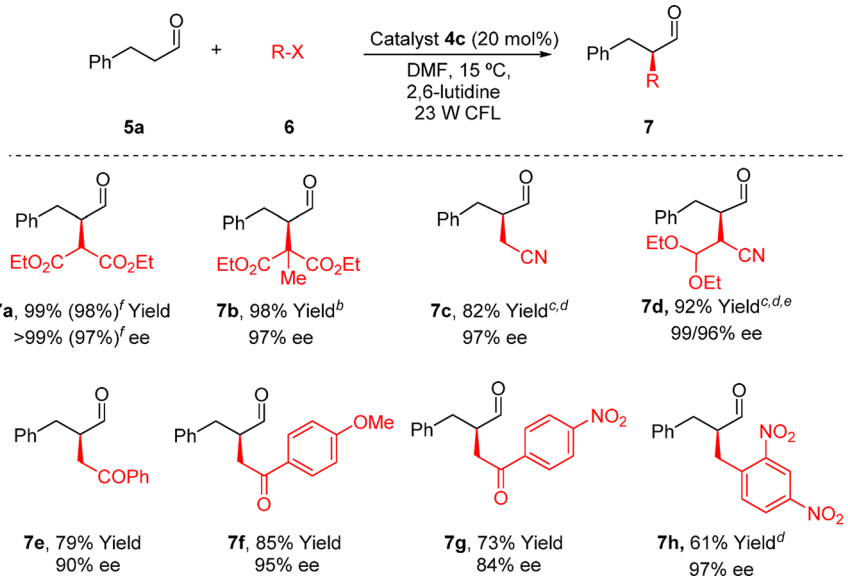

[a]**5a** (0.24 mmol), **6** (0.12 mmol), 2,6-lutidine (0.24 mmol), and catalyst **4** in 0.24 mL of DMF were stirred at 15 °C under visible light irradiation (CFL-23 W). [b]Based on a 30% conversion by ^{1}H NMR. [c]Five equivalents of **5a** was employed. [d]DMSO used as solvent. [e]Overall yield of both diastereoisomers (dr 2:1). [f]Reaction performed on a 1 mmol scale.

Table 4. Scope of the Reaction of Different Aldehydes (5) with Diethyl Bromomalonate (6a)[a]

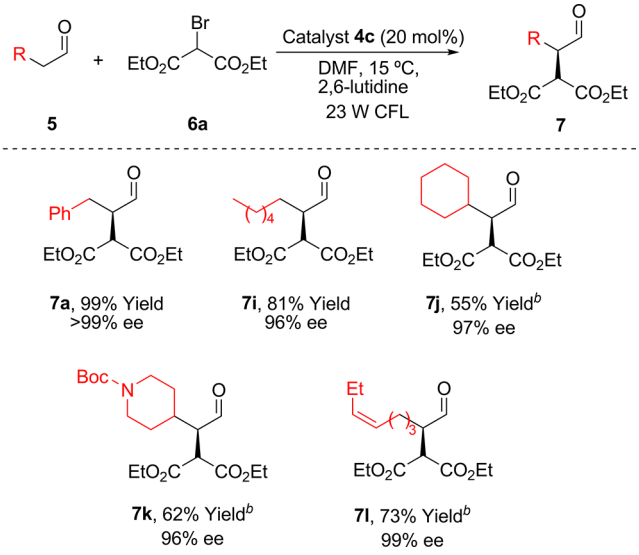

[a]**5** (0.24 mmol), **6a** (0.12 mmol), 2,6-lutidine (0.24 mmol), and catalyst **4** in 0.24 mL of DMF were stirred at 15 °C under visible light irradiation (CFL-23 W). [b]Five equivalents of the corresponding aldehyde **5** was used.

to MacMillan's catalyst **4e** (compare entries 3, 4, 7, and 16 of Table 2).

Mechanistic Considerations. *Originally Proposed Photocatalytic Cycle.* According to the original mechanism proposed by MacMillan and others,[3,7−11] we postulate the mechanism outlined in Scheme 2 for the photoalkylation of aldehydes using bifunctional catalyst **4c**. The reaction starts with the condensation of catalyst **4c** with aldehyde **5** to give the first enamine intermediate **A**. The thioxanthone moiety of intermediate **A** can absorb light to reach excited intermediate **A*** (step 1). It is well-known that thioxanthones can promote a single electron-transfer process (SET).[14] Therefore, this excited intermediate **A*** can

Scheme 2. Proposed Mechanism for the α-Alkylation of Aldehydes Employing Catalyst 4c in Accordance with the Original Mechanism Proposed by MacMillan[3a]

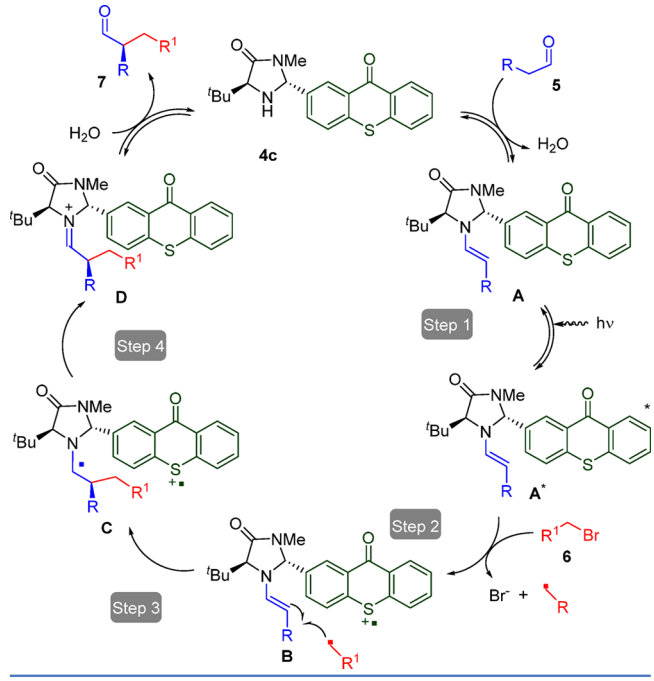

reduce the bromoalkane derivative **6** (step 2) through a SET reduction, to give intermediate **B** and the alkyl radical. Then, the alkyl radical is added to the nucleophilic enamine **B** to yield α-amino radical **C** that can be intramolecularly oxidized by the thioxanthone radical cation. Finally, the resultant iminium **D** is hydrolyzed to give the final α-alkylated aldehyde **7**. To confirm this mechanistic proposal, different experiments involved in the process, and related to the different steps, were performed.

Initiation Process (step 2). Three different mechanisms have been proposed in the literature for the photochemical initiation

DOI: 10.1021/acscatal.8b01331
ACS Catal. 2018, 8, 5928−5940

Scheme 3. Three Different Pathways for the Initiation Process of the α-Alkylation of Aldehydes

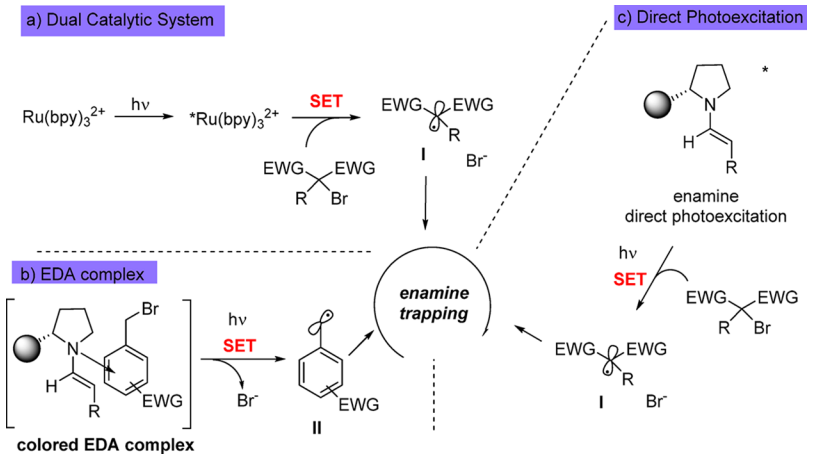

Scheme 4. α-Alkylation of Hydrocinnamaldehyde Using Catalysts 4e–g in the Absence and Presence of an External Photocatalyst

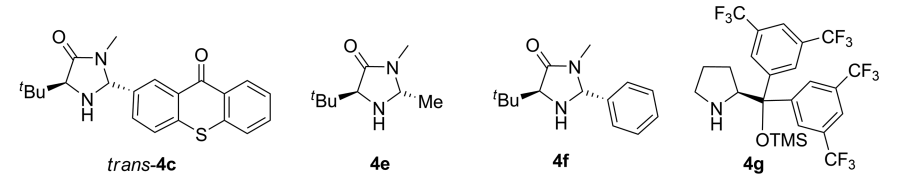

Without External Photocatalyst	4 with $Ru(bpy)_3^{2+}$ (1 mol%)
trans-**4c**, 100% conv. **4e**, 41% conv. **4f**, <5% conv. **4g**, 100% conv.	**4e**, 85% conv. **4f**, 59% conv.

process of this reaction, depending on the organocatalyst employed, the presence of an external photosensitizer, and/or the type of bromo derivative (Scheme 3). The first was proposed by MacMillan[3] and co-workers for the dual catalytic system, using iridium(III) or ruthenium(II) complexes and MacMillan's imidazolidinone catalyst (Scheme 3, top left). In this case, the reducing excited state of the metal photocatalyst can reduce the bromoalkane via a SET process, giving radical intermediate **I** (Scheme 3, top left). The second mechanism was described by Melchiorre and coworkers.[25] In the latter case, a colored EDA complex intermediate between the enamine and an electron deficient benzyl bromide is formed and can be photoexcited to give a SET from the enamine to the bromobenzyl derivative, yielding radical intermediate **II** (Scheme 3, bottom left). The third and most recent mechanism proposed is related to the direct photoexcitation of the enamine,[26] generated upon condensation of an aldehyde and Jørgensen-Hayashi's catalyst, which is able to reach an excited state and to undergo a SET with bromo malonates to form radical intermediate **I** (Scheme 3, right). Once radical intermediate **I** or **II** was formed by some of these mechanisms,[27] the enamine could trap the intermediate (**I** or **II**) as described in step 3 of Scheme 2.

To distinguish which of the initiation mechanisms from the three different pathways was applicable, and to elucidate the role of the thioxanthone in our catalytic system, we studied the α-alkylation of hydrocinnamaldehyde using three different catalysts, **4e–g** (Scheme 4). We chose diethyl bromomalonate as the reagent to eliminate the EDA complex type mechanism because this requires an electron deficient bromobenzyl (equation b, Scheme 3). Catalyst **4f** was chosen because it has an aromatic substituent with a steric hindrance around the secondary amine active center similar to that of our bifunctional catalyst (**4c**), but without the thioxanthone moiety. The results obtained using **4f** will allow us to distinguish the role of the thioxanthone moiety in bifunctional catalyst **4c**. In addition, imidazolidinone catalyst **4e** and Jørgensen-Hayashi's catalyst (**4g**) were also studied for comparison with the mechanisms reported in the literature.[3,27] First, the reaction was performed in the presence of catalysts **4e–g**, without any external photocatalyst (Scheme 4). As Melchiorre reported,[25] Jørgensen-Hayashi catalyst **4g** and catalyst **4e** afforded alkylated product **7a**, with 100 and 41% conversion, respectively, caused by the photoexcitation of the intermediate enamine (Scheme 3, eq c). By contrast, catalyst **4f** did not produce any alkylated product. On the other hand, the addition of the ruthenium(II) complex as an external photocatalyst in combination with aminocatalyst **4e** or **4f** increased the level of formation of α-alkylated product **7a** up to 85 and 59%, respectively. These results indicate that the enamine formed upon condensation of catalyst **4f** and aldehyde **5a** cannot generate the alkyl radical (through a SET between the photoexcited enamine and the bromo derivative) and that the reaction needs an external photocatalyst to proceed.

DOI: 10.1021/acscatal.8b01331
ACS Catal. 2018, 8, 5928–5940

To obtain more information and to understand the differences in terms of the reactivity in the reaction conducted with catalysts **4e**−**g**, three different enamines [**4e-En**, **4f-En**, and **4g-En** (Figure 4)][28] were synthesized by condensation of

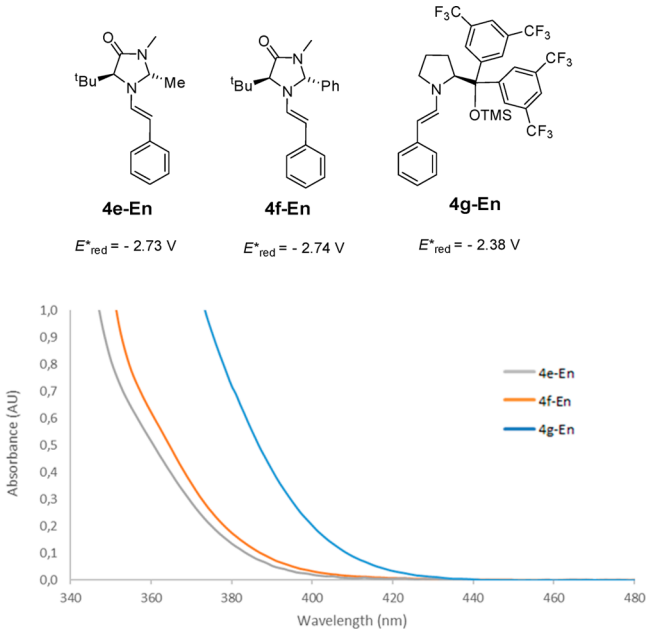

Figure 4. Spectroscopic and CV studies of enamines **4e-En**, **4f-En**, and **4g-En** (volts vs SCE in CH_3CN).

phenylacetaldehyde with the different aminocatalysts.[27] CV and UV−Vis spectra of the enamines were recorded, and the excited redox potentials of the enamines were calculated (see the Supporting Information and Figure 4). According to the excited reduction potential of the three enamines (E^*_{red} from −2.38 to −2.74 V vs SCE in CH_3CN), all should be able to reduce the diethyl bromomalonate (E_{red} = −1.0 V vs SCE in CH_3CN) without needing an external photocatalyst. The UV−Vis spectra of the enamines were also compared. Enamine **4g-En** derived from Jørgensen-Hayashi's catalyst has a significant absorption around 400 nm that guarantees the visible light absorption of the enamine, which can act as a photoinitiator and reduce bromomalonate **6a**. However, this cannot be the reason for the different behavior between enamines **4e-En** and **4f-En** because they have almost identical UV−Vis absorption spectra but a different reactivity (41 and <5% conversion, respectively). An additional factor must be involved in the null conversion realized in the case of catalyst **4f** (with a phenyl substituent). We think that in the case of catalyst **4f** the steric hindrance of the phenyl group is responsible for the lack of any initiation process needed to generate the alkyl radical from the bromo derivative through the direct photoexcitation of the enamine. The addition of an external photocatalyst in combination with **4f** overcomes the null contribution of the direct photoexcitation of the enamine, enabling the initiation step of the reaction and giving good conversion [59% (Scheme 4)]. Therefore, taking into account the fact that catalyst **4f** and bifunctional catalyst **4c** possess a similar steric hindrance around the secondary amine active center, we assumed that the thioxanthone group is responsible for any initiation step process in the case of bifunctional catalyst **4c**.

Catalyst Steric Effects in the Initiation Process. As described previously, the reaction under catalyst **4f** led to a null conversion whereas the alkylation took place with 100% conversion under catalyst **4c** (Scheme 4). Because we thought that the steric hindrance around the active center of the catalyst is the main factor responsible for the different observed reactivities, some additional experiments were performed. It is well-known that the SET process proceeds between two spatially close molecules (enamine and bromomalonate derivative), and therefore, the steric factor around the enamine must play an important role in the initiation process. With these ideas in mind, we synthesized a variety of imidazolidinone catalysts **4e**−**i** and performed the alkylation under the same reaction conditions (see Scheme 5).

First, we performed the reaction using each catalyst **4**, without the addition of an external photocatalyst, with the aim of identifying the effect of the steric hindrance of the intermediate enamine on the initiation process. With regard to the catalysts in the *trans* configuration, the conversions obtained using the different catalysts *trans*-**4** show that only the catalyst with the smallest substituent (methyl, *trans*-**4e**) can promote the initiation of the reaction by direct photoexcitation of the enamine. The *trans* disposition of the substituents shielded both faces of the enamine (Scheme 5), and as a consequence, the bulkiest catalysts (*trans*-**4f**, *trans*-**4h**, and *trans*-**4i**) inhibit the SET process from the enamine to bromo derivative **6a**. In these cases, the addition of $Ru(bpy)_3^{2+}$ as an external photocatalyst, responsible for the photoinitiation step process, overcame this inhibition and allowed the reaction to progress with all the catalysts except in the case of the bulkiest catalyst *trans*-**4i** and *cis*-**4i**, indicating that the corresponding enamines *trans*-**4i-En** and *cis*-**4i-En** were not formed. Furthermore, the enamine ratio (vs the secondary amine catalyst) was determined by ^1H NMR (in CD_3CN and DMF-d_7), showing that **4e-En** and **4f-En** are present in comparable quantities under the reaction conditions (see the Supporting Information). These results indicate that a different amount of the enamine intermediate cannot be responsible for the different activity observed for the two catalysts **4e** and **4f**, in the absence of an external photosensitizer. In addition, quenching studies with the two enamines (**4e-En** and **4f-En**) in the presence of diethyl bromomalonate were conducted. These latter studies showed that the Stern−Volmer constant value in the cases of **4e-En** is double than in the case of **4f-En** (see the Supporting Information). Moreover, a similar study was performed in DMF (under the same reaction conditions, concentration and solvent), yielding a negligible quenching of **4f-En**. By contrast, quenching of **4e-En** was observed, suggesting that a different behavior of the two catalysts under reaction conditions is taking place.

Conversely, it is well-known that enamines formed from imidazolidinones with substituents in the *cis* orientation have one of the faces unblocked (bottom of Scheme 5). Therefore, phenyl and cyclopropyl catalysts *cis*-**4f** and *cis*-**4h** were able to perform the α-alkylation of aldehydes even in the absence of an external photocatalyst because the enamine and the bromo derivative can come into closer proximity compared to the *trans* catalysts. Although the reactivity of catalysts *cis*-**4** was higher than that of the corresponding *trans*-**4**, their enantiomeric discrimination was poor, and for this reason, these *cis* catalysts are not usually employed in photoaminocatalysis.[3,7] To conclude this section, the initiation step under bifunctional catalyst **4c** proceeds toward the thioxanthone moiety and the electronic transfer between the enamine and the bromo derivative can be discarded.

Propagation Process and Quantum Yields. In the α-alkylation of aldehydes, Yoon[29] and Melchiorre[27] have shown that a chain propagation mechanism is involved in the reaction. According to these studies, the accepted mechanism of the alkylation of aldehyde is outlined in Scheme 6. Radical **I** is trapped by enamine

DOI: 10.1021/acscatal.8b01331
ACS Catal. 2018, 8, 5928−5940

Scheme 5. Effect of the Size and Disposition of the Catalyst Substituents in the α-Alkylation of Aldehydes

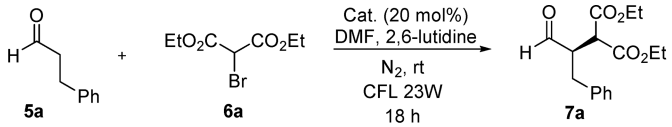

	trans-4e	trans-4f	trans-4h	trans-4i
Conv. (without photocat)	41%	<5%	0%	0%
Conv. (with [Ru])[a]	85%	59%	82%	0%
	cis-4f	**cis-4h**	**cis-4i**	
Conv. (without photocat)	25%	18%	0%	
Conv. (with [Ru])[a]	47%	80%	3%	

[a] 1 mol% of $Ru(bpy)_3^{2+}$ was added

Scheme 6. Accepted Radical Chain Propagation Process for the α-Alkylation of Aldehydes[27,29]

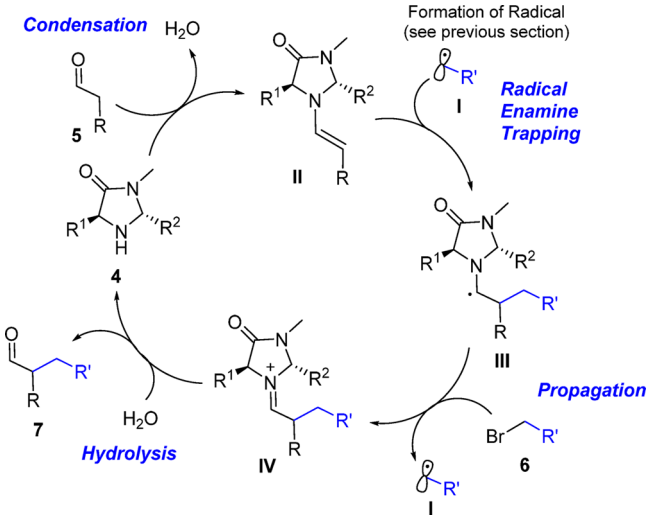

II to form α-amino radical **III** that can be oxidized by bromo derivative **6**. Next, the generated iminium ion **IV** is hydrolyzed to recover catalyst **4**. Therefore, the generation of additional radical species to react with **II**, via the initiation process, is unnecessary because propagation of the process can take place (**6** to **I**). Yoon and Melchiorre have demonstrated the propagation processes by quantum yield measurements (Φ). In Melchiorre's photocatalytic system, Jørgensen-Hayashi's catalyst presented a Φ of 18,[26] whereas Yoon reported that MacMillan's catalyst had a Φ of 22 in that photocatalytic system.[27]

To study the propagation process of our photocatalytic system, we measured the quantum yield of the overall reaction with bifunctional catalyst **4c**. Using our irradiation system, the quantum yield of catalysts **4g** and **4e** or **4f** with thioxanthone as the external photocatalyst was also determined (Figure 5). The quantum yields were measured by the ferrioxalate actinometer methodology, following the procedure described by the IUPAC.[30] A quantum yield of 9.2 was obtained in the reaction catalyzed by Jørgensen-Hayashi's catalyst (**4g**) under our irradiation system (Figure 5). This datum is lower than that reported by Melchiorre because of the different reaction and irradiation conditions but is in agreement with a self-propagation mechanism ($\Phi > 1$). For catalysts **4e** and **4f**, quantum yields of 5.6 and 4.4, respectively, were measured using thioxanthone as the external photocatalyst. By contrast, a quantum yield of 2.4 was obtained using our bifunctional catalyst **4c**. We think that the trend of these values indicates the level of accessibility of α-amino radical **III** by bromo derivative **6**. Indeed, the greatest quantum yield value ($\Phi = 9.2$) was observed for the less hindered intermediate **III** obtained employing catalyst **4g**, which has one of the faces of the pyrrolidine ring plane completely unblocked. On the other hand, the methyl substituent in catalyst **4e** is partially hindering one of the two faces, producing a quantum yield value of 5.6. The presence of a bulkier substituent like phenyl or thioxanthone decreased this value to 4.4 or 2.4, respectively, because of the additional steric hindrance present on one of the faces of the imidazolidinone ring plane, which is blocking the approach of bromo derivative **6** to α-amino radical **III**. This decrease in the overall quantum yield, in the case of our bifunctional catalyst **4c**, can also be attributed to the contribution of the internal redox process (the oxidation of the α-amino radical and the reduction of the radical cation thioxanthone; see intermediate **C** in step 4 of Scheme 2). Therefore, an additional SET between the thioxanthone group of catalyst **4c** and the bromo derivative to initiate the catalytic cycle is necessary (step 2 in Scheme 2), which leads to a further decrease in the observed quantum yield value.[31]

DOI: 10.1021/acscatal.8b01331
ACS Catal. 2018, 8, 5928−5940

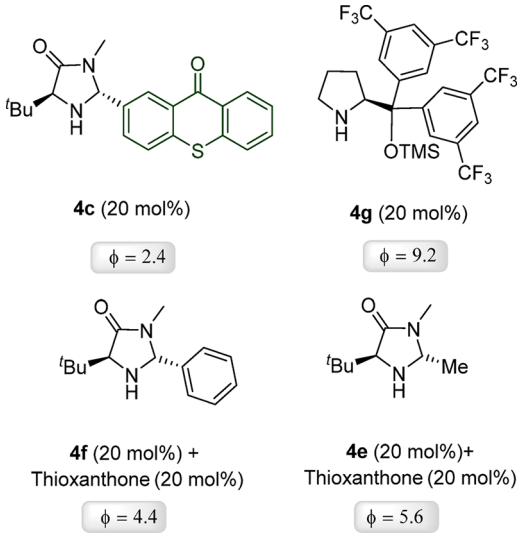

Figure 5. Overall quantum yield of the α-alkylation of hydrocinnamaldehyde with diethyl bromomalonate using different catalytic systems.

Laser Flash Photolysis Experiments. To gain further insight into the mechanism, laser flash photolysis (LFP) experiments were performed to investigate the excited state of bifunctional catalyst **4c** involved in the process, and its comparison with thioxanthone. The transient spectrum of thioxanthone in deoxygenated DMF shows an absorption maximum at 630 nm, which corresponds to the characteristic triplet−triplet band of thioxanthone.[32] Next, we focused our attention on the kinetic decays of both compounds at 630 nm (Figure 6). The decays of

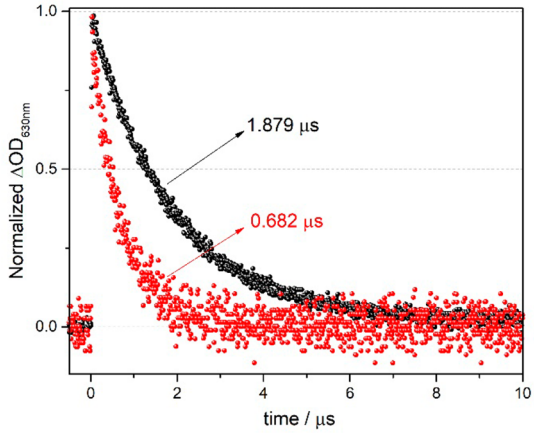

Figure 6. Normalized triplet decay traces of thioxanthone and catalyst **4c** at 630 nm (λ_{exc} = 385 nm).

catalyst **4c** and thioxanthone were markedly different, with triplet lifetime values (τ) being much higher for thioxanthone (1.879 μs) than for bifunctional photocatalyst **4c** (0.682 μs). Therefore, the triplet quenching rate constant (k_q) was determined to be 9.3×10^5 s^{-1}. These results can be explained on the basis of the photochemical studies of thioxanthones as photoinitiators in the polymerization of olefins.[13] In these studies, the thioxanthone triplet excited state is quenched by amines given the corresponding diradicals by an electro-transfer mechanism (Scheme 7). This intermediate could undergo decomposition via proton transfer from the amino radical to the ketone radical or back-electron transfer (BET) to the ground state. We have experimentally confirmed that the degradation of **4c** was negligible, confirming the rapid BET process. Similarly, a decrease in the fluorescence emission of the bifunctional catalyst compared to that of thioxanthone was also observed due to deactivation by the amino moiety (see the Supporting Information).

We then studied the effect of enamine formation on the decay of catalyst **4c**. As indirect proof, we subjected a solution of catalyst **4e** to LFP in the presence and absence of hydrocinnamaldehyde (Figure 7).[28] After the addition of the aldehyde, the solution was

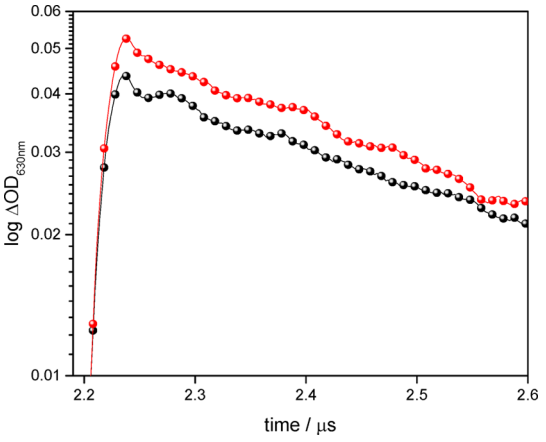

Figure 7. Temporal profiles of catalyst **4c** in deoxygenated DMF monitored at 630 nm (λ_{exc} = 385 nm) in the absence (black) and presence (red) of hydrocinnamaldehyde after stabilization for 20 min.

allowed to stabilize for 20 min. We observed an enhancement in the optical density monitored at 630 nm together with a longer temporal profile after enamine formation. These results seem to indicate that the formation of the enamine could retard the intramolecular electron-transfer process, increasing the amount of thioxanthone triplets. Moreover, the fluorescence of catalyst **4c** after the addition of increasing amounts of aldehyde showed a bathochromic shift and an enhancement of the maximum emission

Scheme 7. Deactivation Mechanism of Bifunctional Catalyst 4c

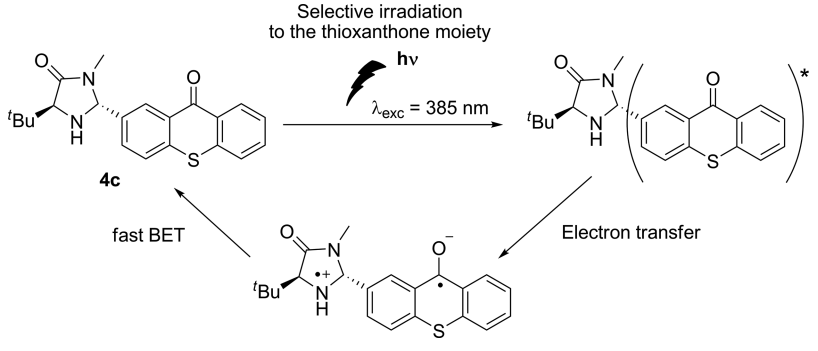

DOI: 10.1021/acscatal.8b01331
ACS Catal. 2018, 8, 5928−5940

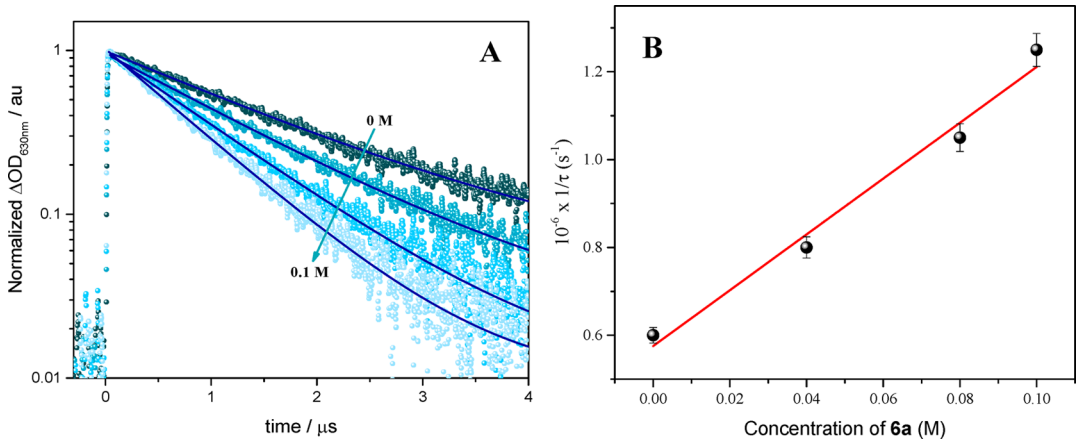

Figure 8. (A) Normalized decay traces of the T−T absorption of **4c** (0.1 mM in N_2/DMF; λ_{exc} = 385 nm) monitored at 630 nm in the presence of increasing amounts of diethyl bromomalonate (**6a**). The blue lines indicate the goodness of the lifetime measurement. (B) Plot of $1/\tau$ vs the concentration of **6a** to obtain $k_q(T_1)$. Experimental errors were <3% of the values obtained.

(see the Supporting Information for graphs). All these experiments demonstrate that the level of intramolecular quenching of the excited state (singlet or triplet) of the thioxanthone moiety by the amino group in the bifunctional catalyst is reduced after enamine formation.

All these experimental studies are in agreement with our TD DFT calculations. The calculations for the **En-4c** intermediate show a behavior similar to that of bifunctional catalyst **4c**, but in this case, the main electronic transitions are from the HOMO−1 orbitals mainly localized over the enamine moiety to LUMO in the thioxanthone (Figure 3). These studies also confirm the presence of a HOMO−LUMO transition in the visible range (484 nm) but with a low oscillation strength. The triplet state shows an energy value of 2.74 eV, which is the same as that of **4c**. In addition, a synergetic effect on the catalyst that leads to a photoinduced charge transfer from the enamine to the thioxanthone is observed, where the carbonyl group could play an important role.

Once it had been established that the enamine derivative (**4c-En**) was a relevant intermediate for the reaction mechanism, we performed quenching investigations to disclose the nature of the thioxanthone excited state involved in the photoinduced electron-transfer mechanism. Fluorescence studies of bifunctional catalyst **4c** in the presence of diethyl bromomalonate do not afford any change in the intensity or shape of the emission spectra (see the Supporting Information). In addition, the triplet decay at 630 nm, in the presence of increasing amounts of diethyl bromomalonate, revealed a dynamic quenching. The corresponding rate constant $k_q(T_1)$ was determined from the decay traces obtained for the T−T absorption of **4c** in the presence of increasing amounts of **6a** (Figure 8A). By plotting the reciprocal lifetime ($1/\tau$) against the concentration of **6a**, we obtained a linear relationship (Figure 8B). The slope of the straight line was 6.4 × 10^6 M^{-1} s^{-1}, which corresponds to $k_q(T_1)$ according to the equation $1/\tau = k_0 + k_q(T_1)[\mathbf{6a}]$. Furthermore, the end-of-pulse absorption in all measurements was clearly the same, being in complete agreement with the results of previously described emission experiments. In conclusion, the combination of fluorescence and LFP studies indicates that the electron-transfer process takes place from the triplet excited state of the thioxanthone moiety of bifunctional catalyst **4c**.

CONCLUSIONS

In this work, we have developed a new bifunctional photoaminocatalyst based on imidazolidinone and thioxanthone in a two-step synthesis, which allows an easy tuning of the steric properties. The photophysical and electrochemical data of the imidazolidinone photocatalyst have been determined, indicating that the catalyst can work under visible light conditions. Therefore, the alkylation of aldehydes with this photoaminocatalyst works with excellent enantioselectivities and yields due to the stereoelectronic properties of the catalyst. Laser flash photolysis experiments showed that the intramolecular quenching of the excited state (singlet or triplet) of the thioxanthone moiety by the amino group in the bifunctional catalyst is reduced after enamine formation. In addition, we have found that bifunctional catalyst **4c** possesses a quantum yield lower than those of other previous photocatalytic systems that can be attributed to the contribution of the internal redox process. Moreover, ground state geometry optimization and energy transition studies of thioxanthone and bifunctional catalyst **4c** were optimized by TD DFT calculations. A rational mechanistic cycle based on different mechanistic experiments, TD DFT calculations, and laser flash photolysis has also been presented.

ASSOCIATED CONTENT

Supporting Information

The Supporting Information is available free of charge on the ACS Publications website at DOI: 10.1021/acscatal.8b01331.

Experimental details, general procedures, optimization of reaction conditions, characterization of products, copies of NMR and HPLC spectra of all products, fluorescence studies, computational details, and theoretical results (PDF)
Crystallographic data (CIF)
Crystallographic data (CIF)

AUTHOR INFORMATION

Corresponding Author

*Departamento de Química Orgánica (Módulo 1), Facultad de Ciencias, Universidad Autónoma de Madrid, 28049 Madrid, Spain. E-mail: jose.aleman@uam.es.

ORCID

Silvia Cabrera: 0000-0002-4907-2932
Raúl Pérez-Ruiz: 0000-0003-1136-3598
Marta Liras: 0000-0002-1724-1586
Víctor A. de la Peña O'Shea: 0000-0001-5762-4787
José Alemán: 0000-0003-0164-1777

DOI: 10.1021/acscatal.8b01331
ACS Catal. 2018, 8, 5928−5940

Notes

The authors declare no competing financial interest.

■ ACKNOWLEDGMENTS

The Spanish Government (CTQ2015-64561-R) and the European Research Council (ERC-CG, Contract 647550) are acknowledged. The authors acknowledge the generous allocation of computing time at the CCC (UAM).

■ REFERENCES

(1) For recent selected reviews, see: (a) Prier, C. K.; Rankic, D. A.; MacMillan, D. W. C. Visible Light Photoredox Catalysis with Transition Metal Complexes: Applications in Organic Synthesis. *Chem. Rev.* **2013**, *113*, 5322−5363. (b) Skubi, K. L.; Blum, T. R.; Yoon, T. P. Dual Catalysis Strategies in Photochemical Synthesis. *Chem. Rev.* **2016**, *116*, 10035−10074. (c) Pitre, S. P.; McTiernan, C. D.; Scaiano, J. C. Library of Cationic Organic Dyes for Visible-Light-Driven Photoredox Transformations. *ACS Omega* **2016**, *1*, 66−76. (d) Romero, N. A.; Nicewicz, D. A. Organic Photoredox Catalysis. *Chem. Rev.* **2016**, *116*, 10075−10166. (e) Narayanam, J. M. R.; Stephenson, C. R. J. Visible light photoredox catalysis: applications in organic synthesis. *Chem. Soc. Rev.* **2011**, *40*, 102−113. (f) Ravelli, D.; Protti, S.; Fagnoni, M. Carbon−Carbon Bond Forming Reactions via Photogenerated Intermediates. *Chem. Rev.* **2016**, *116*, 9850−9913.

(2) Smith, H. D. In *Stereochemistry of Radical Reactions: Concepts, Guidelines, and Synthetic Applications*; Curran, D. P., Porter, N. A., Giese, B., Eds.; VCH: New York, 1996.

(3) For pioneering examples in dual asymmetric photo-organocatalytic systems, see: (a) Nicewicz, D. A.; MacMillan, D. W. C. Merging Photoredox Catalysis with Organocatalysis: The Direct Asymmetric Alkylation of Aldehydes. *Science* **2008**, *322*, 77−80. (b) Nagib, D. A.; Scott, M. E.; MacMillan, D. W. C. Enantioselective α-Trifluoromethylation of Aldehydes via Photoredox Organocatalysis. *J. Am. Chem. Soc.* **2009**, *131*, 10875−10877. (c) Shih, H.-W.; Vander Wal, M. N.; Grange, R. L.; MacMillan, D. W. C. Enantioselective α-Benzylation of Aldehydes via Photoredox Organocatalysis. *J. Am. Chem. Soc.* **2010**, *132*, 13600−13603. (d) Welin, E. R.; Warkentin, A. A.; Conrad, J. C.; MacMillan, D. W. C. Enantioselective α-Alkylation of Aldehydes by Photoredox Organocatalysis: Rapid Access to Pharmacophore Fragments from β-Cyanoaldehydes. *Angew. Chem., Int. Ed.* **2015**, *54*, 9668−9672. (e) Capacci, A. G.; Malinowski, J. T.; McAlpine, N. J.; Kuhne, J.; MacMillan, D. W. C. Direct, enantioselective α-alkylation of aldehydes using simple olefins. *Nat. Chem.* **2017**, *9*, 1073−1077.

(4) Bauer, A.; Westkamper, F.; Grimme, S.; Bach, T. Catalytic enantioselective reactions driven by photoinduced electron transfer. *Nature* **2005**, *436*, 1139−1140.

(5) Ding, W.; Lu, L.-Q.; Zhou, Q.-Q.; Wei, Y.; Chen, J.-R.; Xiao, W.-J. Bifunctional Photocatalysts for Enantioselective Aerobic Oxidation of β-Ketoesters. *J. Am. Chem. Soc.* **2017**, *139*, 63−66.

(6) (a) Huo, H.; Shen, X.; Wang, C.; Zhang, L.; Rose, P.; Chen, L.-A.; Harms, K.; Marsch, M.; Hilt, G.; Meggers, E. Asymmetric photoredox transition-metal catalysis activated by visible light. *Nature* **2014**, *515*, 100−103. (b) Ma, J.; Rosales, A. R.; Huang, X.; Harms, K.; Riedel, R.; Wiest, O.; Meggers, E. Visible-Light-Activated Asymmetric β-C−H Functionalization of Acceptor-Substituted Ketones with 1,2-Dicarbonyl Compounds. *J. Am. Chem. Soc.* **2017**, *139*, 17245−17248. (c) Meggers, E. Exploiting Octahedral Stereocenters: From Enzyme Inhibition to Asymmetric Photoredox Catalysis. *Angew. Chem., Int. Ed.* **2017**, *56*, 5668−5675.

(7) For a review of enantioselective photofunctionalization of aldehydes and ketones, see: Zou, Y.-Q.; Hörmann, F. M.; Bach, T. Iminium and enamine catalysis in enantioselective photochemical reactions. *Chem. Soc. Rev.* **2018**, *47*, 278−290.

(8) Gualandi, A.; Marchini, M.; Mengozzi, L.; Natali, M.; Lucarini, M.; Ceroni, P.; Cozzi, P. G. Organocatalytic Enantioselective Alkylation of Aldehydes with $[Fe(bpy)_3]Br_2$ Catalyst and Visible Light. *ACS Catal.* **2015**, *5*, 5927−5931.

(9) (a) Riente, P.; Matas Adams, M.; Albero, J.; Palomares, E.; Pericàs, M. A. Light-driven organocatalysis using inexpensive, nontoxic Bi_2O_3 as the photocatalyst. *Angew. Chem., Int. Ed.* **2014**, *53*, 9613−9616. (b) Cherevatskaya, M.; Neumann, M.; Füldner, S.; Harlander, C.; Kümmel, S.; Dankesreiter, S.; Pfitzner, A.; Zeitler, K.; König, B. Visible-Light-Promoted Stereoselective Alkylation by Combining Heterogeneous Photocatalysis with Organocatalysis. *Angew. Chem., Int. Ed.* **2012**, *51*, 4062−4066.

(10) Neumann, M.; Füldner, S.; König, B.; Zeitler, K. Metal-free, cooperative asymmetric organophotoredox catalysis with visible light. *Angew. Chem., Int. Ed.* **2011**, *50*, 951−954.

(11) Fidaly, K.; Ceballos, C.; Falguières, A.; Sylla-Iyarreta Veitia, M.; Guy, A.; Ferroud, C. Visible light photoredox organocatalysis: a fully transition metal-free direct asymmetric α-alkylation of aldehydes. *Green Chem.* **2012**, *14*, 1293−1297.

(12) For some contributions of our group in the field of bifunctional organocatalysts, see: (a) Jarava-Barrera, C.; Esteban, F.; Navarro-Ranninger, C.; Parra, A.; Alemán, J. Asymmetric synthesis of trans-dihydroarylfurans in a Friedel−Crafts/substitution domino reaction under squaramide catalysis. *Chem. Commun.* **2013**, *49*, 2001−2003. (b) Parra, A.; Alfaro, R.; Marzo, L.; Moreno-Carrasco, A.; García Ruano, J. L.; Alemán, J. Enantioselective aza-Henry reactions of cyclic α-carbonyl ketimines under bifunctional catalysis. *Chem. Commun.* **2012**, *48*, 9759−9761. (c) Marcos, V.; Alemán, J.; García Ruano, J. L.; Marini, F.; Tiecco, M. Asymmetric Synthesis of α-Alkyl α-Selenocarbonyl Compounds Catalyzed by Bifunctional Organocatalysts. *Org. Lett.* **2011**, *13*, 3052−3055. (d) Frías, M.; Mas-Balleste, R.; Arias, S.; Alvarado, C.; Alemán, J. Asymmetric Synthesis of Rauhut−Currier type Products by a Regioselective Mukaiyama Reaction under Bifunctional Catalysis. *J. Am. Chem. Soc.* **2017**, *139*, 672−679. (e) Frias, M.; Carrasco, A. C.; Fraile, A.; Alemán, J. A General Asymmetric Formal Synthesis of Aza-Baylis−Hillman Type Products under Bifunctional Catalysis. *Chem. - Eur. J.* **2018**, *24*, 3117−3121. (f) Esteban, F.; Cieślik, W.; Arpa, E. M.; Guerrero-Corella, A.; Díaz-Tendero, S.; Perles, J.; Fernández-Salas, J. A.; Fraile, A.; Alemán, J. Intramolecular Hydrogen Bond Activation: Thiourea-Organocatalyzed Enantioselective 1,3-Dipolar Cycloaddition of Salicylaldehyde-Derived Azomethine Ylides with Nitroalkenes. *ACS Catal.* **2018**, *8*, 1884−1890.

(13) Dadashi-Silab, S.; Aydogan, C.; Yagci, Y. Shining a light on an adaptable photoinitiator: advances in photopolymerizations initiated by thioxanthones. *Polym. Chem.* **2015**, *6*, 6595−6615.

(14) Tripathi, C. B.; Ohtani, T.; Corbett, M. T.; Ooi, T. Photoredox ketone catalysis for the direct C−H imidation and acyloxylation of arenes. *Chem. Sci.* **2017**, *8*, 5622−5627.

(15) For selected examples, see: (a) Tröster, A.; Alonso, R.; Bauer, A.; Bach, T. Enantioselective Intermolecular [2 + 2] Photocycloaddition Reactions of 2(1H)-Quinolones Induced by Visible Light Irradiation. *J. Am. Chem. Soc.* **2016**, *138*, 7808−7811. (b) Mayr, F.; Brimioulle, R.; Bach, T. A Chiral Thiourea as a Template for Enantioselective Intramolecular [2 + 2] Photocycloaddition Reactions. *J. Org. Chem.* **2016**, *81*, 6965−6971. (c) Alonso, R.; Bach, T. A chiral thioxanthone as an organocatalyst for enantioselective [2 + 2] photocycloaddition reactions induced by visible light. *Angew. Chem., Int. Ed.* **2014**, *53*, 4368−4371.

(16) Neumann, M. G.; Gehlen, M. H.; Encinas, M. V.; Allen, N. S.; Corrales, T.; Peinado, C.; Catalina, F. Photophysics and photoreactivity of substituted thioxanthones. *J. Chem. Soc., Faraday Trans.* **1997**, *93*, 1517−1521.

(17) (a) Wöll, D.; Smirnova, J.; Galetskaya, M.; Prykota, T.; Bühler, J.; Stengele, K.-P.; Pfleiderer, W.; Steiner, U. E. Intramolecular sensitization of photocleavage of the photolabile 2-(2-nitrophenyl)-propoxycarbonyl (NPPOC) protecting group: photoproducts and photokinetics of the release of nucleosides. *Chem. - Eur. J.* **2008**, *14*, 6490−6497. (b) Harwood, J. S.; Marynick, D. S.; Ternay, A. L., Jr Nuclear magnetic resonance spectra of heterocycles. Analysis of carbon-13 spectra of thioxanthenones using calculated chemical shifts, substituent constants, and PRDDO molecular-orbital calculations. *J. Chem. Soc., Perkin Trans. 2* **1989**, *4*, 325−330.

DOI: 10.1021/acscatal.8b01331
ACS Catal. 2018, 8, 5928−5940

(18) CCDC 1819092 and CCDC 1819093 contain the crystallographic data of compounds **4b** and **4c**, respectively. These data can be obtained free of charge from The Cambridge Crystallographic Data Centre viawww.ccdc.cam.ac.uk/data_request/cif.
(19) Mundt, R.; Villnow, T.; Torres Ziegenbein, Ch.; Gilch, P.; Marian, Ch.; Rai-Constapel, V. Thioxanthone in apolar solvents: ultrafast internal conversion precedes fast intersystem crossing. *Phys. Chem. Chem. Phys.* **2016**, *18*, 6637−6647.
(20) Rai-Constapel, V.; Villnow, T.; Ryseck, G.; Gilch, P.; Marian, C. M. Chimeric Behavior of Excited Thioxanthone in Protic Solvents: II. Theory. *J. Phys. Chem. A* **2014**, *118*, 11708−11717.
(21) Rubio-Pons, Ò.; Serrano-Andrés, L.; Burget, D.; Jacques, P. A butterfly like motion as a clue to the photophysics of thioxanthone. *J. Photochem. Photobiol., A* **2006**, *179*, 298−304.
(22) Rai-Constapel, V.; Kleinschmidt, M.; Salzmann, S.; Serrano-Andres, L.; Marian, C. M. Thioxanthone: on the shape of the first absorption band. *Phys. Chem. Chem. Phys.* **2010**, *12*, 9320−9327.
(23) Ishijima, S.; Higashi, M.; Yamaguchi, H. Magnetic Circular Dichroism and Circular Dichroism Spectra of Xanthones. *J. Phys. Chem.* **1994**, *98*, 10432−10435.
(24) Herkstroeter, W. G.; Lamola, A. A.; Hammond, G. S. Mechanisms of photochemical reactions in solution XXVIII. Values of triplet excitation energies of selected sensitizers. *J. Am. Chem. Soc.* **1964**, *86*, 4537−4540.
(25) For EDA complexes, see: Arceo, E.; Jurberg, I. D.; Álvarez-Fernández, A.; Melchiorre, P. Photochemical activity of a key donor−acceptor complex can drive stereoselective catalytic α-alkylation of aldehydes. *Nat. Chem.* **2013**, *5*, 750−756.
(26) For the visible light absorption of the enamine, see: Silvi, M.; Arceo, E.; Jurberg, I. D.; Cassani, C.; Melchiorre, P. Enantioselective Organocatalytic Alkylation of Aldehydes and Enals Driven by the Direct Photoexcitation of Enamines. *J. Am. Chem. Soc.* **2015**, *137*, 6120−6123.
(27) For a completed studied in the alkylation of enamines with the Jorgensen-Hayashi catalyst, see: Bahamonde, A.; Melchiorre, P. Mechanism of the Stereoselective α-Alkylation of Aldehydes Driven by the Photochemical Activity of Enamines. *J. Am. Chem. Soc.* **2016**, *138*, 8019−8030.
(28) We have tried several conditions for the synthesis of **En-4c**, in all cases with unfruitful results.
(29) Cismesia, M. A.; Yoon, T. P. Characterizing chain processes in visible light photoredox catalysis. *Chem. Sci.* **2015**, *6*, 5426−5434.
(30) Kuhn, H. J.; Braslavsky, S. E.; Schmidt, R. Name and symbol of the element with atomic number 111. *Pure Appl. Chem.* **2004**, *76*, 2105−2146.
(31) To determine the thermodynamic feasibility of radical chain pathways in our photocatalytic system, DFT calculations of **En-4c** were performed (propagation step in Scheme 5). Oxidation of the resultant radical intermediate (intermediate III in Scheme 5) occurs by an exergonic process, leading to an enamine cation (intermediate IV in Scheme 5). See the Supporting Information for further details.
(32) Karasu, F.; Arsu, N.; Jockusch, S.; Turro, N. J. Mechanistic Studies of Photoinitiated Free Radical Polymerization Using a Bifunctional Thioxanthone Acetic Acid Derivative as Photoinitiator. *Macromolecules* **2009**, *42*, 7318.

DOI: 10.1021/acscatal.8b01331
ACS Catal. 2018, 8, 5928−5940

Experimental Part
Chapter 3

(The complete “Supporting Information” documents, with all the characterization data, NMR spectra, SFC or HPLC traces and other experimental procedures have been included in the enclosed USB memory)

General procedure for the α-alkylation of aldehydes

An oven-dried 10 mL vial equipped with a magnetic stir bar was charged with catalyst **4c** (0.024 mmol), the corresponding bromide **6** (0.12 mmol) and the corresponding aldehyde **5** (0.24 mmol or 0.60 mmol in the indicated cases). Then, 0.24 mL of anhydrous DMF (or 0.12 mL of DMSO) were added, followed by 2,6-lutidine (0.24 mmol). The vial was closed with a PTFE/rubber septum and the reaction mixture was degassed by three cycles of "freeze-pump-thaw". Then the vial was placed approximately 5 cm away from a 23 W compact fluorescent light (CFL) bulb and the reaction mixture was stirred at room temperature (20°C). After the reaction was complete, the solvent was eliminated under reduced pressure and the crude mixture was purified by flash chromatography to afford the corresponding α-alkylated aldehyde **7**. For the determination of the enantiomeric excess the crude aldehyde **7** was derivatized through a Wittig reaction. After the elimination of the solvent from the reaction mixture, 4 equivalents of benzyl(triphenylphosphoranylidene)acetate and 1 mL of DCM were added, then the vial was closed and the mixture was stirred at reflux until complete conversion. Finally, the crude mixture was purified by flash chromatography to afford the corresponding pure product which was analyzed by SFC on chiral columns.

Characterization data for the alpha-alkylated compounds (7)

(*R*)-Diethyl 2-(1-oxo-3-phenylpropan-2-yl)malonate (7a)[19]

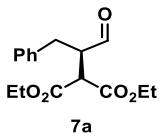

7a

7a was prepared according to the general procedure and purified by flash chromatography (CyHex : EtOAc = 9 : 1) to obtain 34.7 mg of the α-alkylated aldehyde **7a** as a colorless oil (99% yield). The enantiomeric excess was determined by SFC on a *Daicel Chiralpak* IA column after the above described derivatization: CO_2/MeOH 95:5, flow rate 2.0 mL/min, λ = 210 nm, τ_{major} = 5.57 min, τ_{minor} = 6.07 (>99% ee). This compound has been previously described in the literature.[19]

^{1}H NMR ($CDCl_3$): δ 9.78 (s, 1H), 7.35 – 7.17 (m, 5H), 4.26 – 4.15 (m, 4H), 3.68 (d, *J* = 7.0 Hz, 1H), 3.39 (q, *J* = 7.3 Hz, 1H), 3.12 (dd, *J* = 14.2, 7.5 Hz, 1H), 2.83 (dd, *J* = 14.2, 7.3 Hz, 1H), 1.27 (t, *J* = 7.1 Hz, 6H).

(*R*)-Diethyl 2-methyl-2-(1-oxo-3-phenylpropan-2-yl)malonate (7b)

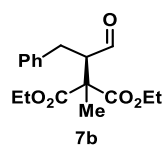

7b

7b was prepared according to the general procedure and purified by flash chromatography (CyHex : EtOAc = 9 : 1) to obtain 10.8 mg of the α-alkylated aldehyde **7b** as a colorless oil (98% yield based on a 30% conversion by ^{1}H NMR). The enantiomeric excess was determined by SFC on a *Daicel Chiralpak* IG-3 column after the

above described derivatization: CO_2/MeOH 90:10, flow rate 3.0 mL/min, λ = 210 nm, τ_{major} = 1.43 min, τ_{minor} = 1.64 min (97% ee).

^{1}H NMR ($CDCl_3$): δ 9.73 (d, *J* = 1.3 Hz, 1H), 7.33-7.16 (m, 5H), 4.13-4.25 (m, 4H), 3.46 (ddd, *J* = 10.2, 3.7, 1.4 Hz, 1H), 3.04 (dd, *J* = 14.1, 10.1 Hz, 1H), 2.74 (dd, *J* = 14.1, 3.6 Hz, 1H), 1.56 (s, 3H), 1.30-1.22 (m, 6H).

^{13}C NMR ($CDCl_3$): δ 201.5, 170.8, 139.0, 129.2, 128.7, 126.7, 62.1, 56.7, 56.3, 32.0, 18.1, 14.1 (2C).

HRMS (ESI): calculated for $C_{17}H_{23}O_5^+$, $[M+H]^+$ = 307.1540; found = 307.1527.

(*R*)-3-Benzyl-4-oxobutanenitrile (7c)[123c]

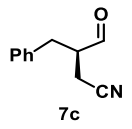

7c

7c was prepared according to the general procedure employing 5 equiv of aldehyde **5a** and DMSO as the solvent. The crude mixture was purified by flash chromatography (CyHex : EtOAc = 9 : 1) to obtain 17.0 mg of the α-alkylated aldehyde **7c** as a colorless oil (82% yield). The enantiomeric excess was determined by SFC on a *Daicel Chiralpak* IG-3 column after the above described derivatization: CO_2/MeOH 90:10, flow rate 3.0 mL/min, λ = 210 nm, τ_{minor} = 4.33 min, τ_{major} = 5.20 min (97% ee). This compound has been previously described in the literature.[123c]

^{1}H NMR ($CDCl_3$)**:** δ 9.77 (s, 1H), 7.46 – 7.13 (m, 5H), 3.26 – 3.14 (m, 1H), 3.05 – 2.94 (m, 2H), 2.53 (dd, *J* = 17.2, 5.6 Hz, 1H), 2.44 (dd, *J* = 16.9, 5.8 Hz, 1H).

(*R*)-3-Benzyl-2-(diethoxymethyl)-4-oxobutanenitrile (7d)

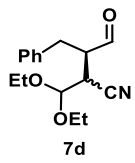

7d

7d was prepared according to the general procedure employing 5 equiv of aldehyde **5a** and DMSO as the solvent. The crude mixture was purified by flash chromatography (CyHex : EtOAc = 9 : 1) to obtain 30.4 mg of the α-alkylated aldehyde **7d** (*dr* 2:1) as a colorless oil (92% combined yield). The enantiomeric excess was determined by SFC on a *Daicel Chiralpak* IG-3 column after the above described derivatization.

Major diastereoisomer: CO_2/MeOH 95:5, flow rate 3.0 mL/min, λ = 210 nm, τ_{major} = 3.38 min, τ_{minor} = 3.87 min (99% ee).

Minor diastereoisomer: CO_2/MeOH 95:5, flow rate 3.0 mL/min, λ = 210 nm, τ_{minor} = 2.60 min, τ_{major} = 2.82 min (96% ee).

(*mix of diastereoisomers, dr = 2:1*)

^{1}H NMR ($CDCl_3$): δ 9.76 (d, *J* = 2.0 Hz, 1H, *minor*), 9.60 (d, *J* = 0.7 Hz, 1H, *major*), 7.37-7.19 (m, 5H), 4.75 (d, *J* = 6.0 Hz, 1H, *minor*), 4.45 (d, *J* = 5.9 Hz, 1H, *major*), 3.75 – 2.83 (m, 8H), 1.26 – 1.12 (m, 6H).

^{13}C NMR ($CDCl_3$): δ 200.0 (*major*), 199.9 (*minor*), 136.9 (*major*), 136.8 (*minor*), 129.3 (*major*), 129.2 (*minor*), 129.1 (*minor*), 129.0 (*major*), 127.4 (*major*), 127.3 (*minor*), 117.6 (*major*), 117.2 (*minor*), 100.3 (*minor*), 100.1 (*major*), 65.0 (*minor*), 64.3 (2C, *major*), 63.8 (*minor*), 50.4 (*minor*), 50.2 (*major*), 37.0 (*major*), 36.9 (*minor*), 34.2 (*major*), 33.5 (*minor*), 15.2 (*minor*), 15.1 (*major*).

HRMS (ESI): calculated for $C_{16}H_{25}N_2O_3^+$, $[M+NH_4]^+$ = 293.1860; found = 293.1871.

(*R*)-2-Benzyl-4-oxo-4-phenylbutanal (7e)[128b]

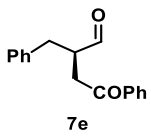

7e

7e was prepared according to the general procedure and purified by flash chromatography (CyHex : EtOAc = 9 : 1) to obtain 23.9 mg of the α-alkylated aldehyde **7e** as a colorless oil (79% yield). The enantiomeric excess was determined by SFC on a *Daicel Chiralpak* IG-3 column after the above described derivatization: CO_2/MeOH 85:15, flow rate 3.0 mL/ min, λ = 210 nm, τ_{minor} = 9.67 min, τ_{major} = 19.07 min (90% ee). This compound has been previously described in the literature.[128b]

^{1}H NMR ($CDCl_3$): δ 9.90 (s, 1H), 7.96 – 7.87 (m, 2H), 7.60 – 7.53 (m, 1H), 7.49 – 7.41 (m, 2H), 7.34 – 7.17 (m, 5H), 3.49 – 3.35 (m, 2H), 3.23 – 3.13 (m, 1H), 3.07 – 2.96 (m, 1H), 2.88 – 2.78 (m, 1H).

(*R*)-2-Benzyl-4-(4-methoxyphenyl)-4-oxobutanal (7f)

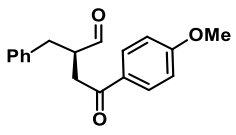

7f

7f was prepared according to the general procedure and purified by flash chromatography (CyHex : EtOAc = 9 : 1) to obtain 28.8 mg of the α-alkylated aldehyde **7f** as a colorless oil (85% yield). The enantiomeric excess was determined by SFC on a *Daicel Chiralpak* ID column after the above described derivatization: CO_2/MeOH 90:10, flow rate 3.0 mL/ min, λ = 210 nm, τ_{major} = 14.77 min, τ_{minor} = 17.66 min (95% ee).

^{1}H NMR ($CDCl_3$): δ 9.90 (bs, 1H), 7.89 (d, *J* = 8.9 Hz, 2H), 7.34-7.16 (m, 5H), 6.91 (d, *J* = 8.9 Hz, 2H), 3.86 (s, 3H), 3.43-3.30 (m, 2H), 3.16 (dd, *J* = 13.9, 6.0 Hz, 1H), 3.06-2.92 (m, 1H), 2.82 (dd, *J* = 14.0, 7.5 Hz, 1H).

^{13}C NMR ($CDCl_3$): δ 203.4, 196.4, 163.8, 138.4, 130.5, 129.7, 129.2, 128.8, 126.8, 113.9, 55.6, 48.6, 37.1, 34.9.

HRMS (ESI): calculated for $C_{18}H_{19}O_3^+$, $[M+H]^+$ = 283.1329; found = 283.1338.

(*R*)-2-Benzyl-4-(4-nitrophenyl)-4-oxobutanal (7g)

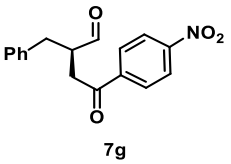

7g

7g was prepared according to the general procedure and purified by flash chromatography (CyHex : EtOAc = 9 : 1) to obtain 30.3 mg of the α-alkylated aldehyde **7g** as a low-melting yellow solid (73% yield). The enantiomeric excess was determined by SFC on a *Daicel Chiralpak* IB column after the above described derivatization: CO_2/MeOH 90:10, flow rate 3.0 mL/ min, λ = 210 nm, τ_{minor} = 11.53 min , τ_{major} = 12.26 min (84% ee).

^{1}H NMR ($CDCl_3$): δ 9.89 (bs, 1H), 8.31-8.25 (m, 2H), 8.07-8.01 (m, 2H), 7.35-7.17 (m, 5H), 3.50-3.38 (m, 2H), 3.21 (dd, *J* = 14.0, 5.9 Hz, 1H), 3.00-2.79 (m, 2H).

^{13}C NMR ($CDCl_3$): δ 202.4, 196.7, 150.6, 141.1, 137.8, 129.2, 129.1, 129.0, 127.1, 124.0, 48.7, 37.5, 34.7.

HRMS (ESI): calculated for $C_{17}H_{15}NO_4^+$, $[M]^+$ = 297.0996; found = 297.0966.

(*R*)-2-Benzyl-3-(2,4-dinitrophenyl)propanal (7h)

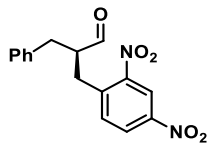

7h

7h was prepared according to the general procedure employing DMSO (1M) as the solvent. The crude mixture was purified by flash chromatography (CyHex : EtOAc = 9 : 1) to obtain 25.1 mg of the α-alkylated aldehyde **7h** as a yellow oil (61% yield). The enantiomeric excess was determined by SFC on a *Daicel Chiralpak* IC column after the above described derivatization: CO_2/MeOH 90:10, flow rate 3.0 mL/min, λ = 210 nm, τ_{minor} = 7.50 min, τ_{major} = 8.54 min (97% ee).

^{1}H NMR ($CDCl_3$): δ 9.70 (d, *J* = 1.1 Hz, 1H), 8.77 (d, *J* = 2.4 Hz, 1H), 8.30 (dd, *J* = 8.5, 2.4 Hz, 1H), 7.57 (d, *J* = 8.6 Hz, 1H), 7.36-7.15 (m, 5H), 3.45-3.33 (m, 1H), 3.23-3.05 (m, 3H), 2.99-2.87 (m, 1H).

^{13}C NMR ($CDCl_3$): δ 202.2, 149.3, 146.8, 141.8, 137.1, 134.8, 129.1, 129.0, 127.2, 126.9, 120.6, 53.9, 36.3, 32.1.

HRMS (ESI): calculated for $C_{16}H_{18}N_3O_5^+$, $[M+NH_4]^+$ = 332.1241; found = 332.1240.

(*R*)-Diethyl 2-(1-oxooctan-2-yl)malonate (7i)[19]

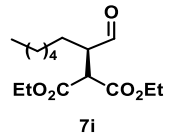

7i

7i was prepared according to the general procedure and purified by flash chromatography (CyHex : EtOAc = 9 : 1) to obtain 27.8 mg of the α-alkylated aldehyde **7i** as a colorless oil (81% yield). The enantiomeric excess was determined by SFC on a *Daicel Chiralpak* IC column after the above described derivatization: CO_2/MeOH gradient from 98:2 to 95:5 in 30 min, flow rate 2.0 mL/min, λ = 210 nm, τ_{minor} = 17.89 min, τ_{major} = 18.29 min (96% ee). This compound has been previously described in the literature.[19]

^{1}H NMR ($CDCl_3$): δ 9.77 (s, 1H), 4.29 – 4.15 (m, 4H), 3.74 (d, *J* = 8.6 Hz, 1H), 3.16 – 3.07 (m, 1H), 1.78 – 1.52 (m, 2H), 1.43 – 1.20 (m, 14H), 0.92 – 0.83 (m, 3H).

(*R*)-Diethyl 2-(1-cyclohexyl-2-oxoethyl)malonate (7j)[19]

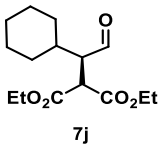

7j

7j was prepared according to the general procedure employing 5 equiv of aldehyde **5j** and purified by flash chromatography (CyHex : EtOAc = 9 : 1) to obtain 18.8 mg of the α-alkylated aldehyde **7j** as a colorless oil (55% yield). The enantiomeric excess was determined by SFC on a *Daicel Chiralpak* IC column after the above described derivatization: CO_2/MeOH 95:5, flow rate 2.0 mL/min, λ = 210 nm, τ_{minor} = 16.46 min, τ_{major} = 17.26 min (97% ee). This compound has been previously described in the literature.[19]

^{1}H NMR ($CDCl_3$): δ 9.84 (d, J = 1.4 Hz, 1H), 4.30 – 4.14 (m, 4H), 3.86 (d, *J* = 9.9 Hz, 1H), 3.16 (ddd, *J* = 9.8, 4.5, 1.5 Hz, 1H), 1.90 – 1.56 (m, 5H), 1.39 – 0.84 (m, 12H).

(2*R,Z*)-Diethyl 2-(1-oxonon-6-en-2-yl)malonate (7k)[19]

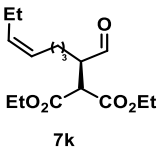

7k

7k was prepared according to the general procedure employing 5 equiv of aldehyde **5k** and purified by flash chromatography (CyHex : EtOAc = 9 : 1) to obtain 26.1 mg of the α-alkylated aldehyde **7k** as a colorless oil (73% yield). The enantiomeric excess was determined by SFC on a *Daicel Chiralpak* IC column after the above described derivatization: CO_2/MeOH gradient from 98:2 to 95:5 in 20 min, flow rate 2.0 mL/min, λ = 210 nm, τ_{minor} = 5.64 min, τ_{major} = 6.01 min (99 % ee). This compound has been previously described in the literature.[19]

^{1}H NMR ($CDCl_3$): δ 9.77 (d, *J* = 1.1 Hz, 1H), 5.45 – 5.34 (m, 1H), 5.32 – 5.19 (m, 1H), 4.28-4.15 (m, 4H), 3.73 (d, *J* = 8.5 Hz, 1H), 3.17 – 3.06 (m, 1H), 2.12 – 1.93 (m, 4H), 1.79 – 1.63 (m, 1H), 1.63 – 1.52 (m, 1H), 1.52 – 1.33 (m, 2H), 1.30 – 1.23 (m, 6H), 0.95 (t, *J* = 7.6 Hz, 3H).

(*R*)-Diethyl 2-(1-(1-(*tert*-butoxycarbonyl)piperidin-4-yl)-2-oxoethyl)malonate (7l)[19]

7l was prepared according to the general procedure employing 5 equiv of aldehyde **5l** and purified by flash chromatography (*n*-Hex : acetone = 4 : 1) to obtain 28.7 mg of the α-alkylated aldehyde **7l** as a colorless oil (62% yield). The enantiomeric excess was determined by SFC on a *Daicel Chiralpak* IC column after the above described derivatization: CO_2/MeOH 90:10, flow rate 3.0 mL/min, λ = 210 nm, τ_{minor} = 4.49 min , τ_{major} = 4.95 min (96% ee). This compound has been previously described in the literature.[19]

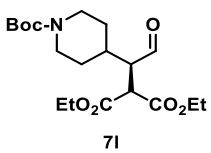

7l

^{1}H NMR ($CDCl_3$): δ 9.84 (d, *J* = 1.4 Hz, 1H), 4.30 – 4.04 (m, 6H), 3.84 (d, *J* = 9.0 Hz, 1H), 3.15 (ddd, *J* = 9.1, 5.0, 1.4 Hz, 1H), 2.72 – 2.53 (m, 2H), 1.91 – 1.56 (m, 3H), 1.48 – 1.39 (m, 11H), 1.30 – 1.24 (m, 6H).

Enantioselective [2+2] Photocycloaddition of Enones

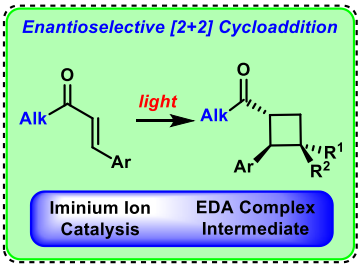

Chapter 4

4. Enantioselective [2+2] Photocycloaddition of Enones

4.1 Introduction to [2+2] Photocycloadditions

The [2+2] photocycloaddition is undoubtedly one of the most important photochemical reactions and, in the last decades, it has found widespread use in organic synthesis and for the preparation of natural products.[129] The unique features of this photochemical reaction, which enables the construction of multiple bonds in a single step, are allowing the access to uncommon reactivities and transformations that would be difficult to achieve by other conventional strategies. Moreover, in many cases, the simplicity of the required reaction partners is permitting the construction of carbocyclic compounds from common and commercially available precursors.

The first example of a sunlight-driven [2 + 2] photocycloaddition was reported by Liebermann in 1877, obtaining a photodimeric product from a *para*-quinone derivative (Scheme 70a).[130] In 1902, with a groundbreaking example, Ciamician reported the first intramolecular [2+2] photocycloaddition reaction, obtaining carvonecamphor from carvone upon sunlight exposure (Scheme 70b).[3a] Nevertheless, the first intermolecular photocycloadditions, obtained through the employment of an appropriate olefin as the reaction partner, were achieved more than half a century later by Schenck's,[131] Eaton's[132] and De Mayo's[133] research groups (Scheme 70c). In 1963, Corey's group employed for the first time an intermolecular [2 + 2] photocycloaddition as a key step in the total synthesis of caryophyllene (Scheme 70d).[134] Since then, a myriad of cyclobutanes have been synthetized, mainly through [2+2] photocycloaddition reactions, and they have been employed as useful building blocks in the synthesis of several natural products.[129]

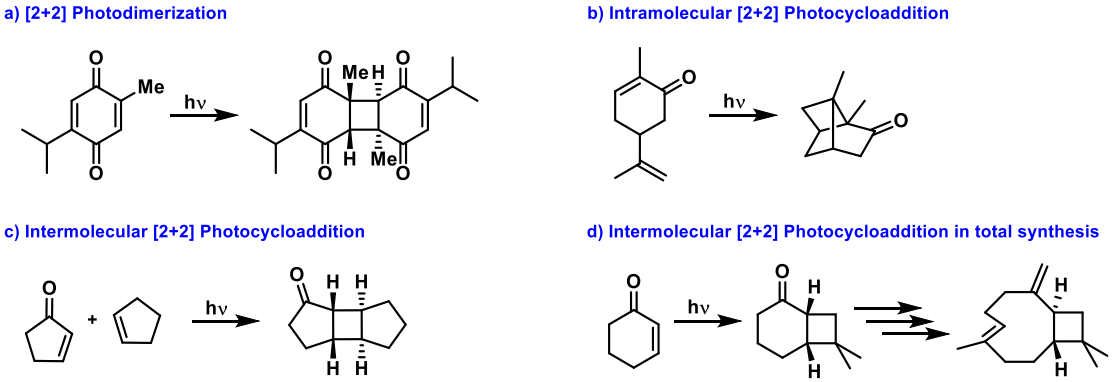

Scheme 70. Pioneering examples in [2+2] photocycloaddition reactions.

The regioselectivity of the [2+2] photocycloaddition of enones is determined by the electronic characteristics of the olefin that is employed as the reaction partner. Indeed, upon light absorption, the enone reaches an excited state that presents an umpolung of polarity in comparison with the ground state. As a consequence, the reaction of an enone and an olefin with an electron-donating or an electron-withdrawing group is leading to an opposite regioselectivity, affording the head-to-tail or the head-to-head product, respectively (Scheme 71).[129]

[129] S. Poplata, A. Tröster, Y.-Q. Zou, T. Bach, *Chem. Rev*. **2016**, *116*, 9748-9815.
[130] C. Liebermann, *Ber. Dtsch. Chem. Ges*. **1877**, *10*, 2177-2179.
[131] G. O. Schenck, W. Hartmann, S.-P. Mannsfeld, W. Metzner, C. H. Krauch, *Chem. Ber*. **1962**, *95*, 1642-1647.
[132] P. E. Eaton, *J. Am. Chem. Soc*. **1962**, *84*, 2454-2455.
[133] P. De Mayo, H. Takeshita, A. B. M. A. Sattar, *Proc. Chem. Soc.* **1962**, 119.
[134] E. J. Corey, R. B. Mitra, H. Uda, *J. Am. Chem. Soc.* **1963**, *85*, 362-363.

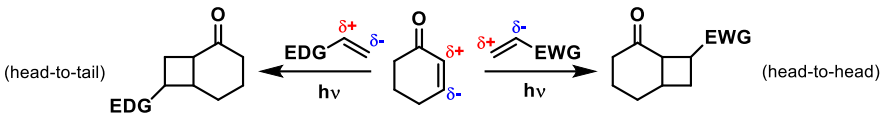

Scheme 71. Regioselectivity in the [2+2] photocycloaddition of enones with electronically different alkenes.

4.2 Enantioselective Strategies in [2+2] Photocycloadditions

In the last decades, an increasing interest in [2+2] photocycloadditions was aimed at the achievement of asymmetric photocatalytic strategies for the obtainment of enantioenriched cyclobutanes. A pioneering example of a highly enantioselective [2+2] photocycloaddition was reported by Bach's research group in 2009 (Scheme 72).[40] The employment of a xanthone organocatalyst allowed an efficient coordination of the quinolone substrate through hydrogen bonding interactions to give a catalyst-coordinated complex. The light-induced excitation of the xanthone chromophore leads, after ISC, to an excited triplet state that can efficiently photosensitize the substrate through a triplet energy transfer mechanism. Indeed, the triplet energy of the xanthone chromophore (E^T = 74 kcal/mol) is above the required value for an efficient triplet sensitization of the quinolone (E^T = 67 kcal/mol). Furthermore, the close spatial proximity of the chromophore to the coordinated substrate is leading to a preferential energy transfer between them in comparison with intermolecular triplet sensitization.

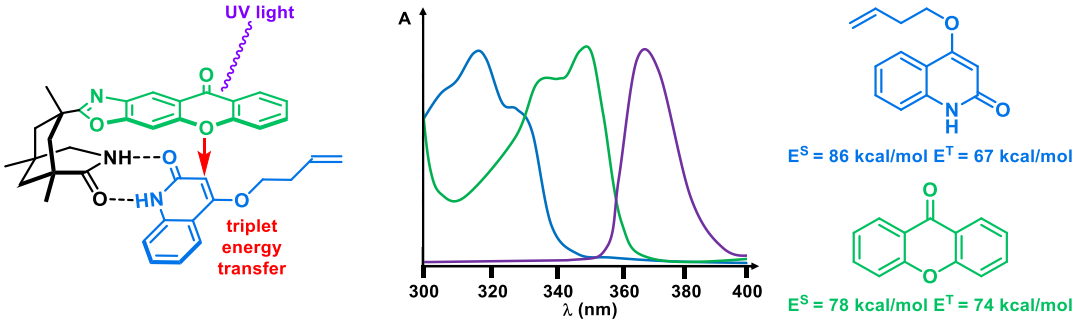

Scheme 72. Pioneering example of an enantioselective [2+2] photocycloaddition achieved by means of a triplet energy transfer.

A further development of this activation mode by Bach's group led to the synthesis of a thioxanthone catalyst, which permitted to carry out an analogous [2+2] photocycloaddition under visible light irradiation (Scheme 73).[62] Indeed, due to the enhanced absorption of the thioxanthone chromophore the asymmetric transformation has been achieved over alkyl quinolone derivatives at longer wavelengths. The lower triplet energy of these substrates, in comparison with 4-alkoxy substituted quinolones is allowing the efficient triplet sensitization of them by the thioxanthone moiety (E^T = 65 kcal/mol), affording the corresponding products in high enantioselectivity and yield.

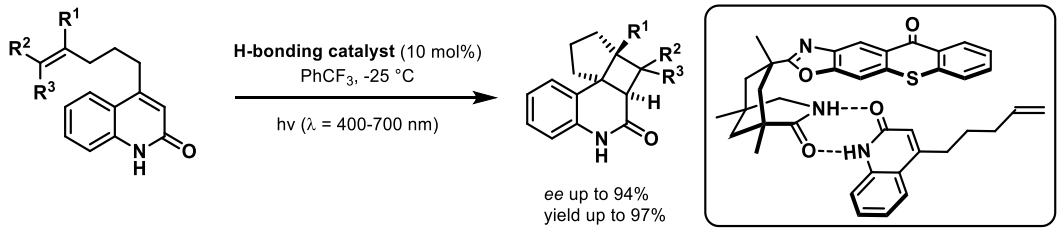

Scheme 73. Development of a visible light absorbing thioxanthone photocatalyst for enantioselective [2+2] photocycloadditions through a triplet energy transfer mechanism.

Another activation strategy in asymmetric [2+2] photocycloadditions was reported by Bach's research group through the employment of Lewis acid catalysis. In 2010, a highly enantioselective [2+2] of coumarins was achieved by means of an oxazaborolidine-mediated photocycloaddition (Scheme 74a).[63] Indeed, the background [2+2] photocycloaddition of coumarins is poorly efficient through direct irradiation of the substrate, due to rapid deactivation of its excited state. However, through the employment of an oxazaborolidine-based catalyst as the Lewis acid, the excited state lifetime is increased, as it is the overall ISC rate to the triplet excited active state, affording the desired enantioenriched products. The same strategy has been applied to the asymmetric [2+2] photocycloaddition of enones, leading to the corresponding products in high enantioselectivity, although with huge differences regarding the activation mechanism (Scheme 74b).[64,135] Indeed, in this case, a triplet excited state is involved even in the background reaction of the unbounded enone, which presents an higher ISC rate in comparison with the Lewis acid-substrate complex. Nevertheless, due to a strong bathochromic shift in the visible light region observed upon coordination, the Lewis acid-substrate complex can be selectively photoexcited with an appropriate irradiation source, avoiding any racemic background reaction. The synthetic value of this strategy has been highlighted through the accomplished enantioselective total synthesis of natural products.

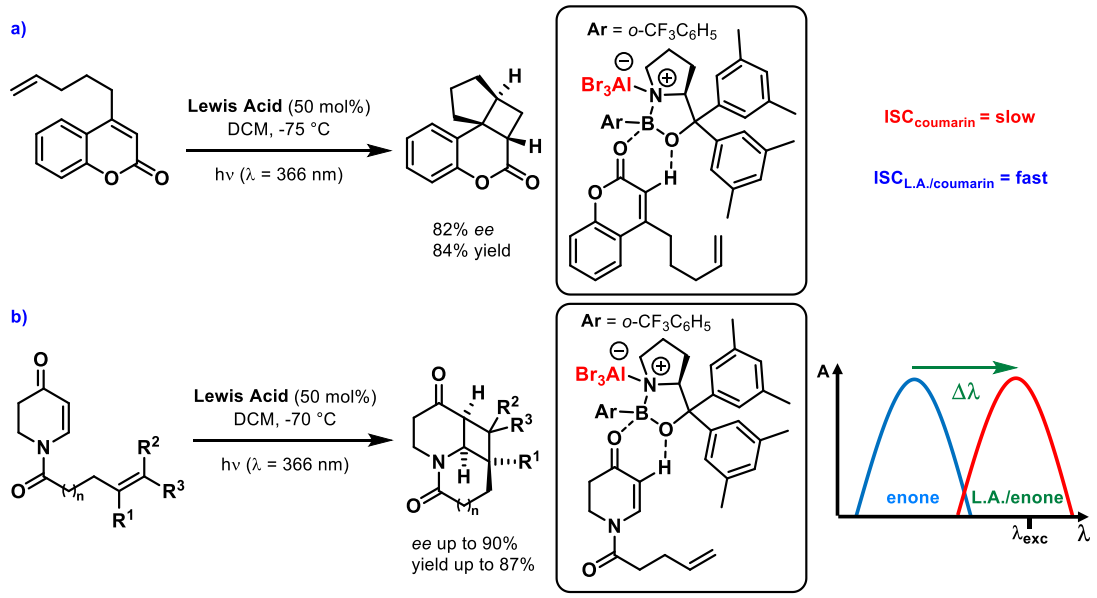

Scheme 74. Lewis acid-mediated enantioselective [2+2] photocycloadditions of coumarins (a) and enones (b).

Another outstanding intramolecular photocycloaddition of cyclic enones was reported by Bach's group through Lewis acid catalysis, achieving interesting enantioenriched tricyclic products (Scheme 75).[136] Whereas, the related asymmetric intermolecular version was reported by the same research group in 2018 (Scheme 76).[137] A wide range of simple unactivated alkenes, such as ethylene, could be employed as the olefin partner, obtaining the corresponding products in high efficiency and impressive enantioselectivity, although it usually required a high excess of the alkene. The synthetic value of this reaction was showcased through the application of it in the total synthesis of grandisol, which was accomplished by means of an intermolecular [2+2] photocycloaddition as the stereodefining key step (Scheme 76, right).

[135] R. Brimioulle, A. Bauer, T. Bach, *J. Am. Chem. Soc*. **2015**, *137*, 5170-5176.
[136] R. Brimioulle, T. Bach, *Angew. Chem. Int. Ed.* **2014**, *53*, 12921-12924.
[137] S. Poplata, T. Bach, *J. Am. Chem. Soc.* **2018**, *140*, 3228-3231.

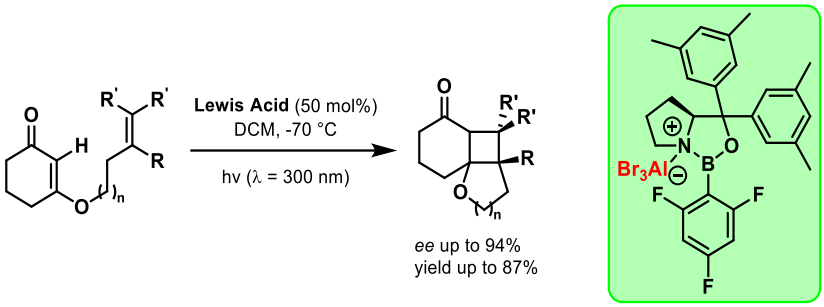

Scheme 75. Lewis acid-mediated asymmetric intramolecular [2+2] photocycloaddition of enones.

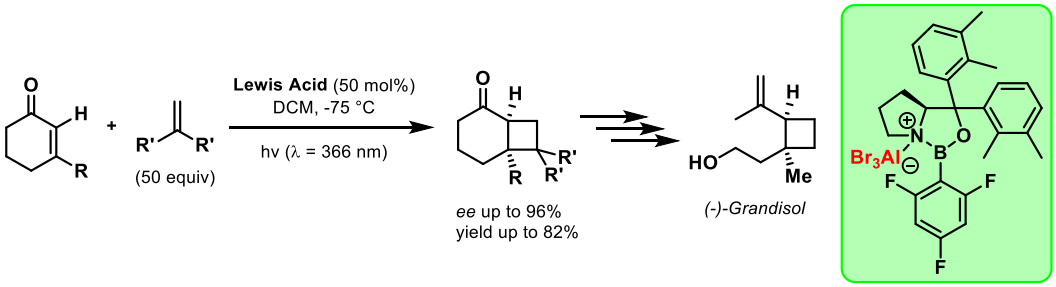

Scheme 76. Lewis acid-mediated enantioselective intermolecular [2+2] photocycloaddition of enones and its application in the asymmetric total synthesis of a natural product.

Due to the fact that enones have a weak *n*-π^* transition bathochromically shifted in comparison with the π-π^* transition, the exclusive excitation of a chiral Lewis acid-substrate complex is challenging despite the observed bathochromic shift. Moreover, since the ISC rate from ^1n-π^* to $^3\pi$-π^* is several orders of magnitude higher than the corresponding ISC rate from $^1\pi$-π^* to $^3\pi$-π^* (El Sayed's rule),[138] the racemic background reaction, for a [2+2] photocycloaddition that is taking place from the triplet excited state, is becoming competitive with the Lewis acid-mediated reaction, leading to a required high catalyst loading. A special case, in which just a 20 mol% of oxazaborolidine-based catalyst could be employed, was reported by Bach's group in the asymmetric *ortho*-photocycloaddition of 9-phenanthrene carboxaldehyde derivatives, which led to the corresponding dearomatized products (Scheme 77).[139] This result has been achieved as a consequence of two factors: the greater displacement to longer wavelengths ($\Delta\lambda$ of the bathochromic shift) for substrates that present a π-π^* transition at lower energy and the fact that the *ortho*-photocycloaddition proceeded via an excited singlet state.

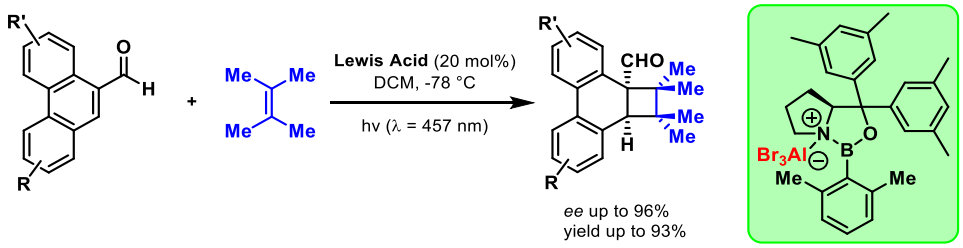

Scheme 77. Lewis acid-mediated asymmetric *ortho*-photocycloaddition of 9-phenanthrene carboxaldehydes.

In 2014, Yoon's research group reported a highly enantioselective intermolecular [2+2] photocycloadditions of acyclic enones through visible light irradiation (Scheme 78).[65] Upon carefully choosing the appropriate reaction partners, the corresponding crossed products could be obtained in high efficiency. This brilliant dual-catalytic strategy strictly requires an aryl enone

[138] (a) M. A. El-Sayed, *Acc. Chem. Res.* **1968**, *1*, 8-16; (b) P. Klán, J. Wirz, "Photochemistry of Organic Compounds", Wiley, Chichester **2009**, 38-39.
[139] S. Stegbauer, C. Jandl, T. Bach, *Angew. Chem. Int. Ed.* **2018**, *57*, 14593-14596.

as the substrate, which can be reduced through a Lewis acid-mediated photoredox process to the corresponding radical anion. An electron-deficient alkene, which cannot be reduced under the reaction conditions, has to be employed as the reaction partner.

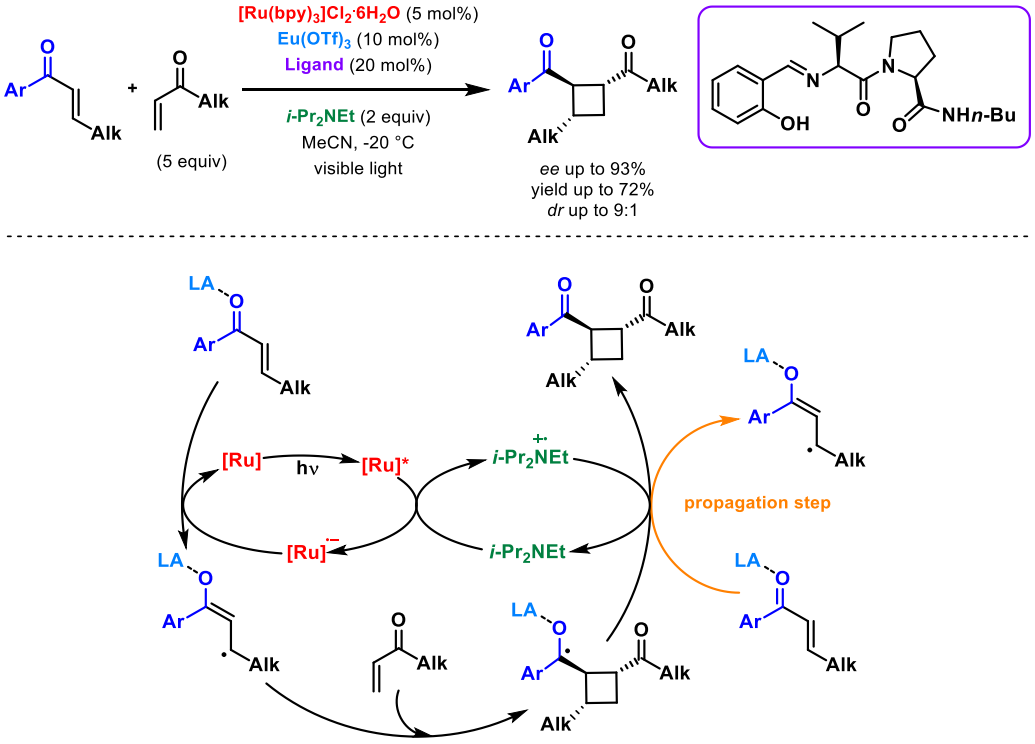

Scheme 78. Enantioselective intermolecular [2+2] cycloaddition achieved through a dual-catalytic photoredox strategy.

In 2016, Yoon's research group reported the first enantioselective intermolecular [2+2] photocycloaddition enabled by a triplet energy transfer mechanism (Scheme 79).[66] The use of a ruthenium complex as an external photocatalyst allowed the exclusive photosensitization of a Lewis acid-substrate complex in comparison with the unbounded hydroxychalcone. This has been achieved since upon coordination the Lewis acid is lowering the triplet energy of the substrate (from E^T = 54 kcal/mol to 33 kcal/mol), unlocking a thermodynamic favorable energy transfer from the photosensitizer (E^T = 46 kcal/mol), which is, on the other hand, unable of catalyzing the racemic background process. Through the exploitation of this triplet photosensitization strategy, dienes and styrene derivatives could be employed as the olefin partner in the [2+2] photocycloaddition of hydroxychalcones, obtaining the desired enantioenriched products in high efficiency.[66,67]

Another outstanding activation mode in asymmetric [2+2] photocycloaddition was reported by the group of Yoon in 2019 (Scheme 80).[68] Through the employment of an oxazaborolidine-based Lewis acid catalyst, an intermolecular [2+2] photocycloaddition between highly versatile cinnamic esters and styrene derivatives was accomplished in high enantioselectivity. Although the reaction worked even in this case through a triplet energy transfer photosensitization, there are some important differences that are worth to mention. Indeed, the triplet energy lowering observed upon oxazaborolidine-based Lewis acid coordination was of only 7 kcal/mol and, with other Lewis acid catalysts, any decrease of the triplet energy was observed. Nevertheless, these Lewis acids still worked as efficient catalysts, demonstrating that triplet energy lowering is not the activation mode in this reaction. On the other hand, the analysis of the relevant frontier molecular orbitals for the cinnamate ester, the Lewis-acid substrate complex and the photocatalyst evidenced that a significant orbital overlap was required to achieve an efficient

photosensitization. Moreover, the Lewis acid could also catalyze the [2+2] photocycloaddition through the stabilization of the excited triplet state.

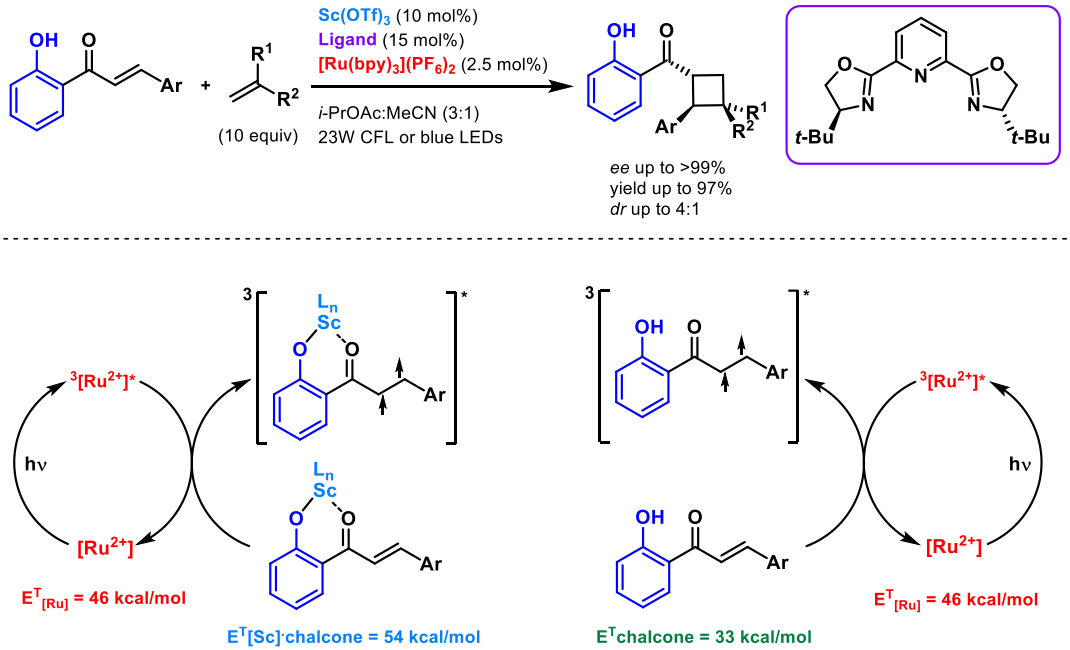

Scheme 79. Enantioselective intermolecular [2+2] photocycloaddition enabled by a dual-catalytic system through a triplet energy transfer mechanism.

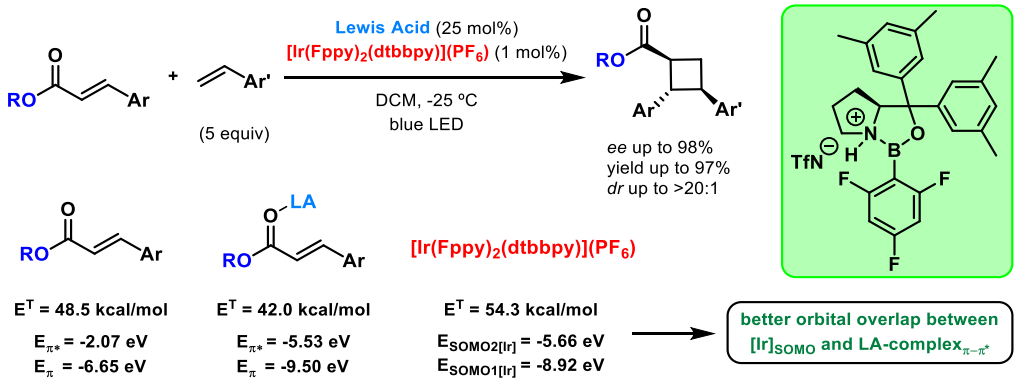

Scheme 80. Enantioselective intermolecular [2+2] photocycloaddition of cinnamate esters and styrenes enabled by a dual-catalytic system.

The research group of Meggers developed a chiral-at-metal rhodium catalyst and demonstrated that it can be efficiently employed in a variety of [2+2] photocycloadditions, obtaining the desired cyclobutane derivatives with outstanding enantioselectivity (Scheme 81).[84] The rhodium catalyst is acting as a Lewis acid capable of undergoing an efficient binding with N-acyl imidazole and pyrazole derivatives. Thus, the resulting rhodium-substrate complex can be selectively photoexcited, due to an increased absorption at the irradiation wavelength, to reach a reactive excited triplet state that can carry out the enantioselective [2+2] photocycloaddition with diene and styrene derivatives.[84a] The same strategy has been applied in the asymmetric photo-dearomatization of benzofuran and benzothiophene derivatives.[84b] Moreover, a highly efficient and enantioselective [3+2] photocycloaddition was achieved by the same group employing vinyl azides as the reaction partners.[84c]

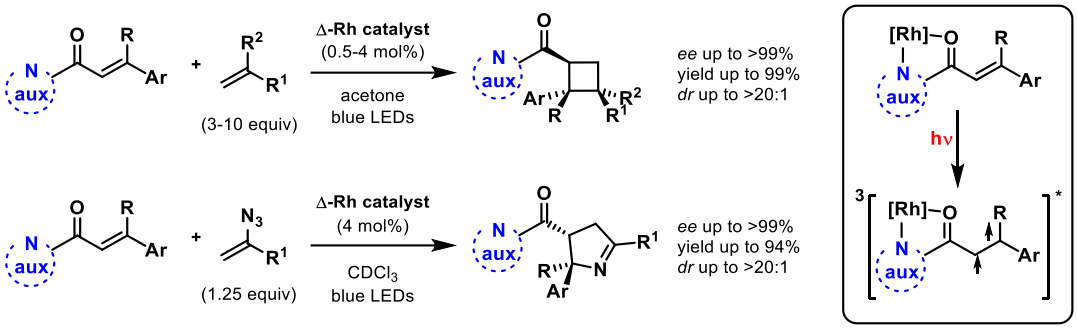

Scheme 81. Asymmetric [2+2] and [3+2] photocycloadditions achieved through the employment of a chiral-at-metal rhodium catalyst.

In this context, the Yoon's research group developed chiral-at-metal iridium complexes that have allowed the achievement of highly enantioselective [2+2] photocycloadditions (Scheme 82).[69] These catalysts have the particular feature that they have been properly designed to permit hydrogen-bonding interactions with the substrate, allowing the obtainment of stereocontrolled transformations. In the first intramolecular example, the catalyst is selectively binding to the lactam motif of the quinolone, employing the nitrogen and hydrogen atoms of the pyrazole ring (Scheme 82a). The energy transfer from the iridium catalyst to the coordinated substrate permits to carry out the stereocontrolled [2+2] reaction.[69a] On the other hand, in the intermolecular reaction with maleimide, the iridium catalyst is coordinating the two oxygen atoms of the quinolone just through the hydrogen of the pyrazole ring (Scheme 82b). This represents a rare example of an enantioselective photocatalytic reaction that was achieved through the catalytic binding of a ground state substrate, which is reacting with an excited state reaction partner.[69b] Indeed, they demonstrated that the energy transfer occurs from the iridium catalyst to the uncoordinated maleimide, leading to a highly efficient stereoinduced process.

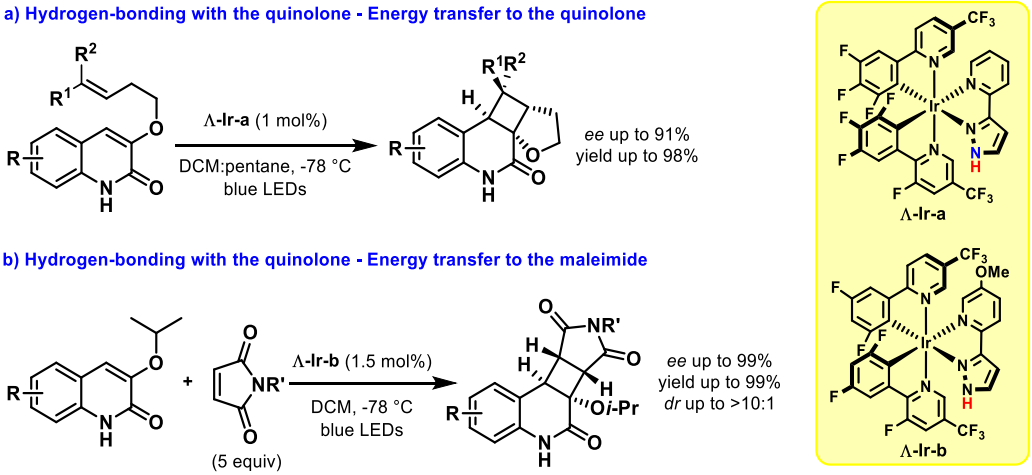

Scheme 82. Asymmetric [2+2] photocycloadditions enabled by the use of chiral-at-metal iridium catalysts through hydrogen bonding catalysis.

4.3 Objectives of this Chapter

Although different enantioselective strategies for the achievement of efficient [2+2] photocycloadditions have been reported in the last decade, the reaction over simple acyclic unfunctionalized enones remained an elusive topic due to reactivity limitations of dual-catalytic photoredox approaches and limited reported activation modes. For this purpose, we envisioned that iminium ion catalysis could provide a suitable activation of simple unfunctionalized acyclic enones overcoming the requirement of a bidentate coordination for the substrate as in the

reported Lewis acid strategies or the employment of a specifically tailored hydrogen-bond catalyst. The only two examples of stereoinduced photocycloaddition over iminium ions have been reported by Mariano's and Bach's groups, using UV light or an external ruthenium photosensitizer, respectively (Scheme 83a,b).[140,141] Nevertheless, both approaches required pre-formation of a stoichiometric iminium ion by condensation of a chiral amine, which is merely acting as a chiral auxiliary.

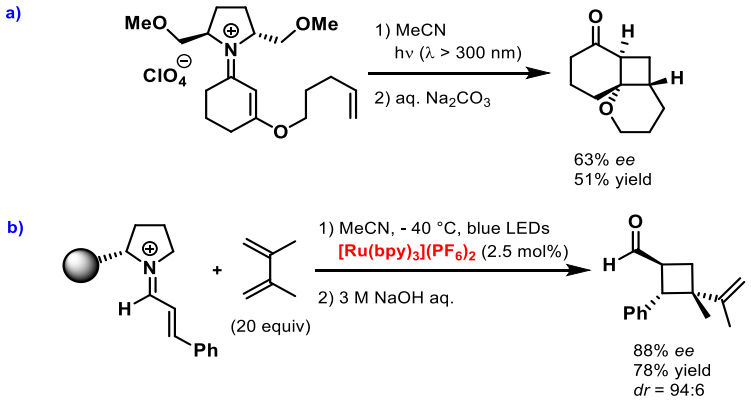

Scheme 83. Previously reported asymmetric [2+2] photocycloadditions over stoichiometric iminium ions.

The development of a catalytic version of Mariano's strategy is obstructed by the fact that enones have an *n*-π^* transition bathochromically shifted in comparison with the π-π^* transition of an iminium ion, leading to an impossible selective excitation of a catalytic iminium ion and provoking a racemic background reaction of the enone. This is essentially due to the high ISC rate from ^{1}*n*-π^* to $^3\pi$-π^* which, despite the low molar absorption coefficient of the *n*-π^* transition of enones, is permitting a symmetry-allowed ISC (El Sayed's rule) that unlocks the population of a reactive excited triplet state.[138] Therefore, to overcome this intrinsic challenge, we thought about the possibility of taking advantage of the appearance of a new absorption band (bathochromically shifted in comparison with the enone transition) upon formation of an electron-donor acceptor (EDA) complex. Indeed, EDA complexes have been elegantly employed by Melchiorre's group for enantioselective photo-redox reactions,[54a-c] and recently the formation of an intramolecular EDA complex has been exploited for the achievement of an asymmetric radical conjugate addition over enones (Scheme 84).[54d]

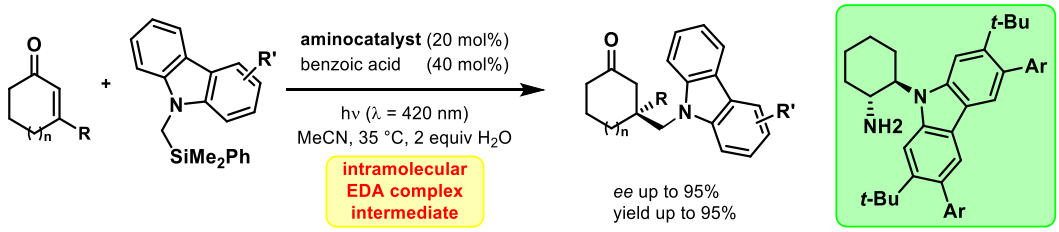

Scheme 84. Asymmetric radical conjugate addition over enones through an intramolecular EDA complex intermediate.

Nevertheless, the catalytic formation of EDA complexes in enantioselective intermolecular cycloaddition reactions has been maintained unexplored. The only example of an intramolecular [2+2] photocycloaddition was reported by Sivaguru's research group, but it is more likely involving an intermolecular exciplex formation than an EDA complex, at least at the catalyst loading employed for the reaction scope (Scheme 85).[142]

[140] C. Chen, V. Chang, X. Cai, E. Duesler, P. S. Mariano, *J. Am. Chem. Soc*. **2001**, *123*, 6433-6434.
[141] F. M. Hörmann, T. S. Chung, E. Rodriguez, M. Jakob, T. Bach, *Angew. Chem. Int. Ed*. **2018**, *57*, 827-831.
[142] N. Vallavoju, S. Selvakumar, S. Jockusch, M. P. Sibi, J. Sivaguru, *Angew. Chem. Int. Ed*. **2014**, *53*, 5604-5608.

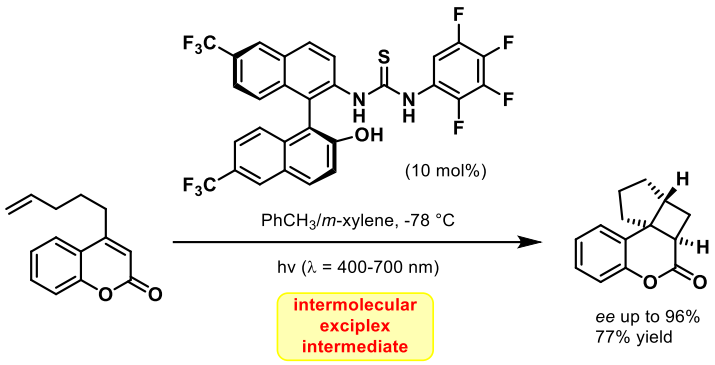

Scheme 85. Enantioselective intramolecular [2+2] photocycloaddition of coumarins mediated by an exciplex intermediate.

Therefore, the exploitation of iminium ion catalysis and EDA complex photoactivity seemed to be a novel complementary alternative for the synthesis of enantioenriched cyclobutanes via [2+2] photocycloaddition starting from standard acyclic enones (Scheme 86).

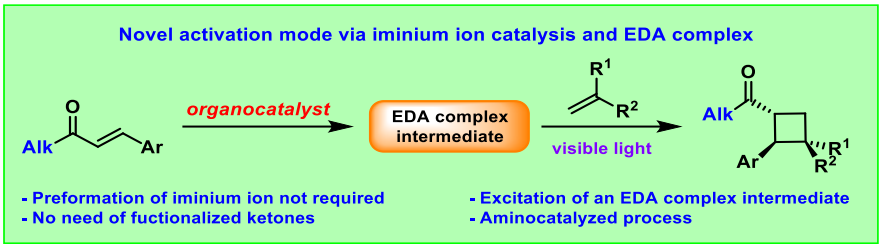

Scheme 86. Proposed aminocatalytic enantioselective strategy for the obtainment of enantioenriched cyclobutanes by means of an EDA complex intermediate.

For the achievement of this goal we proposed the following sub-objectives:

1) Searching of an appropriate aminocatalyst which is enabling the photocatalytic [2+2] cycloaddition.
2) Evaluation of the reaction scope and of the limitations of this strategy.
3) DFT calculations and appropriate experiments to support the corresponding mechanistic proposal.

4.4 Publications and Experimental Section

Enantioselective Aminocatalytic [2+2] Cycloaddition through Visible Light Excitation

Thomas Rigotti, Rubén Mas-Ballesté and José Alemán*

Unpublished Results

(Submitted to ACS Catalysis)

The experimental section was taken from the "Supporting Information" document associated with the specific publication and is including the corresponding numeration. The characterization data have been shown only for the final products that appear in the scope of the reaction. The complete "Supporting Information" documents, with all the characterization data, NMR spectra, SFC or HPLC traces and other experimental procedures have been included in the enclosed USB memory.

Enantioselective Aminocatalytic [2+2] Cycloaddition through Visible Light Excitation

Thomas Rigotti,[†] *Rubén Mas-Ballesté,*[§,‡] *and José Alemán**[,†,‡]

[†]Organic Chemistry Department, Universidad Autónoma de Madrid, 28049 Madrid (Spain)

[§]Inorganic Chemistry Department, Universidad Autónoma de Madrid, 28049 Madrid (Spain)

[‡]Institute for Advanced Research in Chemical Sciences, Universidad Autónoma de Madrid, 28049 Madrid (Spain)

KEYWORDS photocatalysis, enantioselective [2+2] photocycloaddition, iminium ion catalysis, EDA complex photoactivity, cyclobutanes, aminocatalysis

ABSTRACT. An asymmetric aminocatalytic activation strategy to obtain enantioenriched cyclobutanes through [2+2] photocycloaddition under visible light irradiation is presented. This metal-free process does not require the use of any external photocatalyst, as it is catalyzed by a simple diamine, which upon condensation with an enone substrate, forms an iminium ion intermediate that absorbs in the visible light region. The direct excitation of such an intermediate (EDA complex) leads to an excited state that can undergo a stereocontrolled intermolecular photocycloaddition with good enantio- and diastereo-meric ratios and excellent yields. Finally,

DFT calculations and experiments were performed to support the EDA behaviour and the mechanistic proposal.

INTRODUCTION

Visible light photocatalysis has received growing interest during the last decades because of its ability to achieve bond constructions that are generally not feasible using conventional and established thermal catalysis.[1] Nevertheless, enantioselective photocatalysis has found limited applications because the achievement of high levels of stereoinduction have been obstructed by various factors that are intrinsic to the nature of photochemical reactions.[2] Indeed, the high reactivity of open-shell intermediates and the low energy barrier of short-lived electronic excited states leads to a rapid evolution of the reaction course, challenging the possibility of a triggered and stereocontrolled transformation induced by a chiral catalyst. Additionally, the presence of non-catalysed background racemic processes has further complicated the achievement of this goal.

In this context, the [2+2] photocycloaddition represents a powerful multiple bond construction approach for the synthesis of chiral cyclobutanes in a single step. However, despite their abundance in natural product backbones, and their importance as synthetic intermediates only a few enantioselective photocatalytic strategies to achieve enantioenriched cyclobutanes have been described to date.[3] The pioneering works of Bach's group[4,5] on catalytic enantioselective [2+2] photocycloadditions employed different strategies to achieve stereoinduction. Lactam hydrogen bonding interactions were used as a stereocontrol element, leading to a preferential energy transfer towards the catalyst-coordinated substrate (Figure 1a).[2e,4] A second strategy relied on the exclusive photoexcitation of a chiral oxazaborolidine Lewis acid-substrate complex due to a bathochromic

absorption shift observed upon coordination.[5] In this regard, the first intermolecular enantioselective [2+2] reaction enabled by a Lewis acid-catalysed triplet energy transfer has been reported,[6] whereas a chiral-at-rhodium complex has been employed to efficiently promote the [2+2] photocycloaddition over acyclic compounds (Figure 1b).[7] Therefore, we hypothesised whether another catalytic activation mode might be feasible to obtain enantioenriched cyclobutanes derivatives, overcoming the requirement of a bidentate coordination for the substrate, as in the strategies reported (Figure 1a-b).[4-7] Indeed, the achievement of an enantioselective [2+2] photocycloaddition over simple acyclic unfunctionalised enones is still an elusive topic due to the reactivity limitations of dual-catalytic photoredox approaches and limited reported activation modes to provide the stereocontrol.[3]

For this purpose, we envisioned that iminium ion catalysis could provide the suitable activation of simple unfunctionalised acyclic enones. Only two substrate-specific examples of stereoinduced photocycloaddition over iminium ions have been reported by Mariano's and Bach's groups, using UV light or an external ruthenium photosensitiser, respectively.[8,9] Nevertheless, both approaches required pre-formation of a stoichiometric iminium ion by condensation of a chiral amine, which is merely acting as a chiral auxiliary. The development of a catalytic version of Mariano's strategy is obstructed by the fact that enones have an n-π^* transition bathochromically shifted by comparison with the π- π^* transition of an iminium ion, leading to an almost impossible selective excitation of a catalytic iminium ion and provoking a racemic background reaction of the enone.[9] Therefore, we considered the possibility of taking advantage of the possible appearance of a new absorption band upon the formation of an EDA complex between an electron poor fragment (**C=NH$^+$**-CH$_n$-Ar) and an electron rich moiety (C=NH$^+$-CH$_n$-**Ar**) present in the iminium ion intermediate. Although electron-donor acceptor (EDA) complexes have been elegantly employed

for enantioselective photo-redox reactions,[10] their catalytic employment in intermolecular [2+2] photocycloadditions remains unexplored.[10f] Therefore, the exploitation of iminium ion catalysis and EDA complex photoactivity seemed to be a novel complementary alternative for the synthesis of enantioenriched cyclobutanes via [2+2] photocycloaddition starting from standard acyclic enones.

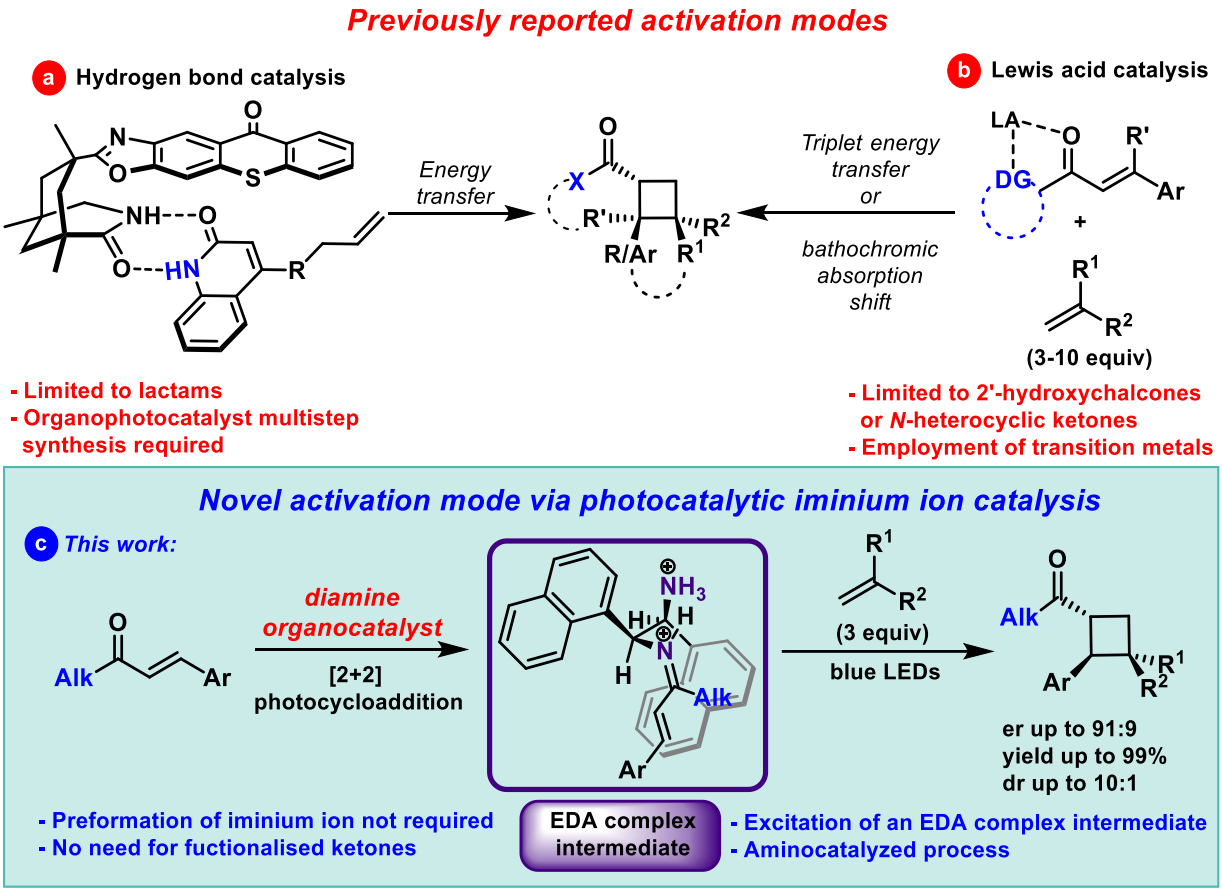

Figure 1. Enantioselective catalytic activation strategies in [2+2] photocycloadditions: a-b) previous and c) present work (DG= directing group, LA= Lewis Acid).

Herein we disclose the first enantioselective aminocatalytic activation strategy to obtain cyclobutanes through a stereocontrolled [2+2] photocycloaddition by the irradiation of an intramolecular EDA complex intermediate (Figure 1c). We found that this reaction can be applied

to a variety of unfunctionalised acyclic enones and different double bonds with good yields and good enantiomeric and diastereomeric ratios. In addition, we have proven by mechanistic experiments that the reaction is catalysed by a simple diamine through the direct excitation of an iminium ion intermediate triggered by the red shift absorption of a transient intramolecular EDA complex.

RESULTS AND DISCUSSION

In the search for an aminocatalytic activation strategy for the development of an enantioselective [2+2] photocycloaddition, we envisioned that the *in situ* generation of an intramolecular iminium ion EDA complex could have permitted the preferential visible light excitation of this intermediate over the carbonyl species, avoiding any racemic background process. In addition, the recently reported photoactivity of an intramolecular EDA complex for single-electron transfer (SET) reactions encouraged us to evaluate a new activation mode for the development of an enantioselective [2+2] photocycloaddition.[10d] Taking advantage of this bathochromic shift in the visible light region (see below), the excitation of the transient EDA complex species would lead to an excited state chiral intermediate which could carry out a stereocontrolled [2+2] photocycloaddition. 4-Phenyl-3-buten-2-one **1a** was chosen as a model substrate (Table 1) to obtain an enantioenriched cyclobutane **4a** that is not possible to achieve employing the previously reported catalytic activation strategies.[3-7] Gratifyingly, we achieved the product of interest employing diene **2a** (3 equiv), a diamine catalyst **3a** (0.4 equiv) and TFA (trifluoroacetic acid, 1 equiv) as an acid promoter while running the reactions in acetonitrile under blue LED irradiation

Table 1. Optimisation studies for the [2+2] photocycloaddition.

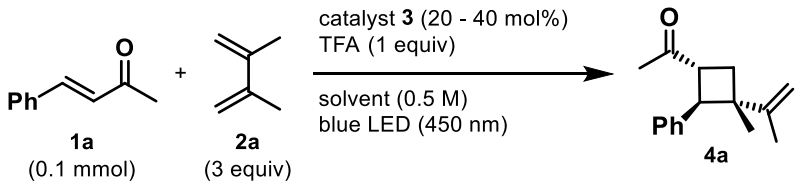

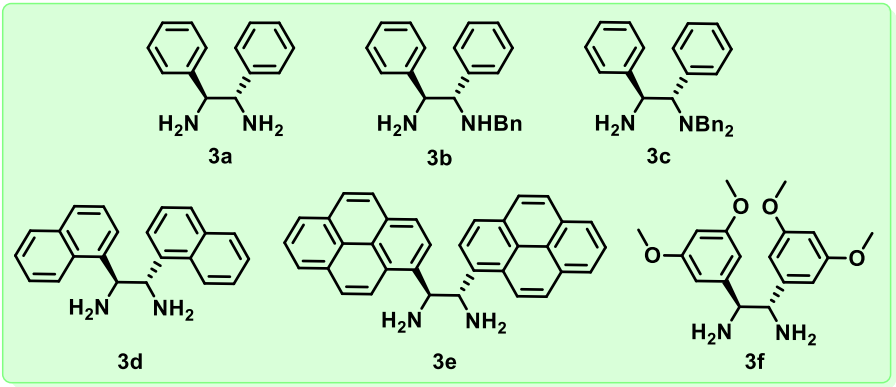

Entry	Organocatalyst (mol%)	Solvent	Conversion[a](%)	*er*[b]
1	3a (40)	MeCN	27	73:27
2	3b (40)	MeCN	19	63:37
3	3c (40)	MeCN	8	51:49
4	3d (40)	MeCN	53	80:20
5	3e (40)	MeCN	21	72:28
6	3f (40)	MeCN	45	71:29
7	**3d (20)**	**Et_2O**	**100**	**90:10**
8[c]	3d (20)	Et_2O	0	-
9	-	Et_2O	9	-
10[d]	3d (20)	Et_2O	100	82:18

[a] Determined by ^{1}H NMR of the crude mixture after 17h. [b] Determined by chiral SFC analysis of the isolated product. [c] Reaction carried out in the dark.[d] Reaction carried out under air.

(entry 1). Diphenylethylene diamine (DPEN) **3a** afforded the product with a low conversion and moderate enantiomeric ratio (*er* = 73:27, entry 1). The use of mono-benzylated and di-benzylated catalysts **3b** and **3c** decreased the reactivity and lowered the *er* (entries 2 and 3) indicating the need for a primary diamine catalyst in order to reach higher levels of stereoinduction. We then studied

the effect of the stereoelectronic nature of the aromatic backbone of the catalyst testing different C_2 symmetric diamines (entries 4-6). We found that the use of 1-naphthyl as the aryl moiety (catalyst **3d**) had a beneficial impact on both reactivity, as expected with a better donor moiety for the formation of the EDA complex, and stereoselectivity (*er* = 80:20, entry 4). After a final screening of the reaction conditions (see the Supporting Information), cyclobutane **4a** was obtained in excellent yields and good enantioselectivity (99 % yield, *er* = 90:10, entry 7) employing a 20 mol % of catalyst loading (**3d**) and diethyl ether as the solvent. Furthermore, the exclusion of light, or the organocatalyst, suppressed the reaction almost completely (entries 8 and 9). In addition, the presence of oxygen (air) did not inhibit the reaction, and full conversion was achieved under the reaction conditions (entry 10).

The different reactivity observed in the presence of the various catalysts can be explained by the formation of an intramolecular EDA complex between the electron-rich moiety of catalyst **3** and the transient generated electron-poor iminium ion. As an initial observation, we noticed that a coloured intramolecular EDA complex was clearly forming upon preparation of the reaction mixtures (Figure 2, top) and their absorption spectra was recorded (Figure 2, bottom). Indeed, a 0.05 M solution of substrate **1a** and TFA showed negligible absorption in the visible light region, explaining the low conversion observed for the racemic background process (entry 9, Table 1). The use of diamine catalyst **3a** led to a small increase in the absorbance due to the slight generation of a pale colored EDA complex.[11] Conversely, when electron-rich catalysts **3d-f** were employed, a strong bathochromic shift in the visible light region was observed, turning the reaction mixture bright yellow, or orange in the case of **3e** (Figure 2).[12] This strongly indicates that the formation of an EDA complex is taking place and that it can lead to the preferential excitation of this

intermediate over the carbonyl substrate, permitting the enantioselective reaction to proceed under visible light irradiation without the use of any external photosensitiser.

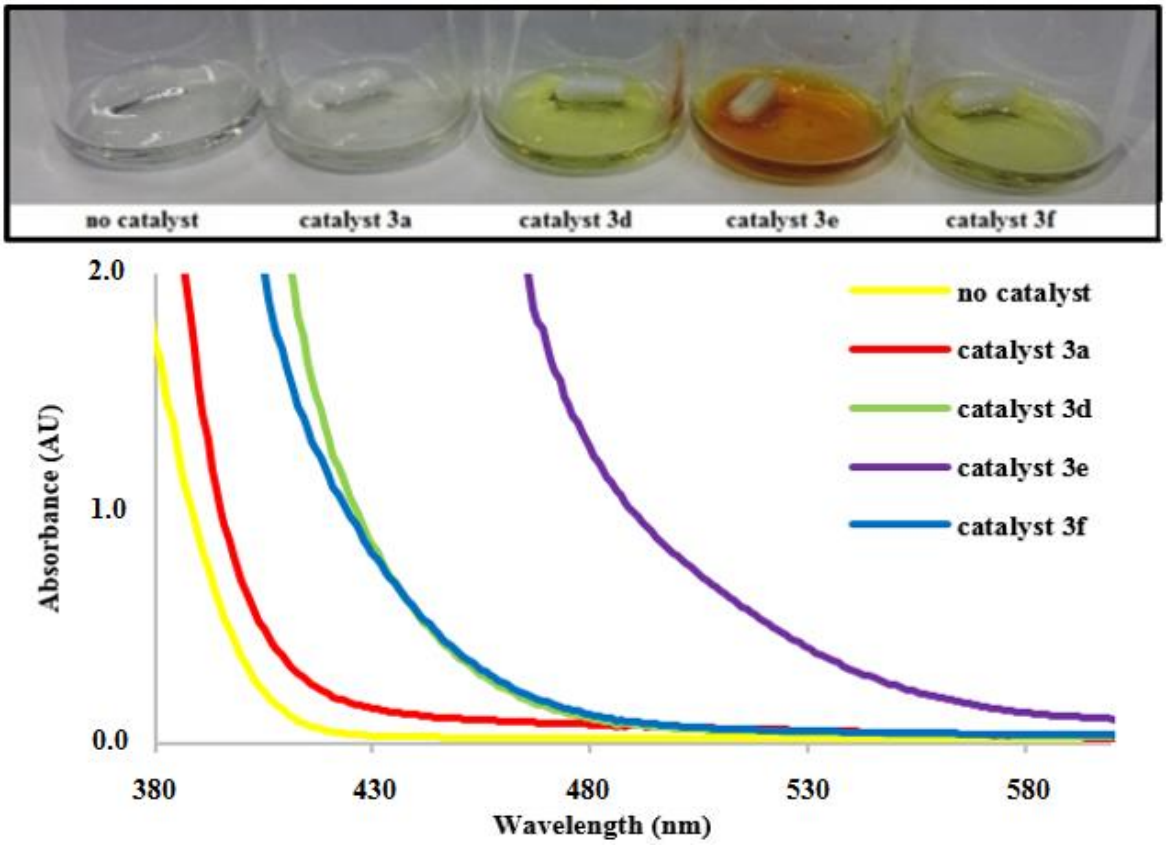

Figure 2. Top: Visual appearance of the reaction mixtures with the different catalysts. Bottom: Absorption spectra (0.05 M solutions in 1 cm quartz cell; see the Supporting Information for further details).

After optimizing the reaction conditions, we studied the scope of the reaction considering both enones **1** and alkenes **2** (Table 2). The reaction proceeded efficiently with enone **1b**, obtaining the corresponding product **4b** with a high yield and good enantioselectivity (99 % yield, *er* = 88:12). Enone **1c** led to the desired cyclobutane adduct **4c**, although with slightly lower *er* values, probably due to an inefficient condensation of the primary diamine catalyst and hence, a more consistent racemic background process. The substitution on the aryl moiety was well tolerated and different

cyclobutanes (**4d-j**) could be obtained using this methodology. The reaction tolerated the presence of different *ortho* substituents at the aryl ring of the ketone leading to the corresponding more sterically hindered cyclobutanes **4d-f**. Indeed, *ortho*-methyl and *ortho*-isopropyl substituents can be present in the starting enone leading to the corresponding cyclobutanes **4d** and **4e** in high yields and good enantiomeric ratios (93 % yield, *er* = 88:12 and 94 % yield, *er* = 91:9, respectively). Furthermore, *ortho* disubstituted and *metha* disubstituted cyclobutane **4f** and **4g** were obtained without a significant erosion in the yield and enantioselectivity (76 % yield, *er* = 81:19 and 86 % yield, *er* = 87:13, respectively). The presence of electron-donating (MeO-, **1h**) and electron-withdrawing (CF_3-, **1i**) groups had little impact on the reaction, isolating the products **4h** and **4i** with good enantioselectivities (60 % yield, *er* = 82:18 and 62 % yield, *er* = 82:18, respectively). The *para*-Br substituted enone **1j** led to the halogenated cyclobutane **4j** (88 % yield, *er* = 88:12), which could be further manipulated by cross-coupling methodologies. Gratifyingly, other aryl moieties such as 1-naphthyl and 3-furanyl can be introduced in the final product with comparable enantioselectivity, giving cyclobutanes **4k** and **4l**. The reaction was also tested with different olefins to prove the generality of the protocol. When isoprene was employed as the alkene partner, cyclobutane **4m** was obtained with a 77 % yield, while styrene proceeded smoothly to product **4n** with an 84 % yield and 82:18 *er*. Electron-poor styrene **1l** led to the CF_3-containing cyclobutane **4o** with a 72 % yield and 78:22 *er*. The employment of indene led to the production of cyclobutane **4p**, which contains an interesting tricyclic scaffold. On the other hand, the quaternary carbon-containing product **4q** could be obtained with a 75 % yield when 1,1-diphenylethylene was employed as the olefin partner. The absolute configuration of the enantioenriched cyclobutanes **4** was determined by derivatisation of **4a** to hydrazone **5a**, which was unambiguously confirmed by

single crystal X-ray crystallography (See Table 1 and the Supporting Information for further details).[13]

Table 2. Scope of the reaction in the [2+2] photocycloaddition[a]

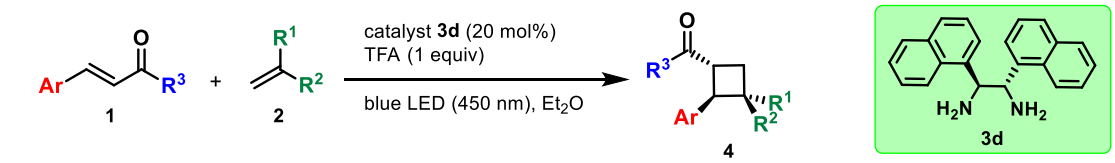

enone scope

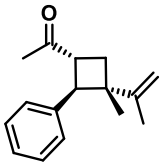

4a

99% yield
8:1 *dr*
90:10 *er*

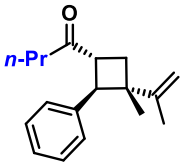

4b

99% yield
10 :1 *dr*
88:12 *er*

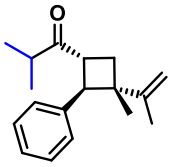

4c

76% yield
9:1 *dr*
73:27 *er*

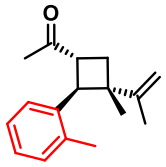

4d

93% yield
8:1 *dr*
88:12 *er*

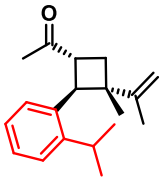

4e

94% yield
10:1 *dr*
91:9 *er*

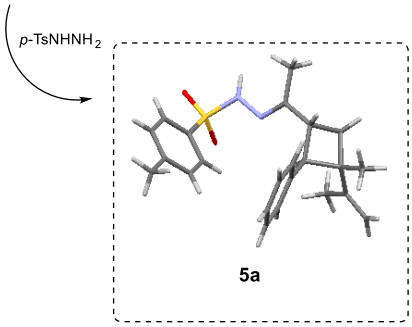

5a

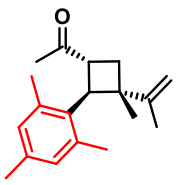

4f

76% yield
2:1 *dr*
81:19 *er*

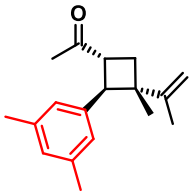

4g

86% yield
8:1 *dr*
87:13 *er*

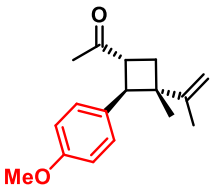

4h

60% yield
3:1 *dr*
82:18 *er*

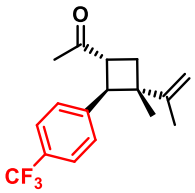

4i

62% yield
6:1 *dr*
82:18 *er*

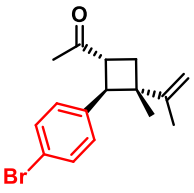

4j

88% yield
8:1 *dr*
88:12 *er*

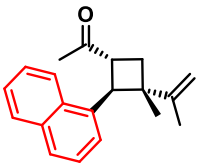

4k

49% yield
2:1 *dr*
81:19 *er*

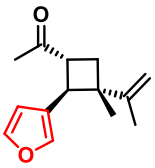

4l

45% yield
10:1 *dr*
76:24 *er*

olefin scope

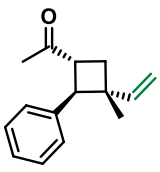

4m

77% yield
8:2:1 *dr*
81:19 *er*

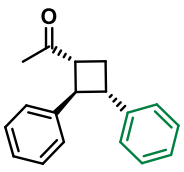

4n

84% yield
4:1 *dr*
82:18 *er*

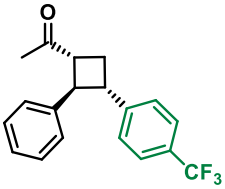

4o

72% yield
5:1 *dr*
78:22 *er*

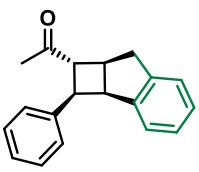

4p

43% yield
3:1 *dr*
72:28 *er*

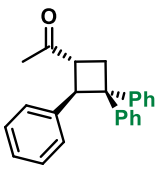

4q

75% yield
20:1 *dr*
81:19 *er*

[a]Reaction conditions: **1** (0.1 mmol), **2** (0.3 mmol), **3d** (0.02 mmol), TFA (0.1 mmol) and 0.2 mL of Et_2O (see the Supporting Information for further details). [b]*0.9 mmol of* ***2*** *were* employed. [c]MTBE used as the solvent.

MECHANISTIC PROPOSAL

The proposed reaction mechanism (Figure 3) would start with the acid-promoted condensation of diamine catalyst **3d** with enone **1a** to form the ketiminium ion intermediate **A-1**, which due to the contiguous presence of donor (naphthyl) and acceptor (iminium ion) moieties, gives a coloured EDA complex. The latter can reach the excited states **B-1** or **B-2** under blue LED irradiation. Indeed, from the ground state **A-1**, a SET between the donor and the acceptor moieties can give an unproductive excited state **B-2**,[14] that would successively restore **A-1** by BET (back electron transfer) or lead to an excited species **B-1** by means of a thermal equilibrium in the excited state (*vide infra*).[10e] Furthermore, the singlet excited state species **B-1** can react with alkene **2a** in a [2+2] photocycloaddition to give the biradical intermediate **C-1**. [8,15,16] The latter evolves to the cyclobutyl iminium ion **D-1**, which after hydrolysis, gives the cyclobutane product **4a** and catalyst **3d**. The singlet excited state reactivity is supported by the fact that the reaction was not inhibited by the presence of oxygen (entry 10, Table 1), which would suppress the reaction if a triplet excited state would be the reactive species. In addition, when the reaction was performed employing the triplet photosensitiser $Ru(bpy)_3Cl_2 \cdot 6H_2O$ the reaction could be further catalysed by triplet energy transfer.[6a-b,9,17] Under these conditions, the stereochemical outcome (diastereomeric ratio) of the reaction was significantly different from the singlet reactivity that we have proposed, since an excited triplet iminium ion induced by the metal photocatalyst is supposed to be the reactive species (see the Supporting Information for a full explanation and further details).

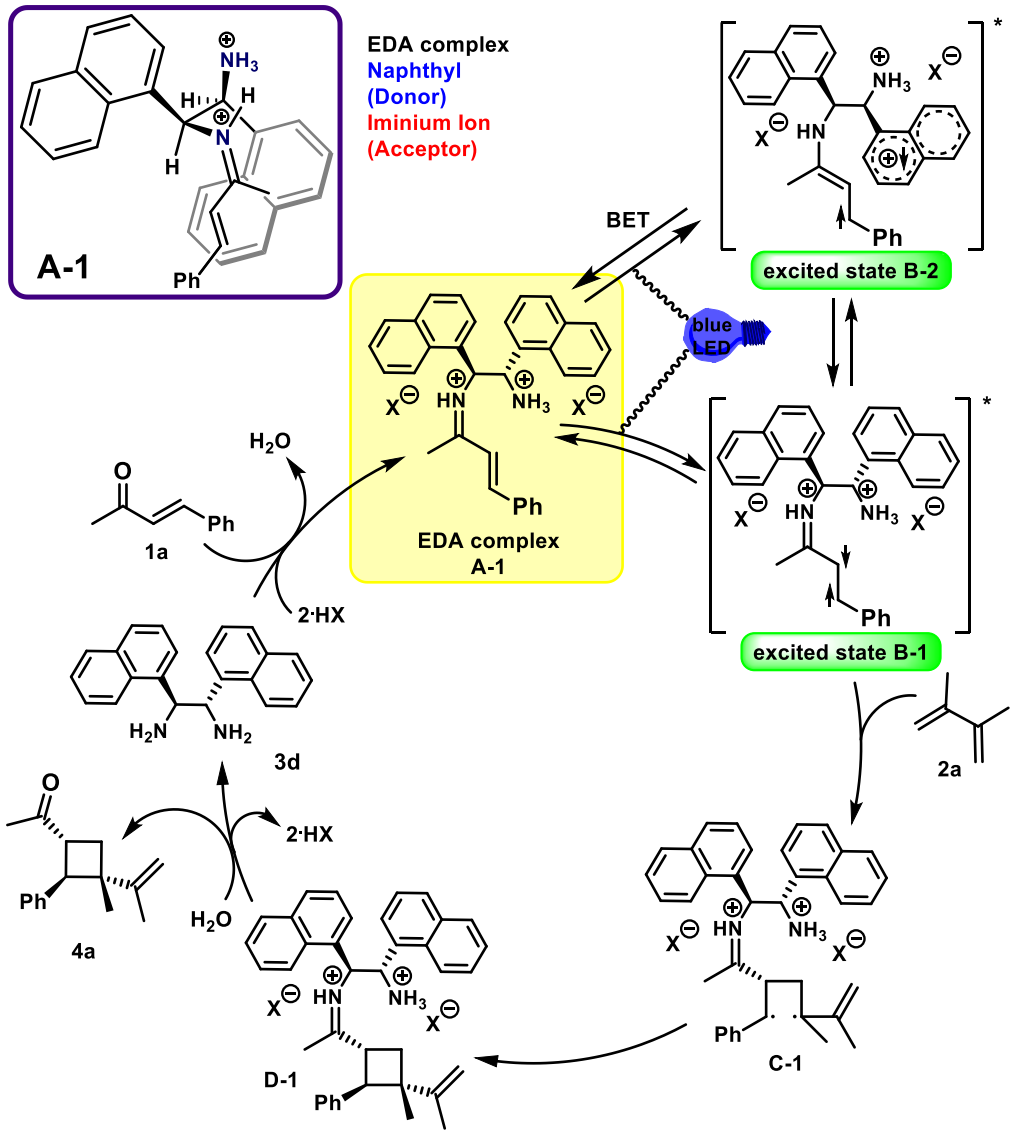

Figure 3. Mechanistic proposal for the [2+2] photocycloaddition via EDA complex.

In order to provide further insights into the molecular and electronic structures of the iminium ion formed upon condensation of enone **1a** and catalyst **3d** (**A-1**, Figure 3), DFT calculations at the M062X/6311G** level were performed. We thoroughly explored the potential energy surface, and different conformations have been isolated as local minimums (see the Supporting Information). However, as a consequence of the inherent geometric constrictions of the molecule considered, none of the conformers found included π-staking between the naphthyl moiety and the

iminium fragment. Nevertheless, the intramolecular EDA behaviour is suggested from the analysis of the electronic structure of the more stable conformer, which indicates that the HOMO orbital is located in the naphthyl moiety and the corresponding LUMO is found in the iminium fragment (Figure 4, top). Therefore, excitation of this intermediate can lead to an intramolecular single-electron transfer from the naphthyl to the iminium moieties. Indeed, optimisation of the same structure in the triplet spin state at the same calculation level indicates that the SOMO orbitals correspond exactly to the HOMO and LUMO orbitals found in the singlet spin state (see the Supporting Information). Furthermore, we analysed the possible electronic transitions by means of single point TDDFT calculations (CAMB3LYP/631G*) on the optimised structure at the M062X/6311G** level (Figure 4, top). Indeed, the first allowed $S_0 \rightarrow S_1$ transition is found at approximately 380 nm and it is mainly described as an internal single electron transfer from the HOMO in the naphthyl to the LUMO in the iminium fragment.

Although the intramolecular EDA behavior is well established from the DFT analysis, the lower energy singlet charge transfer excited state (**B-2**) cannot be responsible for the reaction outcome.[14] In fact, a singlet excited state with two unpaired electrons in the iminium fragment (**B-1**) is expected to be the active species in the [2+2] photocycloaddition observed.[8,15] Interestingly, further analysis of our TDDFT data reveals that we can expect a more intense second $S_0 \rightarrow S_2$ transition found at close energy from the first transition (350 nm). This second transition is mainly described as a HOMO-3/LUMO excitation, as both orbitals are involved localised on the iminium fragment. This excited state (**B-1**) is supposed to produce the biradical species **C-1**, which has also been studied by DFT calculations at the M062X/6311G** level at both triplet and open-shell singlet spin states. Remarkably, the **C-1** species is 20.6 kcal/mol more stable than the other biradical species that could putatively be formed from a charge transfer excited state **B-2** (**C-1'**;

Figure 4, bottom). Therefore, as expected, excited state **B-1** must be the reactive species in the [2+2] photocycloaddition. However, open-shell singlet species can be located as a local minimum in the potential energy surface, readily evolving exothermically (-30.3 kcal/mol) to the postulated cyclobutane intermediate **D-1** through a very shallow kinetic barrier (<1 Kcal/mol).

The combination of the experimental results and theoretical data suggests that although intramolecular EDA behavior is observed for **A-1**, the charge transfer species is unproductive for the reaction. Indeed, the reaction should proceed from an iminium-localized singlet excited state that appears close in energy to the charge transfer transition. In order to study the role of the naphthyl group at the iminium ion for the EDA behavior, we optimised the structure of an **A-1** analogue but replacing the naphthyl fragments by methyl groups (see the Supporting Information). According to the theoretical results, we should expect an intense first $S_0 \rightarrow S_1$ transition at 353 nm, which essentially corresponds to the $S_0 \rightarrow S_2$ transition for compound **A-1**. Therefore, the appearance of a new absorption band in the visible light region, due to the formation of the EDA complex **A-1**, enables its excitation to the excited state **B-2** at longer wavelengths, which can convert through a thermal equilibrium to the iminium-localized singlet excited state (**B-1**).[10e] Once the iminium-localized singlet excited state has been populated, the stereocontrolled [2+2] photocycloaddition can be carried out.

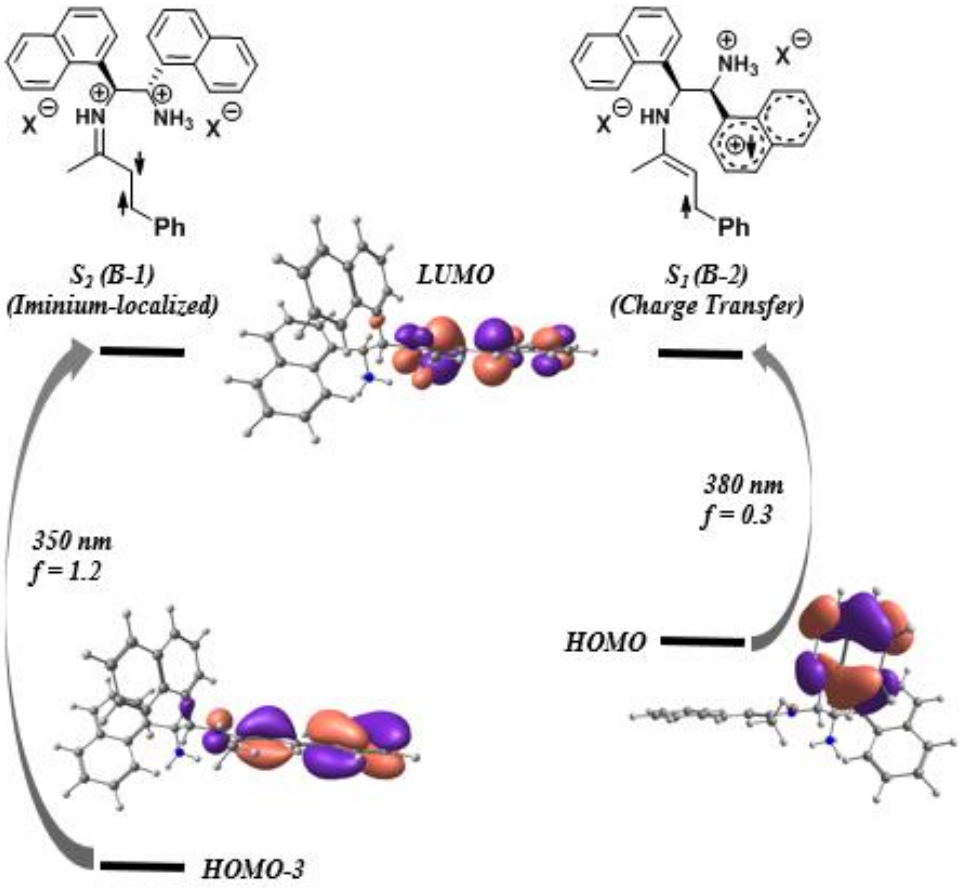

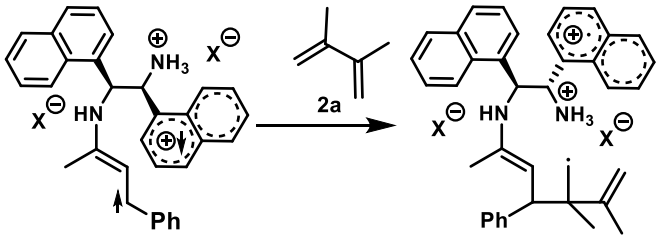

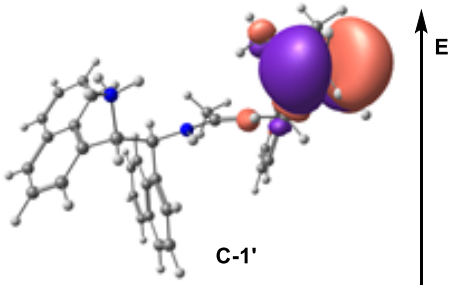

$\Delta\Delta G_{(C\text{-}1)\text{-}(C\text{-}1')}$ = -20.6 kcal/mol

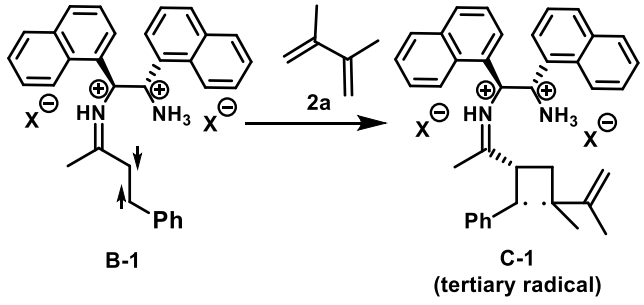

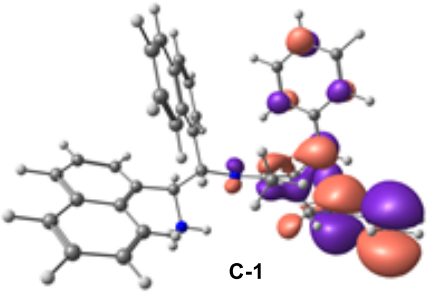

Figure 4. Top) $S_0 \rightarrow S_1$ and $S_0 \rightarrow S_2$ transitions found from TDDFT calculations at the CAMB3LYP/631G* level on the optimised structure at M062X/6311G** level of the **A-1** species. The orbitals found at the M062X/6311G** level are drawn at 97 % probability. Bottom) Two possible pathways leading to the experimentally observed product and relative energy of the two corresponding radicals (SOMO-2 orbitals).

The representation of the energy diagram for the different species involved in the excitation process is illustrated in Figure 5. The ground state EDA complex **A-1** can reach a charge transfer excited state **B-2** (singlet charge transfer, $\mathbf{CT^S}$), which can convert to the excited species **B-1** (singlet iminium-localized, $\mathbf{LE^S}$) by means of a thermal equilibrium in the excited state.[10e] In principle, the singlet excited species could undergo an intersystem crossing (ISC) to the triplet analogues. However, as expected according to El-Sayed's rule,[15b,18] and the well-known observed trend that organic photocatalysts preferentially work as active species at the singlet excited state upon direct light excitation,[1c] the ISC rate would be extremely slow for an iminium-ion, discarding any contribution of triplet excited species in this system. Therefore, the singlet iminium-localized excited species **B-1** ($\mathbf{LE^S}$) is proposed as the only active intermediate.[14]

The TDDFT calculations revealed that, although spin-forbidden through direct excitation, the most favourable (and lowest in energy) of the singlet-triplet transitions is localised over the iminium fragment (HOMO-3/LUMO), with an energy gap of 46 kcal/mol.[17] Thus, through the use of an external ruthenium photosensitiser, the reaction can be further catalysed by means of triplet photosensitisation, populating the iminium-localised triplet excited state, as observed experimentally (see blue line, right-Figure 5).

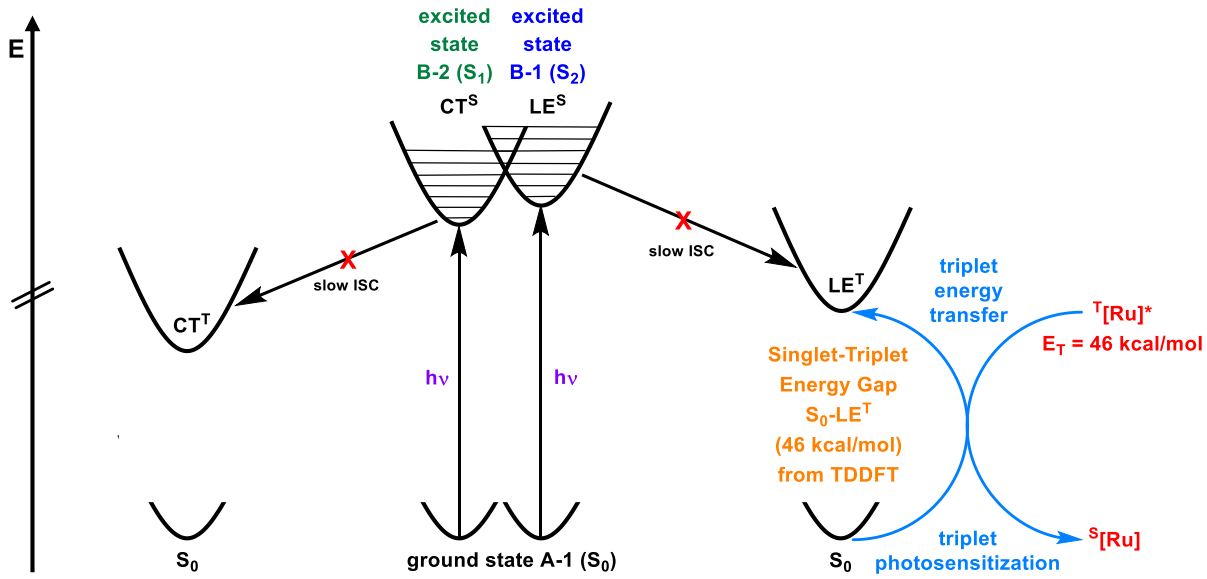

Figure 5. Representation of the energy diagram for the ground state and excited state species that are involved in the EDA complex-mediated [2+2] photocycloaddition or in the triplet photosensitized analogous reaction.

To gain further evidence in support of the mechanistic proposal, some additional experiments were performed (Scheme 1). The employment of alkyl catalyst **3g** or catalyst **3h** predictably led to negligible conversion and to a racemic product, because they are unable to form an EDA complex due to the lack of electron-rich (donor) moieties (Scheme 1a,b).[19] On the other hand, when a ruthenium photocatalyst was employed as an external photosensitiser the reaction was able to proceed through a triplet energy transfer mechanism, indicating that, even if not capable of forming any EDA complexes, the catalysts **3g** and **3h** can properly condensate with enone **1a** to carry out the reaction, albeit with a low enantioselectivity.[6a-b,9,20]

Scheme 1. Additional proof supporting the mechanistic proposal and the EDA complex formation.

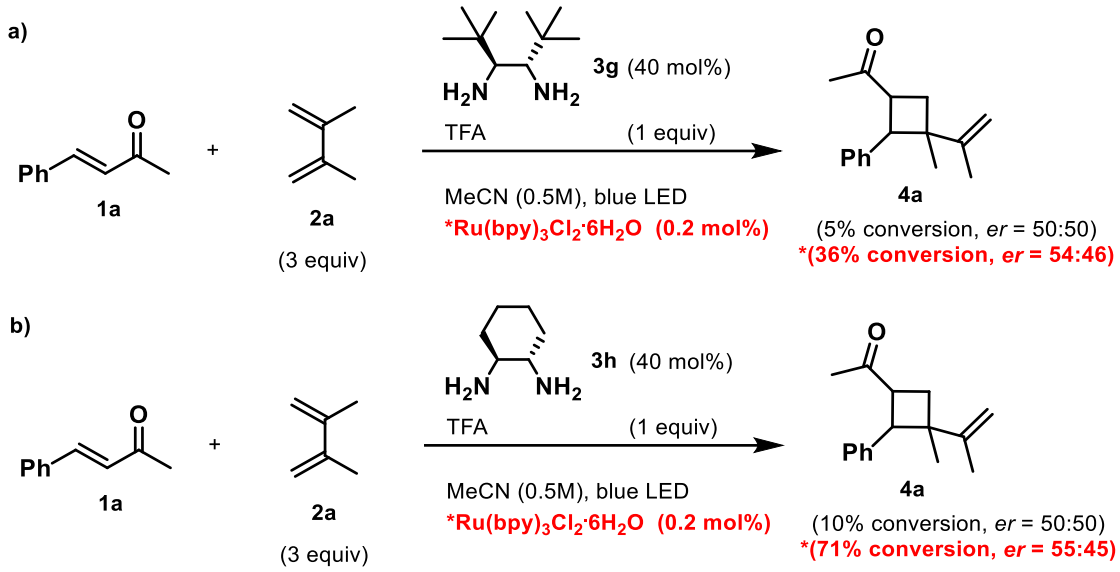

CONCLUSIONS

In conclusion we have described an aminocatalytic activation strategy to obtain enantioenriched cyclobutane derivatives. The direct excitation of an intramolecular EDA complex allows the use of visible light irradiation in the [2+2] photocatalytic cycloaddition, avoiding uncatalysed pathways between enones and dienes, which enables an asymmetric iminium ion catalysed reaction. The combination of the experimental data and DFT calculations reveal that the EDA behaviour results from a low energy charge transfer excited state (**B-2**). Furthermore, such an intermediate makes accessible, through a thermal equilibrium, a localised excited state (**B-1**), which is the active species in the [2+2] cycloaddition. This is the first aminocatalytic enantioselective [2+2] reaction that enables the preparation of enantioenriched cyclobutanes, which are inaccessible by Lewis acid activation strategies reported up until now.

ASSOCIATED CONTENT

Supporting Information. The following files are available free of charge.

Experimental details, characterization data of compounds, NMR spectra, SFC traces, mechanistic discussion and DFT calculations data (PDF)

X-Ray Crystallographic Data (CIF)

AUTHOR INFORMATION

Corresponding Author

Prof. Dr. José Alemán*

e-mail: jose.aleman@uam.es

Author Contributions

All authors have given approval to the final version of the manuscript.

ACKNOWLEDGMENT

Financial support was provided by the European Research Council (ERC-CoG, contract number: 647550), Spanish Government (RTI2018-095038-B-I00), "Comunidad de Madrid" and European Structural Funds (S2018/NMT-4367). We thank Prof. Olga García Mancheño for helpful discussion about the manuscript.

REFERENCES

1. (a) C. Prier, D. Rankic, D. W. C. MacMillan "Visible Light Photoredox Catalysis with Transition Metal Complexes: Applications in Organic Synthesis", *Chem. Rev*. **2013**, *113*, 5322-5363; (b) J. M. R. Narayanam, C. R. J. Stephenson "Visible Light Photoredox Catalysis: Applications in Organic Synthesis", *Chem. Soc. Rev*. **2011**, *40*, 102-113; (c) N. A. Romero, D. A. Nicewicz "Organic Photoredox Catalysis", *Chem. Rev.* **2016**, 116, 10075-10166; (d) Q.-Q. Zhou, Y.-Q. Zou, L.-Q. Lu, W.-J. Xiao "Visible-Light-Induced Organic Photochemical Reactions via Energy Transfer Pathways", *Angew. Chem. Int. Ed.* **2019**, *58*, 1586-1604; *Angew. Chem*. **2019**, *131*, 1600-1619; (e) C. R. J. Stephenson, T. P. Yoon, D. W. C. MacMillan "Visible Light Photocatalysis in Organic Chemistry", **2018,** Wiley-VCH.

2. (a) R. Brimioulle, D. Lenhart, M. M. Maturi, T. Bach "Enantioselective Catalysis of Photochemical Reactions", *Angew. Chem. Int. Ed*. **2015**, *54*, 3872-3890; (b) E. Meggers "Asymmetric Catalysis Activated by Visible Light", *Chem. Commun*. **2015**, *51*, 3290-3301; (c) A. F. Garrido-Castro, M. C. Maestro, J. Alemán "Asymmetric Induction in Photocatalysis - Discovering a New Side to Light-Driven Chemistry", *Tetrahedron Lett.* **2018**, *59*, 1286-1294; (d) A. Bauer, F. Westkamper, S. Grimme, T. Bach "Catalytic Enantioselective Reactions Driven by Photoinduced Electron Transfer", *Nature* **2005**, *436*, 1139-1140; (e) C. Müller, A. Bauer, T. Bach "Light-Driven Enantioselective Organocatalysis", *Angew. Chem. Int. Ed*. **2009**, *48*, 6640-6642; *Angew. Chem*. **2009**, *121*, 6767-6769.

3. (a) S. Poplata, A. Tröster, Y.-Q. Zou, T. Bach "Recent Advances in the Synthesis of Cyclobutanes by Olefin [2 + 2] Photocycloaddition Reactions", *Chem. Rev*. **2016**, *116*, 9748-9815; (b) J. Du, K. L. Skubi, D. M. Schultz, T. P. Yoon "A Dual-Catalysis Approach to Enantioselective [2 + 2] Photocycloadditions Using Visible Light", *Science* **2014**, *344*, 392-396; (c) T. P. Yoon

"Photochemical Stereocontrol Using Tandem Photoredox–Chiral Lewis Acid Catalysis", *Acc. Chem. Res*. **2016**, *49*, 2307−2315.

4. (a) R. Alonso, T. Bach "A Chiral Thioxanthone as an Organocatalyst for Enantioselective [2+2] Photocycloaddition Reactions Induced by Visible Light", *Angew. Chem. Int. Ed*. **2014**, *53*, 4368-4371; *Angew. Chem*. **2014**, *126*, 4457-4460. For an example employing a chiral thiourea as the catalyst in an intramolecular [2+2] photocycloaddition of 2,3-dihydropyridone-5-carboxylates, see (b) F. Mayr, R. Brimioulle, T. Bach "A Chiral Thiourea as a Template for Enantioselective Intramolecular [2+2] Photocycloaddition Reactions", *J. Org. Chem*. **2016**, *81*, 6965-6971.

5. (a) R. Brimioulle, T. Bach "Enantioselective Lewis Acid Catalysis of Intramolecular Enone [2+2] Photocycloaddition Reactions", *Science* **2013**, *342*, 840–843. For an intermolecular version, see: (b) S. Poplata, T. Bach "Enantioselective Intermolecular [2+2] Photocycloaddition Reaction of Cyclic Enones and Its Application in a Synthesis of (−)-Grandisol", *J. Am. Chem. Soc.* **2018**, *140*, 3228-3231.

6. (a) T. R. Blum, Z. D. Miller, D. M. Bates, I. A. Guzei, T. P. Yoon "Enantioselective Photochemistry through Lewis Acid–Catalyzed Triplet Energy Transfer", *Science* **2016**, *354*, 1391-1395; (b) Z. D. Miller, B. J. Lee, T. P. Yoon "Enantioselective Crossed Photocycloadditions of Styrenic Olefins by Lewis Acid Catalyzed Triplet Sensitization", *Angew. Chem. Int. Ed*. **2017**, *56*, 11891-11895; *Angew. Chem*. **2017**, *129*, 12053-12057. Very recently the Yoon's group reported an enantioselective [2+2] photocycloaddition over cinnamate esters: (c) M. E. Daub, H. Jung, B. J. Lee, J. Won, M.-H. Baik, T. P. Yoon "Enantioselective [2+2] Cycloadditions of Cinnamate Esters: Generalizing Lewis Acid Catalysis of Triplet Energy Transfer", *J. Am. Chem. Soc*. **2019**, *141*, 9543-9547.

7. (a) X. Huang, T. R. Quinn, K. Harms, R. D. Webster, L. Zhang, O. Wiest, E. Meggers "Direct Visible-Light-Excited Asymmetric Lewis Acid Catalysis of Intermolecular [2+2] Photocycloadditions", *J. Am. Chem. Soc.* **2017**, *139*, 9120−9123; (b) N. Hu, H. Jung, Y. Zheng, J. Lee, L. Zhang, Z. Ullah, X. Xie, K. Harms, M.-H. Baik, E. Meggers "Catalytic Asymmetric Dearomatization by Visible-Light-Activated [2+2] Photocycloaddition", *Angew. Chem. Int. Ed.* **2018**, *57*, 6242-6246; *Angew. Chem*. **2018**, *130*, 6350-6354. For an example of [3+2] photocycloaddition developed by the same group, see: (c) X. Huang, X. Li, X. Xie, K. Harms, R. Riedel, E. Meggers "Catalytic Asymmetric Synthesis of a Nitrogen Heterocycle through Stereocontrolled Direct Photoreaction from Electronically Excited State", *Nat. Commun*. **2017**, *8*, 2245. For examples of the use of a chiral hydrogen-bonding Iridium photocatalyst reported by the Yoon's lab, see: (d) K. L. Skubi, J. B. Kidd, H. Jung, I. A. Guzei, M.-H. Baik, T. P. Yoon "Enantioselective Excited-State Photoreactions Controlled by a Chiral Hydrogen-Bonding Iridium Sensitizer",*J. Am. Chem. Soc.* **2017**, *139*, 17186-17192; (e) J. Zheng, W. B. Swords, H. Jung, K. L. Skubi, J. B. Kidd, G. J. Meyer, M.-H. Baik, T. P. Yoon "Enantioselective Intermolecular Excited-State Photoreactions Using a Chiral Ir Triplet Sensitizer: Separating Association from Energy Transfer in Asymmetric Photocatalysis", *J. Am. Chem. Soc*. **2019**, *141*, 13625-13634.

8. C. Chen, V. Chang, X. Cai, E. Duesler, P. S. Mariano "A General Strategy for Absolute Stereochemical Control in Enone−Olefin [2 + 2] Photocycloaddition Reactions", *J. Am. Chem. Soc*. **2001**, *123*, 6433-6434.

9. F. M. Hörmann, T. S. Chung, E. Rodriguez, M. Jakob, T. Bach "Evidence for Triplet Sensitization in the Visible-Light-Induced [2+2] Photocycloaddition of Eniminium Ions", *Angew. Chem. Int. Ed*. **2018**, *57*, 827-831; *Angew. Chem*. **2018**, *130*, 835-839.

10. (a) E. Arceo, I. D. Jurberg, A. Álvarez-Fernández, P. Melchiorre "Photochemical Activity of a Key Donor–Acceptor Complex Can Drive Stereoselective Catalytic α-Alkylation of Aldehydes", *Nat. Chem*. **2013**, *5*, 750-756; (b) E. Arceo, A. Bahamonde, G. Bergonzini, P. Melchiorre "Enantioselective Direct α-Alkylation of Cyclic Ketones by Means of Photo-Organocatalysis", *Chem. Sci*., **2014**, *5*, 2438–2442; (c) Ł. Woźniak, J. J. Murphy, P. Melchiorre "Photo-organocatalytic Enantioselective Perfluoroalkylation of β-Ketoesters", *J. Am. Chem. Soc*. **2015**, *137*, 5678-5681; (d) Z.-Y. Cao, T. Ghosh, P. Melchiorre "Enantioselective Radical Conjugate Additions Driven by a Photoactive Intramolecular Iminium-Ion-Based EDA Complex", *Nat. Commun*. **2018**, *9*, 3274. For a review regarding applications of EDA complexes in organic synthesis, see: (e) C. G. S. Lima, T. de M. Lima, M. Duarte, I. D. Jurberg, M. W. Paixão "Organic Synthesis Enabled by Light-Irradiation of EDA Complexes: Theoretical Background and Synthetic Applications", *ACS Catal*. **2016**, *6*, 1389-1407. For an example of an intramolecular [2+2] photocycloaddition over 4-akenyl-substituted coumarins enabled by an intermolecular exciplex formation, see: (f) N. Vallavoju, S. Selvakumar, S. Jockusch, M. P. Sibi, J. Sivaguru "Enantioselective Organo-Photocatalysis Mediated by Atropisomeric Thiourea Derivatives", *Angew. Chem. Int. Ed.* **2014**, *53*, 5604-5608.

11. EDA complexes between substituted benzenes (as electron donors) and quinones are reported in the literature: P. C. Dwivedi, A. Gupta, A. K. Banga "Electron Donor-Acceptor Complexes of Substituted Benzenes with Quinones", *Curr. Sci*. **1982**, *51*, 651-653.

12. Catalyst **3d** showed as well a negligible absorption, indicating that only the intramolecular EDA complex is responsible of the increased absorption and of the photoactivity (see Supporting Information for further details).

13. CCDC 1923032 (**5a**) contains the crystallographic data. These data can be obtained free of charge at www.ccdc.cam.ac.uk.

14. We can discard **B-2** from being the reactive species in the [2+2] photocycloaddition because of the observed experimental regioselectivity and because of the results of DFT calculations (see the Supporting Information for a full explanation and details).

15. For examples of singlet state reactivity of iminium ions, see: (a) C. Brenninger, J. D. Jolliffe, T. Bach "Chromophore Activation of α,β-Unsaturated Carbonyl Compounds and Its Application to Enantioselective Photochemical Reactions", *Angew. Chem. Int. Ed*. **2018**, *57*, 14338-14349; *Angew. Chem*. **2018**, *130*, 14536-14547; (b) P. Klán, J. Wirz "*Photochemistry of Organic* Compounds", Wiley, Chichester, **2009**; (c) X. Cai, V. Chang, C. Chen, H.-J. Kim, P. S. Mariano "A Potentially General Method to Control Relative Stereochemistry in Enone–Olefin 2+2-Photocycloaddition Reactions by using Eniminium Salt Surrogates", *Tetrahedron Lett.* **2000**, 4*1*, 9445-9449.

16. A concerted [2+2] reaction in which the two C-C bonds were formed simultaneously, leading directly to cyclobutyl iminium ion **D-1**, is an alternative plausible pathway. Nevertheless, the possibility of the presence of a biradical intermediate was indicated by DFT calculations (see the Supporting Information for the details).

17. In the presence of an external photosensitizer the reaction can be further catalyzed through a triplet energy transfer mechanism. Indeed, by means of TDDFT calculations (Figure 5, see the Supporting Information for further details), the singlet-triplet energy gap for the EDA complex **A-1** has been found being 46 kcal/mol which is in accordance with the triplet energy of $Ru(bpy)_3Cl_2 \cdot 6H_2O$ that has been reported in the literature (46 kcal/mol). On the other hand, the

enone substrate **1a** presents a higher energy gap that does not allow the reaction to proceed in the absence of a diamine catalyst, which enables the formation of the iminium ion (conversion <10%). This has been supported by further experimental evidences (Scheme 1a,b).

18. M. A. El-Sayed, *Acc. Chem. Res.* **1968**, *1*, 8-16.

19. This suggests that the low conversion was simply due to background processes.

20. This clearly demonstrate that the iminium ion obtained from the condensation of an alkyl diamine catalyst with enone **1a** can reach a triplet excited state by triplet energy transfer from an external ruthenium photocatalyst. Indeed, by means of TDDFT calculations (see the Supporting Information), the singlet-triplet energy gap for an analogous iminium ion, unable of forming any EDA complex due to the lack of naphthyl moieties (replaced by methyl groups), has been found being 46 kcal/mol which is in accordance with the triplet energy of $Ru(bpy)_3Cl_2{\cdot}6H_2O$ that has been reported in the literature (46 kcal/mol). On the other hand, the enone substrate **1a** presents a higher energy gap that does not allow the reaction to proceed in the absence of a diamine catalyst, which enables the formation of the iminium ion, leading to a negligible conversion (<10%). This is in accordance with the reported results of triplet sensitization over stoichiometric iminium ions reported by Bach's research group (see ref. 9).

Experimental Part
Chapter 4

(The complete “Supporting Information” documents, with all the characterization data, NMR spectra, SFC or HPLC traces and other experimental procedures have been included in the enclosed USB memory)

General procedure for the enantioselective [2+2] photocycloaddition

An oven-dried 10 mL vial, equipped with a magnetic stir bar, was charged with catalyst **3d** (0.02 mmol), and the corresponding ketone **1** (0.10 mmol). Then, 200 µL of a TFA solution (0.10 mmol, 0.5 M) in diethyl ether were added, followed by the corresponding alkene partner (0.30 mmol). The vial was closed with a PTFE/rubber septum and the reaction mixture was deoxygenated by three cycles of "freeze-pump-thaw". The reaction mixture was stirred at room temperature under blue LED irradiation (450 nm) in a photoreactor, as illustrated in the reaction setup, until reaction completion (as judged by TLC or ^{1}H NMR). The solvent was removed under reduced pressure and the crude mixture was purified by flash chromatography to afford the corresponding cyclobutane **4** in stated yield (sum of both major and minor diastereoisomers) and enantiomeric purity. Unless otherwise noted, characterization data and enantiomeric ratios are reported for the major cyclobutane diastereoisomer.

Characterization data for the enantioenriched cyclobutanes (4a-q)

1-((1*R*,2*R*,3*S*)-3-Methyl-2-phenyl-3-(prop-1-en-2-yl)cyclobutyl)ethan-1-one (4a)

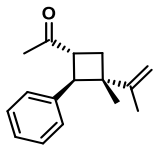

4a

1a was prepared according to the general procedure and purified by flash chromatography (CyHex : EtOAc = 95 : 5) to obtain 22.6 mg of product as a colorless oil (99% yield). The enantiomeric excess was determined by SFC on a *Daicel Chiralpak* IB-3 column: CO_2/MeOH 95:5, flow rate 1.0 mL/min, λ = 210 nm, τ_{major} = 2.78 min, τ_{minor} = 2.59 (*er* = 90:10).

$[\alpha]^{20}_D$ = - 82 (*c* = 0.37, $CHCl_3$).

^{1}H NMR (300 MHz, $CDCl_3$): δ 7.36 – 7.29 (m, 2H), 7.28 – 7.20 (m, 3H), 4.83 (br s, 1H), 4.79 (br p, *J* = 1.4 Hz, 1H), 3.73 (d, *J* = 10.2 Hz, 1H), 3.50 (q, *J* = 9.7 Hz, 1H), 2.31 (t, *J* = 10.2 Hz, 1H), 2.05 (s, 3H), 1.92 (dd, *J* = 10.8, 8.7 Hz, 1H), 1.71 (br s, 3H), 1.03 (s, 3H).

^{13}C NMR (75 MHz, $CDCl_3$): δ 209.3, 152.6, 139.5, 128.4, 128.3, 126.7, 108.9, 50.2, 44.9, 44.8, 33.1, 28.4, 21.7, 19.0.

HRMS (ESI): calculated for $C_{16}H_{21}O^+$, $[M+H]^+$ = 229.1587; found = 229.1595.

1-((1*R*,2*R*,3*S*)-3-Methyl-2-phenyl-3-(prop-1-en-2-yl)cyclobutyl)butan-1-one (4b)

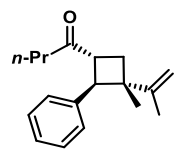

4b

4b was prepared according to the general procedure and purified by flash chromatography (CyHex : EtOAc = 97 : 3) to obtain 25.4 mg of product as a colorless oil (99% yield). The enantiomeric excess was determined by SFC on a *Daicel Chiralpak* IC column: CO_2/MeOH 95:5, flow rate 2.0 mL/min, λ = 230 nm, τ_{major} = 6.85 min, τ_{minor} = 6.63 (*er* = 88:12).

$[\alpha]^{20}_D$ = - 86 (*c* = 0.40, $CHCl_3$).

^{1}H NMR (300 MHz, $CDCl_3$): δ 7.37 – 7.28 (m, 2H), 7.27 – 7.20 (m, 3H), 4.83 (br s, 1H), 4.79 (br p, *J* = 1.5 Hz, 1H), 3.74 (d, *J* = 10.1 Hz, 1H), 3.49 (q, *J* = 9.7 Hz, 1H), 2.36 – 2.24 (m, 3H), 1.90 (dd, *J* = 10.6, 8.8 Hz, 1H), 1.71 (s, 3H), 1.55 (sxt, *J* = 7.3 Hz, 2H), 1.03 (s, 3H), 0.84 (t, *J* = 7.4 Hz, 3H).

^{13}C NMR (75 MHz, $CDCl_3$): δ 211.2, 152.6, 139.7, 128.3 (2C), 126.7, 108.9, 50.0, 44.9, 44.1, 43.2, 33.2, 21.7, 19.0, 17.2, 13.9.

HRMS (ESI): calculated for $C_{18}H_{25}O^+$, $[M+H]^+$ = 257.1900; found = 257.1902.

2-Methyl-1-((1*R*,2*R*,3*S*)-3-methyl-2-phenyl-3-(prop-1-en-2-yl)cyclobutyl)propan-1-one (4c)

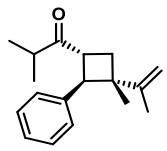

4c

4c was prepared according to the general procedure and purified by flash chromatography (CyHex : EtOAc = 97 : 3) to obtain 19.5 mg of product (as a mixture of diastereoisomers) as a colorless oil (76% yield). The enantiomeric excess was determined by SFC on a *Daicel Chiralpak* IA column: CO_2/MeOH 95:5, flow rate 1.0 mL/min, λ = 210 nm, τ_{major} = 12.16 min, τ_{minor} = 11.57 (*er* = 73:27).

^{1}H NMR (300 MHz, $CDCl_3$, *major diastereoisomer*): δ 7.34 – 7.18 (m, 5H), 4.83 (br s, 1H), 4.78 (br p, *J* = 1.5 Hz, 1H), 3.81 (d, *J* = 10.0 Hz, 1H), 3.64 (q, *J* = 9.5 Hz, 1H), 2.55 (hept, *J* = 7.2 Hz, 1H), 2.28 (t, *J* = 10.0 Hz, 1H), 1.92 (dd, *J* = 10.7, 8.6 Hz, 1H), 1.71 (s, 3H), 1.07 – 1.00 (m, 9H).

^{13}C NMR (75 MHz, $CDCl_3$, *major diastereoisomer*): δ 214.7, 152.6, 139.8, 128.30, 128.28, 126.6, 108.9, 49.6, 45.0, 42.4, 39.6, 34.1, 21.8, 19.0, 18.6, 18.2.

HRMS (ESI): calculated for $C_{18}H_{25}O^+$, $[M+H]^+$ = 257.1900; found = 257.1880.

1-((1*R*,2*S*,3*S*)-3-Methyl-3-(prop-1-en-2-yl)-2-(o-tolyl)cyclobutyl)ethan-1-one (4d)

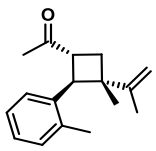

4d

4d was prepared according to the general procedure and purified by flash chromatography (CyHex : EtOAc = 95 : 5) to obtain 22.5 mg of product as a colorless oil (93% yield). The enantiomeric excess was determined by SFC on a *Daicel Chiralpak* IC column: CO_2/MeOH 95:5, flow rate 2.0 mL/min, λ = 210 nm, τ_{major} = 7.84 min, τ_{minor} = 7.34 (*er* = 88:12).

$[\alpha]^{20}_D$ = - 93 (*c* = 0.175, $CHCl_3$).

^{1}H NMR (300 MHz, $CDCl_3$): δ 7.36 (d, *J* = 7.6 Hz, 1H), 7.25 – 7.16 (m, 1H), 7.15 – 7.12 (m, 2H), 4.78 (br p, *J* = 1.5 Hz, 1H), 4.76 – 4.74 (m, 1H), 3.88 (d, *J* = 10.3 Hz, 1H), 3.60 (q, *J* = 9.3 Hz, 1H), 2.57 – 2.49 (m, 1H), 2.26 (s, 3H), 2.00 (s, 3H), 1.81 – 1.80 (m, 3H), 1.76 (dd, *J* = 11.2, 8.9 Hz, 1H), 1.07 (s, 3H).

^{13}C NMR (75 MHz, $CDCl_3$): δ 209.2, 151.3, 137.29, 137.26, 130.7, 127.6, 126.6, 125.7, 110.1, 47.3, 45.1, 44.5, 31.3, 28.6, 21.5, 20.3, 19.7.

HRMS (ESI): calculated for $C_{17}H_{23}O^+$, $[M+H]^+$ = 243.1743; found = 243.1716.

1-((1*R*,2*S*,3*S*)-2-(2-Isopropylphenyl)-3-methyl-3-(prop-1-en-2-yl)cyclobutyl)ethan-1-one (4e)

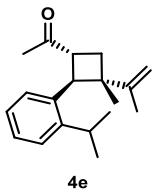
4e

4e was prepared according to the general procedure and purified by flash chromatography (CyHex : EtOAc = 95 : 5) to obtain 25.4 mg of product as a colorless oil (94% yield). The enantiomeric excess was determined by SFC on a *Daicel Chiralpak* IC column: CO_2/MeOH 96:4, flow rate 2.0 mL/min, λ = 210 nm, τ_{major} = 5.94 min, τ_{minor} = 5.67 (*er* = 91:9).

$[\alpha]^{20}_D$ = - 177 (*c* = 0.885, $CHCl_3$).

^{1}H NMR (300 MHz, $CDCl_3$): δ 7.39 – 7.32 (m, 1H), 7.30 – 7.15 (m, 3H), 4.80 (br p, *J* = 1.5 Hz, 1H), 4.72 (s, 1H), 3.93 (d, *J* = 10.2 Hz, 1H), 3.63 (q, *J* = 9.3 Hz, 1H), 3.05 (hept, *J* = 6.8 Hz, 1H), 2.59 – 2.49 (m, 1H), 2.00 (s, 3H), 1.80 – 1.71 (m, 4H), 1.18 (d, *J* = 6.8 Hz, 3H), 1.11 (d, *J* = 6.8 Hz, 3H), 1.04 (s, 3H).

^{13}C NMR (75 MHz, $CDCl_3$): δ 209.1, 150.7, 148.1, 135.4, 127.7, 127.0, 125.6, 125.4, 110.1, 46.6, 45.3, 44.7, 31.1, 28.6, 28.5, 25.5, 22.9, 21.5, 19.7.

HRMS (ESI): calculated for $C_{19}H_{27}O^+$, $[M+H]^+$ = 271.2056; found = 271.2056.

1-((1*R*,2*S*,3*S*)-2-Mesityl-3-methyl-3-(prop-1-en-2-yl)cyclobutyl)ethan-1-one (4f)

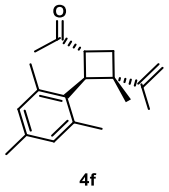
4f

4f was prepared according to the general procedure and purified by flash chromatography (CyHex : EtOAc = 95 : 5) to obtain 20.5 mg of product as a colorless oil (76% yield). The enantiomeric excess was determined by SFC on a *Daicel Chiralpak* IB column: CO_2/MeOH 95:5, flow rate 1.0 mL/min, λ = 210 nm, τ_{major} = 3.51 min, τ_{minor} = 3.20 (*er* = 81:19).

$[\alpha]^{20}_D$ = - 103 (*c* = 0.48, $CHCl_3$).

^{1}H NMR (300 MHz, $CDCl_3$): δ 6.79 (s, 2H), 4.78 – 4.73 (m, 2H), 4.18 (dt, *J* = 10.7, 8.6 Hz, 1H), 4.04 (d, *J* = 10.8 Hz, 1H), 2.53 (dd, *J* = 11.2, 8.5 Hz, 1H), 2.43 (s, 6H), 2.22 (s, 3H), 2.05 (s, 3H), 1.84 (dd, *J* = 11.2, 8.8 Hz, 1H), 1.76 (s, 3H), 1.24 (s, 3H).

^{13}C NMR (75 MHz, $CDCl_3$): δ 209.6, 151.5, 138.1, 135.8, 132.2, 130.9, 110.0, 49.1, 46.8, 46.2, 32.2, 28.0, 23.0, 21.7, 20.7, 20.5.

HRMS (ESI): calculated for $C_{19}H_{27}O^+$, $[M+H]^+$ = 271.2056; found = 271.2047.

1-((1*R*,2*R*,3*S*)-2-(3,5-Dimethylphenyl)-3-methyl-3-(prop-1-en-2-yl)cyclobutyl)ethan-1-one (4g)

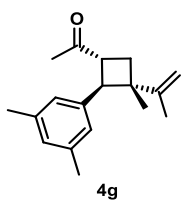
4g

4g was prepared according to the general procedure and purified by flash chromatography (CyHex : EtOAc = 95 : 5) to obtain 22.1 mg of product as a colorless oil (86% yield). The enantiomeric excess was determined by SFC on a *Daicel Chiralpak* IB column: CO_2/MeOH 98:2, flow rate 1.0 mL/min, λ = 210 nm, τ_{major} = 3.68 min, τ_{minor} = 3.37 (*er* = 87:13).

$[\alpha]^{20}_D$ = - 115 (*c* = 1.095, $CHCl_3$).

^{1}H NMR (300 MHz, $CDCl_3$): δ 6.88 – 6.83 (m, 3H), 4.84 – 4.82 (m, 1H), 4.78 (br p, *J* = 1.4 Hz, 1H), 3.65 (d, *J* = 10.2 Hz, 1H), 3.47 (q, *J* = 9.6 Hz, 1H), 2.32 – 2.25 (m, 7H), 2.04 (s, 3H), 1.90 (dd, *J* = 10.7, 8.8 Hz, 1H), 1.71 – 1.70 (m, 3H), 1.03 (s, 3H).

^{13}C NMR (75 MHz, $CDCl_3$): δ 209.4, 152.7, 139.4, 137.7, 128.4, 126.2, 108.8, 50.2, 44.9, 44.8, 33.1, 28.4, 21.7, 21.6, 19.0.

HRMS (ESI): calculated for $C_{18}H_{25}O^+$, $[M+H]^+$ = 257.1900; found = 257.1913.

1-((1*R*,2*R*,3*S*)-2-(4-Methoxyphenyl)-3-methyl-3-(prop-1-en-2-yl)cyclobutyl)ethan-1-one (4h)

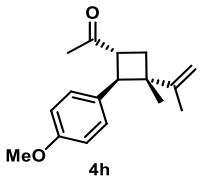

4h

4h was prepared according to the general procedure (employing MTBE as the solvent) and purified by flash chromatography (CyHex : EtOAc = 95 : 5) to obtain 15.5 mg of product as a colorless oil (60% yield). The enantiomeric excess was determined by SFC on a *Daicel Chiralpak* IA column: CO_2/MeOH 95:5, flow rate 2.0 mL/min, λ = 230 nm, τ_{major} = 8.37 min, τ_{minor} = 7.96 (*er* = 82:18).

$[\alpha]^{20}_D$ = - 51 (*c* = 0.32, $CHCl_3$).

^{1}H NMR (300 MHz, $CDCl_3$): δ 7.19 (d, *J* = 8.7 Hz, 2H), 6.87 (d, *J* = 8.8 Hz, 2H), 4.81 – 4.79 (m, 1H), 4.77 (br p, *J* = 1.4 Hz, 1H), 3.81 (s, 3H), 3.62 (d, *J* = 10.3 Hz, 1H), 3.44 (q, *J* = 9.5 Hz, 1H), 2.31 (t, *J* = 10.2 Hz, 1H), 2.02 (s, 3H), 1.93 – 1.84 (m, 1H), 1.69 (br s, 3H), 1.02 (s, 3H).

^{13}C NMR (75 MHz, $CDCl_3$): δ 209.3, 158.5, 152.8, 131.6, 129.4, 113.8, 108.7, 55.4, 50.1, 45.3, 44.9, 32.8, 28.4, 21.7, 19.0.

HRMS (ESI): calculated for $C_{17}H_{23}O_2^+$, $[M+H]^+$ = 259.1693; found = 259.1659.

1-((1*R*,2*R*,3*S*)-3-Methyl-3-(prop-1-en-2-yl)-2-(4-(trifluoromethyl)phenyl)cyclobutyl)ethan-1-one (4i)

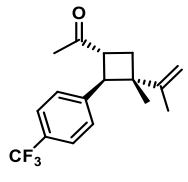

4i

4i was prepared according to the general procedure and purified by flash chromatography (CyHex : EtOAc = 95 : 5) to obtain 18.4 mg of product as a colorless oil (62% yield). The enantiomeric excess was determined by SFC on a *Daicel Chiralpak* IG-3 column: CO_2/MeOH 95:5, flow rate 2.0 mL/min, λ = 230 nm, τ_{major} = 2.66 min, τ_{minor} = 3.26 (*er* = 82:18).

$[\alpha]^{20}_D$ = - 40 (*c* = 0.175, $CHCl_3$).

^{1}H NMR (300 MHz, $CDCl_3$): δ 7.57 (d, *J* = 8.1 Hz, 2H), 7.33 (d, *J* = 8.4 Hz, 2H), 4.86 – 4.81 (m, 2H), 3.84 (d, *J* = 10.2 Hz, 1H), 3.49 (q, *J* = 9.6 Hz, 1H), 2.28 (t, *J* = 10.2 Hz, 1H), 2.09 (s, 3H), 2.00 (ddd, *J* = 10.7, 8.9, 0.8 Hz, 1H), 1.72 (dd, *J* = 1.4, 0.7 Hz, 3H), 1.03 (s, 3H).

^{13}C NMR (75 MHz, $CDCl_3$): δ 208.7, 151.9, 143.83, 143.82, 128.4 (2C), 125.39, 125.34, 125.29, 125.24, 109.4, 49.0, 44.9, 44.8, 33.7, 28.2, 21.6, 19.0.

^{19}F NMR (282 MHz, $CDCl_3$): δ -62.44.

HRMS (ESI): calculated for $C_{17}H_{20}F_3O^+$, $[M+H]^+$ = 297.1461; found = 297.1430.

1-((1*R*,2*R*,3*S*)-2-(4-Bromophenyl)-3-methyl-3-(prop-1-en-2-yl)cyclobutyl)ethan-1-one (4j)

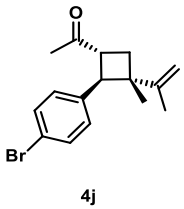

4j

4j was prepared according to the general procedure and purified by flash chromatography (CyHex : EtOAc = 95 : 5) to obtain 27.0 mg of product as a colorless oil (88% yield). The enantiomeric excess was determined by SFC on a *Daicel Chiralpak* IA column: CO_2/MeOH 95:5, flow rate 2.0 mL/min, λ = 230 nm, τ_{major} = 10.02 min, τ_{minor} = 9.59 (*er* = 88:12).

$[\alpha]^{20}_D$ = - 57 (*c* = 0.475, $CHCl_3$).

^{1}H NMR (300 MHz, $CDCl_3$): δ 7.44 (d, *J* = 8.4 Hz, 2H), 7.11 (d, *J* = 8.5 Hz, 2H), 4.83 – 4.76 (m, 2H), 3.70 (d, *J* = 10.2 Hz, 1H), 3.43 (q, *J* = 9.6 Hz, 1H), 2.28 (t, *J* = 10.2 Hz, 1H), 2.06 (s, 3H), 1.95 (dd, *J* = 10.8, 8.8 Hz, 1H), 1.72 – 1.69 (m, 3H), 1.01 (s, 3H).

^{13}C NMR (75 MHz, $CDCl_3$): δ 208.8, 152.2, 138.6, 131.5, 129.9, 120.6, 109.1, 49.2, 44.9, 44.7, 33.4, 28.3, 21.6, 18.9.

HRMS (ESI): calculated for $C_{16}H_{23}NBrO^+$, $[M+NH_4]^+$ = 324.0958; found = 324.0926.

1-((1*R*,2*S*,3*S*)-3-Methyl-2-(naphthalen-1-yl)-3-(prop-1-en-2-yl)cyclobutyl)ethan-1-one (4k)

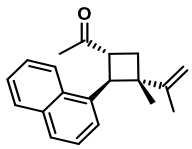

4k

4k was prepared according to the general procedure and purified by flash chromatography (CyHex : EtOAc = 95 : 5) to obtain 13.6 mg of product as a colorless oil (49% yield). The enantiomeric excess was determined by SFC on a *Daicel Chiralpak* IG-3 column: CO_2/MeOH 95:5, flow rate 2.0 mL/min, λ = 230 nm, τ_{major} = 7.73 min, τ_{minor} = 7.20 (*er* = 81:19).

$[\alpha]^{20}_D$ = - 120 (*c* = 0.40, $CHCl_3$).

^{1}H NMR (300 MHz, $CDCl_3$): δ 8.00 – 7.92 (m, 1H), 7.87 – 7.81 (m, 1H), 7.78 – 7.73 (m, 1H), 7.56 – 7.39 (m, 4H), 4.91 – 4.88 (m, 1H), 4.85 – 4.83 (m, 1H), 4.41 (d, *J* = 10.1 Hz, 1H), 3.79 (q, *J* = 9.4 Hz, 1H), 2.73 – 2.64 (m, 1H), 2.04 (s, 3H), 1.83 – 1.81 (m, 4H), 1.01 (s, 3H).

^{13}C NMR (75 MHz, $CDCl_3$): δ 209.1, 150.9, 135.5, 134.1, 132.6, 128.7, 127.5, 125.9, 125.8, 125.2, 125.0, 124.7, 111.2, 47.5, 44.8, 44.7, 31.5, 28.6, 21.4, 20.3.

HRMS (ESI): calculated for $C_{20}H_{23}O^+$, $[M+H]^+$ = 279.1743; found = 279.1757.

1-((1*R*,2*S*,3*S*)-2-(Furan-3-yl)-3-methyl-3-(prop-1-en-2-yl)cyclobutyl)ethan-1-one (4l)

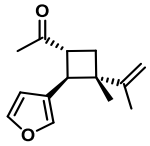

4l

4l was prepared according to the general procedure and purified by flash chromatography (CyHex : EtOAc = 95 : 5) to obtain 9.8 mg of product as a colorless oil (45% yield). The enantiomeric excess was determined by SFC on a *Daicel Chiralpak* IG-3 column: CO_2/MeOH 95:5, flow rate 2.0 mL/min, λ = 210 nm, τ_{major} = 3.97 min, τ_{minor} = 3.70 (*er* = 76:24).

$[\alpha]^{20}_D$ = - 16 (*c* = 0.125, $CHCl_3$).

^{1}H NMR (300 MHz, $CDCl_3$): δ 7.39 (t, *J* = 1.7 Hz, 1H), 7.36 – 7.31 (m, 1H), 6.34 (dd, *J* = 1.8, 0.9 Hz, 1H), 4.74 – 4.71 (m, 2H), 3.46 (d, *J* = 10.2 Hz, 1H), 3.26 – 3.15 (m, 1H), 2.27 (t, *J* = 10.3 Hz, 1H), 2.06 (s, 3H), 1.90 (ddd, *J* = 10.8, 8.5, 0.8 Hz, 1H), 1.67 (dd, *J* = 1.4, 0.8 Hz, 3H), 1.10 (s, 3H).

^{13}C NMR (75 MHz, $CDCl_3$): δ 208.9, 152.89, 143.1, 140.1, 124.2, 111.0, 108.3, 46.2, 44.2, 42.1, 33.2, 28.4, 22.2, 18.4.

HRMS (ESI): calculated for $C_{14}H_{19}O_2^+$, $[M+H]^+$ = 219.1380; found = 219.1342.

1-((1*R*,2*S*,3*R*)-3-Methyl-2-phenyl-3-vinylcyclobutyl)ethan-1-one (4m)

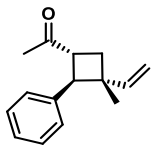

4m

4m was prepared according to the general procedure and purified by flash chromatography (CyHex : EtOAc = 95 : 5) to obtain 16.5 mg of product (as a mixture of diastereoisomers) as a colorless oil (77% yield). The enantiomeric excess was determined by SFC on a *Daicel Chiralpak* IG-3 column: CO_2/MeOH 95:5, flow rate 2.0 mL/min, λ = 210 nm, τ_{major} = 4.10 min, τ_{minor} = 5.38 (*er* = 81:19).

^{1}H NMR (300 MHz, $CDCl_3$, *major diastereoisomer*): δ 7.36 – 7.12 (m, 5H), 6.04 (dd, *J* = 17.1, 10.8 Hz, 1H), 5.06 – 4.95 (m, 2H), 3.65 – 3.41 (m, 2H), 2.36 – 2.23 (m, 1H), 2.11 (s, 3H), 1.97 – 1.88 (m, 1H), 0.90 (s, 3H).

^{13}C NMR (75 MHz, $CDCl_3$, *major diastereoisomer*): δ 209.2, 147.0, 138.9, 128.4, 127.4, 126.7, 111.8, 51.2, 44.4, 41.7, 33.5, 28.5, 20.4.

HRMS (ESI): calculated for $C_{15}H_{19}O^+$, $[M+H]^+$ = 215.1430; found = 215.1442.

1-((1*R*,2*R*,3*S*)-2,3-Diphenylcyclobutyl)ethan-1-one (4n)

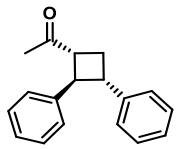

4n

4n was prepared according to the general procedure and purified by flash chromatography (CyHex : EtOAc = 95 : 5) to obtain 20.5 mg of product as a colorless oil (82% yield). The enantiomeric excess was determined by SFC on a *Daicel Chiralpak* IB-3 column: CO_2/MeOH 95:5, flow rate 1.0 mL/min, λ = 210 nm, τ_{major} = 6.40 min, τ_{minor} = 5.88 (*er* = 82:18).

$[\alpha]^{20}_D$ = + 2.3 (*c* = 0.325, $CHCl_3$).

^{1}H NMR (300 MHz, $CDCl_3$): δ 7.38 – 7.16 (m, 10H), 3.68 (t, *J* = 9.6 Hz, 1H), 3.56 (td, *J* = 10.0, 8.0 Hz, 1H), 3.31 (td, *J* = 9.7, 8.2 Hz, 1H), 2.65 – 2.53 (m, 1H), 2.33 (q, *J* = 10.1 Hz, 1H), 2.08 (s, 3H).

^{13}C NMR (75 MHz, $CDCl_3$): δ 208.5, 143.3, 142.3, 128.8, 128.6, 127.1, 127.0, 126.8, 126.7, 50.9, 50.1, 43.0, 28.52, 28.50.

HRMS (ESI): calculated for $C_{18}H_{19}O^+$, $[M+H]^+$ = 251.1430; found = 251.1401.

1-((1*R*,2*R*,3*S*)-2-Phenyl-3-(4-(trifluoromethyl)phenyl)cyclobutyl)ethan-1-one (4o)

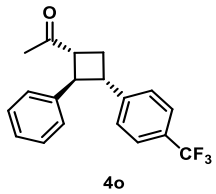

4o

4o was prepared according to the general procedure and purified by flash chromatography (CyHex : EtOAc = 95 : 5) to obtain 22.9 mg of product as a colorless oil (72% yield). The enantiomeric excess was determined by SFC on a *Daicel Chiralpak* IC column: CO_2/MeOH 95:5, flow rate 2.0 mL/min, λ = 230 nm, τ_{major} = 6.89 min, τ_{minor} = 6.48 (*er* = 78:22).

$[\alpha]^{20}_D$ = - 4.1 (*c* = 0.455, $CHCl_3$).

^{1}H NMR (300 MHz, $CDCl_3$): δ 7.54 (d, *J* = 8.1 Hz, 2H), 7.38 – 7.22 (m, 7H), 3.73 – 3.55 (m, 2H), 3.42 – 3.31 (m, 1H), 2.69 – 2.55 (m, 1H), 2.46 – 2.27 (m, 1H), 2.08 (s, 3H).

^{13}C NMR (75 MHz, $CDCl_3$): δ 208.1, 147.26, 147.25, 141.7, 128.9, 127.3, 127.2, 127.0 (2C), 125.60, 125.55, 125.50, 125.45, 50.9, 50.0, 42.7, 28.6, 28.1.

^{19}F NMR (282 MHz, $CDCl_3$): δ -62.43.

HRMS (ESI): calculated for $C_{19}H_{21}NF_3O^+$, $[M+NH_4]^+$ = 336.1570; found = 336.1625.

1-((1*R*,2*R*,2a*R*,7a*S*)-2-phenyl-2,2a,7,7a-tetrahydro-1H-cyclobuta[a]inden-1-yl)ethan-1-one (4p)

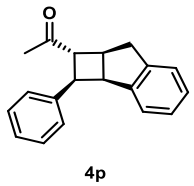

4p

4p was prepared according to the general procedure and purified by flash chromatography (CyHex : EtOAc = 95 : 5) to obtain 11.2 mg of product (as a mixture of diastereoisomers) as a colorless oil (43% yield). The enantiomeric excess was determined by SFC on a *Daicel Chiralpak* IG-3 column: CO_2/MeOH 80:20, flow rate 2.0 mL/min, λ = 210 nm, τ_{major} = 3.06 min, τ_{minor} = 2.63 (*er* = 72:28).

$[\alpha]^{20}_D$ = - 69 (*c* = 0.35, $CHCl_3$).

^{1}H NMR (300 MHz, $CDCl_3$, *major diastereoisomer*): δ 7.29 (d, *J* = 7.8 Hz, 1H), 7.22 – 7.13 (m, 4H), 6.94 – 6.85 (m, 3H), 6.37 – 6.33 (m, 1H), 4.09 – 3.95 (m, 2H), 3.38 – 3.18 (m, 3H), 2.95 (d, *J* = 16.2 Hz, 1H), 2.02 (s, 3H).

^{13}C NMR (75 MHz, $CDCl_3$, *major diastereoisomer*): δ 208.6, 144.1, 141.4, 138.9, 128.15, 128.08, 127.7, 127.3, 126.8, 126.1, 125.5, 55.3, 48.4, 46.2, 39.0, 36.6, 28.6. HRMS (ESI): calculated for $C_{19}H_{19}O^+$, $[M+H]^+$ = 263.1430; found = 263.1440.

1-((1*R*,2*R*)-2,3,3-Triphenylcyclobutyl)ethan-1-one (4q)

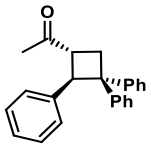

4q

4q was prepared according to the general procedure and purified by flash chromatography (CyHex : EtOAc = 95 : 5) to obtain 24.5 mg of product as a white solid (75% yield). The enantiomeric excess was determined by SFC on a *Daicel Chiralpak* IB-3 column: CO_2/MeOH 95:5, flow rate 2.0 mL/min, λ = 210 nm, τ_{major} = 3.24 min, τ_{minor} = 2.85 (*er* = 81:19).

$[\alpha]^{20}_D$ = + 13 (*c* = 0.785, $CHCl_3$).

^{1}H NMR (300 MHz, $CDCl_3$): δ 7.30 – 7.24 (m, 4H), 7.17 – 7.09 (m, 7H), 7.00 – 6.95 (m, 2H), 6.90 – 6.85 (m, 2H), 4.35 (d, *J* = 10.7 Hz, 1H), 3.59 (td, *J* = 10.6, 7.9 Hz, 1H), 3.24 (dd, *J* = 11.7, 7.9 Hz, 1H), 2.67 (dd, *J* = 11.8, 10.5 Hz, 1H), 1.93 (s, 3H).

^{13}C NMR (75 MHz, $CDCl_3$): δ 208.5, 150.9, 141.6, 138.8, 129.0, 128.7, 128.5, 128.1, 127.9, 127.1, 126.31, 126.27, 126.0, 53.7, 53.4, 47.8, 32.6, 28.7.

HRMS (ESI): calculated for $C_{24}H_{26}NO^+$, $[M+H]^+$ = 327.1743; found = 327.1746.

Imide-Acridinium Organophotocatalysts

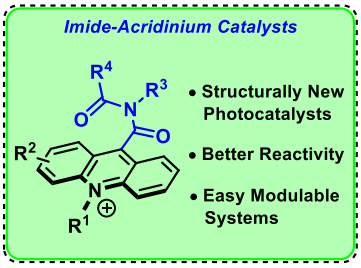

Chapter 5

5. Imide-Acridinium Organophotocatalysts

5.1 Introduction to Acridinium-based Organic Photocatalysts

Acridinium-based compounds are an interesting family of organic photoredox catalysts that present optimal photophysical properties and excited state reduction potentials, being extremely powerful oxidants.[8c] Although the simpler acridinium photocatalyst (**Acr-Me$^+$**) has a singlet excited state reduction potential of +2.32 eV (vs SCE), a fluorescence quantum yield of 1, and a relatively high lifetime of 34 ns, it has found very limited use in organic photoredox catalysis due to its poor stability under the required reaction conditions. Indeed it suffers both nucleophilic and radical addition at the 9-position in the ground state or, after a SET, at the acridinyl radical, respectively (Scheme 87). Although the related 9-phenyl substituted derivative (**Ph-Acr-Me$^+$**) can survive radical additions it can be deactivated by nucleophilic attack and, more importantly, it presents highly reduced photophysical properties due to possible non-radiative decay pathways originating from the rotation of the phenyl ring, leading to vibrational deactivation of its excited state. A major breakthrough in acridinium-based organic photocatalysts has been reported by Fukuzumi's research group with the synthesis of a 9-mesityl substituted derivative (**Mes-Acr-Me$^+$**).[143] The presence of a mesityl moiety is tremendously enhancing the stability of this catalyst, preventing nucleophilic and radical addition at the 9-position due to the increased steric hindrance provided by the *ortho*-methyl substituents and to the required orthogonality of the mesityl ring in respect to the acridinium scaffold (Scheme 87). Moreover, *N*-phenyl substituted analogues and alkyl substitutions on the acridinium scaffold led to an increased stability, limiting dealkylation pathways and degradation of the catalyst. After the above mentioned pioneering work of Fukuzumi, this class of catalysts has found widespread use in organic synthesis with an increasing interest in the last decade mainly due to the outstanding properties of acridinium-based photocatalysts.[8c] Furthermore, a large variety of structurally related compounds have been developed with the aim of enhancing or modulating the photophysical properties of the catalysts.

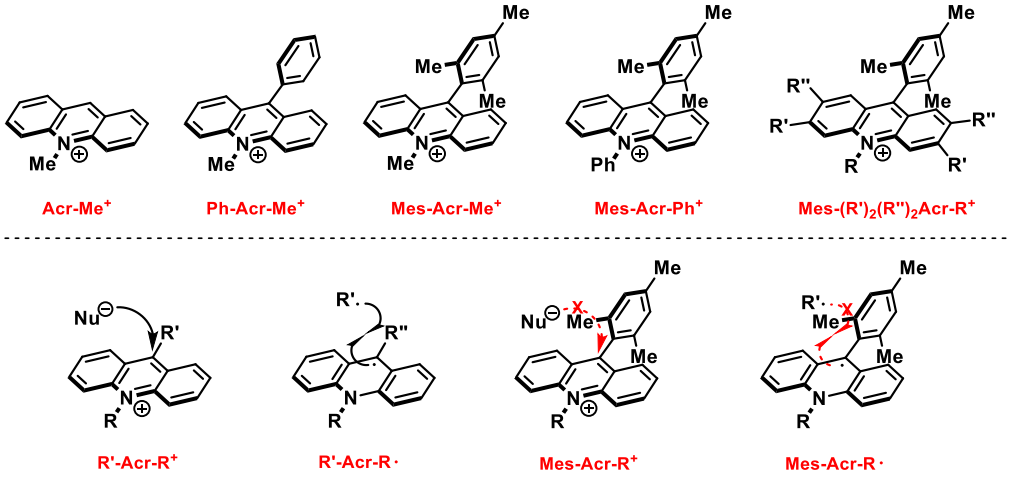

Scheme 87. Development of acridinium-based photocatalysts and possible deactivation of them by nucleophilic or radical additions.

[143] S. Fukuzumi, H. Kotani, K. Ohkubo, S. Ogo, N. V. Tkachenko, H. Lemmetyinen, *J. Am. Chem. Soc.* **2004**, *126*, 1600-1601.

5.2 Initial Development and Applications of Acridinium-based Photocatalysts

One of the first applications of an acridinium-based catalyst in organic photoredox catalysis was reported by Fukuzumi's research group in 2003. The oxygenation of α-methylstyrene was accomplished under aerobic conditions and visible light irradiation employing 10-methylacridinium as the organic photocatalyst (Scheme 88).[144]

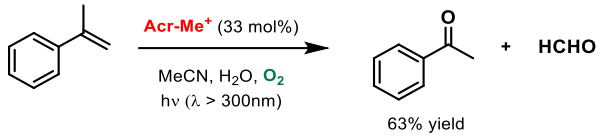

Scheme 88. Photooxygenation of α-methylstyrene by an acridinium catalyst.

A major advance, that rapidly expanded the use of acridinium-based catalysts in photocatalysis, has been achieved with the development of a 9-mesityl substituted acridinium catalyst by Fukuzumi's research group.[143] The high potentiality and increased stability of this new catalyst has been highlighted in the last decades with a myriad of reported applications in photoredox catalysis.[8c] The first of them was disclosed by Fukuzumi's group showing that it could be employed in the photooxygenation of anthracenes and alkenes (Scheme 89a,b).[145] The epidioxyanthracene derivatives could be obtained in excellent yields when side reactions and further undesired oxidations could be avoided, such in the case of dimethyl substituted anthracene. On the other hand the oxygenation of tetrasubstituted alkenes led to a mixture of dioxetane and photocleaved products.

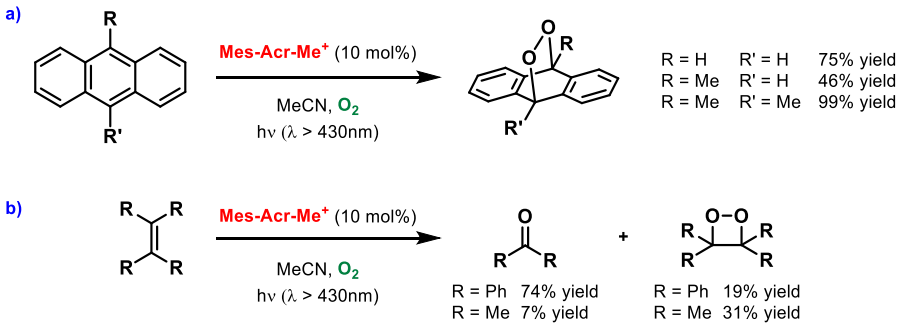

Scheme 89. Photooxygenation of anthracenes and alkenes.

The same research group reported that a 9-phenyl substituted catalyst could be employed in the photooxidation of primary alcohols,[146] whereas the Feng's group expanded this methodology to secondary alcohols (Scheme 90a).[147] In addition, an interesting bromination of aromatic compounds has been achieved in high efficiency employing the 9-mesityl substituted catalyst through an aryl radical cation intermediate (Scheme 90b).[148]

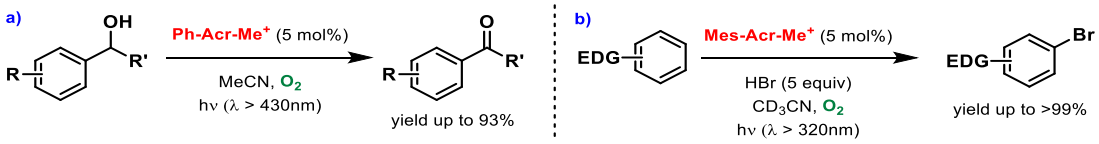

Scheme 90. Photocatalytic oxidation of benzylic alcohols and bromination of aromatic compounds.

[144] K. Suga, K. Ohkubo, S. Fukuzumi, *J. Phys. Chem. A* **2003**, *107*, 4339-4346.
[145] H. Kotani, K. Ohkubo, S. Fukuzumi, *J. Am. Chem. Soc.* **2004**, *126*, 15999-16006.
[146] K. Ohkubo, K. Suga, S. Fukuzumi, *Chem. Commun*. **2006**, 2018-2020.
[147] H. J. Xu, X. L. Xu, Y. Fu, Y. S. Feng, *Chin. Chem. Lett*. **2007**, *18*, 1471-1475.
[148] K. Ohkubo, K. Mizushima, R. Iwata, S. Fukuzumi, *Chem. Sci*. **2011**, *2*, 715-722.

On the other hand, a related modified catalyst was employed by Fukuzumi's group in the benzylic oxidation of *para*-xylene (Scheme 91a),[149] although a similar oxidation had been already reported by Griesbeck's group over methyl naphthalenes (Scheme 91b).[150] A further example that is worth to mention is the oxygenation of cyclohexane, which is involving a radical mechanism deriving from the photooxidation of chloride anions to furnish a reactive specie that is abstracting a hydrogen atom through the cleavage of a carbon-hydrogen bond.[151]

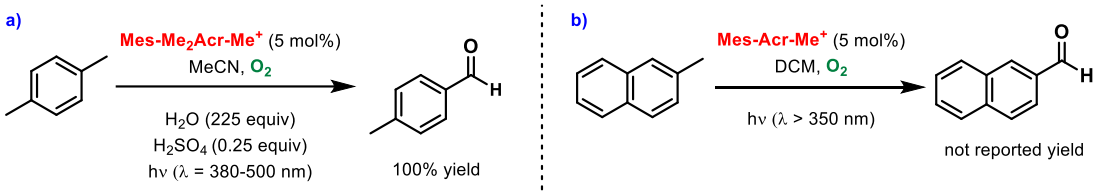

Scheme 91. Photocatalytic oxidation of benzylic positions.

5.3 Recent Advances in the Use of Acridinium Photocatalysts in Organic Synthesis

After all the above described seminal examples, the potentiality of this class of catalysts has been tremendously expanded by the Nicewicz's research group in the last decade.[27a] The excellent photophysical properties and excited state reduction potentials of 9-mesityl acridinium catalysts have been brilliantly exploited by the Nicewicz's group to achieve outstanding and unique transformations. The first example of a photocatalytic anti-Markovnikov hydrofunctionalization reaction was reported in 2012 leading to the intramolecular and intermolecular hydroetherification of alkenes (Scheme 92a),[26] while the related hydroamination reactions were reported by Nicewicz in the following years (Scheme 92b).[152]

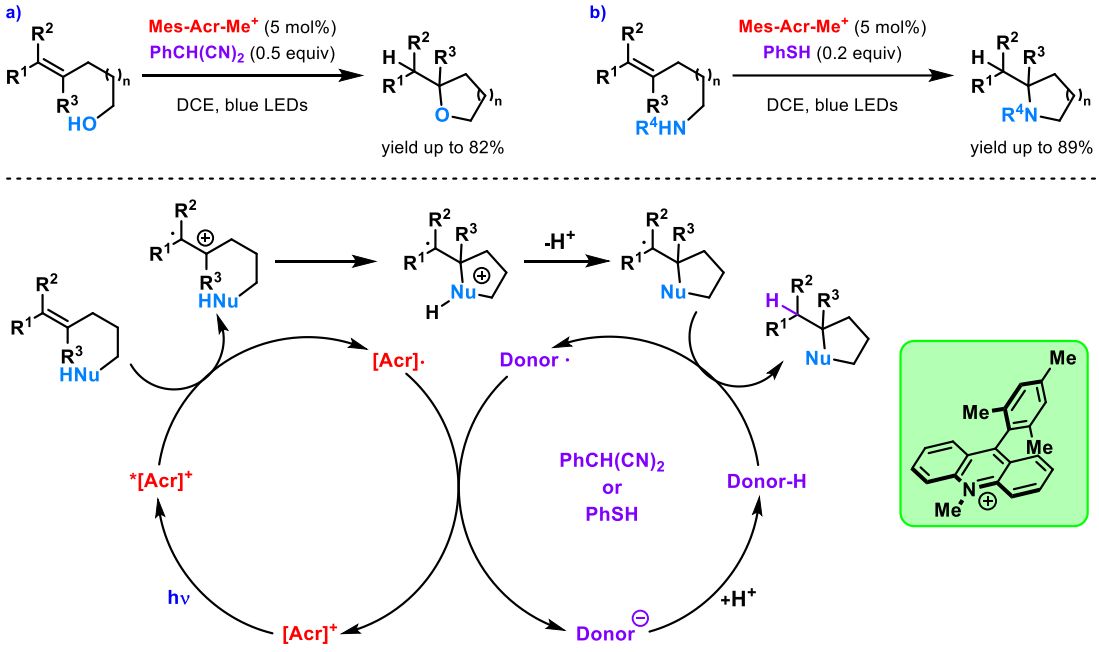

Scheme 92. Anti-Markovnikov hydrofunctionalization of alkenes via organic photoredox catalysis and corresponding proposed reaction mechanism.

[149] K. Ohkubo, K. Mizushima, R. Iwata, K. Souma, N. Suzuki, S. Fukuzumi, *Chem. Commun*. **2010**, *46*, 601-603.
[150] A. G. Griesbeck, M. Cho, *Org. Lett*. **2007**, *9*, 611-613.
[151] K. Ohkubo, A. Fujimoto, S. Fukuzumi, *Chem. Commun*. **2011**, *47*, 8515-8517.
[152] (a) T. M. Nguyen, D. A. Nicewicz, *J. Am. Chem. Soc*. **2013**, *135*, 9588-9591; (b) T. M. Nguyen, N. Manohar, D. A. Nicewicz, *Angew. Chem. Int. Ed*. **2014**, *53*, 6198-6201.

The anti-Markovnikov hydrofunctionalization is due to the selective formation of a radical cation intermediate upon photooxidation of the alkene by the acridinium-based catalyst, leading to the sole formation of a benzylic radical and showcasing the high synthetic value of photoredox catalysis in achieving unique products. The corresponding carbocation can be trapped by a nucleophilic species both in an intramolecular or intermolecular fashion, whereas a hydrogen atom donor has to be employed to furnish the desired product (through a HAT) and to restore the ground state of the catalyst (through a SET). Further interesting examples reported by Nicewicz's group are the anti-Markovnikov addition of carboxylic acids to alkenes (Scheme 93) and the hydrofunctionalization of unsaturated amides and thioamides.[153]

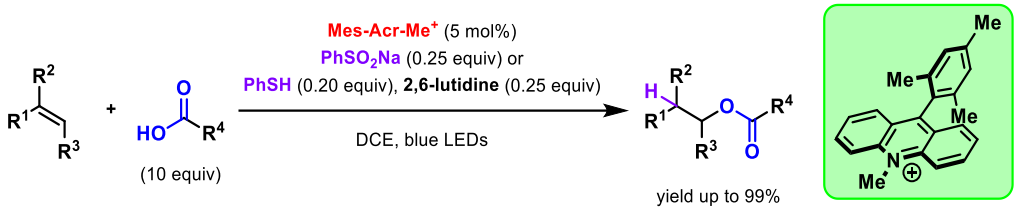

Scheme 93. Anti-Markovnikov addition of carboxylic acids to alkenes via organic photoredox catalysis.

The same strategies could also be applied in redox-neutral polar radical crossover cycloaddition reactions (Scheme 94).[154] The nucleophilic attack of an allyl alcohol over the photo-generated radical cation results in a radical intermediate, which can undergo a cyclization, providing a wide range of functionalized compounds. The reaction between alkenes and alkenols led to the obtainment of highly substituted tetrahydrofuranes (Scheme 94), while lactones could be synthetized employing unsaturated acids.[154a,b]

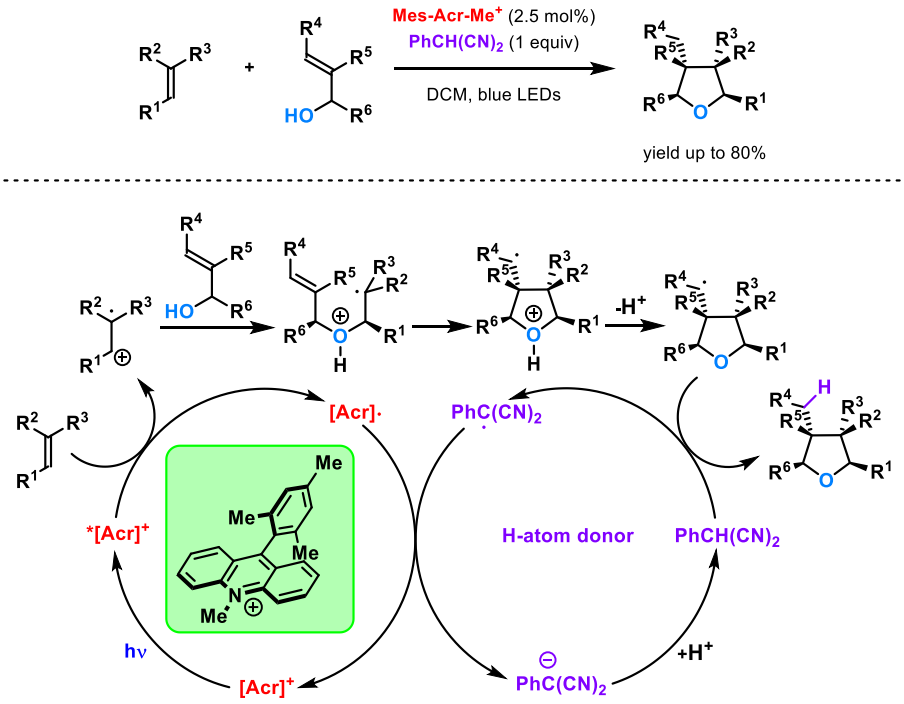

Scheme 94. Redox-neutral polar crossover cycloaddition and relative reaction mechanism.

[153] A. J. Perkowski, D. A. Nicewicz, *J. Am. Chem. Soc*. **2013**, *135*, 10334-10337; (b) P. D. Morse, D. A. Nicewicz, *Chem. Sci*., **2015**, *6*, 270-274.

[154] (a) J.-M. M. Grandjean, D. A. Nicewicz, *Angew. Chem. Int. Ed*. **2013**, *52*, 3967-3971; (b) M. A. Zeller, M. Riener, D. A. Nicewicz, *Org. Lett*. **2014**, *16*, 4810-4813; (c) N. J. Gesmundo, J.-M. M. Grandjean, D. A. Nicewicz, *Org. Lett*. **2015**, *17*, 1316-1319; (d) C. L. Cavanaugh, D. A. Nicewicz, *Org. Lett*. **2015**, *17*, 6082-6085.

An outstanding example provided by the Nicewicz's research group involves the addition of mineral acids to styrene derivatives employing the appropriate amine salt as a source of halogen anions and obtaining the corresponding anti-Markovnikov functionalized products in high yield (Scheme 95).[155]

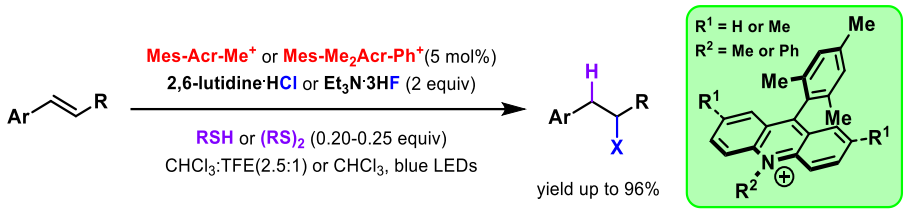

Scheme 95. Anti-Markovnikov addition of mineral acids to alkenes unlocked by photoredox catalysis.

Another brilliant methodology for the C-H amination of arenes and heteroarenes via organic photoredox catalysis was reported by Nicewicz's research group, highlighting the undoubtedly value of it through the successful accomplished late-stage functionalization of complex molecules (Scheme 96).[156] The reaction works through the photooxidation of electron-rich aromatic and heteroaromatic compounds to give an aryl radical cation intermediate, which undergoes a nucleophilic attack by the amine nucleophile to furnish the desired product after proton loss and rearomatization. Shortly after, a corresponding detailed study regarding the C-H functionalization of aromatic and heteroaromatic scaffolds, which are common cores in pharmaceutically relevant compounds, was accomplished.[157] Electron density calculations permitted to predict the site-selectivity of the majority of these functionalizations over a wide range of electron-rich aromatic compounds that could be oxidized by the appropriate ditert-butyl substituted catalyst (E_{red}*= 2.15 eV vs SCE). Furthermore, a related C-H cyanation[158] and an important C–H fluorination,[159] employing $^{18}F^-$ as the nucleophile, were achieved through similar strategies via aryl radical cation intermediates, whereas the hydrodecarboxylation of carboxylic acid derivatives have been carried out through the use of acridinium-based organic photoredox catalysts.[160]

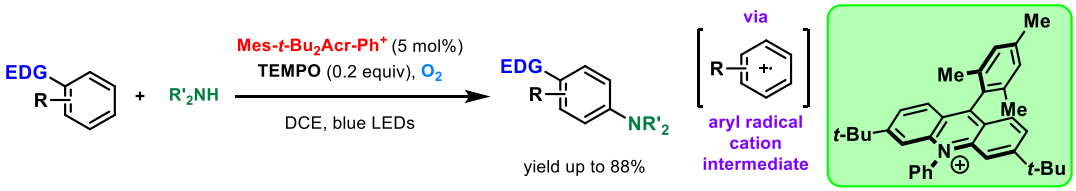

Scheme 96. C-H amination strategy allowed by organic photoredox catalysis.

An interesting example of the versatility of acridinium catalysts has been highlighted by Nicewicz's and DiRocco's research groups through the development of a catalyst with enhanced stability and modulated ground state and excited state redox potentials.[161] The synthesis of an appropriately designed catalyst, with a relatively electron-rich acridinium core, permitted the achievement of a transformation that relies on the one-electron reduction of an α-acyl radical generated upon radical conjugate addition over dimethyl fumarate (Scheme 97). Indeed, it is not possible to carry out this reaction employing the highly oxidizing Fukuzumi's catalyst due to its weakly negative ground state reduction potential. On the other hand, the electron-rich

[155] D. J. Wilger, J.-M. M. Grandjean, T. R. Lammert, D. A. Nicewicz, *Nat. Chem*. **2014**, *6*, 720-726.
[156] N. A. Romero, K. A. Margrey, N. E. Tay, D. A. Nicewicz, *Science* **2015**, *349*, 1326-1330.
[157] K. A. Margrey, J. B. McManus, S. Bonazzi, F. Zecri, D. A. Nicewicz, *J. Am. Chem. Soc.* **2017**, *139*, 11288-11299.
[158] J. B. McManus, D. A. Nicewicz, *J. Am. Chem. Soc.* **2017**, *139*, 2880-2883.
[159] W. Chen, Z. Huang, N. E. S. Tay, B. Giglio, M. Wang, H. Wang, Z. Wu, D. A. Nicewicz, Z. Li, *Science* **2019**, *364*, 1170-1174.
[160] J. D. Griffin, M. A. Zeller, D. A. Nicewicz, *J. Am. Chem. Soc.* **2015**, *137*, 11340-11348.
[161] A. Joshi-Pangu, F.Lévesque, H. G. Roth, S. F. Oliver, L.-C. Campeau, D. Nicewicz, D. A. DiRocco, *J. Org. Chem.* **2016**, *81*, 7244-7249.

acridinium catalyst presents a more negative ground-state reduction potential that allows to carry out a SET giving the necessary ester enolate and its subsequent protonation.

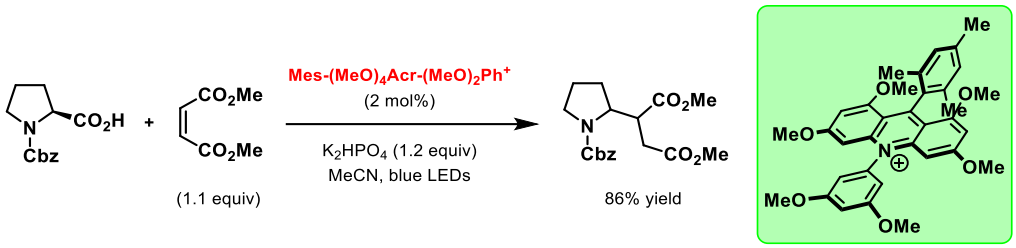

Scheme 97. Synthetic application of an electron-rich acridinium-based photocatalyst.

Another example of the incomparable potentiality of acridinium-based photocatalysts has been showcased by the Nicewicz's lab through the development of nucleophilic aromatic substitution transformations via cation radical intermediates under visible light irradiation (Scheme 98).[162] The one-electron photooxidation of electron-rich aromatic and heteroaromatic compounds allowed to carry out a nucleophilic aromatic substitution reaction employing a wide range of nucleophilic species such as nitrogen-based compounds and cyanide anions.

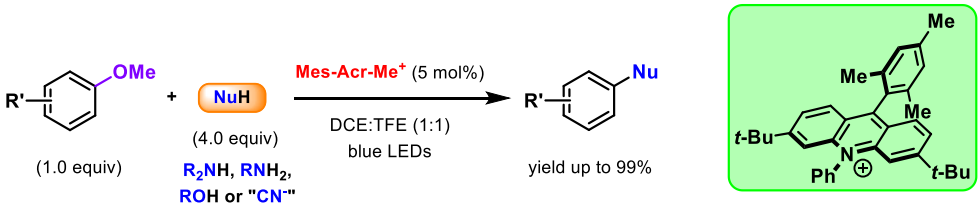

Scheme 98. Nucleophilic aromatic substitution reaction via a cation radical intermediate.

Another important application of this class of catalysts is regarding the synthesis of polysubstituted aldehydes starting from styrene derivatives and ethyl vinyl ethers (Scheme 99),[163] whereas a C-H functionalization strategy was developed through the use of an acridinium photocatalyst and a phosphate base.[164]

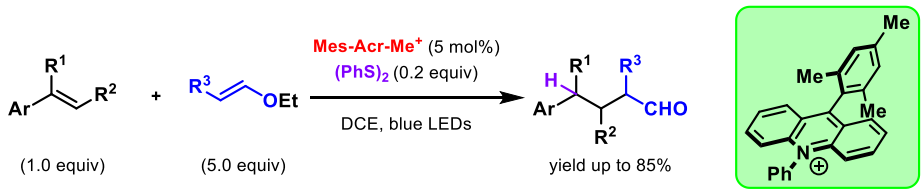

Scheme 99. Photocatalytic strategy for the synthesis of aldehydes.

The unique features of acridinium-based photocatalysts, and their employment as extremely powerful oxidants, can be highlighted by the successful unlocked generation and alkylation of α-carbamyl radicals from carbamates, which present very high oxidation potentials (E around -2 eV) and allowing the reaction being carried out only with this class of catalysts (Scheme 100).[165]

[162] (a) N. E. S. Tay, D. A. Nicewicz, *J. Am. Chem. Soc*. **2017**, *139*, 16100-16104; (b) N. Holmberg-Douglas, D. A. Nicewicz *Org. Lett*. **2019**, *21*, 7114-7118.
[163] F. Wu, L. Wang, J. Chen, D. A. Nicewicz, Y. Huang, *Angew. Chem. Int. Ed*. **2018**, *57*, 2174-2178.
[164] K. A. Margrey, W. L. Czaplyski, D. A. Nicewicz, E. J. Alexanian, *J. Am. Chem. Soc*. **2018**, *140*, 4213-4217.
[165] J. B. McManus, N. P. R. Onuska, D. A. Nicewicz, *J. Am. Chem. Soc*. **2018**, *140*, 9056-9060.

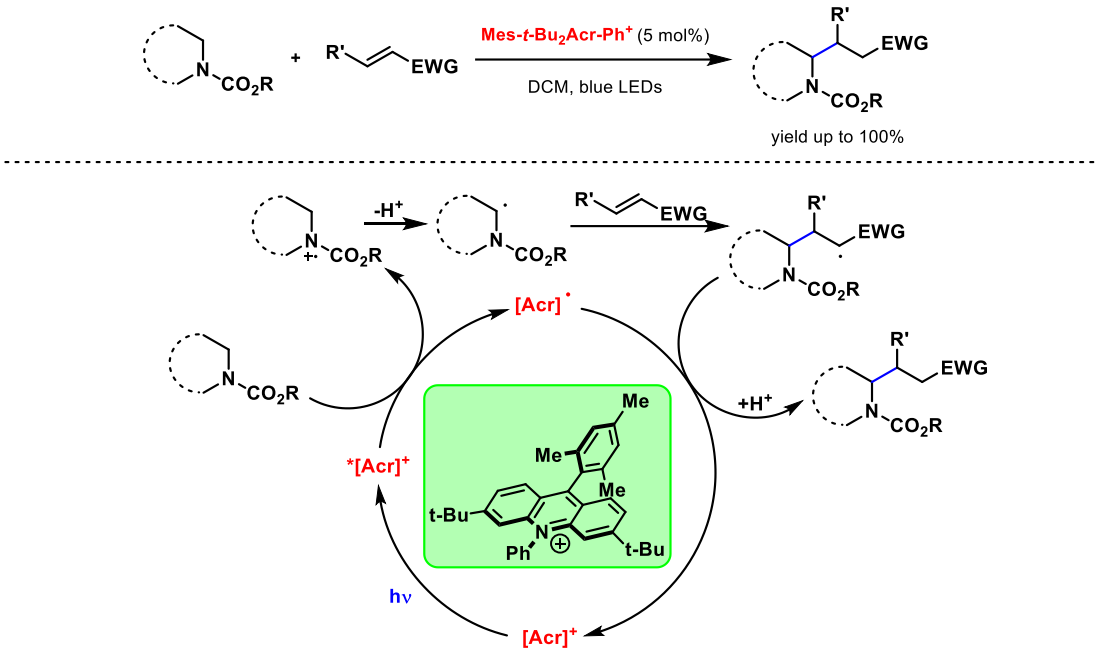

Scheme 100. α-Alkylation of carbamates through the use of an acridinium-based photocatalyst.

Two other important examples regarding the use of acridinium photocatalysts were reported by Molander's research group in a Minisci-type alkylation reaction, showcasing an outstanding application in the late-stage functionalization of Camptothecin (Scheme 101a),[166] and by Xiao's group in the synthesis of tetrasubstituted pyrroles (Scheme 101b).[48]

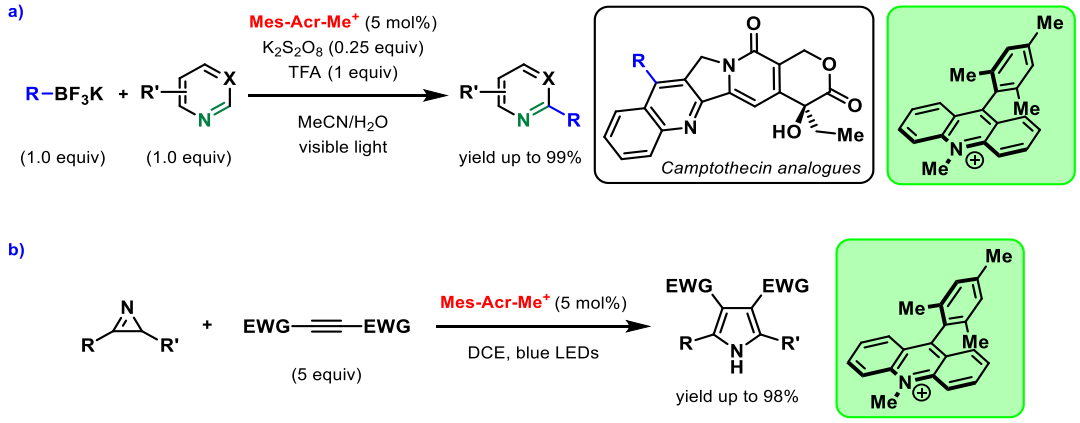

Scheme 101. (a) Minisci-type reaction and late-stage functionalization of a complex molecule under visible light irradiation. (b) Formal [3+2] cycloaddition for the synthesis of polysubstituted pyrroles.

5.4 Introduction to Multicomponent Reactions (MCRs)

Although an outstanding strategy for the synthesis of acridinium-based organophotocatalysts was recently reported by Nicewicz's group,[27b] until 2018 the commonly employed synthesis for this class of catalysts relied on high temperature and following oxidation or the employment of organometallic highly nucleophilic species, which limited the substrate scope and the functional group tolerance (Scheme 102).[167] Due to the lack of methodologies that

[166] J. K. Matsui, D. N. Primer, G. A. Molander, *Chem. Sci*. **2017**, *8*, 3512-3522.

[167] (a) A. Baeyer, *Ber. Dtsch. Chem. Ges*. **1871**, *4*, 555-558; (b) A. V. Dubrovskiy, R. C. Larock, *J. Org. Chem*. **2012**, *77*, 11232-11256; (c) T. Tsudaka, H. Kotani, K. Ohkubo, T. Nakagawa, N. V. Tkachenko, H. Lemmetyinen, S. Fukuzumi, *Chem. Eur. J*. **2017**, *23*, 1306-1317; (d) C. Fischer, C. Sparr, *Angew. Chem. Int. Ed*. **2018**, *57*, 2436-2440.

enabled the synthesis of acridinium-based photocatalysts through a mild C-H functionalization reaction, we envisioned that a multicomponent reaction could have provided an efficient, modulable and versatile strategy for this purpose.

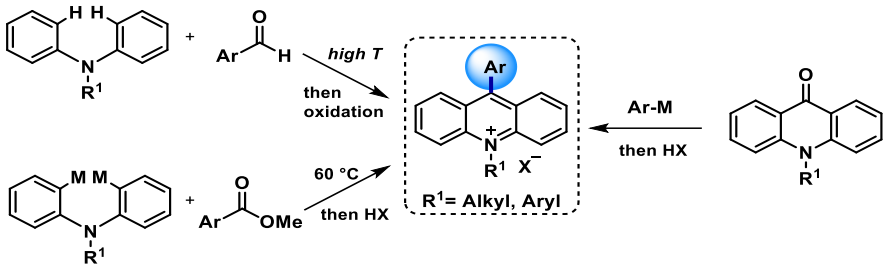

Scheme 102. Commonly employed synthesis to obtain an acridinium-based catalyst.

A multicomponent reaction (MCR) is a useful methodology in which three or more reactants are employed in a single step to form a new product in which they are almost fully incorporated in the final structure, making the multicomponent reaction an efficient, atom economical methodology for the construction of highly versatile products, with minimal or any generation of by-products (Scheme 103).[168] Due to these particular features, multicomponent reactions have been intensively used in combinatorial chemistry or in the preparation of library of compounds, allowing the employment of a wide range of different substrates.

The first multicomponent reaction that was reported in the literature was the Strecker reaction that was discovered in 1850 and, since then, it has been intensively employed for the synthesis of α-amino acids (Scheme 103a).[169] This three-component reaction relies on the nucleophilic attack of a cyanide anion over an *in-situ* generated iminium ion, leading to an aminonitrile that can be successively hydrolyzed to obtain the corresponding amino acid. Another important example of a three-component reaction is the Hantzsch dihydropyridine synthesis that was reported in 1881 and that is involving an aldehyde, ammonia and two equivalents of a β-keto ester (Scheme 103b).[170] In addition, the dihydropyridine products can be oxidized to obtain the corresponding pyridines. The Biginelli reaction is another closely related MCR that permits the synthesis of dihydropyrimidinones from β-keto esters, aldehydes and ureas in the presence of an acid catalyst (Scheme 103c).[171] On the other hand, the Passerini reaction is accomplishing the synthesis of α-acyloxy amides from carboxylic acids, aldehydes, and isonitriles (Scheme 103d).[172] Both Biginelli's and Passerini's reactions have been widely employed in the pharmaceutical industry due to the various bioactivities of the corresponding products. A relatively recent multicomponent reaction was reported by Ugi's research group in 1959, being the first four-component reaction that appeared in the literature (Scheme 103e).[168,173] By means of a an efficient and atom economical reaction between carbonyl compounds, amines, isonitriles and carboxylic acids the corresponding α-acylamino amides could be obtained. The importance and versatility of this reaction can be highlighted by the successful employment that it has found in the pharmaceutical industry for the preparation of library of compounds and in the synthesis of specific drugs. In addition, 3-component Ugi-type reactions have been reported, as well as 5-, 6-, 7-, and 8-component analogous reactions.[168]

[168] R. P. Herrera, E. Marqués-López, "Multicomponent Reactions: Concepts and Applications for Design and Synthesis", **2015**, John Wiley and Sons.
[169] A. Strecker, *Justus Liebigs Ann. Chem*. **1850**, *75*, 27-45.
[170] A. Hantzsch, *Ber. Dtsch. Chem. Ges*. **1881**, *14*, 1637-1638.
[171] P. Biginelli, *Ber. Dtsch. Chem. Ges*. **1891**, *24*, 1317-1319.
[172] (a) M. Passerini, *Gazz. Chim. Ital*. **1921**, *51*, 126-129; (b) M. Passerini, *Gazz. Chim. Ital.* **1921**, *51*, 181-188.
[173] I. Ugi, R. Meyr, U. Fetzer, C. Steinbrückner, *Angew. Chem*. **1959**, *71*, 386-386.

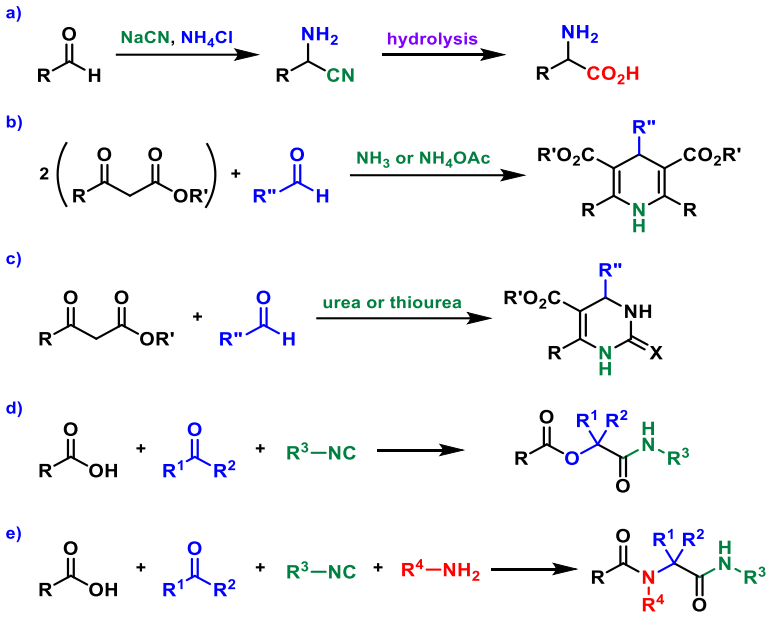

Scheme 103. Selected examples of multicomponent reactions (MCRs): (a) Strecker reaction, (b) Hantzsch dihydropyridine synthesis, (c) Biginelli reaction, (d) Passerini reaction and (e) Ugi reaction.

The Ugi reaction consists in a sequence of simple elementary steps that permit the obtainment of a wide range of differently substituted products from simple starting materials (Scheme 104).[168] It relies on the nucleophilic addition of an isocyanide anion over a usually transient generated imine or iminium ion, which is formed upon condensation of a primary amine with a carbonyl compound. Nevertheless, depending on the reactions conditions, the imine itself can be the electrophilic species that is taking part in the process, and in some cases it can be appropriately activated by external agents such as Lewis acid catalysts. The key intermediate that is being formed is the nitrilium ion. Indeed, a second nucleophilic addition over this species can be carried out by a carboxylate anion to give, after a rearrangement, the desired α-acylamino amide.

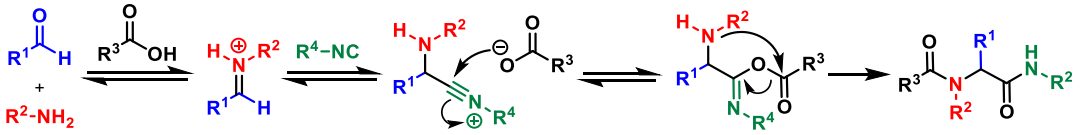

Scheme 104. Commonly accepted mechanism for the Ugi Reaction.

Oxidative processes can be employed as alternative strategies in Ugi-type reactions, allowing the obtainment of the electrophilic imine (or the corresponding iminium ion) without the required condensation step. For instance, the use of different oxidative methodologies permitted the achievement of various functionalizations over tetrahydroisoquinoline and pyrrolidine derivatives. An efficient Ugi-type reaction was reported by Zhu's group through the employment of IBX as an external oxidant (Scheme 105a),[174a] whereas the use of an oxidative enzyme allowed an efficient catalytic desymmetrization of pyrrolidine derivatives to the corresponding enantiopure cyclic imines, which carried out a following highly diastereoselective Ugi reaction (Scheme 105b).[174b]

[174] (a) T. Ngouansavanh, J. Zhu, *Angew. Chem. Int. Ed.* **2007**, *46*, 5775-5778; (b) A. Znabet, E. Ruijter, F. J. J. de Kanter, V. Khler, M. Helliwell, N. J. Turner, R. V. A. Orru, *Angew. Chem. Int. Ed*. **2010**, *49*, 5289-5292.

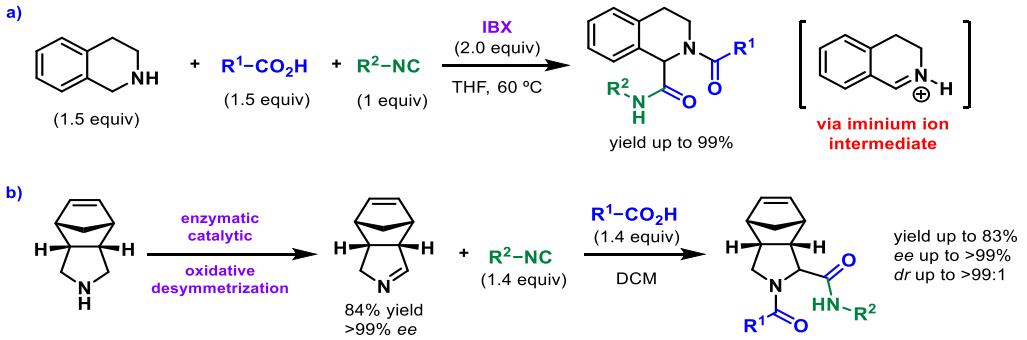

Scheme 105. (a) T. Ngouansavanh, J. Zhu, *Angew. Chem. Int. Ed.* **2007**, *46*, 5775-5778; (b) A. Znabet, E. Ruijter, F. J. J. de Kanter, V. Khler, M. Helliwell, N. J. Turner, R. V. A. Orru, *Angew. Chem. Int. Ed*. **2010**, *49*, 5289-5292.

5.5 Background of the Group in Oxidation Processes

In the last years our group reported an unprecedented efficient strategy for the synthesis of dibenzoxepines and dibenzoazepines through a copper-catalyzed oxidative approach starting from simple xanthenes and acridanes, respectively (Scheme 106).[175] The use of a copper catalyst allowed a C-H bond functionalization by means of an oxidative process that led to the obtainment of a carbocation intermediate. The presence of the nucleophilic trimethylsilyldiazomethane permitted the trapping of this transient-generated carbocationic species to give a three-membered ring intermediate through displacement of molecular nitrogen as the leaving group. This cyclopropane-containing intermediate could then undergo a ring-expansion reaction, leading to the rearranged seven-membered tricyclic structure. In the end, the removal of the trimethylsilyl group furnished the desired dibenzoxepine or dibenzoazepine scaffolds. Furthermore, the mechanistic proposal was supported by DFT calculations and deuterium labelling experiments.

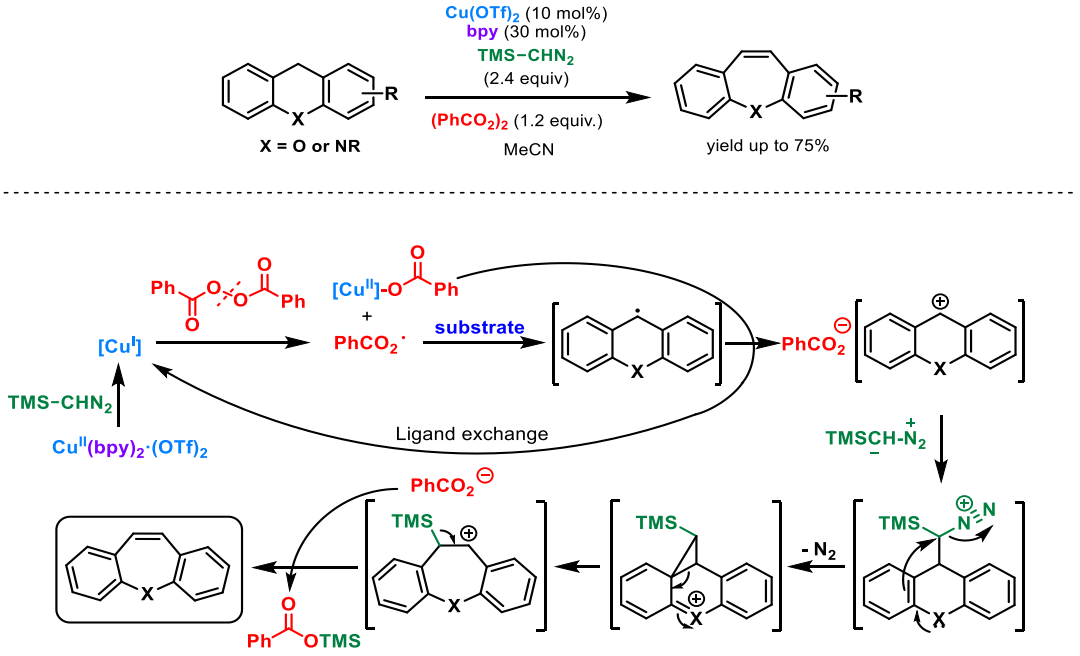

Scheme 106. Previous work of our group regarding the synthesis of dibenzoxepines and dibenzoazepines through a copper-catalyzed oxidative process.

[175] T. Stopka, L. Marzo, M. Zurro, S. Janich, E.-U. Würthwein, C. G. Daniliuc, J. Alemán, O. García Mancheño, *Angew. Chem. Int. Ed.* **2015**, *54*, 5049-5053.

A related metal-free strategy which unlocked the functionalization of C-H bonds was applied by our group in the synthesis of 3-benzazepines (Scheme 107).[176] In this case, 2,2,6,6-tetramethylpiperidine 1-oxyl (TEMPO) oxoammonium salt was successfully employed as the active oxidant species to furnish the corresponding iminium ion of tetrahydroisoquinolines. Then, this intermediate could be efficiently trapped by the trimethylsilyldiazomethane to give a cyclopropane-containing species which rearranged through a ring-expansion reaction to furnish a seven-membered ring compound. Even in this case, DFT calculations were carried out to support the mechanistic proposal, while the synthetic value of this strategy was highlighted by the synthesis of a biologically active 3-benzazepine (*Lorcaserin*).

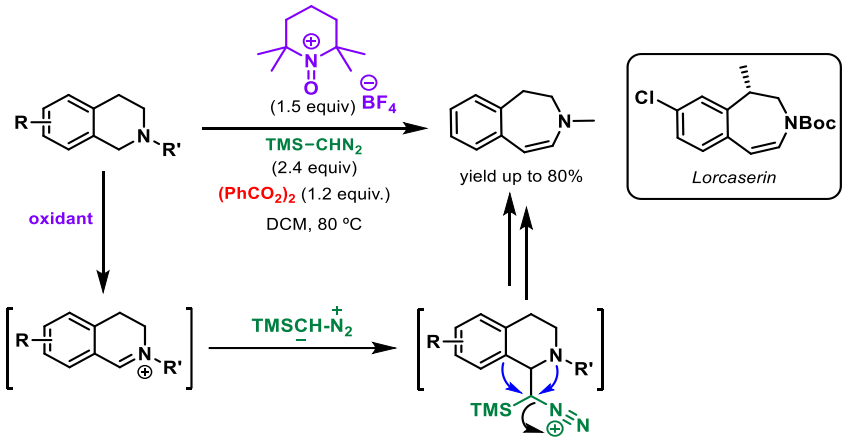

Scheme 107. Previous work of our group regarding the synthesis of 3-benzazepines through a metal-free oxidative process.

5.6 Objectives of this Chapter

Due to the expertise that our group has in C-H functionalization strategies, we wondered if a similar activation of normally inert C-H bonds of acridanes could have provided a novel methodology for a modulable synthesis of structurally related derivatives. For this purpose we envisioned that, by means of a selective functionalization of the benzylic position of acridanes, we could have carried out an Ugi-type multicomponent reaction (Scheme 108). Moreover, the subsequent oxidation of these acridanes derivatives would have afforded novel acridinium-based compounds that could have been tested as possible organophotocatalysts in different reactions.

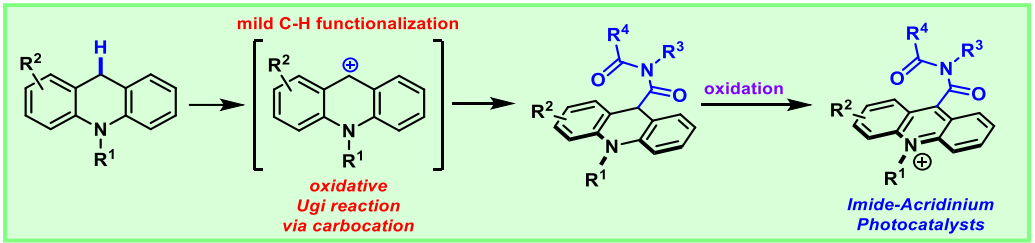

Scheme 108. Proposed strategy for the synthesis of novel imide-acridinium organophotocatalysts.

For the achievement of this goal the following sub-objectives have been identified:

1) Development of an Ugi-type oxidative reaction which would permit an easy modulable synthesis of structurally different acridane derivatives.

[176] A. Gini, J. Bamberger, J. Luis-Barrera, M. Zurro, R. Mas-Ballesté, J. Alemán, O. García Mancheño, *Adv. Synth. Catal.* **2016**, *358*, 4049-4056.

2) Evaluation of the reaction scope and elucidation of the mechanism.
3) Searching of the appropriate oxidant for the synthesis of the corresponding acridinium derivatives.
4) Evaluation of the photocatalytic properties and efficiency of these new photocatalysts through the employment of them in some model reactions.
5) Additional DFT calculations and fluorescence quenching experiments to evaluate possible differences between the novel photocatalysts and the ones reported in the literature.

5.7 Publications and Experimental Section

Novel Oxidative Ugi-Reaction for the Synthesis of Highly Active, Visible Light, Imide-Acridinium OrganoPhotocatalysts

Andrea Gini, Mustafa Uygur, Thomas Rigotti, José Alemán,* and Olga García Mancheño*

Chem. Eur. J. **2018**, *24*, 12509-12514

(*Highlighted* in *Synfacts* **2018**, *14*, 1133)

The experimental section was taken from the "Supporting Information" document associated with the specific publication and is including the corresponding numeration. The characterization data have been shown only for the final products that appear in the scope of the reaction. The complete "Supporting Information" documents, with all the characterization data, NMR spectra, SFC or HPLC traces and other experimental procedures have been included in the enclosed USB memory.

Mesityl or Imide Acridinium PhotoCatalysts: Accessible or not Accessible Charge-Transfer State in Photoredox Catalysis

Andrea Gini, Thomas Rigotti, Raúl Pérez-Ruiz, Mustafa Uyugur, Rubén Mas-Ballesté, Inés Corral, Lara Martínez-Fernández, Victor A. de la Peña O'Shea, Olga García Mancheño* and José Alemán*

Chem. Photo. Chem. **2019**, *3*, 609-612

The experimental section was taken from the "Supporting Information" document associated with the specific publication and is including the corresponding numeration. The characterization data have been shown only for the final products that appear in the scope of the reaction. The complete "Supporting Information" documents, with all the characterization data, NMR spectra, SFC or HPLC traces and other experimental procedures have been included in the enclosed USB memory.

ChemPubSoc Europe

DOI: 10.1002/chem.201802830

CHEMISTRY
A European Journal
Communication

Synthetic Methods

Novel Oxidative Ugi Reaction for the Synthesis of Highly Active, Visible-Light, Imide-Acridinium Organophotocatalysts

Andrea Gini,[b] Mustafa Uygur,[a] Thomas Rigotti,[c] José Alemán,*[c, d] and Olga García Mancheño*[a, b]

Abstract: A newly designed class of acridinium-based organophotocatalysts bearing an imide group at the C9-position is presented. To achieve these unprecedented structures, a synthetic strategy based on a novel straightforward oxidative Ugi-type reaction at the benzylic position of C9-unsubstituted acridanes was developed. The introduction of the imide-unit affords a notable photocatalytic activity enhancement, allowing efficient transformations in different oxidative and reductive visible-light catalytic reactions.

Visible-light photoredox catalysis has been established as a powerful tool for the synthesis of molecules by selective activation of bonds under mild conditions. Therefore, access to unique reactivities are possible, including those thermally forbidden or difficult to carry out by other methodologies.[1] The catalysts involved in most of the photocatalytic processes are based on Ru^{II} and Ir^{III} complexes.[2] More recently, the possibility of using organic photoredox catalysts for synthetic transformations has been extensively investigated.[3] These photocatalysts are suitable for industrial applications because of their remarkable photophysics and electrochemical properties (e.g. as powerful oxidant).[3] In addition, the low price and low toxicity of these photoredox active organic dyes compared to the commonly used transition metal-based photocatalysts make them very attractive.

Among well-established organophotocatalysts, acridinium derivatives represent a specific family that contains extended conjugated π-systems and absorb light in the visible region (Figure 1, left).[4] In the excited state, acridinium ions are usually

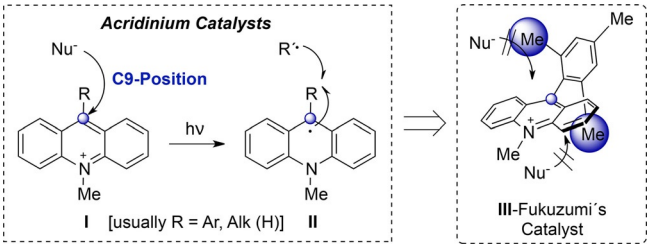

Figure 1. Previous acridinium-photocatalysts and reactivity at the C9-position.

powerful oxidants, whereas they are weak reductants. In addition, they show good quantum yields in some reactions and extremely long lifetime of fluorescence.[4d, 5] However, the first generation of this group of photocatalysts, unsubstituted or C9-aryl substituted *N*-methyl acridinium ions (type **I**), has only found limited use due to its susceptibility to the nucleophile addition at the 9-position in the ground state, or by the addition of radical species to its corresponding acridinyl radical (Figure 1, **I** and **II** respectively).[6, 7] In order to avoid this drawback, in 2004 Fukuzumi introduced a mesityl group at the C9-position. Therefore, the stability of the photocatalyst under the reaction conditions was increased by blocking the access of the nucleophiles and radical species to the photocatalyst (Figure 1 **III**).[8] Although the stability of the Fukuzumi's catalyst **III** was substantially enhanced to respect to the first generation, the kinetic of the reactions was significantly diminished. The negative impact of this substitution in the kinetics of photocatalytic reactions can be attributed to the steric hindrance imposed by the mesityl group. Although there are several publications related to the use of acridinium salts as photocatalysts, only compounds that present alkyl and aryl substituents at the C9-position have been reported.[9, 10] Therefore, in order to achieve a higher performance and broaden synthetic applicability, new acridinium-type catalysts bearing different functional groups are needed.

Based on our extended experienced on oxidative C–H functionalization[11] for the synthesis of biological and important

[a] *M. Uygur, Prof. O. García Mancheño*
Organic Chemistry Institute
University of Münster
48149 Münster (Germany)
E-mail: olga.garcia@uni-muenster.de

[b] *A. Gini, Prof. O. García Mancheño*
Institute for Organic Chemistry
University of Regensburg
93053 Regensburg (Germany)

[c] *T. Rigotti, Prof. J. Alemán*
Organic Chemistry Department
Módulo 1
Universidad Autónoma de Madrid
28049 Madrid (Spain)www.uam.es/jose.aleman
E-mail: jose.aleman@uam.es

[d] *Prof. J. Alemán*
Institute for Advanced Research in Chemical Sciences (IAdChem)
Universidad Autónoma de Madrid
28049 Madrid (Spain)

Supporting information and the ORCID identification number(s) for the author(s) of this article can be found under: https://doi.org/10.1002/chem.201802830.

pharmaceutical compounds,[12] we decided to introduce a polar group at C9 by exploiting the direct C–H bond functionalization technology on acridane scaffolds, followed by an oxidative aromatization to the corresponding acridinium salts (Scheme 1).[12a] For this purpose, we focused on the Ugi multicomponent reaction (Ugi-MCR), as one of the most potent and convenient methodology for the synthesis of a large variety of bisamides and imides.[13] The Ugi reaction implies a cascade of elementary chemical transformations between amines, aldehydes (or ketones), isocyanides and carboxylic acids to assemble, via the formation of a key iminium intermediate, a single amide-type product. Despite the outstanding applications developed in the past decades, all the few reported examples on oxidative Ugi multicomponent reactions (Ox-Ugi-MRC), which proceed by a (sp^3)C–H bond oxidation at the substrate, relay on the formation of a key iminium salt.[14] Moreover, as far as we know, the synthesis of acridinium imide derivatives has not been reported to date. In addition, the synthesis of these acridinium derivatives (top, Scheme 1) required the use of Grignard or organolithium derivatives, high temperatures or strong acids,[15] making essentially these methodologies functional group non-tolerant. Concern by the lack of precedents, and in order to achieve our targeted imide-photocatalyst, we envisioned the development on a novel Ugi multicomponent reaction based on an in situ generated key carbocation electrophilic intermediate (or arylogous iminium ion), which will allow to easily tune the substitution on the final structure (Scheme 1, bottom).

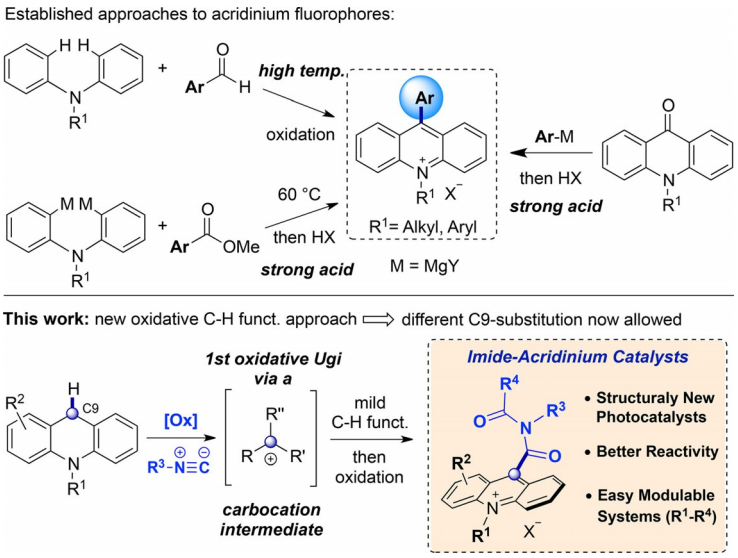

Scheme 1. Described synthesis of acridinium salts and our synthetic approach.

Herein, the straightforward synthesis of a novel family of imide-acridinium photocatalysts based on the first modular, mild oxidative Ugi-type reaction on dibenzylic substrates is presented. Furthermore, their photochemical properties, applications as highly potent organophotocatalyst, and their distinct reactivity respect to a commercially available and well-established acridinium salt, are discussed.

We started the optimization of the oxidative Ugi-type reaction with *N*-methyl acridane (**1a**) as model substrate and commercially available cyclohexyl isocyanide (**2a**) in acetonitrile at room temperature (Table 1). Initially, several common peroxides were tested as oxidants (Table 1, entries 1–4). Unexpectedly, the use of hydroperoxides such as *t*BuOOH (TBHP) in the presence of benzoic acid as additive, which was already described in previous oxidative Ugi reactions with amine-substrates,[14,16] did not lead to the desired product **3a** (entry 1). Similarly, the aprotic dialkylperoxide *t*BuOO*t*Bu or PhCO-OO-*t*Bu were also unsuccessful (entries 2 and 4). Next, our recently developed $Cu(OTf)_2$/bipyridyl/benzoyl peroxide (BPO) oxidative system for C(sp^3)–H bond functionalization reactions was employed (entry 3).[11a] In this case, the reagent BPO had a double role as both the oxidant and the carboxylic acid or carboxylate source. Therefore, the addition of an external carboxylic acid was not required to obtain the imide Ugi products **3**. Accordingly, the desired product **3a** was obtained in a promising 29% yield. However, two of the main issues of this reaction are the low stability of the products **3** under oxidative conditions and the competition between the desired Ugi-type reaction and the over-oxidation of the substrate to the acridone or the aromatic acridine. Therefore, to avoid the formation of undesired by-products, both shorter reaction times and an excess of isocyanide were explored. We found that the use of two equivalents of **2a** and 4 hours reaction time led to the best results, providing **3a** in a synthetically useful 61% yield, which was improved

Table 1. Optmization of the conditions for the oxidative Ugi reaction with **1a**.[a]

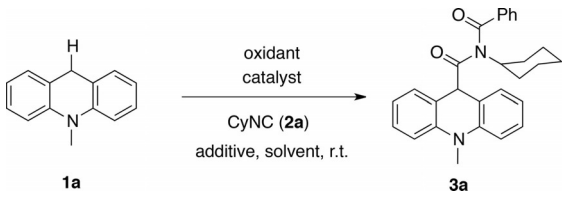

	Catalyst [mol%][b]	Oxidant [equiv]	**2a** [equiv]	*t* [h]	Yield **3a** [%][c]
1	$Cu(OTf)_2$ (10)/bpy (30)	*t*BuOOH (1.2)	1.2	18	–[d]
2	$Cu(OTf)_2$ (10)/bpy (30)	*t*BuOO*t*Bu (1.2)	1.2	18	–[d]
3	$Cu(OTf)_2$ (10)/bpy (30)	$(PhCO_2)_2$ (1.2)	1.2	18	29
4	$Cu(OTf)_2$ (10)/bpy (30)	$(PhCO_2)$O*t*Bu (1.2)	1.2	18	–
5	$Cu(OTf)_2$ (10)/bpy (30)	$(PhCO_2)_2$ (1.2)	2.0	18	36
6	$Cu(OTf)_2$ (10)/bpy (30)	$(PhCO_2)_2$ (1.2)	2.0	4	61(66)[e]
7	$Cu(OTf)_2$ (10)/bpy (30)	$(PhCO_2)_2$ (1.2)	2.0	4	35[f]
8	$Cu(OTf)_2$ (15)/bpy (45)	$(PhCO_2)_2$ (1.2)	2.0	4	42
9	$Cu(OTf)_2$ (5)/bpy (15)	$(PhCO_2)_2$ (1.2)	2.0	4	52
10	$Cu(OTf)_2$ (10)/bpy (30)	$(PhCO_2)_2$ (1.5)	2.0	4	22
11	$[Ru(bpy)_3](PF_6)_2$ (1)	air, blue LEDs	2.0	18	30[d,g]

[a] **1a** (0.1–0.2 mmol), oxidant, catalyst, CyNC in MeCN (0.1 M) at room temperature in a sealed tube. [b] $Cu(OTf)_2$ was pre-dried under vacuum at 60 °C. [c] Isolated yields. [d] Reaction in the presence of 1.2 equiv of $PhCO_2H$. [e] 2 mmol scale reaction in brackets. [f] $Cu(OTf)_2$ was not pre-dried. [g] Full conversion observed after 18 h (30% conv., 3.5 h). A mixture of **3a**, acridone and acridine was obtained.

to 66% when the reaction was scaled up 20 times (entry 6). It is important to mention that the reaction was sensitive to moisture (entry 7), being needed anhydrous conditions to achieve satisfactory results.[17] Finally, the increase or decrease of the catalyst loading (15 or 5 vs. 10 mol%, entries 8 and 9), the increase of the oxidant (entry 10), or the use of standard oxidative aerobic photocatalytic conditions with $[Ru(bpy)_3](PF_6)_2$ (entry 11), led to significant less efficient reactions.

With the best conditions in hand, $Cu(OTf)_2$/bipyridyl as catalytic system and benzoyl peroxide as oxidant in acetonitrile at room temperature (Table 1, entry 6), the reaction with different substituted acridanes **1** was investigated (Table 2). Acridanes with various N-protecting groups such as methyl, benzyl and phenyl efficiently reacted, giving the desired products **3a**–**c** in good yields (61–70%). The reaction also tolerated different electron donating (R^2 = Me, Ph, MeO; **3d**–**g**, 41–68%,) and electron withdrawing (R^2 = Br, F; **3h**–**j**, 32–63%) groups at the acridane core. It is also interesting to note that the steric hindered substrate **1k** (1,4-dimethyl substituted) was also well tolerated, leading to **3k** in a good 57% yield. Regarding the isocyanide reagent, the system worked well with other alkyl groups such as *n*Bu (**3l**,**m**), *t*Bu (**3n**,**o**) and benzyl (**3p**,**q**), as well as aryl (**3r**,**s**) substituents, providing the corresponding imides in moderate to good yields.

Aiming to shed some light into the mechanism of the oxidative Ugi reaction, several experiments were carried out (Scheme 2). Firstly, the *N*-methyl acridinium salt **1a′** was prepared by simple oxidation of the acridane **1a** with trityl perchlorate.[12a] The carbocation salt **1a′** was then enrolled in the Ugi-type reaction with cyclohexyl isocyanide (**2a**) with two different reagents: *p*-toluic acid (Scheme 2, equation i-a) or sodium *p*-toluate (Scheme 2, equation i-b). While no reaction was observed with *p*-toluic acid, the imide derivative **3t** was obtained in moderate yield (39%) when *p*-$TolCO_2^-$ was used as the corresponding carboxylate. The lower yield obtained compared to the reaction with the in situ generated cationic species could be explained due to the high instability of the stoichiometrically employed C9-unsubstituted acridinium salt **1a′**, showing the more synthetic utility of our employed oxidative C–H functionalization approach. Therefore, under the catalytic conditions the reactive carbocation intermediate is formed and present in the media in low amounts, allowing an efficient and

Table 2. Scope for the oxidative Ugi multicomponent reaction.[a,b]

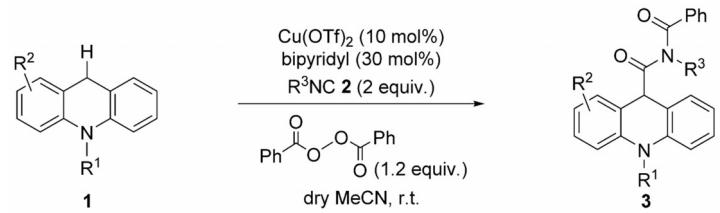

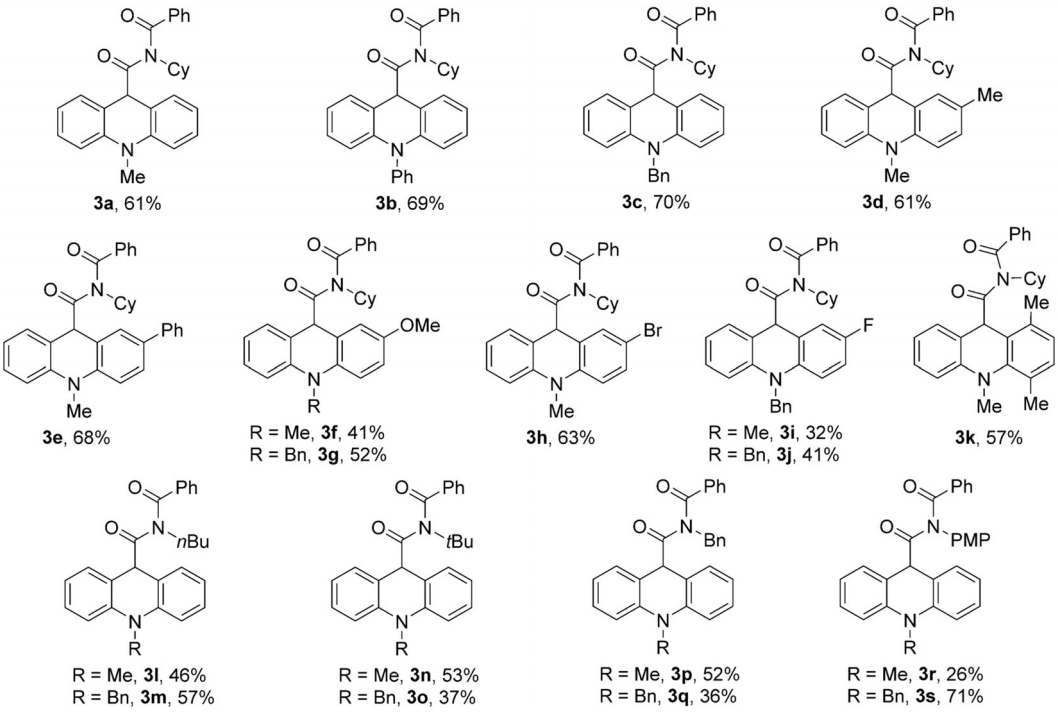

[a] The reactions were performed in a 0.1–0.4 mmol scale in CH_3CN (see Supporting Information). [b] Isolated yields after flash chromatography. PMP = *p*-methoxylphenyl.

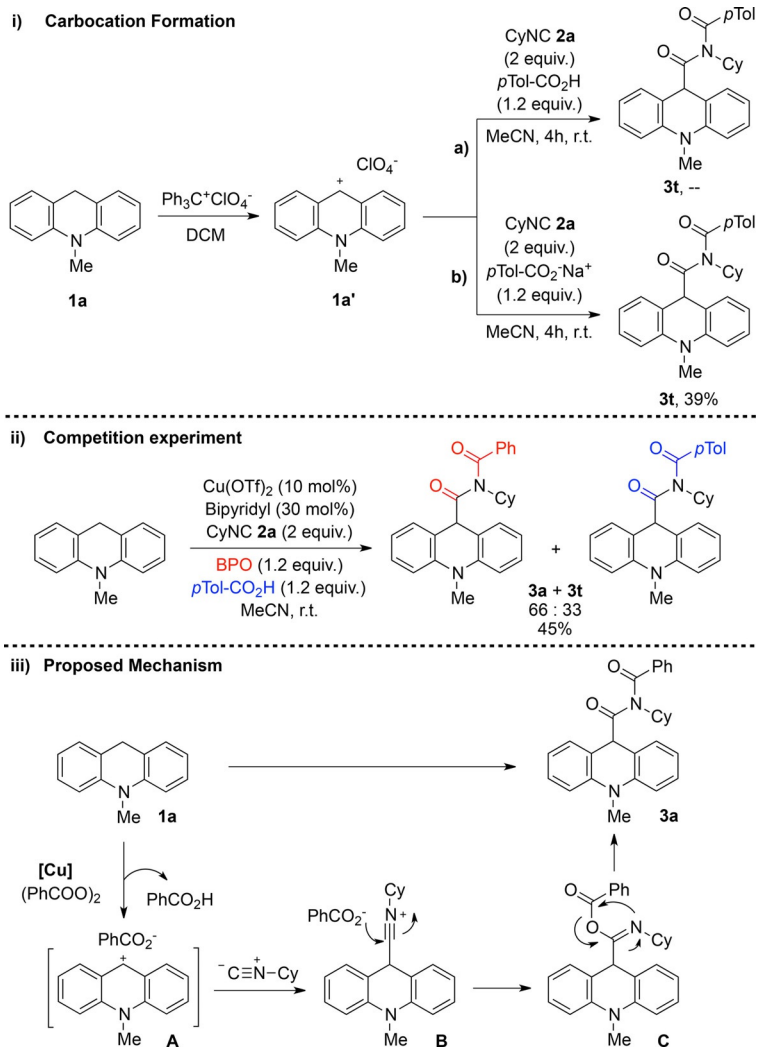

Scheme 2. Oxidative Ugi reaction: Mechanistic experiments and proposal.

selective conversion into the desired product **3**. Next, a competition experiment was performed between the in situ formed benzoate from the bezoyl peroxide and an external added carboxylic acid with a similar pKa, such as *p*-toluic acid (Scheme 2, equation ii). The reaction involved 1.2 equivalent of benzoyl peroxide, forming at most 2.4 equivalents of benzoic acid/benzoate, and 1.2 equivalents of the *p*-toluic acid. The two possible Ugi-type products **3a** and **3t** were then obtained in a perfect statistical 2:1 ratio (**3a:3t**, 66:33) in a 45% overall yield. Based on the experimental observations, a plausible reaction mechanism was postulated (Scheme 2, equation iii). Consequently, the reaction occurs via a copper-catalyzed radical-initiated oxidation of the benzylic C9-position to produce the carbocation **A**.[18] Then, the addition of the isocyanide (to form **B**) and sequential attack of the in situ formed benzoate, provides the neutral intermediate **C**, which rapidly undergoes an Ugi-type rearrangement process to give the desired product **3**.

For the synthesis of the photoactive acridinium salts, the final aromatization process was carried out for some selected imide-acridanes **3** with tritylperchlorate as mild hydride abstractor in dry acetonitrile,[19] yielding the corresponding acridinium perchlorate salts **4** in a range from 36 to 79% yield (Scheme 3, top). The photochemical properties of the newly obtained acridiniums were next investigated. The acridinium salts **4** display two maximum absorption bands (355–380 nm and 420–460 nm), which depend on the substituents at the imide and acridinium nitrogen-atom (Scheme 3, top right; see Supporting Information for further details). As a result, modifications of the substituents (R^1, R^2 and R^3) allowed an easy tuning of the excited state properties of these acridinium salts. Interestingly, when a methoxy substituent was present (R^2 = MeO), acridiniums **4f** and **4g** showed a strong bathochromic shift of both characteristic bands up to λ_{max} = 380 and 460 nm. Moreover, the ground-state redox potentials of the catalysts were determined by cyclic voltammetry (CV) in acetonitrile as solvent (see Supporting Information). The ground state reduction of catalysts **4** occurs at low potentials (around −0.3 V vs. SCE) with a relative excited state reduction potential around 2.4 V (showing slightly variations depending on the substituents), which are above the values of the Fukuzumi's photocatalyst **III** ($E_{1/2}$ = +2.18 V vs. SCE).[3] After obtaining these appealing results, the catalytic activity of **4** was then investigated in the dehydrogenative lactonization of 2-phenylbenzoic acid (**5**) as model reaction (see the optimization Table S2).[20] This transformation is known to proceed through a reductive quenching cycle and was already reported with the Fukuzumi's commercial catalyst **III**. In fact, when other less oxidative catalysts like $[Ru(bpy)_3](BF_4)_2$ ($E^*_{1/2}$ = +0.77 V vs. SCE)[2] or Eosin-Y ($E^*_{1/2}$ = +0.83 or 1.23 vs. SCE)[3] were employed, no conversion was found. On the contrary, the stronger oxidant catalyst **III** ($E^*_{1/2}$ = +2.18 V vs. SCE)[3] gave the lactone **6** with a moderate 30% yield (Scheme 3, equation a). Outstandingly, our designed acridinium catalysts **4** led to the lactone **6** in notable higher yields (46–93%, see Table S2 in the Supporting Information) under the same conditions and reaction time. In particular, **4a** and **4b** turned out to be the optimal photo-organocatalysts, providing **6** in 83 and 93% yield, respectively (Scheme 3, equation a). In order to generalize the good catalytic performance of catalysts **4**, the activity of both the parent *N*-methyl derivative **4a** and the best catalyst **4b** was compared with the Fukuzumi's catalyst **III** in different photoredox reactions (equations b–d). Initially, oxidative transformations such as the oxidation of alcohols to aldehydes and ketones were explored. Acridinium catalysts such as **III** can oxidize primary and secondary benzylic alcohols under oxygen atmosphere[21] by oxidation of the arene to its radical cation and subsequent deprotonation.[3] To our delight, after one hour the alcohol **7** was oxidized to **8** in 28% conversion with catalyst **III**, whereas **4a** and **4b** gave a significant improved 75% and 92% conversion, respectively (Scheme 3, equation b). Furthermore, the *anti*-Markovnikov hydro-functionalization of alkenes, which has extensively been studied employing mesityl acridinium type catalysts,[3] was in-

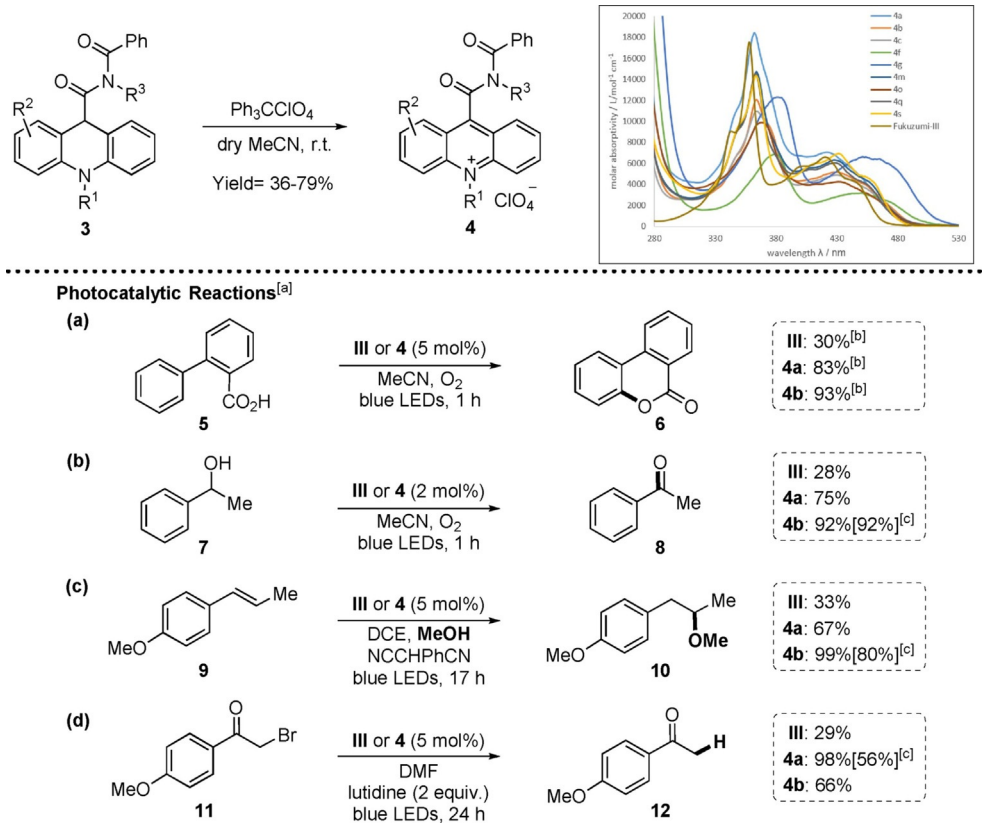

Scheme 3. Comparative photocatalytic reactions with **III**, **4a** and **4b**. [a] NMR conversions. [b] Isolated yields. [c] NMR yields in brackets.

vestigated. In the chosen case of the intermolecular hydroetherification of alkenes such as **9** with methanol (10 equiv), a redox-active hydrogen atom transfer agent such as 2-phenyl malononitrile (0.5 equiv) was used to improve the yields.[22] As in the previous reaction, the photocatalysts **4a** and **4b** gave higher conversions than the Fukuzumi's catalyst **III** under the same conditions (17 h, 67 and 99% vs. 33%; Scheme 3, equation c). In addition, although acridinium salts are known to be weak reductants, the reduction of the bromo-ketone derivative **11** ($E_{1/2} = -0.49$ V vs. SCE) with **4** was also challenged.[2] Surprisingly, excellent results were also obtained in this type of reaction, in which the *N*-methyl derivative **4a** showed better results than **4b** (98 vs. 66% conversion). Moreover, both photocatalysts **4** proved again to be more active than **III** (29% conversion) (Scheme 3, equation d).

In conclusion, the designed novel imide-acridinium organophotocatalysts **4** were prepared in a simple 2-steps approach by a new oxidative C–H functionalization/Ugi-type reaction of acridanes, followed by an aromatization process. The developed oxidative Ugi reaction with benzoyl peroxide, used as both oxidant and carboxylate source, has allowed the introduction of a polar functional group at the C9-position. Furthermore, the methodology is rather flexible and tolerates a wide range of substituents. In terms of reactivity, the imide-acridiniums **4** led to a notable higher activity than the commercially available, commonly used Fukuzumi's catalyst in both oxidative and reductive reactions.

Acknowledgements

The Boehringer Ingelheim Stiftung (Exploration Grant), the Deutsche Forschungsgemeinschaft (DFG), the COST Action "C–H activation in organic Synthesis (CHAOS)" (CA15106) and Spanish Government (CTQ2015-64561-R) are gratefully acknowledged for generous support.

Conflict of interest

The authors declare no conflict of interest.

Keywords: acridinium salts · C–H functionalization · multicomponent reactions · oxidation · photocatalysis

[1] a) M. Fagnoni, D. Dondi, D. Ravelli, A. Albini, *Chem. Rev.* **2007**, *107*, 2725; b) S. Fukuzumi, K. Ohkubo, *Chem. Sci.* **2013**, *4*, 561–574; c) J. M. R. Narayanam, C. R. J. Stephenson, *Chem. Soc. Rev.* **2011**, *40*, 102; d) E. Meggers, *Chem. Commun.* **2015**, *51*, 3290; e) M. H. Shaw, J. Twilton, D. W. C. MacMillan, *J. Org. Chem.* **2016**, *81*, 6898–6926; f) A. F. Garrido-Castro, M. C. Maestro, J. Alemán, *Tetrahedron Lett.* **2018**, *59*, 1286.

[2] K. P. Christopher, D. A. Rankic, D. W. C. MacMillan, *Chem. Rev.* **2013**, *113*, 5322.

[3] N. A. Romero, D. A. Nicewicz, *Chem. Rev.* **2016**, *116*, 10075.

[4] a) K. A. Margrey, D. A. Nicewicz, *Acc. Chem. Res.* **2016**, *49*, 1997; b) A. J. Perkowski, D. A. Nicewicz, *J. Am. Chem. Soc.* **2013**, *135*, 10334; c) K. Ohkubo, T. Kobayashi, S. Fukuzumi, *Angew. Chem. Int. Ed.* **2011**, *50*, 8652; *Angew. Chem.* **2011**, *123*, 8811.

[5] a) G. Weber, F. W. J. Teale, *Trans. Faraday Soc.* **1957**, *53*, 646–655; b) A. C. Benniston, A. Harriman, P. Li, J. P. Rostron, H. J. van Ramesdonk, M. M. Groeneveld, H. Zhang, J. W. Verhoeven, *J. Am. Chem. Soc.* **2005**, *127*, 16054.

[6] a) T. M. Bockman, J. K. Kochi, *J. Phys. Org. Chem.* **1997**, *10*, 542; b) K. Suga, K. Ohkubo, S. Fukuzumi, *J. Phys. Chem. A* **2006**, *110*, 3860.

[7] Even if the Ph-Acr-Me^+ catalyst did not show radical-radical reactivity it is subject to nucleophilic deactivation: D. Zhou, R. Khatmullin, J. Walpita, N. A. Miller, H. L. Luk, S. Vyas, C. M. Hadad, K. D. Glusac, *J. Am. Chem. Soc.* **2012**, *134*, 11301.

[8] a) S. Fukuzumi, H. Kotani, K. Ohkubo, S. Ogo, N. Tkachenko, H. Lemmetyinen, *J. Am. Chem. Soc.* **2004**, *126*, 1600; b) Y.-C. Lin, C.-T. Chen, *Org. Lett.* **2009**, *11*, 4858.

[9] For acridinium C-9-esters with chemiluminescence applications, see e.g.: K. A. Browne, D. D. Deheyn, G. A. El-Hiti, K. Smith, I. Weeks, *J. Am. Chem. Soc.* **2011**, *133*, 14637.

[10] For phenyl-C9-acridinium derivatives in photocatalysis, see: L. Chen, H. Li, P. Li, L. Wang, *Org. Lett.* **2016**, *18*, 3646, and references therein.

[11] Selected reviews: a) C. Liu, H. Zhang, W. Shi, A. Lei, *Chem. Rev.* **2011**, *111*, 1780; b) S. A. Girard, T. Knauber, C.-J. Li, *Angew. Chem. Int. Ed.* **2014**, *53*, 74; *Angew. Chem.* **2014**, *126*, 76; c) Special issue on C–H activation, R. H. Crabtree, *Chem. Rev.* **2017**, *117*, 8481.

[12] a) T. Stopka, L. Marzo, M. Zurro, S. Janich, E. U. Würthwein, C. G. Daniliuc, J. Alemán, O. García Mancheño, *Angew. Chem. Int. Ed.* **2015**, *54*, 5049; *Angew. Chem.* **2015**, *127*, 5137; b) H. Richter, R. Fröhlich, C. G. Daniliuc, O. García Mancheño, *Angew. Chem. Int. Ed.* **2012**, *51*, 8656; *Angew. Chem.* **2012**, *124*, 8784; c) A. Gini, J. Bamberger, J. Luis-Barrera, M. Zurro, R. Mas-Ballesté, J. Alemán, O. García Mancheño, *Adv. Synth. Catal.* **2016**, *358*, 4049, and references therein.

[13] a) I. Ugi, R. Meyr, U. Fetzer, C. Steinbrückner, *Angew. Chem.* **1959**, *71*, 386; b) J. Alemán, S. Cabrera, C. Alvarado, *Recent Advances in the Ugi Multicomponent Reaction in Multicomponent Reactions: Concepts and Applications for Design and Synthesis* (Eds.: R. P. Herrera, E. Marqués López), Wiley, NJ, **2015**, pp. 245.

[14] a) T. Ngouansavanh, J. Zhu, *Angew. Chem. Int. Ed.* **2007**, *46*, 5775; *Angew. Chem.* **2007**, *119*, 5877; b) X. Ye, C. Xie, Y. Pan, L. Han, T. Xie, *Org. Lett.* **2010**, *12*, 4240; c) M. Rueping, C. Vila, *Org. Lett.* **2013**, *15*, 2092; d) Y. Chen, G. Feng, *Org. Biomol. Chem.* **2015**, *13*, 4260; e) S. U. Dighe, S. Kolle, S. Batra, *Eur. J. Org. Chem.* **2015**, 4238; f) K. Singh, A. Kaur, V. S. Mithu, S. Sharma, *J. Org. Chem.* **2017**, *82*, 5285.

[15] a) A. Baeyer, *Ber. Dtsch. Chem. Ges.* **1871**, *4*, 555; b) A. V. Dubrovskiy, R. C. Larock, *J. Org. Chem.* **2012**, *77*, 11232; c) T. Tsudaka, H. Kotani, K. Ohkubo, T. Nakagawa, N. V. Tkachenko, H. Lemmetyinen, S. Fukuzumi, *Chem. Eur. J.* **2017**, *23*, 1306; d) C. Fischer, C. Sparr, *Angew. Chem. Int. Ed.* **2018**, *57*, 2436, and references therein.

[16] C. de Graaff, L. Bensch, M. J. van Lint, E. Ruijter, R. V. A. Orru, *Org. Biomol. Chem.* **2015**, *13*, 10108.

[17] The $Cu(OTf)_2$ catalyst was pre-dried at 50–60 °C under high vacuum for several hours prior use.

[18] a) T. Saegusa, Y. Ito, S. Kobayashi, K. Hirota, N. Takeda, *Can. J. Chem.* **1969**, *47*, 1217; b) B. L. Tran, B. Li, M. Driess, J. F. Hartwig, *J. Am. Chem. Soc.* **2014**, *136*, 2555.

[19] a) Alternative electrochemical oxidation: A. V. Shchepochkin, O. N. Chupakhin, V. N. Charushin, D. V. Steglenko, V. I. Minkin, G. L. Rusinov, I. A. Matern, *RSC Adv.* **2016**, *6*, 77834; b) Alternative catalytic oxidation: S. Fukuzumi, K. Okamoto, Y. Tokuda, C. P. Gros, R. Guilard, *J. Am. Chem. Soc.* **2004**, *126*, 17059.

[20] N. P. Ramirez, I. Bosque, J. C. Gonzalez-Gomez, *Org. Lett.* **2015**, *17*, 4550.

[21] H. J. Xu, X. L. Xu, Y. Fu, Y. S. Feng, *Chin. Chem. Lett.* **2007**, *18*, 1471.

[22] D. S. Hamilton, D. A. J. Nicewicz, *J. Am. Chem. Soc.* **2012**, *134*, 18577.

Manuscript received: June 1, 2018
Accepted manuscript online: June 8, 2018
Version of record online: July 25, 2018

ChemPubSoc Europe

DOI: 10.1002/cptc.201900116

CHEMPHOTOCHEM Communications

Special Issue

Mesityl or Imide Acridinium Photocatalysts: Accessible Versus Inaccessible Charge-Transfer States in Photoredox Catalysis

Andrea Gini,[a] Thomas Rigotti,[a] Raúl Pérez-Ruiz,[b] Mustafa Uygur,[c] Rubén Mas-Ballesté,[d, e] Inés Corral,[e, f, g] Lara Martínez-Fernández,[f] Victor A. de la Peña O'Shea,[b] Olga García Mancheño,*[c] and José Alemán*[a, e]

A study on C9-imide acridinium photocatalysts with enhanced photoredox catalytic activity with respect to the well-established C9-mesityl acridinium salt is presented. The differences observed rely on the diverse accessibility of singlet charge-transfer excited states, which have been proven by CASPT2/CASSCF calculations, fluorescence and quenching studies.

In recent years, visible-light organo-photoredox catalysis[1] has arisen as a valid and potent alternative for the commonly used photoredox catalysts based on ruthenium and iridium polypyridyl complexes.[2] Indeed, these organo-catalysts have opened new paths in visible light-induced photoredox processes, due to their versatility, the wide range of reductive and oxidative potentials and their reasonable prices.[3] In this regard, the acridinium-based photoredox catalysts **1**[1] (Figure 1, top) have attracted a vast interest, especially in the form of the corresponding 9-mesityl derivatives. Indeed, from the pioneering work of Fukuzumi and co-workers,[4] the 9-mesityl *N*-methyl acridinium salt (**1 b**) was found to be one of the most powerful photoredox catalysts.[5] In the last decade, **1 b** became the most widely used acridinium-based photoredox catalyst due to its stability and its high oxidative potential (~2.2 V vs. SCE). However, it still presents substantial reactivity and stability limitations.[1,4,5] Aiming at overcoming some of these restraints, we recently developed a new class of C9-imide acridinium-based photoredox catalysts **2** (Figure 1, top).[6] In this manner, a vast library of imide-acridinium derivatives with comparable or even improved properties than **1 b** was achieved. The *N*-methyl and *N*-phenyl cyclohexyl derivatives (**2 a** and **2 b**) showed the highest efficiency as photoredox catalysts in all the reactions we tested, showing in all the cases better results than employing **1 b** (Figure 1, bottom). The mesityl group of **1 b** is

[a] A. Gini, T. Rigotti, Prof. J. Alemán
Organic Chemistry Department, Módulo 1
Universidad Autónoma de Madrid, Facultad de Ciencias
Calle Francisco Tomás y Valiente, 7, 28049 Madrid (Spain)
E-mail: jose.aleman@uam.es
[b] R. Pérez-Ruiz, V. A. de la Peña O'Shea
Photoactivated Process Unit
IMDEA Energy
Av. Ramón de la Sagra 3, 28935 Madrid (Spain)
[c] M. Uygur, Prof. O. García Mancheño
Organic Chemistry Institute
University of Münster
Corrensstraße 40, 48149 Münster (Germany)
E-mail: olga.garcia@uni-muenster.de
[d] R. Mas-Ballesté
Inorganic Chemistry Department, Módulo 7
Universidad Autónoma de Madrid, Facultad de Ciencias
Calle Francisco Tomás y Valiente, 7, 28049 Madrid (Spain)
[e] R. Mas-Ballesté, I. Corral, Prof. J. Alemán
Institute for Advanced Research in Chemical Sciences (IAdChem)
Universidad Autónoma de Madrid, Facultad de Ciencias
Calle Francisco Tomás y Valiente, 7, 28049 Madrid (Spain)
[f] I. Corral, L. Martínez-Fernández
Condensed Matter Physics Center (IFIMAC)
Universidad Autónoma de Madrid, Facultad de Ciencias
Calle Francisco Tomás y Valiente, 7, 28049 Madrid (Spain)
[g] I. Corral
Chemistry Department, Módulo 13
Universidad Autónoma de Madrid, Facultad de Ciencias
Calle Francisco Tomás y Valiente, 7, 28049 Madrid (Spain)

Supporting information for this article is available on the WWW under https://doi.org/10.1002/cptc.201900116

Special Issue An invited contribution to a Special Issue on Photochemical Synthesis. This is a joint project with our sister journal *Eur. J. Org. Chem.*

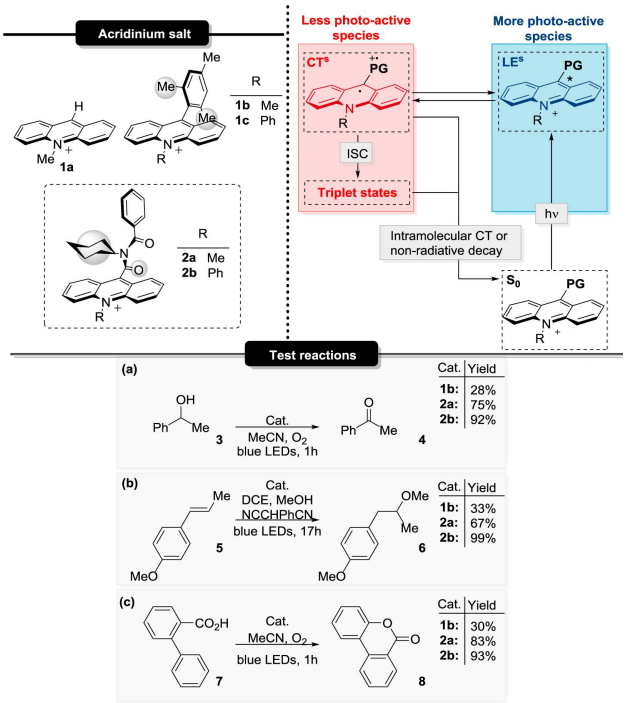

Figure 1. Top: Acridinium salt catalysts and their theoretical photo-excited species (PG = protecting group). Bottom: Test reactions.[6]

responsible of the low susceptibility to nucleophilic and radical addition on the acridinium core of **1b**, increasing its chemical stability. However, this orthogonal electron-rich aromatic ring in the C9-position opens the access to inactive charge transfer species (CT).[4,7–10] The role of these charge-transfer states has been a matter of debates,[7] but at the moment it is accepted that the singlet charge transfer (CT^s) state is irrelevant in electron-transfer processes and it is an unproductive photoredox pathway.[1,8] Therefore, its tendency is to decay *via* non-radiative pathways or to perform the intersystem-crossing.

In this work, in order to get some insight on the better performance of the novel class of acridinium salt catalysts **2** respect to the classical mesityl derivatives **1**, we have investigated the photophysics of both the Fukuzumi's catalyst **1b** and the acridinium salts **2** with the help of steady state spectroscopy and excited state ab initio simulations.

We started measuring and comparing the properties connected to long life and active singlet excited species of **1** and **2** (Table 1). In principle, both triplet-states, the charge transfer triplet state (CT^T) and the locally excited triplet (LE^T) could take part on electron transfer (ET) processes.[4,10] However, under the standard concentrated conditions the quenching of the triplet state by the reactants was not observed, even when the CT^T state of C9-mesityl acridinium photocatalyst was recently reported to be active in particular cases, exhibiting both oxidizing and reducing abilities.[11] Therefore, the triplet contribution is almost negligible.[8a] As a result, it is evident that the insertion of a mesityl group in the 9-position on an acridinium scaffold is at the same time an advantage and a drawback: on one hand it enhances the stability of the acridinium core; on the other hand it decreases the fluorescence quantum yield and life time of excited species due to the access to unproductive CT states (Table 1). As a matter of fact, we wondered about the effect of introducing the bulky C9-imide group of **2a–b** in the population of CT states. Therefore, additional experimental and theoretical evidences were needed in order to clarify this issue.

The absorption spectra were first recorded for all the acridinium salts (Figure 2, top). The maximum absorbance in the visible light region for all the catalysts is in the range of 420–450 nm. Moreover, since **1a** is known to have an extremely high fluorescence quantum yield ($\Phi_F = \sim 1$),[12] the four catalysts were compared based on this information. When the catalysts **2a** and **2b** were separately excited with monochromatic light at 430 nm, a significant emission band centred at 500 and 530 nm was observed, respectively (Figure 2, bottom). The large bathochromic shift of **2b** could be related to the partial planarization of the N–Ph caused by the hindrance of the rotation of the bulky imide protecting group.[13]

The fluorescence quantum yield (Φ_F) of **2a** and **2b** resulted consistently higher ($\Phi_F = 0.10$ and 0.25, respectively) compared to the Fukuzumi acridinium salt **1b** ($\Phi_F = 0.02$) (Table 1). Such characteristics, as the fluorescence lifetime and quantum yield, were substantially lower for **1b** than for **1a**. This is ascribed to the impossibility of **1a** to form CT_s species due to the absence of substituents at the C9 position (R = H) (Table 1 and see computational studies below).[1,4,7] Interestingly, the fluorescence lifetime (τ_F) for **2b** was 12.4 ns, which is notably longer than the τ_F for **1b** (5.1 ns) but still lower than the extremely long lifetime of 21. **1a** excited species (34.7 ns) (Table 1). However, the *N*-Me analogue **2a** presents a lower fluorescence lifetime than the other considered catalysts. Nonetheless, the less rigid 9-imide-based protecting group of the acridinium scaffold has various vibrational and rotational paths that may dissipate the excited state in a non-radiative manner. In this perspective, taking into account that the excited 9-substituted acridinium scaffold performs a forced bending of the protecting groups in both the 9-position and in the nitrogen,[16] excited **2a*** could have a higher rotation-freedom than the excited *N*-Ph derivative **2b***, in which the phenyl group could prevent and block the free rotation of the imide group. This opens more non-radiative decay pathways

Table 1. Photophysical and photoredox data of **1a–b** and **2a–b** photocatalysts considered in this work, and **1c** for comparison reasons.

Cat.	$E^{1/2}_{red}$ [a] [V] vs SCE	E^{S}_{red} [b] [V] vs SCE	$\lambda_{em\,max}$ [nm]	Φ_F [c]	τ_F [d] [ns]
1a	−0.46	+2.32	490	~1	34.7
1b	−0.49	+2.18	507	0.02	5.1
1c[14]	−0.55	+2.00	509[e]	n.a.	0.49/5.5[f]
2a	−0.33	+2.36	500	0.10	2.1[g]
2b	−0.28	+2.40	525	0.25	12.4

[a] Ground state reduction potential. [b] Singlet excited state reduction potential. [c] Calculated comparing the fluorescence intensity of **1a**.[15] [d] Fluorescence half-lifetime in the presence of air in MeCN. [e] Reported in DCE. [f] Reported in MeOH. [g] Fitting component: 2.1 ns (>99%),

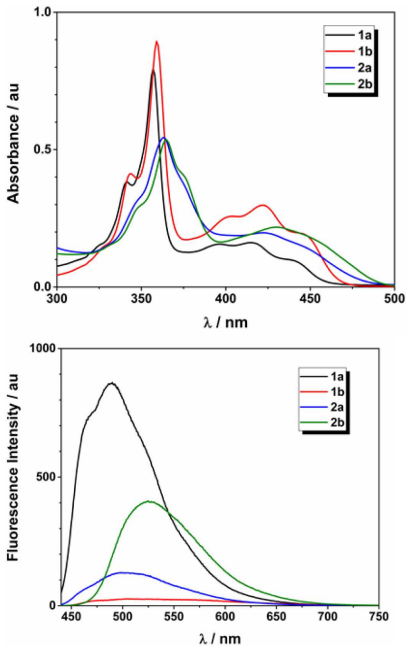

Figure 2. UV/Vis absorption and emission spectra. Top: Absorption spectra of the corresponding acridinium salt derivatives in acetonitrile under air. All concentrations were fixed at 50 μM; Bottom: Steady-state emission spectra (λ_{exc} = 430 nm) of the corresponding acridinium salt derivatives in acetonitrile under air. All concentrations were fixed at 50 μM.

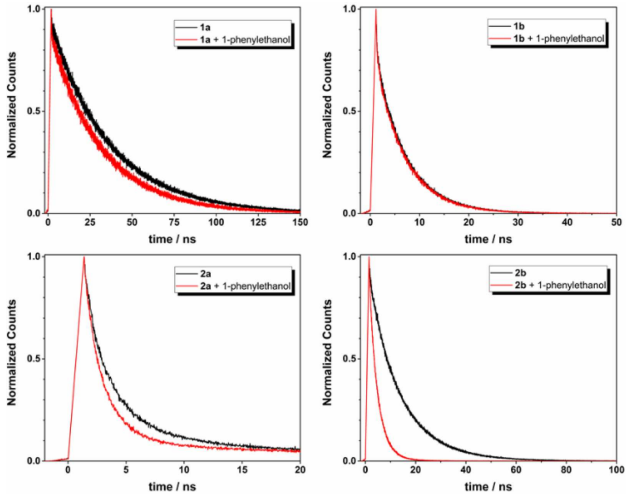

Figure 3. Normalized time-resolved emission spectra (λ_{exc} = 445 nm) of the catalysts **1a-b** and **2a-b** (50 μM) in the presence of 0.2 M 1-phenylethanol (**3**) as quencher in acetonitrile under air.

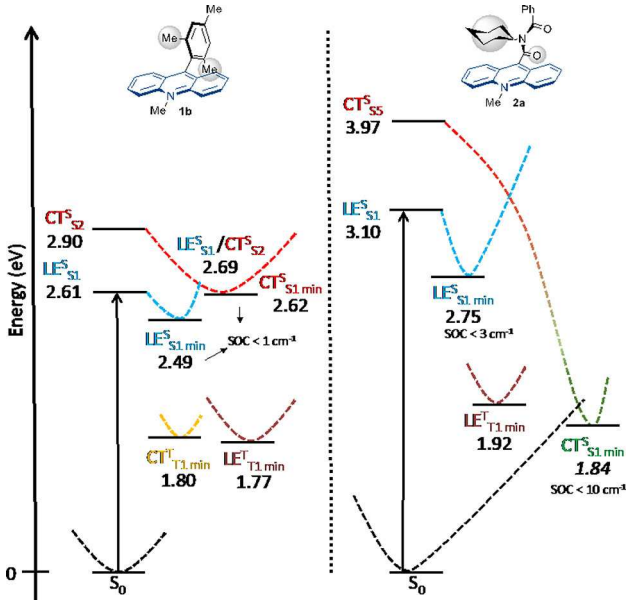

Figure 4. CASPT2/ANO-S//TD-M062X/6-31G* gas-phase potential energy profiles for **1b** and **2a**. Energies relative to the S_0 are given in eV and spin-orbit couplings in cm^{-1}.

and, therefore, leads to a lower fluorescence lifetime for the *N*-Me derivative.

Then, the fluorescence of the catalysts **1a**–**b** and **2a**–**b** was studied in the presence of a 0.2 M solution of an appropriate quencher such as 1-phenylethanol (**3**, ~ +2.11 V vs. SCE)[17] (Figure 3). The normalized time-resolved emission spectra showed a correlation between the quenching intensity and the light-induced oxidation reaction results when employing different photocatalysts. Indeed, alcohol **3** quenches the excited state of catalyst **2b** (τ_F (**3**) 3.3 ns vs. τ_F 12.4 ns) and slightly that of **1a** and **2a** (Figure 3). This significant dynamic quenching of the singlet excited state for **2b** may rely on its high quantum yield and the initial hypothesis of non-accessible CT and triplet states for this catalyst. Moreover, the emission temporal profile of **1b** retained its characteristic shape under the presence of **3**. This behaviour could be due to the low concentration of singlet excited state of **1b**, which is related to its low fluorescence quantum yield. It is worth to mention that further emission studies under argon showed that **1b** was affected by the presence of air (see S.I.). Therefore, the active excited state from **1b** is less stable under the aerobic reaction conditions, which could contribute to its poor catalytic performance in some systems. Nevertheless, under identical conditions the product **4** is still formed in the presence of **1b** (Figure 1(a), 28%), for which the thermodynamic driving force for an electron transfer process became important.

In addition, the reduction potential of the excited state of the new catalysts **2** was estimated by combining cyclic-voltammetry and spectroscopic data.[6] Despite the lower reduction potential of **2a** and **2b** ground states compared to **1a** and **1b**, the two imide-based catalysts showed a comparable excited state reduction potential with **1a** and, to our delight, higher than the 9-mesityl derivative **1b** (see Table 1).

Further insight into the nature of the reactive excited states of **2a** or **1b** was obtained from CASPT2/CASSCF calculations (see Figure 4 and the Supporting Information for more details). Regarding the Fukuzumi's catalyst **1b**, the calculations asserted the proposal previously inferred from the experimental data (Figure 4, left). Therefore, two excited species LE^s_{S1} (localized, S_1) and CT^s_{S2} (charge transfer, S_2) very close in energy (0.3 eV) were calculated at Franck Condon region, with oscillator strengths amounting to 0.1397 and 0.0068, respectively, indicating much higher absorption for LE^s_{S1} than for CT^s_{S2}. The geometry optimization of these excited states resulted in two new S_1 minima close in energy ($CT^s_{S1\text{-}min}$ and $LE^s_{S1\text{-}min}$, 2.62 and 2.49 eV, respectively), with the localized species being slightly more stable (Figure 4).

Our calculations also revealed that the CT^s_{S2}/LE^s_{S1} internal conversion funnel lies close to the two optimized minima. This translates into an almost negligible energy barrier interconnecting both the excited localized and charge transfer species, which is in agreement with the previously reported equilibrium between LE and CT species from experimental data.[9b] The very small spin orbit coupling (SOC) (<1 cm^{-1}) calculated at the two S_1 minima also points to a small probability of population transfer to the triplet manifold, where the stability order of the CT^T and LE^T minima is maintained. Here, still the localized and CT triplet minima present similar energies (1.77 and 1.80 eV). Therefore, these data are fully consistent with the scenario describing an equilibrium between the LE and CT singlet excited minima, being the former species the active one, with the latter corresponding to a CT unproductive intermediate.

In contrast, the replacement of the mesityl by the imide group at the C-9 position results in a considerable destabilization of the CT electronic excited species, delocalized between the acridinium and phenyl moieties (Figure 4, right). In fact, the energy difference between the two states at the Franck Condon region amounts to 0.87 eV in the gas phase. The optimization of the localized excited state leads to a minimum with an

energy of 2.75 eV relative to the ground state. The lowest lying CT state (S_5) at Franck Condon region evolves to a very stable CT minimum of different character, delocalized over the acridinium and imide moieties. The probability of transferring population to the triplet manifold from the LE minimum is predicted to be small (SOC < 3 cm^{-1}). The couplings of the most stable CT state at the position of the minimum CT^{S}_{S1min} are however not negligible (SOC ca. 10 cm^{-1} with the T_1). Still, the chances to leak population to the triplet manifold are small considering that the barrier to indirectly access the CT^{S}_{S1min} from LE^{S}_{S1min} is very large. Therefore, the larger energy barrier of **2** compared to **1** interconnecting the LE and CT minima makes the imide derivative a more active and efficient photocatalyst.

In conclusion, the herein studied novel class of photoredox catalysts **2** have showed the tendency of forming LE species, being CT states quite inaccessible, whereas in **1 b** these CT and LE species are equally accessible. Considering that CT states are unproductive species in the catalytic system, our observations explain the better performances observed for **2 a** and **2 b** compared to the widely used 9-mesityl acridinium salt catalyst **1 b**.

Acknowledgements

The Boehringer Ingelheim Stiftung (Exploration Grant), the Deutsche Forschungsgemeinschaft (DFG), Spanish Government (CTQ2015-64561-R, CTQ2015-63997-C2, ENE2016-79608-C2-1-R) and Community of Madrid (2016-T1/AMB-1275) are acknowledged. I.C. and L.M.F acknowledge the "Ramón y Cajal" and "Juan de la Cierva-Incorporación" to the Spanish government (MINECO). We thank the generous allocation of computing time at the CCC (UAM). The authors wish to thank ''Comunidad de Madrid'' for its support to the FotoArt-CM Project (S2018/NMT-4367) through the Program of R&D activities between research groups in Technologies 2013, co-financed by European Structural Funds.

Conflict of Interest

The authors declare no conflict of interest.

Keywords: acridinium catalyst · charge transfer · excited state · photocatalysis · quenching studies

[1] N. A. Romero, D. A. Nicewicz, *Chem. Rev.* **2016**, *116*, 10075–10166 and references cited therein.

[2] a) J. M. R. Narayanam, C. R. J. Stephenson, *Chem. Soc. Rev.* **2011**, *40*, 102–113; b) K. P. Christopher, D. A. Rankic, D. W. C. MacMillan, *Chem. Rev.* **2013**, *113*, 5322–5363; c) M. H. Shaw, J. Twilton, D. W. C. MacMillan, *J. Org. Chem.* **2016**, *81*, 6898–6926.

[3] a) M. Fagnoni, D. Dondi, D. Ravelli, A. Albini, *Chem. Rev.* **2007**, *107*, 2725–2756; b) S. Fukuzumi, K. Ohkubo, *Chem. Sci.* **2013**, *4*, 561–574; c) A. F. Garrido Castro, M. C. Maestro, J. Alemán, *Tetrahedron Lett.* **2018**, *59*, 1286–1294.

[4] a) S. Fukuzumi, H. Kotani, K. Ohkubo, N. V. Tkachenko, H. Lemmetyinen, *J. Am. Chem. Soc.* **2004**, *126*, 1600–1601; b) H. Kotani, K. Ohkubo, S. Fukuzumi, *J. Am. Chem. Soc.* **2004**, *126*, 15999–16006; c) S. Fukuzumi, K. Ohkubo, T. Suenobu, *Acc. Chem. Res.*, **2014**, *47*, 1455–1464.

[5] a) K. A. Margrey, D. A. Nicewicz, *Acc. Chem. Res.* **2016**, *49*, 1997–2006; b) A. J. Perkowski, D. A. Nicewicz, *J. Am. Chem. Soc.* **2013**, *135*, 10334–10337; c) K. Ohkubo, T. Kobayashi, S. Fukuzumi, *Angew. Chem. Int. Ed.* **2011**, *50*, 8652–8655; *Angew. Chem.* **2011**, *123*, 8811–8814.

[6] A. Gini, M. Uygur, T. Rigotti, J. Aléman, O. García Mancheño, *Chem. Eur. J.* **2018**, *24*, 12509–12514.

[7] a) A. C. Benniston, A. Harriman, P. Li, J. P. Rostron, J. W. Verhoeven, *Chem. Commun.* **2005**, 2701–2703; b) J. W. Verhoeven, H. J. van Ramesdonk, M. M. Groenveld, A. C. Benniston, A. Harriman, *ChemPhysChem*, **2005**, *6*, 2251–2260; c) K. Ohkubo, H. Kotani, S. Fukuzumi, *Chem. Commun.* **2006**, 4520–4522; d) . S. Fukuzumi, *Phys. Chem. Chem. Phys.* **2008**, *10*, 2283–2297; e) A. C. Benniston, A. Harriman, J. W. Verhoeven, *Phys. Chem. Chem. Phys.* **2008**, *10*, 5156–5158; f) S. Fukuzumi, H. Kotani, K. Ohkubo, *Phys. Chem. Chem. Phys.* **2008**, *10*, 5159–5162; g) T. Tsukada, H. Kotani, K. Ohkubo, T. Nakagawa, N. V. Tkachenko, G. Lemmetyinen, S. Fukuzumi, *Chem. Eur. J.* **2017**, *23*, 1306–1317.

[8] a) N. A. Romero, D. A. Nicewicz, *J. Am. Chem. Soc.* **2014**, *136*, 17024–17035; b) D. J. Wilger, J.-M. M. Grandjean, T. R. Lammert, D. A. Nicewicz, *Nat. Chem.* **2014**, *6*, 720–726; c) A. Joshi-Pangu, F. Lévesque, H. G. Roth, S. F. Oliver, L.-C. Campeu, D. Nicewicz, D. A. DiRocco, *J. Org. Chem.* **2016**, *81*, 7244–7249.

[9] a) J. W. Verhoeven, H. J. van Ramesdonk, H. Zhang, M. M. Groeneveld, A. C. Benniston, A. Harriman, *Int. J. Photoenergy*, **2005**, *7*, 103–108; b) A. C. Benniston, A. Harriman, P. Li, J. P. Rostron, H. J. van Ramesdonk, M. M. Groeneveld, H. Zhang, J. W. Verhoeven, *J. Am. Chem. Soc.* **2005**, *127*, 16054–16064.

[10] a) S. A. Jonker, F. Ariese, J. W. Verhoeven, *Recl. Trav. Chim. Pays-Bas*, **1989**, *108*, 109–115; b) G. Jones II, D. Yan, J. Hu, J. Wan, B. Xia, V. I. Vullev, *J. Phys. Chem. B* **2007**, *111*, 6921–6929; c) E. Kuruvilla, D. Ramaiah, *J. Phys. Chem. B* **2007**, *111*, 6549–6556; d) J. Hu, B. Xia, D. Bao, A. Ferreira, J. Wan, G. Jones II, V. I. Vullev, *J. Phys. Chem. A.* **2009**, *113*, 3096–3107.

[11] See e.g.: a) X. Hu, G. Zhang, F. Bu, X. Luo, K. Yi, H. Zhang, A. Lei, *Chem. Sci.* **2018**, *9*, 1521–1526; b) X. Hu, G. Zhang, F. Bu, A. Lei, *Angew. Chem. Int. Ed.* **2018**, *57*, 1286–1290; c) W. Cao, C. Wu, T. Lei, X. Yang, B. Chen, C. Tung, L. Wu, *J. Catal.* **2018**, *39*, 1194–1201; d) M. Xiang, Z.-K. Xin, B. Chen, C.-H. Tung, L.-Z. Wu, *Org. Lett.* **2017**, *19*, 3009–3012; e) T. Tsudaka, H. Kotani, K. Ohkubo, T. Nakagawa, N. V. Tkachenko, H. Lemmetyinen, S. Fukuzumi, *Chem. Eur. J.* **2017**, *23*, 1306–1317; f) T. Tsudaka, K. Ohkubo, S. Fukuzumi, *Chem. Commun.* **2016**, *52*, 6178–6180; g) S. Fukuzumi, K. Ohkubo, *Org. Biomol. Chem.* **2014**, *12*, 6059–6071.

[12] a) A. G. Griesbeck, M. Cho, *Org. Lett.* **2007**, *9*, 611–613; b) K. Ohkubo, K. Mizushima, R. Iwata, K. Souma, N. Suzuki, S. Fukuzumi, *Chem. Commun.* **2010**, *46*, 601–603; c) K. Ohkubo, A. Fujimoto, S. Fukuzumi, *Chem. Commun.* **2011**, *47*, 8515–8517.

[13] a) A. S. Klymchenko, *Acc. Chem. Res.* **2017**, *50*, 366–375; b) S.-C. Lee, J. Heo, H. C. Woo, J.-A. Lee, Y. H. Seo, C.-L. Lee, S. Kim, O.-P. Kwon, *Chem. Eur. J.* **2018**, *24*, 13706–13718.

[14] Reported photophysical and photoredox data of **1 c**: a) J. D. Griffin, M. A. Zeller, D. A. Nicewicz, *J. Am. Chem. Soc.* **2015**, *137*, 11340–11348; b) D. J. Wilger, J.-M. M. Grandjean, T. R. Lammert, D. A. Nicewicz, *Nat. Chem.* **2014**, *6*, 720–726.

[15] G. Weber, F. W. J. Teale, *Trans. Faraday Soc.* **1957**, *53*, 646–655.

[16] a) G. Weber, F. W. J. Teale, *Trans. Faraday Soc.* **1957**, *53*, 646–655. b) M. Hoshno, H. Uekusa, A. Tomita, S. Koshihara, T. Sato, S. Nozawa, S. Adachi, K. Ohkubo, H. Kotani, S. Fukuzumi, *J. Am. Chem. Soc.* **2012**, *134*, 4569–4572.

[17] H. G. Roth Nathan, A. Romero, D. A. Nicewicz, *Synlett* **2016**, *27*, 714–723.

Manuscript received: April 16, 2019
Revised manuscript received: May 12, 2019
Accepted manuscript online: May 13, 2019
Version of record online: June 7, 2019

Experimental Part
Chapter 5

(The complete “Supporting Information” documents, with all the characterization data, NMR spectra, SFC or HPLC traces and other experimental procedures have been included in the enclosed USB memory)

General procedure for the oxidative Ugi-reaction:

In an oven-dried screw cap Schlenk under nitrogen atmosphere, anhydrous $Cu(OTf)_2$ (7.2 mg, 0.02 mmol, 10 mol%) (note: avoid moisture, copper(II) triflate is slightly hydroscopic. The catalyst was pre-dried at 50 °C for several hours under high vacuum), 2,2'-bipyridyne (9.4 mg, 0.06 mmol, 30 mol%) and acridane **1** (0.2 mmol, 1 equiv.) were added following this order. The mixture was dissolved in acetonitrile (0.1 M), and the isocyanide **2** (2 equiv.) and benzoyl peroxide (58.1 mg, 0.24 mmol, 1.2 equiv.) were then added. The obtained mixture was stirred at room temperature for 4 h. After evaporating the solvent, the crude product was purified by flash column chromatography using a hexane/ethyl acetate mixture as eluent.

***N*-Benzoyl-*N*-cyclohexyl-10-methyl-acridane-9-carboxamide (3a)**

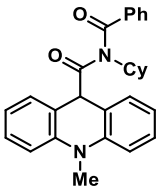

3a

According to the general procedure, the reaction of acridane **1a** (39.0 mg, 0.2 mmol, 1 equiv.) with cyclohexyl isocyanide **2a** (49.7 µL, 0.40 mmol, 2.0 equiv.), provided the title compound after flash column chromatography (hexane/EtOAc, 9:1) as a white solid (51.8 mg, 0.122 mmol, 61%).

^{1}H NMR (400 MHz, $CDCl_3$): δ 7.77 – 7.73 (m, 2H), 7.70 – 7.64 (m, 1H), 7.59 – 7.52 (m, 2H), 7.26 – 7.20 (m, 2H), 6.96 – 6.91 (m, 2H), 6.88 – 6.83 (m, 2H), 6.76 – 6.71 (m, 2H), 4.95 (s, 1H), 4.03 (tt, *J* = 12.0, 3.5 Hz, 1H), 3.40 (s, 3H), 1.80 – 1.67 (m, 2H), 1.65 – 1.56 (m, 2H), 1.52 – 1.42 (m, 1H), 1.32 – 1.25 (m, 2H), 1.16 – 0.96 (m, 3H).

^{13}C NMR (100 MHz, CDCl3): δ 176.8, 174.5, 142.7, 137.8, 132.9, 129.5, 129.2, 128.5, 128.4, 120.7, 120.5, 112.8, 59.4, 53.5, 33.3, 29.6, 26.3, 25.2.

HRMS (ESI-MS): Mass calc. for $[C_{28}H_{29}N_2O_2]^+$: *m/z* = 425.2224, found: *m/z* = 425.2228.

***N*-Benzoyl-*N*-cyclohexyl-10-phenyl-acridane-9-carboxamide (3b)**

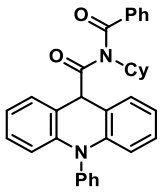

3b

According to the general procedure, the reaction of acridane **1c** (51.5 mg, 0.2 mmol, 1.0 equiv.) with cyclohexyl isocyanide **2a** (49.7 µL, 0.40 mmol, 2.0 equiv.), provided the title compound after flash column chromatography (hexane/EtOAc, 9:1) as slightly yellow solid (68.1 mg, 0.138 mmol, 69%).

^{1}H NMR (400 MHz, $CDCl_3$):δ 7.83 – 7.77 (m, 2H), 7.71 – 7.65 (m, 1H), 7.63 – 7.54 (m, 4H), 7.53 – 7.45 (m, 1H), 7.42 – 7.35 (m, 2H), 7.03 – 6.95 (m, 2H), 6.85 – 6.76 (m, 4H), 6.33 (d, *J* = 8.0 Hz, 2H), 5.09 (s, 1H), 4.15 – 3.99 (m, 1H), 1.84 – 1.73 (m, 2H), 1.66 – 1.59 (m, 2H), 1.55 – 1.46 (m, 1H), 1.35 – 1.27 (m, 2H), 1.18 – 0.99 (m, 3H).

^{13}C NMR (100 MHz, $CDCl_3$): δ 176.4, 174.8, 142.2, 140.7, 137.8, 133.0, 131.3, 130.7, 129.5, 129.2, 128.5, 128.4, 128.1, 120.6, 118.6, 114.8, 59.4, 52.7, 29.7, 26.3, 25.3.

HRMS (ESI-MS): Mass calc. for $[C_{33}H_{31}N_2O_2]^+$: *m/z* = 487.2380, found: *m/z* = 487.23874.

_N_-Benzoyl-_N_-cyclohexyl-10-benzyl-acridane-9-carboxamide (3c)

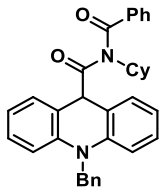

3c

According to the general procedure, the reaction of acridane **1b** (54.3 mg, 0.2 mmol, 1.0 equiv.) with cyclohexyl isocyanide **2a** (49.7 µL, 0.40 mmol, 2.0 equiv.), provided the title compound after flash column chromatography (hexane/EtOAc, 9:1) as a white solid (70.1 mg, 0.140 mmol, 70%).

^{1}H NMR (400 MHz, $CDCl_3$): δ 7.85 – 7.75 (m, 2H), 7.75 – 7.67 (m, 1H), 7.64 – 7.55 (m, 2H), 7.33 – 7.21 (m, 3H), 7.20 – 7.15 (m, 2H), 7.14 – 7.05 (m, 2H), 6.89 – 6.82 (m, 2H), 6.79 – 6.73 (m, 4H), 5.20 (s, 2H), 5.02 (s, 1H), 4.14 – 4.02 (m, 1H), 1.82 – 1.69 (m, 2H), 1.67 – 1.60 (m, 2H), 1.56 – 1.47 (m, 1H), 1.34 – 1.26 (m, 2H), 1.17 – 0.99 (m, 3H).

^{13}C NMR (100 MHz, $CDCl_3$): δ 176.4, 174.7, 141.6, 137.9, 137.0, 133.0, 129.5, 129.3, 128.8, 128.6, 128.5, 127.0, 126.2, 120.7, 120.3, 114.0, 59.4, 53.1, 51.0, 29.7, 26.3, 25.2.

HRMS (ESI-MS): Mass calc. for $[C_{34}H_{33}N_2O_2]^+$: *m/z* = 501.2537, found: *m/z* = 501.2544.

_N_-Benzoyl-_N_-cyclohexyl-2,10-dimethyl-acridane-9-carboxamide (3d)

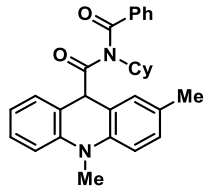

3d

According to the general procedure, the reaction of acridane **1d** (41.9 mg, 0.2 mmol, 1.0 equiv.) with cyclohexyl isocyanide **2a** (49.7 µL, 0.40 mmol, 2.0 equiv.), provided the title compound after flash column chromatography (hexane/EtOAc, 9:1) as white solid (53.5 mg, 0.122 mmol, 61%).

^{1}H NMR (400 MHz, $CDCl_3$): δ 7.77 – 7.72 (m, 2H), 7.71 – 7.65 (m, 1H), 7.60 – 7.52 (m, 1H), 7.27 – 7.20 (m, 1H), 7.06 – 7.02 (m, 1H), 6.95 – 6.78 (m, 4H), 6.45 – 6.41 (m, 1H), 4.95 (s, 1H), 4.01 (tt, *J* = 12.0, 3.6 Hz, 1H), 3.39 (s, 3H), 2.21 (s, 3H), 1.90 – 1.57 (m, 4H), 1.52 – 1.43 (m, 1H), 1.39 – 1.23 (m, 3H), 1.10 – 1.00 (m, 2H).

^{13}C NMR (100 MHz, $CDCl_3$): δ 176.4, 174.6, 142.7, 140.4, 137.8, 132.8, 129.6, 129.4, 129.1, 129.0, 128.8, 128.6, 128.3, 120.6, 120.4, 120.1, 112.6, 112.5, 59.3, 53.5, 33.1, 29.9, 29.2, 26.2, 26.2, 25.1, 20.4.

HRMS (ESI-MS): Mass calc. for $[C_{29}H_{30}N_2O_2Na]^+$: *m/z* = 461.2199, found: *m/z* = 461.2198.

_N_-Benzoyl-_N_-cyclohexyl-2,10-dimethyl-acridane-9-carboxamide (3e)

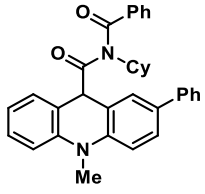

3e

According to the general procedure, the reaction of acridane **1i** (54.3 mg, 0.2 mmol, 1.0 equiv.) with cyclohexyl isocyanide **2a** (49.7 µL, 0.40 mmol, 2.0 equiv.), provided the title compound after flash column chromatography (hexane/EtOAc, 9:1) as white solid (68.1 mg, 0.136 mmol, 68%).

^{1}H NMR (400 MHz, $CDCl_3$): δ 7.82 – 7.75 (m, 2H), 7.67 – 7.60 (m, 1H), 7.55 – 7.39 (m, 7H), 7.34 – 7.23 (m, 2H), 7.02 (d, *J* = 8.5 Hz, 1H), 6.97 (d, *J* = 8.0 Hz, 1H), 6.93 – 6.83 (m,

3H), 5.03 (s, 1H), 4.06 (tt, *J* = 12.0, 3.5 Hz, 1H), 3.46 (s, 3H), 1.87 – 1.69 (m, 2H), 1.62 – 1.50 (m, 4H), 1.39 – 1.32 (m, 2H), 1.09 – 1.01 (m, 2H).

^{13}C NMR (100 MHz, $CDCl_3$): δ 176.1, 174.6, 142.3, 141.9, 140.5, 137.8, 133.1, 133.0, 129.5, 129.2, 128.7, 128.6, 128.5, 127.1, 126.9, 126.6, 126.5, 120.8, 120.6, 120.5, 113.1, 112.8, 59.3, 53.5, 33.3, 29.8, 26.2, 26.2, 25.1.

HRMS (ESI-MS): Mass calc. for $[C_{34}H_{33}N_2O_2]^+$: *m/z* = 501.2537, found: *m/z* = 501.2540.

_N_-Benzoyl-_N_-cyclohexyl-2-methoxy-10-methyl-acridane-9-carboxamide (3f)

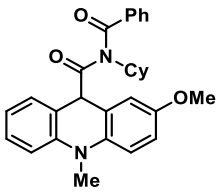

3f

According to the general procedure, the reaction of acridane **1f** (45.1 mg, 0.2 mmol, 1.0 equiv.) with cyclohexyl isocyanide **2a** (49.7 µL, 0.40 mmol, 2.0 equiv.), provided the title compound after flash column chromatography (hexane/EtOAc, 4:1) as white solid (37.3 mg, 0.082 mmol, 41%).

^{1}H NMR (400 MHz, $CDCl_3$): δ HAr should be 12!! 8.15 – 8.09 (m, 1H), 7.79 – 7.73 (m, 2H), 7.71 – 7.63 (m, 1H), 7.62 – 7.53 (m, 2H), 7.52 – 7.44 (m, 1H), 7.26 – 7.19 (m, 1H), 6.93 – 6.89 (m, 1H), 6.87 – 6.81 (m, 2H), 6.28 (d, *J* = 2.8 Hz, 1H), 4.94 (s, 1H), 4.03 (tt, *J* = 12.0, 3.6 Hz, 1H), 3.70 (s, 3H), 3.38 (s, 3H), 1.87 – 1.27 (m, 8H), 1.08 – 1.01 (m, 2H).

^{13}C NMR (100 MHz, $CDCl_3$): 176.0, 174.6, 154.0, 142.9, 137.8, 137.0, 133.8, 133.0, 130.3, 129.5, 129.2, 128.7, 128.6, 128.5, 121.6, 120.1, 114.4, 113.7, 113.5, 112.5, 59.5, 55.8, 53.7, 33.3, 30.0, 29.2, 26.3, 26.7, 25.2.

HRMS (ESI-MS): Mass calc. for $[C_{29}H_{30}N_2O_3Na]^+$: *m/z* =477.2149, found: *m/z* = 477.2152.

_N_-Benzoyl-_N_-cyclohexyl-2-methoxy-10-benzyl-acridane-9-carboxamide (3g)

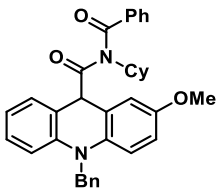

3g

According to the general procedure, the reaction of acridane **1j** (60.3 mg, 0.2 mmol, 1.0 equiv.) with cyclohexyl isocyanide **2a** (49.7 µL, 0.40 mmol, 2.0 equiv.), provided the title compound after flash column chromatography (hexane/EtOAc, 4:1) as white solid (55.2 mg, 0.101 mmol, 52%).

^{1}H NMR (400 MHz, $CDCl_3$): δ 7.84 – 7.79 (m, 2H), 7.72 – 7.66 (m, 1H), 7.62 – 7.57 (m, 2H), 7.32 – 7.26 (m, 2H), 7.25 – 7.21 (m, 1H), 7.18 – 7.13 (m, 2H), 7.11 – 7.06 (m, 1H), 6.86 – 6.82 (m, 2H), 6.73 – 6.69 (m, 1H), 6.69 – 6.66 (m, 2H), 6.33 – 6.26 (m, 1H), 5.16 (s, 2H), 5.01 (s, 1H), 4.07 (t, *J* = 12.0, 3.5 Hz, 1H), 3.70 (s, 3H), 1.87 – 1.60 (m, 5H), 1.54 – 1.47 (m, 1H), 1.41 – 1.33 (m, 1H), 1.18 – 0.99 (m, 3H).

^{13}C NMR (100 MHz, $CDCl_3$): δ 176.2, 174.8, 154.1, 141.9, 137.9, 137.3, 135.9, 133.1, 129.6, 129.3, 128.9, 128.7, 128.6, 127.0, 126.3, 121.3, 120.2, 119.8, 114.9, 114.6, 113.7, 113.4, 59.4, 55.8, 53.3, 51.1, 30.2, 29.3, 26.4, 26.3, 25.3.

HRMS (ESI-MS): Mass calc. for $[C_{35}H_{34}N_2O_3Na]^+$: *m/z* =531.2642, found: *m/z* = 531.238.

***N*-Benzoyl-*N*-cyclohexyl-2-bromo-10-methyl-acridane-9-carboxamide (3h)**

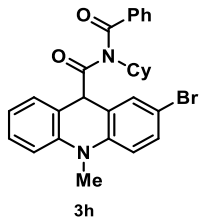

3h

According to the general procedure, the reaction of acridane **1g** (54.6 mg, 0.2 mmol, 1.0 equiv.) with cyclohexyl isocyanide **2a** (49.7 µL, 0.40 mmol, 2.0 equiv.), provided the title compound after flash column chromatography (hexane/EtOAc, 9:1) as white solid (63,7 mg, 0.126 mmol, 63%). ^{1}H NMR (400 MHz, $CDCl_3$): δ 7.79 – 7.67 (m, 3H), 7.64 – 7.55 (m, *J* = 10.3, 4.5 Hz, 2H), 7.30 (dd, *J* = 8.7, 2.3 Hz, 1H), 7.28 – 7.22 (m, 1H), 6.98 – 6.88 (m, *J* = 7.6, 5.6 Hz, 3H), 6.80 (d, *J* = 8.8 Hz, 1H), 6.56 (d, *J* = 2.3 Hz, 1H), 4.90 (s, 1H), 4.01 (tt, *J* = 11.9, 3.6 Hz, 1H), 3.38 (s, 3H), 1.92 – 1.77 (m, 1H), 1.72 – 1.57 (m, 4H), 1.52 – 1.36 (m, 2H), 1.15 – 1.00 (m, 3H).

^{13}C NMR (100 MHz, $CDCl_3$): δ 175.8, 174.6, 141.9, 141.8, 137.4, 133.2, 130.9, 129.5, 129.2, 128.7, 128.6, 122.5, 120.8, 120.3, 114.3, 112.9, 112.4, 59.4, 53.0, 33.3, 30.4, 28.8, 26.2, 26.1, 25.1.

HRMS (ESI-MS): Mass calc. for $[C_{28}H_{28}BrN_2O_2]^+$: *m/z* =503.1329, found: *m/z* = 503.1309.

***N*-Benzoyl-*N*-cyclohexyl-2-fluoro-10-methyl-acridane-9-carboxamide (3i)**

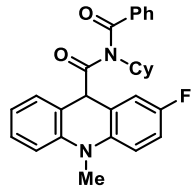

3i

According to the general procedure, the reaction of acridane **1h** (42.6 mg, 0.2 mmol, 1.0 equiv.) with cyclohexyl isocyanide **2a** (49.7 µL, 0.40 mmol, 2.0 equiv.), provided the title compound after flash column chromatography (hexane/EtOAc, 9:1) as white solid (28.4 mg, 0.06 mmol, 32%).

^{1}H NMR (400 MHz, $CDCl_3$): δ 7.76 – 7.71 (m, 2H), 7.71 – 7.66 (m, 1H), 7.60 – 7.54 (m, 2H), 7.23 – 7.20 (m, 1H), 6.97 – 6.82 (m, 5H), 6.35 (dd, *J* = 8.6, 2.8 Hz, 1H), 4.92 (s, 1H), 4.01 (tt, *J* = 12.0, 3.6 Hz, 1H), 3.40 (s, 3H), 1.87 – 1.75 (m, 1H), 1.73 – 1.64 (m, 1H), 1.56 – 1.35 (m, 4H), 1.15 – 0.93 (m, 4H).

^{13}C NMR (100 MHz, $CDCl_3$): δ 175.8, 174.6, 157.5 (d, *JC-F* = 239.1 Hz), 142.6, 139.4, 137.6, 133.2, 129.6, 129.2, 128.8, 128.7, 122.2 (d, *JC-F* = 7.4.1 Hz), 120.6, 120.1, 115.1 (d, *JC-F* = 23.0.1 Hz), 114.8 (d, *JC-F* = 22.4 Hz), 113.6 (d, *JC-F* = 7.8 Hz), 112.8, 59.6, 53.3, 33.6, 30.4, 29.0, 26.4.

^{19}F NMR (376 MHz, $CDCl_3$): δ - 124.7.

HRMS (ESI-MS): Mass calc. for $[C_{28}H_{28}FN_2O_2]^+$: *m/z* =443.2129, found: *m/z* = 443.2136.

***N*-Benzoyl-*N*-cyclohexyl-2-fluoro-10-benzyl-acridane-9-carboxamide (3j)**

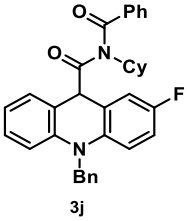

3j

According to the general procedure, the reaction of acridane **1k** (43.4 mg, 0.150 mmol, 1.0 equiv.) with cyclohexyl isocyanide **2a** (37.2 µL, 0.300 mmol, 2.0 equiv.), provided the title compound after flash column chromatography (hexane/EtOAc, 9:1) as white solid (55.2 mg, 0.104 mmol, 52%).

^{1}H NMR (400 MHz, $CDCl_3$): δ 7.83 – 7.78 (m, 2H), 7.74 – 7.68 (m, 1H), 7.62 – 7.57 (m, 2H), 7.32 – 7.26 (m, 2H), 7.24 – 7.21 (m, 1H), 7.17 – 7.13 (m, 2H), 7.12 – 7.06 (m, 1H),

6.92 – 6.84 (m, 2H), 6.80 (dt, *J* = 8.7, 3.0 Hz, 1H), 6.74 (d, *J* = 8.2 Hz, 1H), 6.67 (dd, *J* = 9.1, 4.6 Hz, 1H), 6.36 (dd, *J* = 8.7, 2.9 Hz, 1H), 5.17 (s, 2H), 4.99 (s, 1H), 4.06 (tt, *J* = 12.0, 3.5 Hz, 1H), 1.91 – 1.78 (m, 1H), 1.74 – 1.61 (m, 2H), 1.59 – 1.47 (m, 2H), 1.44 – 1.38 (m, 1H), 1.14 – 0.98 (m, 4H).

^{13}C NMR (100 MHz, $CDCl_3$): δ 176.1, 174.8, 157.5 (d, *JC-F* = 239.3 Hz), 153.9, 141.6, 138.4, 137.6, 136.9, 133.4, 129.7, 129.3, 129.0, 128.8 (d, *JC-F* = 7.8 Hz), 127.2, 126.2, 121.8 (d, *JC-F* = 7.3 Hz), 120.8, 119.7, 115.0 (d, *JC-F* = 23.0 Hz), 114.9 (d, *JC-F* = 22.9 Hz), 114.0, 59.6, 52.9, 51.4, 30.4, 29.1, 26.3.

^{19}F NMR (376 MHz, $CDCl_3$): δ - 124.2.

HRMS (ESI-MS): Mass calc. for $[C_{34}H_{31}FN_2O_2Na]^+$: *m/z* =519.2442, found: *m/z* = 519.2446.

_N_-Benzoyl-_N_-cyclohexyl-1,4,10-trimethyl-acridane-9-carboxamide (3k)

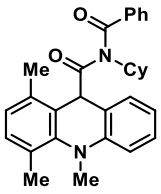

3k

According to the general procedure, the reaction of acridane **1l** (44.3 mg, 0.2 mmol, 1.0 equiv.) with cyclohexyl isocyanide **2a** (49.7 µL, 0.40 mmol, 2.0 equiv.), provided the title compound after flash column chromatography (hexane/EtOAc, 9:1) as white solid (51.6 mg, 0.114 mmol, 57%).

^{1}H NMR (400 MHz, $CDCl_3$): δ 7.64 – 7.45 (m, 5H), 7.25 – 7.19 (m, 1H), 7.13 – 7.08 (m, 1H), 7.01 – 6.95 (m, 1H), 6.83 – 6.74 (m, 2H), 6.53 – 6.47 (m, 1H), 5.35 (s, 1H), 3.83 (tt, *J* = 12.0, 3.6 Hz, 1H), 3.55 (s, 3H), 2.39 (s, 3H), 2.33 (s, 3H), 1.91 – 1.71 (m, 2H), 1.62 (s, 2H), 1.51 – 1.43 (m, 1H), 1.37 – 1.23 (m, 2H), 1.12 – 0.95 (m, 3H).

^{13}C NMR (100 MHz, $CDCl_3$): δ 177.0, 174.6, 147.3, 144.0, 136.9, 133.3, 132.3, 131.1, 129.1, 128.7, 128.0, 127.0, 125.8, 125.7, 124.2, 120.9, 117.3, 60.1, 49.7, 41.8, 29.9, 29.3, 26.3, 25.1, 20.7, 19.4.

HRMS (ESI-MS): Mass calc. for $[C_{29}H_{30}N_2O_2Na]^+$: *m/z* = 461.2199, found: *m/z* = 461.2198.

_N_-Benzoyl-_N_-benzyl-10-methyl-acridane-9-carboxamide (3l)

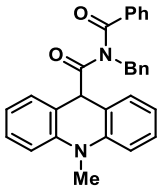

3l

According to the general procedure, the reaction acridane **1a** (39.0 mg, 0.2 mmol, 1.0 equiv.) with benzyl isocyanide **2b** (46.8 mg, 0.40 mmol, 2.0 equiv.), provided the title compound after flash column chromatography (hexane/EtOAc, 9:1) as white solid (45.0 mg, 0.104 mmol, 52%).

^{1}H NMR (400 MHz, $CDCl_3$): δ 7.64 – 7.55 (m, 3H), 7.51 – 7.44 (m, 2H), 7.31 – 7.24 (m, 2H), 7.17 – 7.10 (m, 3H), 7.05 – 7.01 (m, 2H), 6.98 – 6.87 (m, 6H), 5.58 (s, 1H), 4.78 (s, 2H), 3.38 (s, 3H).

^{13}C NMR (100 MHz, $CDCl_3$): δ 175.1, 173.8, 142.6, 137.9, 134.0, 130.6, 129.5, 128.3, 128.2, 121.0, 120.4, 112.8, 60.0, 53.3, 28.8.

HRMS (ESI-MS): Mass calc. for $[C_{29}H_{25}N_2O_2Na]^+$: *m/z* = 433.1911, found: *m/z* = 433.1920.

_N_-Benzoyl-_N_,10-dibenzyl--acridane-9-carboxamide (3m)

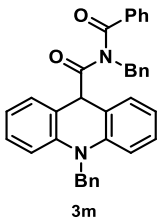

3m

According to the general procedure, the reaction of acridane **1b** (40.7 mg, 0.15 mmol, 1.0 equiv.) with benzyl isocyanide **2b** (35.1 mg, 0.30 mmol, 2.0 equiv.), provided the title compound after flash column chromatography (hexane/EtOAc, 9:1) as white solid (27.4 mg, 0.054 mmol, 36%).

^{1}H NMR (400 MHz, $CDCl_3$): δ 7.63 – 7.56 (m, 3H), 7.49 – 7.44 (m, 2H), 7.30 – 7.21 (m, 3H), 7.17 – 7.08 (m, 7H), 7.04 – 7.01 (m, 2H), 6.96 – 6.92 (m, 2H), 6.89 – 6.82 (m, 2H), 6.77 – 6.73 (m, 2H), 5.64 (s, 1H), 5.14 (s, 2H), 4.82 (s, 2H).

^{13}C NMR (100 MHz, $CDCl_3$): δ 176.4, 174.9, 141.9, 137.2, 136.9, 136.0, 134.5, 132.9, 129.2, 128.9, 128.6, 128.5, 127.8, 127.3, 127.0, 126.3, 120.9, 120.8, 116.3, 114.2, 51.1, 50.7, 50.4.

HRMS (ESI-MS): Mass calc. for $[C_{35}H_{29}N_2O_2]^+$: *m/z* = 509.2229, found: *m/z* = 509.2231.

_N_-Benzoyl-_N_-*tert*-butyl-10-methyl-acridane-9-carboxamide (3n)

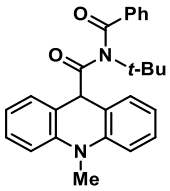

3n

According to the general procedure, the reaction of acridane **1a** (39.0 mg, 0.2 mmol, 1.0 equiv.) with *tert*-butyl isocyanide **2c** (45.2 µL, 0.40 mmol, 2.0 equiv.), provided the title compound after flash column chromatography (hexane/EtOAc, 9:1) as white solid (42.2 mg, 0.106 mmol, 53%).

^{1}H NMR (400 MHz, $CDCl_3$): δ 8.04 – 7.98 (m, 2H), 7.76 – 7.68 (m, 1H), 7.64 – 7.53 (m, 2H), 7.25 – 7.17 (m, 2H), 6.95 – 6.88 (m, 2H), 6.87 – 6.79 (m, 2H), 6.68 – 6.60 (m, 2H), 4.63 (s, 1H), 3.39 (s, 3H), 1.37 (s, 9H).

^{13}C NMR (100 MHz, $CDCl_3$): δ 175.1, 173.8, 142.6, 137.9, 134.0, 130.6, 129.5, 128.3, 128.2, 121.0, 120.4, 112.8, 60.0, 53.3, 33.3, 28.8.

HRMS (ESI-MS): Mass calc. for $[C_{26}H_{27}N_2O_2]^+$: *m/z* = 399.2067, found: *m/z* = 399.2072.

_N_-Benzoyl-_N_-*tert*-butyl-10-benzyl-acridane-9-carboxamide (3o)

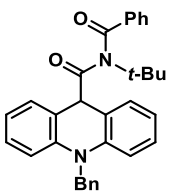

3o

According to the general procedure, the reaction of acridane **1b** (54.3 mg, 0.2 mmol, 1.0 equiv.) with *tert*-butyl isocyanide **2c** (45.2 µL, 0.40 mmol, 2.0 equiv.), provided the title compound after flash column chromatography (hexane/EtOAc, 9:1) as white solid (35.5 mg, 0.075 mmol, 37%).

^{1}H NMR (400 MHz, $CDCl_3$): δ 8.07 – 7.97 (m, 2H), 7.78 – 7.68 (m, 1H), 7.64 – 7.55 (m, 2H), 7.31 – 7.27 (m, 2H), 7.25 – 7.20 (m, 1H), 7.18 – 7.10 (m, 2H), 7.11 – 6.98 (m, 2H), 6.81 – 6.75 (m, 2H), 6.73 – 6.68 (m, 2H), 6.68 – 6.62 (m, 2H), 5.18 (s, 2H), 4.76 (s, 1H), 1.39 (s, 9H).

^{13}C NMR (100 MHz, $CDCl_3$): δ 173.9, 173.2, 141.6, 140.1, 137.2, 134.2, 130.7, 129.5, 128.8, 128.3, 128.2, 126.9, 126.2, 120.7, 120.5, 113.9, 59.9, 52.8, 51.2, 28.7.

HRMS (ESI-MS): Mass calc. for $[C_{32}H_{30}N_2O_2]^+$: *m/z* = 475.2380, found: *m/z* = 475.2385.

_N_-Benzoyl-_N_-butyl-10-methyl-acridane-9-carboxamide (3p)

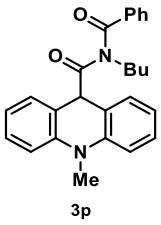

3p

According to the general procedure, the reaction of acridane **1a** (29.3 mg, 0.15 mmol, 1.0 equiv.) with *n*-butyl isocyanide **2d** (31.4 µL, 0.30 mmol, 2.0 equiv.), provided the title compound after flash column chromatography (hexane/EtOAc, 9:1) as white solid (26.3 mg, 0.066 mmol, 44%).

^{1}H NMR (400 MHz, $CDCl_3$): δ 7.68 – 7.60 (m, 3H), 7.55 – 7.50 (m, 2H), 7.29 – 7.23 (m, 2H), 7.06 – 7.02 (m, 2H), 6.99 – 6.94 (m, 2H), 6.92 – 6.86 (m, 2H), 5.47 (s, 1H), 3.56 – 3.49 (m, 2H), 3.43 (s, 3H), 1.30 – 1.20 (m, 2H), 1.16 – 1.02 (m, 2H), 0.71 (t, *J* = 7.3 Hz, 3H).

^{13}C NMR (100 MHz, $CDCl_3$): δ 176.4, 174.9, 142.8, 136.2, 132.7, 129.2, 128.9, 128.6, 128.4, 121.3, 120.6, 112.9, 50.9, 47.8, 33.3, 30.7, 20.1, 13.7.

HRMS (ESI-MS): Mass calc. for $[C_{26}H_{27}N_2O_2]^+$: *m/z* = 399.2067, found: *m/z* = 399.2067.

_N_-Benzoyl-_N_-butyl-10-benzyl-acridane-9-carboxamide (3q)

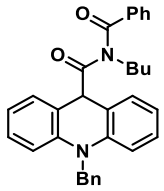

3q

According to the general procedure, the reaction of acridane **1b** (40.7 mg, 0.15 mmol, 1.0 equiv.) with *n*-butyl isocyanide **2d** (31.4 µL, 0.30 mmol, 2.0 equiv.), provided the title compound after flash column chromatography (hexane/EtOAc, 9:1) as white solid (40.7 mg, 0.085 mmol, 57%).

^{1}H NMR (400 MHz, $CDCl_3$): δ 7.75 – 7.69 (m, 2H), 7.68 – 7.62 (m, 1H), 7.59 – 7.53 (m, 2H), 7.34 – 7.23 (m, 3H), 7.22 – 7.16 (m, 2H), 7.16 – 7.05 (m, 4H), 6.93 – 6.84 (m, 2H), 6.83 – 6.72 (m, 2H), 5.55 (s, 1H), 5.22 (s, 2H), 3.62 – 3.53 (m, 2H), 1.35 – 1.21 (m, 2H), 1.19 – 1.01 (m, 2H), 0.73 (t, *J* = 7.2 Hz, 3H).

^{13}C NMR (100 MHz, $CDCl_3$): δ 177.0, 175.0, 142.0, 137.1, 136.2, 132.8, 129.3, 129.0, 128.9, 128.6, 127.0, 126.3, 121.0, 120.8, 114.1, 51.2, 50.4, 47.9, 30.7, 20.1, 13.7.

HRMS (ESI-MS): Mass calc. for $[C_{32}H_{30}N_2O_2]^+$: *m/z* = 475.2380, found: *m/z* = 475.2381.

_N_-Benzoyl-_N_-(4-methoxyphenyl)-10-methyl-acridane-9-carboxamide (3r)

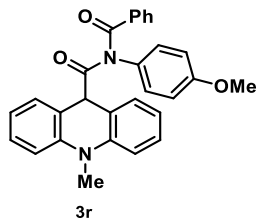

3r

According to the general procedure, the reaction of acridane **1a** (29.3 mg, 0.15 mmol, 1.0 equiv.) with 4-methoxyphenyl isocyanide **2e** (39.0 mg, 0.30 mmol, 2.0 equiv.), provided the title compound after flash column chromatography (hexane/EtOAc, 4:1) as white solid (17.5 mg, 0.039 mmol, 26%).

^{1}H NMR (400 MHz, $CDCl_3$): δ 7.41 – 7.20 (m, 10H), 7.02 – 6.94 (m, 4H), 6.84 (s, 3H), 5.68 (s, 1H), 3.76 (s, 3H), 3.39 (s, 3H).

^{13}C NMR (100 MHz, $CDCl_3$): δ 176.4, 173.4, 159.1, 142.8, 135.0, 132.1, 131.9, 129.6, 128.9, 128.7, 128.6, 128.3, 121.1, 120.6, 114.9, 113.0, 55.5, 50.3, 33.3.

HRMS (ESI-MS): Mass calc. for $[C_{29}H_{24}N_2O_3]^+$: *m/z* = 449.1860, found: *m/z* = 449.1870.

_N_-Benzoyl-_N_-(4-methoxyphenyl)-10-benzyl-acridane-9-carboxamide (3s)

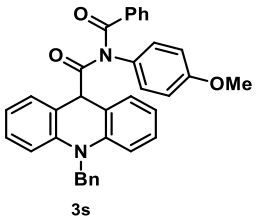

3s

According to the general procedure, the reaction of acridane **1b** (40.7 mg, 0.15 mmol, 1.0 equiv.) with 4-methoxyphenyl isocyanide **2e** (39.0 mg, 0.30 mmol, 2.0 equiv.), provided the title compound after flash column chromatography (hexane/EtOAc, 4:1) as white solid (55.9 mg, 0.106 mmol, 71%).

^{1}H NMR (400 MHz, $CDCl_3$): δ 7.45 – 7.37 (m, 3H), 7.35 – 7.27 (m, 5H), 7.25 – 7.13 (m, 6H), 7.00 – 6.94 (m, 2H), 6.87 – 6.83 (m, 4H), 6.80 – 6.76 (m, 2H), 5.73 (s, 1H), 5.12 (s, 2H), 3.78 (s, 3H).

^{13}C NMR (100 MHz, $CDCl_3$): δ 177.0, 173.5, 159.2, 141.7, 137.1, 135.0, 132.1, 132.0, 129.7, 129.0, 128.9, 128.8, 128.7, 128.4, 127.0, 126.2, 120.9, 120.8, 114.9, 114.2, 55.6, 51.3, 50.0.

HRMS (ESI-MS): Mass calc. for $[C_{35}H_{28}N_2O_3]^+$: *m/z* = 525.2173, found: *m/z* = 525.2178.

General procedure for the synthesis of acridinium salts

In a Schlenk-flask under nitrogen atmosphere, the corresponding imide-acridane derivative **3** (0.050 - 0.100 mmol, 1 equiv.) and tritylperchlorate (1.1 equiv.) were dissolved in dry MeCN (0.06 M) and stirred for 18 h at room temperature. Diethyl ether was added and the formed suspension was stirred for further 10 minutes at room temperature. The reaction mixture was stored in the freezer for 30 minutes to complete the precipitation. The solid was filtered off, washed with diethyl ether and dried under vacuo to give the corresponding acridinium perchlorate **4**.

9-(Benzoyl(cyclohexyl)carbamoyl)-10-methylacridinium perchlorate (4a)

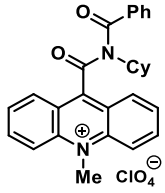

4a

According to the general procedure, the reaction of **3a** (42.4 mg, 0.100 mmol, 1 equiv.) and tritylperchlorate (37.7 mg, 0.110 mmol, 1.1 equiv.), provided the title compound **4a** as a yellow-greenish solid (41.8 mg, 0.080 mmol, 80%).

^{1}H NMR (400 MHz, CD_3CN): δ 8.45 (d, *J* = 10.0 Hz, 2H), 8.39 – 8.31 (m, 4H), 8.07 – 7.96 (m, 2H), 7.28 – 7.20 (m, 1H), 7.14 (dd, *J* = 8.3, 1.3 Hz, 2H), 7.05 – 6.97 (m, 2H), 4.63 (s, 3H), 4.45 (tt, *J* = 12.1, 3.7 Hz, 1H), 2.45 (dd, *J* = 12.2, 3.3 Hz, 2H), 2.35 – 2.25 (m, 2H), 1.78 – 1.68 (m, 1H), 1.49 – 1.20 (m, 5H).

^{13}C NMR (100 MHz, CD3CN): δ 175.9, 167.4, 154.6, 143.2, 140.7, 135.4, 134.6, 132.3, 130.8, 130.1, 130.0, 129.9, 129.6, 124.1, 120.5, 62.4, 40.7, 31.3, 27.7, 26.7.

HRMS (ESI-MS): Mass calc. for $C_{21}H_{23}N_2O^+$ [M+H -PhCO]$^+$: *m/z* = 319.1805, found: *m/z* = 319.1813.

9-(Benzoyl(cyclohexyl)carbamoyl)-10-phenylacridinium perchlorate (4b)

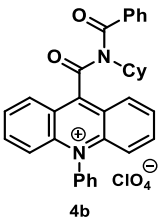

4b

According to the general procedure, the reaction with **3b** (48.7 mg, 0.100 mmol, 1 equiv.) and tritylperchlorate (37.7 mg, 0.110 mmol, 1.1 equiv.), provided the title compound **4b** as a yellow-greenish solid (31.6 mg, 0.054 mmol, 54%).

^{1}H NMR (400 MHz, CD_3CN): δ 8.43 (d, *J* = 8.7 Hz, 2H), 8.17 – 8.12 (m, 2H), 8.05 – 7.99 (m, 2H), 7.94 – 7.89 (m, 2H), 7.89 – 7.83 (m, 1H), 7.51 – 7.46 (m, 1H), 7.44 (d, *J* = 9.2 Hz, 2H), 7.40 – 7.35 (m, 1H), 7.25 (ddd, *J* = 7.7, 2.5, 1.2 Hz, 1H), 7.18 (dd, *J* = 8.3, 1.2 Hz, 2H), 7.02 (t, *J* = 7.8 Hz, 2H), 4.60 (tt, *J* = 11.8, 3.5 Hz, 1H), 2.50 (dd, *J* = 12.2, 3.2 Hz, 1H), 2.44 (dd, *J* = 12.1, 3.3 Hz, 1H), 2.40 – 2.30 (m, 2H), 1.82 – 1.73 (m, 2H), 1.56 – 1.42 (m, 2H), 1.42 – 1.29 (m, 2H).

^{13}C NMR (100 MHz, CD3CN): δ 174.2, 165.5, 142.1, 139.3, 136.8, 134.1, 133.1, 132.0, 131.5, 131.5, 129.6, 128.7, 128.4, 127.6, 127.5, 127.0, 122.5, 120.0, 60.5, 29.7, 26.1, 25.1.

HRMS (ESI-MS): Mass calc. for $C_{26}H_{25}N_2O^+$ [M+H -PhCO]$^+$: *m/z* = 381.1961, found: *m/z* = 381.1969.

9-(Benzoyl(cyclohexyl)carbamoyl)-10-benzylacridinium perchlorate (4c)

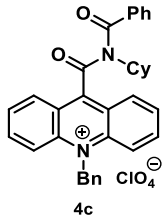

4c

According to the general procedure, the reaction of **3c** (25.0 mg, 0.050 mmol, 1 equiv.) and tritylperchlorate (18.3 mg, 0.055 mmol, 1.1 equiv.), provided the title compound **4c** as a yellow-greenish solid (20.1 mg, 0.030 mmol, 61%).

^{1}H NMR (400 MHz, CD_3CN): δ 8.42 (d, *J* = 8.4 Hz, 2H), 8.35 – 8.21 (m, 4H), 8.03 (dd, *J* = 8.7, 2.0 Hz, 1H), 8.01 (dd, *J* = 8.6, 2.0 Hz, 1H), 7.45 – 7.35 (m, 3H), 7.26 – 7.12 (m, 3H), 7.06 – 6.90 (m, 4H), 6.37 (s, 2H), 4.57 (tt, *J* = 11.7, 3.8 Hz, 1H), 2.52 – 2.25 (m, 4H), 1.80 – 1.67 (m, 2H), 1.56 – 1.22 (m, 4H).

^{13}C NMR (100 MHz, CD3CN): δ 175.2, 166.3, 154.7, 142.7, 141.0, 135.0, 134.1, 134.1, 131.7, 130.4, 130.3, 129.8, 129.6, 129.4, 129.4, 126.8, 123.8, 119.8, 61.5, 55.8, 30.7, 27.0, 26.1.

HRMS (ESI-MS): Mass calc. for $C_{27}H_{27}N_2O^+$ [M+H - PhCO]$^+$: *m/z* = 395.2118, found: *m/z* = 395.2117.

9-(Benzoyl(cyclohexyl)carbamoyl)-2-methoxy-10-methylacridinium perchlorate (4f)

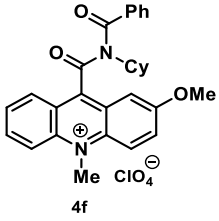

4f

According to the general procedure, the reaction of **3f** (22.7 mg, 0.050 mmol, 1 equiv.) and tritylperchlorate (18.8 mg, 0.055 mmol, 1.1 equiv.), provided the title compound **4f** as a yellow-greenish solid (19.9 mg, 0.036 mmol, 72%).

^{1}H NMR (400 MHz, CD_3CN): δ 8.36 (dd, *J* = 9.7, 5.6

Hz, 2H), 8.31 – 8.20 (m, 2H), 8.03 – 7.91 (m, 2H), 7.37 (d, *J* = 2.7 Hz, 1H), 7.10 (t, *J* = 7.4 Hz, 1H), 6.97 (dd, *J* = 8.2, 1.2 Hz, 2H), 6.84 (t, *J* = 7.8 Hz, 2H), 4.73 – 4.61 (m, 1H), 4.57 (s, 3H), 4.09 (s, 3H), 2.49 – 2.20 (m, 4H), 1.76 (bd, *J* = 13.0 Hz, 2H), 1.61 – 1.41 (m, 2H), 1.42 – 1.28 (m, 2H).

^{13}C NMR (100 MHz, CD3CN): δ 173.9, 165.1, 158.6, 137.1, 134.5, 134.1, 132.9, 132.4, 128.9, 127.9, 127.7, 127.1, 123.9, 122.6, 120.4, 118.4, 102.5, 59.2, 56.2, 38.9, 35.3, 29.7, 29.2, 25.7, 24.8.

HRMS (ESI-MS): Mass calc. for $C_{29}H_{29}N_2O_3^+$ [M+H -PhCO]$^+$: *m/z* = 453.2173, found: *m/z* = 453.2172.

9-(Benzoyl(cyclohexyl)carbamoyl)-10-benzyl-2-methoxyacridinium perchlorate (4g)

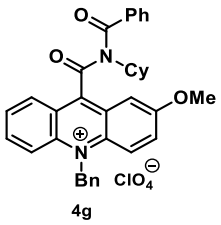

4g

According to the general procedure, the reaction of **3g** (26.5 mg, 0.050 mmol, 1 equiv.) and tritylperchlorate (18.8 mg, 0.055 mmol, 1.1 equiv.), provided the title compound **4g** as a yellow-greenish solid (19.2 mg, 0.030 mmol, 61%).

^{1}H NMR (400 MHz, CD_3CN): δ 8.37 (d, *J* = 8.6 Hz, 1H), 8.21 – 8.13 (m, 3H), 8.00 – 7.89 (m, 2H), 7.46 – 7.36 (m, 4H), 7.13 – 7.02 (m, 3H), 7.00 – 6.90 (m, 2H), 6.83 (t, *J* = 7.8 Hz, 2H), 6.31 (s, 2H), 4.88 – 4.67 (m, 1H), 4.10 (s, 3H), 2.47 – 2.30 (m, 2H), 2.30 – 2.20 (m, 2H), 2.01 (br.s., 1H), 1.84 – 1.72 (m, 1H), 1.54 (m, 2H), 1.42 – 1.23 (m, 2H).

^{13}C NMR (100 MHz, CD3CN): δ 174.2, 165.0, 159.2, 138.4, 138.3, 134.7, 134.1, 133.1, 133.0, 129.4, 129.3, 128.8, 128.6, 128.2, 128.1, 125.8, 123.4, 120.6, 118.6, 103.2, 59.4, 56.7, 55.0, 30.3, 29.5, 26.1, 26.0, 25.2.

HRMS (ESI-MS): Mass calc. for $C_{27}H_{26}N_2O_2^+$ [M+H –PhCO, -Me]$^+$: *m/z* = 410.1989, found: *m/z* = 409.2286.

9-(Benzoyl(*n*-butyl)carbamoyl)-10-benzylacridinium perchlorate (4m)

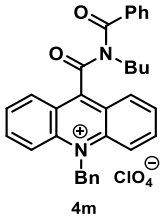

4m

According to the general procedure, the reaction of **3m** (23.7 mg, 0.050 mmol, 1 equiv.) and tritylperchlorate (18.8 mg, 0.055 mmol, 1.1 equiv.), provided the title compound **4m** as a yellow-greenish solid (17.3 mg, 0.030 mmol, 55%).

^{1}H NMR (400 MHz, CD_3CN): δ 8.43 (d, *J* = 8.4 Hz, 2H), 8.38 – 8.27 (m, 4H), 8.02 (ddd, *J* = 8.5, 5.9, 1.8 Hz, 2H), 7.47 – 7.34 (m, 6H), 7.27 – 7.22 (m, 2H), 7.16 – 7.07 (m, 2H), 6.46 (s, 2H), 4.27 (t, *J* = 7.3 Hz, 2H), 1.98 – 1.90 (m, 2H, signal under the solvent peak), 1.52 – 1.38 (m, 2H), 0.97 (t, *J* = 7.3 Hz, 3H).

^{13}C NMR (100 MHz, CD3CN): δ 173.3, 164.1, 139.9, 133.2, 132.8, 132.1, 129.4, 129.3, 129.0, 128.7, 128.6, 128.3, 128.2, 126.5, 125.9, 123.2, 122.8, 118.9, 54.8, 46.9, 30.4, 19.9, 12.9.

HRMS (ESI-MS): Mass calc. for $C_{32}H_{29}N_2O_2^+$ [M]$^+$: *m/z* = 473.2224, found: *m/z* = 473.2248.

9-(Benzoyl(*tert*-butyl)carbamoyl)-10-benzylacridinium perchlorate (4o)

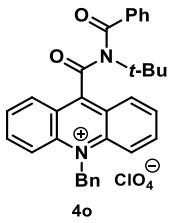

4o

According to the general procedure, the reaction of **3o** (23.7 mg, 0.050 mmol, 1 equiv.) and tritylperchlorate (18.8 mg, 0.055 mmol, 1.1 equiv.), provided the title compound **4o** as a yellow-greenish solid (10.3 mg, 0.018 mmol, 36%).

^{1}H NMR (400 MHz, CD_3CN): δ 8.38 (dd, *J* = 8.7, 0.8 Hz, 2H), 8.24 (ddd, *J* = 9.2, 6.5, 1.4 Hz, 2H), 8.19 (d, *J* = 9.0 Hz, 2H), 7.99 (ddd, *J* = 8.5, 6.6, 1.1 Hz, 2H), 7.41 – 7.36 (m, 3H), 7.19 – 7.14 (m, 3H), 6.95 – 6.87 (m, 4H), 6.32 (s, 2H), 1.91 (s, 9H).

^{13}C NMR (100 MHz, CD3CN): δ 175.1, 163.6, 153.0, 142.2, 140.6, 134.9, 133.6, 131.4, 130.5, 130.0, 129.9, 129.6, 129.2, 126.5, 126.3, 123.3, 119.1, 63.0, 55.3, 28.5.

HRMS (ESI-MS): Mass calc. for $C_{32}H_{29}N_2O_2^+$ $[M]^+$: *m/z* = 473.2224, found: *m/z* = 473.2237.

9-(Benzoyl)(benzyl)carbamoyl)-10-benzylacridinium perchlorate (4q)

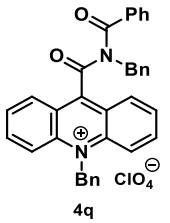

4q

According to the general procedure, the reaction of **3q** (25.4 mg, 0.050 mmol, 1 equiv.) and tritylperchlorate (18.8 mg, 0.055 mmol, 1.1 equiv.), provided the title compound **4q** as a yellow-greenish solid (16.7 mg, 0.027 mmol, 55%).

^{1}H NMR (400 MHz, CD_3CN): δ 8.35 – 8.27 (m, 6H), 8.01 – 7.94 (m, 2H), 7.52 – 7.46 (m, 4H), 7.45 – 7.32 (m, 5H), 7.28 (dd, *J* = 8.3, 1.2 Hz, 2H), 7.17 – 7.04 (m, 4H), 6.44 (s, 2H), 5.53 (s, 2H).

^{13}C NMR (100 MHz, CD3CN): δ 174.9, 166.7, 154.2, 141.8, 140.0, 136.2, 133.1, 132.9, 132.8, 129.5, 129.3, 129.0, 128.8, 128.6, 128.5, 128.3, 128.0, 125.8, 122.9, 119.0, 54.9, 50.0.

HRMS (ESI-MS): Mass calc. for $C_{35}H_{27}N_2O_2^+$ $[M]^+$: *m/z* = 507.2067, found: *m/z* = 507.2071.

9-(Benzoyl(4-methoxyphenyl)carbamoyl)-10-benzylacridinium perchlorate (4s)

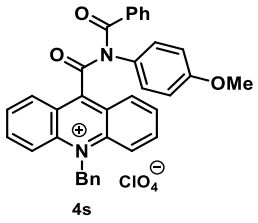

4s

According to the general procedure, the reaction of **3s** (26.2 mg, 0.050 mmol, 1 equiv.) and tritylperchlorate (18.8 mg, 0.055 mmol, 1.1 equiv.), provided the title compound **4s** as a yellow-greenish solid (21.2 mg, 0.034 mmol, 68%).

^{1}H NMR (400 MHz, CD_3CN): δ 8.65 (d, *J* = 8.5 Hz, 2H), 8.44 (d, *J* = 9.2 Hz, 2H), 8.40 – 8.32 (m, 2H), 8.08 (dd, *J* = 7.9, 6.9 Hz, 2H), 7.61 (br.s, 2H), 7.52 (br.s, 2H), 7.45 – 7.36 (m, 4H), 7.28 (br.s., 2H), 7.17 (br.s., 2H), 7.04 (br.s., 2H), 6.56 (s, 2H), 3.82 (s, 3H).

^{13}C NMR (100 MHz, CD3CN): δ 171.2, 160.2, 142.0, 140.0, 133.4, 132.7, 130.3, 129.4, 129.3, 129.2, 128.7, 128.4, 128.3, 125.9, 122.6, 119.0, 114.8, 55.4, 54.8.

HRMS (ESI-MS): Mass calc. for $C_{28}H_{23}N_2O_2^+$ $[M+H\ -PhCO]^+$: *m/z* = 419.1754, found: *m/z* = 419.1761.

Different photocatalytic procedures and characterization data

6*H*-Benzo[*c*]chromen-6-one (6)[177]

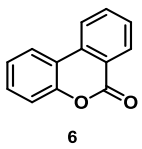
6

2-Biphenylcarboxylic acid **5** (19.8 mg, 0.1 mmol, 1 equiv) and the corresponding photocatalyst (5 mol%) were dissolved in a 4:1 mixture of acetonitrile and water (1.2 and 0.3 mL) and irradiated from the bottom side by 455 nm LEDs for 18 hours. A saturated solution of $NaHCO_3$ was added and the reaction was extracted with EtOAc (3x). The combined organic phases were washed with brine (3x) and dried over $MgSO_4$. The solvent was evaporated and the crude mixture was purified by flash column chromatography (petroleum ether:EtOAc = from 19:1 to 4:1) to obtain **6** as a white solid. This compound has been previously described in the literature.[177]

^{1}H NMR (300 MHz, $CDCl_3$): δ 8.43 (dd, *J* = 8.0, 1.4 Hz, 1H), 8.15 (d, *J* = 8.1 Hz, 1H), 8.09 (dd, *J* = 7.9, 1.4 Hz, 1H), 7.89 – 7.80 (m, 1H), 7.64 – 7.56 (m, 1H), 7.50 (ddd, *J* = 8.4, 7.1, 1.5 Hz, 1H), 7.42 – 7.31 (m, 2H).

1-Phenylethanone (8)[147]

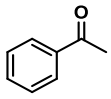
8

An oven-dried 10 mL vial equipped with a magnetic stir bar was charged with the appropriate (0.004 mmol, 2 mol%) and 1-phenylethanol **7** (0.2 mmol). Then 1 mL of CH_3CN was added, the vial was closed with a PTFE/rubber septum ensuring the exposure to air through a needle. Subsequently the vial was irradiated under stirring with a single blue LED (λ = 455 nm) placed at approximately 0.5 cm of distance and maintaining the reaction mixture at room temperature (20 °C) with a refrigerating system. After 1 hour the reaction reached full conversion and the yield was determined by ^{1}H NMR vs. 9-bromophenanthrene as the internal standard. This compound has been previously described in the literature.[147]

^{1}H NMR (300 MHz, $CDCl_3$): δ 8.02 – 7.88 (m, 2H), 7.64 – 7.52 (m, 1H), 7.51 – 7.43 (m, 2H), 2.62 (s, 3H).

1-Methoxy-4-(2-methoxypropyl)benzene (10)[26]

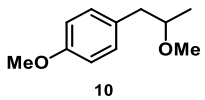
10

An oven-dried 10 mL vial equipped with a magnetic stir bar was charged with the corresponding catalyst (0.01 mmol, 5 mol%), *trans*-anethole **9** (0.2 mmol), 2-phenylmalononitrile (0.1 mmol) and MeOH (2.0 mmol). Then 0.4 mL of anhydrous DCE were added, the vial was closed with a PTFE/rubber septum and the reaction mixture was degassed by three cycles of "freeze-pump-thaw. Subsequently the vial was

[177] N. P. Ramirez, I. Bosque, J. C. Gonzalez-Gomez, *Org. Lett.* **2015**, *17*, 4550-4553.

irradiated under stirring with a single blue LED (λ = 455 nm) placed at approximately 0.5 cm of distance and maintaining the reaction mixture at room temperatura (20 °C) with a refrigerating system. After 17 hours the reaction reached full conversion and the yield was determined by ^{1}H NMR vs. 9-bromophenanthrene as the internal standard. This compound has been previously described in the literature.[26]

^{1}H NMR (300 MHz, $CDCl_3$) δ 7.11 (d, *J* = 8.7 Hz, 2H), 6.83 (d, *J* = 8.7 Hz, 2H), 3.79 (s, 3H), 3.54 – 3.42 (m, 1H), 3.34 (s, 3H), 2.85 (dd, *J* = 13.7, 5.9 Hz, 1H), 2.56 (dd, *J* = 13.7, 6.8 Hz, 1H), 1.11 (d, *J* = 6.1 Hz, 3H).

1-(4-Methoxyphenyl)ethanone (12)

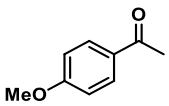

12

An oven-dried 10 mL vial equipped with a magnetic stir bar was charged with the corresponding catalyst (0.005 mmol, 5 mol%), 2-bromo-1-(4-methoxyphenyl)ethanone **11** (0.1 mmol) and lutidine (0.2 mmol). Then 0.5 mL of anhydrous DMF were added, the vial was closed with a PTFE/rubber septum and the reaction mixture was degassed by three cycles of “freeze-pumpthaw. Subsequently the vial was irradiated under stirring with a single blue LED (λ = 455 nm) placed at approximately 0.5 cm of distance and maintaining the reaction mixture at room temperature (20 °C) with a refrigerating system. After 24 hours the reaction reached full conversion and the yield was determined by ^{1}H NMR vs. 9-bromophenanthrene as the internal standard. The analytical data were in accordance with the ones of the commercially available compound.

^{1}H NMR (300 MHz, $CDCl_3$) δ 7.93 (d, *J* = 8.9 Hz, 2H), 6.92 (d, *J* = 8.9 Hz, 2H), 3.86 (s, 3H), 2.55 (s, 3H).

Metal-Catalyzed Asymmetric [3+2] Cycloaddition

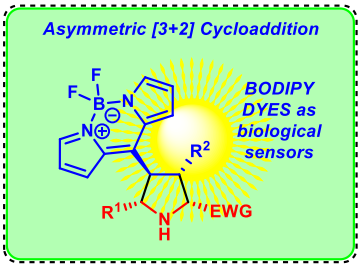

Chapter 6

6. Metal-Catalyzed Asymmetric [3+2] Cycloaddition

6.1 Introduction to the BODIPY Chromophore

4,4-Difluoro-4-bora-3a,4a-diaza-*s*-indacenes (BODIPYs) are a family of organoboron compounds that rely on a boron-dipyrromethene core which have found widespread use as fluorescent dyes in the last decades (Figure 4).[178] This is essentially due to their excellent photophysical properties and to their high chemical and photo-stability. Indeed, they present strong absorption bands in the UV-visible light region (high molar absorption coefficients) and outstanding emission properties, presenting in many cases high fluorescence quantum yields.[178] Moreover, the relatively high stability at different pH and physiological conditions make them suitable as fluorescent probes and labelling agents for proteins and DNA in biochemistry.[178,179] Various methodologies for the synthesis of BODIPY dyes and for the post-functionalization of the BODIPY core have been reported to date, allowing the obtainment of structurally different compounds with an impressive range of substitutions at the various positions of the BODIPY.[178,180] Indeed, small modifications of the BODIPY structure have a huge impact on the photophysical properties of the corresponding dye, permitting an easy-tuning of them. Due to this particular feature, simple synthetic procedures and derivatizations of the structure allow the access to a large number of compounds with different fluorescence characteristics that can be appropriately chosen depending on the specific required application.

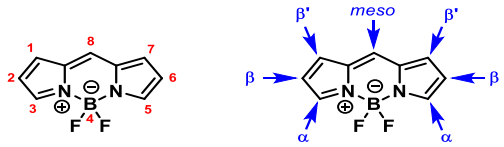

Figure 4. BODIPY core and relative positions at which it can be functionalized.

As expected, the electronic nature of the substituents is changing the corresponding wavelengths of maximum absorption and emission of the specific BODIPY derivative (Figure 5).[178,181] In addition, due to the particular electronic characteristics of the BODIPY core, the substitution position (α, β, β' or *meso*) can lead to different photophysical properties and quantum yield values.[178,181] For instance, the introduction of a phenyl group at the 8-position (*meso*) led to an impressive diminished fluorescence quantum yield value (ϕ = 0.19), due to the allowed free rotation of the phenyl which is leading to non-radiative vibrational deactivation pathways of the singlet excited state. On the other hand, if two methyl substituents are present at the 1,7-positions of the BODIPY core, the axial rotation is attenuated by the steric hindrance provided by the two methyl groups (ϕ = 0.65). Furthermore, if the phenyl substituent is replaced by a mesityl group, the increased steric constrains leads to an almost quantitative fluorescence quantum yield (ϕ = 0.97), which is the same value observed for a simple *meso*-methyl substitution. In addition, a significantly more attenuated effect can be observed for the

[178] (a) A. Loudet, K. Burgess, *Chem. Rev*. **2007**, *107*, 4891-4932; (b) G. Ulrich, R. Ziessel, A. Harriman, *Angew. Chem. Int. Ed*. **2008**, *47*, 1184-1201; (c) N. Boens, V. Leen, W. Dehaen, *Chem. Soc. Rev*. **2012**, *41*, 1130-1172.

[179] (a) S. Kolemen, E. U. Akkaya, *Coord. Chem. Rev*. **2018**, *354*, 121-134; (b) S. Krajcovicova, J. Stankova, P. Dzubak, M. Hajduch, M. Soural, M. A. Urban, *Chem. Eur. J*. **2018**, *24*, 4957-4966; (c) T. Kowada, H. Maeda, K. Kikuchi, *Chem. Soc. Rev*. **2015**, *44*, 4953-4972; (d) P. Rivera-Fuentes, S. J. Lippard, *Acc. Chem. Res*. **2015**, *48*, 2927-2934; (e) Y. Ni, J. Wu, *Org. Biomol. Chem*. **2014**, *12*, 3774-3791; (f) R. Lincoln, L. E. Greene, W. Zhang, S. Louisia, G. Cosa, *J. Am. Chem. Soc*. **2017**, *139*, 16273-16281.

[180] (a) N. Boens, B. Verbelen, W. Dehaen, *Eur. J. Org. Chem.* **2015**, 6577-6595. (b) N. Boens, B. Verbelen, M. J. Ortiz, L. Jiao, W. Dehaen, *Coord. Chem. Rev.* **2019**, *399*, 213024.

[181] (a) L. Wang, B. Verbelen, C. Tonnelé, D. Beljonne, R. Lazzaroni, V. Leen, W. Dehaena, N. Boens, *Photochem. Photobiol. Sci.* **2013**, *12*, 835-847; (b) Y. Gabe, T. Ueno, Y. Urano, H. Kojima, T. Nagano, *Anal. Bioanal. Chem.* **2006**, *386*, 621-626; (c) A. B. Nepomnyashchii, M. Bröring, J. Ahrens, A. J. Bard, *J. Am. Chem. Soc*. **2011**, *133*, 8633-8645; (d) E. Palao-Utiel, L. Montalvillo-Jiménez, I. Esnal, R. Prieto-Montero, A. R. Agarrabeitia, I. García-Moreno, J. Bañuelos, I. López-Arbeloa, S. de la Moya, M. J. Ortiz, *Dyes Pigm*. **2017**, *141*, 286-298.

substitution at different positions. Indeed, phenyl substitutions at 3,5-positions is lowering the quantum yield just by a slight extend (ϕ = 0.16) in comparison with the related methyl substituted compound described above (ϕ = 0.19).

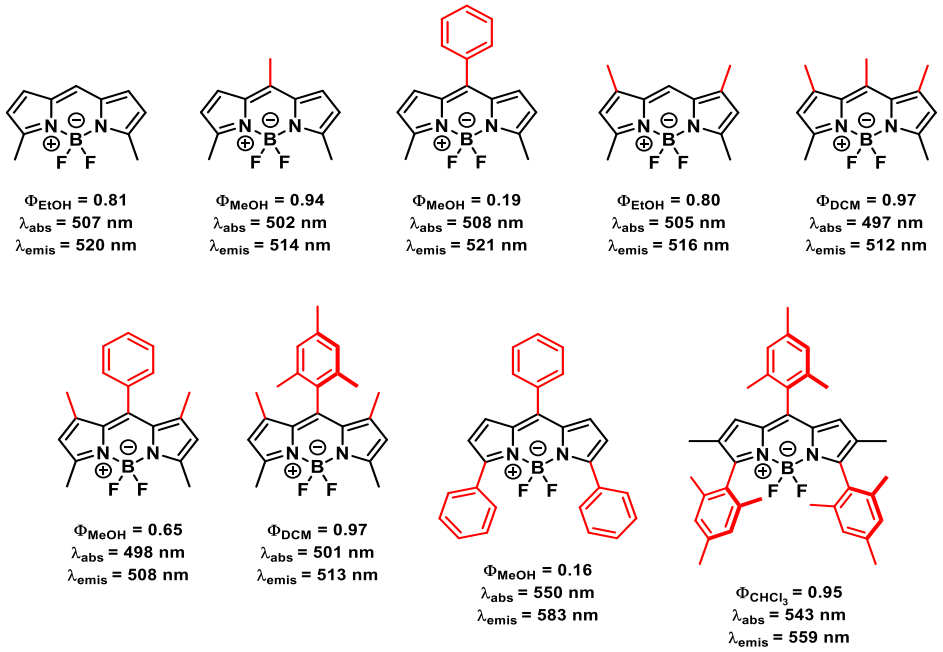

Figure 5. Selected examples of BODIPY derivatives and their photophysical properties.

The substitution at the boron center is possible through the use of organolithium compounds or methoxy anions, although the photophysical properties are not strongly affected (Figure 6). The introduction of two sulfonate electron-withdrawing groups is blue-shifting the absorption and emission bands but it has the great advantage of rendering the compound highly soluble in water. Electrophilic aromatic substitution at the 2,6-positions is easily carried out to give the corresponding di-halogenated products, which have strongly diminished fluorescence quantum yield values. Indeed, the presence of heavy halogen atoms, such as bromine or iodine, is favoring a higher intersystem crossing rate (ISC) to the triplet excited state due to the higher spin-orbit coupling (SOC). The di-brominated BODIPY shows some fluorescence (ϕ = 0.45) whereas the di-

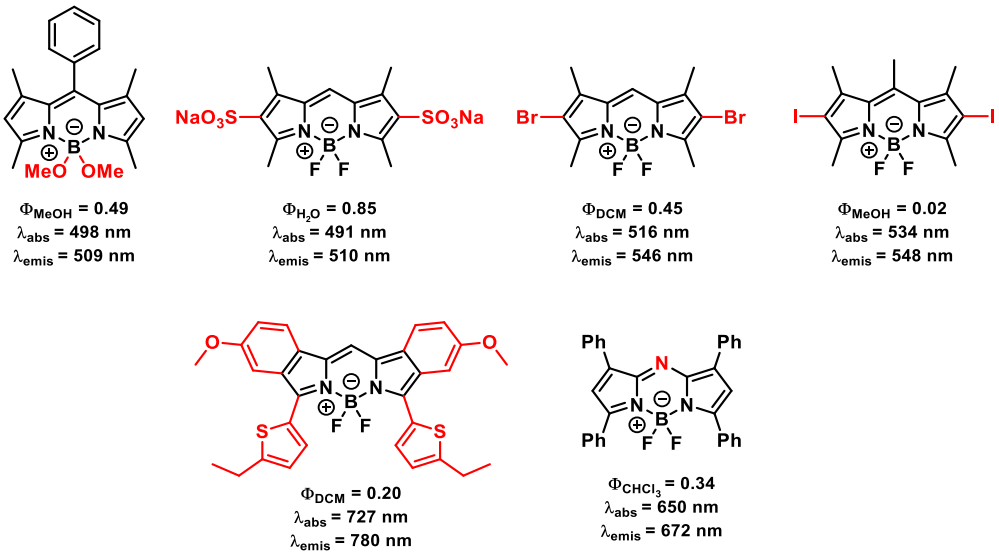

Figure 6. Selected examples of BODIPY derivatives and their photophysical properties.

iodinated one has almost no emission from the singlet excited state (ϕ = 0.02). In the end, through a rational design and empirically-driven observations, the synthesis of near-IR absorbing BODIPYs has been achieved, such as the representative thiophene-containing BODIPY (λ_{abs} = 727 nm) and the aza-BODIPY (λ_{abs} = 650 nm).

The presence of intramolecular single-electron transfers between the BODIPY core and a *meso*-substituted aryl moiety are leading to charge transfer excited states which are more prone to be deactivated by non-radiative pathways, leading to a decreased fluorescence quantum yield (Scheme 109).[178,182] The single-electron transfer can take place from the aryl moiety towards the BODIPY core or vice versa. In the first case the charge transfer can be favored by the presence of electron-donating substituents on the aryl ring, which are stabilizing the corresponding radical cation intermediate, or by the presence of electron-withdrawing substituents on the BODIPY core, which are stabilizing the relative radical anion. On the other hand, for a single-electron transfer from the BODIPY core to the aryl moiety the obvious opposite considerations are favoring the charge transfer species.

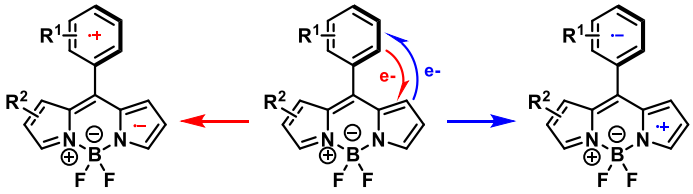

Scheme 109. Intramolecular single-electron transfers leading to charge transfer species.

This feature can be seen as an undesired or appropriately chosen effect, depending on the specific application. Indeed, a non-emissive BODIPY-based compound can be used as a fluorescent probe if upon coordination or specific chemical reaction is turning on its fluorescence becoming a useful tool for imaging techniques. This effect can be highlighted by the different quantum yields values of the diamine- (ϕ = 0.001) and benzotriazole-containing (ϕ = 0.40) BODIPYs (Figure 7). Indeed, the diamine-containing BODIPY does not show any emission due to the presence of an electron-rich aryl moiety which is unlocking a charge transfer event. However, upon reaction with nitric oxide a benzotriazole BODIPY is formed which can emit from its singlet excited state due to the suppression of the charge transfer state. Therefore, the diamine-containing BODIPY can be used as an efficient fluorescent probe for nitric oxide. A similar effect can be observed in the two parental 2,6-substituted BODIPYs. The presence of electron-withdrawing ester groups is diminishing the fluorescence quantum yield (ϕ = 0.41) in comparison with the di-ethyl substituted analogue (ϕ = 0.67) due to the more favorable electron transfer event.

On the other hand, the presence of an electron-poor *meta*-nitrobenzene substituent is unlocking a charge transfer species through an opposite electron transfer from the BODIPY core to the *meso*-substituent, leading to low values of fluorescence quantum yield (ϕ = 0.004) (Figure 8). This effect can be attenuated by the insertion of a methoxy substituent on the aryl moiety (ϕ = 0.023) or through removal of electron density from the BODIPY core by means of 2,6-di-acetyl substitution (ϕ = 0.529).

[182] (a) Y. Gabe, Y. Urano, K. Kikuchi, H. Kojima, T. Nagano, *J. Am. Chem. Soc*. **2004**, *126*, 3357-3367; (b) T. Ueno, Y. Urano, H. Kojima, T. Nagano, *J. Am. Chem. Soc*. **2006**, *128*, 10640-10641.

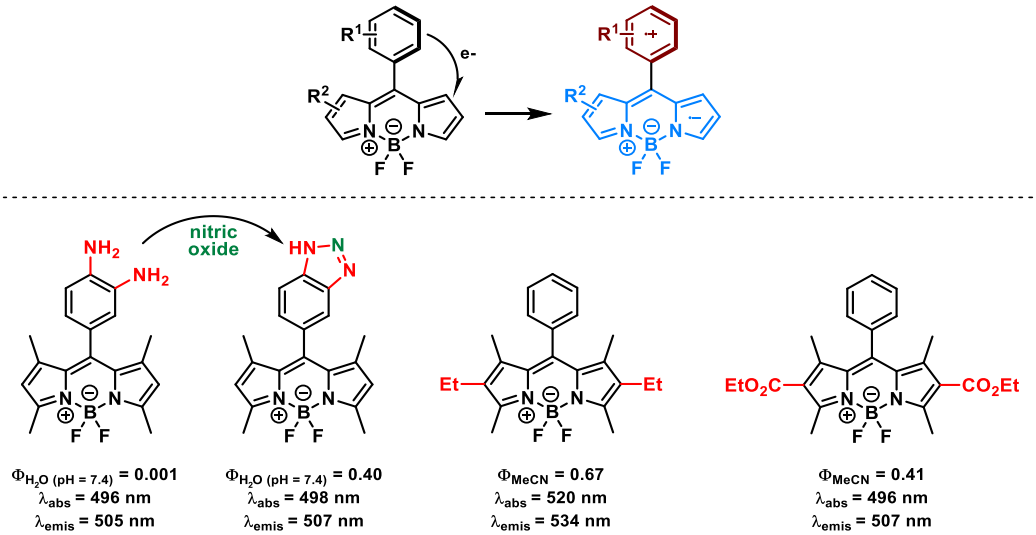

Figure 7. Selected examples of BODIPY derivatives and their photophysical properties to show the possible SET from the aryl moiety to the BODIPY core.

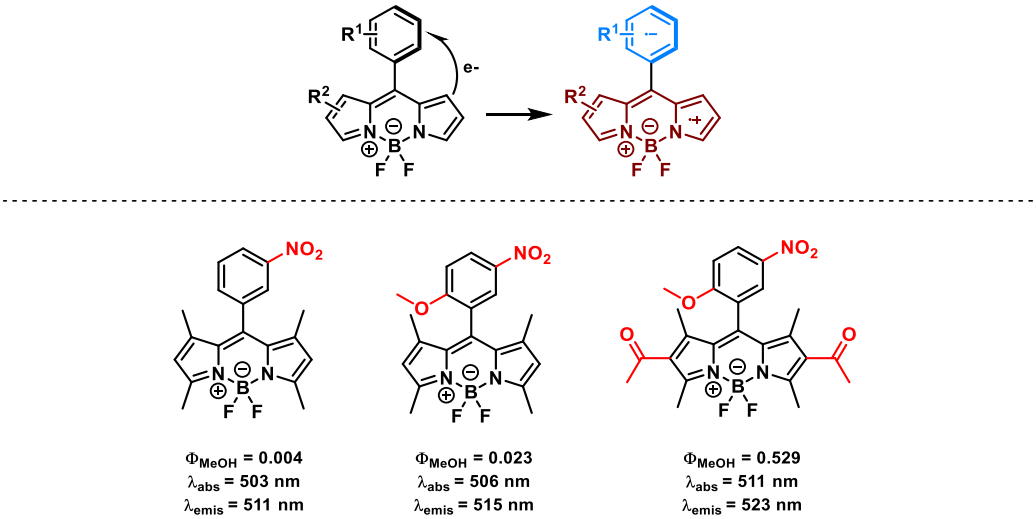

Figure 8. Selected examples of BODIPY derivatives and their photophysical properties to show the possible SET from the BODIPY core to the aryl moiety.

Although BODIPY dyes are visible light absorbing molecules with high fluorescent quantum yields and tunable photophysical properties that make them suitable candidates as photocatalysts, these organoboron compounds have found only extremely limited use in photoredox catalysis.[7a,8c,183] Indeed, even if the first examples have been reported several years ago, BODIPy dyes have only been employed by few of the research groups that are currently working in photocatalysis. The modest excited state energies and excited state redox potentials of BODIPYs have probably obstructed their implementation as photocatalysts. Furthermore, in the majority of the reported examples, the BODIPY dyes had to be appropriately adorned with heavy halogen atoms which allowed the ISC to the reactive triplet excited state, working as photosensitizers or photoredox catalysts. Nevertheless, BODIPY dyes have been extensively used in biochemistry as fluorescent labelling agents as we describe in the next section.

[183] (a) I. K. Sideri, E. Voutyritsa, C. G. Kokotos, *Org. Biomol. Chem.* **2018**, *16*, 4596-4614; (b) L. Huang, J. Zhao, S. Guo, C. Zhang, J. Ma, *J. Org. Chem*. **2013**, *78*, 5627-5637 ; (c) We. Li, L. Li, H. Xiao, R. Qi, Y. Huang, Z. Xie, X. Jing, H. Zhang, *RSC Adv*. **2013**, *3*, 13417-13421.

6.2 BODIPY Derivatives in Biochemistry and as Fluorescent Labelling Agents

BODIPY dyes have been intensively investigated and employed in biochemistry and bioimaging as specific biosensors and probes, in photodynamic therapy or as potentially circularly polarized luminescence-inducing compounds.[178,179,184] Through the appropriate functionalization, the BODIPY-based compound can be adorned with a specific moiety to work as a pH, nitrite, nitric oxide or amine probes or for the detection of a myriad of metal ions, among many other uses (Figure 8). The ability of generating reactive singlet oxygen has allowed the use of BODIPY derivatives in photodynamic therapy, in which they work from their triplet excited state. In addition, if the BODIPY core is found into close proximity of a stereogenic center in an appropriately synthetized enantioenriched compound, circularly polarized luminescence (CPL) properties can be observed.[184]

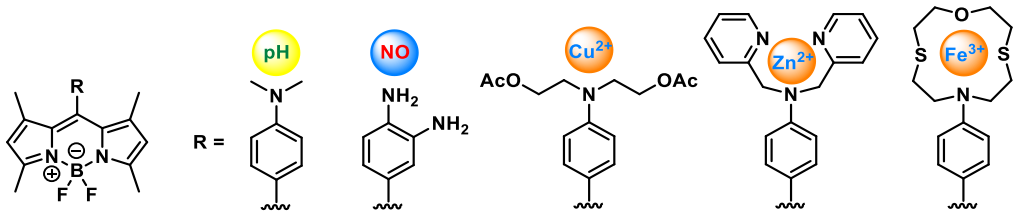

Figure 8. Selected examples of BODIPY derivatives employed as biological probes.

Moreover, since there is a great interest in the use of fluorescent moieties for the functionalization of proteins,[185] due to their excellent and easily tunable photophysical properties, BODIPYs have been widely employed for this purpose (Scheme 110).[186] The copper-catalyzed 1,3 dipolar cycloaddition between azides and alkynes is one of the most widely employed strategies to achieve this goal (Scheme 110a,b), whereas another interesting example can be observed in the bioconjugation achieved over a isocyanate-containing BODIPY (Scheme 110c). Many other different strategies for the conjugation of BODIPY derivatives with proteins have been reported and, in most of the cases, they have been achieved through reaction of a functionalized protein and an appositely functionalized BODIPY. Moreover, in all these strategies, it is common to employ an appropriate conformationally flexible linker to join the fluorescent moiety and the biomolecule, which is usually connected through one of the terminal amino acids which are composing it. The presence of the linker and the terminal connection with the protein are often desired since this permit to place the bulky fluorescent dye relatively far away from the protein structure, avoiding any undesired interaction or steric hindrance provided by the BODIPY. Indeed, this could have an impact on the three-dimensional structure of the protein and, as a consequence, leading to undesired modifications of the targeted interactions inside the biological systems. Nevertheless, direct C-H functionalization strategies became available in the last decade to permit the easy connection of fluorescent moieties with amino acids and peptides, without the required prefunctionalization of both coupling partners. A representative example of these oustanding C-H activation methodologies has been reported by the Vendrell's research group with the incorporation of a BODIPY unit into the tryptophan amino acid structure (Scheme 111a).[187] In addition, Ackermann and coworkers have reported

[184] (a) P. Kaur, K. Singh, *J. Mater. Chem. C* **2019**, *7*, 11361-11405; (b) A. Kamkaew, S. H. Lim, H. B. Lee, L. V. Kiew, L. Y. Chung, K. Burgess, *Chem. Soc. Rev.* **2013**, *42*, 77-88; (c) H. Tanaka, Y. Inoue, T. Mori, *ChemPhotoChem* **2018**, *2*, 386-402.

[185] (a) W. Xu, K. M. Chan, E. T. Kool, *Nat. Chem.* **2017**, *9*, 1043-1055; (b) J. Wang, J. Zhang, Y. M. Lee, S. Ng, Y. Shi, Z.-C. Hua, Q. Lin, H.-M. Shen, *Nat. Protoc.* **2017**, *12*, 279-288; (c) X. Chen, Y.-W. Wu, *Org. Biomol. Chem.* **2016**, *14*, 5417-5439; (d) J. M. Chalker, G. J. L. Bernardes, B. G. Davis, *Acc. Chem. Res*. **2011**, *44*, 730-741.

[186] (a) M. Albrecht, A. Lippach, M. P. Exner, J. Jerbi, M. Springborg, N. Budisab, G. Wenz, *Org. Biomol. Chem.* **2015**, *13*, 6728-6736; (b) M. H. Y. Cheng, H. Savoie, F. Bryden, R. W. Boyle, *Photochem. Photobiol. Sci.* **2017**, *16*, 1260-1267; (c) N. Zhao, T. M. Williams, Z. Zhou, F. R. Fronczek, M. Sibrian-Vazquez, S. D. Jois, M. G. H. Vicente, *Bioconjugate Chem*. **2017**, *28*, 1566-1579; (d) P. S. Deore, D. V. Soldatov, R. A. Manderville, *Scientific Reports* **2018**, *8*, 16874; (e) L. C. D. de Rezende, F. A. da Silva Emery, *Orbital Elec. J. Chem.* **2013**, *5*, 62-83.

[187] L. Mendive-Tapia, C. Zhao, A. R. Akram, S. Preciado, F. Albericio, M. Lee, A. Serrels, N. Kielland, N. D. Read, R. Lavilla, M. Vendrell, *Nat. Commun*. **2016**, *7*, 10940.

the direct modification of peptides by means of a BODIPY-labelling C-H activation strategy which works over alanine and phenylalanine derivatives, without the requirement of the usually scarcely present tryptophan building block (Scheme 111b).[188]

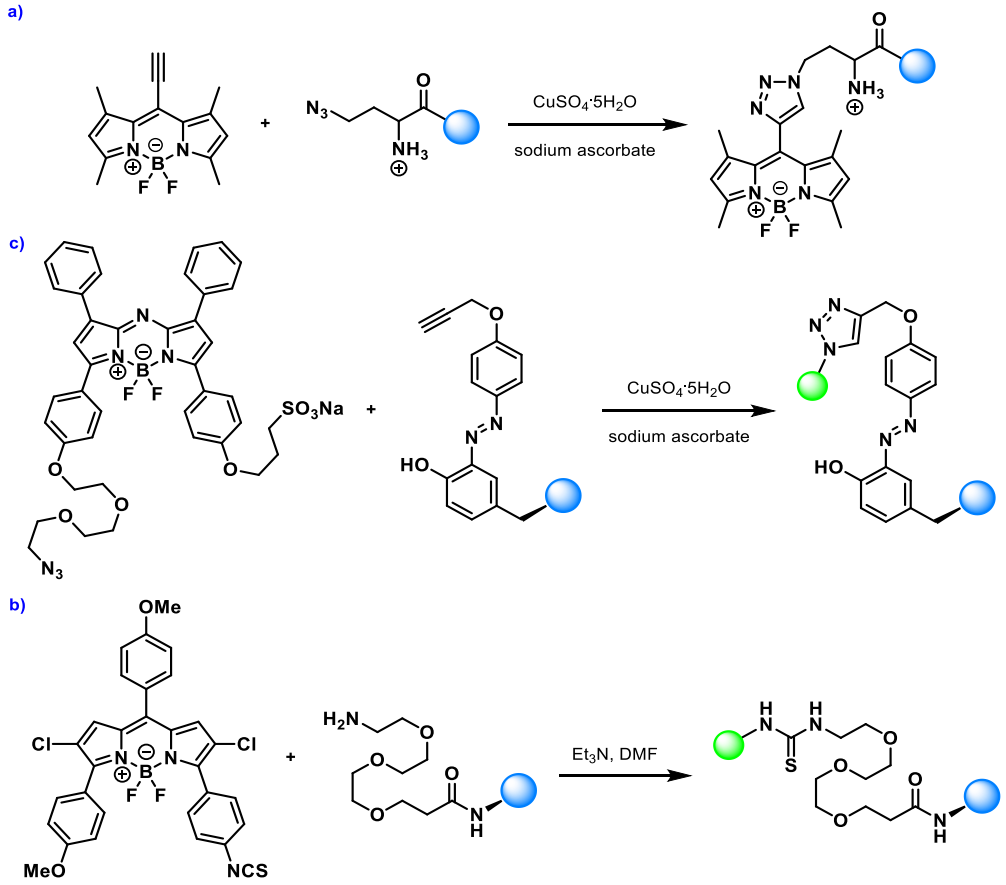

Scheme 110. Selected examples of strategies that are allowing the BODIPY-labelling of proteins.

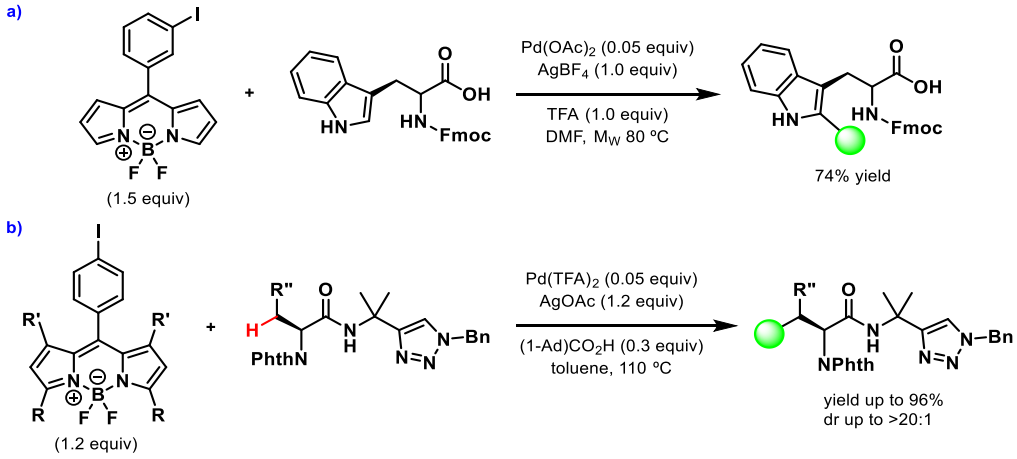

Scheme 111. Direct C-H activation strategies to functionalize tryptophan (a) or alanine and phenylalanine (b) residues with a BODIPY.

In summary, BODIPYs have been widely employed in biochemistry as fluorescent labelling agents for their incorporation in proteins by means of different functionalization strategies. This

[188] (a) W. Wang, M. M. Lorion, O. Martinazzoli, L. Ackermann, *Angew. Chem. Int. Ed.* **2018**, *57*, 10554-10558; for a similar strategy regarding a BODIPY-labeling over cyclobutane derivatives, see: (b) M. Virelli, W. Wang, R. Kuniyil, J. Wu, G. Zanoni, A. Fernandez, J. Scott, M. Vendrel, L. Ackermann, *Chem. Eur. J.* **2019**, *25*, 12712-12718.

has mainly been achieved by C-H activation, standard coupling reactions or 1,3-dipolar cycloadditions over unactivated alkynes. Therefore, due their electron-deficient properties we wondered about the possible use of these moieties as electron-withdrawing, activating groups in [3+2] cycloadditions over otherwise unreactive alkene double bonds. In the next section, we will briefly discuss this cycloaddition reaction and the corresponding alkene dipolarophiles which have been normally employed.

6.3 Introduction to Metal-Catalyzed Asymmetric [3+2] Cycloadditions

Metal-catalyzed asymmetric [3+2] cycloadditions of azomethine ylides with activated alkenes have been intensively investigated, showcasing its potential as a straightforward and efficient methodology for the preparation of enantioenriched pyrrolidines.[189] This strategy has been widely employed in the last decades with an impressive number of different metal-ligand-based catalytic systems being developed. The use of a metal salt as a Lewis acid is allowing the activation of the azomethine ylide through the formation of a metal complex, which presents an increased acidity for the hydrogen atoms that are at the α-position to the carbonyl group (Scheme 112). Then, an appropriate weak base can abstract a proton to give a reactive 1,3-dipole that can be added to an electron-poor alkene by means of a concerted cycloaddition or through a stepwise mechanism, involving an initial Michael addition and a following ring-closing event. Indeed, during the last decades, numerous functionalized alkenes have been used as efficient dipolarophiles exploiting the presence of an appropriate electron-withdrawing group, which is activating the double bond towards the dipolar cycloaddition. The first example of a stoichiometrically metal-promoted enantioselective [3+2] cycloaddition reaction of azomethine ylides was reported by Grigg's research group in 1991, achieving excellent enantioselectivities and employing cobalt (II) chloride as the Lewis acid (Scheme 113).[190]

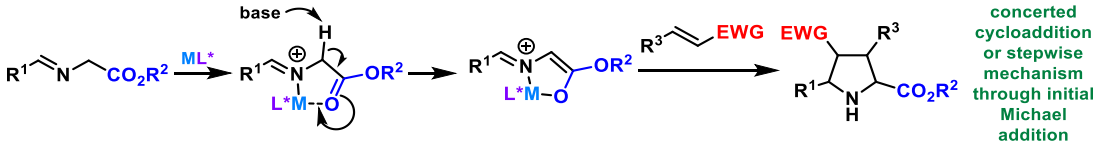

Scheme 112. Representative metal-catalyzed mechanism of 1,3-dipolar cycloadditions of azomethine ylides and activated alkenes.

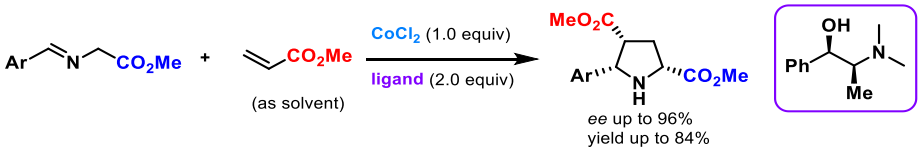

Scheme 113. Pioneering example regarding an asymmetric [3+2] cycloaddition of azomethine ylides.

The relative first catalytic examples were independently reported by Zhang's and Jørgensen's groups in 2002 (Scheme 114 and 115).[191,192] Zhang's methodology relied on silver (I) acetate as the Lewis acid (Scheme 114), while Jørgensen's group employed a zinc (II)/BOX catalytic system (Scheme 115), observing in both cases high levels of stereoinduction. Furthermore, the generality of the silver-catalyzed reaction has been demonstrated through the successful employment of structurally different dipolarophiles as the reaction partner.

[189] For recent reviews on the topic, see: (a) J. Adrio, J. C. Carretero, *Chem. Commun.* **2014**, *50*, 12434-12446; (b) T. Hashimoto, K. Maruoka, *Chem. Rev*. **2015**, *115*, 5366-5412.
[190] P. Allway, R. Grigg, *Tetrahedron Lett*. **1991**, *32*, 5817-5820.
[191] J. M. Longmire, B. Wang, X. Zhang, *J. Am. Chem. Soc.* **2002**, *124*, 13400-13401.
[192] A. S. Gothelf, K. V. Gothelf, R. G. Hazell, K. A. Jørgensen, *Angew. Chem., Int. Ed*. **2002**, *41*, 4236-4238.

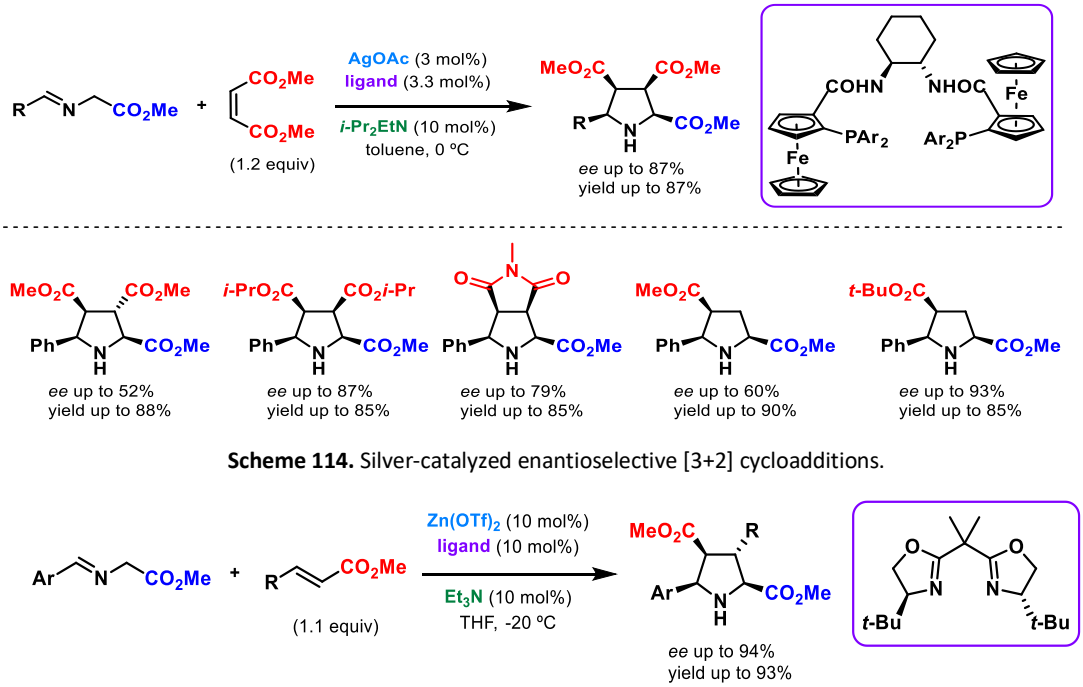

Scheme 114. Silver-catalyzed enantioselective [3+2] cycloadditions.

Scheme 115. Zinc-catalyzed enantioselective [3+2] cycloadditions.

Another interesting example which employs a copper (I) salt as the Lewis acid was reported by the Carretero's research group in 2005 (Scheme 116).[193] Even in this case, the generality of the reaction has been highlighted through the use of different dipolarophiles, accomplishing the synthesis of pyrrolidine-containing products with excellent enantioselectivity.

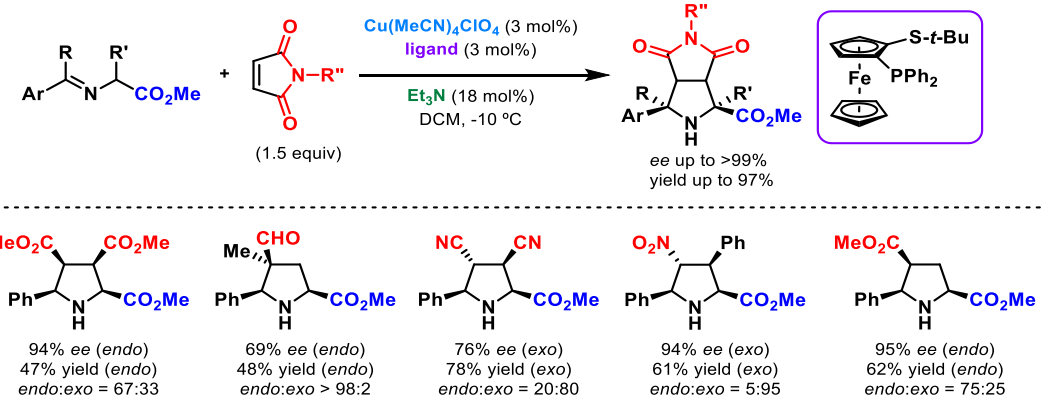

Scheme 116. Copper-catalyzed enantioselective [3+2] cycloaddition of azomethine ylides.

Almost simultaneously, a copper-catalyzed reaction, in which nitrostyrenes were employed as the activated alkenes, was reported by the group of Wu, achieving the corresponding enantioenriched pyrrolidines in high yield and enantioselectivity (Scheme 117).[194]

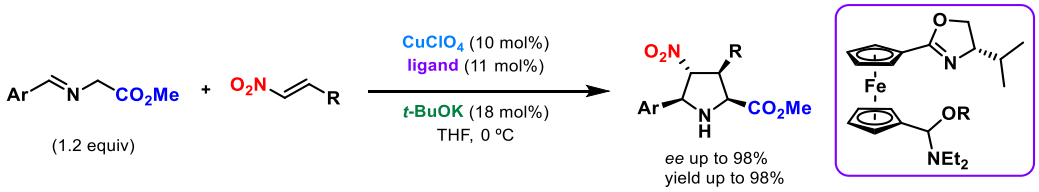

Scheme 117. Copper-catalyzed asymmetric [3+2] cycloaddition with nitrostyrene derivatives as the dipolarophiles.

[193] S. Cabrera, R. G. Arrayás, J. C. Carretero, *J. Am. Chem. Soc.* **2005**, *127*, 16394-16395.
[194] X.-X. Yan, Q. Peng, Y. Zhang, K. Zhang, W. Hong, X.-L. Hou, Y.-D. Wu, *Angew. Chem., Int. Ed*. **2006**, *45*, 1979-1983.

Shortly after, the group of Carretero reported two brilliant examples in which vinyl sulfone and bis-sulfonyl ethylene were employed as masked ethylene and acetylene analogues, respectively (Scheme 118a,b).[195] Indeed, after appropriate removal of the sulfonyl groups, the corresponding 2,5-substituted pyrrolidines could be obtained with high enantioselectivity.

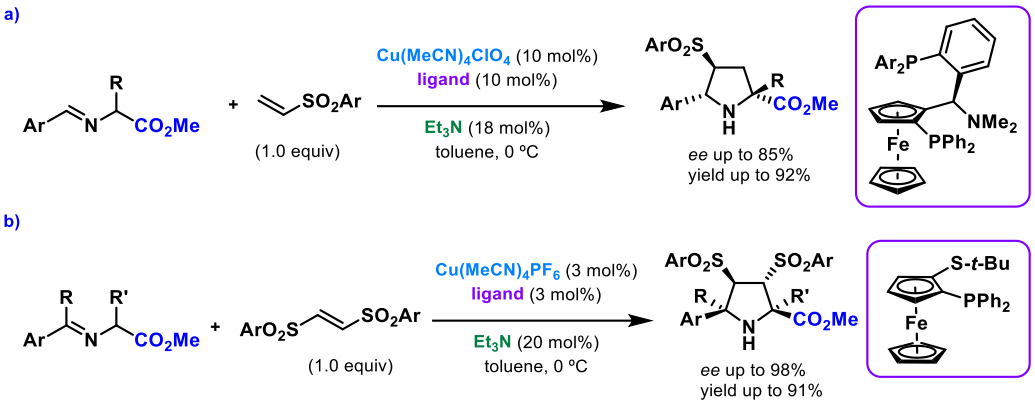

Scheme 118. Copper-catalyzed asymmetric [3+2] cycloaddition employing vinyl sulfone and bis-sulfonyl ethylene.

Another important example regarding the use of cyclic or acyclic enones as the dipolarophiles has been reported by the same research group in 2009 (Scheme 119a),[196] whereas a highly efficient copper-catalyzed [3+2] cycloaddition, that permitted the synthesis of enantioenriched spirooxindoles, was reported by the Waldmann group (Scheme 119b).[197]

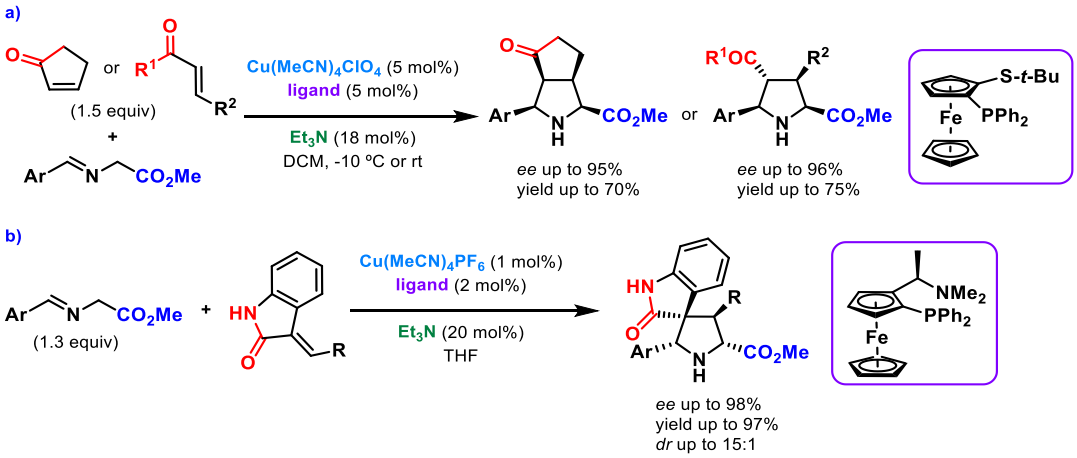

Scheme 119. Enantioselective [3+2] cycloadditions: (a) enones as the dipolarophiles, (b) preparation of spirooxindoles.

A brilliant strategy for the achievement of 5-unsubstituted pyrrolidines was described by Carretero's group through the employment of α-silylimines as 1,3-dipole precursors (Scheme 120a).[198] Indeed, upon a base-assisted removal of the trimethylsilyl group, a zwitterionic species was generated, leading to the desired 5-unsubstituted enantioenriched pyrrolidines. Furthermore, the same group reported the use of simple electron-poor styrene derivatives as unprecedented efficient dipolarophiles in copper-catalyzed [3+2] cycloadditions, achieving outstanding yields and enantioselectivities (Scheme 120b).[199]

[195] (a) T. Llamas, R. Gómez Arrayás, J. C. Carretero, *Org. Lett*. **2006**, *8*, 1795-1798; (b) A. López-Pérez, J. Adrio, J. C. Carretero, *J. Am. Chem. Soc.* **2008**, *130*, 10084-10085.

[196] J. Hernández-Toribio, R. Gómez Arrayás, B. Martín-Matute, J. C. Carretero, *Org. Lett*. **2009**, *11*, 393-396.

[197] P. Antonchick, C. Gerding-Reimers, M. Catarinella, M. Schürmann, H. Preut, S. Ziegler, D. Rauh, H. Waldmann, *Nat. Chem*. **2010**, *2*, 735-740.

[198] J. Hernández-Toribio, S. Padilla, J. Adrio, J. C. Carretero, *Angew. Chem. Int. Ed*. **2012**, *51*, 8854-8858.

[199] A. Pascual-Escudero, A. de Cózar, F. P. Cossío, J. Adrio, J. C. Carretero, *Angew. Chem. Int. Ed*. **2016**, *55*, 15334-15338.

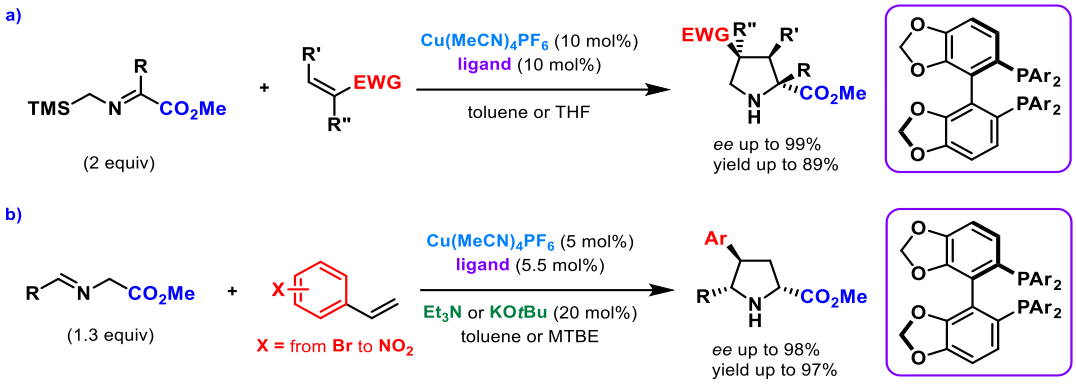

Scheme 120. Copper-catalyzed enantioselective [3+2] cycloadditions to give 5-unsubstituted pyrrolidines (a) and employing electron-deficient styrene derivatives as the dipolarophiles (b).

Therefore, although different enantioselective strategies have been reported in the last decades, there is still a high interest in the further developing of efficient electron-withdrawing groups, which could unlock the possibility of obtaining a dipolar cycloaddition over otherwise unreactive alkenes.

6.5 Objectives of this Chapter

The particular photophysical and electronic properties of *meso*-substituted alkenyl BODIPYs make them attractable building blocks for the incorporation of BODIPY-containing fluorescent moieties into more complex structures (Scheme 121).[200] Indeed, the presence of an alkenyl substituent at the 8-position of the BODIPY core is deactivating almost completely its fluorescence (ϕ = 0.05) due to low rotational and vibrational energy barriers, which are leading to non-radiative thermal deactivation pathways. On the other hand, the alkyl substituted analogue presents a remarkable high fluorescence quantum yield (ϕ = 0.91), which makes it suitable for bioimaging purposes. Moreover, the electron-poor properties of the *meso*-position of the BODIPY moiety were highlighted by Peña Cabrera's group through an accomplished conjugated addition of 1-dodecanethiol at the alkene double bond, with the BODIPY core working as an efficient electron-withdrawing group in a racemic uncatalyzed process (Scheme 121).[200] As expected, even in this case, the corresponding product was found to be highly fluorescent (ϕ = 0.75), showcasing the potentiality of alkenyl BODIPYs as precursors of fluorescent dyes.

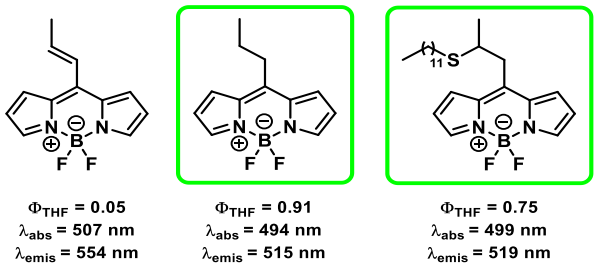

Scheme 121. Different photophysical properties of *meso*-substituted alkenyl and alkyl BODIPYs and electron-withdrawing characteristics of the BODIPY core.

Taking into account these characteristics, our group reported the first enantioselective transformation to obtain a BODIPY-containing enantioenriched compound, starting from alkenyl

[200] I. J. Arroyo, R. Hub, B. Zhong Tang, F. I. López, E. Peña-Cabrera, *Tetrahedron* **2011**, *67*, 7244-7250.

BODIPYs (Scheme 122).[201] This result was achieved through an aminocatalytic strategy which relied on the use of a pyrrolidine-based organocatalyst to carry out a stereocontrolled [4+2] cycloaddition exploiting transient generated trienamine intermediates as the reactive species.[202] In addition, DFT calculations revealed that the process proceeded through a stepwise mechanism and a combination of experimental and theoretical evidenced supported the stronger electron-withdrawing character of the BODIPY moiety in comparison with other electron-deficient activating groups.

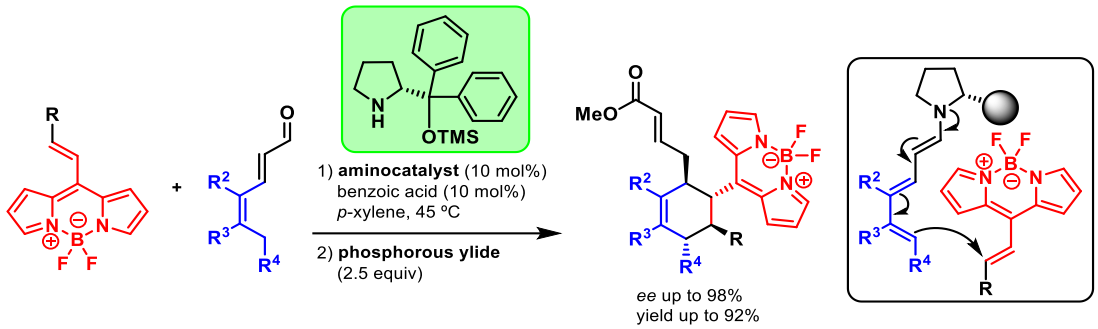

Scheme 122. Aminocatalytic enantioselective [4+2] cycloaddition over alkenyl BODIPYs.

For the above mentioned reasons, and inspired by the successful development of an aminocatalytic strategy based on a [4+2] cycloaddition,[201] we thought that other functionalization reactions could have been carried out over *meso*-alkenyl BODIPY exploiting the electron-withdrawing character of the BODIPY at the 8-position and obtaining a highly fluorescent compound. For this purpose we envisioned that an asymmetric metal-catalyzed [3+2] cycloaddition, employing azomethine ylides and BODIPY as a new electron withdrawing group, could have been a possible strategy to achieve an enantioenriched BODIPY-labeled pyrrolidine (Scheme 123). The resulting fluorescent pyrrolidine could then be employed as a biological sensor or linked to amino acids and peptides due to its proline-based structure. To achieve this goal the following sub-objectives have been identified:

1) Development and optimization of the reaction conditions for a metal-catalyzed [3+2] cycloaddition in which the BODIPY could work as a novel electron-withdrawing group.
2) Evaluation of the reaction scope and of the relative substrate limitations.
3) DFT studies concerning the reaction mechanism and the characteristic electron-withdrawing features of the BODIPY moiety.
4) Biological studies employing the BODIPY-containing pyrrolidines to test their use as biological sensors in cell imaging.

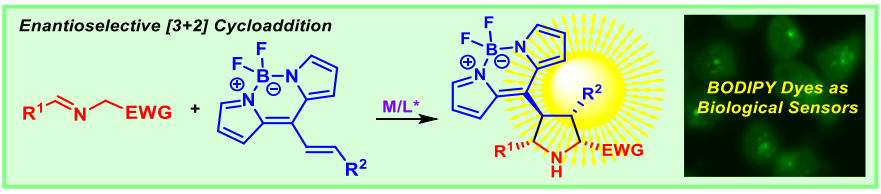

Scheme 123. Proposed asymmetric strategy for the obtainment of BODIPY-containing enantioenriched pyrrolidines.

[201] A. Guerrero-Corella, J. Asenjo-Pascual, T. Janardan Pawar, S. Díaz-Tendero, A. Martín-Sómer, C. Villegas Gómez, J. L. Belmonte-Vázquez, D. E. Ramírez-Ornelas, E. Peña-Cabrera, A. Fraile, D. Cruz Cruz, J. Alemán, *Chem. Sci.* **2019**, *10*, 4346-4351.
[202] V. Marcos, J. Alemán, *Chem. Soc. Rev*. **2016**, *45*, 6812-6832.

6.5 Publications and Experimental Section

Boron Dipyrromethene (BODIPY) as Electron-Withdrawing Group in Asymmetric Copper-Catalyzed [3+2] Cycloadditions for the Synthesis of Pyrrolidine-Based Biological Sensors

Thomas Rigotti, Juan Asenjo-Pascual, Ana Martín-Somer, Paula Milán Rois, Marco Cordani, Sergio Díaz-Tendero, Álvaro Somoza, Alberto Frailea,* and José Alemán*

Adv. Synth. Catal. **2020** (DOI: 10.1002/adsc.201901465)

The experimental section was taken from the "Supporting Information" document associated with the specific publication and is including the corresponding numeration. The characterization data have been shown only for the final products that appear in the scope of the reaction. The complete "Supporting Information" documents, with all the characterization data, NMR spectra, SFC or HPLC traces and other experimental procedures have been included in the enclosed USB memory.

10.1002/adsc.201901465

FULL PAPER

DOI: 10.1002/adsc.201((will be filled in by the editorial staff))

Boron Dipyrromethene (BODIPY) as Electron-Withdrawing Group in Asymmetric Copper-Catalyzed [3+2] Cycloadditions for the Synthesis of Pyrrolidine-Based Biological Sensors

Thomas Rigotti,[a,f] Juan Asenjo-Pascual,[a,f] Ana Martín-Somer,[b] Paula Milán Rois,[c] Marco Cordani,[c] Sergio Díaz-Tendero,[b,d,e] Álvaro Somoza,[c] Alberto Fraile[a,d,*] and José Alemán[a,d,*]

[a] Department of Organic Chemistry (module 01), Universidad Autonoma de Madrid, Cantoblanco, 28049 Madrid, Spain. Webpage: www.uam.es/jose.aleman. E-mail: alberto.fraile@uam.es; jose.aleman@uam.es
[b] Department of Chemistry (module 13), Universidad Autonoma de Madrid, Cantoblanco, 28049 Madrid, Spain.
[c] IMDEA Nanociencia, Cantoblanco, 28049 Madrid, Spain.
[d] Institute for Advanced Research in Chemical Sciences (IAdChem), Universidad Autónoma de Madrid, 28049 Madrid, Spain.
[e] Condensed Matter Physics Center (IFIMAC), Universidad Autónoma de Madrid, Cantoblanco, 28049 Madrid, Spain.

Received: ((will be filled in by the editorial staff))

Supporting information for this article is available on the WWW under http://dx.doi.org/10.1002/adsc.201######.((Please delete if not appropriate))

Abstract. In this work, we describe the use of Boron Dipyrromethene (BODIPY) as electron-withdrawing group for activation of double bonds in asymmetric copper-catalyzed [3+2] cycloaddition reactions with azomethine ylides. The reactions take place under smooth conditions and with high enantiomeric excess for a large number of different substituents, pointing out the high activation of the alkene by using a boron dipyrromethene as electron-withdrawing group. Experimental, theoretical studies and comparison with other common electron-withdrawing groups in asymmetric copper-catalyzed [3+2] cycloadditions show the reasons of the different reactivity of the boron dipyrromethene derivatives, which can be exploited as a useful activating group in asymmetric catalysis. Additional experiments show that the so obtained pyrrolidines can be employed as biocompatible biosensors, which can be located in the endosomal compartments and do not present toxicity in three cell lines.

Keywords: asymmetric catalysis; pyrrolidines; Electron-Withdrawing Group; bioimaging cell; Frontier Molecular Orbitals; BODIPY; cycloaddition

Introduction

Boron dipyrromethene derivatives (BODIPYs) are a very remarkable family of fluorescent dyes that have been employed as powerful tools for labeling strategies in biochemistry and molecular biology.[1] The reasons for their success are related to their high cell permeability, impressive spectroscopic properties[2] as well as excellent robustness and chemical- and photo-stability.[2a,3] Owing to their unique optical and chemical properties, BODIPYs have been used as biological sensors and for cell imaging. However, although some recent methodologies allow the direct labelling of biomolecules with the BODIPY unit,[4] generally, it is necessary to use approaches that are based on conventional coupling reactions from two functionalized substrates,[5] thus requiring tedious modifications of the target biomolecule, including the corresponding linker.

Proline and its derivatives constitute a remarkable family of natural and synthetic compounds with very interesting chemical and bioactive applications.[6] Furthermore, proline plays a crucial role in peptides by limiting their conformational freedom, which modulates the nucleation of their secondary structures. Those spatial arrangements tune their biological behavior and protect them against degradation. Such changes are especially relevant in therapeutic peptides, where their selectivity and activity can be enhanced.[7] Moreover, proline core is present in the structure of kainoid natural neurotoxins such as α-Kainic acid (I),[8] (-)-Domoic acid (II),[9] and Acromelic acid (III),[10] which promote potent stimulation of the central nervous system, cause brain damage, and neurological disorders (Figure 1). Another related family of synthetic molecules such as IV[11] has been identified as potent hepatitis C virus (HCV) inhibitors (Figure 1).

Plenty of novel strategies and methods have been developed in recent years to synthesize these heterocycles. Among them, catalytic asymmetric 1,3-dipolar cycloadditions of azomethine ylides with activated alkenes have turned out to be one of the most straightforward and efficient methods for the preparation of enantioenriched prolines,[12] from which, and by simple transformations, it is possible to obtain highly functionalized pyrrolidines.[13]

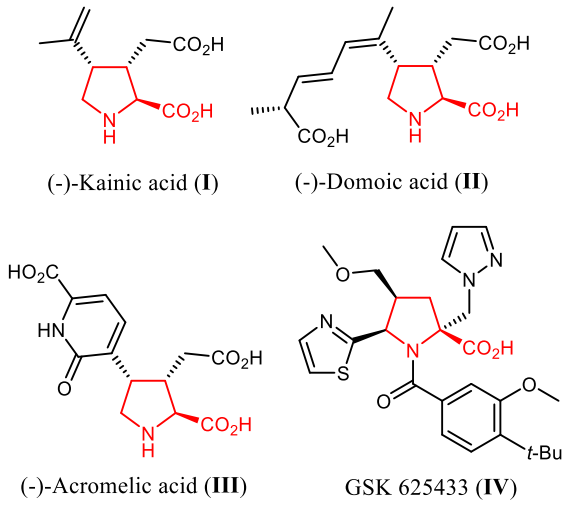

Figure 1. Different biologically active proline derivatives described in the literature.

Usually, strong electron-withdrawing groups (EWG) (e.g. nitro, ester, sulfone, amide, phosphonate, etc) at the alkene are needed to achieve the desired reactivity (Scheme 1a). In a very recent report, the activation of a double bond was achieved by a very electron-poor aryl group, such as nitrophenyl styrenes, allowing their use as dipolarophiles in [3+2] cycloadditions.[14] Nevertheless, the range of suitable dipolarophile partners is still limited, and most of them are related to the common EWGs in asymmetric catalysis.

Since BODIPY core is known for its electron-withdrawing character,[15] and can be used as fluorescent moiety for bioimaging techniques,[1] we wondered if it would be possible to use this interesting group as EWG for alkene activation in asymmetric [3+2] cycloaddition reactions. Taking into account that BODIPYs and pyrrolidines moieties are very important structures, this [3+2] cycloaddition will give access to enantiomerically enriched pyrrolidines incorporating a fluorophore dye (Scheme 1b). In this work, we show that BODIPY units can be used as EWG in asymmetric catalysis for the synthesis of pyrrolidines thus adding a new EWG to the range of suitable dipolarophiles in [3+2] cycloaddition reactions. Quantum chemistry calculations, comparing the reactivity with other common EWGs, demonstrate that BODIPY is able to activate the double bond better than any other. Besides, we show that the so obtained pyrrolidines incorporating a fluorophore moiety (BODIPY) could be applied to live-cell imaging in three different cellular cell lines.

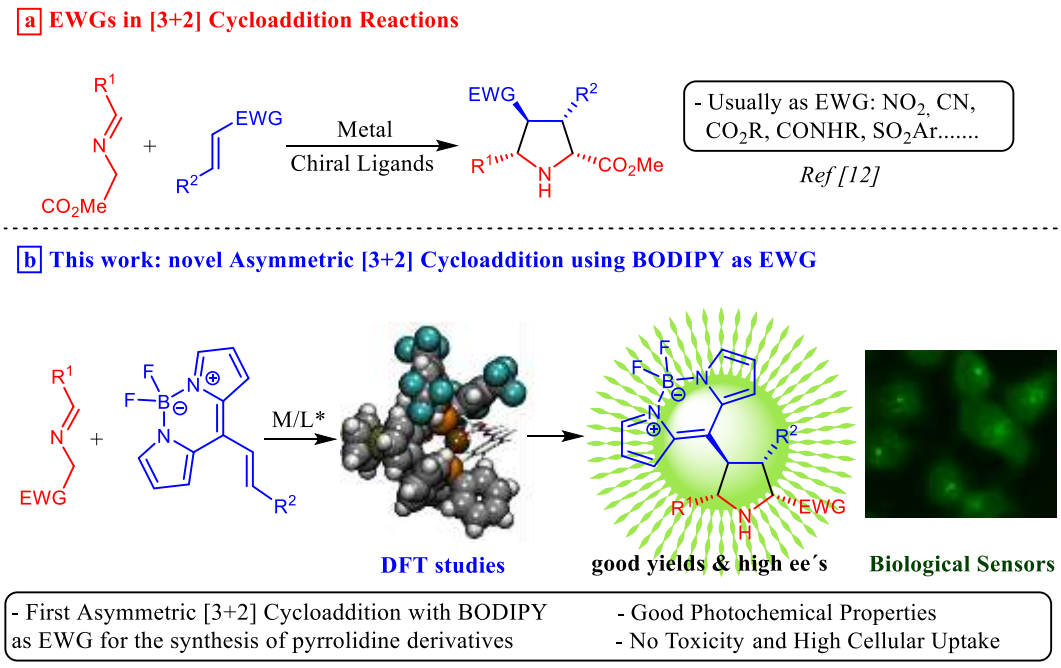

Scheme 1. Comparison of the previously used approaches and present work (M/L*: Metal/Chiral Ligands).

Results and Discussion

Synthesis of BODIPY pyrrolidines, screening and scope. We began our investigations carrying out the cycloaddition reaction between iminoester **1a** and alkenyl-BODIPY **2a** in the presence of $[Cu(CH_3CN)_4][PF_6]$ (15 mol%), triethylamine (30 mol%) as base, toluene as solvent and several chiral ligands (**L1-L6**) (15 mol%) at room temperature (Table 1, entries 1-6). It should be noted that in all trials a complete *exo* selectivity was obtained (*dr*>98:2). The best result was achieved using Walphos (**L6**) as the ligand (entry 6, Table 1), obtaining the *exo*-**3a** adduct in 90% *ee* and complete

diastereoselectivity (*dr*>98:2) but with low yield. In order to improve this result, we tested different solvents (see S.I. for further details), obtaining the desired product in 85% yield and with a 96% of enantiomeric excess (*ee*) when the reaction was performed in DCM (entry 7). Then, the influence of the catalyst loading on the reaction outcome was evaluated. The use of 10 mol% of catalyst maintained the *ee* values previously obtained (entry 8), but a lower catalytic loading (5 mol%) provoked a slight decrease in the final enantioselectivity (90% *ee*, entry 9, Table 1). Considering these results, we decided to decrease the temperature to 4 ºC, achieving the final adduct *exo*-**3a** in high yield (89%) and excellent enantioselectivity (98%) (entry 10, table 1).[16] However, the use of even lower catalyst loading (2.5 mol%, entry 11, table 1) gave low *ee*.

Table 1. Catalysts screening and optimization of reaction conditions.[a]

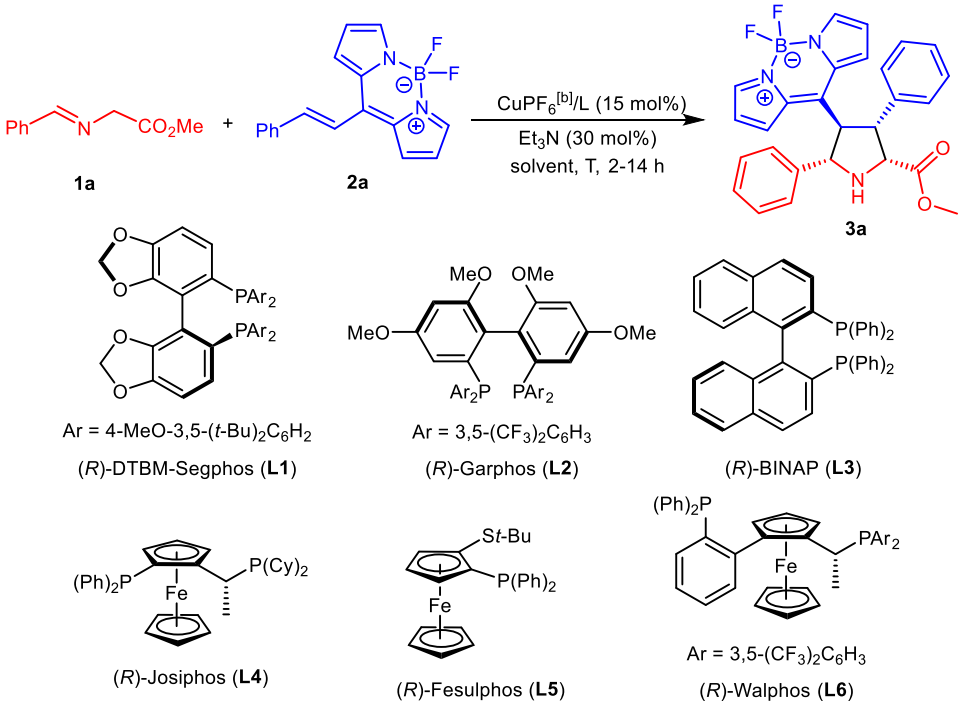

Entry	L (%mol)	Solvent	T (ºC)	Yield (%)[c]	*Exo*/*endo*[d]	*ee* (%)[e]
1	**L1** (15)	Toluene	25	64	>98:2	-84
2	**L2** (15)	Toluene	25	58	>98:2	6
3	**L3** (15)	Toluene	25	60	>98:2	-75
4	**L4** (15)	Toluene	25	49	>98:2	-70
5	**L5** (15)	Toluene	25	34	>98:2	-76
6	**L6** (15)	Toluene	25	33	>98:2	90
7	**L6** (15)	DCM	25	85	>98:2	96
8	**L6** (10)	DCM	25	nd	>98:2	97
9	**L6** (5)	DCM	25	nd	>98:2	90
10	**L6 (5)**	**DCM**	**4**	**89**	**>98:2**	**98**
11	**L6** (2.5)	DCM	4	nd	>98:2	90

[a] All the reactions were performed on a 0.07 mmol scale of **2a** using a dry solvent (0.5 mL) under air atmosphere. [b] $CuPF_6$: $[Cu(CH_3CN)_4][PF_6]$. [c] Isolated yield after flash-chromatography. [d] Ratio determined by ^1H NMR spectroscopy of the crude mixture. [e] Determined by chiral HPLC.

Once the best conditions were determined (entry 10, Table 1), we carried out the scope of the reaction using different iminoesters **1** and alkenyl-BODIPYs **2** (Table 2). Firstly, we tested the influence of the electronic properties and the steric effect of substituents at the dipole precursor **1**. The presence of an electron-donating group (EDG, *p*-MeO, **1b**) or an EWG (*p*-CF_3, **1c**) in the aryl moiety yielded pyrrolidines **3b-c** in high yield (79-84%) and high *ee* (93-98%), which indicates that the reaction tolerates imines with different electronic properties. A more sterically hindered imine such as **1d** allowed the synthesis of **3d** with excellent enantioselectivity and without erosion of the final yield (88%). Similarly, the cycloaddition reactions of imines **1e-f**, containing a heteroaromatic ring, gave the corresponding adducts **3e** and **3f** with high *ee*. The reaction also proceeded with very high enantioselectivity (98% *ee*) but with a lower yield (40%) with the cycloalkyl substituent (**1g**). The reaction worked properly even

when the ester group of the imine was substituted for an amide group, obtaining the pyrrolidine **3h** in very high yield and excellent *ee* (83% yield, 98% *ee*). Then, a variety of different alkenyl-BODIPYs **2d-f** were also studied (third and fourth row). Indeed, electron-donating and electron-withdrawing groups on the aryl moiety of the dipolarophile were tolerated, leading to pyrrolidines **3i** (*p*-MeO), **3j** (*p*-CF_3) and **3k** (*p*-Cl) with very high enantioselectivities (93-97% *ee*). The presence of two ethyl groups at C-3 and C-5 positions of the BODIPY core did not affect the stereoselectivity (91% *ee*) but provoked a decrease of the yield (53%). Finally, we were delighted to find that alkenyl-BODIPY **2f,** which contains a primary alkyl chain substituent, also led to the pyrrolidine **3m** in high yield and very high enantioselectivity. In addition, pyrrolidine **3n** with a quaternary center was obtained, but in low yield and enantiomeric excess.

Table 2. Scope for the synthesis of BODIPY pyrrolidines **3** from different imines **1** and double bonds **2**.[a]

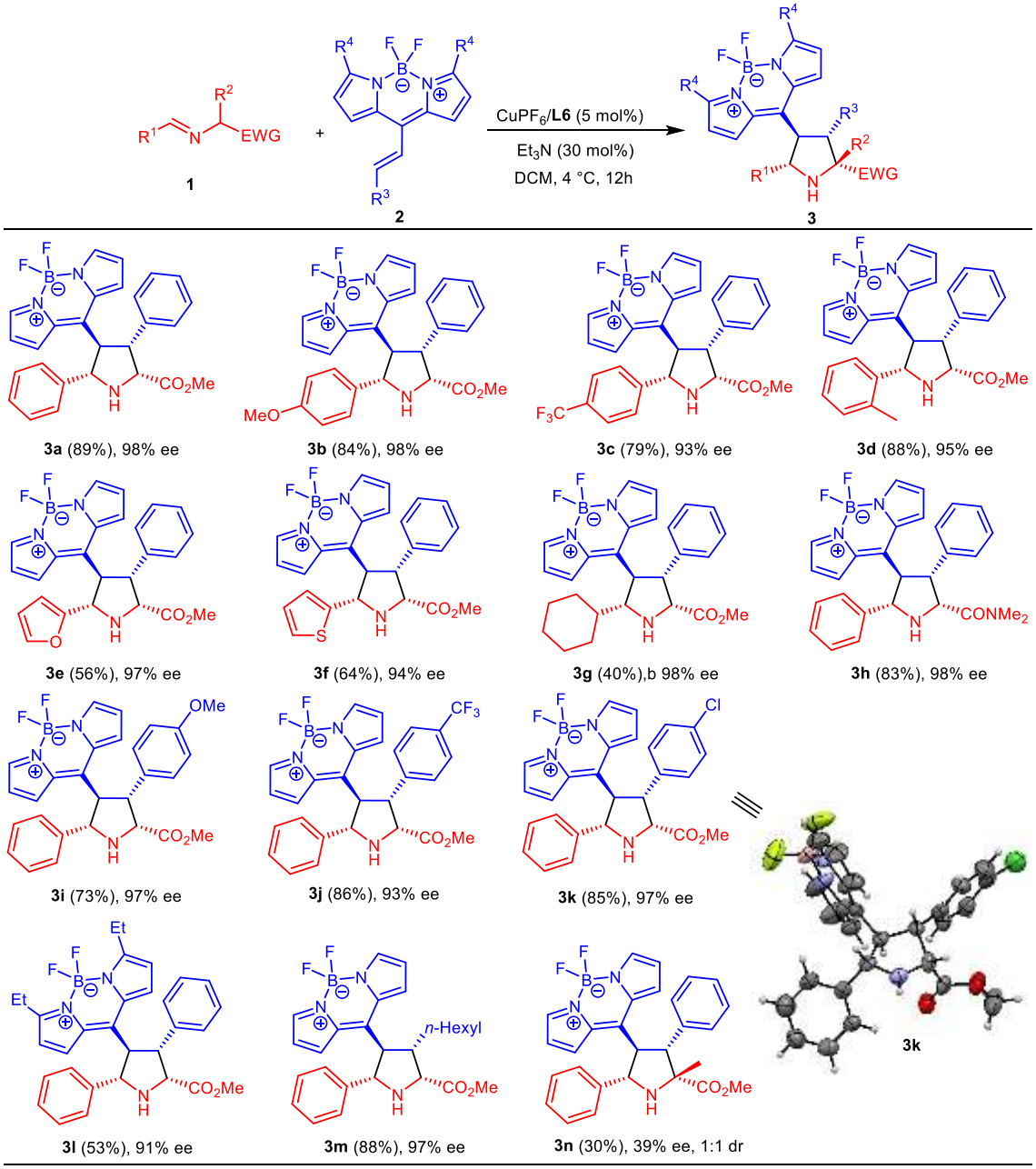

[a] All reactions were performed in 0.1 mmol scale of **2** using dry DCM (0.75 mL) under air atmosphere. Isolated yields were calculated after flash-chromatography. *ee* were determined by chiral HPLC. [b] Yield determined by ^{1}H NMR using an internal standard.

The spatial arrangement of all the substituents of the pyrrolidine moiety was determined from the absolute configuration of the asymmetric centers of pyrrolidine **3k**, which was unequivocally assigned as 2*R*, 3*R*, 4*R*, 5*S* by X-Ray crystallographic analysis (see bottom-right, Table 2).[17] This configuration can be explained by an *exo* approach, (the more favorable when copper salts are used)[12b] of the dipolarophile **2**

to the bottom prochiral face (2*Re*,4*Si*) of dipole **1** (see explanation in next section).

DFT calculations: BODIPY as EWG, thermodynamics and kinetics.[18] In order to shed light into the reaction mechanism, additional experiments and DFT calculations were carried out.[19] We modeled the reaction between dipole **1a** and dipolarophile **2a** in the presence of the catalyst complex: $[Cu(CH_3CN)_4][PF_6]$/Walphos (Cu/**L6**). We started the computational study analyzing the most favorable way for the dipole to coordinate to the catalyst complex. As it can be seen in Figure 2a, once the metalloazomethine ylide is formed in presence of the base (dipole), it can coordinate with Cu/**L6** in two different ways: complex **I** or **II**; both of them having the top prochiral face blocked by the 3,5-ditrifluoromethylaryl substituents of the Walphos ligand. The Gibbs free energy difference (ΔG) between **I** and **II** is 4.15 kcal/mol, being complex **I** the most stable.

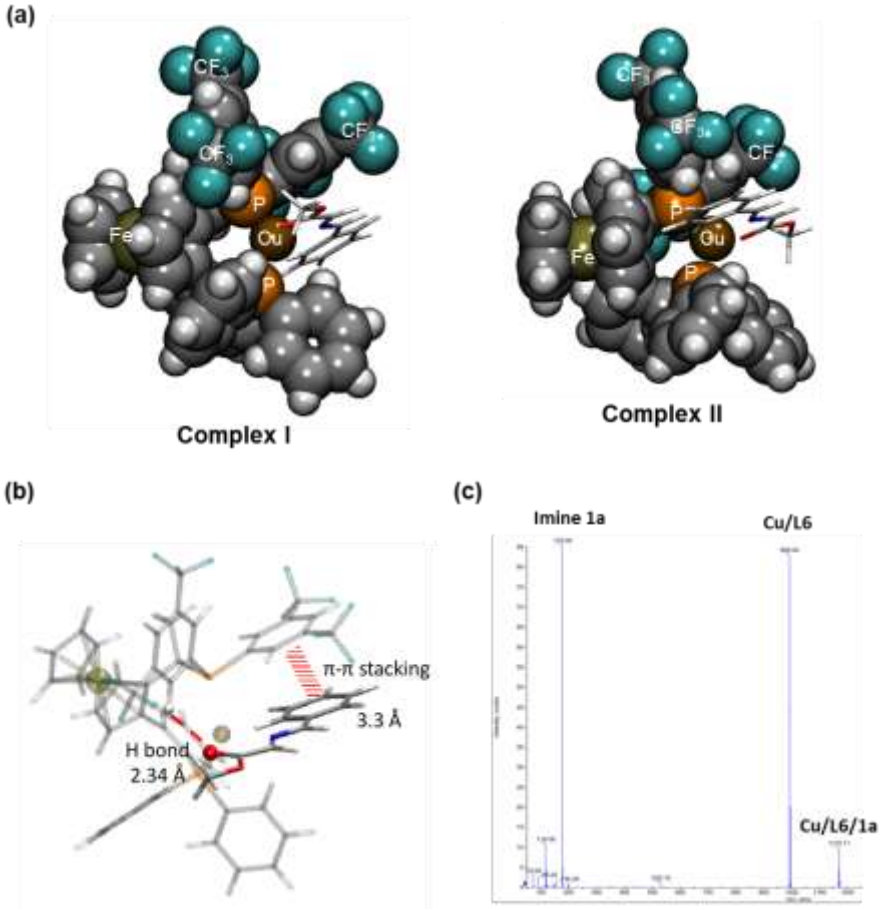

Figure 2. a) Optimized structures (at B3LYP/6-31G(d,p) level of theory) for the two possible orientations of the complex between the catalyst and dipole: Cu/**L6**/dipole (see Figure S4 in the Supporting Information for more details). The Gibbs free energy difference (ΔG) between them is 4.15 kcal/mol, being complex **I** the most stable. **(b)** Stabilizing interactions present in complex **I**. **(c)** Mass spectrum of a mixture of Cu, ligand **L6** and imine **1a** (see S.I. for full mass-spectrum).

This could be attributed to a stabilizing π-π interaction between the phenyl group of the imine and a 3,5-$(CF_3)_2$Ph ring of the ligand, which is absent in complex **II** (Figure 2b). In addition, an intramolecular hydrogen bond between the carbonyl oxygen of the imine and a hydrogen of the other 3,5-$(CF_3)_2$Ph ring of the ligand could further stabilize complex **I**. In order to check that a complex Cu/**L6**/**1a** was formed and stable, we carried out a mass spectroscopy study (see Supporting Information). We detected a peak at *m/z* 1170.11 amu corresponding to the Cu/**L6**/**1a** complex and a peak at *m/z* 993.04 amu, which corresponds to the Cu/**L6** complex (Figure 2c). This evidences the existence and stability of the Cu/**L6**/**1a** complex.

In a second step, we studied the attack of several dipolarophiles to the previously formed dipole-catalyst complex (complex-**I**). Frontier Molecular Orbital Theory is often employed to explain the reactivity on this kind of reactions.[20] Thus, the HOMO-LUMO gap energy difference between the HOMO of the dipole and the LUMO of the dipolarophile can be related to the reaction rate constant, being faster the reaction as the HOMO-

10.1002/adsc.201901465

LUMO gap decreases. Experimental conversions,[21] after 30 minutes at r.t., and values of HOMO-LUMO gap for different dipolarophiles are shown in Figure 3 together with the LUMO of the dipolarophiles considered.

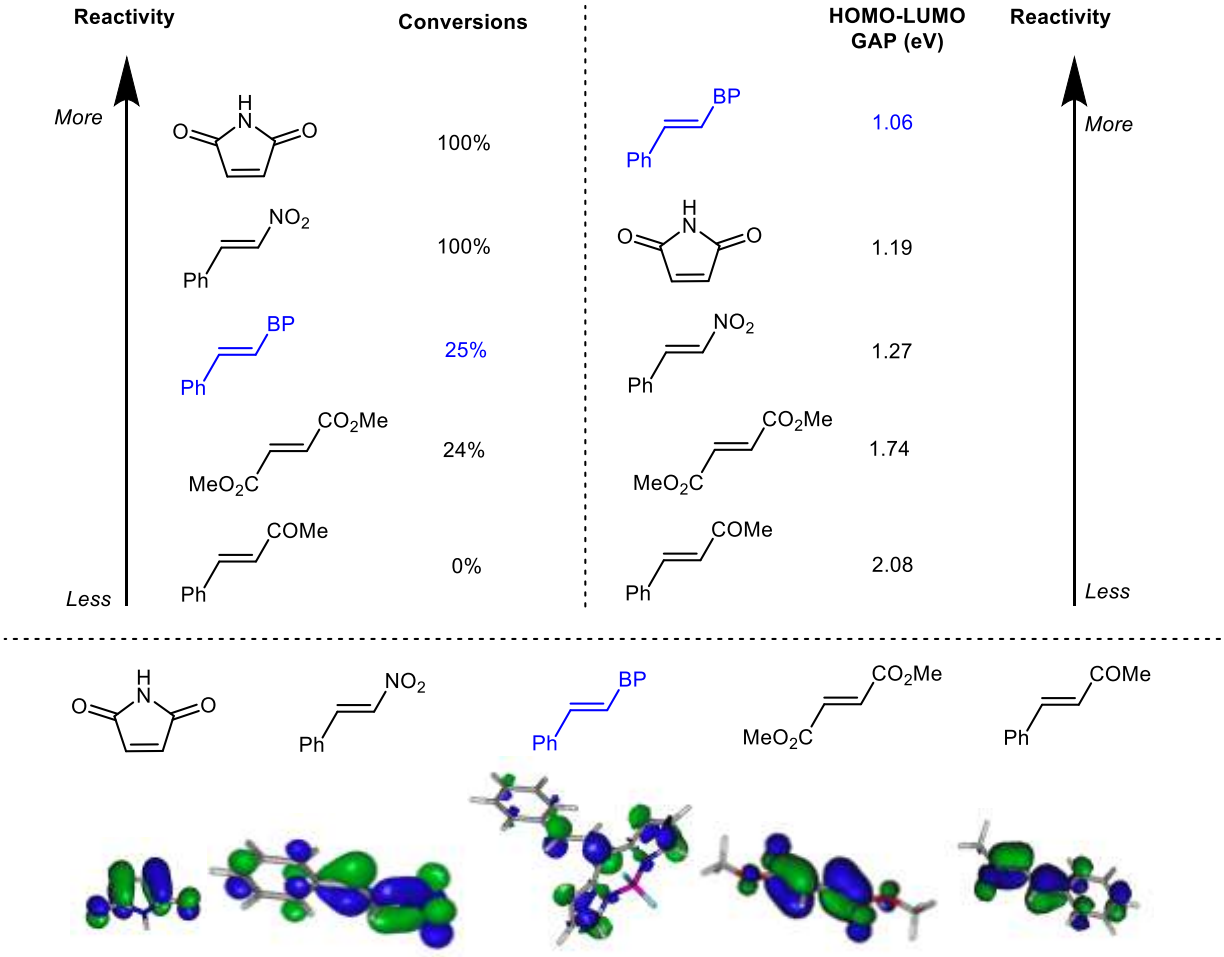

Figure 3. Conversions and HOMO-LUMO gap for the reaction of Cu/**L6**/dipole with different dipolarophiles. We have used Kohn-Sham orbitals computed at B3LYP/6-31G(d,p) level of theory. The LUMO of the different dipolarophiles is also shown in the bottom.

In general, we found a good correspondence between conversion and HOMO-LUMO gap. However, for the derivative **2a** with the BODIPY unit as EWG, the low HOMO-LUMO gap (1.06 eV) does not correspond to the low conversion found experimentally (25%). The BODIPY is a better EWG than the nitro group since it triggers a larger decrease of the LUMO energy than the nitro group (and consequently the HOMO-LUMO gap is smaller for the BODIPY derivative). However, conversion to product is one quarter of that obtained with β-nitrostyrene. Therefore, these differences between LUMO and HOMO cannot explain the observed trend and other factors must influence the reactivity, affecting the conversion.

This leads us to evaluate whether kinetic factors control the reactivity. Figure 4a shows the potential energy surface (PES) for the [3+2] cycloaddition reaction of ylide **1a** with **2a** in the presence of catalyst (Cu/**L6**). Figure 4b shows the corresponding PES using β-nitrostyrene as dipolarophile in the presence of catalyst (Cu/**L6**) and ylide **1a**. Therefore, a direct comparison of the reaction of BODIPY **2a** and β-nitrostyrene with **1a** is shown (Figure 4).

10.1002/adsc.201901465

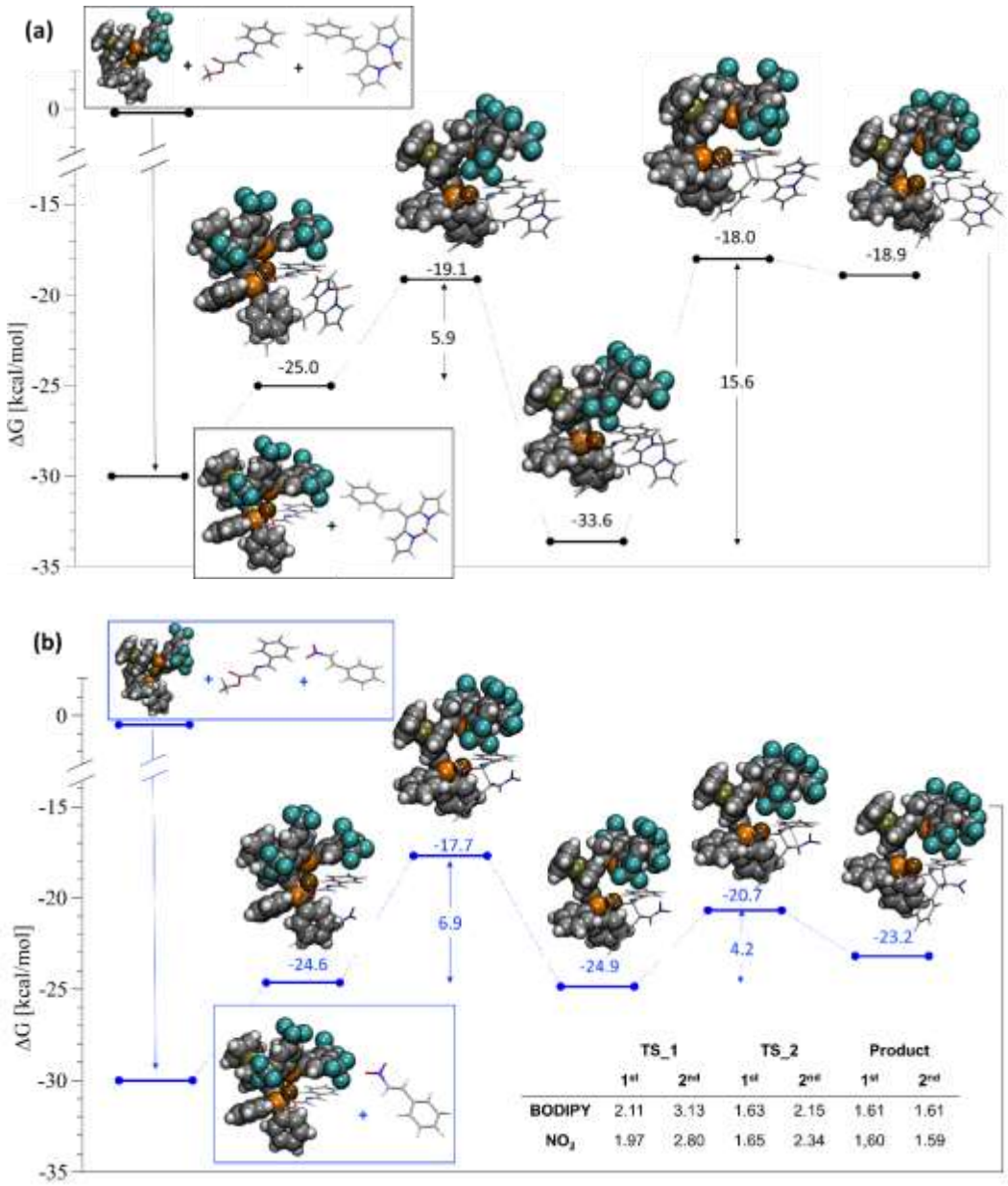

Figure 4. Potential energy surface for the [3+2] cycloaddition reaction of ylide **1a** in the presence of catalyst ($CuPF_6$/**L6**) with BODIPY alkene **2a (a)**, or with β-nitrostyrene **(b)**. PES computed at $SMD_{(Dichloromethane)}$/wB97X-D/6-311+G(d,p)//B3LYP/6-31G(d,p) level of theory. Relative Gibbs free energies are referred to the separate reactants (ylide **1a**, catalyst and dipolarophile (**(a)** BODIPY alkene **2a, (b)** β-nitrostyrene)). From left to right: separate reactants, PAC, 1st transition state (TS), intermediate, 2nd TS and final pyrrolidine product. A table with the distances of the 1st and 2nd C-C forming bonds for key structures is also shown.

The zero corresponds to the separated catalyst, dipole and dipolarophile. The first step is the exothermic formation of complex **I** between the catalyst and the dipole (Cu/**L6**/ylide-**1a**) as previously stated, which is 30 kcal/mol more stable than the separate reactants. Then, complex **I** forms, together with the dipolarophile (**2a** or β-nitrostyrene), a pre-association complex (PAC),[22] which is about 5 kcal/mol above in energy.

The mechanism for BODIPY substituted alkene **2a** and β-nitrostyrene is qualitatively similar. The [3+2] cycloaddition reaction is stepwise in both cases. Thus, the first energy barrier corresponds to the formation of the first new C-C bond leading to an intermediate. The second energy barrier corresponds to cyclization of the intermediate through the formation of a 2nd C-C bond, yielding the final products. Also in both cases this second step is reversible since the product is less stable than the intermediate. However, there are several quantitatively essential differences between the reaction mechanisms of the two considered dipolarophiles. For BODIPY derivative, the rate-

limiting step is the formation of the 2nd C-C bond. On the contrary, for β-nitrostyrene, the highest barrier corresponds to 1st C-C bond formation being this the rate-limiting step.

The intermediate is markedly more stable for **2a** (BODIPY) than for β-nitrostyrene. Moreover, β-nitrostyrene intermediate has about the same energy as the PAC while BODIPY intermediate is significantly more stable than its PAC (about 9 kcal/mol). This could be explained by the more significant charge separation found for the BODIPY derivative (see Figure S5 in the Supporting Information). Since BODIPY is a better EWG than nitro, the negative charge located in the alkene moiety is larger for the first one (0.74 vs. 0.60, respectively). Concomitantly, the positive charge located in the catalyst moiety is equivalently more substantial. The greater charge separation leads to a more significant dipole moment in the BODIPY alkene (21.6 D vs. 16.2 D) and a larger electrostatic stabilization of the BODIPY intermediate.

We can also explain these quantitative differences using the orbital picture. Thus, the 1st step is favored for BODIPY **2a** because the HOMO-LUMO gap is smaller (1.06 vs. 1.27 eV for **2a** and nitrostyrene, respectively). However, this interaction leads to the formation of a very stable intermediate compared to β-nitrostyrene. In addition, orbital overlap for formation of the product from the intermediate (2nd C-C bond) is much better for β-nitrostyrene (see Figure 5), making this process -and the overall reaction- faster for the latter one. Furthermore, β-nitrostyrene product is more stable than BODIPY product **3a**. Probably due to higher steric congestion at the BODIPY product.

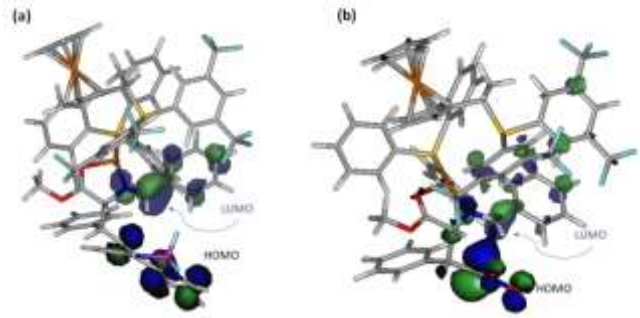

Figure 5. Frontier molecular orbitals in the intermediate of the reaction pathway computed at the B3LYP/6-31G(d,p). (a) BODIPY alkene **2a**; (b) β-nitrostyrene.

Overall, BODIPY is able to activate the double bond in the first C-C bond formation better than other typical EWGs used for [3+2] cycloaddition reactions in spite of its bulkiness. However, the second C-C bond requires more energy due to the high stabilization of the intermediate provided by the BODIPY group.

BODIPY pyrrolidine derivatives as probes for imaging. Taking into account that the synthesized pyrrolidines-BODIPYs **3a-n** showed excellent absorption and emission properties (see Figure 7b), similar to those described in the literature for other BODIPY derivatives,[3] we thought that it would be very interesting to evaluate the applicability of these pyrrolidine-BODIPYs **3** for live-cell imaging. We interrogated representative derivatives (**3a** and **3h**) for their ability to penetrate in three cellular lines, MEL 202 (uveal melanoma cell line), PANC-1 (pancreatic cancer cell line) and MCF7 (breast cancer cell line), and their propensity for nonspecific background staining. The results obtained with BODIPYs **3a** and **3h** were compared with the derivative **4**,[23] to determinate the influence of the pyrrolidine moiety and to show the advantage of having this structure joined to the BODIPY core.

First, we studied their toxicity by incubation during 24 h in the three cell lines mentioned at different concentrations. The BODIPY derivatives **3a**, **3h** and **4** were non-toxic up to 10 μM (Figure 6 and S6 in the Supporting Information). We observed a decrease in the viability of the cells when treated with the compounds at high concentrations (100 μM). However, this result is due to the presence of DMSO, required to solubilize the compounds at such concentration, since the viability reduction is the same when exposed only to DMSO in the three cell lines tested. Therefore, we selected 10 μM concentration for the next experiments.

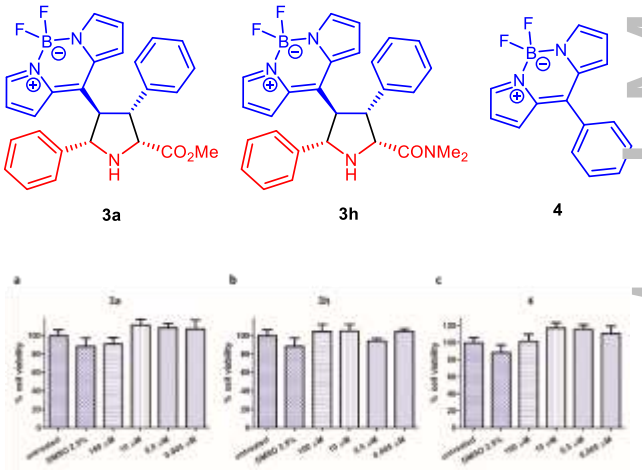

Figure 6. BODIPYs toxicity in PANC-1 cell line. The highest DMSO concentration employed was 2.5 %, the same DMSO amount present in the samples at 100 μM concentration. **(a)** BODIPY **3a**, **(b)** BODIPY **3h**, **(c)** BODIPY **4**.

We studied BODIPYs accumulation in the cell using lysotracker, as an endosomal probe (Figure 7a). The images show that BODIPYs were colocalized with the lysotracker in PANC-1, revealing that BODIPYs were accumulated in endosomal compartments. Moreover, the internalization of the BODIPY derivatives was also studied by flow cytometry (Figure 7c). In this assay, the peaks at the right imply better uptake by the cells. Therefore, the

internalization in PANC-1 was higher with BODIPY **3a** than BODIPY **3h**, and the latter was better uptaken than BODIPY **4** (Figure 7c). The same behavior was observed in MEL 202 and MCF-7 cell lines (see Supporting Information).

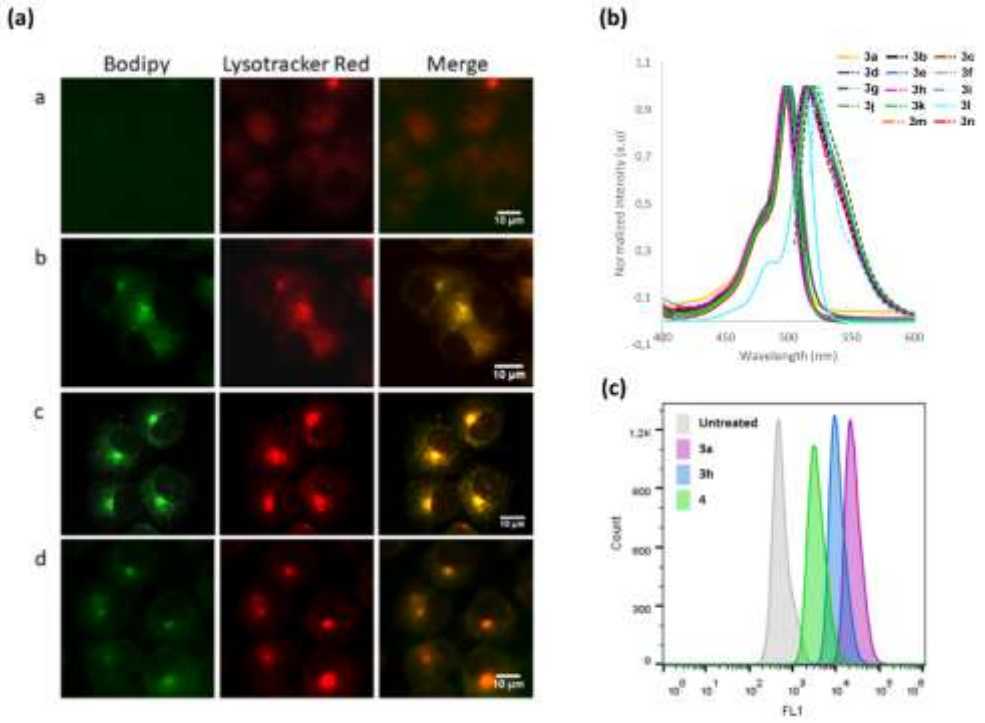

Figure 7. (a) BODIPYs localization in PANC-1 cells. In the first column, BODIPY fluorescence is showed in green, in the second one a lysotracker Red labeling to show the endosomal compartment and in the third column the merge. *Row a* corresponds to untreated PANC-1 cells. *Row b* to PANC-1 cells treated with 10 µM of BODIPY **3a**. *Row c* to PANC-1 cells treated with 10 µM of BODIPY **3h** and *Row d* to PANC-1 cells treated with 10 µM of BODIPY **4**. **(b)** Absorption and emission (dash-line) spectra of BODIPYs **3a-n** (see S.I. for details). **(c)** BODIPY uptake in PANC-1. The further to the right, the better the uptake.

This study highlights the potential use of the newly synthesized pyrrolidines-BODIPYs for imaging lysosomes in cells. All of them were localized in the endosomal compartment but the cellular uptake was very different between the different BODIPYs, obtaining the best result with the proline BODIPY **3a** in the three different tumoral cells.

Conclusion

In summary, we have reported an easy and versatile approach for preparation of pyrrolidine-BODIPY derivatives in high yields and excellent stereoselectivities by an asymmetric metal-catalyzed [3+2] cycloaddition reaction. Also, it has been shown that the BODIPY group is capable of activating double bonds in this type of reactions acting as an electron-withdrawing group. DFT studies show that, in this specific [3+2] cycloaddition, the BODIPY moiety, although it should work as a better EWG, is less reactive than a nitro group. This is because the intermediate generated in the first step of the cycloaddition is very stable in the case of the BODIPY-alkene because of the high charge separation between the catalyst/**L6**/dipole complex and the dipolarophile, leading to a great electrostatic stabilization. The derivatives were tested in three different cell lines revealing a selective accumulation in the lysosomes. Therefore, due to their inherent excellent fluorescent properties, the synthesized BODIPY derivatives could be used for the imaging of these organelles in live cells.

Experimental Section

General procedure for the [3+2] cycloaddition

An oven-dried 10 mL vial equipped with a magnetic stir bar was charged with $[Cu(CH_3CN)_4]PF_6$ (0.005 mmol, 5 mol%), (*R*)-Walphos ligand **L6** (0.006 mmol, 6 mol%) and the corresponding BODIPY substrate **2** (0.1 mmol). Then, anhydrous DCM (0.75 mL) were added, followed by the corresponding imine **2** (0.15 mmol, 1.5 equiv). The vial was closed with a PTFE/rubber septum and the reaction mixture was stirred at 4 °C for 15 minutes prior adding triethylamine (0.03 mmol, 30 mol%). Stirring was maintained at the same temperature for 12 hours. The solvent was removed under reduced pressure and the crude mixture was purified by flash chromatography (eluent indicated in each case) affording the corresponding pyrrolidines **3**.

Methyl (2*R*,3*R*,4*R*,5*S*)-4-(5,5-difluoro-5*H*-4λ^4,5λ^4-dipyrrolo[1,2-*c*:2',1'-*f*][1,3,2] diazaborinin-10-yl)-3,5-diphenylpyrrolidine-2-carboxylate (3a)

Pyrrolidine **3a** was obtained following the general procedure, from BODIPY **2a** and imine **1a**, after purification by flash chromatography (CyHex:EtOAc = 2:1) as a red solid (42 mg, 89% yield). $[\alpha]^{20}_D$ = - 139 (*c* = 0.035, $CHCl_3$). ^{1}H NMR (500 MHz, $CDCl_3$, 278 K): δ 7.80 (br s, 1H), 7.73 (br s, 1H), 7.62 (br s, 1H), 7.45 – 7.41 (m, 2H), 7.33 – 7.18 (m, 8H), 6.65 (br s, 2H), 6.20 (br s, 1H), 4.87 (d, *J* = 9.8 Hz, 1H), 4.68 (d, *J* = 9.4 Hz, 1H), 4.33 (t, *J* = 9.5 Hz, 1H), 3.87 (t, *J* = 9.7 Hz, 1H), 3.25 (s, 3H), 3.02 (br s, 1H). ^{13}C NMR (126 MHz, $CDCl_3$, 278 K): δ 172.6, 148.2, 145.8, 141.8, 139.5, 139.0, 137.2, 132.3, 129.7, 129.0, 128.7, 128.5, 127.8, 127.7, 127.6, 126.4, 118.8, 118.0, 72.5, 65.9, 59.7, 58.8, 51.9. ^{19}F NMR (282 MHz, $CDCl_3$, 298 K): δ -145.6 – -145.9 (m, 2F). HRMS (ESI+): calculated for $C_{27}H_{25}BF_2N_3O_2^+$, $[M+H]^+$ = 472.2002; found = 472.2008. The enantiomeric excess was determined by HPLC on a *Chiralpak* IB column: *n*-Hex/*i*-PrOH 40:60, flow rate 1.0 mL/min, λ = 495 nm, τ_{major} = 12.06 min, τ_{minor} = 7.06 min (98% *ee*).

Computational details

Geometry optimizations, orbital energies, harmonic frequency calculations, thermodynamic corrections and intrinsic reaction coordinate (IRC) calculations were computed with B3LYP functional combined with Pople's double-ξ basis set 6-31G(d,p), which includes polarization functions. Harmonic vibrational frequencies were computed to characterize minima and transition states (TS) and IRCs to verify connectivity between TSs and adjacent minima at the same level of theory - B3LYP/6-31G(d,p). More accurate values for the final energies were computed by means of single point calculations with ω-B97X-D functional and a larger, triple-ξ, basis set including diffuse functions, 6-311+G(d,p), over the geometries previously optimized. The range-separated hybrid functional ω-B97X-D includes Grimme's D2 dispersion correction, absent in B3LYP functional. The effect of the solvent (CH_2Cl_2) was also taken into account using the SMD continuum solvation model.

Biological studies

Viability assays: alamar blue. After treating the cells with the solutions of the compounds, a stock solution of resazurin sodium salt (Sigma-Aldrich, St. Louis, MO, USA) (1 mg/mL) in PBS was diluted 1% (v/v) in complete RPMI medium and added to the cells. After 3 h in the incubator (37 ˚C), the fluorescence was measured at 25 ˚C in a plate reader Synergy H4 Hybrid reader (BioTEK) λex = 550 nm, λem = 590 nm. The fluorescent intensity measurements were processed using the following equation: % Cell viability = ((Sample data - Negative control) / (Positive control - Negative control)) ×100. The positive control corresponds with untreated cells. A resazurin solution without cells was used as negative control.

Localization assay. The cells were harvested on coverslips. Then the bodipys were added in a final concentration of 10 µM. 24h later the cells were washed twice with PBS. Finally, 48 h after the treatment LisoTracker red DND-99 was dissolved in optiMEM to 50 nM final concentration. The solution was incubated 5 min with the cells at room temperature and the cells were then washed twice with PBS. Then, the samples were studied in a Leica DMI3000 M inverted microscope (Leica, Wetzlar, Germany) at 800 exposure units. The bodibys signal was observed with the green filter of the microscope (λ_{ex} 460-500 nm; λ_{em} 515-545 nm) and the lysotracker with the red filter (λ_{ex} 540-580 nm; λ_{em} 615-680 nm). The images were modified for a correct visualization with Fiji-Image J program.

Flow cytometry assay. After the treatment the cells were trypsinized for 5 min, then the process stopped with complete medium. The cells were washed with PBS and centrifugated with 177× g for 5 min in an Eppendorf centrifuge 5804 R (Eppendorf, Hamburg, Germany). The process was done twice. After that, the cells were analyzed in a Beckman Coulter Cytomics 500 Flow Cytometer (Beckman Coulter, Indianapolis, IN, USA) using 20000 cells.

Acknowledgements

This work was supported by the Spanish Government (RTI2018-095038-B-I00, CTQ2016-76061-P, SAF2017-87305-R), Comunidad de Madrid (IND2017/IND-7809), and co-financed by European Structural and Investment Fund. We acknowledge the generous allocation of computing time at the CCC (UAM). Financial support from the Spanish Ministry of Economy and Competitiveness, through the ''Maria de Maeztu'' Program of Excellence in R&D (MDM-2014-0377), is also acknowledged. Asociación Española Contra el Cáncer, and IMDEA Nanociencia acknowledge support from the 'Severo Ochoa' Programme for Centres of Excellence in R&D (MINECO, Grant SEV-2016-0686). F. E. and A. G. thank the Spanish Government for FPI-PhD. fellowships and E.M.A for FPU-PhD fellowship. P.M.R thanks the Ministry of Economy, Industry and competitiveness of Spain for the FPI grant (BES-2017.082521). A.M.S. thanks CAM for a postdoctoral contract (2016-T2/IND-1660).

References

[1] a) S. Kolemen, E. U. Akkaya, *Coord. Chem. Rev.* **2018**, *354*, 121-134; b) S. Krajcovicova, J. Stankova, P. Dzubak, M. Hajduch, M. Soural, M. A. Urban, *Chem. Eur. J.* **2018**, *24*, 4957-4966; c) R. Lincoln, L. E. Greene, W. Zhang, S. Louisia, G. Cosa, *J. Am. Chem. Soc.* **2017**, *139*, 16273-16281; d) T. Kowada, H. Maeda, K. Kikuchi, *Chem. Soc. Rev.* **2015**, *44*, 4953-4972; e) P. Rivera-Fuentes, S. J. Lippard, *Acc. Chem. Res.* **2015**, *48*, 2927-2934; f) Y. Ni, J. Wu, *Org. Biomol. Chem.* **2014**, *12*, 3774-3791.

[2] a) G. Ulrich, R. Ziessel, A. Harriman, *Angew. Chem. Int. Ed.* **2008**, *47*, 1184-1201; b) N. Boens, V. Leen, W. Dehaen, *Chem. Soc. Rev.* **2012**, *41*, 1130-1172; c) A. Loudet, K. Burgess, *Chem. Rev.* **2007**, *107*, 4891-4932.

[3] N. Boens, B. Verbelen, W. Dehaen, *Eur. J. Org. Chem.* **2015**, 6577-6595.

[4] a) W. Wang, M. M. Lorion, O. Martinazzoli, L. Ackermann, *Angew. Chem. Int. Ed.* **2018**, *57*, 10554-10558; b) L. Mendive-Tapia, C. Zhao, A. R. Akram, S. Preciado, F. Albericio, M. Lee, A. Serrels, N. Kielland, N. D. Read, R. Lavilla, M. Vendrell, *Nat. Commun* **2016**, *7*, 10940.

[5] a) P. S. Deore, D. V. Soldatov, R. A. Manderville, *Sci. Rep.* **2018**, *8*, 16874; b) M. H. Y. Cheng, H. Savoie, F. Bryden, R. W. Boyle, *Photochem. Photobiol. Sci.* **2017**, *16*, 1260-1267; c) N. Zhao, T. M. Williams, Z. Zhou, F. R. Fronczek, M. Sibrian-Vazquez, S. D. Jois, M. G. H. Vicente, *Bioconjugate Chem.* **2017**, *28*, 1566−1579; d) L. C. D. de Rezende, F. A. da Silva Emery, *Orbital Elec. J. Chem.* **2013**, *5*, 62-83.

[6] a) A. A. Morgan, E. Rubenstein, *PLOS One* **2013**, *8*, e53785; b) G. Wu, F. W. Bazer, R. C. Burghardt, G. A.

Johnson, S. Woo Kim, D. A. Knabe, P. Li, X. Li, J. R. McKnight, M. Carey Satterfield, T. E. Spencer, *Amino Acids* **2011**, *40*, 1053-1063; c) S Kaul, S. S. Sharma, I. K. Mehta, *Amino Acids* **2008**, *34*, 315-320.

[7] a) Y. Che, G. R. Marshall, *Biopolymers* **2006**, *81*, 392-406; b) S. M. Cowell, Y. S. Lee, J. P. Cain, V. J. Hruby, *Curr. Med. Chem.* **2004**, *11*, 2785-2798; c) P. Karoyan, S. Sagan, O. Lequin, J. Quancard, S. Lavielle, G. Chassaing in: *Targets in Heterocyclic Systems Vol. 8* (Eds.: O. A. Attanasi, D. Spinelli), RSC, Cambridge, **2004**, pp 216-273; d) C. Toniolo, M. Crisma, F. Formaggio, C. Peggion, *Biopolymers (Pept. Sci.)* **2001**, *60*, 396-419.

[8] X.-Y. Zheng, H.-L. Zhang, Q. Luo, J. Zhu, *J. Biomed. Biotechnol.* **2011**, *2011*, Article ID 457079.

[9] O. M. Pulido, *Mar. Drugs* **2008**, *6*, 180-219.

[10] H. Shinozaki, M. Ishida, Y. Gotoh, S. Kwak in: *Amino Acids* (Eds.: G. Lubec, G. A. Rosenthal), Springer, Dordrecht, **1990**, pp 281-293.

[11] F. Gray, L. Amphlett, H. Bright, L. Chambers, A. Cheasty, R. Fenwick, D. Haigh, D. Hartley, P. Howes, R. Jarvest, F. Mirzai, F. Nerozzi, N. Parry, M. Slater, S. Smith, P. Thommes, C. Wilkinson, E. Williams, *42nd Meeting of the European Association for the Study of Liver Diseases*, Barcelona, Spain, April 11–15, **2007**.

[12] a) G. Pandey, P. Banerjee, S. R. Gadre, *Chem. Rev.* **2006**, *106*, 4484-4517; b) J. Adrio, J. C. Carretero, *Chem. Commun.* **2011**, *47*, 6784-6794; c) J. Adrio, J. C. Carretero, *Chem. Commun.* **2014**, *50*, 12434-12446; d) T. Hashimoto, K. Maruoka, *Chem. Rev.* **2015**, *115*, 5366-5412.

[13] a) C. Bhat, S. G. Tilve, *RSC Adv.* **2014**, *4*, 5405-5452; b) M. I. Calaza, C. Cativiela, *Eur. J. Org. Chem.* **2008**, 3427-3448.

[14] a) A. Pascual-Escudero, A. de Cózar, F. P. Cossío, J. Adrio, J. C. Carretero, *Angew. Chem. Int. Ed.* **2016**, *55*, 15334-15338; b) K. Liu, Y. Xiong, Z.-F. Wang, H.-Y. Taoa, C.-J. Wang, *Chem. Commun.* **2016**, *52*, 9458-9461.

[15] a) A. Guerrero-Corella, J. Asenjo-Pascual, T. Janardan Pawar, S. Díaz-Tendero, A. Martín-Sómer, C. Villegas Gómez, J. L. Belmonte-Vázquez, D. E. Ramírez-Ornelas, E. Peña-Cabrera, A. Fraile, D. Cruz Cruz, J. Alemán, *Chem. Sci.* **2019**, *10*, 4346-4351; b) Y. Liu, X. Lv, M. Hou, Y. Shi, W. Guo, *Anal. Chem.* **2015**, *87*, 11475-11483.

[16] We carried out the reaction at -30 ºC but the conversion was very low and the ee value was similar to the obtaining at 4 ºC.

[17] CCDC 1899217 (**3k**) contains the crystallographic data. These data can be obtained free of charge at www.ccdc.cam.ac.uk.

[18] a) All the optimized structures computed can be visualized and download from http://dx.doi.org/10.19061/iochem-bd-8-6; b) M. Álvarez-Moreno, C. de Graaf, N. Lopez, F. Maseras, J. M. Poblet, C. Bo, *J. Chem. Inf. Model.* **2015**, *55*, 95-103.

[19] Gaussian 09, Revision E.01, M. J. Frisch et al., Gaussian, Inc., Wallingford CT, **2013**.

[20] I. Fleming, *Frontier Orbitals and Organic Chemical Reactions*, Wiley, London, **1978**.

[21] For cycloaddition with maleimide, β-nitrostyrene and dimethyl fumarate, see: S. Cabrera, R. Gómez Arrayás, J. C. Carretero, *J. Am. Chem. Soc.* **2005**, *127*, 16394-16395. For cycloaddition with (*E*)-4-phenylbut-3-en-2-one, see: b) J. Hernández-Toribio, R. Gómez Arrayás, B. Martín-Matute, J. C Carretero, *Org. Lett.* **2009**, *11*, 393-396.

[22] The importance of pre-association complexes (PAC) was studied in an aminocatalytic case, see: a) E. Arpa. M. Frías, C. Alvarado, J. Alemán, S. Díaz-Tendero, *J. Mol. Cat. A.* **2016**, *423*, 308-318; b) F. Aguilar- Galindo, A. M. Tuñón, A. Fraile, J. Alemán, S. Diaz- Tendero, *Theor. Chem. Acc.* **2019**, *138*, 59; c) A. Martín-Somer, E. M. Arpa, S. Díaz-Tendero, J. Alemán, *Eur. J. Org. Chem.* **2019**, 574-581.

[23] V. Leen, P. Yuan, L. Wang, N. Boens, W. Dehaen, *Org. Lett.* **2012**, *14*, 6150-6153.

Experimental Part
Chapter 6

(The complete “Supporting Information” documents, with all the characterization data, NMR spectra, SFC or HPLC traces and other experimental procedures have been included in the enclosed USB memory)

General procedure B for the [3+2] cycloaddition

An oven-dried 10 mL vial equipped with a magnetic stir bar was charged with $[Cu(CH_3CN)_4]PF_6$ (1.9 mg, 0.005 mmol, 0.05 equiv.), (*R*)-Walphos ligand **L6** (5.6 mg, 0.006 mmol, 0.06 equiv.) and the corresponding BODIPY substrate **2** (0.10 mmol). Then, anhydrous DCM (0.75 mL) were added, followed by the corresponding imine **1** (0.15 mmol, 1.5 equiv.). The vial was closed with a PTFE/rubber septum and the reaction mixture was stirred at 4 °C for 15 minutes prior adding triethylamine (4.2 µL, 0.03 mmol, 0.3 equiv.). Stirring was maintained at the same temperature for 12 hours. The solvent was removed under reduced pressure and the crude mixture was purified by flash chromatography (eluent indicated in each case) affording the corresponding pyrrolidines **3**.

Methyl (2*R*,3*R*,4*R*,5*S*)-4-(5,5-difluoro-5*H*-4λ^4,5λ^4-dipyrrolo[1,2-*c*:2',1'-*f*][1,3,2] diazaborinin-10-yl)-3,5-diphenylpyrrolidine-2-carboxylate (3a)

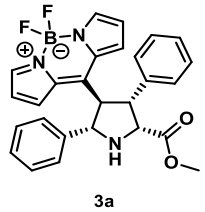

3a

Pyrrolidine **3a** was obtained following the general procedure B, from BODIPY **2a** and imine **1a**, after purification by flash chromatography (CyHex:EtOAc = 2:1) as an amorphous red solid (42 mg, 89% yield). The enantiomeric excess was determined by HPLC on a *Chiralpak* IB column: *n*-Hex/*i*-PrOH 40:60, flow rate 1.0 mL/min, λ = 495 nm, τ_{major} = 12.06 min, τ_{minor} = 7.06 min (98% *ee*).

$[\alpha]^{20}_D$ = - 139 (*c* = 0.035, $CHCl_3$).

^{1}H NMR (500 MHz, $CDCl_3$, 278 K): δ 7.80 (br s, 1H), 7.73 (br s, 1H), 7.62 (br s, 1H), 7.45 – 7.41 (m, 2H), 7.33 – 7.18 (m, 8H), 6.65 (br s, 2H), 6.20 (br s, 1H), 4.87 (d, *J* = 9.8 Hz, 1H), 4.68 (d, *J* = 9.4 Hz, 1H), 4.33 (t, *J* = 9.5 Hz, 1H), 3.87 (t, *J* = 9.7 Hz, 1H), 3.25 (s, 3H), 3.02 (br s, 1H).

^{13}C NMR (126 MHz, $CDCl_3$, 278 K): δ 172.6, 148.2, 145.8, 141.8, 139.5, 139.0, 137.2, 132.3, 129.7, 129.0, 128.7, 128.5, 127.8, 127.7, 127.6, 126.4, 118.8, 118.0, 72.5, 65.9, 59.7, 58.8, 51.9.

^{19}F NMR (282 MHz, $CDCl_3$, 298 K): δ -145.6 – -145.9 (m, 2F).

HRMS (ESI+): calculated for $C_{27}H_{25}BF_2N_3O_2^+$, $[M+H]^+$ = 472.2002; found = 472.2008.

Methyl (2*R*,3*R*,4*R*,5*S*)-4-(5,5-difluoro-5*H*-4λ^4,5λ^4-dipyrrolo[1,2-*c*:2',1'-*f*][1,3,2] diazaborinin-10-yl)-5-(4-methoxyphenyl)-3-phenylpyrrolidine-2-carboxylate (3b)

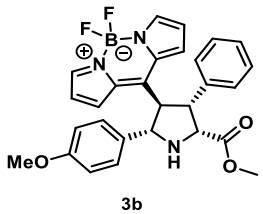

3b

Pyrrolidine **3b** was obtained following the general procedure B, from BODIPY **2a** and imine **1b**, after purification by flash chromatography (CyHex:EtOAc = 2:1) as an amorphous red solid (42 mg, 84% yield). The enantiomeric excess was determined by HPLC on a *Daicel Chiralpak* ID column: *n*-Hex/*i*-PrOH 40:60, flow rate 1.0 mL/min, λ = 495 nm, τ_{major} = 18.80 min, τ_{minor} = 12.09 min (98% *ee*).

$[\alpha]^{20}_D$ = - 74 (*c* = 0.040, $CHCl_3$).

^{1}H NMR (500 MHz, $CDCl_3$, 278 K): δ 7.79 (br s, 1H), 7.73 (br s, 1H), 7.60 (br s, 1H), 7.35 (d, *J* = 8.7 Hz, 2H), 7.28 – 7.17 (m, 5H), 6.81 (d, *J* = 8.7 Hz, 2H), 6.71 (br s, 1H), 6.63 (br s, 1H), 6.23 (br s, 1H), 4.83 (d, *J* = 9.8 Hz, 1H), 4.65 (d, *J* = 9.4 Hz, 1H), 4.32 (t, *J* = 9.6 Hz, 1H), 3.86 (t, *J* = 9.8 Hz, 1H), 3.74 (s, 3H), 3.24 (s, 3H), 2.92 (br s, 1H). ^{13}C NMR (126 MHz, $CDCl_3$, 278 K): δ 172.7, 159.5, 148.4, 145.7, 141.7, 139.0, 137.2, 132.3, 131.5, 129.7, 129.3, 128.7, 127.8, 127.7, 127.6, 118.8, 117.9, 114.2, 72.2, 65.8, 59.6, 58.9, 55.3, 51.9.

^{19}F NMR (471 MHz, $CDCl_3$, 278 K): δ -144.9 – -145.7 (m, 2F).

HRMS (ESI+): calculated for $C_{28}H_{27}BF_2N_3O_3^+$, $[M+H]^+$ = 502.2108; found = 502.2124.

Methyl (2*R*,3*R*,4*R*,5*S*)-4-(5,5-difluoro-5*H*-4λ^4,5λ^4-dipyrrolo[1,2-*c*:2',1'-*f*][1,3,2] diazaborinin-10-yl)-3-phenyl-5-(4-(trifluoromethyl)phenyl)pyrrolidine-2-carboxylate (3c)

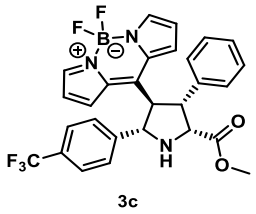

3c

Pyrrolidine **3c** was obtained following the general procedure B, from BODIPY **2a** and imine **1c**, after purification by flash chromatography (CyHex:EtOAc = 2:1) as an amorphous red solid (43 mg, 79% yield). The enantiomeric excess was determined by HPLC on a *Daicel Chiralpak* ID column: *n*-Hex/*i*-PrOH 40:60, flow rate 1.0 mL/min, λ = 495 nm, τ_{major} = 6.38 min, τ_{minor} = 5.28 min (93% *ee*).

$[\alpha]^{20}_D$ = + 10 (*c* = 0.055, $CHCl_3$).

^{1}H NMR (500 MHz, $CDCl_3$, 278 K): δ 7.82 (br s, 1H), 7.77 (br s, 1H), 7.61 (br s, 1H), 7.58 (d, *J* = 8.4 Hz, 2H), 7.55 (d, *J* = 8.5 Hz, 2H), 7.30 – 7.17 (m, 5H), 6.66 (br s, 1H), 6.59 (br d, *J* = 2.8 Hz, 1H), 6.23 (br d, *J* = 2.1 Hz, 1H), 4.95 (d, *J* = 9.8 Hz, 1H), 4.70 (d, *J* = 9.3 Hz, 1H), 4.33 (t, *J* = 9.4 Hz, 1H), 3.85 (t, *J* = 9.7 Hz, 1H), 3.27 (s, 3H), 2.99 (br s, 1H).

^{13}C NMR (126 MHz, $CDCl_3$, 278 K): δ 172.6, 147.2, 146.3, 144.0, 142.1, 138.7, 137.1, 132.2, 130.5 (q, J_{C-F} = 32.6 Hz), 129.6, 128.8, 127.9, 127.7, 127.6, 126.9, 125.9 (q, J_{C-F} = 3.6 Hz), 124.0 (q, J_{C-F} = 272.1 Hz), 119.1, 118.2, 71.4, 65.6, 59.2, 58.3, 51.9.

^{19}F NMR (471 MHz, $CDCl_3$, 278 K): δ -62.44 (s, 3F), -145.1 (ddd, *J* = 104.6, 56.9, 28.2 Hz, 1F), -145.70 (ddd, *J* = 106.1, 56.6, 28.0 Hz, 1F).

HRMS (ESI+): calculated for $C_{28}H_{24}BF_5N_3O_2^+$, $[M+H]^+$ = 540.1876; found = 540.1865.

Methyl (2*R*,3*R*,4*R*,5*S*)-4-(5,5-difluoro-5*H*-4λ^4,5λ^4-dipyrrolo[1,2-*c*:2',1'-*f*][1,3,2] diazaborinin-10-yl)-3-phenyl-5-(*o*-tolyl)pyrrolidine-2-carboxylate (3d)

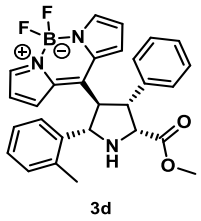

3d

Pyrrolidine **3d** was obtained following the general procedure B, from BODIPY **2a** and imine **1d**, after purification by flash chromatography (CyHex:EtOAc = 2:1) as an amorphous red solid (43 mg, 88% yield). The enantiomeric excess was determined by HPLC on a *Daicel Chiralpak* ID column: *n*-Hex/*i*-PrOH 40:60, flow rate 1.0 mL/min, λ = 495 nm, τ_{major} = 10.47 min, τ_{minor} = 8.12 min (95% *ee*).

$[\alpha]^{20}_D$ = + 3 (*c* = 0.034, $CHCl_3$).

^{1}H NMR (500 MHz, $CDCl_3$, 278 K): δ 7.99 (d, *J* = 7.5 Hz, 1H), 7.77 (br s, 1H), 7.74 (br s, 1H), 7.68 (br s, 1H), 7.32 (t, *J* = 7.5 Hz, 1H), 7.29 – 7.24 (m, 4H), 7.23 – 7.19 (m, 1H), 7.13 (td, *J* = 7.5, 1.1 Hz, 1H), 6.99 (d, *J* = 7.5 Hz, 1H), 6.70 (br s, 1H), 6.65 (br s, 1H), 6.22 (br s, 1H), 5.18 (d, *J* = 9.8 Hz, 1H), 4.69 (d, *J* = 9.4 Hz, 1H), 4.39 (t, *J* = 9.5 Hz, 1H), 3.92 (t, *J* = 9.8 Hz, 1H), 3.25 (s, 3H), 1.95 (s, 3H).

^{13}C NMR (126 MHz, $CDCl_3$, 278 K): δ 172.7, 148.0, 145.8, 141.7, 139.1, 137.9, 137.0, 136.5, 132.4, 130.9, 129.7, 128.7, 128.0, 127.8, 127.7, 127.3, 127.0, 125.0, 118.8, 118.0, 67.7, 66.0, 59.8, 58.9, 51.9, 19.5.

^{19}F NMR (471 MHz, $CDCl_3$, 278 K): δ -144.97 – -145.95 (m, 2F).

HRMS (ESI+): calculated for $C_{28}H_{27}BF_2N_3O_2^+$, $[M+H]^+$ = 486.2159; found = 486.2152.

Methyl (2*S*,3*S*,4*S*,5*R*)-4-(5,5-difluoro-5*H*-4λ^4,5λ^4-dipyrrolo[1,2-*c*:2',1'-*f*][1,3,2] diazaborinin-10-yl)-5-(furan-2-yl)-3-phenylpyrrolidine-2-carboxylate (3e)

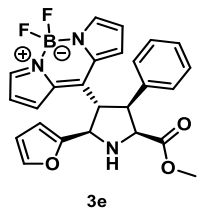

3e

Pyrrolidine **3e** was obtained following the general procedure B, from BODIPY **2a** and imine **1e**, using the (*S*)-Walphos as catalyst, after purification by flash chromatography (gradient of CyHex:EtOAc = from 2:1 to 1:1) as an amorphous red solid (26 mg, 56% yield). The enantiomeric excess was determined by HPLC on a *Daicel Chiralpak* ID column: *n*-Hex/*i*-PrOH 40:60, flow rate 1.0 mL/min, λ = 495 nm, τ_{major} = 12.15 min, τ_{minor} = 15.70 min (97% *ee*).

$[\alpha]^{20}_D$ = + 91 (*c* = 0.05, $CHCl_3$).

^{1}H NMR (500 MHz, $CDCl_3$, 243 K): δ 7.81 (br s, 2H), 7.52 (br s, 1H), 7.47 (s, 1H), 7.33 – 7.27 (m, 2H), 7.27 – 7.20 (m, 3H), 6.99 (br s, 1H), 6.66 (br s, 1H), 6.37 (br s, 1H), 6.29 – 6.27 (m, 1H), 6.24 (d, *J* = 2.9 Hz, 1H), 4.90 (d, *J* = 9.8 Hz, 1H), 4.67 (d, *J* = 9.5 Hz, 1H), 4.34 (t, *J* = 9.5 Hz, 1H), 4.25 (t, *J* = 9.6 Hz, 1H), 3.21 (s, 3H).

^{13}C NMR (126 MHz, $CDCl_3$, 243 K): δ 171.7, 150.2, 148.1, 146.0, 143.1, 142.1, 138.7, 137.0, 132.1, 129.6, 128.8, 128.0, 127.8, 127.3, 119.2, 118.3, 110.7, 109.2, 66.3, 66.2, 59.6, 56.6, 52.3.

^{19}F NMR (471 MHz, $CDCl_3$, 243 K): δ -143.98 – -144.49 (m, 1F), -145.32 – -145.82 (m, 1F).

HRMS (ESI+): calculated for $C_{25}H_{23}BF_2N_3O_3^+$, $[M+H]^+$ = 462.1795; found = 462.1784.

Methyl (2*R*,3*R*,4*R*,5*S*)-4-(5,5-difluoro-5*H*-4λ^4,5λ^4-dipyrrolo[1,2-*c*:2',1'-*f*][1,3,2] diazaborinin-10-yl)-3-phenyl-5-(thiophen-2-yl)pyrrolidine-2-carboxylate (3f)

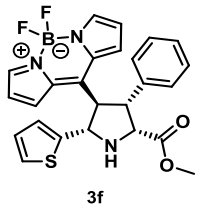

3f

Pyrrolidine **3f** was obtained following the general procedure B, from BODIPY **2a** and imine **1f**, after purification by flash chromatography (gradient of CyHex:EtOAc = from 2:1 to 1:1) as an amorphous red solid (31 mg, 64% yield). The enantiomeric excess was determined by HPLC on a *Daicel Chiralpak* IB column: *n*-Hex/*i*-PrOH 40:60, flow rate 1.0 mL/min, λ = 495 nm, τ_{major} = 16.93 min, τ_{minor} = 9.10 min (94% *ee*).

$[\alpha]^{20}_D$ = - 97 (*c* = 0.034, $CHCl_3$).

^{1}H NMR (500 MHz, $CDCl_3$, 243 K): δ 7.82 (br s, 2H), 7.55 (br d, J = 4.3 Hz, 1H), 7.32 – 7.20 (m, 6H), 6.89 – 6.86 (m, 3H), 6.66 (br dd, *J* = 4.4, 2.0 Hz, 1H), 6.33 (br dd, *J* = 4.4, 1.9 Hz, 1H), 5.16 (d, *J* = 9.7 Hz, 1H), 4.69 (d, *J* = 9.4 Hz, 1H), 4.30 (t, *J* = 9.4 Hz, 1H), 3.95 (t, *J* = 9.5 Hz, 1H), 3.24 (s, 3H), 3.14 (br s, 1H).

^{13}C NMR (126 MHz, $CDCl_3$, 243 K): δ 172.0, 147.6, 146.1, 142.8, 142.0, 138.7, 137.1, 132.0, 129.9, 128.7, 127.7, 127.6, 127.4, 127.1, 125.6, 125.3, 119.1, 118.1, 68.0, 65.8, 60.0, 59.0, 52.0.

^{19}F NMR (471 MHz, $CDCl_3$, 243 K): δ -144.33 – -145.35 (m, 2F).

HRMS (ESI+): calculated for $C_{25}H_{23}BF_2N_3O_2S^+$, $[M+H]^+$ = 478.1567; found = 478.1576.

Methyl (2*R*,3*R*,4*R*,5*R*)-5-cyclohexyl-4-(5,5-difluoro-5*H*-4λ^4,5λ^4-dipyrrolo[1,2-*c*:2',1'-*f*][1,3,2]diazaborinin-10-yl)-3-phenylpyrrolidine-2-carboxylate (3g)

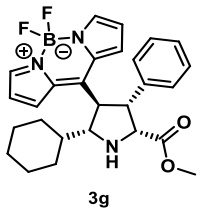

3g

Pyrrolidine **3g** was obtained following the general procedure B, from BODIPY **2a** and imine **1g**, (40% yield by ^{1}H NMR employing 9-bromo phenanthrene as the internal standard). An analytical sample of **3g** was obtained after various purifications by flash chromatography (gradient of CyHex:EtOAc = from 2:1 to 1:1) as an amorphous red solid (5 mg, 10% yield). The enantiomeric excess was determined by HPLC on a *Daicel Chiralpak* ID column: *n*-Hex/*i*-PrOH 80:20, flow rate 1.0 mL/min, λ = 495 nm, τ_{major} = 9.03 min, τ_{minor} = 6.39 min (98% *ee*).

^{1}H NMR (500 MHz, $CDCl_3$, 278 K): δ 7.77 (br s, 2H), 7.45 – 7.40 (m, 2H), 7.35 – 7.27 (m, 3H), 7.26 – 7.19 (m, 4H), 4.88 (d, *J* = 9.8 Hz, 1H), 4.68 (d, *J* = 9.4 Hz, 1H), 4.33 (t, *J* = 9.5 Hz, 1H), 3.87 (t, *J* = 9.7 Hz, 1H), 3.26 (s, 3H), 1.33 – 1.18 (m, 7H), 0.93 – 0.77 (m, 4H).

HRMS (ESI+): calculated for $C_{27}H_{31}BF_2N_3O_2^+$, $[M+H]^+$ = 478.2472; found = 472.2503.

(2*R*,3*R*,4*R*,5*S*)-4-(5,5-Difluoro-5*H*-4λ^4,5λ^4-dipyrrolo[1,2-*c*:2',1'-*f*][1,3,2]diazaborinin-10-yl)-*N*,*N*-dimethyl-3,5-diphenylpyrrolidine-2-carboxamide (3h)

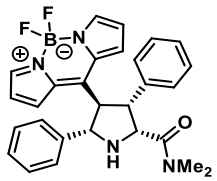

3h

Pyrrolidine **3h** was obtained following the general procedure B, from BODIPY **2a** and imine **1h**, after purification by flash chromatography (EtOAc) as an amorphous red solid (40 mg, 83% yield). The enantiomeric excess was determined by HPLC on a *Daicel Chiralpak* IC column: *n*-Hex/*i*-PrOH 0:100, flow rate 1.0 mL/min, λ = 495 nm, τ_{major} = 12.11 min, τ_{minor} = 7.07 min (98% *ee*).

$[\alpha]^{20}_D$ = - 211 (*c* = 0.042, $CHCl_3$).

^{1}H NMR (500 MHz, $CDCl_3$, 278 K): δ 7.75 (br s, 1H), 7.66 (br s, 2H), 7.48 (d, *J* = 7.0 Hz, 2H), 7.29 (t, *J* = 7.4 Hz, 2H), 7.25 – 7.20 (m, 1H), 7.22 – 7.14 (m, 5H), 6.83 (br d, *J* = 4.4 Hz, 1H), 6.63 (br s, 1H), 6.21 (br d, *J* = 2.8 Hz, 1H), 4.92 (d, *J* = 10.3 Hz, 1H), 4.84 (d, *J* = 9.6 Hz, 1H), 4.42 (dd, *J* = 11.6, 9.5 Hz, 1H), 3.88 (t, *J* = 11.0 Hz, 1H), 2.64 (s, 3H), 2.42 (s, 3H).

^{13}C NMR (126 MHz, $CDCl_3$, 278 K): δ 171.2, 148.3, 145.5, 141.4, 139.0, 137.2, 137.1, 132.2, 129.8, 129.1, 128.5 (2C), 128.2, 128.0, 127.4, 126.5, 118.7, 117.8, 73.2, 62.5, 61.4, 60.6, 36.4, 35.8.

^{19}F NMR (471 MHz, $CDCl_3$, 278 K): δ -145.08 – -145.82 (m, 2F).

HRMS (ESI+): calculated for $C_{28}H_{28}BF_2N_4O^+$, $[M+H]^+$ = 485.2319; found = 485.2322.

Methyl (2*R*,3*R*,4*R*,5*S*)-4-(5,5-difluoro-5*H*-4λ^4,5λ^4-dipyrrolo[1,2-*c*:2',1'-*f*][1,3,2] diazaborinin-10-yl)-3-(4-methoxyphenyl)-5-phenylpyrrolidine-2-carboxylate (3i)

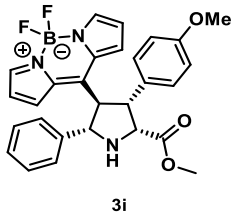

3i

Pyrrolidine **3i** was obtained following the general procedure B, from BODIPY **2b** and imine **1a**, after purification by flash chromatography (CyHex:EtOAc = 2:1) as an amorphous red solid (37 mg, 73% yield). The enantiomeric excess was determined by HPLC on a *Daicel Chiralpak* IB column: *n*-Hex/*i*-PrOH 40:60, flow rate 1.0 mL/min, λ = 495 nm, τ_{major} = 12.70 min, τ_{minor} = 7.19 min (97% *ee*).

$[\alpha]^{20}_D$ = - 222 (*c* = 0.040, $CHCl_3$).

^{1}H NMR (500 MHz, $CDCl_3$, 278 K): δ 7.80 (br s, 1H), 7.73 (br s, 1H), 7.61 (br s, 1H), 7.46 – 7.41 (m, 2H), 7.33 – 7.21 (m, 3H), 7.15 (d, *J* = 8.8 Hz, 2H), 6.78 (d, *J* = 8.7 Hz, 2H), 6.67 (br s, 1H), 6.64 (br s, 1H), 6.22 (br s, 1H), 4.86 (br d, *J* = 9.6 Hz, 1H), 4.64 (br s, 1H), 4.29 (t, *J* = 9.4 Hz, 1H), 3.83 (t, *J* = 9.7 Hz, 1H), 3.74 (s, 3H), 3.31 (s, 3H).

^{13}C NMR (126 MHz, $CDCl_3$, 278 K): δ 172.8, 158.9, 148.4, 145.7, 141.7, 139.6, 137.2, 132.4, 130.8, 129.7, 129.0, 128.8, 128.5, 127.6, 126.4, 118.8, 117.9, 113.9, 72.4, 65.8, 59.9, 58.3, 55.3, 52.0.

^{19}F NMR (471 MHz, $CDCl_3$, 278 K): δ -145.10 (ddd, *J* = 102.9, 57.1, 27.9 Hz, 1F), -145.64 (ddd, *J* = 105.9, 56.3, 27.5 Hz, 1F).

HRMS (ESI+): calculated for $C_{28}H_{27}BF_2N_3O_3$+, $[M+H]^+$ = 502.2108; found = 502.2100.

Methyl (2*R*,3*R*,4*R*,5*S*)-4-(5,5-difluoro-5*H*-4λ^4,5λ^4-dipyrrolo[1,2-*c*:2',1'-*f*][1,3,2] diazaborinin-10-yl)-5-phenyl-3-(4-(trifluoromethyl)phenyl)pyrrolidine-2-carboxylate (3j)

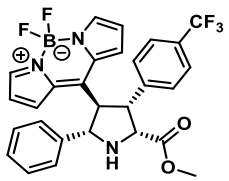

3j

Pyrrolidine **3j** was obtained following the general procedure B, from BODIPY **2c** and imine **1a**, after purification by flash chromatography (CyHex:EtOAc = 2:1) as an amorphous red solid (46 mg, 86% yield). The enantiomeric excess was determined by HPLC on a *Daicel Chiralpak* IB column: *n*-Hex/*i*-PrOH 40:60, flow rate 1.0 mL/min, λ = 495 nm, τ_{major} = 9.62 min, τ_{minor} = 5.96 min (93% *ee*).

$[\alpha]^{20}_D$ = - 149 (*c* = 0.038, $CHCl_3$).

^{1}H NMR (500 MHz, $CDCl_3$, 278 K): δ 7.83 (br s, 1H), 7.76 (br s, 1H), 7.60 (br s, 1H), 7.54 (d, *J* = 8.1 Hz, 2H), 7.43 – 7.39 (m, 4H), 7.32 – 7.23 (m, 3H), 6.67 (br s, 1H), 6.56 (br s, 1H), 6.22 (br s, 1H), 4.86 (d, *J* = 9.7 Hz, 1H), 4.73 (d, *J* = 9.2 Hz, 1H), 4.35 (t, *J* = 9.2 Hz, 1H), 3.79 (t, *J* = 9.4 Hz, 1H), 3.28 (s, 3H), 3.02 (br s, 1H).

^{13}C NMR (126 MHz, $CDCl_3$, 278 K): δ 172.1, 147.3, 146.2, 143.8, 142.1, 139.3, 137.1, 132.3, 129.9 (q, J_{CF} = 32.7 Hz), 129.5, 129.0, 128.6, 128.2, 127.6, 126.3, 125.7 (q, J_{CF} = 3.6 Hz), 124.0 (q, J_{CF} = 272.1 Hz), 119.1, 118.2, 72.2, 65.5, 59.9, 57.8, 52.0.

^{19}F NMR (471 MHz, $CDCl_3$, 278 K): δ -62.46 (s, 3F), -144.72 (ddd, *J* = 105.4, 57.2, 28.2 Hz, 1F), -145.98 (ddd, *J* = 106.1, 56.1, 27.7 Hz, 1F).

HRMS (ESI+): calculated for $C_{28}H_{24}BF_5N_3O_2^+$, $[M+H]^+$ = 540.1876; found = 540.1871.

Methyl (2*R*,3*R*,4*R*,5*S*)-3-(4-chlorophenyl)-4-(5,5-difluoro-5*H*-4λ^4,5λ^4-dipyrrolo[1,2-*c*:2',1'-*f*][1,3,2]diazaborinin-10-yl)-5-phenylpyrrolidine-2-carboxylate (3k)

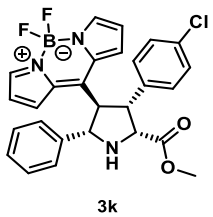

3k

Pyrrolidine **3k** was obtained following the general procedure B, from BODIPY **2d** and imine **1a**, after purification by flash chromatography (CyHex:EtOAc = 2:1) as an amorphous red solid (43 mg, 85% yield). The enantiomeric excess was determined by HPLC on a *Daicel Chiralpak* IB column: *n*-Hex/*i*-PrOH 40:60, flow rate 1.0 mL/min, λ = 495 nm, τ_{major} = 8.89 min, τ_{minor} = 6.26 min (97% *ee*).

$[\alpha]^{20}_D$ = - 157 (*c* = 0.040, $CHCl_3$).

^{1}H NMR (500 MHz, $CDCl_3$, 278 K): δ 7.81 (br s, 1H), 7.76 (br s, 1H), 7.59 (br s, 1H), 7.41 (d, *J* = 7.1 Hz, 2H), 7.33 – 7.18 (m, 7H), 6.65 (br s, 1H), 6.59 (br s, 1H), 6.22 (br s, 1H), 4.85 (d, *J* = 9.7 Hz, 1H), 4.68 (d, *J* = 9.3 Hz, 1H), 4.27 (t, *J* = 9.3 Hz, 1H), 3.75 (t, *J* = 9.5 Hz, 1H), 3.33 (s, 3H), 2.99 (br s, 1H).

^{13}C NMR (126 MHz, $CDCl_3$, 278 K): δ 172.3, 147.6, 146.1, 142.0, 139.4, 138.0, 137.1, 133.5, 132.3, 129.6, 129.1, 129.0, 128.9, 128.6, 127.6, 126.3, 119.0, 118.1, 72.1, 65.5, 60.0, 57.8, 52.0.

^{19}F NMR (471 MHz, $CDCl_3$, 278 K): δ -144.92 (ddd, *J* = 105.0, 57.2, 28.1 Hz, 1F), -145.80 (ddd, *J* = 106.0, 56.2, 27.8 Hz, 1F).

HRMS (ESI+): calculated for $C_{27}H_{24}BClF_2N_3O_2^+$, $[M+H]^+$ = 506.1613; found = 506.1604.

Methyl (2*R*,3*R*,4*R*,5*S*)-4-(3,7-diethyl-5,5-difluoro-5*H*-4λ^4,5λ^4-dipyrrolo[1,2-*c*:2',1'-*f*][1,3,2]diazaborinin-10-yl)-3,5-diphenylpyrrolidine-2-carboxylate (3l)

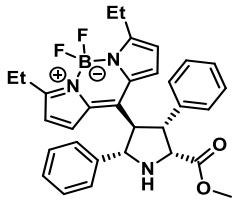

3l

Pyrrolidine **3l** was obtained following the general procedure B, from BODIPY **2e** and imine **1a**, after purification by flash chromatography (CyHex:EtOAc = 2:1) as an amorphous red solid (28 mg, 53% yield). The enantiomeric excess was determined by HPLC on a *Daicel Chiralpak* IB column: *n*-Hex/*i*-PrOH 40:60, flow rate 1.0 mL/min, λ = 495 nm, τ_{major} = 12.24 min, τ_{minor} = 5.75 min (91% *ee*).

$[\alpha]^{20}_D$ = - 62 (*c* = 0.10, $CHCl_3$).

^{1}H NMR (500 MHz, $CDCl_3$, 278 K): δ 7.48 – 7.43 (m, 3H), 7.33 – 7.28 (m, 2H), 7.28 – 7.22 (m, 5H), 7.22 – 7.17 (m, 1H), 6.53 (br d, *J* = 4.4 Hz, 1H), 6.46 (br d, *J* = 4.2 Hz, 1H), 6.04 (br d, *J* = 4.4 Hz, 1H), 4.86 (d, *J* = 9.9 Hz, 1H), 4.66 (d, *J* = 9.4 Hz, 1H), 4.28 (t, *J* = 9.4 Hz, 1H), 3.78 (t, *J* = 9.7 Hz, 1H), 3.24 (s, 3H), 3.03 (q, *J* = 7.5 Hz, 2H), 2.92 – 2.86 (m, 2H), 1.34 (t, *J* = 7.6 Hz, 3H), 1.18 (t, *J* = 7.6 Hz, 3H).

^{13}C NMR (126 MHz, $CDCl_3$, 278 K): δ 172.7, 165.2, 160.7, 142.7, 139.9, 139.6, 136.4, 131.6, 128.90, 128.6, 128.5, 128.3, 127.9, 127.6, 126.6 (2C), 117.6, 116.4, 71.8, 65.8, 58.9, 58.5, 51.9, 22.1, 21.9, 12.7, 12.3.

^{19}F NMR (471 MHz, $CDCl_3$, 278 K): δ -145.65 – -146.48 (m, 2F).

HRMS (ESI+): calculated for $C_{31}H_{33}BF_2N_3O_2^+$, $[M+H]^+$ = 528.2628; found = 528.2629.

Methyl (2*R*,3*S*,4*R*,5*S*)-4-(5,5-difluoro-5*H*-4λ^4,5λ^4-dipyrrolo[1,2-*c*:2',1'-*f*][1,3,2]diazaborinin-10-yl)-3-octyl-5-phenylpyrrolidine-2-carboxylate (3m)

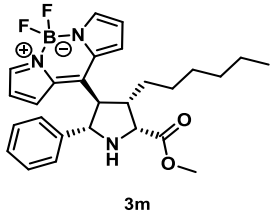

3m

Pyrrolidine **3m** was obtained following the general procedure B, from BODIPY **2f** and imine **1a**, after purification by flash chromatography (gradient of CyHex:EtOAc from 3:1 to 1:1) as an amorphous red solid (42 mg, 88% yield). The enantiomeric excess was determined by HPLC on a *Daicel Chiralpak* ID column: *n*-Hex/*i*-PrOH 80:20, flow rate 1.0 mL/min, λ = 495 nm, τ_{major} = 24.58 min, τ_{minor} = 20.30 min (97% *ee*).

$[\alpha]^{20}_D$ = + 86 (*c* = 0.06, $CHCl_3$).

^{1}H NMR (500 MHz, $CDCl_3$, 278 K): δ 7.81 (s, 2H), 7.54 (br s, 1H), 7.37 (d, *J* = 7.6 Hz, 2H), 7.28 – 7.18 (m, 3H), 6.89 (br s, 1H), 6.60 (br s, 1H), 6.32 (br s, 1H), 4.75 (d, *J* = 8.9 Hz, 1H), 4.41 – 4.36 (m, 1H), 3.83 (s, 3H), 3.44 (t, *J* = 10.3 Hz, 1H), 3.25 – 3.16 (m, 1H), 2.90 (br s, 1H), 1.40 – 1.02 (m, 10H), 0.79 (t, *J* = 7.0 Hz, 3H).

^{13}C NMR (126 MHz, $CDCl_3$, 278 K): δ 174.6, 149.1, 145.3, 142.0, 140.2, 137.2, 132.5, 129.3, 128.9, 128.3, 127.9, 126.5, 118.6, 118.0, 72.6, 63.6, 57.7, 53.6, 52.2, 31.5, 30.9, 29.3, 27.7, 22.5, 14.1.

^{19}F NMR (471 MHz, $CDCl_3$, 278 K): δ -144.12 (ddd, *J* = 104.7, 57.8, 28.2 Hz, 1F), -147.05 (ddd, *J* = 105.6, 55.6, 27.0 Hz, 1F).

HRMS (ESI+): calculated for $C_{27}H_{33}BF_2N_3O_2^+$, $[M+H]^+$ = 480.2628; found = 480.2633.

Methyl (2*R*,3*R*,4*R*,5*S*)-4-(5,5-difluoro-5*H*-4λ^4,5λ^4-dipyrrolo[1,2-*c*:2',1'-*f*][1,3,2]diazaborinin-10-yl)-2-methyl-3,5-diphenylpyrrolidine-2-carboxylate (3n)

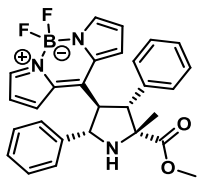

3n

Pyrrolidine **3n** was obtained following the general procedure B, from BODIPY **2a** and imine **1n**, after purification by flash chromatography (gradient of CyHex:EtOAc from 3:1 to 1:1) as an amorphous red solid (15 mg, 30% yield). The enantiomeric excess was determined by HPLC on a *Daicel Chiralpak* ID column: *n*-Hex/*i*-PrOH 40:60, flow rate 1.0 mL/min, λ = 495 nm, τ_{major} = 8.32 min, τ_{minor} = 7.44 min (39% *ee*).

$[\alpha]^{20}_D$ = - 6 (*c* = 0.034, $CHCl_3$).

^{1}H NMR (500 MHz, $CDCl_3$, 278 K): δ 7.73 (br s, 1H), 7.71 – 7.65 (m, 2H), 7.50 – 7.46 (m, 2H), 7.32 – 7.26 (m, 2H), 7.26 – 7.18 (m, 4H), 7.13 – 7.10 (m, 2H), 7.05 (br s, 1H), 6.63 (br s, 1H), 6.30 (br s, 1H), 4.99 (d, *J* = 10.1 Hz, 1H), 4.23 (dd, *J* = 12.5, 10.2 Hz, 1H), 4.10 (d, *J* = 12.5 Hz, 1H), 3.26 (s, 3H), 1.77 (s, 2H).

^{13}C NMR (126 MHz, $CDCl_3$, 278 K): δ 176.0, 147.3, 145.5, 141.6, 139.4, 137.2, 135.9, 132.3, 129.7, 129.0, 128.7, 128.5, 128.1, 127.6, 127.4, 126.5, 118.7, 118.0, 71.7, 71.5, 68.0, 57.7, 52.4, 26.6.

^{19}F NMR (471 MHz, $CDCl_3$, 278 K): δ -144.95 (ddd, J = 104.0, 57.0, 28.0 Hz), -145.79 (ddd, J = 110.0, 58.0, 27.7 Hz).

HRMS (ESI+): calculated for $C_{28}H_{27}BF_2N_3O_2^+$, $[M+H]^+$ = 486.2159; found = 486.2208.

Summary of Results

Summary of Results

During this PhD thesis, we have dealt with the development of novel photocatalytic processes and new photocatalysts, which allowed us to report the following results:

Photocatalytic Cyclopropane Ring Expansion (Chapter 2)

Angew. Chem. Int. Ed. **2017**, *56*, 7826-7830

The photocatalytic ring-opening of enantioenriched vinyl cyclopropane derivatives has led to the obtainment of a ring-expansion reaction through a vinyl cyclopropane rearrangement. Furthermore, retention of the chiral information of the starting materials has been observed in the corresponding dihydrofurane and cyclopentene derivatives. The ring-expansion reaction worked through a triplet energy transfer mechanism, allowed by the employment of a specific iridium photocatalyst. Indeed, the triplet energy of the photosensitizer was in accordance with the theoretically calculated singlet-triplet energy gap of the nitrocyclopropane obtained from DFT studies. By means of experimental and theoretical evidences, it has been demonstrated that the nitrocyclopropane derivative required the presence of a nitro group in its structure to unlock the desired triplet photosensitization. Indeed, the cyclopropanes that were substituted by other electron-withdrawing groups presented an increased triplet energy that did not permit the ring-opening with the employed photocatalyst. Furthermore, DFT calculations revealed the reasons behind the observed regioselectivity of the process.

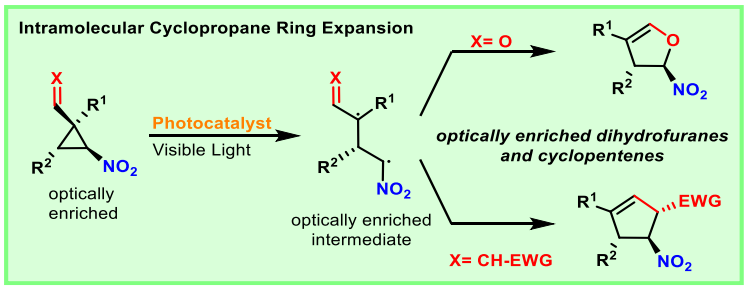

Scheme 124. Summary of results of Chapter 2.

Synthesis of a Bifunctional Photo-aminocatalyst (Chapter 3)

ACS Catal. **2018**, *8*, 5928-5940

The synthesis of a bifunctional photo-aminocatalyst based on an imidazolidinone-like structure and a thioxanthone photocatalytic moiety has been carried out. The bifunctional system worked in the asymmetric α-alkylation of aldehydes as a photoredox catalyst for the generation of radical species from bromo derivatives and as an efficient aminocatalyst, delivering the desired enantioenriched products. Although in this reaction the bifunctional catalyst has not been found advantageous over dual catalytic systems, the differences between the two processes have been studied through additional mechanistic experiments. In this case we have demonstrated that the steric hindrance around the active center of the involved

intermediates had a huge impact over the single-electron transfer events from both radical and excited species, which should be taken into account for the development of future catalysts.

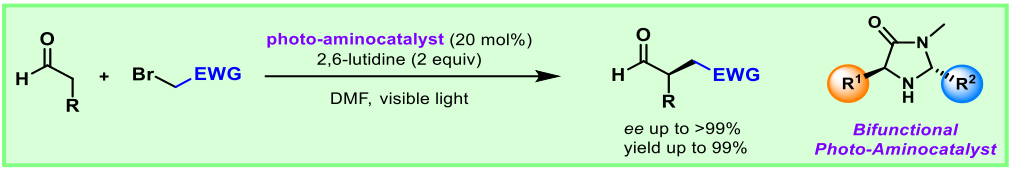

Scheme 125. Summary of results of Chapter 3.

Enantioselective [2+2] Photocycloaddition of Enones (Chapter 4)

Submitted

The first aminocatalytic enantioselective [2+2] photocycloaddition of enones has been achieved through the development of a new activation mode which relies on the formation of an intramolecular iminium ion-based EDA complex intermediate. The direct excitation of this transient generated species at the charge transfer absorption band permitted the exclusive excitation of the chiral iminium ion employing visible light irradiation and avoiding any undesired racemic background process. Indeed, the charge transfer state can be converted to an iminium-localized singlet excited species by means of an equilibrium in the excited state, leading to a stereocontrolled [2+2] photocycloaddition. This iminium ion catalytic strategy allowed the synthesis of enantioenriched cyclobutanes that would be inaccessible through the employment of the activation modes reported in the literature. Furthermore, the mechanistic proposal has been supported by DFT and TDDFT calculations and additional experiments.

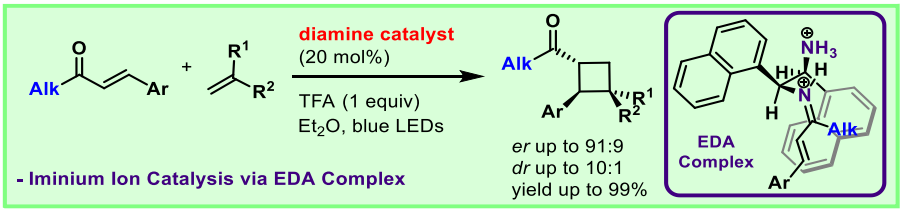

Scheme 126. Summary of results of Chapter 4.

Acridinium-based Organophotocatalysts (Chapter 5)

Chem. Eur. J. **2018**, *24*, 12509-12514

Chem. Photo. Chem. **2019**, *3*, 609-612

In the context of photoredox catalysis, the synthesis of new structurally different acridinium-based photocatalysts have been achieved by replacing the normally employed electron-donating mesityl moiety for an imide-based scaffold. This apparently minor change permits to avoid an intramolecular single-electron transfer that unlocks the generation of a charge transfer species, which is easily deactivated by thermal processes through non-radiative pathways. The new imide-acridinium photocatalysts have been efficiently employed in some photocatalytic reactions showing better performances in comparison with the normally used acridinium

catalysts. The reasons of this being essentially attributable to the lack of charge transfer species in the new catalysts which are working from a localized singlet excited state. Fluorescence quenching measurements and DFT calculations have provided a strong support to the different behavior of the studied acridinium-based systems, helping the possible future development of this kind of photocatalysts.

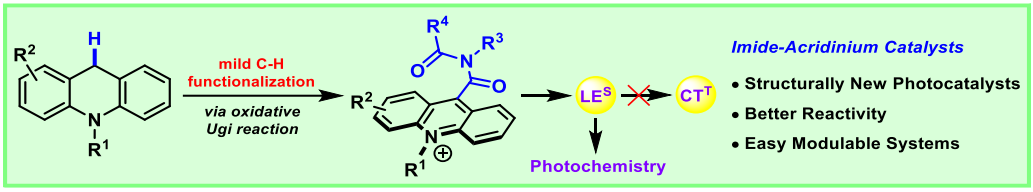

Scheme 127. Summary of results of Chapter 5.

Metal-catalyzed Asymmetric [3+2] Cycloaddition (Chapter 6)

Adv. Synth. Catal. **2020** (DOI: 10.1002/adsc.201901465)

A copper-catalyzed asymmetric 1,3 dipolar cycloaddition has been developed, permitting the obtainment of enantioenriched BODIPY-containing pyrrolidines. The incorporation of the fluorescent BODIPY moiety has been achieved employing azomethine ylides and *meso*-substituted alkenyl BODIPY derivatives through a [3+2] cycloaddition. Indeed, the alkene double bond resulted highly activated through nucleophilic addition by means of the particular electronic properties of the BODIPY core. Furthermore the corresponding cyclized products showed a remarkable fluorescence which was not observed in the starting BODIPY derivatives. The copper-catalytic system and the electron-withdrawing properties of the BODIPY moiety have been investigated by means of theoretical calculations, whereas the five-membered enantioenriched products have been employed as efficient biosensors for cell imaging purposes, giving the opportunity for a future development in the functionalization of peptides.

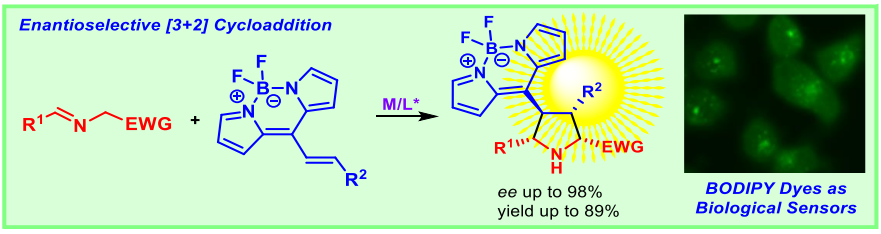

Scheme 128. Summary of results of Chapter 6.

Conclusions

Conclusiones

En la presente tesis doctoral se han investigado dos campos bien diferenciados, el desarrollo de nuevos procesos fotocatalíticos y la síntesis de nuevos fotocatalizadores. En una primera parte (capítulo 2), hemos desarrollado una expansión fotocatalítica estereoespecifica de ciclopropanos enantioenriquecidos, permitiéndonos obtener dihidrofuranos y ciclopentenos con retención de la información quiral. La reacción se ha llevado a cabo a través de una transferencia de energía desde un estado excitado triplete de un fotocatalizador de iridio. La energía del triplete de este último es de hecho comparable con la energía requerida para una fotosensitización del ciclopropano, probando mediante cálculos DFT y pruebas experimentales que el proceso tenía lugar a través de una transferencia de energía. Adicionalmente, pruebas experimentales y teóricas han demostrado que el ciclopropano necesita la presencia de un grupo nitro en su estructura, ya que con otros grupos electrón atractores la energía requerida para una fotosensitización vía triplete no es alcanzada por ninguno de los fotocatalizadores estudiados.

En el tercer capítulo hemos llevado a cabo la síntesis de un foto-aminocatalizador bifuncional que está basado en una estructura de imidazolidinona y que contiene como unidad fotocatalítica una tioxantona. Esta última actúa como fotocatalizador en un proceso redox y, además, constituye uno de los sustituyentes que se necesitan alrededor del centro catalítico para llevar a cabo la reacción de α-alquilación asimétrica de aldehídos. Si bien es cierto que en esta reacción no se han encontrado ventajas en el uso de un sistema bifuncional en comparación a un sistema de múltiples catalizadores, las diferencias entre ambos sistemas se han investigados mediante pruebas mecanísticas adicionales. En este caso, se ha observado que el impedimento estérico de los intermedios de reacción tiene una gran importancia en procesos de transferencia de un electrón entre especies radicalarias o especies excitadas, lo cual se debería tener en cuenta en el desarrollo de futuros catalizadores y sistemas catalíticos.

En la presente tesis doctoral (capítulo 4) también se ha desarrollado una nueva estrategia para la formación de ciclobutanos gracias a una fotocicloadición [2+2] enantioselectiva. En la bibliografía, solo han sido publicadas algunas versiones catalíticas enantioselectivas, todas ellas basadas en el uso de ácidos de Lewis o catalizadores de enlace de hidrógeno. Durante esta tesis se ha desarrollado una fotocicloadición [2+2] asimétrica empleando la catálisis de ion iminio como nuevo modo de activación de enonas. Esta estrategia tiene la ventaja de no necesitar ningún sustrato prefuncionalizado para dar una coordinación bidentada con el ácido de Lewis o con el catalizador de enlace de hidrogeno y, además, de no requerir ningún fotocatalizador externo. Este resultado se logró mediante la utilización de un intermedio electrón dador-aceptor (EDA) quiral que se forma en el medio de reacción entre el aminocatalizador y la enona. La transferencia de un electrón intramolecularmente da lugar en el compuesto a una nueva banda de absorción en el espectro visible, permitiendo la excitación de este intermedio quiral y evitando la irradiación de la enona, la cual daría lugar a la reacción racémica.

En el contexto de la catálisis fotoredox se han sintetizado también diferentes fotocatalizadores de acridinio basados en una nueva estructura en la que el grupo electrón donador normalmente usado se ha reemplazado por un grupo imídico (capítulo 5). Este aparente pequeño cambio de la estructura permite bloquear una transferencia intramolecular de un electrón que da lugar a una especie a transferencia de carga, la cual es fácilmente desactivada por procesos térmicos no radiativos. Los nuevos catalizadores de acridinio han sido eficazmente empleados en algunas reacciones fotocatalíticas, demostrando su mayor

fotoactividad en comparación con los que están reportados en la bibliografía. Las razones de esta mejora pueden ser explicadas mediante el análisis de las propiedades fotofísicas y por cálculos computacionales, ayudando un posible futuro desarrollo de catalizadores basados en acridinio.

Por último, en el capítulo 6, hemos desarrollado una reacción 1,3 dipolar asimétrica catalizada por cobre, la cual ha permitido obtener unas pirrolidinas funcionalizadas con cromóforos fluorescentes basados en una estructura de BODIPY. Las pirrolidinas se han obtenido con excelentes enantioselectividades empleando iluros de azometino y derivados de BODIPY sustituidos en la posición *meso* por un grupo alquenilo. De esta manera, el doble enlace del alqueno resulta fuertemente activado gracias a las propiedades electrón-atractoras que el cromóforo ejerce en esta posición. Además, debido a las propiedades fotofísicas de los BODIPYs, el derivado alquenil-sustituido no presenta fluorescencia alguna, mientras que los compuestos finales son altamente fluorescentes. Aprovechando este hecho, las correspondientes pirrolidinas que han sido sintetizadas se han empleado en distintas líneas celulares, demostrando su alta fluorescencia en un cultivo real, y su aplicación como biosensores.

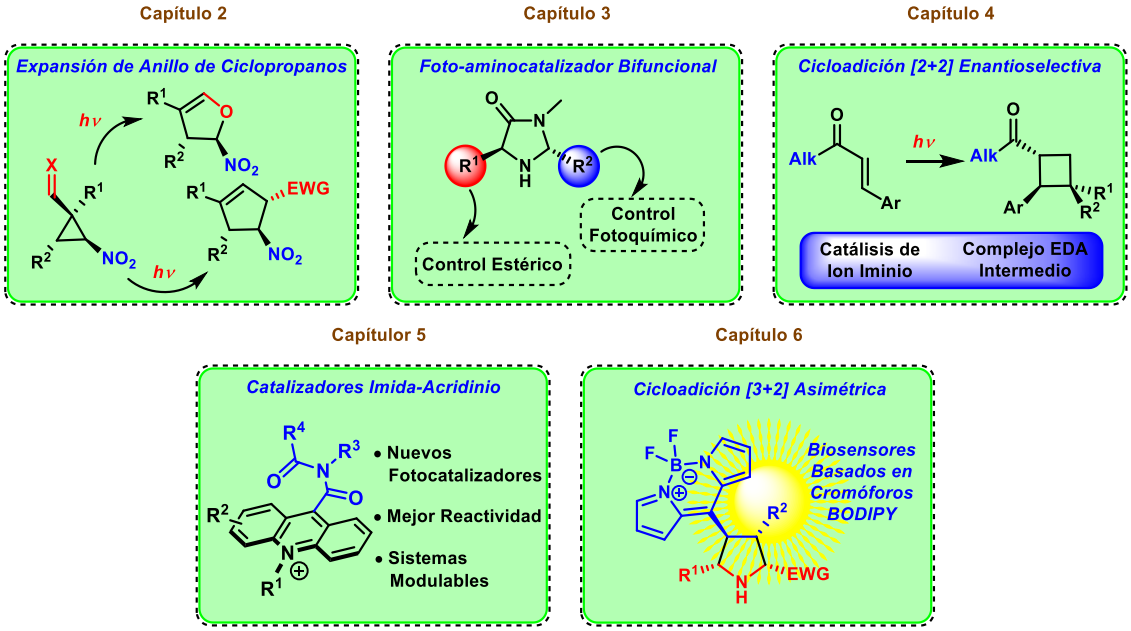

Figura 9. Resultados de la presente tesis doctoral.

References:

1. M. Oelgemöller, *Chem. Rev*. **2016**, *116*, 9664-9682.
2. A. Albini, V. Dichiarante, *Photochem. Photobiol. Sci*. **2009**, *8*, 248-254.
3. (a) G. Ciamician, P. Silber, *Ber. Dtsch. Chem. Ges.* **1908**, *41*, 1928-1935; the structure of the cyclobutane was confirmed by subsequent studies: (b) G. Büchi, I. M. Goldman, *J. Am. Chem. Soc*. **1957**, *79*, 4741-4748; (c) J. Meinwald, R. A. Schneider, *J. Am. Chem. Soc*. **1965**, *87*, 5218-5229.
4. G. Ciamician, P. Silber, *Ber. Dtsch. Chem. Ges*. **1900**, *33*, 2911-2913.
5. G. Ciamician, *Science* **1912**, *36*, 385-394.
6. M. D. Kärkäs, J. A. Porco Jr., C. R. J. Stephenson, *Chem. Rev*. **2016**, *116*, 9683-9747.
7. (a) C. R. J. Stephenson, T. P. Yoon, D. W. C. MacMillan "Visible Light Photocatalysis in Organic Chemistry", **2018**, Wiley-VCH; (b) R. Brimioulle, D. Lenhart, M. M. Maturi, T. Bach, *Angew. Chem. Int. Ed*. **2015**, *54*, 3872-3890; (c) E. Meggers, *Chem. Commun*. **2015**, *51*, 3290-3301; (d) A. F. Garrido-Castro, M. C. Maestro, J. Alemán, *Tetrahedron Lett.* **2018**, *59*, 1286-1294. (e) C. Jiang, W. Chen, W.-H. Zheng, H. Lu, *Org. Biomol. Chem*. **2019**, *17*, 8673-8689.
8. (a) C. Prier, D. Rankic, D. W. C. MacMillan, *Chem. Rev*. **2013**, *113*, 5322-5363; (b) J. M. R. Narayanam, C. R. J. Stephenson, *Chem. Soc. Rev*. **2011**, *40*, 102-113; (c) N. A. Romero, D. A. Nicewicz, *Chem. Rev.* **2016**, 116, 10075-10166; (d) M. H. Shaw, J. Twilton, D. W. C. MacMillan, *J. Org. Chem.* **2016**, *81*, 6898-6926. (e) b) J. Twilton, C. Le, P. Zhang, M. H. Shaw, R. W. Evans, D. W. C. MacMillan, *Nat Rev Chem*. **2017**, *1*, 0052.
9. E. C. Gentry and R. R. Knowles, *Acc. Chem. Res*. **2016**, *49*, 1546-1556.
10. G. J. Kavarnos, N. J. Turro, *Chem. Rev.* **1986**, *86,* 401-449.
11. Q.-Q. Zhou, Y.-Q. Zou, L.-Q. Lu, W.-J. Xiao, *Angew. Chem. Int. Ed.* **2019**, *58*, 1586-1604.
12. C. G. S. Lima, T. de M. Lima, M. Duarte, I. D. Jurberg, M. W. Paixão, *ACS Catal*. **2016**, *6*, 1389-1407.
13. D. M. Hedstrand, W. M. Kruizinga, R. M. Kellogg, *Tetrahedron Lett*. **1978**, *19*, 1255-1258.
14. H. Cano-Yelo, A. Deronzier, *Tetrahedron Lett*. **1984**, *25*, 5517-5520.
15. H. Cano-Yelo, A. Deronzier, *J. Chem. Soc., Perkin Trans. 2* **1984**, 1093-1098.
16. K. Okada, K. Okamoto, N. Morita, K. Okubo, M. Oda, *J. Am. Chem. Soc.* **1991**, *113*, 9401-9402.
17. A. Bauer, F. Westkamper, S. Grimme, T. Bach, *Nature* **2005**, *436*, 1139-1140.
18. (a) M. A. Ischay, M. E. Anzovino, J. Du, T. P. Yoon, *J. Am. Chem. Soc.* **2008**, *130*, 12886-12887; for a closely related intermolecular version reported by the same research group see: (b) J. Du, T. P. Yoon, *J. Am. Chem. Soc.* **2009**, *131*, 14604-14605.
19. D. A. Nicewicz, D. W. C. MacMillan, *Science* **2008**, *322*, 77-80.
20. J. M. R. Narayanam, J. W. Tucker, C. R. J. Stephenson, *J. Am. Chem. Soc.* **2009**, *131*, 8756-8757.
21. M. A. Cismesia, T. P. Yoon, *Chem. Sci.*, **2015**, *6*, 5426-5434.
22. (a) M. A. Ischay, Z. Lu, T. P. Yoon, *J. Am. Chem. Soc.* **2010,** *132*, 8572-8574; for a closely related intermolecular version reported by the same research group see: (b) M. A. Ischay, M. S. Ament, T. P. Yoon, *Chem. Sci*., **2012**, *3*, 2807-2811.
23. (a) S. Lin, M. A. Ischay, C. G. Fry, T. P. Yoon, *J. Am. Chem. Soc*. **2011**, *133*, 19350-19353; for a closely related intramolecular version reported by the same research group see: (b) S. Lin, C. E. Padilla, M. A. Ischay, T. P. Yoon, *Tetrahedron Lett.* **2012**, *53*, 3073-3076.
24. S. Maity, M. Zhu, R. S. Shinabery, N. Zheng, *Angew. Chem. Int. Ed.* **2012**, *51*, 222-226.
25. J. Wang, N. Zheng, *Angew. Chem. Int. Ed.* **2015**, *54*, 11424-11427.
26. D. S. Hamilton, D. A. Nicewicz, *J. Am. Chem. Soc.* **2012**, *134*, 18577-18580.
27. (a) K. A. Margrey, D. A. Nicewicz, *Acc. Chem. Res.* **2016**, *49*, 1997-2006; (b) A. R. White, L. Wang, D. A. Nicewicz, *Synlett* **2019**, *30*, 827-832.
28. E. H. Discekici, N. J. Treat, S. O. Poelma, K. M. Mattson, Z. M. Hudson, Y. Luo, C. J. Hawker, J. Read de Alaniz, *Chem. Commun.,* **2015**, *51*, 11705-11708.
29. N. Noto, T. Koike, M. Akita, *ACS Catal.* **2019**, *9*, 4382-4387.
30. T. Koike, M. Akita, *Chem* **2018**, *4*, 409-437.
31. B. Schweitzer-Chaput, M. A. Horwitz, E. de Pedro Beato, P. Melchiorre, *Nat. Chem.* **2019**, *11*, 129-135.
32. (a) J. C. Tellis, D. N. Primer, G. A. Molander, *Science,* **2014***, 345*, 433-436; (b) Z. Zuo, D. T. Ahneman, L. Chu, J. A. Terrett, A. G. Doyle, D. W. C. MacMillan, *Science,* **2014***, 345*, 437-440.
33. S. Y. Reece, J. M. Hodgkiss, J. Stubbe, D. G. Nocera, *Philos. Trans. R. Soc., B* **2006**, *361*, 1351-1364.
34. K. T. Tarantino, P. Liu, R. R. Knowles*, J. Am. Chem. Soc.* **2013**, *135*, 10022-10025.
35. G. J. Choi, R. R. Knowles, *J. Am. Chem. Soc*. **2015**, *137*, 9226-9229.
36. (a) A. J. Musacchio, L. Q. Nguyen, G. H. Beard, R. R. Knowles, *J. Am. Chem. Soc.* **2014**, *136*, 12217-12220; (b) A. J. Musacchio, B. C. Lainhart, X. Zhang, S. G. Naguib, T. C. Sherwood, R. R. Knowles, *Science* **2017**, *355*, 727-730; (c) D. C. Miller, J. M. Ganley, A. J. Musacchio, T. C. Sherwood, W. R. Ewing, R. R. Knowles, *J. Am. Chem. Soc.* **2019**, *141*, 16590-16594; (d) David C. Miller, G. J. Choi, H. S. Orbe, R. R. Knowles, *J. Am. Chem. Soc.* **2015**, *137*, 13492-13495; (e) K. Zhao, K. Yamashita, J. E. Carpenter, T. C. Sherwood, W. R. Ewing, P. T. W. Cheng, R. R. Knowles, *J. Am. Chem. Soc*. **2019**, *141*, 8752-8757; (f) G. J. Choi, Q. Zhu, D. C. Miller, C. J. Gu, R. R. Knowles, *Nature* **2016**, *539*, 268-271.
37. D. A. DiRocco, K. Dykstra, S. Krska, P. Vachal, D. V. Conway, M. Tudge, *Angew. Chem. Int. Ed.* **2014**, *53*, 4802-4806.
38. H. Ikezawa, C. Kutal, K. Yasufuku, H. Yamazaki, *J. Am. Chem. Soc.* **1986,** *108,* 1589-1594.
39. R. R. Islangulov, F. N. Castellano, *Angew. Chem.* **2006**, *118*, 6103-6105.
40. C. Müller, A. Bauer, T. Bach, *Angew. Chem. Int. Ed*. **2009**, *48*, 6640-6642.
41. Z. Lu, T. P. Yoon, *Angew. Chem. Int. Ed*. **2012**, *51*, 10329-10332.
42. Y.-Q. Zou, S.-W. Duan, X.-G. Meng, X.-Q. Hu, S. Gao, J.-R. Chen, W.-J. Xiao, *Tetrahedron* **2012**, *68*, 6914-6919.

43. T. Lei, C. Zhou, M.-Y. Huang, L.-M. Zhao, B. Yang, C. Ye, H. Xiao, Q.-Y. Meng, V. Ramamurthy, C.-H. Tung, L.-Z. Wu, *Angew. Chem. Int. Ed*. **2017**, *56*, 15407-15410.
44. N. Münster, N. A. Parker, L. van Dijk, R. S. Paton, M. D. Smith, *Angew. Chem. Int. Ed.* **2017**, *56*, 9468-9472.
45. D. R. Heitz, J. C. Tellis, G. A. Molander, *J. Am. Chem. Soc.* **2016**, *138*, 12715-12718.
46. E. R. Welin, C. Le, D. M. Arias-Rotondo, J. K. McCusker, D W. C. MacMillan, *Science* **2017**, *355*, 380-385.
47. (a) M. Osawa, H. Nagai, M. Akita, *Dalton Trans.* **2007**, *8*, 827-829; (b) W.‑J., Yoo, T. Tsukamoto, S. Kobayashi, *Org. Lett.* **2015**, *17*, 3640-3642.
48. J. Xuan, X.-D. Xia, T.-T. Zeng, Z.-J. Feng, J.-R. Chen, L.-Q. Lu, W.-J. Xiao, *Angew. Chem. Int. Ed*. **2014**, *53*, 5653-5656.
49. R. S. Mulliken, *J. Am. Chem. Soc*. **1950**, *72*, 600-608. (b) R. S. Mulliken, *J. Am. Chem. Soc*. **1952**, *74*, 811-824.
50. For some selected examples see: (a) S. Fukuzumi, K. Mochida, J. K. Kochi, *J. Am. Chem. Soc.* **1979**, *101*, 5961-5972; (b) H. C. Gardner, J. K. Kochi, *J. Am. Chem. Soc*. **1976**, *98*, 2460-2469; (c) D. Cantacuzène, R. Dorme, *Tetrahedron Lett.* **1975**, *16*, 2031-2034; (d) M. A. Fox, J. Younathan, G. E. Fryxell, *J. Org. Chem.* **1983**, *48*, 3109-3112; (e) M. Patz, S. Fukuzumi, *J. Phys. Org. Chem*. **1997**, *10*, 129-137.
51. Y. Weia, Q.-Q. Zhou, F. Tan, L.-Q. Lu, W-J Xiao, Synthesis **2019**, *51*, 3021-3054.
52. P. V. Pham, D. A. Nagib, D. W. C. MacMillan, *Angew. Chem. Int. Ed.* **2011**, *50*, 6119-6122.
53. M. Tobisu, T. Furukawa, N. Chatani, *Chem. Lett.* **2013**, *42*, 1203-1205.
54. (a) E. Arceo, I. D. Jurberg, A. Álvarez-Fernández, P. Melchiorre, *Nat. Chem*. **2013**, *5*, 750-756; (b) E. Arceo, A. Bahamonde, G. Bergonzini, P. Melchiorre, *Chem. Sci*., **2014**, *5*, 2438–2442; (c) Ł. Woźniak, J. J. Murphy, P. Melchiorre, *J. Am. Chem. Soc*. **2015**, *137*, 5678-5681; (d) Z.-Y. Cao, T. Ghosh, P. Melchiorre, *Nat. Commun*. **2018**, *9*, 3274.
55. (a) M. Nappi, G. Bergonzini, P. Melchiorre, *Angew. Chem. Int. Ed*. **2014**, *53*, 4921-4925; (b) S. R. Kandukuri, A. Bahamonde, I. Chatterjee, I. D. Jurberg, E. C. Escudero-Adán, P. Melchiorre, *Angew. Chem.Int. Ed.* **2015**, *54*, 1485-1489.
56. I. Bosque, T. Bach, *ACS Catal*. **2019**, *9*, 9103-9109.
57. G. S. Hammond, R. S. Cole, *J. Am. Chem. Soc.* **1965**, *87*, 3256-3257.
58. (a) R. Hoffmann, Y. Inoue, *J. Am. Chem. Soc.* **1999**, *121*, 10702-10710; for a similar pioneering study achieving a 41% of *ee* see: (b) Y. Inoue, T. Yokoyama, N. Yamasaki, A. Tai, *Nature* **1989**, *341*, 225-226.
59. J.-I. Kim, G. B. Schuster, *J. Am. Chem. Soc.* **1990**, *112*, 9635-9637.
60. A. Córdova, H. Sundén, M. Engqvist, I. Ibrahem, J. Casas, *J. Am. Chem. Soc.* **2004**, *126*, 8914-8915.
61. P. Melchiorre, *Angew. Chem. Int. Ed.* **2009**, *48*, 1360-1363.
62. R. Alonso, T. Bach, *Angew. Chem. Int. Ed*. **2014**, *53*, 4368-4371.
63. H. Guo, E. Herdtweck, T. Bach, *Angew. Chem. Int. Ed.* **2010**, *49*, 7782-7785.
64. R. Brimioulle, T. Bach, *Science* **2013**, *342*, 840-843.
65. J. Du, K. L. Skubi, D. M. Schultz, T. P. Yoon, *Science* **2014**, *344*, 392-396.
66. T. R. Blum, Z. D. Miller, D. M. Bates, I. A. Guzei, T. P. Yoon, *Science* **2016**, *354*, 1391-1395.
67. Z. D. Miller, B. J. Lee, T. P. Yoon, *Angew. Chem. Int. Ed*. **2017**, *56*, 11891-11895.
68. M. E. Daub, H. Jung, B. J. Lee, J. Won, M.-H. Baik, T. P. Yoon, *J. Am. Chem. Soc*. **2019**, *141*, 9543-9547.
69. For asymmetric [2+2] photocycloadditions enabled by the use of a chiral hydrogen-bonding Iridium photocatalyst reported by the Yoon's lab, see: (a) K. L. Skubi, J. B. Kidd, H. Jung, I. A. Guzei, M.-H. Baik, T. P. Yoon, *J. Am. Chem. Soc.* **2017**, *139*, 17186-17192; (b) J. Zheng, W. B. Swords, H. Jung, K. L. Skubi, J. B. Kidd, G. J. Meyer, M.-H. Baik, T. P. Yoon, *J. Am. Chem. Soc*. **2019**, *141*, 13625-13634.
70. A. G. Amador, E. M. Sherbrook, T. P. Yoon, *J. Am. Chem. Soc*. **2016**, *138*, 4722-4725.
71. L. Ruiz Espelt, I. S. McPherson, E. M. Wiensch, T. P. Yoon, *J. Am. Chem. Soc.* **2015**, *137*, 2452-2455.
72. D. A. DiRocco, T. Rovis, *J. Am. Chem. Soc*. **2012**, *134*, 8094-8097.
73. G. Bergonzini, C. S. Schindler, C.-J. Wallentin, E. N. Jacobsen, C. R. J. Stephenson, *Chem. Sci.* **2014**, *5*, 112-116.
74. L. J. Rono, H. G. Yayla, D. Y. Wang, M. F. Armstrong, R. R. Knowles, *J. Am. Chem. Soc*. **2013**, *135*, 17735-17738.
75. D. Uraguchi, N. Kinoshita, T. Kizu, T. Ooi *J. Am. Chem. Soc.* **2015**, *137*, 13768-13771 (in this case a PCET mechanism is unlikely as reported by the authors).
76. M. Silvi, E. Arceo, I. D. Jurberg, C. Cassani, P. Melchiorre, *J. Am. Chem. Soc*. **2015**, *137*, 6120-6123.
77. For mechanistic studies regarding the α-alkyation of enamines, see: A. Bahamonde, P. Melchiorre, *J. Am. Chem. Soc.* **2016**, *138*, 8019-8030.
78. G. Filippini, M. Silvi, P. Melchiorre, *Angew. Chem. Int. Ed.* **2017**, *56*, 4447-4451.
79. (a) M. Silvi, C. Verrier, Y. P. Rey, L. Buzzetti, P. Melchiorre, *Nat. Chem*. **2017**, *9*, 868-873; (b) C. Verrier, N. Alandini, C. Pezzetta, M. Moliterno, L. Buzzetti, H. B. Hepburn, A. Vega-Peñaloza, M. Silvi, P. Melchiorre, *ACS Catal*. **2018**, *8*, 1062-1066; (c) L. Woźniak, G. Magagnano, P. Melchiorre, *Angew. Chem. Int. Ed*. **2018**, *57*, 1068-1072; (d) D. Mazzarella, G. E. M. Crisenza, P. Melchiorre, *J. Am. Chem. Soc.* **2018**, *140*, 8439-8443; (e) P. Bonilla, Y. Rey, C. Holden, P. Melchiorre, *Angew. Chem. Int. Ed*. **2018**, *57*, 12819-12823. (f) L. A. Perego, P. Bonilla, P. Melchiorre, *Adv. Synth. Catal.* **2020**, *362*, 302-307.
80. J. J. Murphy, D. Bastida, S. Paria, M. Fagnoni, P. Melchiorre, *Nature* **2016**, *532*, 218-222.
81. X. Huang, E. Meggers, *Acc. Chem. Res.* **2019**, *52*, 833-847.
82. H. Huo, X. Shen, C. Wang, L. Zhang, P. Röse, L.-A. Chen, K. Harms, M. Marsch, G. Hilt, E. Meggers, *Nature* **2015**, *515*, 100-103.
83. (a) C. Wang, Y. Zheng, H. Huo, Philipp Röse, L. Zhang, K. Harms, G. Hilt, E. Meggers, *Chem. Eur. J.* **2015**, *21*, 7355-7359; (b) H. Huo, C. Wang, K. Harms, E. Meggers, *J. Am. Chem. Soc*. **2015**, *137*, 9551-9554; (c) X. Huang, R. D. Webster, K. Harms, E. Meggers, *J. Am. Chem. Soc.* **2016**, *138*, 12636-12642; (d) C. Wang, J. Qin, X. Shen, R. Riedel, K. Harms, E. Meggers, Angew. Chem. Int. Ed. **2016**, *55*, 685-688; (e) H. Huo, K. Harms, and E. Meggers, *J. Am. Chem. Soc.* **2016**, *138*, 6936-6939.
84. (a) X. Huang, T. R. Quinn, K. Harms, R. D. Webster, L. Zhang, O. Wiest, E. Meggers, *J. Am. Chem. Soc.* **2017**, *139*, 9120-9123; (b) N. Hu, H. Jung, Y. Zheng, J. Lee, L. Zhang, Z. Ullah, X. Xie, K. Harms, M.-H. Baik, E. Meggers, *Angew. Chem. Int.*

Ed. **2018**, *57*, 6242-6246. For an example of [3+2] photocycloaddition developed by the same group, see: (c) X. Huang, X. Li, X. Xie, K. Harms, R. Riedel, E. Meggers, *Nat. Commun*. **2017**, *8*, 2245.
85. C. Zhang, S. Chen, C.-X. Ye, K. Harms, L. Zhang, K. N. Houk, E. Meggers, *Angew. Chem. Int. Ed*. **2019**, *58*, 14462-14466.
86. Q. M. Kainz, C. D. Matier, A. Bartoszewicz, S. L. Zultanski, J. C. Peters, G. C. Fu, *Science* **2016**, *351*, 681-684.
87. Z. Zuo, H. Cong, W. Li, J. Choi, G. C. Fu, D. W. C. MacMillan, *J. Am. Chem. Soc.* **2016**, *138*, 1832-1835.
88. E. E. Stache, T. Rovis, A. G. Doyle, *Angew. Chem. Int. Ed*. **2017**, *56*, 3679-3683.
89. A. Hölzl-Hobmeier, A. Bauer, A. Vieira Silva, S. M. Huber, C. Bannwarth, T. Bach, *Nature* **2018**, *564*, 240-243.
90. A. Tröster, A. Bauer, C. Jandl, T. Bach, *Angew. Chem. Int. Ed*. **2018**, *58*, 3538-3541.
91. L. Wimberger, T. Kratz, T Bach, *Synthesis* **2019**, 51, 4417-4416.
92. N. Y. Shin, J. M. Ryss, X. Zhang, S. J. Miller, R. R. Knowles, *Science* **2019**, *366*, 364-369.
93. J. Liu, R. Liu, Y. Wei, M. Shi, *Trends in Chemistry* **2019**, *1*, 779-793.
94. (a) C. Ebner, E. M. Carreira, *Chem. Rev.* **2017**, *117*, 11651-11679; (b) S. J. Gharpure, L. N. Nanda, Tetrahedron Lett. **2017**, *58*, 711-720.
95. (a) T. F. Schneider, J. Kaschel, D. B. Werz, *Angew. Chem. Int. Ed*. **2014**, *53*, 5504-5523; (b) M. A. Cavitt, L. H. Phun, S. France, *Chem. Soc. Rev*. **2014**, *43*, 804-818; (c) H. K. Grover, M. R. Emmett, M. A. Kerr, *Org. Biomol. Chem*. **2015**, *13*, 655-671.
96. G. Stork, P. A. Grieco, *J. Am. Chem. Soc.* **1969**, *91*, 2407-2408.
97. R. B. Beal, M. A. Dombroski, B. B. Snider, *J. Org. Chem*. **1986**, *51*, 4391-4399.
98. A. T. Parsons, J. S. Johnson, *J. Am. Chem. Soc*. **2009**, *131*, 3122-3123.
99. S. Xing, W Pan, C Liu, J Ren, Z. Wang, *Angew. Chem. Int. Ed.* **2010**, *49*, 3215-3218.
100. H. Xiong, H. Xu, S. Liao, Z. Xie, Y. Tang, *J. Am. Chem. Soc*. **2013**, *135*, 7851-7854.
101. (a) K. S. Halskov, F. Kniep, V. H. Lauridsen, E. H. Iversen, B. S. Donslund, K. A. Jørgensen, *J. Am. Chem. Soc.* **2015**, *137*, 1685-1691; (b) J. Blom, A. Vidal-Albalat, J. Jørgensen, C. L. Barløse, K. S. Jessen, M. V. Iversen, K. A. Jørgensen, *Angew. Chem. Int. Ed.* **2017**, *56*, 11831-11835; for an iminium ion strategy reported by Vicario's group, see: (c) E. Sanchez-Diez, D. L. Vesga, E. Reyes, U. Uria, L. Carrillo, J. L. Vicario, *Org. Lett*. **2016**, *18*, 1270-1273.
102. (a) T. Hudlicky, J. W. Reed, *Angew. Chem. Int. Ed*. **2010**, *49*, 4864-4876, (b) M. Meazza, H Guo, R. Rios, *Org. Biomol. Chem*. **2017**, *15*, 2479-2490.
103. (a) N. Neureiter, *J. Org. Chem*. **1959**, *24*, 2044-2046; (b) J. B. Cloke, *J. Am. Chem. Soc*. **1929**, *51*, 1174-1187; (c) C. L. Wilson, *J. Am. Chem. Soc*. **1947**, *69*, 3002-3004.
104. (a) L. A. Paquette, G. V. Meehan, R. P. Henzel, R. F. Eizember, *J. Org. Chem*. **1973**, *38*, 3250-3256. (b) H. R. Sonawane, B. S. Nanjundiah, V. G. Shah, D. G. Kulkarni, J. R. Ahuja, *Tetrahedron Lett.* **1991**, *32*. 1107-1108.
105. R. K. Bowman, J. S. Johnson, *Org. Lett* **2006**, *8*, 573-576.
106. C. D. Schmidt, J. Kaschel, T. F. Schneider, D. Kratzert, D. Stalke, D. B. Werz, *Org. Lett*. **2013**, *15*, 6098-6101.
107. A. Ortega, R. Manzano, U. Uria, L. Carrillo, E. Reyes, T. Tejero, P. Merino, J. L. Vicario, *Angew. Chem. Int. Ed*. **2018**, *57*, 8225-8229.
108. G.-Q. Li, L.-X. Dai, S.-L. You, *Org. Lett*. **2009**, *11*, 1623-1625.
109. O. A. Ivanova, A. O. Chagarovskiy, A. N. Shumsky, V. D. Krasnobrov, I. I. Levina, I. V. Trushkov, *J. Org. Chem.* **2018**, *83*, 543-560.
110. (a) Z. Lu, M. Shen, T. P. Yoon, *J. Am. Chem. Soc*. **2011**, *133*, 1162-1164; (b) A. G. Amador, E. M. Sherbrook, T. P. Yoon, *J. Am. Chem. Soc*. **2016**, *138*, 4722-4725.
111. C. Wang, X. Ren, H. Xie, Z. Lu, *Chem. Eur. J*. **2015**, *21*, 9676-9680.
112. X. Huang, J. Lin, T. Shen, K. Harms, M. Marchini, P. Ceroni, E. Meggers, *Angew. Chem. Int. Ed.* **2018**, *57*, 5454-5458.
113. (a) J. Stavinoha, E. Bay, A. Leone, P. S. Mariano, *Tetrahedron Lett*. **1980**, *21*, 3455-3458; (b) P. S. Mariano, J. Stavinoha, E. Bay, *Tetrahedron* **1981**, *37*, 3385-3395.
114. T. Hashimoto, Y. Kawamata, K. Maruoka, *Nat. Chem*. **2014**, *6*, 702-705.
115. (a) C.-H. Lin, D. Pursley, J. E. M. N. Klein, J. Teske, J. A. Allen, F. Rami, A. Köhn, B. Plietker, *Chem. Sci*. **2015**, *6*, 7034-7043; (b) L. A. Bîldt, X. Guo, A. Prescimone, O. S. Wenger, *Angew. Chem. Int. Ed*. **2016**, *55*, 11247-11250.
116. J. Luis-Barrera, R. Mas-Ballesté, J. Alemán, *ChemPlusChem* **2015**, *80*, 1595-1600.
117. (a) G. S. Bbosa, D. Kitya, A. Lubega, J. Ogwal-Okeng, W. W. Anokbonggo, D. B. Kyegombe, "Review of the Biological and Health Effects of Aflatoxins on Body Organs and Body Systems, Aflatoxins - Recent Advances and Future Prospects (Chapter 12)", *IntechOpen*, **2013**, 239-265. (b) D. H. R. Barton, H. T. Cheung, A. D. Cross, L. M. Jackman, M. Martin-Smith, *J. Chem. Soc.* **1961**, 5061-5072. (c) P. S. Steyn, R. Vleggaar, *J. Chem. Soc., Perkin Trans. 1* **1974**, 2250-2256. (d) R. Kaur, S. K. Chattopadhyay, A. Chatterjee, O. Prakash, F. Khan, N. Suri, D. Priya, A. K. Saxena, *Med. Chem. Res.* **2014**, *23*, 4138-4148.
118. (a) S. Bertelsen, K. A. Jørgensen, *Chem. Soc. Rev*., **2009**, *38*, 2178-2189; (b) G. Lelais, D. W. C. MacMillan, *Aldrichimica Acta* **2006**, *39*, 79-87.
119. (a) A. Erkkilä, I. Majander, P. M. Pihko, *Chem. Rev.* **2007**, *107*, 5416-5470; (b) S. Mukherjee, J. W. Yang, S. Hoffmann, B. List, *Chem. Rev*. **2007**, *107*, 5471-5569; (c) P. Melchiorre, M. Marigo, A. Carlone, G. Bartoli, *Angew. Chem. Int. Ed*. **2008**, *47*, 6138- 6171; (d) D. W. C. MacMillan, *Nature* **2008**, *455*, 304-308.
120. T. D. Beeson, A. Mastracchio, J.-B. Hong, K. Ashton, D. W. C. MacMillan, *Science* **2007**, *316*, 582-585.
121. (a) H.-Y. Jang, J.-B. Hong, D. W. C. MacMillan, *J. Am. Chem. Soc*. **2007**, *129*, 7004-7005; (b) T. H. Graham, C. M. Jones, N. T. Jui, D. W. C. MacMillan, *J. Am. Chem. Soc*. **2008**, *130*, 16494-16495; (c) H. Kim, D. W. C. MacMillan, *J. Am. Chem. Soc*. **2008**, *130*, 398-399; (d) M. Amatore, T. D. Beeson, S. P. Brown, D. W. C. MacMillan, *Angew. Chem. Int. Ed*. **2009**, *48*, 5121-5124; (e) J. C. Conrad, J. Kong, B. N. Laforteza, D. W. C. MacMillan, *J. Am. Chem. Soc*. **2009**, *131*, 11640-11641; (f) A. Mastracchio, A. A. Warkentin, A. M. Walji, D. W. C. MacMillan, *PNAS* **2010**, *107*, 20648-20651.
122. (a) N. Vignola, B. List, *J. Am. Chem. Soc*. **2004**, *126*, 450-451; (b) A. Fu, B. List, W. Thiel, *J. Org. Chem*. **2006**, *71*, 320-326.

123. (a) D. A. Nagib, M. E. Scott, D. W. C. MacMillan, *J. Am. Chem. Soc*. **2009**, *131*, 10875-10877; (b) H.-W. Shih, M. N. Vander Wal, R. L. Grange, D. W. C. MacMillan, *J. Am. Chem. Soc*. **2010**, *132*, 13600-13603; (c) E. R. Welin, A. A. Warkentin, J. C. Conrad, D. W. C. MacMillan, *Angew. Chem. Int. Ed*. **2015**, *54*, 9668-9672; for a photocatalyst-free strategy employing a photoactive radical precursor, see: (d) G. Cecere, C. M. König, J. L. Alleva, D. W. C. MacMillan, *J. Am. Chem. Soc.* **2013**, *135*, 11521-11524.
124. A. G. Capacci, J. T. Malinowski, N. J. McAlpine, J. Kuhne, D. W. C. MacMillan, *Nat. Chem*. **2017**, *6*, 1073-1077.
125. W. Ding, L.-Q. Lu, Q.-Q. Zhou, Y. Wei, J.-R. Chen, W.-J. Xiao, *J. Am. Chem. Soc.* **2017**, *139*, 63-66.
126. X. Shen, Y. Li, Z. Wen, S. Cao, X. Hou, L. Gong, *Chem. Sci*. **2018**, *9*, 4562-4568.
127. Y. Li, K. Zhou, Z. Wen, S. Cao, X. Shen, M. Lei, L. Gong, *J. Am. Chem. Soc.* **2018**, *140*, 15850-15858.
128. (a) A. Gualandi, M. Marchini, L. Mengozzi, M. Natali, M. Lucarini, P. Ceroni, P. G. Cozzi, *ACS Catal*. **2015**, *5*, 5927-5931; (b) P. Riente, M. Matas Adams, J. Albero, E. Palomares, M. A. Pericàs, *Angew. Chem. Int. Ed*. **2014**, *53*, 9613-9616; (c) M. Cherevatskaya, M. Neumann, S. Füldner, C. Harlander, S. Kümmel, S. Dankesreiter, A. Pfitzner, K. Zeitler, B. König, *Angew. Chem. Int. Ed.* **2012**, *51*, 4062-4066; (d) M. Neumann, S. Füldner, B. König, K. Zeitler, *Angew. Chem. Int. Ed*. 2011, *50*, 951-954; (e) K. Fidaly, C. Ceballos, A. Falguières, M. Sylla-Iyarreta Veitia, A. Guy, C. Ferroud, *Green Chem*. **2012**, *14*, 1293-1297.
129. S. Poplata, A. Tröster, Y.-Q. Zou, T. Bach, *Chem. Rev*. **2016**, *116*, 9748-9815.
130. C. Liebermann, *Ber. Dtsch. Chem. Ges*. **1877**, *10*, 2177-2179.
131. G. O. Schenck, W. Hartmann, S.-P. Mannsfeld, W. Metzner, C. H. Krauch, *Chem. Ber*. **1962**, *95*, 1642-1647.
132. P. E. Eaton, *J. Am. Chem. Soc*. **1962**, *84*, 2454-2455.
133. P. De Mayo, H. Takeshita, A. B. M. A. Sattar, *Proc. Chem. Soc.* **1962**, 119.
134. E. J. Corey, R. B. Mitra, H. Uda, *J. Am. Chem. Soc.* **1963**, *85*, 362-363.
135. R. Brimioulle, A. Bauer, T. Bach, *J. Am. Chem. Soc*. **2015**, *137*, 5170-5176.
136. R. Brimioulle, T. Bach, *Angew. Chem. Int. Ed*. **2014**, *53*, 12921-12924.
137. S. Poplata, T. Bach, *J. Am. Chem. Soc.* **2018**, *140*, 3228-3231.
138. (a) M. A. El-Sayed, *Acc. Chem. Res.* **1968**, *1*, 8-16; (b) P. Klán, J. Wirz, "Photochemistry of Organic Compounds", Wiley, Chichester **2009**, 38-39.
139. S. Stegbauer, C. Jandl, T. Bach, *Angew. Chem. Int. Ed.* **2018**, *57*, 14593-14596.
140. C. Chen, V. Chang, X. Cai, E. Duesler, P. S. Mariano, *J. Am. Chem. Soc*. **2001**, *123*, 6433-6434.
141. F. M. Hörmann, T. S. Chung, E. Rodriguez, M. Jakob, T. Bach, *Angew. Chem. Int. Ed*. **2018**, *57*, 827-831.
142. N. Vallavoju, S. Selvakumar, S. Jockusch, M. P. Sibi, J. Sivaguru, *Angew. Chem. Int. Ed*. **2014**, *53*, 5604-5608.
143. S. Fukuzumi, H. Kotani, K. Ohkubo, S. Ogo, N. V. Tkachenko, H. Lemmetyinen, *J. Am. Chem. Soc*. **2004**, *126*, 1600-1601.
144. K. Suga, K. Ohkubo, S. Fukuzumi, *J. Phys. Chem. A* **2003**, *107*, 4339-4346.
145. H. Kotani, K. Ohkubo, S. Fukuzumi, *J. Am. Chem. Soc.* **2004**, *126*, 15999-16006.
146. K. Ohkubo, K. Suga, S. Fukuzumi, *Chem. Commun*. **2006**, 2018-2020.
147. H. J. Xu, X. L. Xu, Y. Fu, Y. S. Feng, *Chin. Chem. Lett*. **2007**, *18*, 1471-1475.
148. K. Ohkubo, K. Mizushima, R. Iwata, S. Fukuzumi, *Chem. Sci*. **2011**, *2*, 715-722.
149. K. Ohkubo, K. Mizushima, R. Iwata, K. Souma, N. Suzuki, S. Fukuzumi, *Chem. Commun*. **2010**, *46*, 601-603.
150. A. G. Griesbeck, M. Cho, *Org. Lett*. **2007**, *9*, 611-613.
151. K. Ohkubo, A. Fujimoto, S. Fukuzumi, *Chem. Commun*. **2011**, *47*, 8515-8517.
152. (a) T. M. Nguyen, D. A. Nicewicz, *J. Am. Chem. Soc*. **2013**, *135*, 9588-9591; (b) T. M. Nguyen, N. Manohar, D. A. Nicewicz, *Angew. Chem. Int. Ed*. **2014**, *53*, 6198-6201.
153. A. J. Perkowski, D. A. Nicewicz, *J. Am. Chem. Soc*. **2013**, *135*, 10334-10337; (b) P. D. Morse, D. A. Nicewicz, *Chem. Sci*., **2015**, *6*, 270-274.
154. (a) J.-M. M. Grandjean, D. A. Nicewicz, *Angew. Chem. Int. Ed*. **2013**, *52*, 3967-3971; (b) M. A. Zeller, M. Riener, D. A. Nicewicz, *Org. Lett*. **2014**, *16*, 4810-4813; (c) N. J. Gesmundo, J.-M. M. Grandjean, D. A. Nicewicz, *Org. Lett*. **2015**, *17*, 1316-1319; (d) C. L. Cavanaugh, D. A. Nicewicz, *Org. Lett*. **2015**, *17*, 6082-6085.
155. D. J. Wilger, J.-M. M. Grandjean, T. R. Lammert, D. A. Nicewicz, *Nat. Chem*. **2014**, *6*, 720-726.
156. N. A. Romero, K. A. Margrey, N. E. Tay, D. A. Nicewicz, *Science* **2015**, *349*, 1326-1330.
157. K. A. Margrey, J. B. McManus, S. Bonazzi, F. Zecri, D. A. Nicewicz, *J. Am. Chem. Soc.* **2017**, *139*, 11288-11299.
158. J. B. McManus, D. A. Nicewicz, *J. Am. Chem. Soc.* **2017**, *139*, 2880-2883.
159. W. Chen, Z. Huang, N. E. S. Tay, B. Giglio, M. Wang, H. Wang, Z. Wu, D. A. Nicewicz, Z. Li, *Science* **2019**, *364*, 1170-1174.
160. J. D. Griffin, M. A. Zeller, D. A. Nicewicz, *J. Am. Chem. Soc.* **2015**, *137*, 11340-11348.
161. A. Joshi-Pangu, F.Lévesque, H. G. Roth, S. F. Oliver, L.-C. Campeau, D. Nicewicz, D. A. DiRocco, *J. Org. Chem.* **2016**, *81*, 7244-7249.
162. (a) N. E. S. Tay, D. A. Nicewicz, *J. Am. Chem. Soc*. **2017**, *139*, 16100-16104; (b) N. Holmberg-Douglas, D. A. Nicewicz *Org. Lett.* **2019**, *21*, 7114-7118.
163. F. Wu, L. Wang, J. Chen, D. A. Nicewicz, Y. Huang, *Angew. Chem. Int. Ed*. **2018**, *57*, 2174-2178.
164. K. A. Margrey, W. L. Czaplyski, D. A. Nicewicz, E. J. Alexanian, *J. Am. Chem. Soc*. **2018**, *140*, 4213-4217.
165. J. B. McManus, N. P. R. Onuska, D. A. Nicewicz, *J. Am. Chem. Soc*. **2018**, *140*, 9056-9060.
166. J. K. Matsui, D. N. Primer, G. A. Molander, *Chem. Sci*. **2017**, *8*, 3512-3522.
167. (a) A. Baeyer, *Ber. Dtsch. Chem. Ges*. **1871**, *4*, 555-558; (b) A. V. Dubrovskiy, R. C. Larock, *J. Org. Chem*. **2012**, *77*, 11232-11256; (c) T. Tsudaka, H. Kotani, K. Ohkubo, T. Nakagawa, N. V. Tkachenko, H. Lemmetyinen, S. Fukuzumi, *Chem. Eur. J*. **2017**, *23*, 1306-1317; (d) C. Fischer, C. Sparr, *Angew. Chem. Int. Ed*. **2018**, *57*, 2436-2440.
168. R. P. Herrera, E. Marqués-López, "Multicomponent Reactions: Concepts and Applications for Design and Synthesis", **2015**, John Wiley and Sons.
169. A. Strecker, *Justus Liebigs Ann. Chem*. **1850**, *75*, 27-45.
170. A. Hantzsch, *Ber. Dtsch. Chem. Ges*. **1881**, *14*, 1637-1638.

171. P. Biginelli, *Ber. Dtsch. Chem. Ges*. **1891**, *24*, 1317-1319.
172. (a) M. Passerini, *Gazz. Chim. Ital.* **1921**, *51*, 126-129; (b) M. Passerini, *Gazz. Chim. Ital.* **1921**, *51*, 181-188.
173. I. Ugi, R. Meyr, U. Fetzer, C. Steinbrückner, *Angew. Chem*. **1959**, *71*, 386-386.
174. (a) T. Ngouansavanh, J. Zhu, *Angew. Chem. Int. Ed.* **2007**, *46*, 5775-5778; (b) A. Znabet, E. Ruijter, F. J. J. de Kanter, V. Khler, M. Helliwell, N. J. Turner, R. V. A. Orru, *Angew. Chem. Int. Ed*. **2010**, *49*, 5289-5292.
175. T. Stopka, L. Marzo, M. Zurro, S. Janich, E.-U. Würthwein, C. G. Daniliuc, J. Alemán, O. García Mancheño, *Angew. Chem. Int. Ed.* **2015**, *54*, 5049-5053.
176. A. Gini, J. Bamberger, J. Luis-Barrera, M. Zurro, R. Mas-Ballesté, J. Alemán, O. García Mancheño, *Adv. Synth. Catal*. **2016**, *358*, 4049-4056.
177. N. P. Ramirez, I. Bosque, J. C. Gonzalez-Gomez, *Org. Lett*. **2015**, *17*, 4550-4553.
178. (a) A. Loudet, K. Burgess, *Chem. Rev*. **2007**, *107*, 4891-4932; (b) G. Ulrich, R. Ziessel, A. Harriman, *Angew. Chem. Int. Ed.* **2008**, *47*, 1184-1201; (c) N. Boens, V. Leen, W. Dehaen, *Chem. Soc. Rev*. **2012**, *41*, 1130-1172.
179. (a) S. Kolemen, E. U. Akkaya, *Coord. Chem. Rev*. **2018**, *354*, 121-134; (b) S. Krajcovicova, J. Stankova, P. Dzubak, M. Hajduch, M. Soural, M. A. Urban, *Chem. Eur. J*. **2018**, *24*, 4957-4966; (c) T. Kowada, H. Maeda, K. Kikuchi, *Chem. Soc. Rev*. **2015**, *44*, 4953-4972; (d) P. Rivera-Fuentes, S. J. Lippard, *Acc. Chem. Res*. **2015**, *48*, 2927-2934; (e) Y. Ni, J. Wu, *Org. Biomol. Chem*. **2014**, *12*, 3774-3791; (f) R. Lincoln, L. E. Greene, W. Zhang, S. Louisia, G. Cosa, *J. Am. Chem. Soc*. **2017**, *139*, 16273-16281.
180. (a) N. Boens, B. Verbelen, W. Dehaen, *Eur. J. Org. Chem.* **2015**, 6577-6595. (b) N. Boens, B. Verbelen, M. J. Ortiz, L. Jiao, W. Dehaen, *Coord. Chem. Rev.* **2019**, *399*, 213024.
181. (a) L. Wang, B. Verbelen, C. Tonnelé, D. Beljonne, R. Lazzaroni, V. Leen, W. Dehaena, N. Boens, *Photochem. Photobiol. Sci.* **2013**, *12*, 835-847; (b) Y. Gabe, T. Ueno, Y. Urano, H. Kojima, T. Nagano, *Anal. Bioanal. Chem*. **2006**, *386*, 621-626; (c) A. B. Nepomnyashchii, M. Bröring, J. Ahrens, A. J. Bard, *J. Am. Chem. Soc*. **2011**, *133*, 8633-8645; (d) E. Palao-Utiel, L. Montalvillo-Jiménez, I. Esnal, R. Prieto-Montero, A. R. Agarrabeitia, I. García-Moreno, J. Bañuelos, I. López-Arbeloa, S. de la Moya, M. J. Ortiz, *Dyes Pigm.* **2017**, *141*, 286-298.
182. (a) Y. Gabe, Y. Urano, K. Kikuchi, H. Kojima, T. Nagano, *J. Am. Chem. Soc*. **2004**, *126*, 3357-3367; (b) T. Ueno, Y. Urano, H. Kojima, T. Nagano, *J. Am. Chem. Soc*. **2006**, *128*, 10640-10641.
183. (a) I. K. Sideri, E. Voutyritsa, C. G. Kokotos, *Org. Biomol. Chem.* **2018**, *16*, 4596-4614; (b) L. Huang, J. Zhao, S. Guo, C. Zhang, J. Ma, *J. Org. Chem*. **2013**, *78*, 5627-5637 ; (c) We. Li, L. Li, H. Xiao, R. Qi, Y. Huang, Z. Xie, X. Jing, H. Zhang, *RSC Adv*. **2013**, *3*, 13417-13421.
184. (a) P. Kaur, K. Singh, *J. Mater. Chem. C* **2019**, *7*, 11361-11405; (b) A. Kamkaew, S. H. Lim, H. B. Lee, L. V. Kiew, L. Y. Chung, K. Burgess, *Chem. Soc. Rev.* **2013**, *42*, 77-88; (c) H. Tanaka, Y. Inoue, T. Mori, *ChemPhotoChem* **2018**, *2*, 386-402.
185. (a) W. Xu, K. M. Chan, E. T. Kool, *Nat. Chem*. **2017**, *9*, 1043-1055; (b) J. Wang, J. Zhang, Y. M. Lee, S. Ng, Y. Shi, Z.-C. Hua, Q. Lin, H.-M. Shen, *Nat. Protoc*. **2017**, *12*, 279-288; (c) X. Chen, Y.-W. Wu, *Org. Biomol. Chem*. **2016**, *14*, 5417-5439; (d) J. M. Chalker, G. J. L. Bernardes, B. G. Davis, *Acc. Chem. Res*. **2011**, *44*, 730-741.
186. (a) M. Albrecht, A. Lippach, M. P. Exner, J. Jerbi, M. Springborg, N. Budisab, G. Wenz, *Org. Biomol. Chem*. **2015**, *13*, 6728-6736; (b) M. H. Y. Cheng, H. Savoie, F. Bryden, R. W. Boyle, *Photochem. Photobiol. Sci.* **2017**, *16*, 1260-1267; (c) N. Zhao, T. M. Williams, Z. Zhou, F. R. Fronczek, M. Sibrian-Vazquez, S. D. Jois, M. G. H. Vicente, *Bioconjugate Chem*. **2017**, *28*, 1566-1579; (d) P. S. Deore, D. V. Soldatov, R. A. Manderville, *Scientific Reports* **2018**, *8*, 16874; (e) L. C. D. de Rezende, F. A. da Silva Emery, *Orbital Elec. J. Chem.* **2013**, *5*, 62-83.
187. L. Mendive-Tapia, C. Zhao, A. R. Akram, S. Preciado, F. Albericio, M. Lee, A. Serrels, N. Kielland, N. D. Read, R. Lavilla, M. Vendrell, *Nat. Commun*. **2016**, *7*, 10940.
188. (a) W. Wang, M. M. Lorion, O. Martinazzoli, L. Ackermann, *Angew. Chem. Int. Ed.* **2018**, *57*, 10554-10558; for a similar strategy regarding a BODIPY-labeling over cyclobutane derivatives, see: (b) M. Virelli, W. Wang, R. Kuniyil, J. Wu, G. Zanoni, A. Fernandez, J. Scott, M. Vendrel, L. Ackermann, *Chem. Eur. J.* **2019**, *25*, 12712-12718.
189. For recent reviews on the topic, see: (a) J. Adrio, J. C. Carretero, *Chem. Commun*. **2014**, *50*, 12434-12446; (b) T. Hashimoto, K. Maruoka, *Chem. Rev*. **2015**, *115*, 5366-5412.
190. P. Allway, R. Grigg, *Tetrahedron Lett*. **1991**, *32*, 5817-5820.
191. J. M. Longmire, B. Wang, X. Zhang, *J. Am. Chem. Soc.* **2002**, *124*, 13400-13401.
192. A. S. Gothelf, K. V. Gothelf, R. G. Hazell, K. A. Jørgensen, *Angew. Chem., Int. Ed*. **2002**, *41*, 4236-4238.
193. S. Cabrera, R. G. Arrayás, J. C. Carretero, *J. Am. Chem. Soc.* **2005**, *127*, 16394-16395.
194. X.-X. Yan, Q. Peng, Y. Zhang, K. Zhang, W. Hong, X.-L. Hou, Y.-D. Wu, *Angew. Chem., Int. Ed*. **2006**, *45*, 1979-1983.
195. (a) T. Llamas, R. Gómez Arrayás, J. C. Carretero, *Org. Lett*. **2006**, *8*, 1795-1798; (b) A. López-Pérez, J. Adrio, J. C. Carretero, *J. Am. Chem. Soc.* **2008**, *130*, 10084-10085.
196. J. Hernández-Toribio, R. Gómez Arrayás, B. Martín-Matute, J. C. Carretero, *Org. Lett*. **2009**, *11*, 393-396.
197. P. Antonchick, C. Gerding-Reimers, M. Catarinella, M. Schürmann, H. Preut, S. Ziegler, D. Rauh, H. Waldmann, *Nat. Chem*. **2010**, *2*, 735-740.
198. J. Hernández-Toribio, S. Padilla, J. Adrio, J. C. Carretero, *Angew. Chem. Int. Ed*. **2012**, *51*, 8854-8858.
199. A. Pascual-Escudero, A. de Cózar, F. P. Cossío, J. Adrio, J. C. Carretero, *Angew. Chem. Int. Ed*. **2016**, *55*, 15334-15338.
200. I. J. Arroyo, R. Hub, B. Zhong Tang, F. I. López, E. Peña-Cabrera, *Tetrahedron* **2011**, *67*, 7244-7250.
201. A. Guerrero-Corella, J. Asenjo-Pascual, T. Janardan Pawar, S. Díaz-Tendero, A. Martín-Sómer, C. Villegas Gómez, J. L. Belmonte-Vázquez, D. E. Ramírez-Ornelas, E. Peña-Cabrera, A. Fraile, D. Cruz Cruz, J. Alemán, *Chem. Sci.* **2019**, *10*, 4346-4351.
202. V. Marcos, J. Alemán, *Chem. Soc. Rev*. **2016**, *45*, 6812-6832.